The Dissertation Committee for Key-Rok Choi
certifies that this is the approved version of the following dissertation:

# Jason-1 Precision Orbit Determination Using GPS Combined with SLR and DORIS Tracking Data

Committee:

Byron D Tapley, Supervisor

John C Ries

Che-Kwan Shum

Bob E Schutz

Robert H Bishop

Wallace T Fowler

# Jason-1 Precision Orbit Determination Using GPS Combined with SLR and DORIS Tracking Data

by

**Key-Rok Choi, B.S.**

**Dissertation**

Presented to the Faculty of the Graduate School of

The University of Texas at Austin

in Partial Fulfillment

of the Requirements

for the Degree of

**Doctor of Philosophy**

The University of Texas at Austin

December 2003

Dedicated to my parents...

# Acknowledgments

I was honored that Dr. Byron Tapley accepted the supervision of my dissertation. He also provided me this wonderful opportunity to study and work at the Center for Space Reseach, University of Texas at Austin as a Graduate Research Assistant. I really appreciate that. I must also thank my committee members, Drs. John Ries, Che-Kwan Shum, Bob Schutz, Robert Bishop and Wallace Fowler for their direction, as well as Drs. Srinivas Bettadpur, Raynor Duncombe, Roger Broucke and the late Dr. Victor Szebehely for their excellent lectures.

Special appreciation and respect has to be expressed to Dr. John Ries for providing this research topic, for being my mentor and for constant availability to answer my numerous questions. I also want to thank Dr. Hyung J. Rim for technical explanations about MSODP (Multi-Satellite Orbit Determination Program). I could not have finished this dissertation successfully without both of you.

This work was also helped by Jason-1 POD (Precision Orbit Determination) group. I want to thank Drs. Bruce Haines and Pascal Willis at NASA's Jet Propulsion Laboratory; Nikita Zelensky and Scott Luthcke at NASA Goddard Space Flight Center; Eelco Doornbos and Remko Scharroo at Delft Institute for Earth-Oriented Space Research (DEOS); and, Jean-Paul

Berthias and others at Centre National d'Etudes Spatiales (CNES) for providing their solutions to be compared. I also would like to thank Dr. Peter Nagel and Rich Risley for proof-reading, and Dr. Ries again for technical review and editing.

I will have to thank my friends for their support and encouragement, and for providing "food and beverage" for my body and mind over the past years living in Austin. They include Sungkoo Bae, Young-Hoon Han, Kwan-Dong Park, Daejong Kim, John NyunGeun Lee and Rich Risley. Especially, I would like to thank the Lees for many home-made Korean dinners and fun time, and to Rich Risley, for introducing many aspects of American life to me. I will cherish your friendship and I wish success for you in your areas. I also hope good luck to a future doctor, Dochul Yang and others.

And finally and most importantly, I would like to express my deepest appreciation to my family, especially to my Mom and Dad, for their love and many sacrifices. I know they are the proudest and happiest people in the world for me because of all that I have accomplished. If there is any glory for me finishing this work, I would give all the glory to them.

Key-Rok Choi
November, 2003

# Jason-1 Precision Orbit Determination Using GPS Combined with SLR and DORIS Tracking Data

Publication No. _____

Key-Rok Choi, Ph.D.
The University of Texas at Austin, 2003

Supervisor: Byron D Tapley

Jason-1, a follow-on altimeter mission to the TOPEX/POSEIDON (T/P) mission, carries receivers for DORIS (Doppler Orbitography and Radiopositioning Integrated by Satellite), SLR (Satellite Laser Ranging) and GPS (Global Positioning System) in support of the Precision Orbit Determination (POD) function. The radial orbit accuracy of the Jason-1 is expected to be 2 cm RMS or better in dynamic approach, with the objective of achieving an accuracy of 1 cm RMS through the improved dynamic models and measurement models. This will require significant improvement in current knowledge of surface force effects as well as improvement in knowledge of gravity field model.

Jason-1 orbits were computed with various combinations of three different types of tracking data to investigate the contribution of each tracking system to the accuracy of orbits. The GPS tracking data were analyzed and

utilized for POD with the DORIS and SLR tracking data using a dynamical approach. Parameterization related to empirical acceleration and antenna phase center was studied, and optimal relative weighting for each tracking system was examined. The effect of ground station selection on the orbit accuracy was also studied and a method of an optimal network selection was developed.

The orbit quality tests were performed through the analysis of tracking residuals, SLR residuals with high-elevation passes, orbit overlap comparisons, and altimeter crossover analysis. The study showed that the contribution of GPS tracking is significant to the improvement of orbit accuracy, especially when GPS tracking is supported by SLR tracking. The SLR residual RMS test, which is an independent and absolute measure of the radial orbit error, clearly indicates that we are approaching the 1-cm radial orbit accuracy for Jason-1.

# Table of Contents

# List of Tables

# List of Figures

# List of Algorithms

# Chapter 1

# Introduction

## 1.1 Overview

Since NASA's satellite altimetry program was first formulated in 1969 [Kaula, 1970], high precision satellite radar altimetry has become a fundamental tool for the study of the ocean surface topography. Previous altimetric satellite missions such as GEOS-3, Seasat, Geosat, ERS-1, ERS-2 and Topex/Poseidon (T/P) demonstrated the usefulness of satellite altimetry for measuring sea level and the ocean topography.

As a satellite altimeter measures the distance above the ocean surface, the usefulness of the measurement depends on the accuracy of the radial component of the satellite altimeter position. The accuracy of the orbit depends on the accuracy of the dynamic force models acting on the satellite, as well as the accuracy and coverage of the satellite tracking data. The errors introduced into the computed altimeter heights due to the radial orbit errors have historically been greater than the magnitude of the altimeter measurement errors before the launch of T/P at 1992, causing a major limitation in the accuracy of the sea surface height. At the time of the launch of Seasat in 1978 (July 1978-October 1978), the radial orbit error attainable from GEOS-

3 (April 1975-December 1978) was about 5 meters [Lerch *et al.*, 1982] and its altimeter measurement precision was 25 cm. The orbit errors for Geosat (March 1985-December 1989) was still at the 30 to 50 cm level in the late 1980s, although its altimeter measurement precision had already reached the 4 cm level [Chelton *et al.*, 2001, see page 2].

Launched on August 12, 1992, the T/P mission has become an example of the state-of-the-art in satellite altimetry. Its altimeter can measure the range from the spacecraft to the instantaneous sea surface with a precision of about 2 cm. The highly successful T/P mission has reduced the radial orbit errors to the level of 2 cm [Tapley *et al.*, 1996; Marshall *et al.*, 1995] from the original radial orbit error requirement of 13 cm rms [Stewart *et al.*, 1986]. The ERS-1 (July 1991-May 1996) and ERS-2 (August 1995-) satellites have also been benefited from the T/P mission to reduce their orbit errors by using crossover techniques and the improved gravity model.

The success of the T/P mission was primarily because of the success of the gravity model improvement. It was also due to the force and measurement model improvement in the POD software, and the precise and robust tracking provided by the satellite laser ranging (SLR) [Tapley *et al.*, 1993] network and the French DORIS doppler tracking system [Nöuel *et al.*, 1988]. The T/P POE is computed from the combined SLR/DORIS data, but the experimental Global Positioning System (GPS) tracking data was also tested to show that it can produce orbits with similar accuracy, if not better, when the GPS security feature such as Anti-Spoofing (A/S) is not active [Bertiger *et al.*, 1994; Schutz

*et al.*, 1994].

The Jason-1 spacecraft, the T/P follow-on, was launched from Vandenverg Air Force Base on December 7, 2001, supported by the state-of-the-art tracking systems: SLR, DORIS and GPS. In order to guarantee a seamless transition between T/P and Jason-1 sea level records, Jason-1 carries a 2.5 cm radial orbit error requirement with an aggressive goal of 1-cm RMS accuracy. The advanced satellite tracking systems, especially with the highly accurate BlackJack GPS receiver, will help the POD community achieve the 1-cm radial accuracy goal. In the following sections, the details of the Jason-1 mission, precision orbit determination concept, and the objectives of this dissertation will be discussed.

## 1.2 Background

### 1.2.1 T/P and Jason-1 Mission

The Jason-1 satellite, a joint project of NASA and CNES, the French space agency, is the follow-on to T/P, a U.S.-French spacecraft that has been making precise measurements of ocean surface topography with an accuracy of 4.2 cm, enabled scientists to forecast the 1997-1998 El Niño. These data are used to map ocean currents, improve the understanding of ocean circulation, measure global sea level change and improve global climate forecasts.

Like T/P, Jason-1 will provide accurate sea surface topography data. Other objectives are to monitor and interpret regional and global sea level change, to improve knowledge of ocean tides and to observe and use wave-

height and wind speed for marine meteorology. Additional contributions of Jason-1 data are foreseen in various domains like geodesy, geophysics, shallow water and coastal environment, enclosed sea circulation, inland water and land topography survey.


Figure 1.1: The Jason-1 Satellite: LRA, DORIS and GPS antennas are equipped for precise orbit determination.

The satellite (see Figure 1.1) includes the launcher adapter, the satellite bus and the instruments constituting the payload. The satellite bus is comprised of a platform and a payload module. Each component of the Jason-1 system has been designed to take into account the evolutions in satellite bus and instrument technology, and the improvements provided by the acquired experience and the highly demanding performance requirements of the scientific community.

The Jason-1 satellite has a design lifetime of three years but the components are built to withstand the expected radiation environment at the 1336-km altitude for five years. Table 1.1 shows the performance specification designed for Jason-1. Consumables are also sized for a five-year mission. The maximum power consumption is about 435 W. The overall satellite mass is less than 500 kg with full load of hydrazine (28 kg) and the satellite is about 3.4 meters high. Due to the high orbit nodal rate (2 per day), the satellite performs yaw-steering attitude control maneuvers to provide the solar arrays with proper solar illumination. The payload science data rate of 25 kbps is continuously stored in the onboard mass memory and is downloaded each time a ground terminal is within view at 613 kbits/s.

| | |
|---|---|
| Satellite mass | 500 kg |
| Satellite power | 450 W |
| Lifetime | Up to 5 years |
| Bus dry mass | 270 kg |
| Bus consumption | 300 W max. |
| Bus size (mm) | 954×954×1000 |
| Payload module size (mm) | 954×954×1218 |
| Storage capacity | 2 Gbits (EOL) |
| Downlink capacity | 650 kbps |
| Uplink capacity | 4 kbps |
| Pointing accuracy | 0.035 |
| V capacity | Up to 120 m/s |

Table 1.1: Jason-1 performance

Jason-1 uses an Earth orbiting satellite equipped with a radar altimeter and other instruments to directly measure sea surface elevation along a

fixed grid of sub-satellite ground tracks and thereby continues the data collection started with T/P. Jason-1 uses the same ground track pattern as T/P. Jason-1 measures the distance from the satellite to the sea surface to within approximately 2.5 cm (averaged over 1 sec). Precise orbit determination allows scientists to locate the spacecraft to within two or three centimeters and a combination with radar measurement allows scientists to achieve the Jason-1 primary mission objective–the production of accurate topographic maps of the world ocean.

The superb performance that the T/P mission has achieved owes much to the efforts made to optimize the satellite system. Jason-1 is adopting the same philosophy, building on the T/P heritage, but with a smaller satellite to reduce costs. Orbit parameters, which are similar to those of T/P, are also designed to fulfill the mission objectives as shown in Table 1.2. The satellite orbits at an altitude of 1336 kilometers above the Earth with a 66 degrees inclination. The orbit inclination of 66 degrees enables the satellite to cover most of the globe's unfrozen oceans. The orbit's repeat cycle is 9.9156 days (i.e., 10 days minus two hours). In approximately 10 days Jason-1 completes 127 passes, which is called a cycle. Thus, the satellite passes over the same point on the Earth's surface every ten days to within one kilometer and records sea-level measurements for the entire globe. The orbit is prograde and not Sun-synchronous. For the study of large-scale ocean variability, this cycle is a trade-off between spatial and temporal resolution.

Jason-1's high altitude (1,336 kilometers) reduces interactions with the

| Orbit characteristics | |
|---|---|
| Semi-major axis | 7714.4278 $km$ |
| Eccentricity | 0.000095 |
| Inclination (non-heliosynchronous) | 66.039° |
| Reference altitude (equatorial) | 1,336 $km$ |
| Nodal period<br>(duration of half-revolution or pass) | 6,745.72 seconds<br>($112'42''$ or 1h52$'$) |
| Repeat cycle | 9.9156 days |
| Number of passes per cycle | 254 |
| Ground track separation at Equator | 315 $km$ |
| Acute angle at Equator crossings | 39.5° |
| Longitude at Equator of pass 1 | 99.9242° |
| Orbital velocity | 7.2 $km/s$ |
| Ground scanning velocity | 5.8 $km/s$ |

Table 1.2: Jason-1 Orbit Characteristics

Earth's atmosphere and gravity field, thus making orbit determination easier and more precise. Significant progress of the general satellite orbit problem are mainly due to the improvement of the mathematical models of the dynamic and kinematic equations used for the satellite orbit computation. In the following section, the satellite orbit determination problem is further discussed.

### 1.2.2 Precise Orbit Determination Problem

The satellite orbit determination problem can be defined as the procedure to compute the state vector (position and velocity) of the center of mass of a satellite whose motion can be expressed by an equation of motion. To compute the state vector, continuous and discrete observations are needed. The clear definition of the time and coordinate reference systems is impor-

tant because the motions of the satellite and observers are often referred to different time and coordinate systems (see Chapter 2.1 for the details). The transformations between the systems should be applied accordingly.

There are various strategies for the satellite ephemerides estimation: 1) kinematic approach, 2) reduced-dynamic approach and 3) dynamic approach. The kinematic approach and the reduced-dynamic approach have been developed especially for GPS tracking and tested on T/P, which was the first user satellite that carried a GPS receiver for orbit determination.

The kinematic or geometric approach [Yunck & Wu, 1986] assumes that pseudorange measurements from at least four GPS satellites are collected continuously at once and also cycle-slip free carrier phase measurements are available for pseudorange smoothing. Since the filter can estimate a three dimensional position independently at each measurement time, this approach does not require a dynamic force model for the user satellite. The kinematic solution, however, is very sensitive to the accuracy of the tracking data and the geometry of the observing GPS satellites.

The reduced dynamic approach [Wu *et al.*, 1989] utilizes both geometric and dynamic information to compensate for the imperfect measurements. This approach is realized by treating unmodeled or mismodeled spacecraft accelerations as stochastic processes to absorb dynamic model errors [Wu *et al.*, 1991; Yunck *et al.*, 1994]. Other data types such as DORIS can be combined with GPS to support certain variations of reduced-dynamic tracking [Barotto, 1995; Willis *et al.*, 2002].

The dynamic orbit determination approach [Tapley, 1973] is the most general method of POD and requires precise force models acting on the satellite. The procedure typically involves an iterative least-squares estimation seeking best fits of selected model parameters and model-predicted satellite position and velocity to the tracking data along an orbit arc. The predicted state at each epoch is integrated by using the satellite equations of motion requiring accurate force models. This least-squares adjustment produces a new initial state vector, which corrects for much of the error in the previous initial conditions and errors in the force model. The resulting solution's accuracy depends on accuracy of the force models and the model parameter adjustment strategy. The estimation of sub-arc empirical acceleration terms in the dynamical POD practice gives the same effect as the stochastic variations in the reduced-dynamic accelerations.

The mathematical models, to describe the motion of an orbiting object in the dynamic orbit determination approach, have been greatly improved over the last decade with better understanding of the nature of the forces on a spacecraft. Also, the intensive post-launch tuning of the T/P force models yielded significant improvement in the ability to model the satellite orbit dynamically. One of the significantly improved force models is the gravity model. With the understanding that the gravity model was the primary error source for the T/P radial orbit, a decade-long gravity model improvement effort was initiated by the T/P project, which resulted in the Joint Gravity Model (JGM-1) [Nerem *et al.*, 1994]. This model, along with other model and

tracking system improvements, resulted in a prelaunch radial orbit accuracy on the order of 6 cm. Post-launch adjustment of the gravity model resulted in JGM-2 [Nerem *et al.*, 1994], which reduced the errors to the 3-4 cm level [Tapley *et al.*, 1994]. The production orbits of T/P are based on the tracking data from SLR and DORIS, but an experimental GPS tracking receiver was also placed onboard [Bertiger *et al.*, 1994; Melbourne *et al.*, 1994]. In 1995, the incorporation of the GPS data led to a new model, JGM-3 [Tapley *et al.*, 1996]. Combined with improved tide models based on the T/P altimeter data, and some additional refinements of the orbit determination strategy, the current orbit accuracy of approximately 2 cm was achieved [Marshall *et al.*, 1995]. In this study for Jason-1 POD, JGM-3 is used for the nominal gravity model.

As further discussed in Section 3.1, one of the principal limitations to further improving the orbit accuracy is the problem of modeling the complex surface forces acting on the spacecraft. The improved design of the GPS processor on Jason-1 may provide the opportunity for further enhancements to the orbit accuracy, since the enhanced GPS receiver on Jason-1 has the potential to allow a more refined parameterization of the force model errors, which is a requirement for orbits at the 1-cm level. In this study, the multi-satellite orbit determination program (MSODP), a dynamic approach which has been developed especially for the GPS data at the University of Texas at Austin (UT) Center for Space Research (CSR), is used. The least square batch filter design and problem formulation for MSODP is described by Rim [1992, see Section 2.5].

### 1.2.3 Measurement Systems: SLR, DORIS and GPS

Like T/P, Jason-1 carries a payload of five instruments to provide measurements for at least three years with full redundancy: the POSEIDON-2 altimeter with two frequencies (13.6 GHz for Ku-band and 5.3 GHz for C-band); the three-frequency Jason-1 microwave radiometer (JMR) with channels at 18.7 GHz, 23.8 GHz, and 34.0 GHz to determine the atmospheric water vapor content in the nadir column in order to correct the radar altimetry measurement; and three tracking systems: DORIS, a Laser Retro-reflector Array (LRA) and a GPS space receiver called the Turbo Rogue Space Receiver (TRSR). The primary tracking systems for T/P were laser ranging and the French DORIS Doppler tracking system. The GPS receiver was flown as a demonstration of the ability of GPS to support high precision POD. With advanced technology, the GPS contribution to the Jason-1 POD is expected to increase.

The DORIS receiver is a radio tracking system developed by CNES, using the Doppler shift of ground beacon signals to provide high precision orbit determination. The onboard package is comprised of the Doppler receiver for Radial Velocity Measurement (MVR), the Ultra Stable Oscillator (USO) housed in a single enclosure providing magnetic shielding, a switch box and an associated antenna. The DORIS receiver on Jason-1 supports the collection of precise Doppler measurements on two radio frequencies (2036.25 MHz and 401.25 MHz). MVR provides a dual terrestrial beacon receiving capability to improve the geometric observability in orbit and an onboard real-time

function called DIODE to compute orbit ephemeris data accurate to 1 meter rms (30 cm for the radial component). Currently, a global network of transmitting beacons is comprised of about 60 stations. In terms of in-flight noise characteristics, the receiver performs better than on T/P ($< 0.4 mm/s$ vs. $0.5\ mm/s$). The DORIS/Jason-1 onboard package, including the Doppler receiver, USO and antenna, was subcontracted to Dassault Electronic (now Thomson Detexis) with CEPE for the USO and Starec for the antenna. These contractors also developed the hardware for DORIS/Topex, DORIS/Spot and DORIS/ENVISAT.

The Laser Retroreflector Array (LRA) provides a target for laser tracking measurements and is used to calibrate the POD system. LRA reflects incoming laser beams from the ground allowing the calibration of the radial position of the satellite. The totally passive array, which was designed to reflect laser pulses back to their point of origin on Earth, is placed on the nadir face of the satellite. The unit consists of nine quartz corner cube retro-reflectors arrayed as a truncated cone with one in the center and the other eight distributed azimuthally around the cone to provide a near-hemispherical response. The retro-reflectors are optimized for a wavelength of 532 nanometers (green), offering a field of view of about 100 degrees. The Jason-1 LRA was manufactured by ITE Inc., under contract to NASA Goddard Space Flight Center (NASA/GSFC). The LRA allows the Jason-1 spacecraft to be tracked with the centimeter accuracy by approximately 40 satellites laser ranging (SLR) stations which make up the International Laser Ranging Service (ILRS).

The Turbo Rogue Space Receiver (TRSR) is a Global Positioning System (GPS) receiver developed by the Jet Propulsion Laboratory (JPL) to provide backup precise orbit determination in post-processing with a radial accuracy of better than 2.5 cm. The "BlackJack" GPS Turbo-Rogue Space Receiver can continuously track up to 12 GPS spacecraft simultaneously on two frequencies. From these signals the instrument acquires measurements of the GPS carrier phase (which can be interpreted as range change) with a precision of about 1 mm and the absolute pseudo-range (defined as the absolute range plus receiver time offset from GPS time) with a precision of about 10 cm. The TRSR will also offer onboard solutions for spacecraft position and time accurate to about 50 m and 150 ns, respectively. The onboard package includes two independent single-string receivers in cold redundancy, each comprising an up-looking antenna which provides a nearly hemispherical field of view, low-noise amplifier, crystal oscillator, sampling downconverter, and baseband digital processor. Fabrication of the TRSR flight units has been subcontracted to Spectrum Astro Inc. of Gilbert, Arizona.

The BlackJack GPS receiver uses advanced-codeless tracking techniques to enable the formation of precise pseudorange and carrier-phase observations on the two principle GPS frequencies (L1 and L2) regardless of the encryption status of the GPS constellation. The experimental versions of the receiver are successfully operating on CHAMP (German scientific mission, July 2000-) and SAC-C (Argentine satellite, November 2000-). Spectrum Astro Inc. built advanced versions of the receivers for Jason-1, ICESat (January 2003-) and the

twin GRACE satellites (March 2002-). More on the measurement precision improvement will be discussed in Section 3.1.

## 1.3 Objectives

Overall objectives of this dissertation are: 1) to evaluate the performance of each measurement type in the combined data to see its advantages and disadvantages, and 2) to maximize each tracking data type for the best accuracy of the Jason-1 orbit. The essential investigations of the dissertation are to determine which combination of measurement types will produce the best orbits, to explore the sensitivity of the orbit to the relative weighting of the data, and to determine the optimal relative weighting of each processed measurement type. Implementation or modification of necessary tools in MSODP to process the combined measurements will be a part of this study. To employ the SLR/DORIS data in MSODP, the SLR/DORIS orbits processed in the MSODP software were verified with the orbits processed in the UTOPIA software used for the T/P orbit determination. Despite its sparseness, SLR tracking is expected to provide an essential role for the orbit centering to constrain the orbit to the reference frame. When the different measurement types are combined, the distinction in the contribution of GPS and DORIS will be an interesting question. The dominant advantage of DORIS tracking is the large number of well-distributed DORIS stations providing near continuous coverage. Since GPS tracking is potentially superior to DORIS as well as its cheap implementation cost, GPS tracking will likely be a significant or primary

tracking type for future altimetric satellites. This study may help to answer the question of whether a GPS receiver should be required on the Ocean Surface Topography Mission (OSTM or Jason-2) scheduled to be launched in 2006 [J. Ries, personal communication, 2002].

The goal of this dissertation for Jason-1 orbit determination is to achieve an orbit accuracy equivalent to or better than currently obtained for T/P, which was ∼2.5 cm, with an aggressive goal of 1-cm RMS accuracy. To achieve this goal, the full potential of each measurement will be utilized in the combined data by optimizing the procedures and models. The important issues that will be discussed in this dissertation can be summarized as follows:

- The optimal parameterization level will be investigated. Selection of an optimal subarc length for estimation of surface force parameters and empirical acceleration parameters will strengthen the contribution of the dense GPS tracking.

- Gravity models for the best performing Jason-1 orbits will be examined.

- Different solar radiation force models for Jason-1 will be tested. Surface model error can be a major orbit error source due to the small mass-to-area ratio of Jason-1.

- The best estimation strategy for the Center-of-Mass (CoM) offset will be investigated. Especially for GPS, the CoM estimation has proved to be beneficial according to T/P experience.

- The optimal relative weight for the measurement combination will be determined.

Additionally the possibility of improving the orbit accuracy with the selection of the optimal station network is explored.

For Jason-1, ITRF2000 coordinates will be applied to all measurements and among all POD groups. Unlike T/P, using the consistent reference system may reduce the miscentering among external orbits, which might be caused by the usage of different reference frames. The orbit solutions will be assessed with the crossover data test and the SLR residual test, as well as compared to orbits determined by external institutes using various approaches.

## 1.4 Outline of Study

Chapter 2 introduces the time and coordinate systems, the dynamic models and measurement models implemented in MSODP. The models include force models specific to the Jason-1 satellite and observation models for all three measurement types.

Chapter 3 presents the model improvement of the Jason-1 satellite over its predecessor, T/P. The impact of the force model and measurement model improvement on the possible orbit accuracy for Jason-1 over the present T/P orbit accuracy will be discussed. The measures to assess the orbit performance will also be summarized in this chapter.

In Chapter 4, the Jason-1 GPS tracking data from cycle 8 to cycle 20

will be examined in detail. The GPS-only orbit will then be obtained through many parameterization experiments. Several important issues such as optimal estimation frequency for empirical parameters, center-of-mass (CoM) offset estimation, GPS satellite orbit element correction (OEC) and solar radiation model to determine a best solution will be discussed.

The orbits presented in Chapter 5 are an essential part of this research. In Chapter 5, the SLR and DORIS tracking data for Jason-1 will be combined with the GPS data to determine 'mixed orbits'. The optimal relative weighting for each measurement type will be explored. Comparison of orbits from each measurement, or from different combinations of each measurement type in MSODP will be conducted to investigate each measurement's contribution to the Jason-1 POD and to find the combination producing the best performing orbit. The external orbit comparison between POD groups will be also performed.

Chapter 6 will examine the effect of the GPS ground station selection on Jason-1 orbits. The effect of selected ground station numbers and the effect of the hemispherical distribution on the orbit quality will be discussed. Then, the optimal distribution set will be determined, and the orbit performance improvement with the optimal distribution sets will be tested.

Finally, Chapter 7 concludes the study and possibilities for the further precision orbit improvement will be discussed.

# Chapter 2

# Dynamics and Kinematics

To estimate the precise orbit of Jason-1 by combining all of three types of tracking data, SLR, DORIS and GPS, the MSODP (Multi-Satellite Orbit Determination Program) software is utilized in this study. MSODP, which was implemented by employing a weighted least squares batch estimation procedure [Tapley, 1973], was developed at UT/CSR as an extension of the UTOPIA software for GPS data processing [Rim, 1992]. With the added implementation to process the different types of measurement data simultaneously, the orbit solutions from MSODP using Jason-1 SLR/DORIS were compared and validated with the solution from UTOPIA. UTOPIA is the single satellite orbit determination program at UT/CSR used primarily to process SLR/DORIS data. MSODP and UTOPIA share the same dynamical force models and measurement models for the SLR/DORIS data processing.

The following sections describe the dynamic force models and measurement models implemented in MSODP. The time and coordinate systems, which are the fundamental concepts to understand the dynamic and measurement models, are also briefly introduced in Section 2.1.

## 2.1 Time and Coordinates

For the orbit determination problem, the descriptions of the motion of the satellite and the tracking system usually involve various time systems and reference frames. For high precision orbit determination, an accurate definition of these reference systems is critical.

***Time System***

Various time systems are defined on basically three types of periodic processes: 1) solar and sidereal times such as UT, UT1, UT2 and UT1R based on the Earth rotation, 2) dynamic times such as TDT or TBT derived from planetary motions in the solar system, and 3) atomic times such as TAI, UTC or GPS Time defined on the basis of atomic oscillations. The UTC, TDT and GPS time system are the ones mostly used in this study.

The Universal Time Coordinated (UTC) system is a uniform time system tied to TAI (International Atomic Time) that is adjusted to adapt Earth rotation rate changes. UTC and TAI differ only by an integer number of seconds. UTC is derived from TAI, but it is kept close to UT2 by introducing leap seconds when needed. The UTC time system is the time system used for observation time tags for SLR, and TAI is used for DORIS. UTC is also used as a broadcast standard time scale to which tracking stations are synchronized, although GPS time is often used as well.

The GPS time system is used for GPS observation time tags. GPS time differs from UTC by an integer number of seconds. Unlike UTC, however, no

additional leap second adjustments are made for the GPS time system. The relation between UTC and GPS time is disseminated in the GPS satellite broadcasting message. The GPS Week, which is often used for the GPS data, is the number of weeks since January 6, 1980.

The Terrestrial Dynamics Time (TDT) system is a uniform and abstract time scale which is used in the equations of motion of a satellite in the geocentric reference frame. In practice, TDT is realized by the relation with TAI as $TDT = TAI + 32^s.184$. Another dynamic time system called Barycentric Dynamical Time (TDB) is commonly used for the planetary ephemerides. For near-Earth satellites such as Jason-1, the geocentric reference frame is completely adequate, and the barycentric reference frame is unnecessary [Ries *et al.*, 1988].

To summarize, the conversion between the time system can be given as:

$$\begin{aligned} TAI &= GPS + 19.^s000 \\ TAI &= TDT - 32.^s184 \\ TAI &= UTC + 1.^s000 \cdot n \end{aligned} \tag{2.1}$$

where integer number $n$ for leap seconds is reported by the the International Earth Rotation Service (IERS). The GPS time was coincident with UTC at the GPS standard epoch 1980, January $6.^d0$.

***Coordinate System***

Coordinate systems are defined according to the origin, the reference plane and the principal direction in the reference plane. Each coordinate system can be used by convenience for each situation. They are transferable to each other.

The J2000 geocentric inertial coordinate system, or Earth-Centered Inertial (ECI) coordinate system, defined by the mean equator and equinox of epoch J2000 (2000 January 1 12:00 UTC), is used for the numerical integration of the equations of motion of a satellite. Many forces on the satellite such as gravitational perturbations, drags, solar radiation perturbations, etc. are expressed in the body-fixed geocentric rotating system, or the Earth-Centered-Earth-Fixed (ECEF), then transformed to the J2000 (or ECI) frame in MSODP. Planetary ephemerides provided by JPL (DE-200) are given in the J2000 barycentric inertial coordinate system, which are transformed to the ECI frame. For the coordinate transformation, precession and nutation of the Earth, polar motion and variations in the rotation of the Earth (UT1-TAI) are considered.

The international terrestrial reference frames (ITRF) for the positions of tracking stations are realized as ECEF. The terrestrial reference frame used in this research is ITRF2000 for tracking stations of all three measurement types. The ITRF2000 reference frame is a new solution for the SLR, DORIS and GPS tracking stations which has made a significant improvement over previous solutions such as CSR95L01, CSR95D02, and ITRF97, which will be

further discussed in Section 3.1.

The body-fixed topocentric rotating system is used for the measurement model. Furthermore, the coordinate systems related to particularly Jason-1 will be discussed in Section 2.5. Additional information about coordinate systems and transformations between each other can be found in Yuan [1991].

## 2.2 Overview of Models

The equations of motion of a near-Earth satellite with respect to the J2000 geocentric inertial frame can be expressed as:

$$\ddot{\vec{r}} = \vec{a}_g + \vec{a}_{non} \tag{2.2}$$

where $\vec{r}$ is the position of the center of mass of the satellite, $\vec{a}_g$ is the sum of the gravitational perturbations acting on the satellite, and $\vec{a}_{non}$ is the sum of the non-gravitational perturbations acting on the satellite.

The gravitational perturbations composed of the perturbations from the Earth, the other bodies such as the Sun, Moon, and other planets and the general relativity effect:

$$\vec{a}_g = \vec{P}_{geo} + \vec{P}_{stides} + \vec{P}_{otides} + \vec{P}_{rotdef} + \vec{P}_{Nbody} + \vec{P}_{rel} \tag{2.3}$$

where $\vec{P}_{geo}$ is the perturbations due to the geopotential of the Earth, $\vec{P}_{stides}$ is the perturbations due to the solid Earth tides, $\vec{P}_{otides}$ is the perturbations

due to the ocean tides, $\vec{P}_{rotdef}$ is the perturbations due to the rotational deformation, $\vec{P}_{Nbody}$ is the perturbations due to the Sun, moon and other planets, and $\vec{P}_{rel}$ is the perturbations due to the general relativity effect. For details of the gravitational perturbations, Appendix A.1 can be referenced. The non-gravitational perturbations will be further discussed in Section 2.3. Table 2.1 summarizes the dynamic models used in this study.

| Dynamic Models | |
|---|---|
| Gravity | JGM-3 truncated 70×70<br>GM=398600.44150 $km^3/sec^2$<br>Re=6378136.3000 m |
| Third-Body | JPL DE200 |
| Solid-Earth tide | IERS 96 [Wahr, 1981] |
| Atmospheric Drag | Density Temperature Model (DTM)<br>[Berger *et al.*, 1998] |
| Solar Radiation Pressure | Box-wing model or Cannonball-wing model<br>Umbra and penumbra earth shadow model |
| Earth Radiation Pressure | Albedo and infrared second-degree zonal model |
| Relativity perturbation | Point-mass (Schwarzschild) term [Ries, 1989] |
| GPS satellite orbits | Fixed with the IGS final solution |
| Numerical integration | Krogh-Shampine-Gorden 14th order,<br>fixed-multi-step integrator.<br>Arc Length: 30 hours with 6 hours overlapped. |

Table 2.1: Dynamic Models

The measurement models for each tracking systems and the correction models to them are described in Appendix A.2. Table 2.2 summarizes the measurement correction models which were employed in this study.

| Measurement Models | |
|---|---|
| SLR | SLR data retrieved from CDDIS<br>- Range bias (per arc) estimated for two stations<br>(7237 and 8834)<br>- Elevation cut-off: 10 deg. |
| DORIS<br>range-rate | DORIS data retrieved from CNES<br>- Frequency bias and tropospheric scale factor estimated<br>for each pass<br>- Elevation cut-off: 5 deg<br>(but all passes must achieve at least 15 deg max elevation)<br>- Timing bias of several microseconds removed from<br>each cycle of DORIS data based<br>on comparison with SLR data |
| GPS<br>double-differenced | GPS data retrieved from CNES<br>- Preprocessing using the TEXGAP software<br>- Elevation cutoff: 0 deg<br>- Sampling rate: 30 sec<br>- Satellite clock biases are eliminated<br>by forming Double-difference |
| Troposphere | Mapping functions for dry and wet for GPS and DORIS<br>- Mapping Temperature Test (MTT) model [Herring, 1992]<br>for GPS<br>- Modified Hopfield model [Goad & Goodman, 1974]<br>for DORIS<br>- Marini & Murray [1973] refraction model for SLR |
| Ionosphere | Not modeled, but eliminated with dual frequencies |
| Plate motions | ITRF2000 |
| Station coordinates | GPS, SLR and DORIS fixed with ITRF2000<br>(with a few exceptions) |
| Station Velocities | ITRF2000 |
| Rot. Deformation | IERS 96 |
| Tide model | IERS 96, ocean loading included |
| Earth Orientation | IERS EOP-C04 Series |
| Center of Mass Offset | a priori: X=−94.2 cm, Y=0.0 cm, Z=0.0 cm |
| Phase Center | a priori:<br>SLR=(22.9, 59.8, 68.3) cm<br>DORIS=(22.9, −59.8, 102.7) cm<br>GPS=(238.91, −21.80, −50.40) cm |

Table 2.2: Measurement Models

## 2.3 Non-gravitational Perturbations

The principal non-gravitational perturbations acting on the near-Earth satellite surfaces may be categorized as:

$$\vec{a}_{non} = \vec{P}_{drag} + \vec{P}_{solar} + \vec{P}_{earth} + \vec{P}_{thermal} + \vec{P}_{empirical} \tag{2.4}$$

where $\vec{P}_{drag}$ is the perturbations due to the atmospheric drag, $\vec{P}_{solar}$ is the perturbations due to the solar radiation pressure, $\vec{P}_{earth}$ is the perturbations due to the Earth radiation pressure, $\vec{P}_{thermal}$ is the perturbations due to the thermal radiation induced by the thermal imbalance in the satellite body, and $\vec{P}_{empirical}$ is the perturbations due to unknown forces which may be represented by the empirical once-per revolution expressions.

For Jason-1, the solar radiation pressure is the main non-gravitational perturbation because of its high altitude, although the drag force is not completely negligible. To model the surface forces properly, the model of the shape and orientation of the satellite is very important. The radiation pressure model for Jason-1 is similar to that used for Topex. The Topex model for the surface forces was developed at the Space Geodesy Branch of NASA Goddard Space Flight Center and the Colorado Center for Astrodynamics Research (CCAR) at the University of Colorado at Boulder [Marshall *et al.*, 1992]. A "micro-model" using a finite element model of the spacecraft was approximated by a relatively simple and less computationally intensive "macro-model", which is more suitable for precision orbit computations. For the macro-model, a box-wing shape was chosen with the plates aligned along the satellite body-fixed

coordinate system. The non-conservative forces acting on each of the surfaces are computed independently, then the vector accelerations were summarized to compute the total effect on the spacecraft center-of mass. In this research, the simple box-wing model was adopted as a nominal model to compute surface forces on Jason-1. The empirical force model is introduced to accommodate the unknown perturbations caused by the surface model errors.

For GPS satellites, several specific models have been devised for the effect of solar radiation pressure known as ROCK models, which are dependent on the satellite design such as BlockI, BlockII, BlockIIa, and BlockIIR. Their models have been implemented in MSODP. For this research, however, IGS GPS precise orbit solutions have been used without computing the GPS satellite ephemerides in MSODP. Especially, to accommodate the errors from the GPS satellite orbits, the empirical orbit element correction parameters are introduced in Section 4.2.3.

### 2.3.1 Solar Radiation Pressure Model

Solar radiation pressure is the main effect on the high altitude satellite like Jason-1. Its effect at altitudes above 800 kilometer exceeds the atmosphere drag effect.

The force due to solar radiation pressure based on a box-wing model can be described as [Luthcke & Marshall, 1992]:

$$\vec{P}_{solar} = -P\frac{\alpha\nu}{m}\sum_{i=1}^{n_f} A_i \cos\theta_i \left[2\left(\frac{\delta_i}{3} + \rho_i \cos\theta_i\right)\hat{n}_i + (1-\rho_i)\hat{s}\right] \qquad (2.5)$$

where $P$ is the solar momentum flux, which is 4.56 $\times 10^{-6} N/m^2$ at a mean distance of 1 A.U. from the Sun; $\alpha$ is the solar radiation scale factor; $\nu$ is the eclipse factor ($\nu = 0$ if the satellite is in full shadow, $\nu = 1$ if the satellite is in full Sun, and $0 < \nu < 1$ if in partial shadow); $m$ is the satellite mass; $A_i$ is the surface area of the $i$-th plate; $\theta_i$ is the angle between surface normal and satellite-Sun vector for the $i$-th plate; $\hat{n}_i$ is the surface normal unit vector for the $i$-th plate; $\hat{s}$ is the satellite-Sun unit vector; $\delta_i$ is the specular reflectivity for the $i$-th plate; $\rho_i$ is the diffuse reflectivity for the $i$-th plate; and, $n_f$ is the total number of plates in the model. Table 2.3 shows the property of each surfaces such as area, specular and diffuse reflectivities. These data in the table was derived from a macro-model for Jason-1, the macro-model with a six-face box was optimally adjusted to reproduce accelerations which already computed using a micro-model. Accelerations due to solar radiation were computed for all possible incoming light directions using the micro-model based on the data provided by the manufacturer. The normal vector for each face (X+, X−, Y+, Y−, Z+, Z−, SA+, SA−) of the box-wing model is specified in the body fixed frame, parallel to the specified coordinate axes and positive in a direction away from the satellite center. The positive solar array normal vector (SA+) is outward from the cell side of the array while the negative normal vector (SA−) is in the opposite direction.

The solar radiation pressure Equation 2.5 can be more simplified by

| Jason-1 visible | | | | | | | | |
|---|---|---|---|---|---|---|---|---|
| surfaces | X+ | X− | Y+ | Y− | Z+ | Z− | SA+ | SA− |
| area [$m^2$] | 1.65 | 1.65 | 3.0 | 3.0 | 3.1 | 3.1 | 9.8 | 9.8 |
| specular ref. | 0.425 | 0.408 | 0.334 | 0.274 | 0.236 | 0.298 | 0.344 | 0.004 |
| diffuse ref. | 0.178 | 0.186 | 0.342 | 0.369 | 0.382 | 0.336 | 0.006 | 0.298 |
| absorbed ref. | -0.26 | -0.12 | 0.249 | 0.297 | 0.309 | 0.240 | 0.647 | 0.697 |

Table 2.3: Jason-1 surface visible characteristics

using a simple cannonball model with a wing as [Tapley *et al.*, 1990]:

$$\vec{P}_{rad-body} = -P(1+\eta)\frac{A}{m}\nu\hat{s} \tag{2.6}$$

where $P$ is the momentum flux due to the Sun; $\eta$ is the reflectivity coefficient of the satellite; $A$ is the cross-sectional area of the satellite normal to the Sun; $m$ is the mass of the satellite; $\nu$ is the eclipse factor; and, $\hat{s}$ is the satellite-Sun unit vector. The solar radiation pressure perturbation on the satellite's solar panels can be also similarly modeled as:

$$\vec{P}_{rad-panels} = -P\nu\frac{|A_p\cos\gamma|}{m}(\hat{s}+\eta_p\hat{n}) \tag{2.7}$$

where $A_p$ is the solar panel area; $\hat{n}$ is the surface normal unit vector of the solar panels; $\gamma$ is the angle between the solar panel surface normal unit vector ($\hat{n}$) and satellite-Sun unit vector ($\hat{s}$); and, $|A_p\cos\gamma|$ is the effective solar panel area perpendicular to $\hat{s}$. The reflectivity coefficients, $\eta$ or $\eta_p$, represent the averaged effect over the whole satellite body and the two panels, respectively. The values of $\eta$, $\eta_p$, $A$, and $A_p$ were derived from the values in Table 2.3. In MSODP, conical and cylindrical shadow models for the Earth and the lunar

shadow are implemented to determine the eclipse factor $\nu$. For this research, the cyclindrical shadow model is applied with the modified back difference (MBD) for integration at shadow boundary. The MBD method [Anderle, 1973; Feulner, 1990] is to account for the numerical integration errors, which can occur for satellites in the shadow because of the discontinuities in the solar radiation perturbation across the shadow boundary.

For this study, the box-wing model was adopted as a nominal surface force model. Orbit comparisons from the box-wing model and the cannonball-wing model in Appendix D show that the orbits from the box-wing model generally perform better than the orbits from the cannonball-wing model.

### 2.3.2 Earth Radiation Model

The radiation pressure from the Earth should be modeled for the precise orbit determination of a near-Earth satellite. Based on the box-wing model, the albedo and infrared accelerations can use a similar acceleration equation to the solar radiation (see Equation 2.5) by changing the radiation flux from the Sun to the Earth and defining $\theta_i$ as the angle between the $i$-th surface normal and the nadir direction. In MSODP, the total perturbation on a satellite of constant cross sectional area and invariant reflective and emissive properties, due to diffuse radiation from all "effective" Earth elements, is implemented as Knocke [1989]:

$$\vec{P}_{earth} = (1+\eta_e)A' \frac{A_c}{mc} \sum_{j=1}^{N} \left[(\tau a E_s \cos\theta_s + e M_b)\hat{r}\right]_j \tag{2.8}$$

where $\eta_e$ is the satellite reflectivity for the Earth radiation pressure; $A^{'}$ is the projected and attenuated area of a surface element of the Earth; $A_c$ is the cross sectional area of the satellite; $m$ is the mass of the satellite; $c$ is the speed of light; $\tau$ is the indication for shadow (0 if the center of element $j$ is in darkness, 1 if it is in daylight); $a$ and $e$ are albedo and emissivity of the element j respectively; $E_s$ is the solar momentum flux density at 1 A.U.; $\theta_s$ is the solar zenith angle; $M_b$ is the exitance of the Earth; $\hat{r}$ is the unit vector from the center of the element $j$ to the satellite; and, $N$ is the total number of effective Earth segments.

The albedo and emissivity are modified using a second degree spherical harmonic expansion to account for latitudinal variation in Earth radiation and the seasonally dependent latitudinal asymmetry [Stephens *et al.*, 1981; Knocke, 1989]:

$$a = a_0 + a_1 P_{10}(\sin\phi) + a_2 P_{20}(\sin\phi) \tag{2.9}$$

$$e = e_0 + e_1 P_{10}(\sin\phi) + e_2 P_{20}(\sin\phi) \tag{2.10}$$

where $a_1 = c_0 + c_1\cos[\omega(t-t_0)] + c_2\sin[\omega(t-t_0)]$; $e_1 = k_0 + k_1\cos[\omega(t-t_0)] + k_2\sin[\omega(t-t_0)]$; $P_{10}$ and $P_{20}$ are the first and second degree Legendre polynomial; $\phi$ is the latitude of the center of the element on the Earth's surface; $\omega$ is the frequency of the periodic terms; and, $t-t_0$ is the time since the epoch of the periodic terms. In this case, only the dominant annual frequency was included.

### 2.3.3 Thermal Radiation Pressure

Thermal radiation pressure is generated by the imbalance of the internal and external heat fluxes. It depends on the shape, the thermal property, the pattern of thermal dumping, orbit characteristics, and the thermal environment of the satellite. Internally, the equipment dissipates radiation which serves to heat the satellite surfaces. Externally, the solar radiation, albedo, andIinfrared fluxes cause surface heating. For T/P, the force exerted on the flat plates due to thermal emission was modeled as [Marshall *et al.*, 1992]:

$$\vec{P}_{thermal} = -\frac{2}{3}\frac{\sigma}{c}\frac{A_i\epsilon_i}{m}T_i^4\hat{n}_i \tag{2.11}$$

where $\sigma$ is the Stefan-Boltzman constant (5.66E-08 $W/m^2/K^4$); $c$ is the speed of light; $m$ is the mass of the satellite; $A_i$ is the surface area of the $i$-th plate; $\epsilon_i$ is the surface emissivity for the $i$-th plate ; $T_i$ is the temperature (Kelvin) for the $i$-th plate ; and, $\hat{n}_i$ is the normal unit vector for the $i$-th plate. For this model, the temperature history algorithm similar to the one defined by Theillier [1988] was used. In order to take into account the thermal emissivity in routine operation, resulting from the energy dissipated by the various instruments and radiated through the radiators, one can also add a constant bias force fixed with respect to the satellite's frame as shown in Table 2.4, which has been provided by CNES for JASON-1 POD.

For this research, Table 2.4 has been adopted as the thermal radiation pressure model[1] for Jason-1 POD instead of using Equation 2.11. However,

[1]In MSODP or UTOPIA, the XBIAS card is assigned as 187 (=90,000/481), the YBIAS

| emissivity | radiated power $[W]$ | force $[\mu N]$ |
|---|---|---|
| $x_s$ | 40 | 0.09 |
| $y_s$ | 80 | 0.18 |
| $z_s$ | 0-8 | 0.0 |

Table 2.4: Jason-1 thermal imbalance provided by CNES

the T/P experience has shown that the thermal radiation pressure may be disregarded when adjusting empirical acceleration parameters.

### 2.3.4 Atmospheric Drag Model

The atmospheric drag model also requires a geometrical model of the spacecraft. For T/P POD, a box-wing model, where the spacecraft is represented as a combination of one box and a connected solar array, was tested. The drag acceleration was computed for each individual plate with the help of the yaw steering model to get the area projected in the direction of the relative wind, and the sum over the box and solar array was used for the net acceleration. With the box-wing model, therefore, the atmospheric drag can be expressed as:

$$\vec{P}_{drag} = -\frac{1}{2}\rho\frac{C_d}{m}V_r\vec{V}_r\sum_{i=1}^{n_f}A_i\cos\theta_i \tag{2.12}$$

where $\rho$ is the atmospheric density; $\vec{V}_r$ is the satellite velocity relative to the atmosphere; $V_r$ is the magnitude of $\vec{V}_r$; $m$ is the satellite mass; $C_d$ is the

card as 374 (=180,000/481). Note that the scale factor of $10^{-12}$ [m/s$^2$] is used in MSODP or UTOPIA.

drag scaling coefficient; $A_i$ is the surface area of the $i$-th plate; $\theta_i$ is the angle between the surface normal of the $i$-th plate and the satellite velocity vector; and, $n_f$ is the number of plates.

By using a cannon-ball model with a panel, equation 2.12 can be simplified as:

$$\vec{P}_{drag} = -\frac{1}{2}\rho\frac{(C_d^B A_B + C_d^P |A_P \cos\gamma|)}{m} V_r \vec{V}_r \tag{2.13}$$

where $C_d^B$ and $C_d^P$ are the drag coefficients for satellite body and panel respectively; $A_B$ and $A_P$ are the cross-sectional area of the main satellite body perpendicular to $\vec{V}_r$ and the solar panel area respectively; $\gamma$ is the angle between the solar panel surface normal unit vector and satellite velocity vector; and, $|A_P \cos\gamma|$ is the effective solar panel area perpendicular to the satellite velocity vector. From the T/P POD experience, using either the box-wing or the cannonball-wing does not make much difference in the orbit solutions. The empirical parameters are able to accommodate the difference.

For the atmospheric density, several empirical density models such as the Jacchia 77 [Jacchia, 1977] and the Density Temperature Model (DTM) [Barlier *et al.*, 1977] are available. The updated DTM model [Berger *et al.*, 1998] has been used for this research.

### 2.3.5 Empirical Force Model

Empirical force modeling is useful in accommodating unmodeled or mismodeled forces by estimating empirical model parameters, when solving

orbital parameters. To accommodate mismodeled constant forces such as drag, the acceleration can be expressed with the constants of radial, transverse and normal components. Many mismodeled forces are known to show a one cycle-per-revolution (1-cpr) frequency associated with the satellite orbital period. To accommodate the periodic mismodeled or unmodeled forces, an empirical acceleration model with periodic coefficients is introduced as:

$$\vec{P}_{empirical} = \begin{bmatrix} (C_R + R_c \cos u + R_s \sin u)\hat{u}_R \\ (C_T + T_c \cos u + T_s \sin u)\hat{u}_T \\ (C_N + N_c \cos u + N_s \sin u)\hat{u}_N \end{bmatrix} \tag{2.14}$$

where $u$ is the argument of latitude of the satellite; $C_R$, $C_T$ and $C_N$ are the constant acceleration of the radial, transverse and normal direction respectively; $R_c$ and $R_s$ are the cosine and sine parts of the 1-cpr radial acceleration; $T_c$ and $T_s$ are the cosine and sine parts of the 1-cpr transverse acceleration; and $N_c$ and $N_s$ are the cosine and sine parts of the 1-cpr normal acceleration. The along-track (or transverse) constant acceleration, $C_T$, is particularly effective in accommodating mismodeled drag forces. In practice, it is not necessary to estimate both the radial and transverse periodic terms, and these can be shown to have the same effect on the orbit when adjusted. In addition, $C_R$ and $C_N$ are typically not estimated. The dramatic improvement of Jason-1 orbits by introduction of the empirical parameters to the two different surface force models, box-wing model and cannonball-wing model, was shown in Appendix D. Further information on the empirical acceleration parameters can be found in Colombo [1989] and Tapley *et al.* [1994].

## 2.4 Center of Mass and Phase Center

Due to the special design and alignment of the fuel tanks on Jason-1, its center of mass as a whole including both body and solar panels is constrained to move only along the x-coordinate during the full longevity of the satellite in orbit.

Table 2.5 shows the spacecraft mass just after deployment in orbit. The spacecraft mass is 489.1 kg, and its center of mass is located at 935 mm from the reference point on the spacecraft body toward the positive x-direction. Once 8 kg of hydrazine have been used, its center of location moves further as much as 7 cm toward the positive x-direction from the original center of mass location. Since the expected cost of the station acquisition for whole longevity is around 5 to 6 kg, Table 2.5 suggests that the center of mass would be somewhere between 935 and 942 mm, unless much more than 8 kg is used for the station acquisition. The engineering estimates of the center of mass was 937 mm, after 1.7 kg of fuel have been consumed to put its final orbit.

| | Mass $[kg]$ | x-center of mass $[mm]$ |
|---|---|---|
| Just after deployment in orbit | 489.1 | 935 |
| After 8 kg hydrazine consumption | 481.1 | 942 |

Table 2.5: x-component of the center of mass with respect to the reference point

The locations of both the center of mass and the phase centers are measured from a fixed reference point on the spacecraft body. Table 2.6 shows the phase centers of the various instruments of Jason-1 in the satellite frame.

| | x [mm] | y [mm] | z [mm] |
|---|---|---|---|
| Altimeter | 1616.0 | 0.0 | 477.5 |
| DORIS 2 GHz | 1171.0 | - 598.0 | 1027.0 |
| DORIS 400 MHz | 1171.0 | - 598.0 | 859.0 |
| LRA (optical center) | 1171.0 | 598.0 | 682.8 |
| GPS 1 - L1 | 2408.0 | 219.7 | -537.2 |
| GPS 1 - L2 | 2420.1 | 220.7 | -558.3 |
| GPS 2 - L1 | 2408.0 | -219.7 | -537.1 |
| GPS 2 - L2 | 2420.2 | -220.8 | -558.5 |

Table 2.6: Instruments phase centers with respect to the reference point

The two DORIS receivers are connected to the same antenna. The export data is referenced to the 2 GHz frequency, but the position of the phase center for the DORIS 400 MHz is not required. For the Turbo-Rogue GPS Space Receiver (TRSR), the two receivers are connected to independent antennas. The GPS-2 receiver is turned on after the launch. The GPS-1 receiver is a redundancy. The receivers are located on the front-up side to direct the GPS satellites. For this research, the ionosphere-free combination of L1 and L2, which is called $L_C$, has been used (see Equation A.45). The GPS phase center estimation is attempted in Section 4.2.1, where the determination of new center of mass location and phase center offset by using the GPS data is further discussed. For the LRA, an additional constant correction of 4.9 cm has been adopted among the POD group.

## 2.5 Jason-1 Coordinate Systems and Yaw Steering

Orbit parameters of a satellite tend to change over time as a result of atmospheric drag. In the long term, more or less periodic variations also occur due to instabilities in the Earth's gravity field, solar radiation pressure, and other forces of smaller magnitude.

Orbit maneuvers for Jason-1 are performed every 40 to 200 days. Intervals between maneuvers depend mainly on solar flux, and each maneuver lasts 20 to 60 minutes. If possible, they are performed above solid earth and at the end of the orbit cycle, as shown in Table 4.1, to minimize altimeter data loss.

Attitude control is based on star tracker, gyros and reaction wheels. The sensors of Jason-1, like its predecessor T/P, require that the satellites be nadir pointing, but rotations about the satellite vertical axis are not constrained. The satellite body yaw motions are controlled by the On-Board Computer (OBC) controls to satisfy the instrument requirements while keeping the solar array pointed towards the sun.

There are three coordinates systems and three angles of interest to understand Jason-1 yaw maneuvers, as illustrated in Figure 2.1. The first is an orbit inertial system, which is earth-centered with

$\vec{X}_0$ normal to the satellite orbit plane

$\vec{Y}_0$ in the orbit plane and normal to the earth-to-sun vector such that $(\vec{X}_0 \times \vec{Y}_0 = \vec{Z}_0)$

$\vec{Z}_0$ along the projection of the earth-to-sun vector into the orbit plane

The second coordinate system is the satellite position system, which is satellite-centered with

$\vec{X}_p$ tangent to the orbit plane such that $(\vec{X}_p \times \vec{Y}_p = \vec{Z}_p)$
$\vec{Y}_p$ normal to the orbit plane $(\vec{Y}_p = \vec{Z}_p \times \vec{V})$
$\vec{Z}_p$ along the satellite-to-earth vector (nadir direction)

$\vec{X}_p$, $\vec{Y}_p$ and $\vec{Z}_p$ directions are also called simply T (or along-track), N (or normal), and R (or radial) direction respectively.

The third coordinate system is the satellite vehicle system or the satellite body-fixed system, which is satellite-centered and fixed to the satellite with

$\vec{X}_v$ along the satellite centerline, positive in the direction from the Multi-Mission Modular Spacecraft (MSS) through the Instrument Module (roll axis)
$\vec{Y}_v$ such that $(\vec{X}_v \times \vec{Y}_v = \vec{Z}_v)$ (pitch axis, parallel to solar array axis)
$\vec{Z}_v$ along the satellite-to-earth vector, positive in the nadir direction (yaw axis)

$\vec{X}_v$ is oriented yaw angle $\Psi$ from $\vec{X}_p$ by positive rotation about $\vec{Z}_p$. The yaw angle $\Psi$ of the satellite is controlled according to $\beta'$ and $\Omega$ to allow

near perfect pointing of the solar array to the Sun. $\beta'$ is the angle between the sun vector and the orbit plane and $\Omega$ is the orbit angle measured from the $\vec{X}_0$ axis by positive rotation about $\vec{X}_0$. "Orbit 6 am" means $\Omega = 0°$, and "Orbit noon" means $\Omega = 90°$. Note that at an orbit altitude of 1334 km, $\beta'$ oscillates between approximately $+88°$ and $-88°$. When $\beta'$ is between $+55.8°$ and $-55.8°$, the satellite will experience solar occultations each orbit. Occultations reach a maximum near 35 minutes at $\beta' = 0°$.

Table 2.7 shows the yaw-angle governing equations for each yaw control mode. The sinusoidal yaw command, which commands the satellite to yaw sinusoidally as a function of satellite orbit angle, was originally adopted for the Topex OBC control to provide for near perfect sun pointing of the solar array, without excessive yaw angular rates for the Dry Rotor Inertial Reference Unit (DRIRU) gyros [Perrygo, 1987]. At low $\beta'$ values, the control gyros are unable to follow the large sinusoidal yaw commands and the OBC switches to a fixed yaw mode of operation. The switch typically occurs at a $\beta'$ value of $15°$ or $-15°$. Note that the solar angles ($\beta'$) and orbit angles ($\Omega$) for yaw steering mode boundary values indicated in the Table 2.7 are adopted as the nominal values for both T/P and Jason-1. However, they may be changed at anytime by ground controllers. Whenever the sun passes through the orbit plane (if $\beta'$ changes sign), the satellite reverses itself performing a $180°$ yaw flip maneuver. This occurs five or six times per year. The ramps and flips are conducted very quickly for Jason-1 compared to T/P, due to Jason-1's smaller inertia. The attitude transition of Jason-1, unlike T/P, can be treated

as nearly instantaneous.

MSODP utilizes a sequence-of-events (SOE) file converted from a satellite attitude events file provided by CNES for the POD team, which is attached in Appendix B.1. Quaternions were also provided. Table 2.8 summarizes Jason-1 yaw transition events occurred during cycle 1 to 20 (see Table 4.1 for the cycle definition). Care needs to be taken when determining the orbits for cycles 13 and 18, because Jason-1 is in the fixed yaw mode since the later part of cycle 12 to cycle 13, and cycle 18 to the early part of cycle 19.

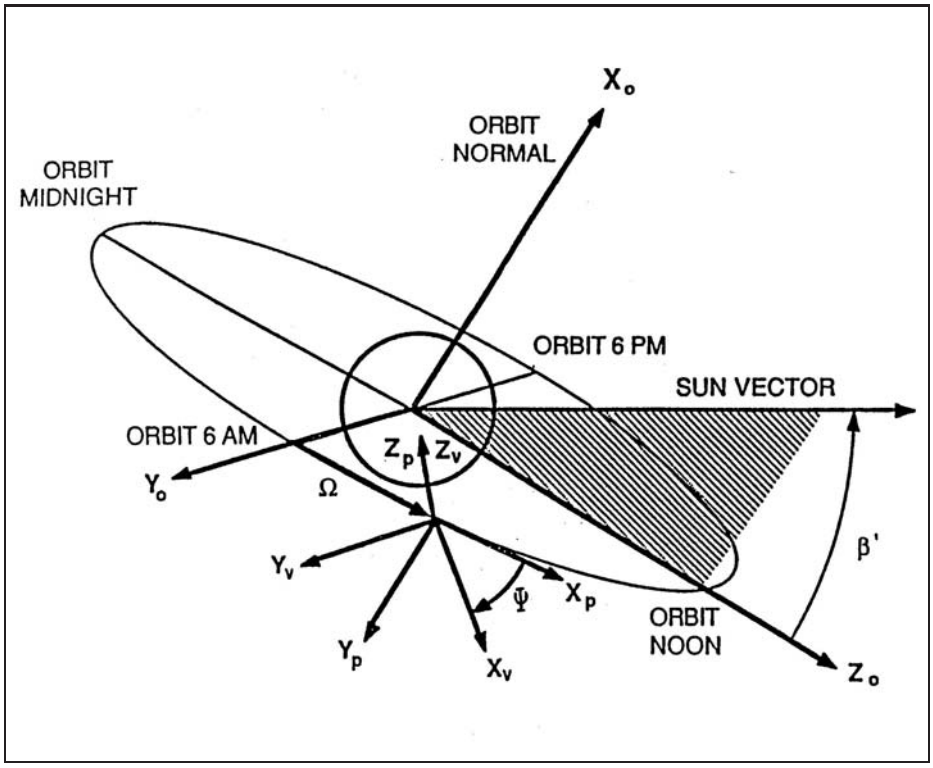


Figure 2.1: Jason-1 Coordinate Systems: orbit inertial system $(\vec{X}_0, \vec{Y}_0, \vec{Z}_0)$, satellite centered position system $(\vec{X}_p, \vec{Y}_p, \vec{Z}_p)$, and satellite body-fixed system $(\vec{X}_v, \vec{Y}_v, \vec{Z}_v)$

| Yaw angle ($\Psi$) | Sun angle ($\beta^{'}$) | Orbit angle ($\Omega$) |
|---|---|---|
| Fixed: | | |
| $\Psi = 0^{\circ}$ | $0.1^{\circ} \leq \beta^{'} < 15^{\circ}$ | |
| $\Psi = 180^{\circ}$ | $-15^{\circ} < \beta^{'} \leq -0.1^{\circ}$ | |
| $\Psi = 90^{\circ}$ | $\beta^{'} \geq 80^{\circ}$ | |
| $\Psi = -90^{\circ}$ | $\beta^{'} \leq -80^{\circ}$ | |
| Ramp Up (fixed yaw to sinusoidal): | | |
| $\Psi = \frac{\beta^{'}}{2}[1 - \cos(2(\Omega + 90^{\circ}))]$ | $\beta^{'} = 15^{\circ}$ | $90^{\circ} \leq \Omega \leq 180^{\circ}$ |
| $\Psi = \frac{\beta^{'}}{2}[1 - \cos(2(\Omega + 90^{\circ}))] - 180^{\circ}$ | $\beta^{'} = -15^{\circ}$ | $270^{\circ} \leq \Omega \leq 360^{\circ}$ |
| Ramp Down (sinusoidal to fixed yaw): | | |
| $\Psi = \frac{\beta^{'}}{2}[1 - \cos(2(\Omega + 90^{\circ}))]$ | $\beta^{'} = 15^{\circ}$ | $180^{\circ} \leq \Omega \leq 270^{\circ}$ |
| $\Psi = \frac{\beta^{'}}{2}[1 - \cos(2(\Omega + 90^{\circ}))] - 180^{\circ}$ | $\beta^{'} = -15^{\circ}$ | $0^{\circ} \leq \Omega \leq 90^{\circ}$ |
| Nominal (sinusoidal): | | |
| $\Psi = [90^{\circ} + (90^{\circ} - \beta^{'})\cos\Omega]$ | $\beta^{'} > 15^{\circ}$ | |
| $\Psi = [-90^{\circ} - (90^{\circ} + \beta^{'})\cos\Omega]$ | $\beta^{'} < -15^{\circ}$ | |
| Flip: | | |
| $\Psi = -90^{\circ}(1 + \cos\Omega)$ | $0^{\circ} \leq \beta^{'} < 0.1^{\circ}$ | $-180^{\circ} \leq \Omega \leq 0^{\circ}$ |
| $\Psi = -90^{\circ}[1 + \cos(\Omega + 180^{\circ})]$ | $-0.1^{\circ} < \beta^{'} < 0^{\circ}$ | $-180^{\circ} \leq \Omega \leq 0^{\circ}$ |

Table 2.7: Governing equations of Yaw Steering Modes for T/P and Jason-1: The ramps and flips of Jason-1 are conducted very quickly for Jason-1 compared to T/P, due to its smaller moment of inertia.

| Date | Time | Transition | | | $\beta'$ |
|---|---|---|---|---|---|
| 2002/01/06 (doy 006) | 15:46 | sinusoidal | to | fix 0° | $\sim -15°$ |
| 2002/01/12 (doy 012) | 16:30 | fix 0° | to | fix 180° | 0° |
| 2002/01/18 (doy 018) | 17:24 | fix 180° | to | sinusoidal | 16° |
| 2002/03/11 (doy 070) | 05:15 | sinusoidal | to | fix 180° | 15° |
| 2002/03/16 (doy 075) | 02:43 | fix 180° | to | fix 0° | 0° |
| 2002/03/21 (doy 080) | 00:27 | fix 0° | to | sinusoidal | $\sim -14°$ |
| 2002/05/11 (doy 131) | 12:16 | sinusoidal | to | fix 0° | $\sim -15.7°$ |
| 2002/05/17 (doy 137) | 16:41 | fix 0° | to | fix 180° | 0° |
| 2002/05/23 (doy 143) | 13:52 | fix 180° | to | sinusoidal | 15° |
| 2002/07/02 (doy 183) | 04:29 | sinusoidal | to | fix 180° | |
| 2002/07/08 (doy 189) | 04:14 | fix 180° | to | fix 0° | |
| 2002/07/14 (doy 195) | 02:20 | fix 0° | to | sinusoidal | |

Table 2.8: Jason-1 Yaw Transition

# Chapter 3

# Model Improvement and Orbit Performance Tests

## 3.1 Model Improvement of Jason-1 over Topex

The radial orbit error for the Jason-1 Geophysical Data Records (GDR), which consist of altimeter measurements, sea surface heights, and nominal orbits predicting the location of the satellite, is required to be less than 2.5 cm with the goal of 1 cm. Table 3.1 shows an estimate of the radial orbit error budget from each error source for T/P. The error budget in the table can also be applied to Jason-1, since the satellite relies upon many of the same models as T/P.

Over the past decade, the orbit error from the gravity model has been significantly reduced due to gravity model improvement. With the knowledge that the gravity model was the primary error source for the radial orbit error, intense efforts had been made during the early T/P project. The efforts resulted in the dramatic reduction of radial orbit error for the T/P orbit to 2.3 cm accuracy level using the Joint Gravity Model (JGM-3) [Tapley *et al.*, 1996] from well above 50 cm level when using the Goddard Earth Model (GEM)-10B [Lerch *et al.*, 1981], the best general gravity models available in the early

| | TOPEX/POSEIDON [Unit: mm] | | | |
|---|---|---|---|---|
| Error source | Mission specification | JGM-2 | JGM-3 | goal |
| Static gravity | 100 | 22 | 9 | 4 |
| Earth and ocean tides | 30 | 13 | 7 | 4 |
| Temporal gravity[1] | N.A. | 8 | 8 | 4 |
| Surface forces[2] | 70 | 15-25 | 10-15 | 5 |
| rad(s,e and thml) | 60 | 20 | | |
| drag | 30 | 10 | | |
| Data errors[3] | 10 | 5-10 | 5-10 | 4 |
| troposphere | | | | |
| cg offset | | | | |
| attitude | | | | |
| Station location[4] | 20 | 10 | 5 | 4 |
| ($\vec{r}$,$\vec{v}$) | | | | |
| geocenter | | | | |
| Radial Orbit RSS | 130 | 35-40 | 20-25 | $\sim$10 |

1 seasonal and other temporal variations other than tides
2 solar, terrestrial and thermal radiation, atmospheric drag, bias forces
3 data noise, biases, troposphere, cg-offset errors, attitude errors
4 includes station position and velocity errors, geocenter motion

Table 3.1: Radial Orbit Error Budget for Topex/Poseidon [Chelton *et al.*, 2001]

1980s. The JGM-3 model was a production from the addition of the T/P GPS tracking data to the previously available JGM-2 model [Nerem *et al.*, 1994] which resulted from the early post-launch T/P SLR and DORIS tracking data.

The GRACE (Gravity Recovery and Climate Experiment) mission, launched on March 17, 2002, is expected to further improve the static and temporal gravity models. This dedicated gravity mission, a joint project between NASA and the Deutsches Zentrum für Luft und Raumfahrt (DLR), has already shown unprecedented improvement in the mean earth gravity field and the seasonal variations. The science data from the GRACE mission will be used to estimate global models for the mean and time variable Earth gravity field approximately every 30 days for the 5 year lifetime of the mission. Analyses of the altimeter data will continue to improve the ocean tidal models. The dominant temporal gravity feature is the seasonal migration of mass between the atmosphere, oceans, and solid earth. To achieve the 1-cm radial rms goal, the error from the temporal gravity may need to be accounted for. In Section 5.5, several gravity models including JGM-3 and a recent preliminary GRACE gravity model will be tested and compared for the Jason-1 radial orbit accuracy.

Because of the significant improvements in the gravity model, the surface force models have become a comparable source of orbit error. The greatest challenge, to achieve the 1-cm orbit accuracy for Jason-1 and altimeter satellites in the future, will be surface force model improvement. As shown in Table 3.1 the error reduction from the surface model improvement has not been suf-

ficient. Due to the high altitude of Jason-1, solar radiation and earth radiation force model are more important than drag forces. Even earth radiation force by itself exceeds the drag acceleration. To make it worse, the mass-to-area ratio of Jason-1 is less than half the mass-to-area ratio of T/P as shown in Table 3.2 and Table 3.3. Table 3.2 compares the masses of Jason-1 and T/P and it shows that the mass of T/P is more than 5 times that of Jason-1. Table 3.3 shows the comparison of the surface sizes of the two spacecraft. The decrease of the mass-to-area ratio means that radiation forces and drag forces become more important than other forces as shown in Equations 2.5, 2.6, 2.7, 2.8 and 2.12. Orbit maneuvers are also affected by the decreased mass-to-area ratio. To satisfy the same constraints and requirements as T/P, more frequent maneuvers are needed for Jason-1. Most of the maneuvers are performed at the cycle boundaries and the ground tracks are maintained within $+/-$ 1 km.

| | Jason-1 | T/P |
|---|---|---|
| platform | 275 | 934 |
| payload module | 64 | 803 |
| payload | 110 | 407 |
| launch vehicle adapter+ballast | 12 | 132 |
| propellant+ pressurant | 28 | 219 |
| total satellite | 489.1 | 2495 |

Table 3.2: Masses of the spacecraft [Unit: kg]

The key factor in overcoming the surface force modeling limitation and more frequent attitude control problem is the dense, continuous and precise

| Area $[m^2]$ | | |
|---|---|---|
| area | T/P | Jason-1 |
| X+ | 4.71 | 1.65 |
| X− | 4.71 | 1.65 |
| Y+ | 8.18 | 3.0 |
| Y− | 8.18 | 3.0 |
| Z+ | 8.32 | 3.1 |
| Z− | 8.32 | 3.1 |
| SA+ | 25.50 | 9.8 |
| SA− | 25.50 | 9.8 |

Table 3.3: Surface Size

tracking data with improved measurement precision and increased coverage. A strategy is typically adopted which consists of estimating a set of empirical accelerations to absorb the errors in the surface model that still remain, which could compromise the orbit accuracy if not accomodated. The more robust GPS data should also support a higher level of parameterization of the surface forces and heavier parameterization for empirical accelerations so that the contribution from this error source to the radial orbit error may be substantially reduced. In Appendex D, the effect of different surface force models and empirical acceleration strategies on the orbit accuracy was examined.

Data errors have been reduced by the improvement of the tracking precision. Table 3.4 shows the precision comparison of each measurement system for T/P and Jason-1. Compared with the GPS receiver on T/P, performance of the GPS TRSR on Jason-1 is significantly improved. For Jason-1, the precision requirement for Lc pseudo range and Lc phase measurement is 30 cm

| type | T/P | Jason-1 |
|---|---|---|
| Laser | 0.5-5 cm | similar to T/P |
| DORIS | 0.45 mm/s | 0.38 mm/s |
| GPS | 50 cm (Lc pseudo)<br>2∼5 mm (Lc phase) | ∼20 cm<br>∼ 1 mm |

Table 3.4: Tracking Precision Improvement

and 2 mm, respectively. Actual measurement precisions satisfy the mission requirement, as shown in Table 3.4.

The strong tracking capability of Low-Earth Orbiters (LEO) is one of the contributions to a more accurate radial RMS orbit. The tracking capability of GPS satellites by Jason-1 has increased to 8.5 satellites on average with a maximum of twelve, which is superior to the hardware-limited tracking capability by T/P that is 5.5 satellites on average with a maximum of six.

Over the last decade, radial accuracies of the GPS satellite orbits provided by IGS, which are generally determined by the inter-comparison between the orbits from seven analysis centers contributing to the final IGS orbits such as Center for Orbit Determination in Europe (CODE) and JPL, have been improved to 8∼10 cm from 25∼30 cm in the 1990s. The large miscentering observed in the GPS orbit solution of T/P [Bertiger *et al.*, 1994] as mentioned in Section 1.3 can be reduced by the improvement of GPS satellite orbits.

DORIS tracking has also improved. Each component of DORIS such as ground beacons, MVR and on-board Ultra Stable Oscillator (OB-USO) has improved. New beacon USOs with improved performances of better short

term relative stability were replaced. Some beacons in Time and Frequency reference beacons were upgraded to improve DORIS on-board time monitoring with respect to TAI. The short-term stability of the OB-USO was increased by about 50% and the short term error on 2 GHz Doppler measurement was improved to 0.11 mm/s from 0.25 mm/s of T/P. The consistency and accuracy of the beacons coordinates (location and velocity) have improved with more DORIS beacons collocated with other geodetic technique ground equipments such as GPS, VLBI and SLR. The beacon numbers have increased to about 60 compared with approximately 50 for T/P. Thus, Jason-1 orbit coverage and geometrical observability by DORIS have improved. However, it has been noted that the USO on Jason-1 is much more susceptible to radiation effects, particularly in the area of the South Atlantic Anomaly, leading to a serious degradation of the DORIS system.

The SLR system also continues to be improved. The addition of a new SLR tracking station in South Africa (Hartebeesthoek) will significantly improve the geographical coverage of SLR tracking. The ultra-mobile French Transportable Laser Ranging Station (FTLRS) which is being developed in co-operation with IGN (Institut Géodynamique National), CNES and OCA/CERGA (Observatoire de la Côte d'Azur/Centre d'Etudes et de Recherches en Géodynamique et Astronomie) will provide inexpensive and more compact SLR network with requirement of 5-photoelectron return at 30-degree elevation in standard clear sky (visibility = 15 km, mean cirrus). The LRA allows the Jason-1 spacecraft to be tracked with centimeter accuracy by approximately 40 satellite laser

ranging (SLR) stations. The LRA on Jason-1 is a heritage of the GFO design and the improved LRA design on Jason-1 leads to smaller target interaction effects. Consequently, SLR fits on Jason-1 are routinely better than T/P. Advances in the DORIS and SLR systems along with the improvement of GPS tracking are expected to help to achieve the challenging 1-cm rms of the radial orbit error.

The accuracy of the terrestrial reference system has also improved, as long time series and multiple geodetic methods are combined to provide better estimates of the tracking station positions and velocities. The determination of the SLR, DORIS and GPS station positions and velocities has steadily improved, and the new ITRF2000 solutions brought the various reference systems into a common frame.

Prior to the Jason-1 mission, CNES and NASA had utilized different station location information for SLR and DORIS. NASA used CSR95L01 for SLR and CSR95D02 for the DORIS station velocities; CNES used ITRF97. Ries *et al.* [2000] has shown that the Z-bias between NASA and CNES orbits for T/P appeared to be caused by using different reference frames. The Z-bias from the comparison between CSR orbits and NASA/GSFC orbits for T/P cycle 120 to 140 is 3 mm on average, ranging between $-2$ mm and 10 mm. The average of the Z-bias between CSR orbits and CNES orbits is $-7$ mm, but ranging between $-30$ mm and 10 mm. A large part of this Z-bias originated from the usage of different reference frames. For Jason-1, ITRF2000 will be used for both SLR/DORIS and GPS stations among all POD groups.

The test of the reference frame transition from CSR95L01/CSR95D02 to ITRF2000 for SLR/DORIS with ten cycles of T/P by Ries *et al.* [2001] has also shown that the orbit performance from ITRF2000 reference system is comparable to the orbit from CSR95L01/CSR95D02 in terms of the altimeter crossover RMS. The fits to the SLR and DORIS were generally as good or better, and the agreement between the CSR and NASA/GSFC orbits was actually improved. There was a small shift of less than a centimeter between the orbits from the reference frames along the Z-direction, translating into a negligible effect on global mean sea level ($< 1$ mm).

## 3.2 Orbit Performance Tests

The orbit accuracy assessment is the estimation of the difference between the computed orbit and the true orbit. Since we cannot know the true orbit, we use other orbits that are assumed to be close to the true orbit as one aspect of this assessment. One can use internal comparisons or external comparisons among independently determined orbits based on independent measurement types or independent software configurations. Comparisons of post-fit residuals and comparisons of two orbits generated with two different tracking data sets sharing a overlapped subset are often used for internal orbit accuracy assessments. For the external assessments, orbits computed from independent tracking systems can be compared. The different measurement types of T/P and Jason-1 provide opportunities for many different independent orbit solutions. Finally, the high elevation SLR data provides a strong

measure of the absolute radial orbit accuracy.

The orbit error in the radial direction is the most critical to the overall altimeter height error budget. The error in the transverse and normal directions is generally on the order of three to five times larger than the radial orbit error, but this is more than adequate for altimeter purposes.

***Post-fit Residual Test***

The post-fit residual RMS is a measure of how well the computed orbit fits the tracking data. Thus, it is indicative both of the model accuracy and of the data quality. For 10-day T/P arcs, the most recent models produced fits of approximately 2 cm for the SLR data, and 0.48∼0.55 mm/s for the DORIS data [see pg. 83 of Chelton *et al.*, 2001; Zelensky *et al.*, 2002]. For Jason-1, the fit residuals for the DORIS data have been reduced to 0.38∼0.42 mm/s [Zelensky *et al.*, 2002]. The post-fit residuals of double-differenced carrier-phase GPS data are typically about 1.3 cm for Jason-1.

A consistent post-fit residual RMS that is not too sensitive to the variability in the amount of tracking data indicates a stable parameterization choice. By introducing enough empirical parameters into the orbit solution, it is possible to reduce the residual RMS to the measurement noise level. However, over-parameterization of the orbit may lead to unstable solutions and poor orbit performance. Thus, the residual RMS as a measure of the orbit accuracy needs to be interpreted cautiously along with other performance tests.

### *Overlap Comparison*

The overlap comparison is a useful test to check the internal orbit consistency, although it needs to be interpreted carefully because some of the tracking data in the overlap periods are used in both orbit fits. The RMS difference in the radial direction should be within a cm level, although it can vary depending on data outage of some stations, GPS satellite performance and the parameterization strategy. Attempting heavy parameterization for an arc without enough tracking data can cause a higher overlap difference. If any GPS satellite passes through the Earth's shadow during the arc, it can also cause inconsistent overlap differences. Since the overlap test usually shows some anomaly in the orbits during the time frame of attitude control or data shortage, the parameterization needs to be varied accordingly.

For the overlap comparison, several-hour overlap lengths are generally chosen to avoid the orbit irregularity near the end points of the arc. In this research, the arc lengths of 30 hours were integrated with the consideration of 3-hour overlap comparison from each arc's ends, and the middle 24-hour solutions were merged to form a full ten-day repeat cycle orbit.

### *High Elevation SLR Residuals Test*

The residual RMS of the SLR range biases is obtained by postprocessing high-elevation SLR passes through the orbit to be tested. The range bias of the SLR data indicates the combined level of radial and cross-track orbit error in the pass at the point of closest approach to the laser observatory. As the

elevation angle of the pass increases, the mean error in the station-to-satellite range approaches the radial orbit error separated from the cross-track errors, assuming that the actual station biases are small enough to be negligible. For high-elevation passes, the cross-track orbit errors contribute very little to the range biases. The global RMS of the range biases from the high-elevation pass test yields a precise and absolute measure of the radial orbit error. It is one of the most accurate and reliable indicators of the radial orbit accuracy, especially when the orbit to be tested did not include any SLR tracking.

The assessment test for this research was restricted to the SLR passes with high-elevation greater than 70 degrees. For each pass, a range bias was determined using laser range observations made over 70 degree elevation. The RMS of the range biases for the high-elevation passes is typically on the order of 2 cm for T/P [Ries & Tapley, 1999].

***External Orbit Comparison***

Another very useful measure of the orbit quality is the comparison of orbits determined from outside institutes independently with different tracking systems and different orbit estimation strategies. Five groups (CNES, DEOS, GSFC, JPL and UT/CSR) contributed multiple solutions as a part of a Jason-1 POD collaboration. The Jet Propulsion Laboratory (JPL) provided GPS orbits from their reduced dynamic approach software, GIPSY/OASIS. Willis *et al.* [2002] from the Institut Géographique National (IGN) also provided independent orbit solutions adapting JPL's analysis software to process DORIS

data with GPS data. The Goddard Space Flight Center (GSFC) of NASA provided GPS-only solutions and SLR/DORIS solutions separately. Centre National d'Etudes Spatiale (CNES) in Toulouse also produced SLR/DORIS and GPS-only orbits by using both the dynamic and the reduced-dynamic approach.

The Center for Space Research of the University of Texas (UT/CSR) at Austin provided separate SLR/DORIS solutions independent of this research. This work contributes additional precise orbits by processing GPS tracking alone or SLR/DORIS/GPS tracking all together simultaneously. Both NASA and CSR employed the dynamic approach. Although each institute's analysis systems were developed independently, they share some common models. The agreement between the various orbits should be a strong indication to the radial orbit error, because they are obtained with different software and configurations, and with almost all of the possible combinations of the available data types of DORIS, SLR and GPS.

The comparison of external orbits also provides a way to examine the orbit miscentering effect possibly caused by using different reference frames or different tracking data types. To examine the orbit centering, the biases in the three directions (X, Y and Z) of the body-fixed frame will be compared. As discussed previously, a Z-bias of larger than 3 cm can sometimes be seen in the comparison between some orbits. The mean values of the altimeter crossover data can also provide a measure of the orbit centering in the inertial frame as discussed in the next section. The actual comparison of external orbits will be

discussed in Section 5.6.

### *Orbit Assessment with Altimeter Crossovers*

The altimeter data serve as an independent check of the orbit accuracy, since they are not used directly in the determination of the satellite orbit. To use the altimeter data as a global independent measure of the satellite orbit assessment, orbit error must be differentiated from other more dominant signals in the altimeter data. To this end, altimeter crossovers are formed by differencing two interpolated altimeter measurements at the crossing point of an ascending and descending track [Shum *et al.*, 1990]. Forming altimeter crossovers can remove the dominant and constant signals in the altimeter residuals such as the marine geoid model error and the quasi-stationary sea surface topography model error. Static errors such as the altimeter height bias and the mean component of the orbit error can also be eliminated. By forming crossovers, however, the effect of temporally varying errors from media, tides, inverted barometer, instrument noise, temporal sea surface changes, etc. may build up instead of being eliminated because of the time differences of the two passes. Thus, the altimeter crossover residuals are influenced by time-varying oceanography.

The magnitude of the crossover residuals can be modeled as the root sum square (RSS) of the uncertainties in the constituent error sources such as the radial orbit errors, ocean tide model errors, the measurement noises of the

| | GDR (T/P) | Goal (Jason-1) |
|---|---|---|
| Altimeter noise | $1.7^a$ | 1.5 |
| EM bias | $2.5^d$ | 1.04 |
| +Skewness | | |
| +tracker bias | | |
| Tropo, dry | $0.7^a$ | 0.7 |
| Tropo, wet | $1.1^b$ | 1 |
| Iono | $0.5^c$ | 0.5 |
| Altimeter meas(range) RSS | 3.3 | 2.25 |

a Based on 1-sec averages of the range estimates for 2-m significant wave height Fu *et al.* [1994]
b Ruf *et al.* [1994]
c Based on 100-km along-track averages of the dual-frequency altimeter estimates of the ionospheric range correction Imel [1994]
d Rodríguez & Martin [1994]

Table 3.5: Single-pass Altimeter Measurement Accuracy for T/P Dual-frequency Altimeter (Side A) [Unit: cm]

crossover, and ocean variability uncertainty.

$$\sigma^2_{xover} = \sigma^2_{orbit} + \sigma^2_{ocean} + \sigma^2_{tide} + \sigma^2_{meas} \tag{3.1}$$

The measurement noise for a crossover is equal to the RSS of the errors of two direct altimeter measurements including ascending and descending. The uncertainty of a direct altimeter measurement is determined as the RSS of errors due to the instrument noise, EM bias, skewness, troposphere corrections, and ionosphere corrections which are shown in Table 3.5. According to Table 3.5, the uncertainty of a direct altimeter measurement is 3.3 cm for T/P GDRs. Therefore, the measurement noise for a crossover becomes 4.7 cm.

The ocean variability is the uncertainty of the two altimeter measurements difference between the ascending and descending passes over the short time interval. The uncertainty of sea surface height due to errors in the ocean

tide model, CSR 3.0 [Eanes & Bettadpur, 1996], is approximately 2 cm, which is much larger than the tide-induced error on the radial orbit of about 0.7 cm as shown in Table 3.1.

| | T/P | Jason-1 |
|---|---|---|
| Radial orbit error | 2.5[d] | 1.0[e] |
| Measurement noise | 4.7[b] | 4.7 |
| Ocean tides | 2.0[c] | 2.0 |
| Ocean variability | 2.2 | 2.2 |
| Crossover residual RMS | 6.1[a] | 5.7 |

a JGM-3 [Tapley *et al.*, 1996]
b From Table 3.5
c [Eanes & Bettadpur, 1996]
d [Ries & Tapley, 1999]
e Goal of radial orbit error for Jason-1

Table 3.6: Altimeter Crossover Error Budget for T/P and Jason-1 [Unit: cm]

Table 3.6 also shows the altimeter crossover error budget for Jason-1, assuming similar errors as T/P but achieving the 1-cm orbit accuracy goal. Using the tabulated values of $\sigma_{orbit}$, $\sigma_{meas}$, $\sigma_{tide}$, and $\sigma_{xover}$ to evaluate Equation 3.1, the ocean variability RMS $\sigma_{ocean}$ is calculated to be approximately 2.2 cm. Applying this value for $\sigma_{ocean}$ for Jason-1, the crossover residual RMS budget is estimated to be approximately 5.7 cm. At this time, however, it is not clear if the Jason-1 measurement noise is as good as T/P. Jason-1 crossover RMS tends to be larger than T/P in spite of better orbits.

The assessment methods discussed above will be applied throughout this dissertation to choose a better parameterization strategy or to select better models by comparing each orbit solution. The radial orbit accuracy for the final solution will be estimated especially based on the crossover residual test

and high elevation SLR residual test. The data spans of the crossover altimeter for the orbit performance assessment purpose are provided in Table 3.7.

| Cycle | start time [UTC] | | stop time [UTC] | | Span Days |
|---|---|---|---|---|---|
| cyc008 | 3/25/2002 | 15: 1: 6. – | 4/04/2002 | 10:35:11. | 9.81534074 |
| cyc009 | 4/04/2002 | 17:46:52. – | 4/14/2002 | 10:57:13. | 9.71551604 |
| cyc010 | 4/14/2002 | 10:57:46. – | 4/24/2002 | 08:55:44. | 9.91525314 |
| cyc011 | 4/24/2002 | 8:56:17. – | 5/04/2002 | 6:54:26. | 9.91537993 |
| cyc012 | 5/04/2002 | 6:54:48. – | 5/14/2002 | 1:55:57. | 9.79247256 |
| cyc013 | 5/14/2002 | 16:59:39. – | 5/24/2002 | 2:42:19. | 9.40462607 |
| cyc014 | 5/24/2002 | 2:51:51. – | 6/03/2002 | 0:49:16. | 9.91486758 |
| cyc015 | 6/03/2002 | 0:50:23. – | 6/12/2002 | 22:47:24. | 9.91459981 |
| cyc016 | 6/12/2002 | 22:49:28. – | 6/22/2002 | 20:40:49. | 9.91065824 |
| cyc017 | 6/22/2002 | 20:50:35. – | 7/02/2002 | 18:13: 1. | 9.89058137 |
| cyc018 | 7/02/2002 | 20: 5:27. – | 7/12/2002 | 16:37:52. | 9.85584870 |
| cyc019 | 7/12/2002 | 16:49:18. – | 7/22/2002 | 14:36:43. | 9.90792129 |
| cyc020 | 7/22/2002 | 14:48:06. – | 8/01/2002 | 12:33:58. | 9.90684214 |

Table 3.7: Altimeter Crossover Data Spans for Performance Assessment

# Chapter 4

# Orbit Solution with GPS

The performance of the BlackJack GPS Turbo-Rogue Space Receiver on Jason-1 has been significantly improved over the experimental GPS receiver on T/P. The robust GPS data will support a higher level of empirical parameterization to accommodate the surface force model errors. The objective of this chapter is to find optimal models and parameterizations to get the best orbit solution by using GPS-only data in the dynamic approach. The solution from GPS-only data will be compared with the solutions from DORIS/SLR to investigate the strength of GPS-only orbits.

Table 4.1 defines each cycle for Jason-1 since January 15, 2002. Prior to the starting epoch of cycle 8, March 13, 2002, the GPS measurement was of lesser quality because of the L2 ramp problem which will be discussed later. In this study, the GPS data from cycles 8 - 20 were utilized. GPS orbits of 30-hour arcs were integrated daily with a 3-hour extension at both ends for the overlap test purpose. Then, each full cycle's orbit was obtained by merging the middle 24-hour arcs of the daily orbits. Table 4.2 shows the orbit spans for orbit performance assessment. However, the orbits from several days for several cycles were excluded in the merging stage, to avoid the anomalous

behaving solutions of some days related to orbit attitude control transition for yaw steering (see Table 2.8). Cycle 12 and cycle 19, for example, are not full cycles. Orbits of the days in the transition of "steering to fix" or "fix to steering" were excluded from each cycle. Inclusion of the orbits from those days into a full cycle orbit for the process of orbit performance assessment significantly degrades the whole cycle's orbit quality, mainly because of the discontinuity of the parameterization for the Center-of-Mass (CoM) in the transition, which will be discussed in Section 4.2.1.

Care also needs to be taken for inclusion of the days near the orbit maintenance maneuver. Day 134 was not included in cycle 12, but the orbit span of 5h:26m:00s-24h:00m:00s (UTC) of day 134 was included in cycle 13. Day 183 was also excluded from cycle 17, but its time span of 19h:19m:30s-24h:00m:00s (UTC) was included in cycle 18. It is best to exclude day 134 and day 183, otherwise the parameterization of day 134 and day 183 should be handled separately from other days with different subarc lengths, and with the integration starting epoch at the cycle starting epoch.

In this chapter, the GPS preprocessing will be described and the effect of the parameter estimation on the orbit solution from GPS-only data will be analyzed. For surface forces, the box-wing model will be compared to the cannonball-wing model. In Chapter 5, the orbit improvement that results from combining SLR/DORIS data with GPS data will be further explored.

| Cycle | start time [UTC] | | | stop time [UTC] | | Days |
|---|---|---|---|---|---|---|
| cyc001 | 1/15/2002 | 5:10:50. | – | 1/25/2002 | 3:09:20. | (day 015 - 025) |
| cyc002 | 1/25/2002 | 3:09:20. | – | 2/04/2002 | 0:45:00. | (day 025 - 035) |
| | orbit maintenance maneuver | | | | | |
| cyc003 | 2/04/2002 | 1:41:40. | – | 2/13/2002 | 23:06:30. | (day 035 - 044) |
| cyc004 | 2/13/2002 | 23:06:30. | – | 2/23/2002 | 21:05:00. | (day 044 - 054) |
| cyc005 | 2/23/2002 | 21:05:00. | – | 3/05/2002 | 18:40:30. | (day 054 - 064) |
| | orbit maintenance maneuver | | | | | |
| cyc006 | 3/05/2002 | 19:36:40. | – | 3/15/2002 | 17:02:00. | (day 064 - 074) |
| cyc007 | 3/15/2002 | 17:02:00. | – | 3/25/2002 | 15:00:30. | (day 074 - 084) |
| cyc008 | 3/25/2002 | 15:00:30. | – | 4/04/2002 | 12:58:60. | (day 084 - 094) |
| cyc009 | 4/04/2002 | 12:59:00. | – | 4/14/2002 | 10:57:30. | (day 094 - 104) |
| cyc010 | 4/14/2002 | 10:57:30. | – | 4/24/2002 | 08:55:60. | (day 104 - 114) |
| cyc011 | 4/24/2002 | 8:56:00. | – | 5/04/2002 | 6:54:30. | (day 114 - 124) |
| cyc012 | 5/04/2002 | 6:54:30. | – | 5/14/2002 | 4:43:00. | (day 124 - 134) |
| | orbit maintenance maneuver | | | | | |
| cyc013 | 5/14/2002 | 5:26:00. | – | 5/24/2002 | 2:43:00. | (day 134 - 144) |
| | gap | | | | | |
| cyc014 | 5/24/2002 | 2:51:40. | – | 6/03/2002 | 0:50:10. | (day 144 - 154) |
| cyc015 | 6/03/2002 | 0:50:10. | – | 6/12/2002 | 22:48:40. | (day 154 - 163) |
| cyc016 | 6/12/2002 | 22:48:40. | – | 6/22/2002 | 20:47:10. | (day 163 - 173) |
| cyc017 | 6/22/2002 | 20:47:10. | – | 7/02/2002 | 8:23:20. | (day 173 - 183) |
| | orbit maintenance maneuver | | | | | |
| cyc018 | 7/02/2002 | 19:19:30. | – | 7/12/2002 | 16:44:10. | (day 183 - 193) |
| cyc019 | 7/12/2002 | 16:44:10. | – | 7/22/2002 | 14:42:40. | (day 193 - 203) |
| cyc020 | 7/22/2002 | 14:42:40. | – | 8/01/2002 | 12:41:20. | (day 203 - 213) |

Table 4.1: Jason-1 Cycle Definition

| Cycle | start 00:00:00 [GPS] | | stop 24:00:00 [GPS] | Days |
|---|---|---|---|---|
| cyc008 | 3/25/2002 | – | 4/04/2002 | (day 084 - 094) |
| cyc009 | 4/04/2002 | – | 4/14/2002 | (day 094 - 104) |
| cyc010 | 4/14/2002 | – | 4/24/2002 | (day 104 - 114) |
| cyc011 | 4/24/2002 | – | 5/04/2002 | (day 114 - 124) |
| cyc012 | 5/04/2002 | – | 5/10/2002 | (day 124 - 130) |
| cyc013 | 5/14/2002 | – | 5/23/2002 | (day 134 - 143) |
| cyc014 | 5/24/2002 | – | 6/03/2002 | (day 144 - 154) |
| cyc015 | 6/03/2002 | – | 6/12/2002 | (day 154 - 163) |
| cyc016 | 6/12/2002 | – | 6/22/2002 | (day 163 - 173) |
| cyc017 | 6/22/2002 | – | 7/01/2002 | (day 173 - 182) |
| cyc018 | 7/02/2002 | – | 7/12/2002 | (day 183 - 193) |
| cyc019 | 7/15/2002 | – | 7/22/2002 | (day 196 - 203) |
| cyc020 | 7/22/2002 | – | 8/01/2002 | (day 203 - 213) |

Table 4.2: Orbit Spans for Performance Assessment. It will be best to exclude days 134 and 183 because of the orbit maintenance maneuver.

## 4.1 GPS preprocessing

The International GPS service for Geodynamics (IGS) provides to the public GPS data files tracked at more than 300 ground stations at present (IGS 2002) in the Receiver Independent EXchange (RINEX) format. At UT/CSR, the tracking data from about 51 stations, which were initially selected based on the ITRF97 reference GPS stations, are routinely archived locally (see Chapter 6 for more details). The tracking data are made available in daily RINEX files by the naming convention of "ssssdddf.yyo.Z", where 'ssss' is the 4-character station code, 'ddd' is the day of the year, 'f' is the file sequence number (0 for 24-hour file), 'yy' is the two-digit year and 'o' indicates the RINEX observation file. The files are compressed using the standard UNIX compression scheme

(*.Z). Currently the standard data rate is 30 seconds for the ground tracking data. Data files contain observations for a 24-hour period, from 00h:00m:00s till 23h:59m:30s GPS time. The RINEX file headers give more information about sites, antennas and signals. For the official site information, the station log files provided by IGS need to be consulted.

The Jason-1 GPS tracking data were made available by CNES at `ftp://spike.cst.cnes.fr`. Initially, the data were restricted to only POD groups but it later became open to the public. The Jason-1 data use the compact RINEX format whose filename extension, 'd' in " *.yyd.Z" instead of 'o', denotes observation files that are additionally compressed using the Hatanaka obs file compression scheme [Hatanaka, 1998]. The Compact RINEX format is a compression format for GPS observation data which is compatible with the RINEX version 2 observation file format. Jason-1's 4-character station code is 'jaso'. Jason-1 collects GPS data every 10 seconds, while the IGS ground stations collect GPS data every 30 seconds.

To process the orbit estimation by employing MSODP, first, the double-differenced GPS data need to be generated by using the ground and Jason-1 tracking data in the preprocessing stage. The main purpose of GPS preprocessing is to edit raw data and generate double-differenced (DD) carrier phase observables with corrected measurement time tags. The files for final DD observables follow the CSR DD ASCII format. The TEXGAP (university of TEXas Gps Analysis Program) software is used for the GPS preprocessing in this study.

After downloading both the raw GPS ground tracking data and Jason-1 tracking data from the IGS and CNES ftp sites, respectively, the sampling time interval is synchronized at 30 seconds for the double-differencing purpose due to their original time interval difference for the data collection, as stated previously. The three day RINEX files were combined to form an 30-hour arc tracking data by merging the centered 24-hour arc of the middle day with the ending 3-hour data from the previous day and the beginning 3-hour data from the following day. The 30 hour observations are needed to estimate 30-hour arc orbits in MSODP. The 3-hour arcs at both ends will be used to compare overlap statistics to assess the orbit solutions. After the sampling rate synchronization and the merging of three 1-day RINEX files, the RINEX files were converted to a machine dependent binary format to handle the intermediate processes because of its disc space economy and efficiency.

A GPS receiver tags its measurements based on its own internal clock, which is not always sufficiently accurate for high-precision geodesy. The next step of preprocessing is, therefore, to correct the GPS receiver time tag of the data with respect to the GPS system time, which was measured by highly accurate GPS satellite on-board atomic clocks and also monitored by ground control stations. By using the original nominal time tag ($t_r$) and the receiver time tag correction ($\delta t_r$), the corrected receiver time tag, $T_r$, can be expressed as $T_r = t_r - \delta t_r$. The receiver time tag correction, $\delta t_r$, is computed as follows:

$$\delta t_r = \frac{\rho}{c} - \frac{\rho_c}{c} + \delta t_s \tag{4.1}$$

where $\rho$ is the pseudo-range observation; $\rho_c$ is the computed range between a GPS satellite and a ground station (or, the user satellite); $\delta t_s$ is the broadcast GPS satellite clock correction; and, $c$ is the speed of light (299,792,458 m/sec). Equation 4.1 requires information such as, 1) observed pseudo-range data from RINEX files for $\rho$, 2) the GPS satellites' clock information provided from the broadcast navigation message for $\delta t_s$, and, 3) the ground station coordinates and the ephemerides of Jason-1 for $\rho_c$. The ephemerides of Jason-1 can be obtained by the SLR/DORIS solution with high precision. The SLR/DORIS solution, however, is not always available because of orbit attitude maneuvers between cycles. In this process, therefore, the navigation solution (NAVSOL) is also used to provide the Jason-1 ephemerides for the gaps between cycles, which existed in the SLR/DORIS orbit solution. To process NAVSOL, Jason-1 pseudo-range data from the RINEX file and the broadcast GPS ephemeris file are required. To improve the precision of the NAVSOL solution, the whole GPS data pre-processing and dynamic GPS orbit estimation process are iterated once. The ephemerides of Jason-1 are expressed in the body-fixed frame with GPS time. The ephemerides files are formatted in the SP1 format to be used in TEXGAP.

GPS satellite clock errors and receiver clock errors which remain in the carrier-phase measurements, even after the time tag correction, can be removed by the differences between the measurements, since they have common error sources. For single-differenced observables, one GPS ground receiver and Jason-1 GPS receiver were paired to form the differences of the raw mea-

surements for a common GPS satellite to eliminate the GPS satellite clock errors (see Equation A.33). Producing double-differenced (DD) observables formed by the differences between the two single-differenced observables from two different GPS satellites (see Equation A.35) can also eliminate the ground receiver clock error and Jason-1 GPS receiver clock error.

The next step is to eliminate the first-order ionospheric effects using the DD carrier phase observables from dual frequencies, L1 and L2. Using the DD carrier phase observables $\phi_{L1}$ at L1 and $\phi_{L2}$ at L2, the ionospheric-free phase observable $\phi_{LC}$ can be formed as [Leick, 1995]:

$$\phi_{LC}(t) = \frac{f_1^2}{f_1^2 - f_2^2}\phi_{L1}(t) - \frac{f_1 f_2}{f_1^2 - f_2^2}\phi_{L2}(t) \tag{4.2}$$

where $f_1$ is the L1 frequency (1575.42 MHz) and $f_2$ is the L2 frequency (1227.60 MHz). In the same way, the ionospheric-free range observable $\rho_{LC}$ can be formed by using $\rho_{L1}$ at L1 and $\rho_{L2}$ at L2 as:

$$\rho_{LC}(t) = \frac{f_1^2}{f_1^2 - f_2^2}\rho_{L1}(t) - \frac{f_1 f_2}{f_1^2 - f_2^2}\rho_{L2}(t) \tag{4.3}$$

The ionospheric-free observables, which will be called DDobs, are the actual GPS data that is to be processed in MSODP.

Finally, the anomalous data points are edited and the cycle-slips are fixed. Data points whose DD residuals are outside of the range of three-times standard deviation of the DD residuals are removed. The DD residual is computed by subtracting the computed DD measurement from the observed DD measurement. The DD passes with less than 6 DDobs were also edited out; the

minimum duration time for DD passes was 3 minutes. In MSODP, DD passes with less than 10 DDobs were further edited. Cycle-slips, which were detected by identifying some anomalies in the differences between the consecutive data points in the DD residuals, are fixed with linear extrapolation. Approximate DD ambiguities are also initially corrected by comparing the computed DD measurement and the observed DD measurement. The approximate correction in the preprocessing stage provides more numerical stability for the dynamic orbit determination process in MSODP to estimate accurate ambiguities. The elevation mask angle of the ground receiver for the DDobs was 15°, and 0° for the Jason-1 elevation cut-off angle. All of the DDobs from about 50 ground stations and Jason-1 were merged together into a file and sorted by the observation time in order to be processed in MSODP.

While the BlackJack receiver on Jason-1 can track up to 12 GPS satellites simultaneously on two frequencies, the actual number of tracked GPS satellites with sufficient signal-to-noise ratio is usually less than 9 as shown in Figure 4.1(a). The figure shows that the average number of tracked satellites is 7-8 since cycle 8, and it is dependent on the yaw regime of Jason-1. The number of satellites tracked in the fixed yaw is reduced to 6, which is the primary reason why the numbers of daily DDobs are reduced in the fixed yaw as shown in Figure 4.2(b). Prior to cycle 8, a higher average number of satellites tracked is shown. During this period, however, the carrier-phase data were not good enough to survive the preprocessing stage because of the L2 ramp, which is a frequency bias on the L2 carrier-phase that affects 7-30% of the data each

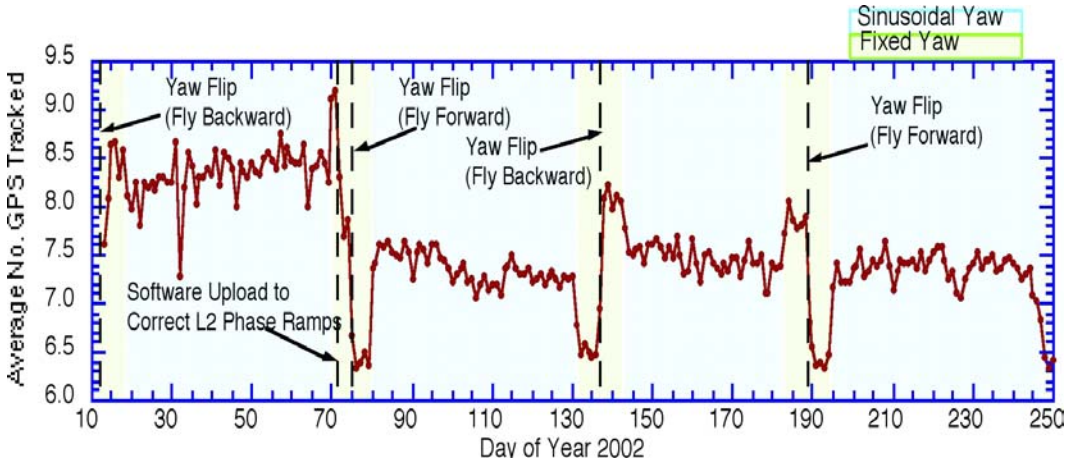


(a) Daily Averaged Number of GPS Satellites

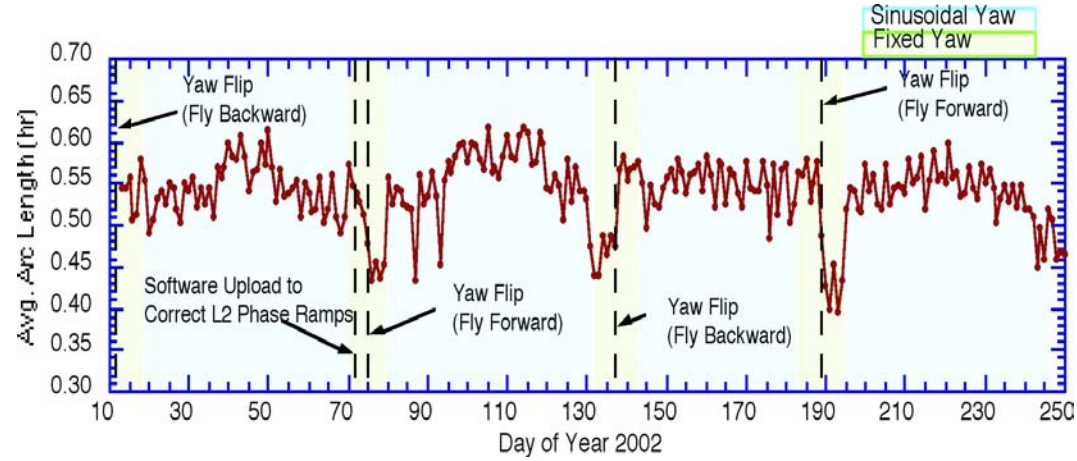


(b) Daily Averaged Arc-length of GPS Track

Figure 4.1: Daily averaged Number of GPS satellites (top) and Arc-length of GPS track (bottom) from Jason-1 [Haines *et al.*, 2002]. The average number of tracked satellites is 7-8 since cycle 8, where the L2 ramp problem was corrected. In the fixed yaw, the number of satellite tracked and the average arc length is reduced. Long and continuous tracking passes are critical for POD.

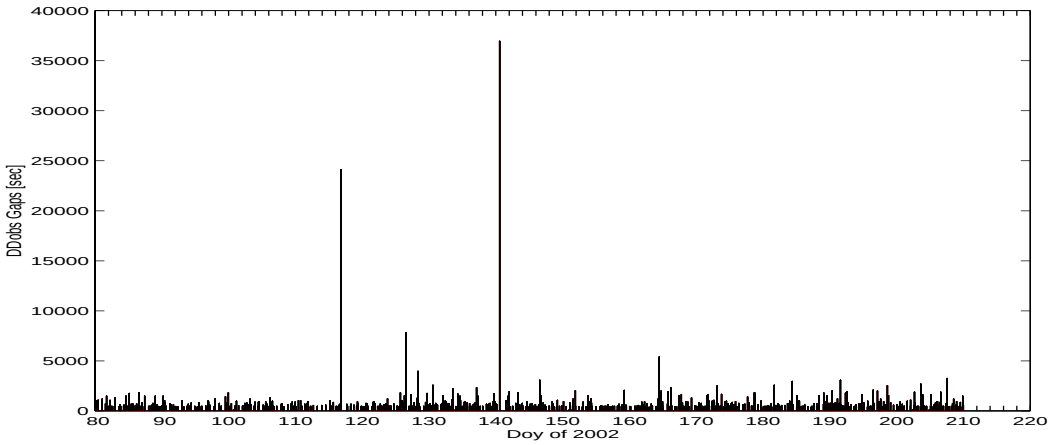


(a) DDobs data gap duration

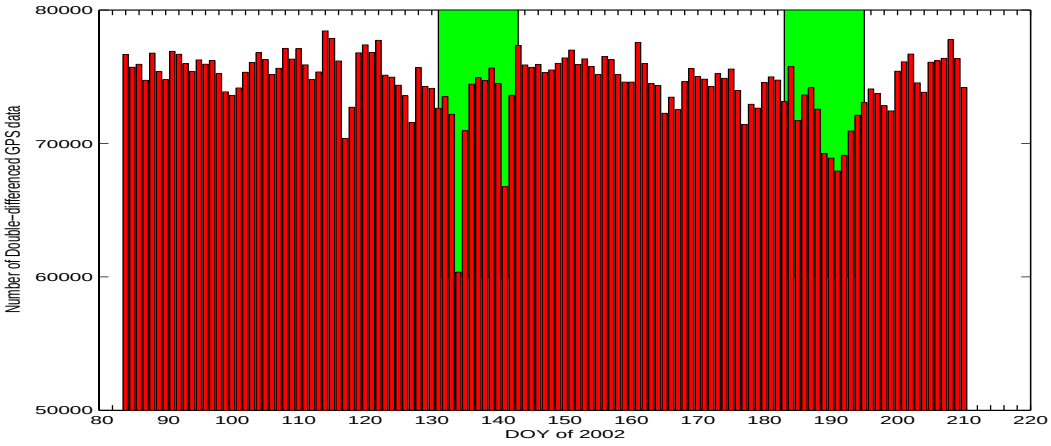


(b) Daily DDobs numbers

Figure 4.2: GPS DDobs gap duration (top) and DDobs numbers (bottom) for cycle 8 to 20. Day 117 has a 7-hour gap and Day 141 has a 10-hour gap. In the fixed yaw (green region), DDobs numbers are significantly reduced.

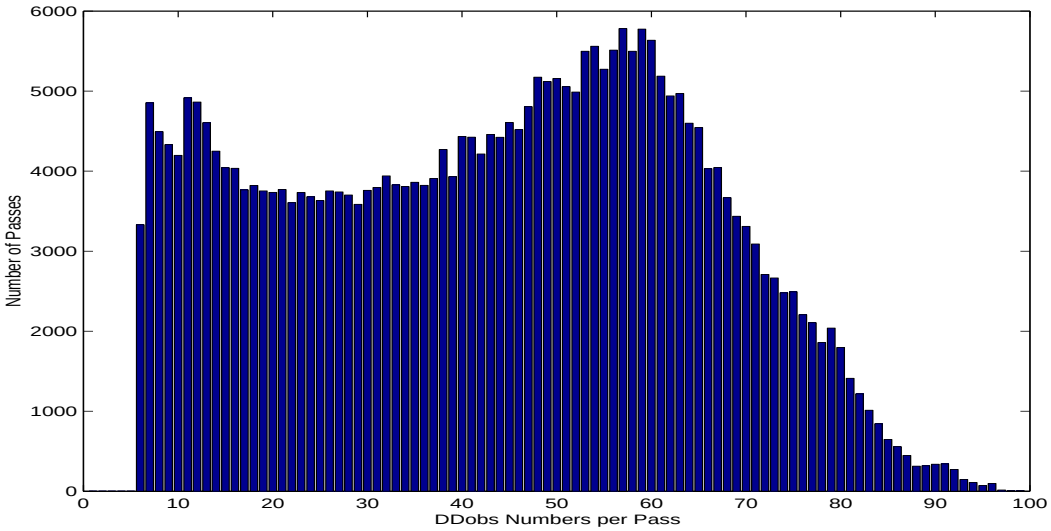


Figure 4.3: DDpass Numbers w.r.t. DDobs per DDpass for cycle 8 - 20. A DDpass with 60 DDobs is 30 minutes long, since 1 DDobs per 30 sec is sampled in a pass.

day depending on the attitude regime [Haines *et al.*, 2002]. A software upload on March 13, 2002, eliminated these L2 phase ramps.

The daily mean length of GPS tracking passes shown in Figure 4.1(b) is 30-35 minutes, also depending on the yaw regime. Long and continuous tracking passes are critical for POD based on GPS tracking. Interrupted tracking usually prevents a heavier parameterization scheme from compensating for the surface model error. The BlackJack receiver on Jason-1 resets approximately 3 to 8 times per day, which results in data gaps with typical duration of 6-12 minutes. The cause of the resets appears to be some correlation with the South Atlantic Anomaly (SAA) implying that they are induced by strong radiation exposure. Figure 4.2(a) and Table 4.3 show that the durations of tracking

| start time [GPS] | Gap duration [sec] | Cycles affected |
|---|---|---|
| 4/27/2002 19:53:00 | 24120 | cycle 011 (day 117) |
| 5/07/2002 14:01:00 | 7830 | cycle 012 (day 127) |
| 5/09/2002 08:15:00 | 3990 | cycle 012 (day 129) |
| 5/21/2002 13:44:00 | 36960 | cycle 013 (day 141) |
| 5/27/2002 13:33:30 | 3090 | cycle 014 (day 147) |
| 6/14/2002 10:50:00 | 5400 | cycle 016 (day 165) |
| 7/11/2002 14:11:00 | 3090 | cycle 018 (day 192) |
| 7/27/2002 14:10:30 | 3270 | cycle 020 (day 208) |

Table 4.3: DDobs gap durations longer than 50 minutes

gaps of longer than one hour have occurred on several days, which can weaken the parameterization. In Table 4.3, day 117 shows a gap longer than 6 hours and day 141 shows a gap longer than 10 hours, which may cause some sub-arc parameterization difficulty, resulting in weakness of the orbits of cycle 11 and cycle 13, respectively. Note that these DDobs gaps of long durations are neither due to the orbit maneuvers between cycles nor due to the yaw steering transitions shown in Table 2.8 or Table 4.1. The effect of the data gaps on the orbit RMS will be discussed later in Section 4.2.2.

## 4.2 Parameterizations

The main components to be estimated in the orbit determination problem are the position and velocity of the satellite [see Appendix C for details of the orbit estimation theory]. The estimation of unknown model parameters is also important to determine precise orbit solutions. In this section, the three independent sets of parameters related to three different issues will be esti-

mated and their effects on the solution will be examined. The three issues are: 1) the parameters related to the Center of Mass of Jason-1, 2) the empirical acceleration parameters to accommodate the surface force model uncertainties, and 3) the parameters related with the orbit element correction of GPS satellites.

### 4.2.1 Center-of-Mass Offset and Phase Center Offset

In this section, 1) the GPS antenna Phase Center Offset is estimated, 2) the best estimation strategy for the GPS phase center offset is investigated by examining each orbit performance, and 3) the estimates of the phase center offset are compared to the original estimates in the lab. Each estimate from different orbit analysis centers using different tracking data is also compared to each other to see whether there is an actual CoM change common to each tracking antenna or whether it is peculiar to the GPS antenna. The satellite body fixed (SBF) coordinate with a reference point as the coordinate origin (see Section 2.5) is used in this section. In MSODP, the phase center offset change, $\Delta\vec{R}_{PC}$, is expressed as:

$$\Delta\vec{R}_{PC} = \vec{R}_{PC}^{new} - \vec{R}_{PC}^{apriori} \tag{4.4}$$

where $\vec{R}_{PC}^{apriori}$ is a priori phase center offset[1] which is a phase center with respect to the CoM, $\vec{R}_{PC}^{new}$ is the new estimated phase center with respect to

[1]The CMOFF card in MSODP means $\vec{R}_{PC}^{apriori}$. The COMDEL card means $(\vec{r}_0 - \vec{r}_{CoM})$, where $\vec{r}_0$ is a reference point vector and $\vec{r}_{CoM}$ is the CoM vector in the satellite body fixed coordinate.

the CoM (see Figure 4.4). The $\Delta X$, $\Delta Y$ and $\Delta Z$ which will be mentioned later are the components of $\Delta\vec{R}_{PC}$.

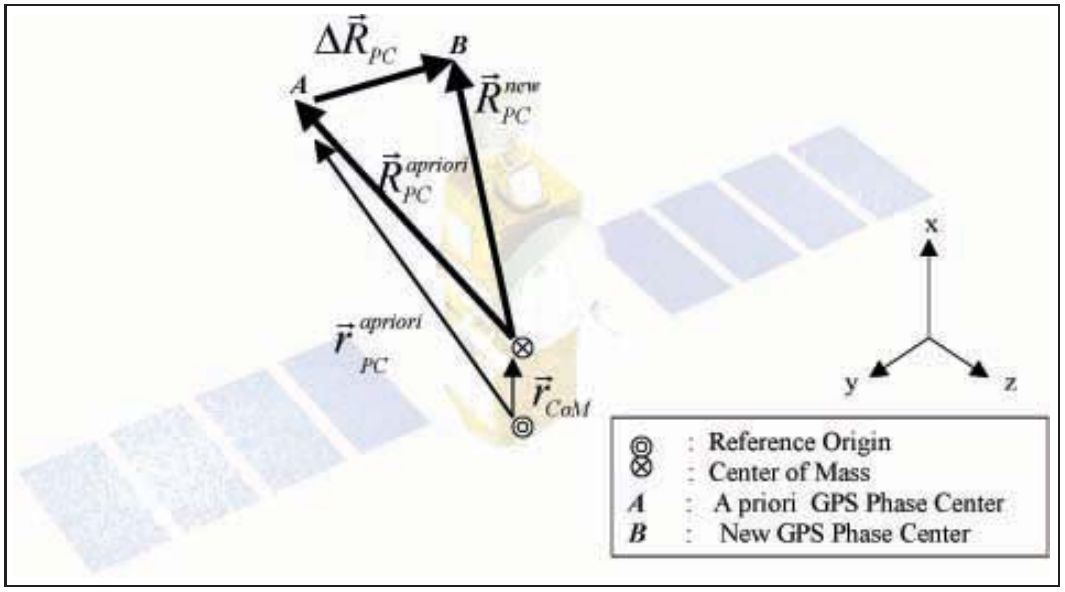


Figure 4.4: Illustration of the Spacecraft Geometry. $\vec{R}_{PC}^{apriori}$ is the vector of a priori phase center location with respect to CoM. $\vec{r}_{CoM}$ is the CoM vector with respect to the reference origin in the satellite body-fixed coordinate and $\vec{r}_{PC}^{apriori}$ is the vector of a priori phase center location with respect to the reference origin. CNES provides information of $\vec{r}_{CoM}$ and $\vec{r}_{PC}^{apriori}$. $\Delta\vec{R}_{PC}$ is estimated in MSODP to obtain $\vec{R}_{PC}^{new}$, which is the vector of new phase center location with respect to the CoM.

The location of CoM is assumed to be 942 mm in the positive X direction with respect to the coordinate origin, which is based on the estimate of 8 $kg$ hydrazine consumption (see Table 2.5). The consumption of fuel is expected to cause the CoM to move forward to the positive X direction, since the fuel tank on the satellite is located on the rear side.

Table 4.4 shows the GPS antenna phase center location of L1 and L2

| | x (mm) | y (mm) | z (mm) |
|---|---|---|---|
| CoM | 942.0 | 0.0 | 0.0 |
| GPS L1 | 2408.0 | -219.7 | -537.1 |
| GPS L2 | 2420.2 | -220.8 | -558.5 |
| GPS $L_C$ | 2389.1 | -218.0 | -504.0 |

Table 4.4: A priori for GPS phase centers and center of mass with respect to the reference origin.

signals measured at a lab before launch. The combined carrier phase signal, $L_C$, is used in this research. The apparent GPS $L_C$ phase center is derived from the lab phase measurements of L1 and L2, by applying Equation A.45 for the ionosphere-free combination. To get the antenna phase center relative to the CoM, one must subtract the CoM from the antenna coordinates.

The experience of T/P showed that the post-launch estimates of the GPS antenna phase center can be very different from the pre-launch estimates, and that estimating the phase center offset can be beneficial to improve the coordinate centering, even though the nature of the discrepancy between the measured location in a lab and the estimated location after launch has not been fully understood. Estimation of the phase center offsets has become standard operating procedure for GPS-based POD because of its contribution to the orbit performance improvement [B. Haines, personal communication, 2002].

The phase center offset relative to the center of mass of the spacecraft can change for two main reasons: one is the actual change of the antenna phase center in space, the other is the change of the center of mass caused

by fuel consumption. The engineers can measure the radiometric phase center location in an anechoic chamber with great accuracy. However, mounting the choke ring on a spacecraft flying at 7 km/s in orbit with a few multipath and potential radio-interference sources around it, can cause some unknown change to the antenna phase center on orbit. In this experiment, the phase center offset change with respect to the CoM is estimated assuming that the CoM is fixed to the nominal value. If the assumption is true, the estimated offset will reflect only the phase center change in space. However, because of the fuel consumption in space, the CoM change is inevitable and must be coupled with the phase offset change in the estimates. If the phase centers can change in the space environment, then the analysis to separate the change of the CoM from the estimates can be even more complicated. In addition to that, if there is any periodic variation in the phase centers in orbit, any variation shorter than 24 hours may not appear in the estimated offset since the short-term variation of the changes of the phase center of less than 24 hours can be averaged during the 1-day arc solution process. However, the variations longer than 1-day could appear in the estimated offset trend.

The question about the estimation of which component of the phase center offset will improve the orbits is investigated in this section. To study the impact on the orbit improvement from the estimation of each component for the change of the phase center offset, several cases were considered as shown in Table 4.5. The estimate of $\Delta X$ can be very critical, because the fuel tank is designed to change the CoM along only the X-direction as fuel is consumed.

| Case | Estimation Strategy for Center-of-Mass Offset |
|---|---|
| **Case NO** | No component of the phase center offsets is estimated. |
| **Case X** | Only $\Delta X$ is estimated. |
| **Case Y** | Only $\Delta Y$ is estimated. |
| **Case Z** | Only $\Delta Z$ is estimated. |
| **Case XZ** | $\Delta X$ and $\Delta Z$ are estimated. |
| **Case XYZ** | All components of the phase center offset, $\Delta X$, $\Delta Y$ and $\Delta Z$ are estimated. |

Table 4.5: Estimation strategy cases for Center-of-Mass Offset

The 30 degree tilt of the GPS antenna in the XZ plane over the XY plane is another reason why the estimation of $\Delta Z$ should be considered seriously as well as the estimation of $\Delta X$ in the experimental cases.

When the CT parameter and the 1-cpr T and N empirical parameters are estimated simultaneously, care needs to be taken for the estimation of $\Delta X$ and $\Delta Y$. It will be difficult to estimate $\Delta X$ if the satellite's X-direction coincides to the along track direction, because it can be correlated to the CT and 1-cpr T empirical parameter. Thus, when the satellite is in fixed yaw, it is impossible to separate the X-directional change of the phase center offset from the along-track empirical parameter. Ideally, the best time to estimate $\Delta X$ is when the X-direction of the satellite is perpendicular to the along-track direction. In the sinusoidal yaw regime, the estimation of $\Delta X$ will be an averaged value over the integration arc length of 30 hours, since the X-direction of the satellite changes sinusoidally relative to the along-track direction. Estimates of $\Delta Y$ can be partially correlated with the 1-cpr empirical

parameters and CT in the sinusoidal yaw regime. In the fixed yaw regime, $\Delta Y$ can not be separated from the 1-cpr N parameter.

The internal consistency test with overlap arcs plays an important role in evaluating orbits from each case with different strategies. The estimation of $\Delta X$ in the fixed yaw mode may cause a meter-level orbit difference in the along-track direction from the overlap orbit comparison because of the correlation of $\Delta X$ and the CT or 1-cpr T parameters. For example, the overlap statistics of **Case XZ** for days in cycle 13 and cycle 18, which are in the fixed yaw regime, were bad, ranging from 4 centimeters to 3 meters in 3-D. However, the orbit of **Case Z** with no estimation of $\Delta X$ significantly improved the overlap consistency to less than 5 cm in 3-D RSS[2]

Tables 4.6 and 4.7 show the orbit performances from each estimation strategy. Note that cycles 8, 9 and 10 are in the sinusoidal yaw regime. Table 4.6 shows that estimating only $\Delta Z$ produced the best internally consistent solution in all of three directions improving $\overline{RMS}$, which is defined as the averaged RMS over all overlaps in a cycle, compared to the $\overline{RMS}$ with no estimation of the phase center offset: its averaged RSS and the averaged RMS in all of three directions was the smallest. Estimating $\Delta X$ possibly hurts the radial and transverse direction consistency of orbit solutions. For all three cycles, estimation of $\Delta X$ produced the largest radial overlap differences which was worse than the **Case NO**. Estimation of $\Delta Y$ made the internal orbit

[2]There were orbit maneuvers for day 134 and day 183. These days were excluded from cycle 13 and 18 for the orbit consistency test.

consistency worse than the **Case NO**, particularly in the transverse or normal direction.

Table 4.7 shows significant reduction of the postfit residuals by estimating $\Delta Z$ for all of the three cycles during sinusoidal yaw. The estimation of $\Delta X$ or $\Delta Y$ did not affect the postfit residuals. Judging by the comparison of the altimeter crossover Means between **Case NO** and **Case Y**, and also between **Case XZ** and **Case XYZ**, the estimation of $\Delta Y$ did not appear to have any noticeable impact on the orbit centering. It is interesting to see that the estimation of $\Delta Z$ increased the crossover Means compared with the **Case NO**. However, estimation of $\Delta X$ appeared to actually help the orbit centering by balancing out with some counter effect from the estimation of $\Delta Z$. To find out the contribution of the $\Delta X$-estimation to the **Case Z**'s orbit centering, the experimental span for the comparison between the **Case Z** and **Case XZ** was extended to additional cycles, with the results shown in Table 4.8.

In Table 4.8, except cycle 16, the orbits from **Case XZ** in the sinusoidal yaw regime show reductions in the crossover Means and the crossover RMSs against the orbits from **Case Z**. All of them show a reduction of SLR residual RMS over the orbits solved using the **Case Z** strategy. However, cycles 13 and 18, which are in the low fixed yaw regime, act differently. Cycle 18 clearly shows the advantage of the **Case Z** strategy. The crossover RMS and the SLR residual RMS of cycle 18 show significant reduction in the orbits of **Case Z** over the orbits of **Case XZ**. The large overlap RSS values of cycles 13 and 18 from **Case XZ**, which are bigger than 1 meter, show the correlation between

| Case | Internal Consistency of Overlaps $\overline{RMS}$ | | | |
|---|---|---|---|---|
| | radial(R) | along-track(T) | normal(N) | RSS |
| NO | 14.0 | 28.5 | 13.3 | 34.7 |
| X | 15.1 | 30.4 | 13.2 | 36.8 |
| Y | 13.9 | 34.1 | 16.7 | 40.8 |
| Z | 12.7 | 25.9 | 13.5 | 32.3 |
| XZ | 14.2 | 28.2 | 13.4 | 34.6 |
| XYZ | 14.4 | 35.7 | 16.9 | 42.5 |

(a) cycle 8

| Case | Internal Consistency of Overlaps $\overline{RMS}$ | | | |
|---|---|---|---|---|
| | radial(R) | along-track(T) | normal(N) | RSS |
| NO | 15.7 | 36.8 | 10.6 | 41.7 |
| X | 17.0 | 39.4 | 10.3 | 44.5 |
| Y | 15.6 | 55.7 | 14.0 | 59.9 |
| Z | 13.6 | 32.2 | 9.9 | 36.6 |
| XZ | 14.7 | 34.1 | 9.7 | 38.6 |
| XYZ | 14.7 | 58.9 | 15.6 | 63.2 |

(b) cycle 9

| Case | Internal Consistency of Overlaps $\overline{RMS}$ | | | |
|---|---|---|---|---|
| | radial(R) | along-track(T) | normal(N) | RSS |
| NO | 13.7 | 26.6 | 10.8 | 32.1 |
| X | 13.8 | 26.6 | 10.8 | 32.2 |
| Y | 13.5 | 58.6 | 14.1 | 62.2 |
| Z | 13.4 | 25.2 | 10.3 | 30.5 |
| XZ | 13.6 | 25.3 | 10.2 | 30.7 |
| XYZ | 13.7 | 56.6 | 12.2 | 60.3 |

(c) cycle 10

Table 4.6: Overlap Arc comparison for the CoM estimation strategy test (Each value represents $\overline{RMS}$, which is averaged RMS over all overlaps in a cycle). Orbits from **Case Z** and **Case XZ** show good internal consistency. [Unit: mm]

| Case | post-fit | SLR residuals(>70°) | | crossover residuals | |
|---|---|---|---|---|---|
| | | Mean | RMS | Mean | RMS |
| NO | 16.2 | 3.2 | 11.0 | 16.3 | 64.6 |
| X | 16.2 | -0.6 | 9.6 | -11.9 | 63.6 |
| Y | 16.2 | 1.7 | 12.2 | 15.5 | 64.3 |
| Z | 15.7 | 2.1 | 11.9 | 20.9 | 65.6 |
| XZ | 15.6 | .0 | 9.4 | 5.7 | 62.4 |
| XYZ | 15.6 | -1.2 | 10.8 | 5.4 | 62.4 |

(a) cycle 8

| Case | post-fit | SLR residuals(>70°) | | crossover residuals | |
|---|---|---|---|---|---|
| | | Mean | RMS | Mean | RMS |
| NO | 14.3 | -1.4 | 15.1 | 10.6 | 60.4 |
| X | 14.3 | -5.1 | 14.8 | -2.0 | 60.4 |
| Y | 14.3 | -1.2 | 15.4 | 10.8 | 60.4 |
| Z | 13.7 | -2.2 | 15.8 | 15.5 | 61.3 |
| XZ | 13.6 | -5.4 | 15.0 | 4.5 | 59.8 |
| XYZ | 13.6 | -5.0 | 15.1 | 4.7 | 59.8 |

(b) cycle 9

| Case | post-fit | SLR residuals(>70°) | | crossover residuals | |
|---|---|---|---|---|---|
| | | Mean | RMS | Mean | RMS |
| NO | 14.1 | -7.8 | 14.3 | -4.2 | 61.2 |
| X | 14.1 | -7.4 | 14.5 | 3.0 | 61.1 |
| Y | 14.1 | -7.6 | 14.5 | -4.3 | 61.3 |
| Z | 13.6 | -8.2 | 13.9 | -3.1 | 60.9 |
| XZ | 13.5 | -7.9 | 14.1 | 3.6 | 60.9 |
| XYZ | 13.5 | -7.8 | 14.3 | 3.6 | 60.9 |

(c) cycle 10

Table 4.7: PostFit, SLR residual, Crossover test for CoM estimation [Unit: mm].

| Cyc | Case | overlap RSS | SLR residuals(>70°) | | crossover residuals | |
|---|---|---|---|---|---|---|
| | | | Mean | RMS | Mean | RMS |
| 8 | Z | 32.3 | 2.1 | 11.9 | 20.9 | 65.6 |
| | XZ | 34.6 | 0.0 | 9.4 | 5.7 | 62.4 |
| 9 | Z | 36.6 | -2.2 | 15.8 | 15.5 | 61.3 |
| | XZ | 38.6 | -5.4 | 15.0 | 4.5 | 59.8 |
| 10 | Z | 30.5 | -8.2 | 13.9 | -3.1 | 60.9 |
| | XZ | 30.7 | -7.9 | 14.1 | 3.6 | 60.9 |
| 11 | Z | 43.8 | -9.7 | 15.7 | -15.5 | 63.6 |
| | XZ | 44.0 | -9.7 | 15.7 | -14.0 | 63.2 |
| 12 | Z | 21.7 | -2.0 | 6.9 | -22.9 | 60.7 |
| | XZ | 24.0 | -2.7 | 6.4 | -18.0 | 59.2 |
| 13† | Z | 33.1 | -3.3 | 12.5 | 4.4 | 63.5 |
| | XZ | 1320.7 | -0.3 | 12.3 | 7.4 | 63.2 |
| 14 | Z | 26.1 | 3.0 | 13.9 | -14.3 | 61.7 |
| | XZ | 28.3 | 4.2 | 12.1 | -4.7 | 59.9 |
| 15 | Z | 29.1 | -6.4 | 17.5 | -10.3 | 60.9 |
| | XZ | 29.9 | -4.3 | 14.7 | -6.3 | 60.3 |
| 16 | Z | 29.6 | 7.6 | 17.6 | -4.2 | 59.6 |
| | XZ | 29.8 | 9.4 | 16.3 | -10.5 | 60.4 |
| 17 | Z | 30.4 | -5.2 | 12.3 | 14.3 | 62.1 |
| | XZ | 30.6 | -4.2 | 11.6 | 7.0 | 60.8 |
| 18† | Z | 31.5 | -5.0 | 8.1 | -2.9 | 55.6 |
| | XZ | 1629.4 | 10.6 | 53.3 | 0.5 | 63.7 |
| 19 | Z | 31.5 | -10.8 | 21.6 | 23.7 | 64.0 |
| | XZ | 31.5 | -10.3 | 19.9 | 12.7 | 61.0 |
| 20 | Z | 25.7 | .6 | 17.5 | 25.7 | 62.9 |
| | XZ | 26.1 | -1.2 | 15.3 | 15.3 | 59.5 |
| Total | Z | 30.7 | -2.8 | 15.0 | 2.7 | 62.1 |
| | XZ | 31.6 | -2.9 | 13.7 | -0.4 | 60.7 |

†: cycle 13 and 18 are in the fixed yaw regime.These two cycles are excluded from the Total average.

Table 4.8: Extended orbit comparison from **Case X** and **Case XZ**. Table shows Overlap statistics, SLR residual, Crossover test for CoM estimation. **Case XZ** works better overall in the sinusoidal yaw regime, but **Case Z** works better in the low fixed yaw regime. [Unit: mm]

CT and $\Delta X$ as previously discussed.

Therefore, the benefit of the estimation of $\Delta Z$ has been clearly shown in the aspects of the internal consistency, postfit residual and crossover statistics of orbits regardless of yaw regimes. The contribution of the estimation of $\Delta X$ is shown for the orbit centering of orbits in the sinusoidal yaw regime. For this research, **Case XZ** was chosen as a nominal estimation strategy for the sinusoidal yaw regime, and **Case Z** for the low fixed yaw regime.

Fig. 4.5(a) shows the postfit residual RMS of MSODP from Day 81 to Day 210. Only $\Delta Z$ is estimated for the fixed yaw regime of cycle 13 and 18. For most of the days, the postfit residual RMS was less than 1.5 cm. The large postfit residual RMS shown around day 134 and day 183 was expected due to the orbit maintenance maneuver at that time. It is interesting to observe the reduction of the postfit residual RMS in the fixed yaw region for both **Case XZ** and **Case Z**. The orbit solution of **Case XZ** in the fixed yaw regime produced bad internal consistency, but its postfit was still as good as the postfit of **Case Z**. This is why the strategy of **Case Z** instead of **Case XZ** is appropriate for the cycles in the fixed yaw regime. The reduction of the postfit residual RMS in the fixed yaw regime against the sinusoidal yaw regime has been commonly observed at CSR and GSFC. (see Fig. 4.5(a) and Fig. 4.7).

Fig. 4.5(b) shows the estimated $\Delta X$ and $\Delta Z$ of the phase center offset from MSODP. The $\Delta X$ varies from $-5$ cm to $+1$ cm, possibly showing a repeating pattern with about a 60 day period. The amplitude variation of

$\Delta X$ also appears to be decreasing to zero over time. The estimates of $\Delta Z$ are fairly stable at $\sim -3.4$ cm for the sinusoidal yaw regime, while the estimates of $\Delta X$ show large variations. For the fixed yaw of cycle 13 and 18 where only $\Delta Z$ was estimated, the estimates of $\Delta Z$ decreased to about $-5$ cm.

For SLR, Zelensky *et al.* [2002] have shown a reduction in the fit of the SLR residuals by correcting the LRA offset. The POD groups with GPS have also shown the orbit performance improvement by correcting the phase center change in X and Z direction. Table 4.9 summarizes the estimates of the phase center change with respect to CoM estimated from several Jason-1 POD groups with different tracking data and softwares. Each center's processing days can vary, and the number of days used to get average values can be different. JPL, UT/CSR and NASA/GSFC participated in the GPS antenna phase center offset comparison with GPS-only data. Among them, UT/CSR and NASA/GSFC participated in the LRA phase center offset comparison with the SLR/DORIS data as well.

| Technique | institute | $\Delta X$ | $\Delta Z$ |
|---|---|---|---|
| GPS | JPL | -15 | -43 |
| | CSR$^{\dagger}$ | -13 | -34 |
| | NASA | -20 | -40 |
| | Average | -16 | -39 |
| | | | |
| SLR | NASA | -13 | 3 |

†: averaged only over days in sinusoidal yaw mode

Table 4.9: Estimates of Phase center change with respect to CoM [unit: mm]

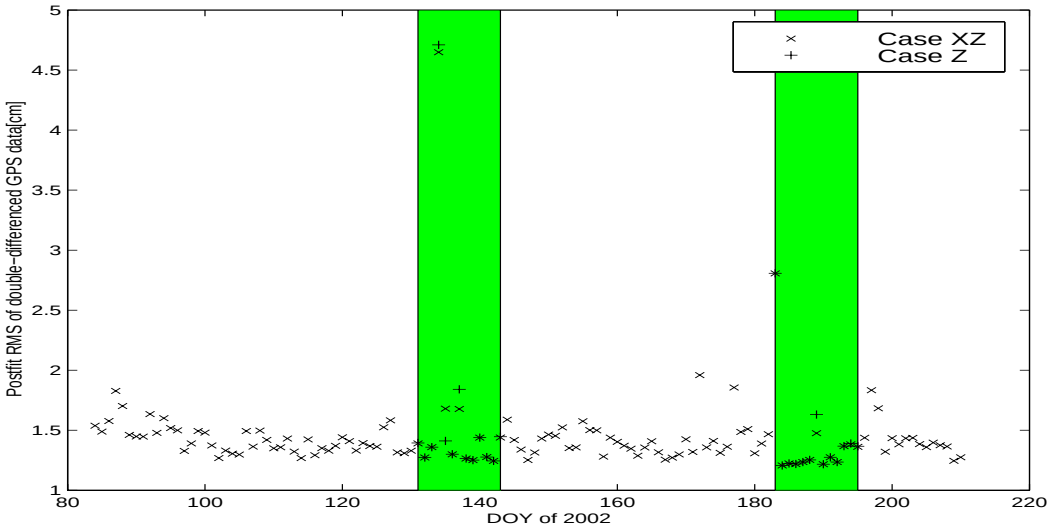


(a) Postfit RMS

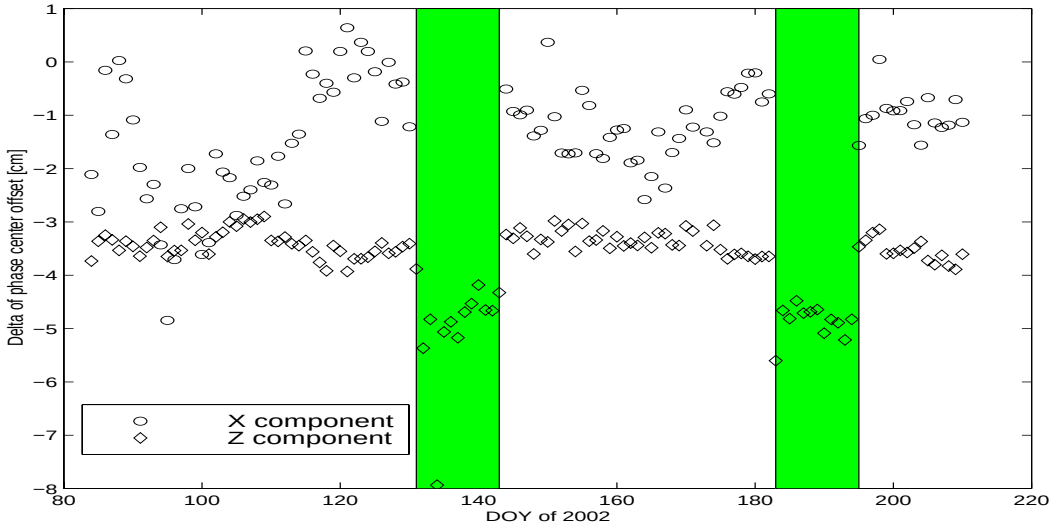


(b) Delta of Phase Center Offset

Figure 4.5: GPS Postfit residuals and $L_C$ Phase Center Offset Estimates at CSR (green region represents the fixed yaw regime)

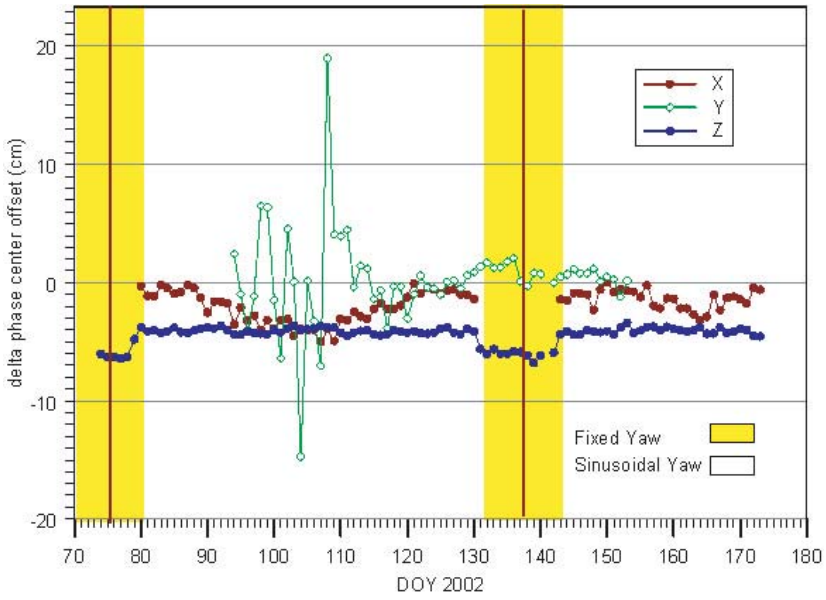


(a) Large scale

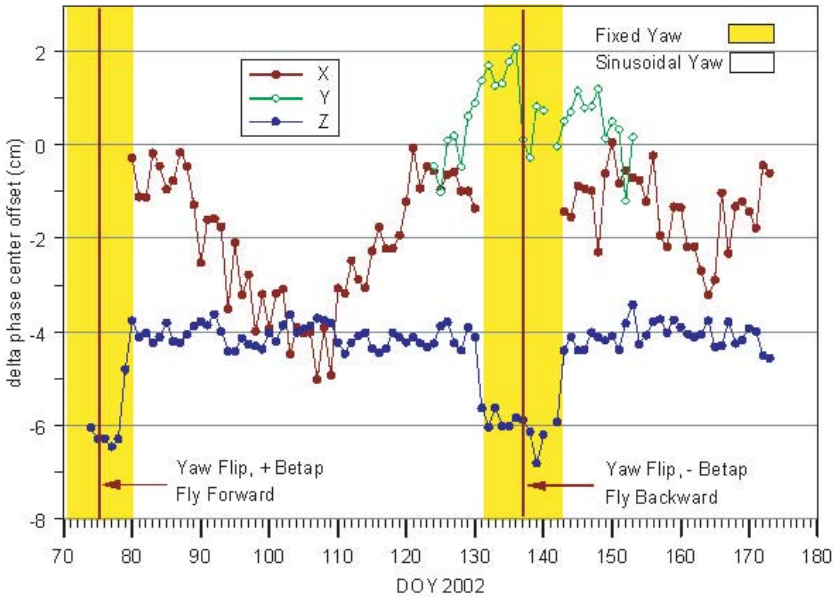


(b) Small scale

Figure 4.6: GPS $L_C$ Phase Center Offset Estimates at GSFC [Luthcke *et al.*, 2002]

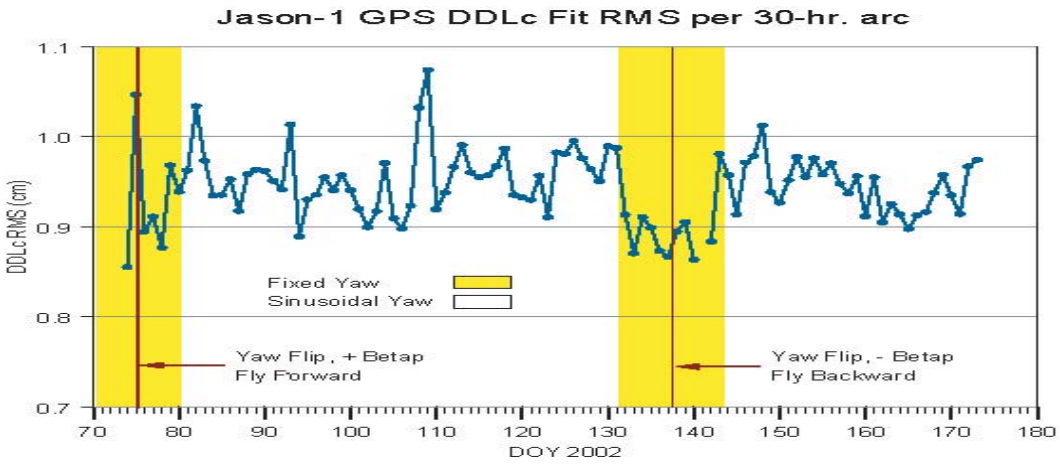


Figure 4.7: GPS DD $L_C$ postfit residual RMS at GSFC

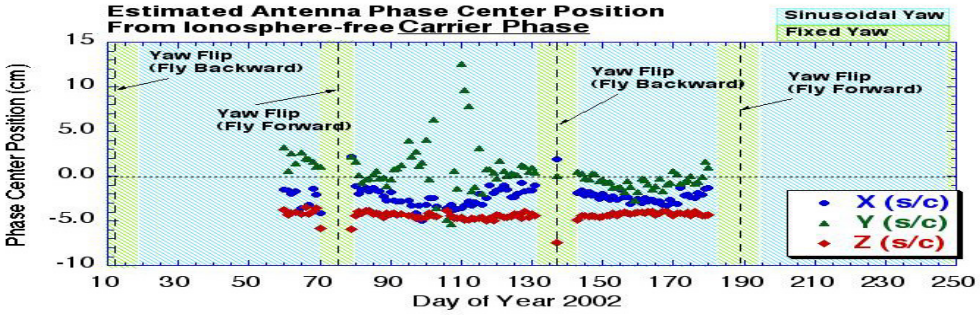


Figure 4.8: GPS $L_C$ Phase Center Center Offset Estimates at JPL

Whether the estimates in Table 4.9 reflect some radiometric phase center anomaly, or whether they account for some real CoM motion is a question. This question may be answered by comparing the estimates of the phase center change from the GPS antenna and the LRA by assuming that the estimates from the GPS antenna reflect the combined change of the CoM and the phase center with respect to the reference origin, while the estimates from LRA reflect solely the change of the CoM. The assumption appears to be supported by the close agreement between the estimates of $\Delta X$ phase center offset from both SLR and GPS: the estimated $\Delta X$ from SLR is $-13$ mm [Zelensky *et al.*, 2002], and the averaged $\Delta X$ of the GPS phase center offset from several GPS POD groups is $-16$ mm as shown in Table 4.9. If the estimates of $\Delta X$ of the GPS $L_C$ phase center reflect purely the CoM change, the $\Delta X$ should not depend on $\beta^{'}$. However, the estimates of $\Delta X$ of the GPS $L_C$ phase center from Haines *et al.* [2002], Luthcke *et al.* [2002] and Choi *et al.* [2002] follow a very consistent pattern of the time series, in which $\Delta X$ appears to depend on the $\beta^{'}$ angle varying between approximately $-5$ and $-50$ mm. The drop of $\Delta X$ during the first high $\beta^{'}$ regime around day 100, which is greater than the drop of $\Delta X$ during the second high $\beta^{'}$ regime around day 160, is observed. The $\Delta X$ variation pattern implies that the estimates of $\Delta X$ probably reflect the actual variation of GPS phase center offset coupled with the shifted CoM. The possible cause of the $\beta^{'}$-dependency of $\Delta X$ of the GPS $L_C$ phase center could be a multipath effect related to $\beta^{'}$ and the solar panel orientation, which is out of the scope of this research.

No significant $\Delta Z$ of phase center offset for the LRA is observed for SLR [Zelensky *et al.*, 2002] at NASA/GSFC. This has been confirmed by Ries *et al.* [2002] at UT/CSR, showing no compelling evidence that the Z offset for the CoM or the LRA requires correction, which implies that the estimated Z-directional change of the GPS antenna phase center mostly reflects the real change of the GPS antenna phase center in Z direction in space without being related to the change of the CoM offset. The estimates of $\Delta Z$ of the GPS phase center offset show a discrepancy depending on the yaw regime. During the sinusoidal yaw regime, $\Delta Z$ of the phase center offset for the GPS $L_C$ combination is approximately $-39$ mm. During the low fixed yaw, however, the $\Delta Z$ of the phase center offset dropped by 15-20 mm as shown in Fig. 4.5(b) The same amount of drop was also observed by Luthcke *et al.* [2002] as shown in Figure 4.6. The reason for the dependency of $\Delta Z$ of the GPS phase center offset on the yaw regime is not clearly understood.

Analysis by Zelensky *et al.* [2002] indicates that there is no reason to change the CoM or LRA offset in the Y direction. For the GPS antenna, the orbits with the estimation of the Y-directional change of the GPS phase center offset performed worse as shown for **Case Y** or **Case XYZ** in Table 4.6 and 4.7. This indicates that there is no need for correction of the CoM or of the GPS phase center offset in the Y direction.

In summary, the orbits with estimation of Z-directional change of the GPS phase center offset performed best in the low fixed yaw regime. For the sinusoidal yaw regime, the X- and Z-directional changes of the GPS phase

| estimates | x [mm] | y [mm] | z [mm] |
|---|---|---|---|
| CoM | 955.0 | 0.0 | 0.0 |
| GPS $L_C$ | 2389.1 | -218.0 | -538.1 |
| LRA | 1171.0 | 598.0 | 682.8 |

Table 4.10: New CoM and Phase Center estimates w.r.t. the reference point at CSR

| estimates | X [mm] | Y [mm] | Z [mm] |
|---|---|---|---|
| GPS $L_C$ | 1434.1 | -218.0 | -538.1 |
| LRA | 216.0 | 598.0 | 682.8 |

Table 4.11: New Phase Center Location relative to new CoM location estimated at CSR

center offset should be estimated simultaneously. The estimated change of GPS phase center offset does not necessarily reflect the actual change of the GPS phase center offset because the estimates might be coupled with the change of CoM. To separate the change of CoM and the actual change of GPS antenna phase center offset, the estimates of phase center offset from the LRA and GPS antenna were compared. The common estimates from both instruments, which are 13 mm in X-direction, are assumed to reflect the actual change of the CoM. Table 4.10 shows the new GPS $L_C$ phase center location with respect to the reference point. By comparing the new estimates with the a priori in Table 4.4, the Z-component of GPS $L_C$ phase center decreased from $-504$ mm to $-538.1$ mm. The LRA phase center (see Table 2.6 for a priori) and the X component of the GPS $L_C$ phase center with respect to the origin did not change. According to Table 2.5, the CoM just after deployment

in orbit should be (935.0, 0.0, 0.0) cm, and it is supposed to be located at (942.0, 0.0, 0.0) mm after 8 kg hydrazine consumption. The increase of the CoM estimate from the nominal value of 942 mm to 955 mm is a surprise, since the best estimate for the actual fuel usage indicates only 1.7 kg, which is far less than 8 kg. Table 4.11 shows the new phase center location of the GPS antenna relative to the new CoM location estimated at CSR.

### 4.2.2 Optimal Subarc Length

One of the benefits that the GPS data can provide for the POD task is its dense and homogeneous tracking capability over time. With the dense observation set, heavier parameterizations are possible to accommodate the force model errors. The heavier parameterization by introducing more subarcs generally will reduce the orbit fit residual RMS, but it does not guarantee a better orbit. On the contrary, too heavy a parameterization can degrade the orbit quality. Thus, finding an optimal frequency for the estimation of empirical acceleration parameters is very important to obtain an orbit solution with better accuracy.

In this section, the optimal subarc length for the estimation of empirical parameters is sought. For the optimal subarc length investigation, the crossover test and SLR residual test for cycle 8 to cycle 20 were performed with different subarc lengths for the empirical acceleration estimation. For the subarc length determination, the attitude mode is important because breaks of the continuity can occur when a thruster is activated. To get a better orbit

solution, that kind of breaking point should be avoided. Thus, as shown in Table 4.2, several days such as day 131-133 and day 194-195 were excluded in this investigation.

The subarc lengths tested for this investigation were chosen by considering several factors such as the Jason-1 orbit period and the integration arc length. Table 4.12 shows the subarc length combinations for each case. Subarc lengths such as 1.8738 hour, 3.7476 hour, 5.6214 hour and 7.4952 hour are exact multiples of the Jason-1 orbit period, which is 1.8738 hour. The subarcs of 3 hour, 6 hour, 10 hour, and 15 hour were chosen because they divide the integration arc length (30 hour) equivalently. For example, the choice of 3 hour for the estimation of Drag (see DRAGL card for MSODP) and 6 hour for the estimation of the empirical acceleration parameters (see RTNPRT card for MSODP) provides ten subarcs for the Drag coefficients and five subarcs for the 1-cpr acceleration in one integration arc. Another set of subarc lengths of 0.1725 day, 0.34492 day and 0.6898 day, which were chosen based on the experience of the T/P orbit process, were also tested.

To decide which experimental cases of the subarc length produced the best orbit, the SLR residual test (see Table 4.15) and the altimeter crossover test (see Table 4.13 and 4.14) were performed for each case's orbit. These two methods serve as independent and absolute indicators to the radial orbit error. In choosing an optimal estimation frequency for the empirical accelerations, the crossover RMS test was the method mainly relied on in this investigation. Table 4.14 shows the crossover RMS from each case for the subarc length

| CT | subarc length for 1-cpr T, N empirical force [unit: hour] | | | | | | | | |
|---|---|---|---|---|---|---|---|---|---|
| | 1.8738* | 3† | 3.7476 | 5.6214 | 6 | 7.4952 | 9 | 10 | 15 |
| 1.8738 | sub1-1 | . | sub1-2 | sub1-3 | . | sub1-4 | . | . | . |
| 3 | . | sub1.5-1.5 | . | . | sub1.5-3 | . | sub1.5-4.5 | sub1.5-10 | . |
| 3.7476 | . | . | sub2-2 | . | . | sub2-4 | . | . | . |
| 6 | . | . | . | . | sub3-3 | . | . | sub3-4 | sub3-5 |

* 1.8738 hour is the orbit period of Jason-1
† 3 hr, 6 hr, 10 hr and 15 hr divide the integration arc length (30 hr) equivalently
Case sub1-2, for example, estimates CT in every 1.8738 hr, and 1-cpr T, N for every 3.7476 hr

(a) Subarc length combination cases

| CT | subarc length of 1-cpr T, N empirical force [unit: day] | |
|---|---|---|
| | 0.34492 | 0.6898 |
| 0.1725 | sub-12 | sub-14 |
| 0.34492 | sub-22 | sub-24 |

(b) Subarc length combination cases based on the experience from Topex SLR/DORIS orbit

Table 4.12: Subarc length combinations for each experiment case.

strategies. For all cases, the crossover RMSs of most of cycles are ∼6 cm. However, the crossover RMSs of cycle 11 and cycle 13, which varied from 6 cm to 18 cm depending on the case, show strong sensitivity to the subarc lengths. As a matter of fact, it will be shown later that the huge crossover RMSs of cycle 11 and cycle 13 occurred due to the long data gaps in day 117 and day 141, or attitude controls in day 134.

Other than the sensitivity of the crossover RMS to the subarc length in cycle 11 and 13, the crossover RMSs in Table 4.14 also show a decreasing tendency, when the subarc length for the estimation of the 1-cpr T and N parameters is increased with the subarc length for the estimation of CT fixed. The tendency can be seen clearly in Figure 4.9. Figure 4.9 shows the comparison of Crossover RMSs from different subarc lengths for the 1-cpr T, N parameters, with the subarc length for CT fixed. The cases with the same subarc lengths for CT and 1-cpr T & N performed the worst. In Figure 4.9(a), the solutions of **Case sub1-1** and **Case sub1-2** performed worse than the solutions of **Case sub1-3** and **Case sub1-4**. The solutions of **Case sub1.5-1.5** and **Case sub1.5-3** did not perform better than **Case sub1.5-4.5** or **Case sub1.5-10** as shown in Figure 4.9(b). This indicates that, to estimate the 1-cpr T & N empirical parameters and CT simultaneously, longer subarc lengths than the subarc length for the estimation of CT are required. The subarc lengths for the estimation of 1-cpr T & N need to be at least twice as long as the subarc length for the estimation of CT.

In addition to the crossover tests and SLR residual tests, the conver-

| Cyc | Crossover Mean for each subarc length strategy | | | | | | | | | | | | | |
|---|---|---|---|---|---|---|---|---|---|---|---|---|---|---|
| | sub1-1 | sub1-2 | sub1-3 | sub1-4 | sub1.5-1.5 | sub1.5-3 | sub1.5-4.5 | sub1.5-10 | sub2-2 | sub2-4 | sub3-3 | sub3-4 | sub3-5 | sub-12 |
| 8 | 6.5 | 6.1 | 5.7 | 7.0 | 5.3 | 5.1 | 5.9 | 4.8 | 5.8 | 7.0 | 6.1 | 4.7 | 5.6 | 6.0 |
| 9 | 4.4 | 4.7 | 4.5 | 4.7 | 3.4 | 4.9 | 6.9 | 6.7 | 5.5 | 5.6 | 5.5 | 7.1 | 8.4 | 5.2 |
| 10 | 5.1 | 4.5 | 3.6 | 2.6 | 4.4 | 4.2 | 5.3 | 4.4 | 4.9 | 2.9 | 4.3 | 5.0 | 4.8 | 4.2 |
| 11 | -11.8 | 3.3 | -14.0 | -12.5 | -7.9 | -14.1 | -11.5 | -11.8 | 3.2 | -12.9 | -8.8 | -11.0 | -11.7 | -12.2 |
| 12 | -16.7 | -16.4 | -18.0 | -16.3 | -16.7 | -17.4 | -17.4 | -16.7 | -17.0 | -16.3 | -17.8 | -16.1 | -17.7 | -16.1 |
| 13 | .9 | -2.7 | 4.4 | 1.4 | 5.6 | 5.0 | 1.0 | 4.2 | .0 | 6.2 | -2.9 | 18.8 | 5.2 | 1.4 |
| 14 | -4.9 | -3.5 | -4.7 | -3.7 | -4.8 | -5.0 | -3.8 | -4.3 | -4.7 | -5.5 | -5.2 | -5.4 | -7.0 | -5.0 |
| 15 | -6.3 | -6.3 | -6.3 | -6.2 | -6.7 | -6.5 | -7.3 | -7.7 | -7.0 | -6.9 | -7.1 | -8.4 | -8.9 | -8.8 |
| 16 | -10.4 | -11.0 | -10.4 | -10.9 | -10.6 | -10.6 | -11.1 | -11.5 | -11.1 | -10.7 | -11.2 | -11.8 | -10.4 | -11.7 |
| 17 | 7.1 | 6.7 | 7.0 | 5.3 | 6.8 | 7.4 | 8.0 | 6.7 | 6.5 | 6.2 | 6.7 | 6.4 | 7.4 | 6.6 |
| 18 | -.5 | -1.7 | -2.9 | -3.3 | -.4 | -1.5 | -2.5 | -2.2 | -1.6 | -2.4 | -1.8 | -1.8 | -2.2 | -2.8 |
| 19 | 17.1 | 15.7 | 12.7 | 14.0 | 16.2 | 16.1 | 16.5 | 17.1 | 15.1 | 13.0 | 16.4 | 19.5 | 18.6 | 15.0 |
| 20 | 15.0 | 14.7 | 15.3 | 15.3 | 13.9 | 14.2 | 17.4 | 15.3 | 14.0 | 13.7 | 14.8 | 16.7 | 17.3 | 15.4 |
| Mean | .4 | 1.1 | -.2 | -.2 | .7 | .1 | .6 | .4 | 1.0 | .0 | -.1 | 1.8 | .7 | -.2 |
| rms | 10.2 | 9.3 | 10.1 | 9.8 | 9.6 | 10.4 | 10.7 | 10.4 | 9.3 | 9.8 | 10.1 | 12.0 | 11.3 | 10.2 |

* Day 117, 134 and 141 are included

Table 4.13: Crossover Mean for each subarc length strategy [Unit: mm]. **Case sub1.5-4.5** (3 hours for CT and 9 hours for 1-cpr T & N) was chosen based on the Averaged Crossover RMS (see Table 4.14). Several cycles show relatively large mis-centering of 1 cm to 2 cm, however the averaged values over the cycles show that GPS-only orbits are well-centered in the long term.

| Cyc | Crossover RMS for each subarc length strategy | | | | | | | | | | | | | |
|---|---|---|---|---|---|---|---|---|---|---|---|---|---|---|
| | sub1-1 | sub1-2 | sub1-3 | sub1-4 | sub1.5-1.5 | sub1.5-3 | sub1.5-4.5 | sub1.5-10 | sub2-2 | sub2-4 | sub3-3 | sub3-4 | sub3-5 | sub-12 |
| 8 | 64.2 | 62.9 | 62.4 | 62.4 | 62.9 | 62.6 | 62.1 | 62.5 | 62.7 | 62.2 | 62.4 | 62.6 | 62.8 | 62.5 |
| 9 | 61.2 | 60.5 | 59.8 | 59.6 | 60.6 | 59.5 | 59.5 | 59.4 | 59.8 | 59.2 | 60.1 | 59.5 | 59.9 | 59.0 |
| 10 | 62.4 | 61.6 | 60.9 | 60.6 | 61.7 | 60.3 | 61.1 | 60.8 | 61.2 | 60.5 | 60.4 | 60.7 | 60.6 | 60.5 |
| 11 | 135.5 | 187.8 | 63.2 | 62.8 | 73.7 | 69.7 | 61.7 | 61.9 | 187.3 | 65.4 | 77.0 | 61.6 | 62.4 | 62.4 |
| 12 | 61.1 | 58.8 | 59.2 | 57.9 | 58.3 | 57.8 | 56.9 | 57.1 | 58.2 | 57.0 | 57.6 | 56.6 | 57.4 | 56.7 |
| 13 | 65.3 | 64.6 | 63.5 | 64.4 | 84.3 | 65.5 | 63.2 | 63.1 | 64.6 | 93.0 | 101.9 | 103.4 | 86.6 | 80.1 |
| 14 | 60.9 | 60.2 | 59.9 | 59.2 | 59.9 | 59.3 | 58.5 | 59.0 | 60.0 | 58.9 | 59.4 | 59.3 | 58.9 | 59.0 |
| 15 | 60.7 | 60.9 | 60.3 | 60.5 | 60.3 | 59.8 | 60.2 | 60.1 | 61.0 | 60.6 | 60.0 | 60.4 | 58.7 | 60.7 |
| 16 | 62.6 | 62.0 | 61.7 | 62.4 | 62.3 | 61.5 | 62.7 | 62.6 | 61.9 | 62.1 | 62.0 | 62.5 | 62.0 | 62.1 |
| 17 | 61.5 | 60.7 | 60.8 | 59.3 | 61.3 | 60.3 | 60.0 | 59.7 | 60.5 | 58.7 | 59.8 | 59.4 | 59.4 | 59.6 |
| 18 | 57.4 | 57.0 | 55.6 | 56.4 | 56.5 | 55.2 | 55.6 | 55.5 | 56.2 | 56.2 | 55.6 | 55.4 | 56.2 | 56.2 |
| 19 | 61.9 | 61.5 | 61.0 | 60.6 | 61.2 | 61.2 | 60.6 | 60.8 | 61.0 | 60.3 | 62.2 | 61.8 | 63.0 | 60.8 |
| 20 | 59.8 | 59.7 | 59.5 | 59.4 | 59.5 | 59.1 | 59.3 | 59.4 | 59.4 | 53.9 | 59.7 | 59.7 | 59.5 | 58.7 |
| Mean | 67.3 | 70.6 | 60.6 | 60.4 | 63.3 | 60.9 | 60.1 | 60.1 | 70.3 | 62.2 | 64.5 | 63.3 | 62.1 | 61.4 |
| (rms) | 20.6 | 35.3 | 2.0 | 2.2 | 7.5 | 3.6 | 2.2 | 2.2 | 35.2 | 9.7 | 12.3 | 12.2 | 7.6 | 6.0 |

* Day 117, 134 and 141 are included.

Table 4.14: Crossover RMS for each subarc length strategy [Unit: mm]. **Case sub1.5-4.5** (3 hours for CT and 9 hours for 1-cpr T & N) and **Case sub1.5-10** (3 hours for CT and 10 hours for 1-cpr T & N) performed best. **Case sub1.5-4.5** was chosen as the subarc length strategy for GPS-only orbits.

| Cyc | SLR residual RMS ($> 70^{o}$) for each subarc length strategy | | | | | | | | | | | | | |
|---|---|---|---|---|---|---|---|---|---|---|---|---|---|---|
| | sub1-1 | sub1-2 | sub1-3 | sub1-4 | sub1.5-1.5 | sub1.5-3 | sub1.5-4.5 | sub1.5-10 | sub2-2 | sub2-4 | sub3-3 | sub3-4 | sub3-5 | sub-12 |
| 8 | 17.5 | 9.7 | 9.4 | 11.5 | 13.3 | 11.8 | 11.5 | 11.4 | 9.4 | 11.6 | 12.8 | 11.1 | 10.0 | 12.6 |
| 9 | 17.0 | 15.8 | 15.0 | 13.5 | 17.6 | 14.1 | 13.2 | 13.1 | 15.9 | 13.8 | 12.8 | 12.8 | 13.3 | 12.3 |
| 10 | 15.5 | 13.4 | 14.1 | 12.5 | 15.1 | 13.5 | 12.6 | 13.1 | 13.3 | 13.1 | 13.1 | 12.5 | 13.5 | 13.2 |
| 11 | 27.3 | 32.6 | 15.7 | 31.2 | 22.9 | 84.1 | 14.6 | 13.3 | 49.6 | 69.7 | 16.8 | 11.1 | 10.4 | 16.4 |
| 12 | 7.7 | 8.0 | 6.4 | 7.2 | 6.9 | 6.4 | 7.4 | 7.5 | 8.0 | 7.6 | 6.3 | 7.5 | 7.2 | 8.0 |
| 13 | 8.6 | 8.8 | 12.5 | 19.9 | 14.1 | 17.8 | 9.6 | 10.2 | 11.7 | 10.8 | 15.8 | 10.2 | 10.1 | 17.4 |
| 14 | 12.5 | 9.9 | 12.1 | 11.0 | 9.3 | 12.2 | 10.4 | 10.5 | 10.4 | 10.0 | 12.2 | 10.7 | 12.8 | 10.8 |
| 15 | 17.3 | 17.7 | 14.7 | 14.9 | 17.1 | 15.1 | 15.5 | 14.2 | 18.5 | 15.5 | 14.2 | 14.1 | 11.9 | 16.2 |
| 16 | 11.3 | 11.4 | 13.5 | 13.2 | 10.8 | 10.3 | 13.4 | 11.9 | 11.4 | 13.2 | 12.0 | 12.1 | 10.7 | 11.6 |
| 17 | 11.9 | 10.8 | 11.6 | 10.7 | 12.1 | 11.5 | 11.5 | 11.0 | 10.4 | 10.1 | 10.7 | 9.2 | 9.5 | 9.9 |
| 18 | 17.6 | 14.1 | 8.1 | 9.4 | 17.1 | 9.1 | 8.8 | 8.6 | 11.1 | 9.9 | 7.5 | 8.3 | 8.2 | 9.0 |
| 19 | 20.7 | 21.0 | 19.9 | 17.8 | 21.2 | 18.8 | 17.8 | 18.4 | 20.3 | 16.4 | 19.4 | 17.5 | 13.3 | 17.5 |
| 20 | 16.8 | 17.3 | 15.3 | 17.1 | 17.7 | 15.9 | 17.2 | 14.5 | 15.7 | 16.0 | 16.3 | 14.9 | 11.7 | 18.6 |
| Mean | 15.5 | 14.7 | 12.9 | 14.6 | 15.0 | 18.5 | 12.6 | 12.1 | 15.8 | 16.7 | 13.1 | 11.7 | 11.0 | 13.3 |
| rms | 5.2 | 6.7 | 3.6 | 6.1 | 4.6 | 20.0 | 3.2 | 2.8 | 10.8 | 16.1 | 3.6 | 2.8 | 2.0 | 3.5 |

* Day 117, 134 and 141 are included

Table 4.15: SLR residual RMS for each subarc length strategy [Unit: mm]. **Case sub1.5-4.5** (3 hours for CT and 9 hours for 1-cpr T & N) was chosen based on the Averaged Crossover RMS (see Table 4.14). The Averaged SLR residual RMSs over the cycles are consistently less than 2 cm.

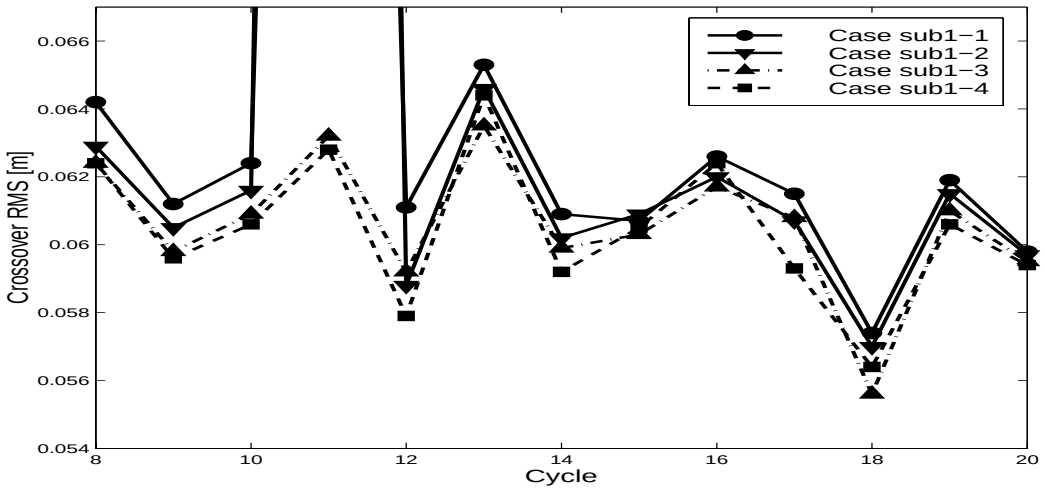


(a) Cases of 1.8738 hour for CT

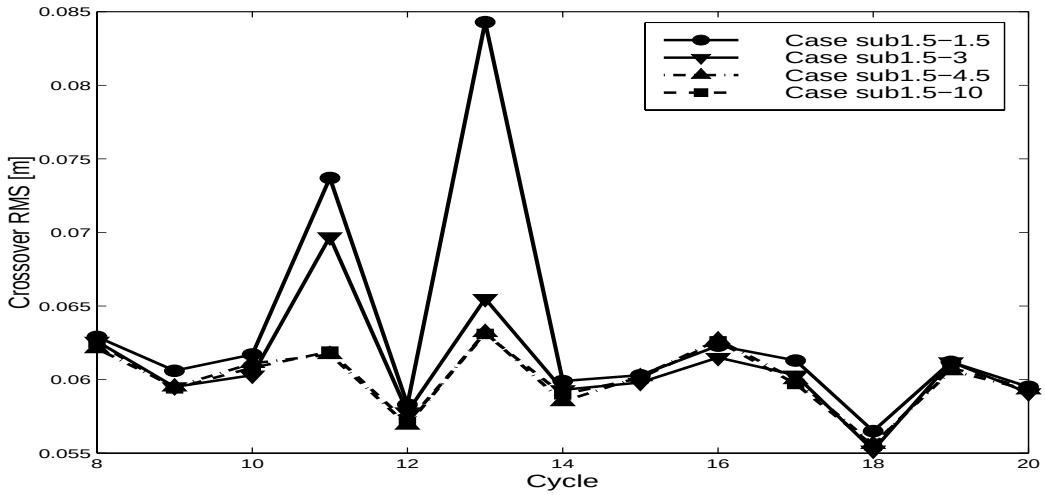


(b) Cases of 3 hours for CT

Figure 4.9: Comparison of Crossover RMSs of different 1-cpr T & N subarc lengths with (a) 1.8738 hour and (b) 3 hours for CT. For each case, it shows that, to estimate the 1-cpr T & N parameters and CT parameter simultaneously, longer subarc lengths for the estimation of 1-cpr T & N parameters than for the CT parameter are required.

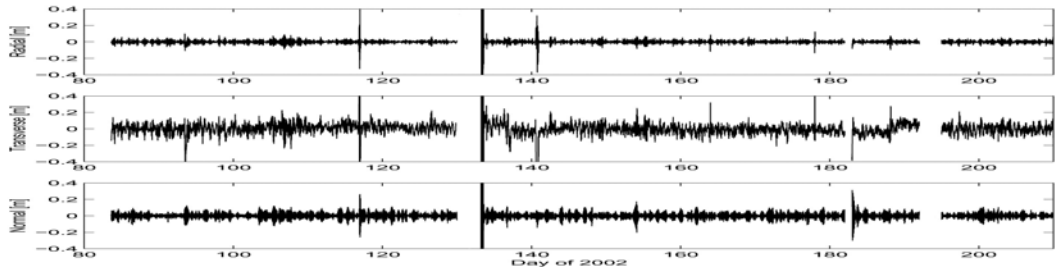


(a) Case **sub1.5-1.5** (3 hours for CT, and 3 hours for 1-cpr T & N)

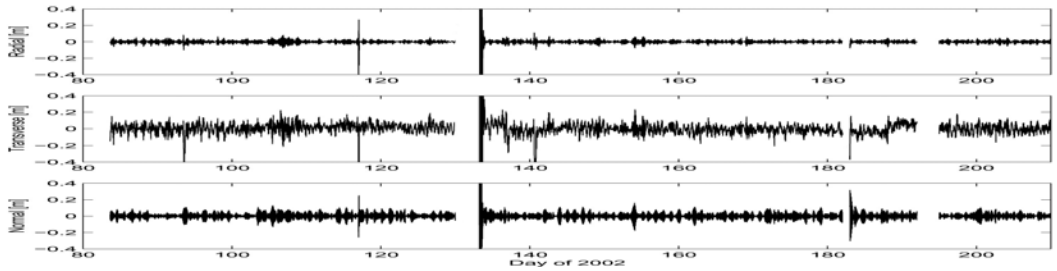


(b) Case **sub1.5-3** (3 hours for CT, and 6 hours for 1-cpr T & N)

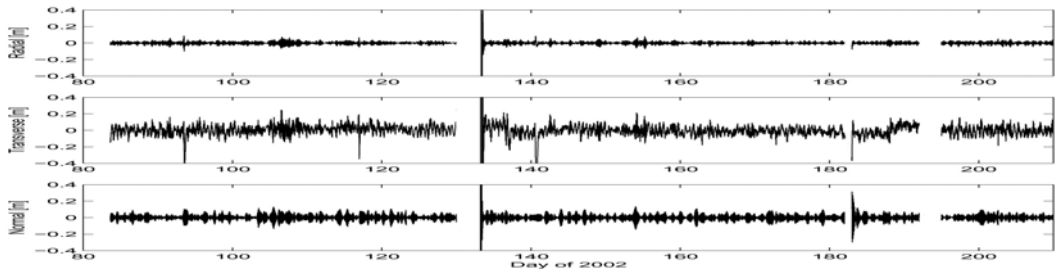


(c) Case **sub1.5-4.5** (3 hours for CT, and 9 hours for 1-cpr T & N)

Figure 4.10: Orbit differences (TRACOM) compared to CSR SLR/DORIS solution. Days 117, 141 and 165 have big DDobs data gaps. Orbit maintenance occurred on Days 134 and 183. As shown, the tracking gaps can be overcome by conservative parameterization, but the orbit maintenance can not be overcome. Days 134 and 183 will be excluded from the full cycles for subsequent analysis.

gence of the estimated parameters in a subarc was examined. Sufficient data in a subarc should give a well converged estimate. Poor convergence may indicate that the subarc is too short to reflect the actual tracking data. For most of these test cases, the estimates of the empirical parameters appear to have converging well with 6 iterations. New converged estimates of the empirical acceleration parameters of each subarc were collected and their dispersion was investigated. For example, the distribution of newly estimated CT parameters of day 90 are shown for each estimation strategy in Figures 4.11(a) and 4.11(b). The concentrated distribution of new empirical parameter estimates for each subarc is desirable, but due to the imperfect tracking, some variation is also likely to be encountered.

Figure 4.11(a) shows new CT estimates for each subarc for day 90 in **Case sub1-1**. The CT estimates (878.4±1426.4) for sixteen 0.079-day subarcs for **Case 1-1** are highly dispersed, compared to the CT estimates for **Case 1-2** (785.6±787.9), and **Case 1-3** (828.3±766.6). It indicates that **Case sub1-1** was too heavily parameterized for the given tracking data. From a more conservative subarc length strategy, **Case sub-24**, the averaged estimate of CT over four 8.28-hour (or 0.345-day) subarcs is 780.8 (±108.1), which shows highly concentrated distribution of the estimates. The estimates of amplitudes and phases of the T & N empirical parameters from **Case sub-24** are also highly concentrated. With moderately aggressive parameterization such as **Case sub1.5-4.5** with 3-hour subarcs for CT, the distribution of the estimates of the CT parameters as well as the T & N parameters appear to

be worsening when compared to conservative parameterizations such as **Case sub-24**. However, the distribution of the estimated CT parameters as shown Figure 4.11(b) is much more consistent than the distribution of the estimated CT parameters with the 1.8738-hour subarcs, and the crossover RMS with **Case sub1.5-4.5** is actually better than those with **Case sub-24** or **Case 1-**series, as shown in Table 4.14.

Comparing the GPS orbits to the SLR/DORIS orbits provides good insight for the orbit performance assessment. Figure 4.10 shows the orbit differences, computed using TRACOM, between CSR's SLR/DORIS solution and GPS solutions. Figure 4.10(a) shows the comparison with the solution from **Case sub1.5-1.5**, Figure 4.10(b) for the comparison with **Case sub1.5-3**, and Figure 4.10(c) for the comparison with **Case sub1.5-4.5**. First of all, it needs to be mentioned that the large orbit differences at the starting epoch of day 134 and day 183 are due to the orbit maintenance as shown in Table 4.1. While CSR's SLR/DORIS solutions were integrated starting from each cycle's starting epoch, the GPS orbits were daily integrated starting at 21h:00m:00s (GPS time), which is a 3-hour advance of each day's zero epoch. Thus, the effects of the maintenance maneuver were inevitable during the GPS processing. However, the large orbit differences shown in Figure 4.10 for day 117, 141 and 165 are caused by the DDobs gaps as shown in Table 4.3 and Figure 4.2(a). Also, unusually large crossover RMSs for cycle 11 from **Case sub1-1**, **Case sub1-2**, **Case sub1.5-1.5**, **Case sub2-2** and **Case sub3-3** as shown earlier in Table 4.14 can be explained by the large gap of DDobs in

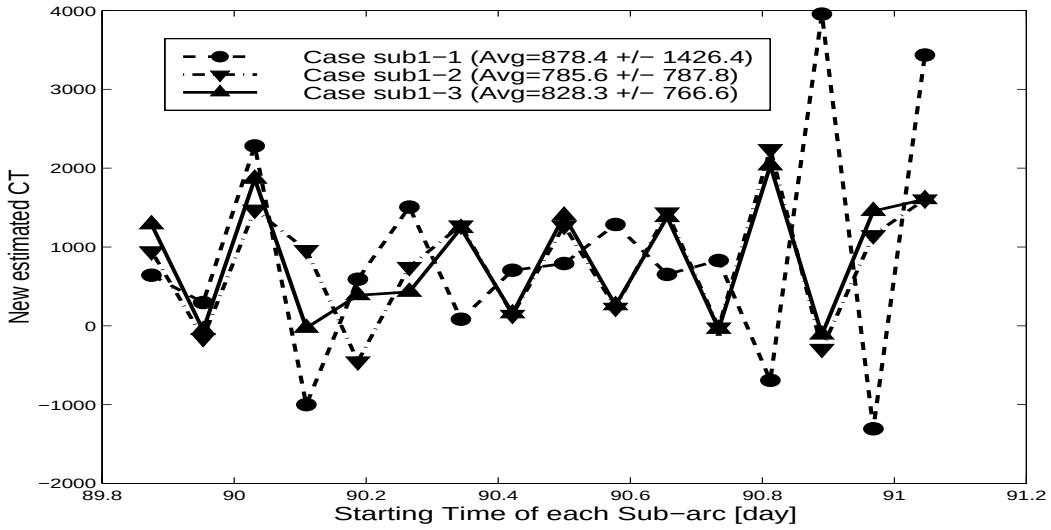


(a) CT estimates for sixteen 1.8738-hour subarcs of day 90

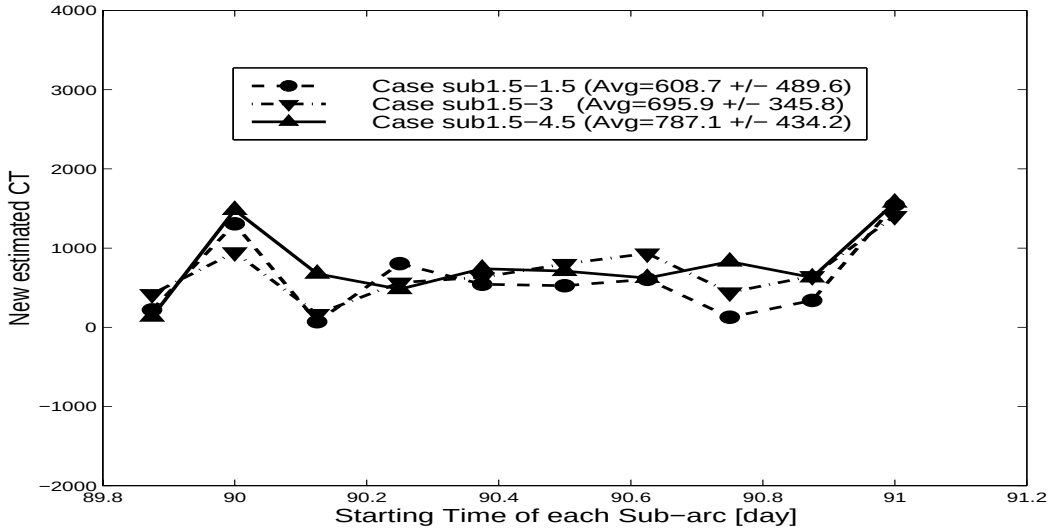


(b) CT estimates for ten 3-hour subarcs of day 90

Figure 4.11: Distribution of new estimated CT parameters of subarcs for day 90. The distribution of the CT estimates from the 3-hour subarc length is more consistent.

day 117 (see Table 4.3). The large crossover RMSs for cycle 13 from **Case sub1.5-1.5**, **Case sub2-4**, **Case sub3-3**, **Case sub3-4**, **Case sub3-5** and **Case sub-12** can also be explained by the large gap of DDobs in day 141 and the attitude control in day 134.

It is difficult to accommodate the model errors caused during the maintenance maneuver by optimizing parameterization. Thus, Days 134 and 183 with the maintenance maneuver will be excluded for subsequent study. However, the large orbit differences caused by the DDobs gaps irrelevant to maintenance maneuver can be reduced by adopting a more conservative parameterization strategy for the empirical acceleration model parameters. Figure 4.10 shows the improvement of the orbits for day 117 and day 141, by applying optimal parameterization. With **Case sub1.5-1.5** (3 hours for CT and 1-cpr T & N), the radial orbit differences for day 117 and 141 are larger than 30 cm. With **Case sub1.5-3** (3 hours for CT and 6 hours for 1-cpr T & N), the radial orbit differences for day 141 are significantly reduced to less than 10 cm. With **Case sub1.5-4.5** (3 hours for CT and 9 hours for 1-cpr T & N), the further orbit improvement is clearly seen for day 117 and 141.

Conclusively, the mean value comparison of crossover RMSs over all cycles in Table 4.14 shows that orbit solutions of **Case sub1.5-4.5** or **Case sub1.5-10** perform best with the crossover RMS of 6.01 ($\pm$0.2) cm. In this study, the subarc parameterization of **Case 1.5-4.5** (3 hours for CT and 9 hours for 1-cpr T & N) will be adopted for the GPS-only nominal orbits.

The overall inertial centering of the GPS orbit solutions for cycles 8 to

20 appear to be not so good, as in Table 4.13. Although the averaged value of the crossover Mean over the cycles is 0.06 cm in **Case sub1.5-4.5**, the magnitudes of the crossover Means of cycle 11, 12, 16, 19 and 20, are larger than 1 cm. The miscentering of orbits for those cycles appears persistently, regardless of the various subarc length strategies, which indicates that the orbits with GPS-only tracking are not inertially well centered, especially over short arcs. However, the crossover Means near or larger than 1 cm can also be caused by the bad altimeter data during those periods. Indeed, the orbits of those cycles from SLR/DORIS also show relatively large crossover Means (see Table 5.6(a) in Chapter 5). The averaged value of the SLR residual RMSs over the cycles as shown in Table 4.15 is 1.3 ($\pm$0.3) cm for **Case sub1.5-4.5**, and the maximal SLR residual RMS is 1.9 cm. For all subarc length cases, the averaged value of the SLR residual RMSs is under 2 cm, which is a promising result for the orbit estimated in the dynamic approach with no SLR data.

### 4.2.3 GPS Satellite Orbits and Orbit Element Correction

To estimate the precise LEO orbit, accurate ephemerides of GPS satellites are needed. In the initial period of the T/P mission, IGS solutions for GPS satellites were not accurate enough to help T/P GPS-only orbits to reach the same level of accuracy of SLR/DORIS orbits. However, over the past decade, the accuracy of IGS solutions has been significantly improved. For this research, GPS satellite orbits are fixed to IGS solutions instead of solving the GPS satellite orbits simultaneously with the Jason-1 orbit.

The improvement of GPS satellite orbits is particularly important to help the inertial centering of the Jason-1 orbits that are processed from GPS-only tracking. Without sufficiently accurate GPS satellite orbits, the already unstable inertial center of the GPS-only orbits due to no support from the SLR tracking might float even further around the actual orbit center. Although the accuracy of IGS solutions for the GPS satellite orbits has been improved, there might be still a possibility for further improvement by introducing the orbit element correction method. The orbit element correction method is introduced to absorb the remaining orbit errors in the ephemerides of the GPS satellites by considering them as a measurement error of the fixed GPS orbits. The computed ranges of GPS satellites can be expressed as:

$$\rho_c = |\vec{\rho}_{sat}| + \frac{\partial \rho}{\partial \alpha}\delta\alpha \tag{4.5}$$

where, $\vec{\rho}_{sat} = \vec{r}_{sat} - \vec{r}_{sta}$, $\vec{r}_{sat}$ and $\vec{r}_{sta}$ are position vectors of the satellite and a tracking station respectively in geocentric coordinates; and $\alpha(t)$ denotes the set of classical Keplerian orbital elements at time $t$, such that the elements of $\alpha \equiv [a\ e\ I\ \omega\ \Omega\ M]^T$ are the semi-major axis, eccentricity, inclination, argument of perigee, longitude of the node and the mean anomaly of each satellite in their respective orbits. The vector of variations of each orbital elements is denoted by $\Delta\alpha$.

The set of kinematic relations between the perturbations of the classical Keplerian orbital elements and the perturbations of position and velocity in the radial, transverse and normal (RTN) directions has been derived previously

[Rosborough, 1986; Casotto, 1993]. The set of the perturbations of position and velocity denoted by $\Delta p(t)$. It is the set composed of six elements of differences in the inertial position and velocity of a satellite from the reference orbit:

$$\begin{aligned} \Delta p &\equiv [\Delta\vec{r}\cdot\hat{\epsilon}_R \quad \Delta\vec{r}\cdot\hat{\epsilon}_T \quad \Delta\vec{r}\cdot\hat{\epsilon}_N \quad \Delta\vec{v}\cdot\hat{\epsilon}_R \quad \Delta\vec{v}\cdot\hat{\epsilon}_T \quad \Delta\vec{v}\cdot\hat{\epsilon}_N]^T \\ &\equiv [\Delta R \qquad \Delta T \qquad \Delta N \qquad \Delta\dot{R} \qquad \Delta\dot{T} \qquad \Delta\dot{N}]^T \end{aligned} \tag{4.6}$$

where the $\hat{\epsilon}$ denotes unit vectors along the radial R, transverse T, and normal N directions of a GPS satellite. The $\vec{r}(t)$ and $\vec{v}(t)$ are the inertial position and velocity of the satellite at time $t$.

The relationship between $\Delta p(t)$ and $\Delta\alpha(t)$, which was derived to the first order in eccentricity, can be expressed as a six dimensional set of linear equations [Eanes, 1995]:

$$\Delta p(t) = Y(t)\cdot\Delta\alpha(t) \tag{4.7}$$

The non-zero elements of matrix $Y(t)$ have been derived to the first order in eccentricity as:

$$Y(t) = \bar{a}\begin{bmatrix} \bar{a}^{-1} & -C_{\bar{M}} & 0 & 0 & 0 & \bar{e}S_{\bar{M}} \\ 0 & 2S_{\bar{M}} & 0 & 1-\bar{e}C_{\bar{M}} & C_{\bar{I}} & 1+\bar{e}C_{\bar{M}} \\ 0 & 0 & S_{\bar{u}} & 0 & -S_{\bar{I}}C_{\bar{u}} & 0 \\ 0 & -\bar{n}S_{\bar{M}} & 0 & -\bar{n}(1+\bar{e}C_{\bar{M}}) & -\bar{n}C_{\bar{I}} & -\bar{n}(1+2\bar{e}C_{\bar{M}}) \\ -\frac{1}{2}\bar{n}\bar{a}^{-1} & \bar{n}C_{\bar{M}} & 0 & \bar{n}\bar{e}S_{\bar{M}} & 0 & 0 \\ 0 & 0 & \bar{n}C_{\bar{u}} & 0 & \bar{e}S_{\bar{I}}S_{\bar{u}} & 0 \end{bmatrix} \tag{4.8}$$

where $C_{\bar{M}} \equiv \cos\bar{M}$, $S_{\bar{M}} \equiv \sin\bar{M}$, $C_{\bar{I}} \equiv \cos\bar{I}$, $S_{\bar{I}} \equiv \sin\bar{I}$, $C_{\bar{u}} \equiv \cos\bar{u}$, $S_{\bar{u}} \equiv \sin\bar{u}$, $\bar{u}(\equiv\bar{\omega}+\bar{M})$ is the mean argument of latitude, and $\bar{n}$ is the average mean-motion of the satellite. The overbars indicate that the quantity is evaluated

on the reference orbit, and $\Delta$ indicates the difference of the reference orbit from the true orbit. From Equation 4.7 and 4.8, the perturbation in the radial direction, $\Delta R$, can be expressed in terms of $\Delta a$, $\Delta e$ and $\Delta M$ as:

$$\Delta R = \bar{a}(\bar{a}^{-1}\Delta a - C_{\bar{M}}\Delta e + \bar{e}S_{\bar{M}}\Delta M) \tag{4.9}$$

The perturbations in the transverse (T), and normal (N) directions are also expressed as:

$$\Delta T = \bar{a}[2S_{\bar{M}}\Delta e + (1 - \bar{e}C_{\bar{M}})\Delta\omega + C_{\bar{I}}\Delta\Omega + (1 + \bar{e}C_{\bar{M}})\Delta M] \tag{4.10}$$

$$\Delta N = \bar{a}(S_{\bar{u}}\Delta I - S_{\bar{I}}C_{\bar{u}}\Delta\Omega) \tag{4.11}$$

| Case | Corrected Orbit Elements |
|---|---|
| **Case Non** | No orbit element correction |
| **Case delA** | Semi-major axis ($a$) |
| **Case delE** | Eccentricity ($e$) |
| **Case delI** | Inclination ($i$) |
| **Case delS** | Argument of perigee ($\omega$) |
| **Case delC** | Longitude of the node ($\Omega$) |
| **Case delM** | Mean Anomaly ($M$) |
| **Case delCI** | ($\Omega$, $i$) |
| **Case delAEM** | ($a$,$e$,$M$) |
| **Case delEISC** | ($e$,$i$,$\omega$,$\Omega$) |
| **Case delAEISCM** | ($a$,$e$,$i$,$\omega$,$\Omega$,$M$) |

Table 4.16: Cases for Orbit Solution with Different Data Combination

Table 4.16 shows the test cases for the study of the orbital element correction. For each case, subarc lengths of 3 hours for the estimation of CT and 9 hours for the estimation of the 1-cpr T and N parameters are employed.

During an experiment for T/P in the early 1990s when the IGS solutions were not accurate enough, a small improvement from **Case delEISC** with the estimation of ($\Delta e$,$\Delta i$,$\Delta\Omega$,$\Delta\omega$) was observed. **Case delAEM** was chosen to see a possible orbit improvement of Jason-1 by adjusting the perturbation along the radial direction $\Delta R$ of the GPS satellite orbits from the relation between $\Delta R$ and ($\Delta a$, $\Delta e$, $\Delta M$) as shown in Equation 4.9.

Table 4.17 shows the comparison of the crossover and SLR residual statistics for each orbit element correction case. Except for $\Delta e$, correcting only one orbit element appears to make little difference from the orbit of **Case Non**. In **Case delE**, the estimation of $\Delta e$ shows clear degradation of the orbit accuracy in all of the three statistics: 1) the crossover RMS of **Case delE** is 6.03 cm, which is larger than 5.97 cm of other cases, 2) the crossover Mean of **Case delE** is 0.9 ($\pm$10.6) mm, which is larger than $\sim$0.4 ($\pm$8.2) mm of other cases, and 3) the SLR residual RMS of **Case delE** is 1.33 cm, which is larger than 1.26 cm of other cases. Furthermore, the orbits of **Case delAEM**, **Case delEISC** and **Case delAEISCM** do not perform better than the orbit of **Case Non**.

Conclusively, the correction of any of GPS satellite orbit elements rarely shows orbit performance improvement, if any, otherwise it degrades the orbit quality. This implies that with the orbit element correction method, the accommodation of the remaining errors in the GPS reference orbits, which are IGS precise solution in this study, may not be efficient.

| Cyc | Crossover Mean for each Case of Orbit Element Correction | | | | | | | | | | |
|---|---|---|---|---|---|---|---|---|---|---|---|
| | Non | delC | delS | delA | delE | delI | delM | delAEM | delCI | delEISC | AEISCM |
| 8 | 2.1 | 4.9 | 5.8 | 2.5 | 10.4 | 5.1 | 5.8 | 13.8 | 5.1 | 13.3 | 19.9 |
| 9 | 5.5 | 4.6 | 7.2 | 5.0 | 8.2 | 6.7 | 7.2 | 8.8 | 5.4 | 9.7 | 10.1 |
| 10 | 6.6 | 6.3 | 8.1 | 5.4 | 9.7 | 6.4 | 8.1 | 10.0 | 6.3 | 10.4 | 9.3 |
| 11 | -7.5 | -6.8 | -5.5 | -9.9 | -9.3 | -8.7 | -5.5 | -9.7 | -7.5 | -7.5 | -13.4 |
| 12 | -13.5 | -14.1 | -13.7 | -13.9 | -19.8 | -14.6 | -13.7 | -19.2 | -16.4 | -21.9 | -24.2 |
| 13 | -.5 | -2.5 | -1.2 | -2.1 | -1.4 | -1.7 | -1.3 | -4.9 | -2.5 | -2.1 | -2.6 |
| 14 | -1.1 | -2.5 | -2.8 | -.3 | -7.6 | -2.4 | -2.8 | -8.1 | -3.1 | -10.8 | -11.6 |
| 15 | -6.5 | -6.3 | -7.3 | -4.8 | -6.8 | -6.9 | -7.3 | -6.3 | -7.1 | -8.9 | -6.3 |
| 16 | -12.0 | -10.2 | -9.2 | -9.8 | -6.3 | -11.3 | -9.1 | -4.9 | -11.8 | -5.1 | -6.4 |
| 17 | 5.6 | 5.6 | 5.7 | 7.5 | 13.0 | 7.1 | 5.6 | 10.1 | 6.5 | 18.3 | 17.5 |
| 18 | -.7 | -1.0 | -1.1 | -.3 | -2.9 | -.8 | -1.1 | -2.0 | -.7 | -2.2 | -1.9 |
| 19 | 12.8 | 12.5 | 13.7 | 13.4 | 12.3 | 13.9 | 13.4 | 16.7 | 11.7 | 16.6 | 24.8 |
| 20 | 13.0 | 11.8 | 8.6 | 13.0 | 12.2 | 11.9 | 8.6 | 11.5 | 9.2 | 7.3 | 18.0 |
| Mean | .3 | .2 | .6 | .4 | .9 | .4 | .6 | 1.2 | -.4 | 1.3 | 2.6 |

(a) Crossover Mean

| Cyc | Crossover RMS for each Case of Orbit Element Correction | | | | | | | | | | |
|---|---|---|---|---|---|---|---|---|---|---|---|
| | Non | delC | delS | delA | delE | delI | delM | delAEM | delCI | delEISC | delAEISCM |
| 8 | 61.8 | 62.4 | 62.2 | 61.8 | 63.3 | 62.0 | 62.2 | 64.4 | 62.1 | 63.7 | 65.6 |
| 9 | 59.3 | 58.9 | 59.1 | 59.4 | 59.4 | 59.3 | 59.1 | 59.4 | 59.0 | 59.6 | 59.7 |
| 10 | 61.3 | 61.4 | 61.6 | 61.0 | 61.9 | 61.3 | 61.6 | 62.0 | 61.5 | 62.3 | 61.7 |
| 11 | 60.9 | 60.8 | 60.7 | 61.2 | 61.7 | 61.0 | 60.7 | 61.9 | 60.7 | 61.5 | 62.8 |
| 12 | 55.7 | 55.9 | 55.6 | 56.0 | 57.9 | 56.0 | 55.6 | 57.9 | 56.8 | 58.9 | 60.1 |
| 13 | 63.1 | 63.3 | 63.1 | 63.3 | 63.4 | 63.1 | 63.1 | 63.9 | 62.2 | 62.4 | 62.9 |
| 14 | 58.4 | 58.4 | 58.5 | 58.4 | 59.5 | 58.3 | 58.5 | 59.6 | 58.4 | 59.9 | 60.1 |
| 15 | 60.1 | 59.2 | 59.4 | 59.8 | 59.6 | 60.2 | 59.5 | 59.4 | 59.3 | 59.7 | 59.4 |
| 16 | 62.9 | 62.8 | 62.6 | 62.2 | 62.2 | 62.9 | 62.6 | 61.6 | 63.2 | 62.2 | 62.0 |
| 17 | 59.6 | 59.7 | 59.5 | 59.8 | 61.4 | 59.9 | 59.5 | 60.6 | 60.0 | 62.9 | 62.7 |
| 18 | 55.6 | 55.9 | 55.7 | 55.7 | 55.7 | 55.8 | 55.7 | 55.7 | 56.0 | 56.1 | 55.9 |
| 19 | 59.6 | 59.7 | 60.2 | 59.7 | 59.7 | 59.9 | 60.0 | 61.2 | 59.4 | 61.3 | 63.9 |
| 20 | 58.2 | 57.8 | 57.3 | 58.3 | 58.2 | 58.1 | 57.2 | 58.0 | 57.6 | 57.8 | 60.0 |
| Mean | 59.7 | 59.7 | 59.7 | 59.7 | 60.3 | 59.8 | 59.6 | 60.4 | 59.7 | 60.6 | 61.3 |

(b) Crossover RMS

| Cyc | SLR residual RMS ($> 70^{o}$) for each Case of Orbit Element Correction | | | | | | | | | | |
|---|---|---|---|---|---|---|---|---|---|---|---|
| | Non | delC | delS | delA | delE | delI | delM | delAEM | delCI | delEISC | delAEISCM |
| 8 | 11.9 | 11.7 | 11.9 | 12.2 | 11.0 | 11.7 | 11.9 | 12.7 | 12.3 | 14.6 | 14.9 |
| 9 | 13.0 | 12.2 | 12.3 | 13.1 | 12.8 | 13.4 | 12.3 | 12.2 | 12.6 | 12.5 | 12.4 |
| 10 | 13.1 | 12.7 | 12.7 | 13.0 | 13.1 | 13.1 | 12.7 | 12.4 | 12.6 | 12.6 | 12.3 |
| 11 | 13.5 | 14.7 | 14.5 | 14.1 | 14.5 | 13.6 | 14.5 | 14.8 | 14.9 | 14.5 | 15.4 |
| 12 | 7.8 | 7.6 | 7.7 | 7.9 | 9.3 | 7.5 | 7.7 | 8.9 | 7.5 | 8.9 | 9.3 |
| 13 | 9.9 | 13.4 | 11.9 | 11.6 | 10.2 | 9.2 | 12.0 | 13.9 | 11.3 | 9.5 | 9.8 |
| 14 | 10.1 | 10.0 | 9.5 | 10.2 | 12.4 | 10.0 | 9.5 | 12.1 | 10.4 | 12.6 | 13.0 |
| 15 | 15.3 | 14.6 | 14.2 | 15.4 | 15.0 | 15.4 | 14.2 | 15.5 | 14.2 | 16.0 | 15.7 |
| 16 | 13.2 | 15.3 | 13.2 | 12.6 | 13.8 | 13.6 | 13.2 | 13.5 | 14.9 | 15.2 | 14.1 |
| 17 | 11.4 | 11.6 | 11.4 | 11.0 | 15.0 | 11.6 | 11.4 | 13.1 | 11.6 | 14.9 | 14.2 |
| 18 | 9.0 | 9.2 | 8.5 | 9.0 | 9.8 | 8.8 | 8.5 | 9.4 | 9.0 | 9.7 | 9.8 |
| 19 | 17.5 | 18.5 | 19.2 | 17.8 | 18.1 | 19.2 | 19.0 | 19.7 | 19.8 | 23.0 | 23.0 |
| 20 | 16.3 | 16.5 | 16.5 | 16.2 | 17.6 | 16.2 | 16.5 | 18.1 | 16.9 | 18.4 | 20.4 |
| Mean | 12.5 | 12.9 | 12.6 | 12.6 | 13.3 | 12.6 | 12.6 | 13.6 | 12.9 | 14.0 | 14.2 |

(c) SLR residual RMS

Table 4.17: Orbit Improvement with Orbit Element Correction [Unit:mm]. The correction of any of GPS satellite orbit elements rarely shows orbit performance improvement, if any. Otherwise, it degrades the orbit quality.

# Chapter 5

# Orbit Improvement by Combining SLR/DORIS with GPS

For T/P, the official orbit solutions were based on SLR and DORIS tracking data. Its experimental orbits from GPS-only were not significantly superior to the SLR/DORIS orbits, presumably because the quality of the GPS data from the Demonstration Receiver was not good enough. In the previous chapter, it was shown that Jason-1 orbit solutions from GPS-only data using the dynamic approach underperformed the orbits from SLR/DORIS data.

However, it is possible that orbits determined with all three measurement types can perform better than the orbits from SLR/DORIS tracking, especially for Jason-1, because of the enhanced quality of GPS tracking. One objective of this chapter is to seek the optimal relative weighting for each measurement type to produce the best performing orbits from combined measurement systems. Another objective is to determine each observation type's contribution and to find the best combination of measurement types. Since it is obvious that SLR tracking is essential to tie the orbits to the reference frame and both DORIS and GPS tracking have the capability of continuous and all-weather coverage, which measurement system among DORIS and GPS

will be better to be combined with SLR is an interesting question especially, if we do not intend to utilize all three of the measurement systems. Orbits from a combination of only two systems may outperform the orbits from combining all three of the systems. The performance of each orbit will be examined using the crossover test and the SLR residual test.

In order to process the combined data of SLR/DORIS and GPS, modified implementations in Fortran 90 were added to MSODP. The version of MSODP for this research is 2001.2, several subroutines of which were modified and improved based on the modsets for the 9408 version [H. Rim, personal communication, 1998]. The modified subroutines for combining data types are described in Appendix E.2 and the job deck is also provided in Appendix E.1. The main change to the code was made to read the tracking data of all three data types from one data file (especially in the codes of OBSERV.f90 and READOB.f90). To obtain the mixed data file combined with SLR/DORIS and GPS tracking data, the Double-Differenced Observation (DDobs) data were converted to the UTOPIA data format [see UTOPIA manual] from the Double-Differenced CSR format [see MSODP manual], then all three type data in the UTOPIA format were merged and sorted in the chronological order based on time-tags (UTC). The subroutine of GPSPAR.f90 was added to process DDobs in the UTOPIA format in MSODP. The mixed data file called 'OBSDAT' contains the observation data type for each data. For SLR and DORIS, there is one observation for one time. However, DDobs data have multiple observation at the same epoch and they all have to be processed at

the same time according to each observation's data type. Also, station information files for all three data types need to be provided to weight each data type differently in the process. The weighting of each data type is further discussed in Section 5.2.

In this chapter, the preprocessing of the SLR/DORIS data will be described. The optimal estimation frequency of the empirical parameters for the processing with the combined data will be investigated in Section 5.3.1. Each observation type's optimal relative weighting will be sought in Section 5.3.2 and each observation type's contribution will be investigated in Section 5.4. Orbits by using different gravity models will be compared in Section 5.5. Finally, the orbit solutions from external institutes will be compared with the orbit solution from the combined data in Section 5.6.

## 5.1 SLR/DORIS data processing

Like the GPS data, raw CNES Jason-1 DORIS data were downloaded from `ftp://spike.cst.cnes.fr`. The downloaded raw data were rearranged from station-ordered to time-ordered. Duplicate observations within 500 microseconds of each other from the same station were checked and removed. CNES's phase solutions were substituted to the phases that were repaired at CSR during the preprocessing stage. Time bias offsets in the DORIS data were also repaired, if needed.

Figure 5.1 shows each DORIS data's station visibility and groundtrack plots for the raw data. During cycle 1 to cycle 20, 55 DORIS stations tracked

Jason-1 as shown in Figure 5.1(a). In Figure 5.1(b), the ground track distribution of the raw data for cycle 15 is shown. In the period of cycle 15, 47 DORIS stations tracked Jason-1. Stations such as ADEA, MORA, GALA, EVEB, GUAB, MARB, AJAB, and ADEB were not active in this period. Although not all of the DORIS stations are always active, the all-weather tracking capability of DORIS provides very dense and vast tracking data for most of time.

On the other hand, SLR tracking are much susceptible to the weather conditions. Figure 5.2 shows SLR data station's visibility and groundtrack plots for the SLR data. Since the Jason-1 launch, 28 SLR stations have been available as shown in Figure 5.2(a). Most of the SLR stations are located in the northern hemisphere. The ground track distribution for the SLR data of cycle 15 in Figure 5.2(b) shows that the distribution of SLR tracking is far less dense and scarce when compared to the DORIS tracking distribution.

The daily passes and observations collected by the DORIS and SLR tracking systems from day-of-year (doy) 80 to 210 of the year 2002 are shown in Figure 5.3 and 5.4 respectively. As shown in Figure 5.4(b), the SLR tracking system provides about 10-20 passes per day, which is about the same number of passes per day tracked by T/P [Tapley *et al.*, 1994]. The weakness of several days for SLR tracking appears to be due to seasonal weather effects and from operator scheduling rather than from orbit maneuvers. Figure 5.3(b) shows that the DORIS tracking system routinely provides about 140 - 160 passes per day, which is almost 40 more passes per day than the daily passes of T/P

[Tapley *et al.*, 1994]. The weakness in DORIS tracking on several days is mainly due to the orbit maneuver between the cycles. Those days are doy 84 (obs # = 4361, pass # = 68), 94 (obs # = 7098, pass # = 105), 134 (obs # = 7493, pass # = 117), and 183 (obs # = 7963, pass # = 113). The tracking weakness on doy 117 (obs # = 8360, pass # = 117) is also observed for DORIS with a gap from 2h:00m:00s to 5h:00m:00s (UTC). This is not related to orbit maneuvers. Remember that the tracking weakness of doy 117 was also observed for GPS with a 7-hour long gap as shown in Figure 4.2. The tracking weakness which occurred in both DORIS and GPS tracking may deteriorate the orbit solution of cycle 11.

Figure 5.5 shows the distribution of pass numbers with respect to the observation numbers per pass in Cycle 8 - 20 for SLR and DORIS. The figure also indicates the pass length distribution, since the observation numbers per pass are linked to the pass lengths. For DORIS, the observation interval in a pass is 10 sec. Therefore, Figure 5.5(b) shows that passes of about 15 minutes long are dominant during cycles 8 - 20, although there are a few passes as long as 40 minutes. Most of DORIS passes are longer than 5 minutes. For SLR, the observation interval in a pass is not regular. At most, approximately 70 observations in a pass are made and about 10 observations in a pass are usually observed as shown in Figure 5.5(a). The minimum number of observations per pass for the processing of SLR and DORIS in MSODP is set to one.

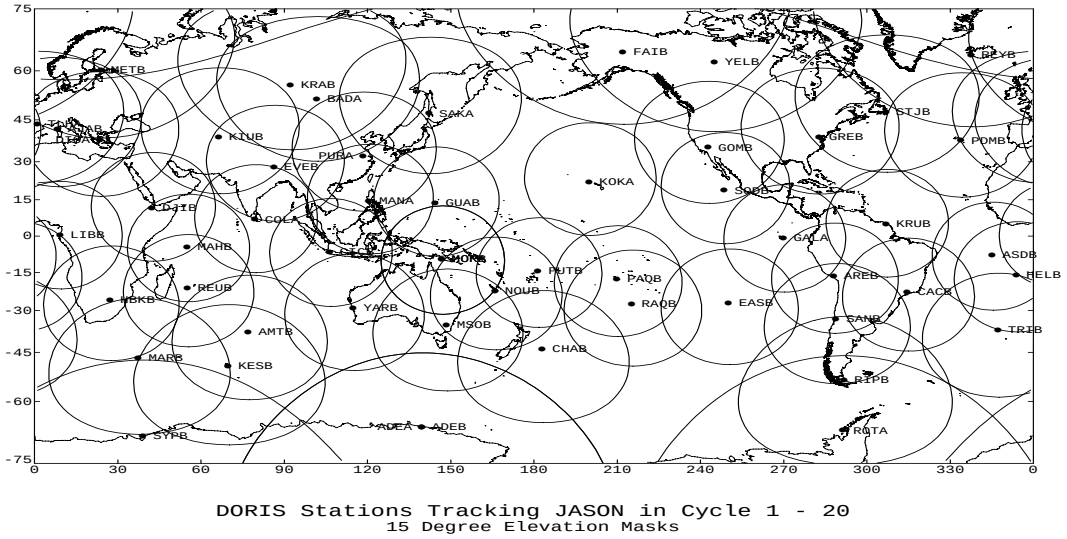


(a) 55 DORIS Stations tracking Jason-1 in cycle 1 - 20 (15° elevation mask)

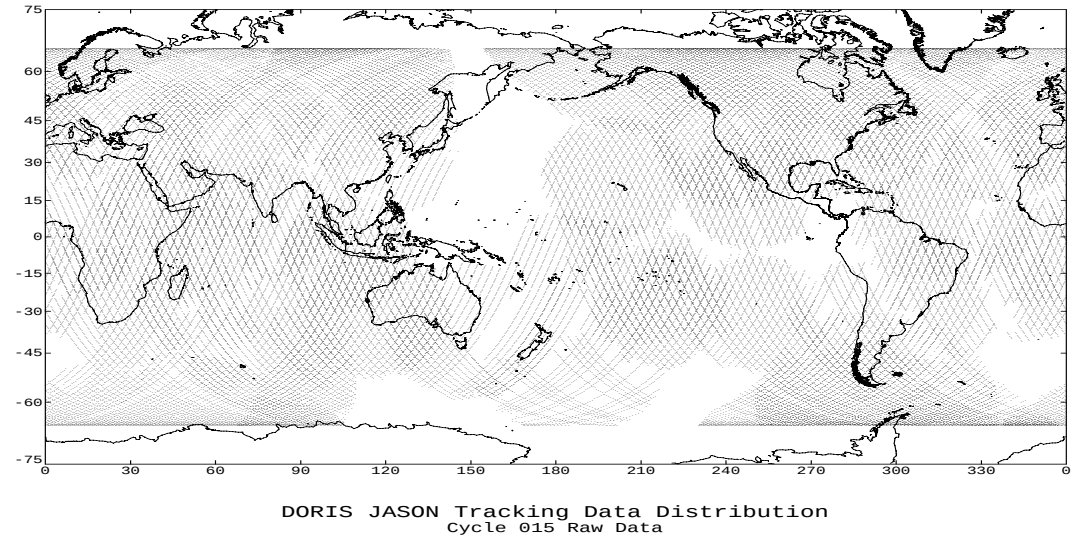


(b) DORIS Jason-1 Tracking Data Distribution for cycle 15

Figure 5.1: 55 DORIS Stations for cycle 1 - 20 (top) and Tracking Data Distribution from 47 stations for cycle 15 (bottom)

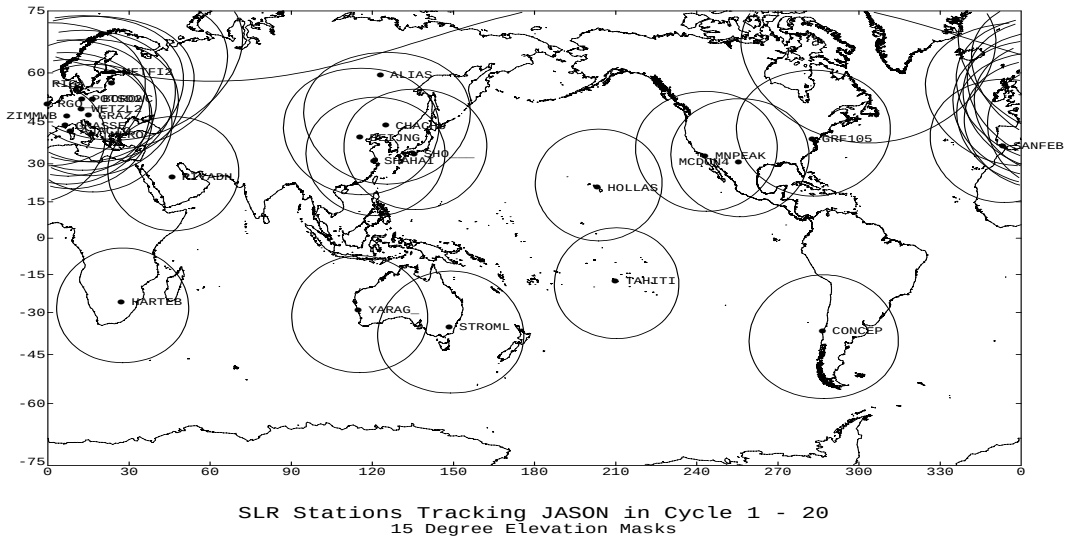


(a) 28 SLR Stations tracking Jason-1 in cycle 1 - 20 (15° elevation mask)

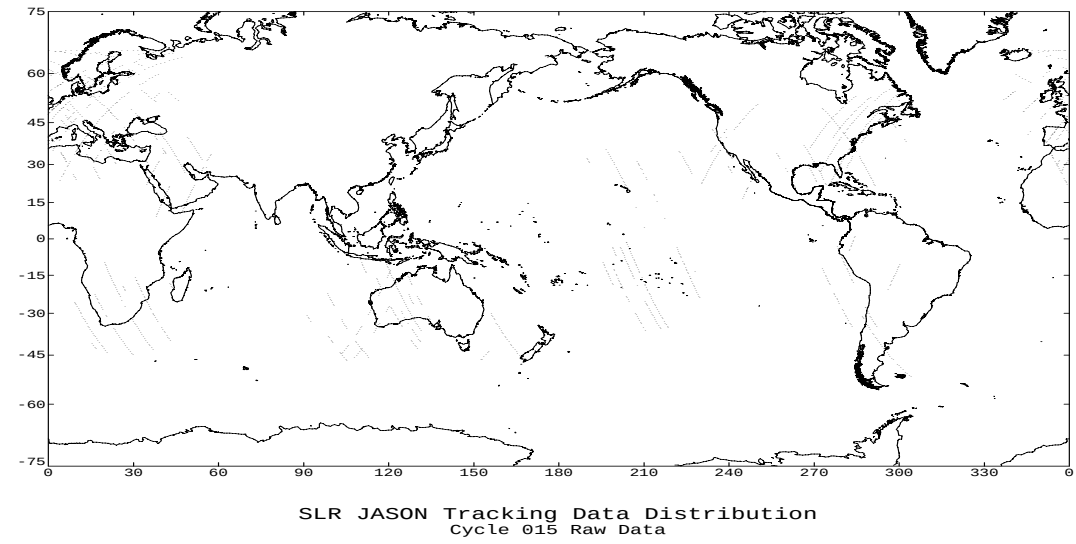


(b) SLR Jason-1 Tracking Data Distribution for cycle 15

Figure 5.2: SLR Stations for cycle 1 - 20 (top) and Tracking Data Distribution for cycle 15 (bottom)

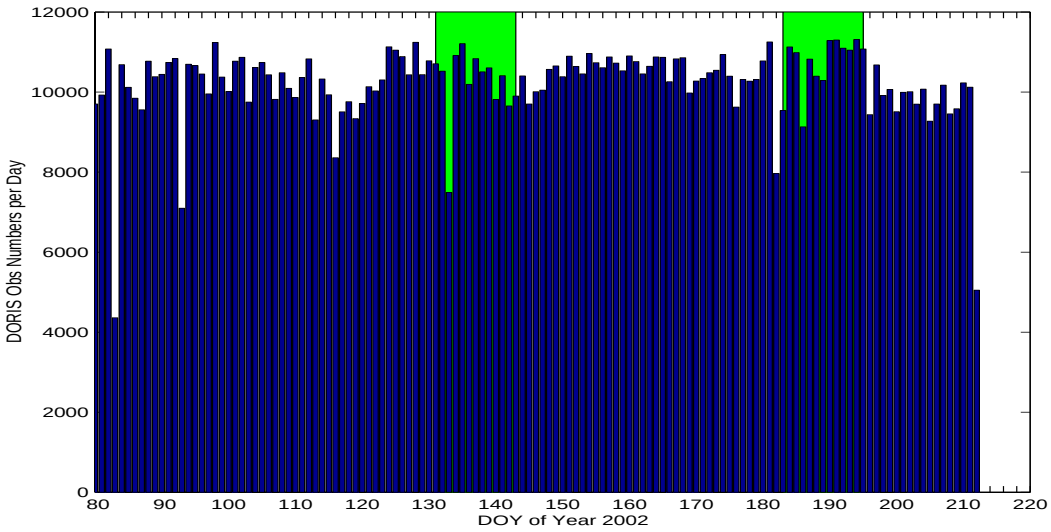


(a) DORIS Obs Numbers per Day

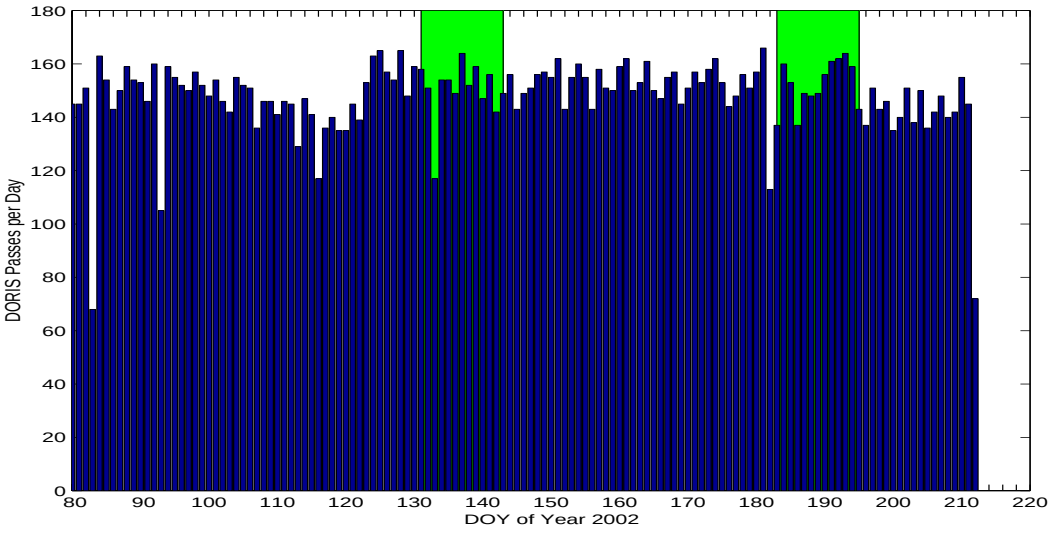


(b) DORIS Passes per Day

Figure 5.3: DORIS Observation Numbers (top) and Pass Numbers (bottom) per Day. There were orbit maneuvers during days 141 and 183. Green region shows the yaw fixed regime.

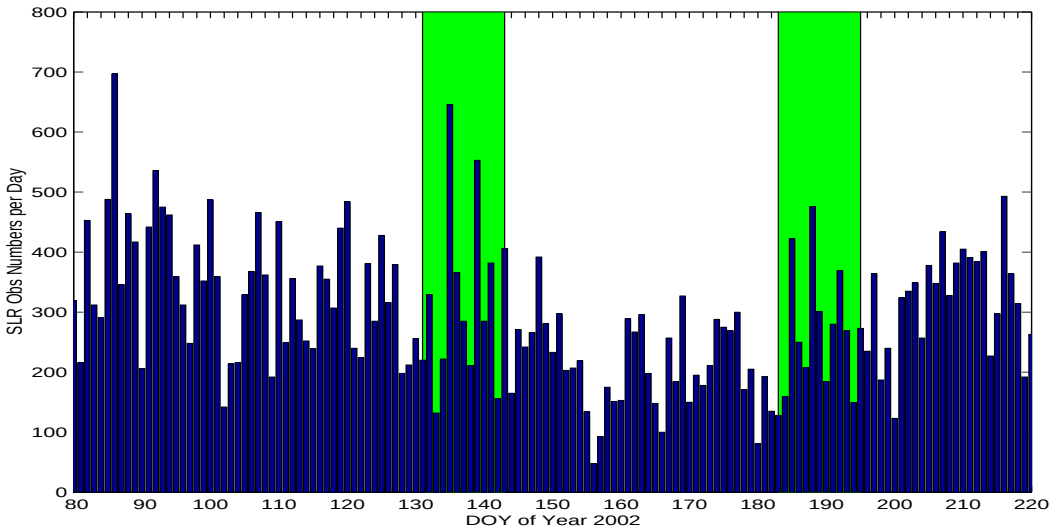


(a) SLR Obs Numbers per Day

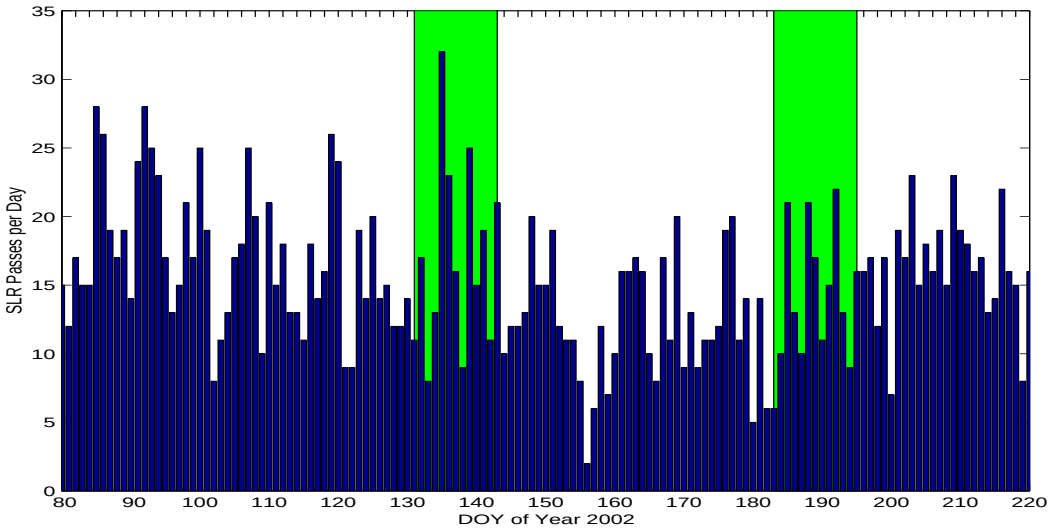


(b) SLR Passes per Day

Figure 5.4: SLR Observation Numbers (top) and Pass Numbers (bottom) per Day

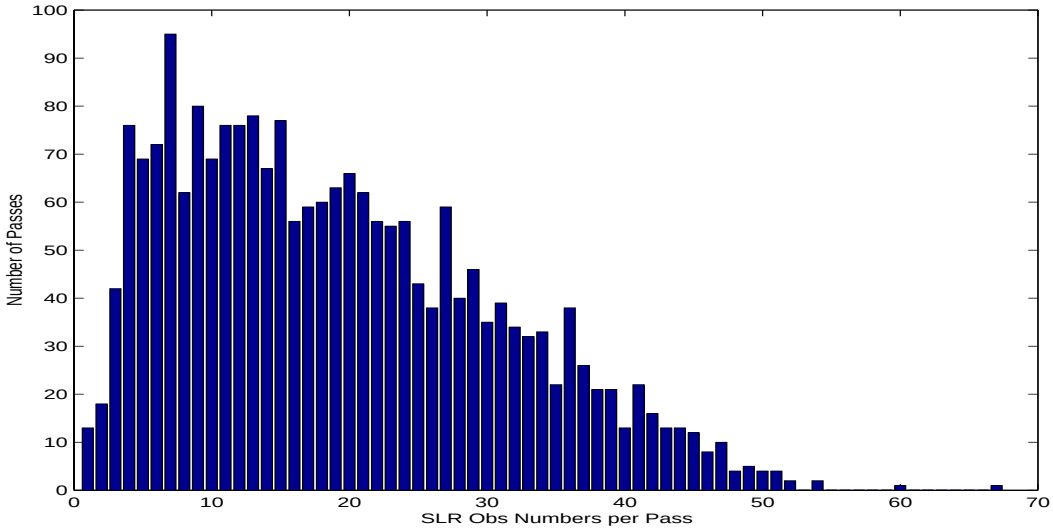


(a) Number of Passes w.r.t. SLR Obs Numbers per Pass

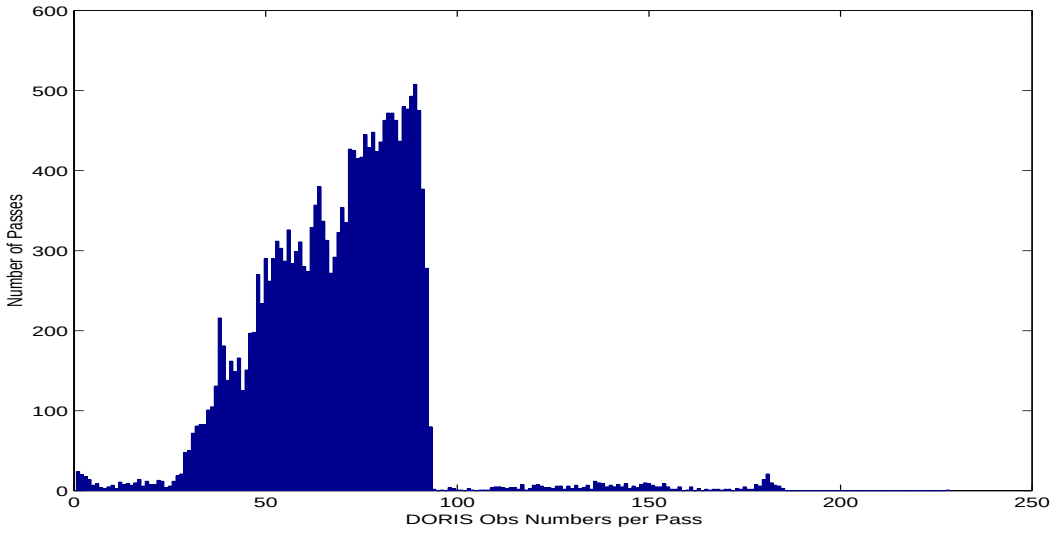


(b) Number of Passes w.r.t. DORIS Obs Numbers per Pass

Figure 5.5: Number of Passes w.r.t. Observation Numbers per Pass for SLR (top) and DORIS (bottom) in Cycle 8 - 20. Observation Numbers per Pass indicates the pass lengths.

## 5.2 Overview of Precise Orbit Determination with the Combined Data

Given a sequence of observations $y_1$, $y_2$, ..., $y_l$ related through the state transition matrix to the state at some general time, $x_k$, and an associated weight $w_i$ for each of the observations, one can write

$$\begin{array}{lcll} y_1 & = & H_1 x_k + \varepsilon_1 & ; w_1 \\ y_2 & = & H_2 x_k + \varepsilon_2 & ; w_2 \\ \vdots & & \vdots & \vdots \\ y_l & = & H_l x_k + \varepsilon_l & ; w_l \end{array} \tag{5.1}$$

where,

$$H_i = \tilde{H}_i \Phi(t_i, t_k) \tag{5.2}$$

and $\varepsilon_l$ is the error for the observation $y_l$. In Equation 5.1, the weights, $w_i$, are assumed to range between zero and one, the observation weighted with one would be given the highest weight while the observations weighted with zero would be neglected. Equation 5.1 can be expressed as:

$$y = H x_k + \varepsilon \ \ ; \ W \tag{5.3}$$

where,

$$y = \begin{bmatrix} y_1 \\ y_2 \\ \vdots \\ y_l \end{bmatrix} ; H = \begin{bmatrix} H_1 \\ H_2 \\ \vdots \\ H_l \end{bmatrix} ; \varepsilon = \begin{bmatrix} \varepsilon_1 \\ \varepsilon_2 \\ \vdots \\ \varepsilon_l \end{bmatrix} ; W = \begin{bmatrix} w_1 & 0 & \cdots & 0 \\ 0 & w_2 & \cdots & 0 \\ & & \ddots & \\ 0 & 0 & \cdots & w_l \end{bmatrix} \tag{5.4}$$

The normal equation form of the weighted least squares problem can be derived as [Tapley, 1973]:

$$(H^T W H)\hat{x}_k = H^T W y \tag{5.5}$$

where, $H^T W H$ is referred to as the normal matrix. If the normal matrix is positive definite, it will have an inverse and the solution to Equation 5.5 is:

$$\hat{x}_k = (H^T W H)^{-1} H^T W y \tag{5.6}$$

By defining the variance-covariance matrix $P_k$, Equation 5.6 can be expressed as:

$$\hat{x}_k = P_k H^T W y \tag{5.7}$$

where, $P_k = (H^T W H)^{-1}$. The value of $\hat{x}_k$ is the weighted least squares estimate and is the estimate which minimizes the sum of the weighted observation errors.

The weighting matrix, $W$, usually results from an initial judgement on the accuracy of the observations followed by a normalization procedure to scale the weights to values between zero and one. $W$ is equal to the inverse of the observation noise covariance matrix, $R$ so that $W = R^{-1}$.

The observation noise covariance matrix, $R$, is defined by assuming that the observation error $\varepsilon$ is random with zero mean such as:

$$R_i = E[\varepsilon_i \varepsilon_i^T] \tag{5.8}$$

In matrix form, the $R$ matrix can be expressed as:

$$R = E[\varepsilon \varepsilon^T] = \begin{bmatrix} R_1 & & & 0 \\ & R_2 & & \\ & & \ddots & \\ 0 & & & R_l \end{bmatrix} \tag{5.9}$$

For the process with the combined measurement types, the weighting matrix should represent each measurement type's relative observation accuracy as well as the observation noise from different stations.

To control the relative weighting of the mixed data types, GPS and DORIS/SLR are weighted in different ways. The data of SLR are weighted according to the individual tracking stations. DORIS is generally weighted the same, but a few stations are downweighted due to poorer performance. GPS double-differenced observations are not weighted for each station individually, since GPS observations from all the stations tend to be relatively homogeneous. In addition, the observation is a combination from two observing stations, and each data is differenced between two different stations with a variety of combinations among many stations each time.

## 5.3 Parameterization and Orbit Solution

A relative weight for each data type which will produce the best orbit solution will be defined as the optimal relative weight. In the process of combining measurement systems, finding an optimal relative weight for each data type is the main goal. In Section 5.3.2, many combinations with different relative weighting for each data type will be explored, then their orbit solutions will be compared by using the altimeter crossover statistics and SLR residuals. All of the orbit solutions compared in this section, in searching for the optimal weight, were processed by using all three data types simultaneously. To see the contribution of each data type to the orbit improvement, the orbit

performance comparison by using combinations with only one or two different data types instead of three data types (i.e. combination of GPS and SLR, or combination of GPS and DORIS) will be discussed in Section 5.4. The best possible combination of data types for the best solution, whether it is the combination of all three data types or not, will also be discussed in Section 5.4.

Before the search for the optimal relative weight in Section 5.3.2, the optimal subarc length for the estimation of the empirical force parameters with the combined measurement system will be determined in Section 5.3.1. To find the optimal subarc length, a priori sigmas for the weights of each measurement type were applied for all of the experimental cases are 10 cm for SLR, 2 mm/s for DORIS and 20 cm for GPS.

### 5.3.1 Optimal Subarc Length

In Section 4.2.2, when only GPS data is used for the orbit determination, optimal subarc lengths for the estimation of the 1-cpr T & N empirical parameters and for the estimation of CT are 9 hours and 3 hours respectively. However, when the SLR/DORIS data are combined with GPS data, it is expected that the optimal subarc lengths can be further shortened with the mutual support of each tracking system. Combining SLR/DORIS with GPS will help to push the parameterization heavier. In this section, the optimal estimation frequency for the empirical force parameters will be re-examined, when the SLR/DORIS data are combined with the GPS data.

Fig 4.2(b) shows that the GPS tracking is much denser than the SLR tracking, and even denser than the DORIS tracking as shown in Figure 5.3(a) and 5.4(a). The dominant DDpass length shown in 4.3 is 30 minutes with the maximal pass length of 50 minutes, while the passes of SLR and DORIS are usually much shorter than DDpasses as shown in 5.5. Figure 5.5(b) indicates that the dominant pass length of DORIS is about 15 minutes. The numbers of observed DDpasses are also much more than the numbers of DORIS passes. This suggests that the addition of SLR/DORIS to GPS may not severely shorten the optimal subarc length for the estimation of empirical force parameters. However, the addition of SLR/DORIS to GPS can still improve the orbit solution compared with the GPS-only solution.

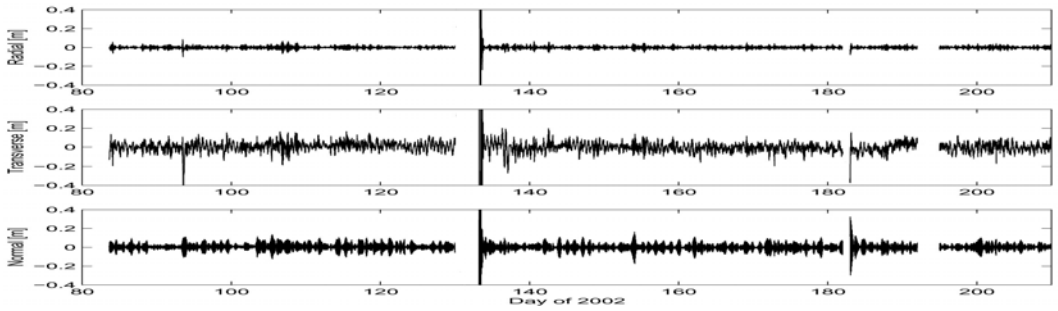


Figure 5.6: Orbit differences (TRACOM) from CSR SLR/DORIS orbit and GPS/SLR/DORIS orbit with 3-hour subarc for CT, and with 6-hour subarc for 1-cpr T & N. The orbits of days 134 and 183 with orbit maneuvers were not improved even by combining measurement systems compared to the GPS-only orbits in Figure 4.10. These two days were excluded for the orbit assessment.

Obvious examples of the orbit improvement by mutual support of GPS and DORIS are the orbit solutions of day 117 and day 141. In Table 4.3,

the GPS data of day 117 show a long gap for 24,120 seconds starting at 19h:53m:00s (GPS time). Also for day 141, there is a long GPS data gap of 36,960 seconds starting at 13h:44m:00s (GPS time). On the other hand, DORIS does not show a long gap in the same periods for day 141, and for day 117, there is a DORIS gap from 2 AM to 5 AM, but it is not the same gap duration as the GPS data. This clearly indicates that for day 117, GPS and DORIS can make up for each other's data gaps. Consequently, the combined data produced a better orbit solution than the solution from only one data type. This can be seen in the comparison of Figure 4.10 and 5.6. For day 117 and 141, it is shown that the orbit differences between GPS/SLR/DORIS and SLR/DORIS in Figure 5.6 were significantly reduced compared to the orbit differences between GPS-only and SLR/DORIS in Figure 4.10. Figure 5.6 also shows that the orbits of days 134 and 183 with orbit maneuvers are not improved even by combining measurement systems. These two days were excluded for the orbit assessment.

To find an optimal subarc length for the estimation of the empirical force parameters, the cases described in Table 4.12 had been tested for cycle 8 to cycle 20. The comparison results of orbit solutions from the experimental cases are shown in Table 5.1. The crossover Mean, crossover RMS and the SLR residual RMS were compared. Among them, the crossover RMS was a critical factor in determining the optimal parameterization.

The averaged crossover RMSs of **Case sub1.5-3** and **sub1.5-4.5** over the cycles appear to be the best among the test cases at 5.87($\pm$0.22) cm and

| Cyc | Crossover Mean for each subarc length strategy | | | | | | | |
|---|---|---|---|---|---|---|---|---|
| | sub1-2 | sub1-3 | sub1-4 | sub1.5-3 | sub1.5-4.5 | sub1.5-10 | sub2-4 | sub3-5 |
| 8 | 2.5 | 3.0 | 3.4 | 3.1 | 2.9 | 2.7 | 4.2 | 4.1 |
| 9 | 2.1 | 3.3 | 2.5 | 2.9 | 2.5 | 2.1 | 2.0 | 4.6 |
| 10 | -.1 | -1.1 | -2.0 | -1.5 | -1.2 | -1.5 | -2.0 | -.6 |
| 11 | -11.7 | -11.4 | -10.7 | -11.2 | -9.5 | -9.9 | -10.8 | -8.5 |
| 12 | -12.7 | -12.7 | -11.6 | -11.4 | -10.9 | -10.9 | -11.4 | -9.4 |
| 13 | -.1 | -.6 | 1.1 | .2 | -2.3 | -1.0 | -3.4 | .8 |
| 14 | -6.1 | -5.7 | -4.9 | -5.7 | -4.8 | -4.9 | -6.7 | -8.6 |
| 15 | -6.0 | -5.9 | -5.4 | -5.7 | -6.2 | -6.1 | -5.6 | -7.5 |
| 16 | -8.8 | -8.4 | -9.7 | -8.0 | -7.9 | -8.2 | -9.6 | -8.8 |
| 17 | 3.7 | 3.5 | 2.9 | 3.8 | 5.9 | 4.6 | 2.6 | 6.4 |
| 18 | -4.4 | -4.7 | -5.1 | -4.3 | -3.8 | -3.8 | -4.9 | -4.5 |
| 19 | 11.4 | 11.2 | 11.1 | 11.4 | 12.5 | 12.1 | 10.2 | 11.8 |
| 20 | 6.4 | 6.4 | 6.6 | 6.0 | 6.8 | 5.6 | 6.9 | 7.8 |
| Mean | -1.8 | -1.8 | -1.7 | -1.6 | -1.2 | -1.5 | -2.2 | -1.0 |
| rms | 7.2 | 7.1 | 7.0 | 6.9 | 7.0 | 6.7 | 6.9 | 7.4 |

(a) Crossover Mean

| Cyc | Crossover RMS for each subarc length strategy | | | | | | | |
|---|---|---|---|---|---|---|---|---|
| | sub1-2 | sub1-3 | sub1-4 | sub1.5-3 | sub1.5-4.5 | sub1.5-10 | sub2-4 | sub3-5 |
| 8 | 61.0 | 61.1 | 60.9 | 61.0 | 61.3 | 61.3 | 61.1 | 62.0 |
| 9 | 59.6 | 58.9 | 59.2 | 58.6 | 58.5 | 58.5 | 58.8 | 59.1 |
| 10 | 59.7 | 59.2 | 59.1 | 58.7 | 59.4 | 59.3 | 59.1 | 59.4 |
| 11 | 61.8 | 61.4 | 61.2 | 61.2 | 61.2 | 61.3 | 61.1 | 61.9 |
| 12 | 55.6 | 55.7 | 55.1 | 54.8 | 54.6 | 54.8 | 54.8 | 54.9 |
| 13 | 61.3 | 61.0 | 60.3 | 61.6 | 61.2 | 61.0 | 62.8 | 60.2 |
| 14 | 59.0 | 58.6 | 58.2 | 58.3 | 58.0 | 58.1 | 58.1 | 58.6 |
| 15 | 58.0 | 57.8 | 57.8 | 57.1 | 57.0 | 57.1 | 57.5 | 57.4 |
| 16 | 61.2 | 61.4 | 62.0 | 61.0 | 61.8 | 62.0 | 61.9 | 61.7 |
| 17 | 58.5 | 58.8 | 58.2 | 58.7 | 59.5 | 59.2 | 58.0 | 59.2 |
| 18 | 55.4 | 55.2 | 55.8 | 54.9 | 55.0 | 55.1 | 55.9 | 56.1 |
| 19 | 59.2 | 58.8 | 59.5 | 59.4 | 59.0 | 59.2 | 59.2 | 60.6 |
| 20 | 57.9 | 57.3 | 57.6 | 57.2 | 56.9 | 57.3 | 57.2 | 57.2 |
| Mean | 59.1 | 58.9 | 58.8 | 58.7 | 58.7 | 58.8 | 58.9 | 59.1 |
| rms | 2.0 | 2.0 | 2.0 | 2.2 | 2.4 | 2.3 | 2.3 | 2.2 |

(b) Crossover RMS

| Cyc | SLR residual RMS (> 70 deg) for each subarc length strategy | | | | | | | |
|---|---|---|---|---|---|---|---|---|
| | sub1-2 | sub1-3 | sub1-4 | sub1.5-3 | sub1.5-4.5 | sub1.5-10 | sub2-4 | sub3-5 |
| 8 | 7.1 | 8.3 | 8.5 | 8.9 | 9.0 | 8.8 | 8.8 | 8.6 |
| 9 | 10.4 | 10.9 | 9.8 | 10.4 | 10.2 | 10.2 | 10.2 | 10.8 |
| 10 | 10.1 | 10.4 | 9.4 | 10.5 | 10.5 | 10.7 | 10.3 | 11.1 |
| 11 | 8.6 | 9.1 | 9.2 | 9.4 | 9.8 | 9.6 | 8.6 | 8.4 |
| 12 | 7.1 | 6.7 | 6.9 | 6.4 | 6.8 | 6.7 | 7.4 | 6.4 |
| 13 | 7.0 | 7.0 | 8.3 | 8.4 | 8.0 | 8.5 | 9.3 | * |
| 14 | 9.0 | 9.7 | 11.0 | 10.9 | 10.5 | 10.4 | 10.5 | 12.2 |
| 15 | 9.6 | 9.6 | 9.8 | 9.7 | 9.7 | 9.8 | 10.3 | 9.3 |
| 16 | 6.8 | 7.4 | 9.7 | 7.1 | 9.6 | 9.5 | 10.2 | 9.4 |
| 17 | 7.6 | 7.8 | 7.6 | 8.5 | 10.3 | 10.3 | 7.6 | 7.8 |
| 18 | 7.0 | 7.6 | 6.6 | 7.5 | 7.9 | 7.9 | 7.2 | 8.0 |
| 19 | 12.9 | 12.2 | 12.6 | 11.8 | 12.8 | 12.5 | 11.9 | 8.8 |
| 20 | 13.4 | 11.7 | 13.3 | 12.7 | 13.2 | 11.6 | 13.3 | 9.1 |
| Mean | 9.0 | 9.1 | 9.4 | 9.4 | 9.9 | 9.7 | 9.7 | * |
| rms | 2.2 | 1.8 | 2.0 | 1.9 | 1.8 | 1.5 | 1.8 | * |

(c) SLR residual RMS

Table 5.1: Optimal Sub-arc Length Strategy. 3-hour subarc for CT and 6-hour subarc for 1-cpr T & N was chosen, however orbits are insensitive to the subarc lengths.

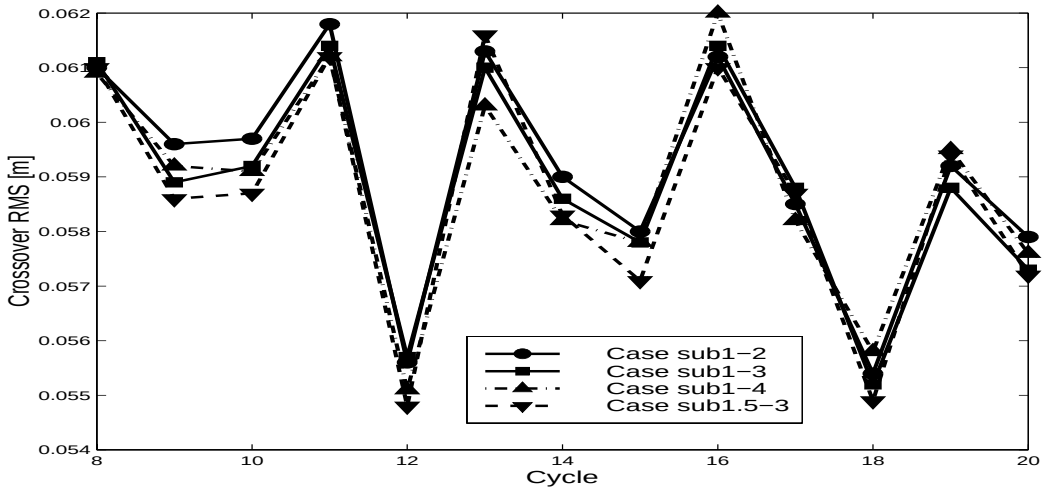


(a) Comparison with several Cases of subarcs

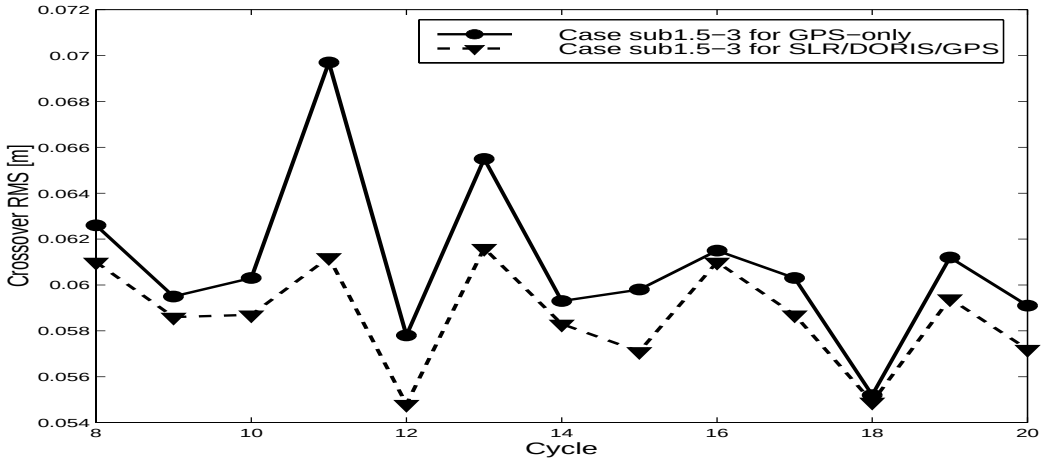


(b) Comparison of GPS-only and GPS/DORIS/SLR with the same subarc strategy

Figure 5.7: Crossover RMS with different subarc lengths, and comparisons for GPS-only and SLR/DORIS/GPS; Orbits with 3-hour subarc for CT (**Case sub1.5-3**) are a little bit better than the orbits with 1.8738-hour subarc for CT (**Case sub1-** series) (top). Orbits with combined data show clear improvement over GPS-only orbits for all cycles (bottom).

5.87($\pm$0.24) cm. The comparison of the crossover RMSs for each cycle shown in Figure 5.7(a) also indicates that the orbits from **Case sub1.5-3**, which is the strategy with 3-hour subarc length for CT and 6-hour subarc length for 1-cpr T & N, perform better than orbits from other cases with heavier parameterization for most of cycles. The crossover RMSs of either heavier parameterizations or lighter parameterizations increased, implying that **Case sub1.5-3** may be an optimal parameterization to estimate the empirical force parameters.

Compared to the crossover RMS of **Case sub1.5-3** from GPS-only tracking (6.09 cm), the orbit from the combined data with SLR/DORIS and GPS with the same estimation strategy for the empirical parameters was significantly improved to 5.91 cm of the crossover RMS. In terms of the radial orbit error, this means the reduction of 1.5 cm over the cycles. Figure 5.7(b) shows that the crossover RMSs were improved over all cycles by combining SLR/DORIS with GPS.

By combining SLR/DORIS with GPS, there is another advantage as well as its contribution to make the heavier parameterization possible. Each measurement system can fill each other system's unexpected data gaps. The orbit of cycle 11 is one of the most benefited orbits from the combined data, because of the improvement by making up of the GPS tracking gap with DORIS tracking data during day 117 as previously stated in Section 5.1.

The crossover Means, which are indicators of the orbit centering, are in the range of $-1\sim-2$ mm for all of the cases. Their standard deviation ($\sim$7

mm in Table 5.1(a)) from cycle to cycle is much smaller than the standard deviation (∼10 mm) of cycles from the GPS-only orbits in Table 4.13, which indicates that the orbits with combined data type are more stable in the sense of the orbit centering with the help of SLR tracking.

Table 5.1(c) shows that the SLR residual RMSs for all of the cases are less than 1 cm. Note that the SLR residual RMSs from GPS-only tracking were 1.2∼1.9 cm for all the cases in Table 4.15, even when the orbits of days 117, 134 and 141 with the tracking weakness or orbit maneuvers were included. This is a very promising result to reach the goal for the 1-cm radial orbit RMS error, since the SLR residual RMS is one of the good independent measures for the orbit accuracy. However, the SLR residual RMSs less than 1 cm in the Table 5.1(c) are likely optimistic measures of the orbit accuracy, because the SLR data are not independent in the fits from the combined data.

### 5.3.2 Optimal Relative Weightings

To find an optimal relative weighting for each measurement type, first, the relative weighting of GPS was sought while the a priori sigmas for weightings of SLR and DORIS were fixed to 10 cm and 2 mm/s respectively, which were the a priori sigmas for CSR's SLR/DORIS solutions [J. Ries, personal communication, 2002]. Since the actual post-fits of the SLR/DORIS orbits were about 2 cm for SLR and 0.5 mm/sec for DORIS, both a priori sigmas for SLR and DORIS are about 4-5 times larger than the post-fit residual RMS of each measurement so that each relative weighting can be balanced for each

measurement type. The higher a priori sigmas than the post-fit residual RMSs is intended to reflect the systematic errors. It is safe not to weight data at its noise level or at the fit level, because it may lead to an optimistic covariance. Once an optimal relative weight of GPS was found, the optimal relative weighting for DORIS was also re-examined with the weightings of SLR and GPS fixed.

Table 5.2 shows each test case with the different a priori sigmas for relative weighting of each measurement type. To find an optimal weighting for GPS, a priori sigmas between 3 cm and 50 cm were applied for GPS, while a priori sigmas for SLR and DORIS were fixed to 10 cm and 2 mm/s respectively as shown in Table 5.2(a). The optimal relative weight for GPS is determined based on the crossover test and the SLR residual test with solutions from each case.

Figure 5.8 and Table 5.3 show the comparison of the crossover test and the SLR residual test for the cases of the relative weighting for GPS. In Table 5.3(a), the averaged crossover Means over the cycles are between 0 and $-2$ mm for all of the cases, which means that orbits from all combined data types are well centered especially due to the contribution of SLR, although they show a scatter of about 8 or 7 mm. The crossover Means of cycle 11, 12 and 19 are persistently larger than 1 cm in amplitude regardless of GPS weightings, which may indicate that the accuracy of the altimeter data for those cycles is bad.

Table 5.3(a) also shows that downweighting GPS by increasing the

| Case | A priori sigmas for each measurement |
|---|---|
| **Case Gw03** | 3 cm for GPS, 10 cm for SLR and 2mm/s for DORIS |
| **Case Gw10** | 10 cm for GPS, 10 cm for SLR and 2mm/s for DORIS |
| **Case Gw20** | 20 cm for GPS, 10 cm for SLR and 2mm/s for DORIS |
| **Case Gw25** | 25 cm for GPS, 10 cm for SLR and 2mm/s for DORIS |
| **Case Gw30** | 30 cm for GPS, 10 cm for SLR and 2mm/s for DORIS |
| **Case Gw35** | 35 cm for GPS, 10 cm for SLR and 2mm/s for DORIS |
| **Case Gw50** | 50 cm for GPS, 10 cm for SLR and 2mm/s for DORIS |

(a) Cases for Orbit Solution with different GPS weightings

| Case | A priori sigmas for each measurement |
|---|---|
| **Case Dw01** | 1 mm/s for DORIS, 10 cm for SLR and 25 cm for GPS |
| **Case Dw02** | 2 mm/s for DORIS, 10 cm for SLR and 25 cm for GPS |
| **Case Dw03** | 3 mm/s for DORIS, 10 cm for SLR and 25 cm for GPS |
| **Case Dw04** | 4 mm/s for DORIS, 10 cm for SLR and 25 cm for GPS |
| **Case Dw05** | 5 mm/s for DORIS, 10 cm for SLR and 25 cm for GPS |
| **Case Dw10** | 10 mm/s for DORIS, 10 cm for SLR and 25 cm for GPS |

(b) Cases for Orbit Solution with different DORIS weightings

Table 5.2: Cases for GPS weightings and DORIS weightings

a priori sigmas from 3 cm to 50 cm interestingly increased the magnitude of crossover Means of orbits with combined data. The degradation of the orbit centering in the GPS-downweighted orbits with combined data might be interpreted as the increased influence of DORIS over SLR or GPS in the combined measurement which can have a negative effect on the orbit centering. Table 5.4(a) shows that the increase of DORIS weighting relative to GPS and SLR actually degrades the orbit centering, indicating that combined orbits with SLR and GPS performs better than the combined orbits with all three measurement types.

The averaged values of the crossover RMSs over cycles 8 to 20 in Figure 5.8(a) and Table 5.3(b) show that all of the crossover RMSs of orbits from **Case Gw15**, **Case Gw20**, **Case Gw25**, **Case Gw30** or **Case Gw35** appear very good, ranging between 5.86 cm and 5.88 cm. The crossover RMSs of either **Case Gw03** or **Case Gw50** are larger than 5.90 cm. This implies that the a priori sigma for the optimal relative weighting of GPS resides somewhere between 15 cm and 35 cm. However, the results are fairly insensitive over the range of weights, with any particular choice not always being the best over all of the cycles. In Figure 5.8(a), the crossover RMS of orbits from **Case Gw25** appears to be near the saddle point, indicating that the a priori sigma of 25 cm for GPS weighting provides the best orbit among the orbits with all three measurement types combined.

The SLR residual RMSs in Table 5.3(c) range from 0.9 to 1.3 cm. The decrease in the SLR residual RMS with the decrease of weighting for GPS

observed in Table 5.3(c) can be explained by considering that the downweight of GPS has the same effect to the upweight of SLR, and that the SLR residual RMS of the orbit always decreases as the weight of SLR to a orbit solution increases. Although the SLR residual RMS is an indicator of orbit accuracy, it reflects the orbit accuracy less and less as the weight of SLR increases.

Finally, with an optimal relative weight for GPS fixed at 25 cm, the contribution of DORIS was also re-examined. The combined data of both SLR and GPS without DORIS are expected to be more than adequate for Jason-1 POD, because of the dense and continuous tracking of GPS. Thus, the concern about DORIS is not only to find an optimal DORIS weighting, but also to find if inclusion of the DORIS data will improve the orbit accuracy. To find optimal weighting for DORIS, a priori sigmas for DORIS ranging from 1 mm/s to 10 mm/s are applied to each DORIS station, while a priori sigmas for SLR and GPS are fixed to 10 cm and 25 cm respectively as shown in Table 5.2(b).

In Figure 5.8(b) and Table 5.4, the results of the crossover test and SLR residual test from each case of DORIS weight are compared. When the crossover RMSs are compared cycle by cycle in Figure 5.8(b) and Table 5.4(b), there is no clear evidence that orbits of any one case of a certain DORIS weight outperform orbits of other cases throughout all cycles. However, the crossover RMS averaged over cycles 8 to 20, as shown in Figure 5.8(b), appears to favor 2 or 3 mm/s for the DORIS weight.

In terms of orbit centering, judged by Table 5.4(a), the orbits from **Case Dw10** with 10 mm/s of a priori sigma for DORIS are better centered

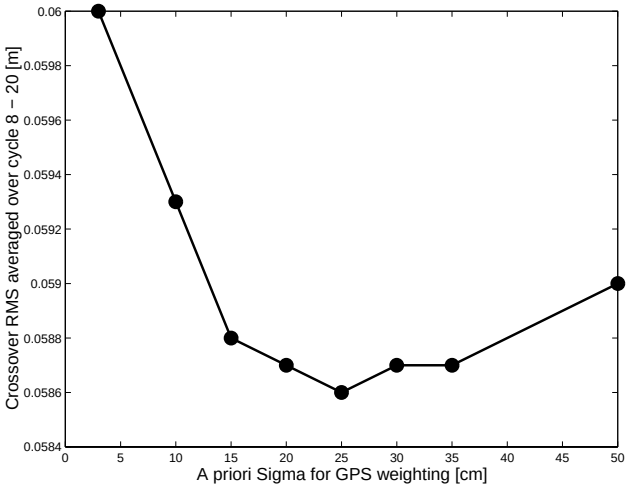


(a) Optimal Weighting for GPS (relative to 10 cm for SLR and 2 mm/s for DORIS)

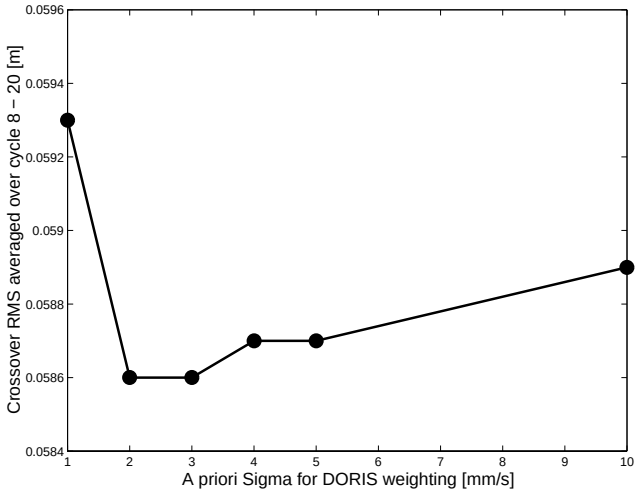


(b) Optimal Weighting for DORIS (relative to 10 cm for SLR and 25 cm for GPS)

Figure 5.8: Crossover RMS as a function of weight of (a) GPS and (b) DORIS. For GPS, a priori sigma of 25 cm appears to be optimal. However, the Crossover RMSs are insensitive to a range of GPS weights between 15 and 35 cm. For DORIS, a priori sigmas of 2 - 3 mm/s appear to be optimal.

| Cyc | Crossover Mean for each relative weighting strategy | | | | | | | |
|---|---|---|---|---|---|---|---|---|
| | Gw03 | Gw10 | Gw15 | Gw20 | Gw25 | Gw30 | Gw35 | Gw50 |
| 8 | 1.3 | 1.8 | 2.4 | 3.1 | 3.7 | 4.3 | 4.9 | 6.3 |
| 9 | 5.3 | 4.2 | 3.5 | 2.9 | 2.5 | 2.2 | 1.9 | 1.5 |
| 10 | 6.9 | 2.8 | .3 | -1.5 | -2.8 | -3.7 | -4.4 | -5.8 |
| 11 | -9.3 | -9.9 | -10.6 | -11.2 | -11.8 | -12.4 | -12.9 | -14.0 |
| 12 | -13.1 | -11.9 | -11.5 | -11.4 | -11.3 | -11.4 | -11.4 | -11.4 |
| 13 | 2.3 | 3.1 | 1.2 | .2 | -.9 | -1.6 | -2.1 | -3.5 |
| 14 | -2.7 | -4.3 | -5.2 | -5.7 | -6.0 | -6.2 | -6.3 | -6.4 |
| 15 | -5.8 | -5.5 | -5.6 | -5.7 | -6.0 | -6.1 | -6.3 | -6.5 |
| 16 | -11.2 | -9.5 | -8.6 | -8.0 | -7.5 | -7.2 | -6.9 | -6.2 |
| 17 | 4.9 | 4.7 | 4.1 | 3.8 | 3.7 | 3.7 | 3.8 | 4.2 |
| 18 | .0 | -1.9 | -3.3 | -4.3 | -5.0 | -5.4 | -5.7 | -6.0 |
| 19 | 12.0 | 11.5 | 11.3 | 11.4 | 11.7 | 12.0 | 12.3 | 12.9 |
| 20 | 9.3 | 7.6 | 6.6 | 6.0 | 5.6 | 5.4 | 5.4 | 5.5 |
| Mean | 0.0 | -0.6 | -1.2 | -1.6 | -1.9 | -2.0 | -2.1 | -2.3 |
| rms | 8.0 | 7.2 | 6.9 | 6.9 | 7.0 | 7.1 | 7.3 | 7.7 |

(a) Crossover Mean

| Cyc | Crossover RMS for each relative weighting strategy | | | | | | | |
|---|---|---|---|---|---|---|---|---|
| | Gw03 | Gw10 | Gw15 | Gw20 | Gw25 | Gw30 | Gw35 | Gw50 |
| 8 | 62.2 | 61.4 | 61.1 | 61.0 | 61.0 | 61.1 | 61.3 | 61.7 |
| 9 | 60.4 | 59.3 | 58.8 | 58.6 | 58.5 | 58.5 | 58.4 | 58.5 |
| 10 | 60.8 | 59.5 | 59.0 | 58.7 | 58.6 | 58.7 | 58.7 | 58.9 |
| 11 | 61.1 | 61.0 | 61.1 | 61.2 | 61.4 | 61.6 | 61.7 | 62.1 |
| 12 | 56.3 | 55.3 | 54.9 | 54.8 | 54.8 | 54.8 | 54.9 | 55.1 |
| 13 | 65.8 | 65.3 | 62.3 | 61.6 | 61.0 | 60.9 | 61.2 | 61.0 |
| 14 | 58.9 | 58.4 | 58.3 | 58.3 | 58.3 | 58.4 | 58.5 | 58.8 |
| 15 | 59.5 | 58.2 | 57.5 | 57.1 | 56.9 | 56.9 | 56.9 | 57.2 |
| 16 | 61.6 | 61.1 | 61.0 | 61.0 | 61.1 | 61.2 | 61.4 | 61.9 |
| 17 | 59.8 | 59.3 | 58.9 | 58.7 | 58.5 | 58.4 | 58.4 | 58.5 |
| 18 | 55.1 | 54.8 | 54.8 | 54.9 | 54.9 | 55.0 | 55.1 | 55.4 |
| 19 | 60.0 | 59.5 | 59.3 | 59.4 | 59.5 | 59.7 | 59.8 | 60.3 |
| 20 | 58.1 | 57.5 | 57.3 | 57.2 | 57.3 | 57.3 | 57.4 | 57.7 |
| Mean | 60.0 | 59.3 | 58.8 | 58.7 | 58.6 | 58.7 | 58.7 | 59.0 |
| rms | 2.7 | 2.7 | 2.3 | 2.2 | 2.2 | 2.2 | 2.3 | 2.3 |

(b) Crossover RMS

| Cyc | SLR residual RMS (> 70 deg) for each relative weighting strategy | | | | | | | |
|---|---|---|---|---|---|---|---|---|
| | Gw03 | Gw10 | Gw15 | Gw20 | Gw25 | Gw30 | Gw35 | Gw50 |
| 8 | 12.1 | 10.5 | 9.5 | 8.9 | 8.5 | 8.2 | 8.0 | 7.6 |
| 9 | 13.3 | 11.6 | 10.8 | 10.4 | 10.1 | 10.0 | 9.8 | 9.6 |
| 10 | 13.4 | 11.6 | 10.8 | 10.5 | 10.4 | 10.3 | 10.3 | 10.2 |
| 11 | 10.5 | 10.1 | 9.7 | 9.4 | 9.1 | 8.9 | 8.7 | 8.4 |
| 12 | 6.9 | 6.6 | 6.5 | 6.4 | 6.4 | 6.5 | 6.5 | 6.6 |
| 13 | 18.0 | 15.8 | 11.2 | 8.4 | 7.7 | 7.4 | 7.3 | 7.5 |
| 14 | 11.4 | 11.1 | 10.9 | 10.9 | 11.0 | 11.0 | 11.1 | 11.2 |
| 15 | 14.5 | 12.4 | 10.9 | 9.7 | 8.9 | 8.4 | 8.0 | 7.3 |
| 16 | 9.4 | 7.7 | 7.2 | 7.1 | 7.1 | 7.2 | 7.3 | 7.6 |
| 17 | 11.3 | 9.9 | 9.1 | 8.5 | 8.2 | 7.9 | 7.8 | 7.6 |
| 18 | 9.3 | 7.9 | 7.6 | 7.5 | 7.5 | 7.5 | 7.5 | 7.4 |
| 19 | 18.1 | 15.1 | 13.2 | 11.8 | 10.7 | 10.0 | 9.4 | 8.5 |
| 20 | 14.9 | 13.8 | 13.1 | 12.7 | 12.4 | 12.2 | 12.1 | 11.9 |
| Mean | 12.5 | 11.1 | 10.0 | 9.4 | 9.1 | 8.9 | 8.8 | 8.6 |
| rms | 3.3 | 2.8 | 2.1 | 1.9 | 1.8 | 1.7 | 1.7 | 1.6 |

(c) SLR residual RMS

Table 5.3: Optimal Weightings for GPS

| Cyc | Crossover Mean for each relative weighting strategy | | | | | |
|---|---|---|---|---|---|---|
| | Dw01 | Dw02 | Dw03 | Dw04 | Dw05 | Dw10 |
| 8 | 7.1 | 3.7 | 2.4 | 1.7 | 1.4 | 1.0 |
| 9 | 1.6 | 2.5 | 2.8 | 3.0 | 3.1 | 3.3 |
| 10 | -6.5 | -2.8 | -1.0 | -.1 | .3 | 1.0 |
| 11 | -17.6 | -11.8 | -9.1 | -7.8 | -7.0 | -5.8 |
| 12 | -13.6 | -11.3 | -10.1 | -9.5 | -9.2 | -8.6 |
| 13 | -2.3 | -.9 | -.5 | -.4 | -.8 | .0 |
| 14 | -7.8 | -6.0 | -5.3 | -5.0 | -4.9 | -4.7 |
| 15 | -7.0 | -6.0 | -5.2 | -4.8 | -4.6 | -4.1 |
| 16 | -7.4 | -7.5 | -7.4 | -7.2 | -7.2 | -7.1 |
| 17 | 3.6 | 3.7 | 4.1 | 4.4 | 4.7 | 5.1 |
| 18 | -6.2 | -5.0 | -4.3 | -4.0 | -3.7 | -3.1 |
| 19 | 14.8 | 11.7 | 10.1 | 9.3 | 8.8 | 8.1 |
| 20 | 8.0 | 5.6 | 4.5 | 4.0 | 3.7 | 3.2 |
| Mean | -2.6 | -1.9 | -1.5 | -1.3 | -1.2 | -0.9 |
| rms | 9.2 | 7.0 | 6.1 | 5.6 | 5.4 | 5.1 |

(a) Crossover Mean

| Cyc | Crossover RMS for each relative weighting strategy | | | | | |
|---|---|---|---|---|---|---|
| | Dw01 | Dw02 | Dw03 | Dw04 | Dw05 | Dw10 |
| 8 | 61.5 | 61.0 | 61.0 | 61.1 | 61.1 | 61.2 |
| 9 | 58.5 | 58.5 | 58.6 | 58.7 | 58.8 | 58.9 |
| 10 | 58.6 | 58.6 | 59.0 | 59.1 | 59.3 | 59.5 |
| 11 | 63.1 | 61.4 | 61.0 | 60.8 | 60.7 | 60.7 |
| 12 | 55.8 | 54.8 | 54.5 | 54.4 | 54.3 | 54.3 |
| 13 | 61.1 | 61.0 | 62.0 | 62.7 | 62.8 | 63.6 |
| 14 | 59.0 | 58.3 | 58.3 | 58.3 | 58.3 | 58.3 |
| 15 | 57.5 | 56.9 | 57.0 | 57.1 | 57.1 | 57.2 |
| 16 | 62.1 | 61.1 | 60.9 | 60.8 | 60.8 | 60.8 |
| 17 | 58.3 | 58.5 | 58.9 | 59.2 | 59.3 | 59.6 |
| 18 | 55.7 | 54.9 | 55.1 | 55.2 | 55.3 | 55.5 |
| 19 | 61.2 | 59.5 | 59.0 | 58.7 | 58.7 | 58.6 |
| 20 | 58.2 | 57.3 | 57.0 | 57.0 | 57.0 | 57.0 |
| Mean | 59.3 | 58.6 | 58.6 | 58.7 | 58.7 | 58.9 |
| rms | 2.3 | 2.2 | 2.3 | 2.4 | 2.4 | 2.5 |

(b) Crossover RMS

| Cyc | SLR residual RMS (> 70 deg) for each strategy | | | | | |
|---|---|---|---|---|---|---|
| | Dw01 | Dw02 | Dw03 | Dw04 | Dw05 | Dw10 |
| 8 | 8.3 | 8.5 | 8.7 | 8.7 | 8.8 | 8.9 |
| 9 | 11.0 | 10.1 | 9.9 | 9.8 | 9.8 | 9.7 |
| 10 | 10.9 | 10.4 | 10.3 | 10.3 | 10.3 | 10.3 |
| 11 | 10.8 | 9.1 | 8.6 | 8.5 | 8.5 | 8.4 |
| 12 | 7.8 | 6.4 | 6.3 | 6.2 | 6.2 | 6.2 |
| 13 | 9.3 | 7.7 | 8.5 | 9.1 | 9.2 | 20.6 |
| 14 | 12.1 | 11.0 | 10.6 | 10.5 | 10.4 | 10.3 |
| 15 | 8.7 | 8.9 | 9.2 | 9.3 | 9.4 | 9.4 |
| 16 | 9.0 | 7.1 | 6.6 | 6.4 | 6.3 | 6.1 |
| 17 | 9.9 | 8.2 | 7.7 | 7.6 | 7.5 | 7.4 |
| 18 | 10.9 | 7.5 | 6.7 | 6.5 | 6.5 | 6.4 |
| 19 | 10.3 | 10.7 | 11.0 | 11.1 | 11.2 | 11.3 |
| 20 | 12.8 | 12.4 | 12.3 | 12.3 | 12.3 | 12.3 |
| Mean | 10.1 | 9.1 | 9.0 | 8.9 | 9.0 | 9.8 |
| rms | 1.5 | 1.8 | 1.8 | 1.9 | 1.9 | 3.8 |

(c) SLR residual RMS

Table 5.4: Optimal Weightings for DORIS

than orbits from other cases with a priori sigmas ranging 1 mm/s to 5 mm/s. For example, the crossover Mean from **Case Dw01** with a priori sigma of 1 mm/s for DORIS is $-3$ mm with a scatter of 9 mm. When the DORIS data is downweighted by a factor of 10, the crossover Mean is reduced to $-1$ mm with a scatter of 5 mm, which strongly indicates that downweighting DORIS with respect to SLR and GPS may help the orbit centering.

Especially, for the cycles having shown large crossover Means, such as cycle 11, 12 and 19, the reduction of the magnitudes of the crossover Means resulted from downweighting DORIS is significant from $-1.8$ cm to $-0.6$ cm for cycle 11, from 1.4 cm to $-0.9$ cm for cycle 12, and from 1.5 cm to 0.8 cm for cycle 19. This implies that DORIS might degrade the orbit quality, when it is combined with SLR and DORIS tracking. The issue of the contribution of DORIS for the orbits with combined data will be discussed further in the next section, where the contribution of each measurement to the orbit quality will be investigated.

However, when GPS tracking is not adequate, DORIS tracking still plays an important role. In Table 5.4(c), overall SLR residual RMS is less than 1.3 cm over the cycles except for the cycle 13 in **Case Dw10**, where the SLR residual RMS is 2.1 cm. The crossover and SLR residual tests for cycle 13 in Table 5.4 included day 141, which is the day suffering from weak GPS tracking. Because of the weakness of GPS tracking, the orbit accuracy of **Case Dw10** for cycle 13 could easily be degraded, if the DORIS tracking is not given sufficient weight.

In summary, the a priori sigmas for an optimal relative weighting for each measurement type are 25 cm for GPS, 10 cm for SLR and 2 mm/s for DORIS. The results were not particularly sensitive over the range of 15 to 35 cm for the GPS weighting. For DORIS, the results were sharply degraded as the a priori sigma for DORIS was reduced to 1 mm/s. Also, it appears that upweighting DORIS, by applying smaller a priori sigmas, degrades the orbit accuracy at least in terms of the orbit centering, which implies that orbits from a combination of SLR and GPS with the exclusion of DORIS may perform better than orbits from a combination of all three measurement types. In the next section, the contribution of each measurement type will be examined and the best measurement combination will be determined.

## 5.4 Contribution of Each Measurement System to Orbit

To study the contribution of each measurement system to the orbit quality, as shown in Table 5.5, several cases with each different measurement combination were processed. The optimal subarc lengths for the estimation of the empirical parameters can be different from each combination of measurement types. For **Case DS**, the subarc lengths to estimate CT and 1-cpr T & N are 0.34492 day and 0.6898 day, respectively (**Case sub-24** in Table 4.12). For GPS-only orbits of **Case G**, the subarc lengths to estimate CT and 1-cpr T & N were 3 hour and 9 hour (**Case sub1.5-4.5**). For other combined orbits of other cases, 3-hour subarc for the estimation of CT and 6-hour subarc for estimation of 1-cpr T & N (**Case sub1.5-3**) were used. For the weight

of each measurement, 10-cm a priori sigma for SLR, 25-cm a priori sigma for GPS and 2-mm/s a priori sigma for DORIS were used. For each case, the same measurement model for each measurement type and the same dynamic models were employed.

| Case | Combined System | Estimation Strategy |
|---|---|---|
| **Case DS** | DORIS+SLR | with **Case sub-24** |
| **Case G** | GPS-only | with **Case sub1.5-4.5** |
| **Case GD** | GPS+DORIS | with **Case sub1.5-3** & **Case Gw25** |
| **Case GS** | GPS+SLR | with **Case sub1.5-3** & **Case Gw25** |
| **Case GDS** | GPS+SLR+DORIS | with **Case sub1.5-3** & **Case Gw25** |

Table 5.5: Cases for Orbit Solution with Different Data Combination

In Table 5.6, the crossover tests and SLR residual tests are compared for the orbits with each different combination of measurement types. In Table 5.6(a), the inertial centering offsets of orbits from **Case G** and **Case GS** are 0.6 mm and $-0.7$ mm, respectively. The orbits of **Case GS** are expected to be well-centered by the contribution of SLR, but the GPS-only orbits also appear to be well-centered, when terms longer than several cycles are considered. While the offset of orbits from **Case G** is highly dispersed cycle by cycle with a 9-mm rms, the offset of orbits from **Case GS** appears to be stable for each cycle with a 5-mm rms. Especially, the orbit centering of cycles 11, 12, 16, 19 and 20 show significant improvement by combining SLR with GPS.

However, addition of DORIS to GPS increased the orbit centering offset from 0.6 mm of **Case G** to $-1.6$ mm of **Case GD**. The scatter of the offset of each cycle also increased by adding DORIS to GPS, which implies that

the contribution of DORIS to GPS is not as significant as the contribution of SLR to GPS. On the contrary, adding DORIS to GPS appears to degrade the centering of orbit. Regardless of the possibility of orbit centering degradation by adding DORIS to GPS, the comparison of the crossover RMSs from **Case G** (5.97 cm) and **Case GD** (5.93 cm) in Table 5.6(b) implies that there might be a marginal contribution to the orbit accuracy when DORIS is combined with GPS. The SLR residual RMSs of **Case G** and **Case GD** in Table 5.6(c) also show the contribution of DORIS to GPS from 1.24 cm to 1.16 cm.

The contribution of SLR to GPS for orbit accuracy, on the other hand, is more significant than the contribution of DORIS to GPS. Table 5.6(b) shows that the crossover RMS of **Case GS** is 5.87 cm, compared to 5.93 cm from **Case GD**. The SLR residual RMSs in Table 5.6(c) also show that SLR contributes to GPS for orbit accuracy more than DORIS from 1.16 cm to 0.87 cm.

Although the significant contribution of SLR to GPS is clearly shown in both the crossover test and the SLR residual test, the contribution of DORIS to GPS is uncertain except particular incidents of big loss of GPS tracking data, which occurred on Day 141 of cycle 13. To find whether DORIS combined with SLR/GPS improves the orbit accuracy or degrades it, the orbits from **Case GS** and **Case GDS** can be compared in Table 5.6. The comparison showed that the addition of DORIS degraded orbit centering from $-0.7$ mm to $-1.9$ mm and the scatter of the crossover Means from each cycle also increased.

The degradation of orbit centering with the increase of DORIS's weight-

| Cyc | Crossover Mean for each Data Combination | | | | |
|---|---|---|---|---|---|
| | Case DS† | Case G | Case GD | Case GS | Case GDS |
| 8 | 4.5 | 2.1 | 6.1 | .9 | 3.7 |
| 9 | 2.2 | 5.5 | 3.8 | 3.4 | 2.5 |
| 10 | -5.4 | 6.6 | -.8 | 1.3 | -2.8 |
| 11 | -10.6 | -7.5 | -17.2 | -4.8 | -11.8 |
| 12 | -9.1 | -13.5 | -15.9 | -8.4 | -11.3 |
| 13 | -2.6 | 3.2 | .4 | .4 | -1.0 |
| 14 | -6.9 | -1.1 | -5.6 | -4.6 | -6.0 |
| 15 | -3.9 | -6.5 | -6.9 | -3.8 | -6.0 |
| 16 | -3.8 | -12.0 | -10.0 | -7.0 | -7.5 |
| 17 | 4.2 | 5.6 | 2.7 | 5.2 | 3.7 |
| 18 | -5.0 | -.7 | -3.2 | -2.8 | -5.0 |
| 19 | 8.2 | 12.8 | 15.3 | 7.9 | 11.7 |
| 20 | 7.9 | 13.0 | 11.0 | 3.1 | 5.6 |
| Mean | -1.6 | 0.6 | -1.6 | -0.7 | -1.9 |
| rms | 6.3 | 8.5 | 9.7 | 4.9 | 7.0 |

(a) Crossover Mean

| Cyc | Crossover RMS for each Data Combination | | | | |
|---|---|---|---|---|---|
| | Case DS† | Case G | Case GD | Case GS | Case GDS |
| 8 | 62.5 | 61.8 | 61.6 | 61.2 | 61.0 |
| 9 | 59.7 | 59.3 | 59.2 | 58.9 | 58.5 |
| 10 | 62.5 | 61.3 | 58.8 | 59.6 | 58.6 |
| 11 | 63.1 | 60.9 | 62.8 | 60.5 | 61.4 |
| 12 | 56.5 | 55.7 | 56.4 | 54.3 | 54.8 |
| 13 | 62.4 | 62.1 | 60.9 | 60.9 | 60.0 |
| 14 | 59.8 | 58.4 | 58.6 | 58.4 | 58.3 |
| 15 | 58.0 | 60.1 | 58.0 | 57.2 | 56.9 |
| 16 | 62.0 | 62.9 | 61.6 | 60.8 | 61.1 |
| 17 | 60.4 | 59.6 | 58.6 | 59.7 | 58.5 |
| 18 | 59.2 | 55.6 | 54.8 | 55.6 | 54.9 |
| 19 | 61.8 | 59.6 | 60.8 | 58.6 | 59.5 |
| 20 | 57.0 | 58.2 | 58.3 | 57.0 | 57.3 |
| Mean | 60.4 | 59.7 | 59.3 | 58.7 | 58.5 |
| rms | 2.2 | 2.3 | 2.2 | 2.1 | 2.1 |

(b) Crossover RMS

| Cyc | SLR residual RMS (> 70 deg) for each Data Combination | | | | |
|---|---|---|---|---|---|
| | Case DS† | Case G | Case GD | Case GS | Case GDS |
| 8 | 10.5 | 11.9 | 10.6 | 8.9 | 8.5 |
| 9 | 11.9 | 13.0 | 12.9 | 9.7 | 10.1 |
| 10 | 10.5 | 13.1 | 12.3 | 10.3 | 10.4 |
| 11 | 8.1 | 13.5 | 11.8 | 8.3 | 9.1 |
| 12 | 7.1 | 7.8 | 8.2 | 6.2 | 6.4 |
| 13 | 10.2 | 8.9 | 10.0 | 6.9 | 7.2 |
| 14 | 12.6 | 10.1 | 11.8 | 10.3 | 11.0 |
| 15 | 9.1 | 15.3 | 11.7 | 9.4 | 8.9 |
| 16 | 7.3 | 13.2 | 9.7 | 6.0 | 7.1 |
| 17 | 7.8 | 11.4 | 12.1 | 7.4 | 8.2 |
| 18 | 8.7 | 9.0 | 10.8 | 6.4 | 7.5 |
| 19 | 8.2 | 17.5 | 15.0 | 11.4 | 10.7 |
| 20 | 10.6 | 16.3 | 14.4 | 12.3 | 12.4 |
| Mean | 9.4 | 12.4 | 11.6 | 8.7 | 9.0 |
| rms | 1.8 | 2.9 | 1.9 | 2.1 | 1.8 |

† For **Case DS**, each full cycle is used for the statistics

(c) SLR residual RMS

Table 5.6: Orbit Improvement with Data Combination. (a) Orbit centering of **Case GS** (GPS+SLR) is best. SLR residual RMSs of less than 1.2 cm are promissing.

| Cyc | X bias ( Case GS VS.) | | | |
|---|---|---|---|---|
| | Case DS | Case G | Case GD | Case GDS |
| 8 | -9.8 | .6 | -4.3 | -3.4 |
| 9 | -6.5 | 1.6 | .1 | -1.8 |
| 10 | -4.7 | 1.7 | -1.0 | -1.9 |
| 11 | -6.3 | .2 | -3.3 | -.4 |
| 12 | -3.0 | -1.5 | -3.5 | -3.1 |
| 13 | .2 | 1.2 | 2.5 | 1.2 |
| 14 | 4.5 | -2.3 | -2.6 | -.4 |
| 15 | 6.7 | -3.1 | -.8 | 1.0 |
| 16 | 5.2 | -3.1 | -.7 | 1.6 |
| 17 | -.5 | -1.6 | -2.8 | -1.5 |
| 18 | -3.1 | -1.2 | -2.5 | -2.1 |
| 19 | -5.2 | 5.0 | -.6 | -2.9 |
| 20 | -7.3 | 3.4 | .5 | 5.0 |
| Mean | -2.3 | .1 | -1.4 | -.7 |
| rms | 5.2 | 2.5 | 1.9 | 2.4 |

(a) X bias

| Cyc | Y bias for each Data Combination | | | |
|---|---|---|---|---|
| | Case DS | Case G | Case GD | Case GDS |
| 8 | -5.5 | 4.4 | 2.9 | -.2 |
| 9 | -3.0 | 7.4 | 2.1 | .1 |
| 10 | -2.8 | 4.9 | 2.6 | 1.6 |
| 11 | -4.9 | 1.0 | 2.5 | 1.2 |
| 12 | -5.4 | .8 | 4.1 | 2.2 |
| 13 | -11.1 | -.5 | 3.4 | 1.8 |
| 14 | 1.0 | -4.5 | .9 | 2.5 |
| 15 | 1.0 | -2.5 | 1.8 | 2.5 |
| 16 | -1.1 | -3.0 | -1.0 | .5 |
| 17 | -7.6 | -8.5 | -3.7 | .9 |
| 18 | -5.5 | -5.0 | -1.5 | .1 |
| 19 | -7.7 | -.6 | -.8 | .0 |
| 20 | -12.7 | -1.8 | -1.9 | -.6 |
| Mean | -5.0 | -.6 | .9 | 1.0 |
| rms | 4.2 | 4.4 | 2.4 | 1.1 |

(b) Y bias

| Cyc | Z bias for each Data Combination | | | |
|---|---|---|---|---|
| | Case DS | Case G | Case GD | Case GDS |
| 8 | -1.8 | .7 | -.7 | -1.3 |
| 9 | .5 | .0 | .2 | -1.2 |
| 10 | -.1 | 1.6 | .1 | -1.1 |
| 11 | -7.4 | 1.6 | .7 | -2.8 |
| 12 | -.7 | 2.8 | 2.0 | 1.1 |
| 13 | 3.7 | -.5 | -2.6 | -1.2 |
| 14 | -5.6 | -2.4 | .5 | .7 |
| 15 | 6.7 | 2.5 | 6.1 | 3.1 |
| 16 | 2.0 | -1.8 | 2.0 | 1.7 |
| 17 | -.5 | 2.6 | 4.3 | 1.6 |
| 18 | 6.2 | .8 | 3.9 | 2.5 |
| 19 | -.2 | 5.7 | 4.4 | 1.6 |
| 20 | -4.5 | 2.2 | 3.5 | 1.2 |
| Mean | -.1 | 1.2 | 1.9 | .4 |
| rms | 4.2 | 2.1 | 2.5 | 1.8 |

(c) Z bias

Table 5.7: Orbit Bias in a Body-fixed Frame with each Data Combination. Each case is compared to **Case GS** (GPS+SLR) assuming that this is probably the best centered solution.

ing in the combined orbits can be also seen in Table 5.4(a). In Table 5.4(a), the magnitudes of the crossover Means increased from −9 mm to −26 mm with the increase of the DORIS' weighting with a priori sigmas from 10 mm/s to 1 mm/s. In fact, DORIS appears to degrade the orbit centering not only in the orbits of **Case GDS**, but also in the orbits of **Case DS**. Table 5.3(a) shows that the magnitude of the crossover Means increased from 0 mm to −2 mm with the decrease of the relative weight of GPS in the orbits of **Case GDS** with all three measurement types, which indicates that GPS is a relatively well-centered system in the long term, unlike DORIS.

In Table 5.6, the comparison of the crossover RMSs and the SLR residual RMSs from **Case GS** and **Case GDS** does not show much difference.

In summary, except for the duration when GPS tracking is not adequate, DORIS appears to be redundant or degrade orbit centering when it is combined with GPS and SLR. For all of the cases with or without a combination of measurement types, the crossover Means range between 0 mm and −2 mm, the crossover RMSs range between 5.9 cm and 6.0 cm, and SLR residual RMSs range between 0.9 cm and 1.3 cm. The SLR residual RMSs from **Case G** and **Case GD** are 1.24 cm and 1.16 cm, respectively, which are quite promising results as an absolute independent measure because **Case G** (GPS-only) and **Case GD** (GPS+DORIS) do not include the SLR data for the POD process.

## 5.5 Gravity Model Comparison with Mixed Orbits

Orbits from a combination of any two systems will be called the 'mixed orbits'. In this section, mixed orbits from each gravity model will be compared. The gravity models tested were 1) JGM-3, 2) EGM96, 3) TEG4 and 4) a preliminary GRACE gravity model (GGM01S) as shown in Table 5.8. All of the orbits in the table were processed with the combination of GPS and SLR systems.

The JGM-3 [Tapley *et al.*, 1996] gravity model contains information from 34 satellites, with a wide spectrum of different inclinations and altitudes. EGM96 [Lemoine *et al.*, 1998] is a geopotential model consisting of: (1) a combination solution to degree and order 70; (2) a block diagonal solution from degree 71 to 359; and (3) the quadrature solution at degree 360. As well as surface gravity data from many different regions of the globe, other data that contributed to EGM96 are direct satellite altimetry from T/P, ERS-1 and GEOSAT, and satellite tracking to over 20 satellites. The TEG4 (the latest in a series of Texas Earth Gravity (TEG) models) gravity model is complete to degree and order 180. The model includes new SLR and DORIS tracking data for 13 satellites, including Lageos I and II, Etalon I and II, Starlette, Stella, Ajisai, BEC, Geos-3, GFZ, SPOT-2, TOPEX and Westpac, and 20 cycles of GPS data for TOPEX, and SLR and PRARE data from ERS-2. Surface gravity anomaly data and satellite altimeter-derived marine geoid undulations were also included. The preliminary GRACE gravity model (GGM01S, 120×120) used in this study was recently developed at CSR based

on GRACE data of 111 days.

| Case | Gravity Model |
|---|---|
| **Case JGM3** | JGM3 |
| **Case EGM96** | EGM96 2000 |
| **Case TEG4** | TEG4 2000 |
| **Case GGM01S** | a preliminary Grace gravity solution |

Table 5.8: Gravity Models

The sensitivity of the orbits to the geopotential depends on the altitude, inclination and eccentricity of the satellite. The satellites with higher altitude are more sensitive to the lower wave length parts of the gravity field. The inclinations of the satellites determine the global coverage of the gravity model.

Table 5.9 summarizes the results of the crossover test and the SLR residual test for the orbits from different gravity models. The averaged crossover RMS of the orbits from EGM96 shows a relatively larger value, 5.92 ($\pm$0.22) cm, compared with orbits from other gravity models. The averaged crossover Mean of the orbits from TEG4, which is -1.6($\pm$4.3) mm, also appeared relatively larger than orbits from other gravity models. Thus, compared among EGM96, TEG4, and JGM3, JGM3 still appears to be a better choice from these three gravity models for Jason-1 POD.

Out of the four gravity models compared, orbits from the GRACE gravity model clearly outperform orbits from other gravity models in both aspects of the crossover test and the SLR residual test. Their averaged crossover RMS over the cycles is 5.83($\pm$0.23) cm, which was reduced modestly from the aver-

| Cyc | Crossover Mean for each Gravity Model | | | |
|---|---|---|---|---|
| | JGM3 | EGM96 | TEG4 | GRACE |
| 8 | .9 | 3.9 | 1.8 | 2.3 |
| 9 | 3.4 | 2.8 | 2.9 | 3.3 |
| 10 | 1.3 | 3.4 | .1 | .9 |
| 11 | -4.8 | -3.2 | -5.0 | -4.3 |
| 12 | -8.4 | -8.9 | -6.9 | -6.5 |
| 13 | .4 | 4.3 | -1.5 | 1.0 |
| 14 | -4.6 | -4.0 | -5.2 | -5.5 |
| 15 | -3.8 | -3.5 | -1.8 | -2.4 |
| 16 | -7.0 | -6.0 | -9.0 | -5.9 |
| 17 | 5.2 | 8.2 | 2.8 | 7.3 |
| 18 | -2.8 | -2.2 | -3.6 | -2.3 |
| 19 | 7.9 | 7.2 | 5.7 | 7.4 |
| 20 | 3.1 | 3.0 | -.8 | 2.0 |
| Mean | -.7 | .4 | -1.6 | -.2 |
| rms | 4.9 | 5.3 | 4.3 | 4.7 |

(a) Crossover Mean

| Cyc | Crossover RMS for each Gravity Model | | | |
|---|---|---|---|---|
| | JGM3 | EGM96 | TEG4 | GRACE |
| 8 | 61.2 | 62.1 | 61.4 | 60.9 |
| 9 | 58.9 | 59.3 | 58.9 | 58.4 |
| 10 | 59.6 | 59.9 | 58.8 | 59.0 |
| 11 | 60.5 | 60.7 | 61.2 | 60.6 |
| 12 | 54.3 | 55.4 | 53.8 | 54.0 |
| 13 | 60.9 | 62.5 | 61.1 | 61.0 |
| 14 | 58.4 | 58.9 | 58.3 | 57.9 |
| 15 | 57.2 | 58.1 | 57.3 | 57.0 |
| 16 | 60.8 | 61.5 | 61.5 | 60.8 |
| 17 | 59.7 | 59.9 | 58.9 | 58.9 |
| 18 | 55.6 | 55.9 | 56.3 | 55.5 |
| 19 | 58.6 | 58.8 | 57.9 | 57.6 |
| 20 | 57.0 | 56.9 | 56.5 | 55.9 |
| Mean | 58.7 | 59.2 | 58.6 | 58.3 |
| rms | 2.1 | 2.2 | 2.3 | 2.3 |

(b) Crossover RMS

| Cyc | SLR residual RMS (> 70 deg) | | | |
|---|---|---|---|---|
| | JGM3 | EGM96 | TEG4 | GRACE |
| 8 | 8.9 | 8.9 | 9.4 | 8.6 |
| 9 | 9.7 | 10.3 | 10.3 | 9.3 |
| 10 | 10.3 | 11.8 | 11.8 | 10.2 |
| 11 | 8.3 | 9.3 | 8.7 | 8.6 |
| 12 | 6.2 | 7.3 | 7.5 | 6.7 |
| 13 | 6.9 | 7.3 | 6.8 | 6.4 |
| 14 | 10.3 | 9.6 | 11.5 | 11.9 |
| 15 | 9.4 | 9.2 | 9.9 | 8.8 |
| 16 | 6.0 | 6.7 | 6.8 | 5.3 |
| 17 | 7.4 | 7.3 | 8.4 | 7.4 |
| 18 | 6.4 | 7.8 | 7.2 | 6.1 |
| 19 | 11.4 | 11.7 | 12.5 | 11.0 |
| 20 | 12.3 | 14.3 | 13.2 | 12.4 |
| Mean | 8.7 | 9.3 | 9.5 | 8.7 |
| rms | 2.1 | 2.2 | 2.2 | 2.3 |

(c) SLR residual RMS

Table 5.9: Gravity Model Comparison

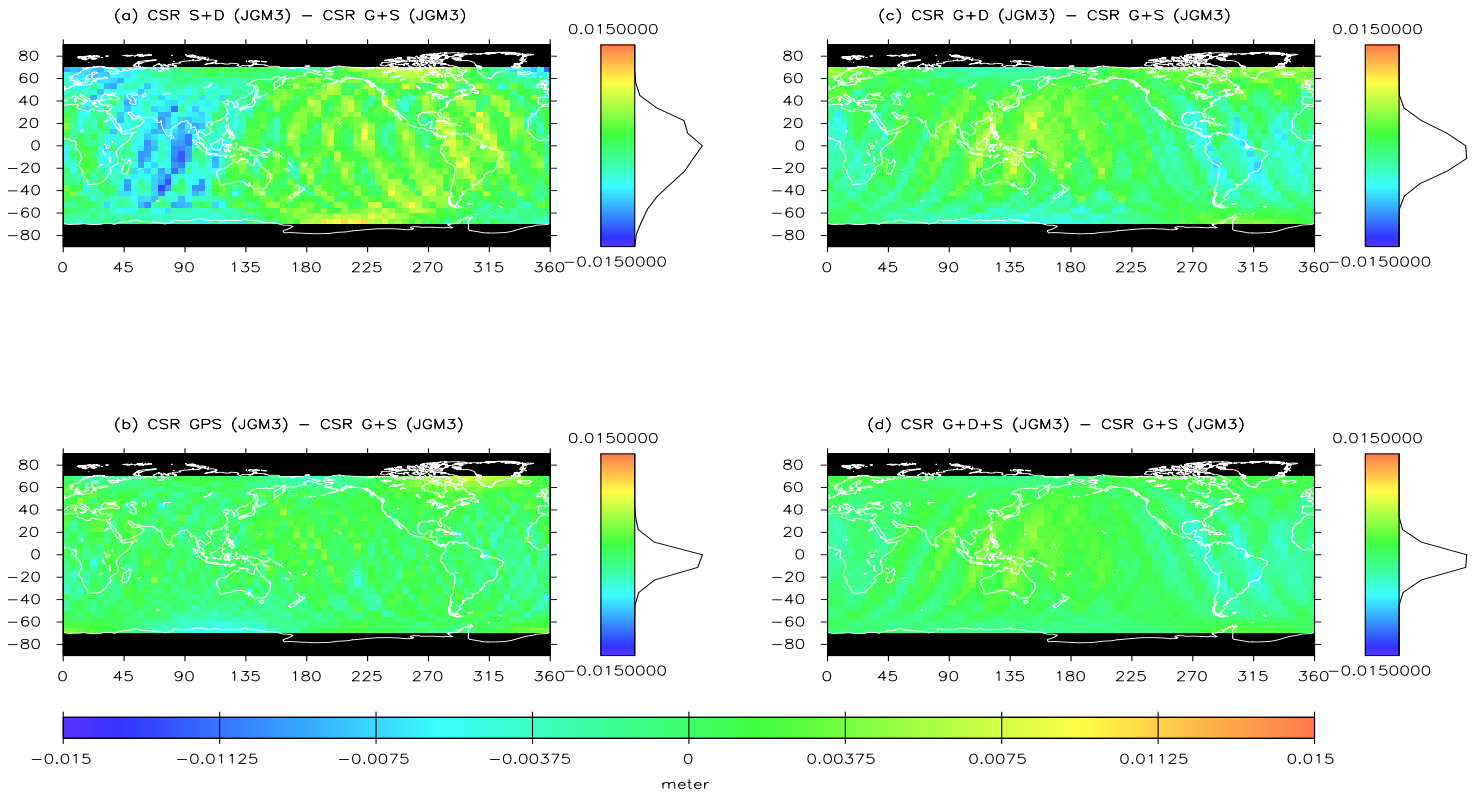


Figure 5.9: Geographically Correlated Orbit Errors in the Radial Component due to Difference of Tracking Data

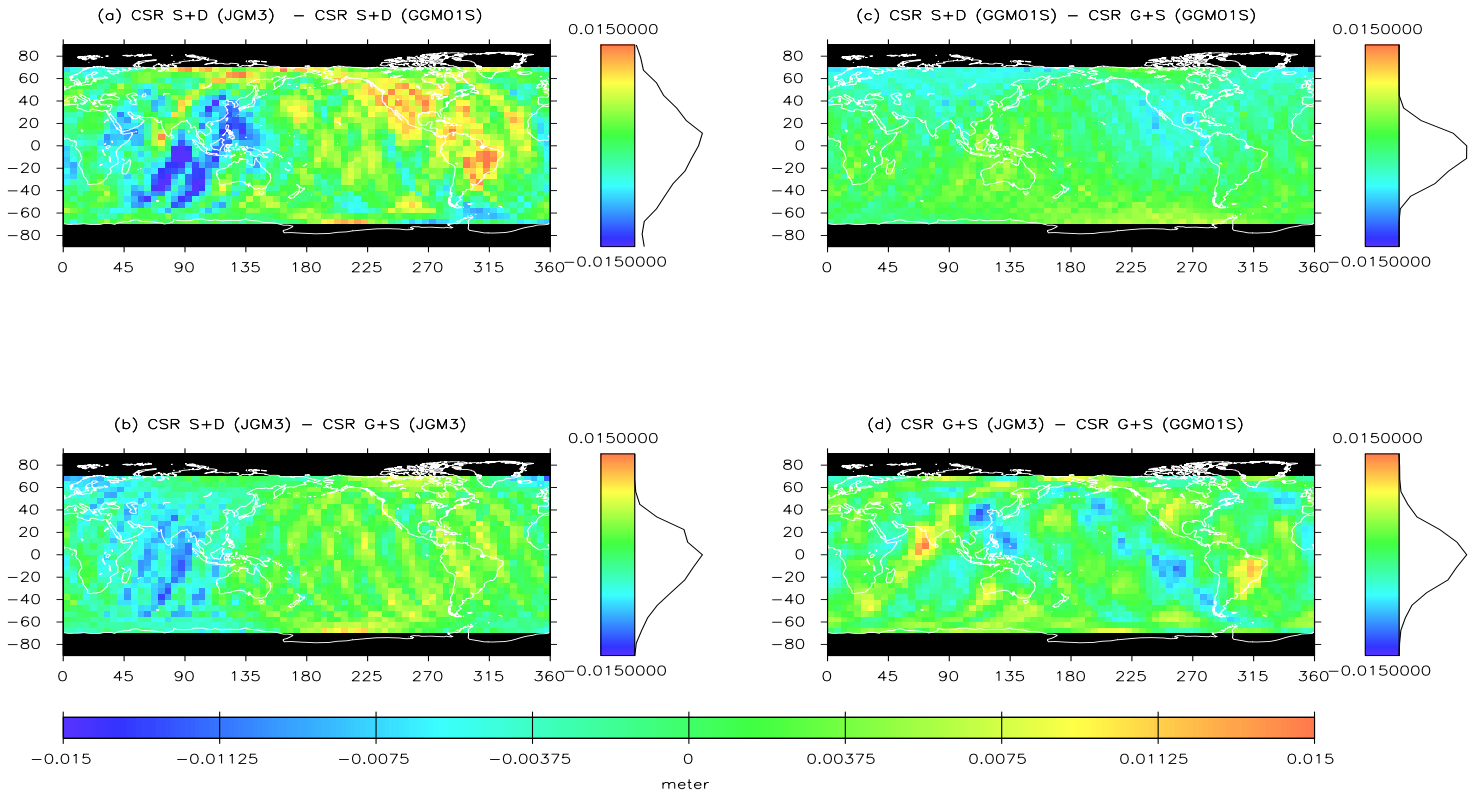


Figure 5.10: Geographically Correlated Orbit Errors in the Radial Component

aged crossover RMS of the orbits from JGM3 (5.87 cm). This is the reduction of 0.7 cm in the variance sense. Their averaged crossover Mean is $-0.2(\pm 4.7)$ mm, which is better than $-0.7(\pm 4.9)$ mm of the orbits from JGM3.

Figure 5.9 shows the Geographically Correlated Orbit Errors (GCE) in the radial component due to different tracking data combination. The mean values of the radial orbit differences were averaged from cycle 8 to cycle 20 using a bin size of 5 degrees by 5 degrees. The pattern in the difference between the CSR SLR+DORIS orbit (S+D) and the CSR GPS+SLR orbit (G+S) (see Figure 5.9(b)) can be ascribed to the geographically correlated orbit errors generated by the JGM3 gravity model used in both orbits. The dynamical SLR+DORIS orbit is subject to the GCE in JGM3 [Rosborough, 1986], whereas the heavy parameterization possible with the dense GPS tracking was able to remove a significant part of the correlated error. The radial differences among the orbits including GPS tracking data is much smaller (see Figure 5.9(b)-(d)).

The GCE between the CSR S+D orbits from the GGM01S model and from the JGM3 model, shown in Figure 5.10(a), indicates a pattern similar to the GCE between the CSR S+D orbit from JGM3 and the CSR G+S orbit from JGM3, as shown in Figure 5.10(b). This means that significant amount of the correlated orbit error left in the CSR S+D orbit from the JGM3 model is removed by using the GRACE gravity solution, GGM01S. When the GGM01S model is used for both orbit solutions, the correlated error between the CSR S+D orbit and the CSR G+S orbit is much smaller (see

Figure 5.10(c)). The GCE between the CSR G+S orbits from JGM3 model and from GGM01S model (see Figure 5.10(d)) shows the short wavelength part of geographically correlated error in JGM3. It appears that some of the small "hot spot" features are generated by the JGM3 gravity model, but even with the heavy parameterization used for the G+S orbit from JGM3 model, they could not be removed. However, these features were removed by using the GGM01S model for the G+S orbit. The GCE between the CSR S+D orbits from JGM3 model and from GGM01S model (Figure 5.10(a)) reflects both the short wavelength geographically correlated error in JGM3 along with additional long wavelength errors in JGM3.

## 5.6 External Orbit Comparison

Five groups such as CNES, DEOS, NASA/GSFC, and NASA/JPL including UT/CSR contributed to Jason-1 POD. Table 5.10 summarizes various orbits from each institute for comparison. Orbit **jpl** is a GPS-only orbit provided by JPL. Orbit **willis** provided by JPL/IGN is an orbit from the GPS data combined with the DORIS data. Both **jpl** and **willis** are based on the reduced dynamic approach implemented in GIPSY-OASIS II. CNES provided an SLR/DORIS orbit (**cnes1**) and two GPS-only orbits. Only one of CNES's GPS-only orbits was included in this comparison as **cnes2**, since the other GPS-only orbit which employed a form of relaxed-dynamics approach (ELFE) appeared to be slightly worse than **cnes2**. DEOS also provided a SLR/DORIS orbit (**deos**) and a GPS-only orbit. Their GPS-only orbit, which was not in-

cluded in this comparison, is similar to **cnes2**.

Orbits processed in CSR with various combination of measurement systems were compared with the external orbits. In Table 5.10, **csr1** is an mixed orbit from GPS and SLR systems, which is the same orbit to the orbit solution from **Case GS** in Section 5.4. Orbit **csr2**, which is the mixed solution of **Case GDS**, was processed by combining all three measurement systems. Orbit **csr3**, which is the solution of **Case DS**, utilized the SLR and DORIS data. Note that, at the time of this comparison, only CSR provided orbits with combination of SLR and GPS, and orbits with all three measurement systems. The orbits from other measurement combinations also can be seen in Section 5.4.

For the comparison on the same condition, each external orbit was interpolated in the same cycle spans with the same interval to the CSR's orbit, which is 10 seconds. Then, the performance test for each external orbit of each cycle was assessed in the overlapped duration of the orbit span and crossover altimeter data span, which are given in Table 4.2 and Table 3.7. For the orbit comparison, day 134 and 183 were further excluded from the orbit spans in Table 4.2.

In Table 5.11(c), SLR/DORIS orbits from CNES and DEOS show large orbit centering offset with the crossover Means of 8 mm and 7 mm respectively, while the crossover Means of SLR/DORIS orbits from CSR and GSFC are below 1 mm. The crossover RMSs of SLR/DORIS orbits from CNES and DEOS are 6.15 cm and 6.22 cm, while the crossover RMSs of SLR/DORIS orbits from

| Case | Combined System | Estimation approach |
|---|---|---|
| **csr1(=GS)** | GPS+SLR | dynamic |
| **csr2(=GDS)** | GPS+DORIS+SLR | dynamic |
| **csr3(=DS)** | SLR+DORIS | dynamic |
| **jpl** | GPS-only | reduced-dynamic |
| **willis** | GPS+DORIS | reduced-dynamic |
| **nasa1** | SLR+DORIS | dynamic |
| **nasa2** | GPS-only | reduced-dynamic |
| **cnes1** | SLR+DORIS | dynamic |
| **cnes2** | GPS-only | dynamic |
| **deos** | SLR+DORIS | dynamic |

Table 5.10: CSR's and External Orbits

CSR and GSFC are 6.07 cm and 6.04 cm with smaller scatter. The SLR residual RMS of Orbit **csr3** is 0.94 cm, and of Orbit **nasa1** is 1.12 cm, while Orbit **cnes1**'s and Orbit **deos**'s are 1.24 and 1.23 cm. Both the altimeter crossover test and SLR residual test show: 1) CSR's and NASA's SLR/DORIS orbits are better than CNES's and DEOS's, 2) CSR's and NASA's SLR/DORIS orbits are very close in quality to each other.

With the dynamic approach, GPS-only orbits generally appear to perform worse than the SLR/DORIS orbits in terms of the crossover RMS, although they appear to provide better orbit centering. However, the reduced-dynamic approach from JPL shows significant improvement compared with GPS-only orbits from other groups, which employed the dynamic approach. All of the statistics of the crossover test and the SLR residual test of Orbit **jpl** are much better than those from SLR/DORIS orbits or other GPS-only orbits.

| Cyc | Crossover Mean for each orbit | | | | | | | | | |
|---|---|---|---|---|---|---|---|---|---|---|
| | csr1 | csr2 | csr3 | jpl | willis | nasa1 | nasa2 | cnes1 | cnes2 | deos |
| 8 | .9 | 3.7 | 5.8 | 5.7 | 9.0 | 10.4 | 21.6 | 13.9 | 5.1 | 20.0 |
| 9 | 3.4 | 2.5 | 3.8 | 4.7 | 2.6 | 2.0 | 2.1 | 7.3 | -7.2 | 13.0 |
| 10 | 1.3 | 2.8 | -2.7 | 2.9 | -1.0 | -2.8 | 8.9 | -3.2 | -6.5 | .2 |
| 11 | -4.8 | -11.8 | -6.8 | -2.5 | -10.1 | -11.2 | -14.6 | -7.8 | -21.6 | -8.7 |
| 12 | -8.4 | -11.3 | -6.5 | -11.7 | -13.6 | -12.6 | -24.8 | -6.9 | -33.1 | -7.1 |
| 13 | .4 | -1.0 | 2.0 | 5.5 | -1.4 | 2.1 | 20.6 | 11.6 | -2.3 | -3.8 |
| 14 | -4.6 | -6.0 | -7.3 | -6.0 | -11.5 | -4.0 | -18.5 | 6.3 | -13.8 | 1.8 |
| 15 | -3.8 | -6.0 | -1.7 | -6.9 | -11.3 | 2.8 | -4.5 | 8.2 | -5.2 | 4.0 |
| 16 | -7.0 | -7.5 | -6.3 | -10.2 | -14.5 | -4.0 | -1.9 | 10.1 | 13.9 | 5.4 |
| 17 | 5.2 | 3.7 | 6.2 | -4.5 | -8.6 | 8.1 | — | 21.3 | 26.3 | 19.8 |
| 18 | -2.8 | -5.0 | -2.9 | -1.8 | -6.1 | -5.6 | — | 6.6 | -8.2 | 4.9 |
| 19 | 7.9 | 11.7 | 14.9 | 9.1 | 10.3 | 15.6 | — | 22.8 | 17.5 | 23.2 |
| 20 | 3.1 | 5.6 | 11.3 | 6.9 | 2.5 | 6.8 | — | 14.1 | 5.5 | 18.7 |
| Mean | -.7 | -1.9 | .8 | -.7 | -4.1 | .6 | -1.2 | 8.0 | -2.3 | 7.0 |
| rms | 4.9 | 7.0 | 7.3 | 6.9 | 8.4 | 8.3 | 16.4 | 9.5 | 16.1 | 10.9 |

- Starting epoch of CNES orbits for cycle 18 is 7/3/2002 03:02:13 (GPS)
- Starting epoch of NASA GPS orbit for cycle 9 is 4/4/2002 17:5:13 (GPS)
- Final epoch of NASA GPS orbit for cycle 13 is 5/21/2002 3:55: 0 (GPS)

(a) Crossover Mean

| Cyc | Crossover RMS for each orbit | | | | | | | | | |
|---|---|---|---|---|---|---|---|---|---|---|
| | csr1 | csr2 | csr3 | jpl | willis | nasa1 | nasa2 | cnes1 | cnes2 | deos |
| 8 | 61.2 | 61.0 | 62.7 | 60.8 | 60.8 | 62.7 | 65.4 | 64.6 | 65.9 | 68.7 |
| 9 | 58.9 | 58.5 | 59.9 | 57.8 | 57.7 | 60.0 | 58.2 | 60.6 | 62.8 | 61.7 |
| 10 | 59.6 | 58.6 | 62.1 | 59.1 | 59.0 | 60.7 | 60.2 | 66.3 | 59.9 | 61.5 |
| 11 | 60.5 | 61.4 | 62.5 | 60.3 | 61.8 | 62.6 | 63.5 | 61.4 | 65.8 | 64.1 |
| 12 | 54.3 | 54.8 | 56.1 | 56.6 | 57.2 | 57.8 | 61.8 | 56.5 | 67.0 | 56.2 |
| 13 | 60.9 | 60.0 | 62.5 | 60.9 | 60.9 | 61.9 | 59.4 | 63.4 | 61.7 | 64.0 |
| 14 | 58.4 | 58.3 | 59.8 | 57.8 | 59.2 | 58.3 | 63.5 | 59.7 | 60.5 | 60.3 |
| 15 | 57.2 | 56.9 | 58.0 | 57.8 | 58.4 | 57.5 | 58.0 | 58.0 | 57.8 | 58.9 |
| 16 | 60.8 | 61.1 | 62.0 | 62.0 | 63.0 | 61.2 | 62.6 | 62.9 | 62.8 | 62.6 |
| 17 | 59.7 | 58.5 | 60.9 | 57.8 | 57.9 | 61.0 | — | 63.8 | 66.1 | 64.1 |
| 18 | 55.6 | 54.9 | 59.4 | 55.2 | 56.7 | 57.7 | — | 56.8 | 57.0 | 58.6 |
| 19 | 58.6 | 59.5 | 61.2 | 58.0 | 58.6 | 62.0 | — | 63.4 | 61.4 | 64.7 |
| 20 | 57.0 | 57.3 | 61.6 | 59.3 | 57.6 | 61.4 | — | 61.5 | 59.9 | 65.0 |
| Mean | 58.7 | 58.5 | 60.7 | 58.7 | 59.1 | 60.4 | 61.4 | 61.5 | 62.2 | 62.3 |
| rms | 2.1 | 2.1 | 2.0 | 1.9 | 1.9 | 1.9 | 2.6 | 3.0 | 3.2 | 3.3 |

(b) Crossover RMS

| Cyc | SLR residual RMS (> 70 deg) for each orbit | | | | | | | | | |
|---|---|---|---|---|---|---|---|---|---|---|
| | csr1 | csr2 | csr3 | jpl | willis | nasa1 | nasa2 | cnes1 | cnes2 | deos |
| 8 | 8.9 | 8.5 | 10.5 | 9.2 | 7.5 | 9.9 | 9.7 | 10.2 | 11.2 | 11.0 |
| 9 | 9.7 | 10.1 | 11.9 | 11.7 | 13.4 | 10.5 | 10.5 | 15.1 | 18.3 | 12.0 |
| 10 | 10.3 | 10.4 | 10.5 | 9.5 | 12.0 | 12.3 | 10.7 | 17.0 | 12.4 | 11.1 |
| 11 | 8.3 | 9.1 | 8.1 | 19.8 | 10.5 | 7.0 | 8.9 | 9.5 | 12.2 | 10.1 |
| 12 | 6.2 | 6.4 | 7.1 | 8.8 | 10.9 | 15.0 | 8.5 | 8.8 | 16.0 | 12.3 |
| 13 | 6.9 | 7.2 | 10.2 | 9.0 | 12.0 | 10.7 | 9.5 | 10.8 | 8.6 | 15.4 |
| 14 | 10.3 | 11.0 | 12.6 | 10.6 | 11.5 | 13.5 | 13.6 | 11.5 | 15.6 | 16.4 |
| 15 | 9.4 | 8.9 | 9.1 | 10.2 | 11.9 | 10.0 | 13.8 | 10.7 | 11.9 | 10.4 |
| 16 | 6.0 | 7.1 | 7.2 | 8.3 | 9.8 | 10.3 | 13.7 | 14.8 | 16.7 | 9.9 |
| 17 | 7.4 | 8.2 | 7.8 | 9.0 | 13.2 | 10.3 | — | 17.3 | 16.1 | 12.3 |
| 18 | 6.4 | 7.5 | 8.7 | 11.5 | 15.0 | 10.7 | — | 8.2 | 8.7 | 10.1 |
| 19 | 11.4 | 10.7 | 8.2 | 12.1 | 14.5 | 11.0 | — | 13.5 | 17.8 | 13.3 |
| 20 | 12.3 | 12.4 | 10.6 | 12.7 | 15.7 | 14.0 | — | 13.7 | 17.7 | 15.9 |
| Mean | 8.7 | 9.0 | 9.4 | 11.0 | 12.1 | 11.2 | 11.0 | 12.4 | 14.1 | 12.3 |
| rms | 2.1 | 1.8 | 1.8 | 3.0 | 2.3 | 2.1 | 2.1 | 3.0 | 3.4 | 2.3 |

(c) SLR residual RMS

Table 5.11: External Orbit Comparison: **csr1** (GPS+SLR) is the best centered orbit. **csr1**, **csr2** (GPS+SLR+DORIS) and **jpl** (GPS-only) are three best orbits in terms of the crossover RMS..

| Cyc | X bias ( Case GS VS.) | | | | | | | | | |
|---|---|---|---|---|---|---|---|---|---|---|
| | csr1 | csr2 | csr3 | jpl | willis | nasa1 | nasa2 | cnes1 | cnes2 | deos |
| 8 | .0 | -3.4 | -9.8 | -8.0 | -7.8 | -8.3 | -9.4 | -6.6 | -5.1 | -10.5 |
| 9 | .0 | -1.8 | -6.5 | -4.6 | -3.9 | -6.2 | -7.3 | -1.4 | -.6 | -10.1 |
| 10 | .0 | -1.9 | -4.7 | -6.2 | -4.0 | -3.7 | -5.3 | -3.4 | -3.6 | -5.1 |
| 11 | .0 | -.4 | -6.3 | -4.7 | -5.2 | -7.3 | -6.1 | -9.2 | -9.3 | -4.5 |
| 12 | .0 | -3.1 | -3.0 | -3.6 | -2.5 | -3.8 | -4.6 | -7.5 | -5.9 | -1.1 |
| 13 | .0 | 1.2 | .2 | 2.3 | 6.0 | -3.0 | 2.8 | -2.6 | -3.2 | 4.5 |
| 14 | .0 | -.4 | 4.5 | 4.5 | 3.2 | 1.5 | 4.1 | -2.1 | -1.0 | 6.8 |
| 15 | .0 | 1.0 | 6.7 | 8.3 | 6.7 | 5.6 | 5.7 | 1.4 | 3.7 | 5.5 |
| 16 | .0 | 1.6 | 5.2 | 10.2 | 9.8 | 6.6 | 12.0 | 1.7 | 1.8 | 1.9 |
| 17 | .0 | -1.5 | -.5 | 6.4 | 5.8 | 1.6 | — | -3.0 | -1.1 | -3.7 |
| 18 | .0 | -2.1 | -3.1 | 1.4 | 4.3 | 2.6 | — | -4.3 | -1.5 | -2.1 |
| 19 | .0 | -2.9 | -5.2 | -.2 | .9 | -1.4 | — | -3.3 | .9 | -4.2 |
| 20 | .0 | 5.0 | -7.3 | -4.9 | -2.0 | -6.5 | — | -5.2 | -1.9 | -14.4 |
| Mean | .0 | -0.7 | -2.3 | .1 | .9 | -1.7 | -.9 | -3.5 | -2.1 | -2.8 |
| rms | .0 | 2.4 | 5.2 | 5.9 | 5.5 | 4.9 | 7.3 | 3.2 | 3.4 | 6.4 |

(a) X bias

| Cyc | Y bias ( Case GS VS.) | | | | | | | | | |
|---|---|---|---|---|---|---|---|---|---|---|
| | csr1 | csr2 | csr3 | jpl | willis | nasa1 | nasa2 | cnes1 | cnes2 | deos |
| 8 | .0 | -.2 | -5.5 | -3.4 | -3.6 | -7.7 | -6.8 | -4.4 | -6.4 | -7.9 |
| 9 | .0 | .1 | -3.0 | -5.8 | -3.2 | -3.2 | -7.1 | 3.4 | 1.9 | -4.4 |
| 10 | .0 | 1.6 | -2.8 | -2.3 | .3 | -1.2 | -6.2 | 5.3 | 5.7 | .9 |
| 11 | .0 | 1.2 | -4.9 | -1.5 | -.9 | -3.7 | -7.1 | 4.9 | 2.6 | -.2 |
| 12 | .0 | 2.2 | -5.4 | -.1 | 2.0 | -2.4 | -4.4 | 1.9 | -1.0 | .0 |
| 13 | .0 | 1.8 | -11.1 | 2.1 | 2.7 | -8.7 | -3.3 | -3.3 | -7.1 | -8.6 |
| 14 | .0 | 2.5 | 1.0 | 2.0 | 5.6 | 3.2 | -4.8 | 3.9 | 1.8 | .5 |
| 15 | .0 | 2.5 | 1.0 | 3.6 | 6.5 | 2.2 | -2.0 | 3.1 | -1.2 | -1.6 |
| 16 | .0 | .5 | -1.1 | .8 | 5.4 | -1.3 | -1.7 | -4.9 | -8.0 | -4.3 |
| 17 | .0 | .9 | -7.6 | .6 | 3.9 | -6.6 | — | -8.8 | -13.3 | -11.7 |
| 18 | .0 | .1 | -5.5 | -1.6 | .2 | -8.9 | — | -10.0 | -13.9 | -13.6 |
| 19 | .0 | .0 | -7.7 | -3.2 | -.8 | -8.3 | — | -8.9 | -12.7 | -9.7 |
| 20 | .0 | -.6 | -12.7 | -6.4 | -3.8 | -10.3 | — | -9.4 | -11.6 | -13.8 |
| Mean | .0 | 1.0 | -5.0 | -1.2 | 1.1 | -4.4 | -4.8 | -2.1 | -4.9 | -5.7 |
| rms | .0 | 1.1 | 4.2 | 3.0 | 3.6 | 4.4 | 2.1 | 6.0 | 6.8 | 5.5 |

(b) Y bias

| Cyc | Z bias ( Case GS VS.) | | | | | | | | | |
|---|---|---|---|---|---|---|---|---|---|---|
| | csr1 | csr2 | csr3 | jpl | willis | nasa1 | nasa2 | cnes1 | cnes2 | deos |
| 8 | .0 | -1.3 | -1.8 | .9 | 5.6 | 1.0 | -4.9 | 1.0 | 2.2 | -1.4 |
| 9 | .0 | -1.2 | .5 | 2.5 | 7.5 | .1 | 2.8 | 3.6 | 5.9 | -.1 |
| 10 | .0 | -1.1 | -.1 | 2.7 | 6.1 | -.3 | 4.3 | 4.6 | 12.1 | -1.5 |
| 11 | .0 | -2.8 | -7.4 | 2.2 | 4.4 | -2.7 | 2.3 | .5 | .3 | -.3 |
| 12 | .0 | 1.1 | -.7 | -1.0 | 3.8 | -2.1 | 3.3 | -4.7 | .4 | -1.6 |
| 13 | .0 | -1.2 | 3.7 | 1.7 | 4.9 | -1.3 | .8 | -8.4 | -1.8 | -2.2 |
| 14 | .0 | .7 | -5.6 | -4.9 | 2.7 | -2.6 | 10.6 | -.7 | 19.7 | 3.2 |
| 15 | .0 | 3.1 | 6.7 | .2 | 10.3 | 8.3 | 11.6 | 11.5 | 20.0 | 8.5 |
| 16 | .0 | 1.7 | 2.0 | -.6 | 11.3 | 5.2 | 13.5 | 5.1 | 11.6 | 5.8 |
| 17 | .0 | 1.6 | -.5 | .1 | 11.4 | 5.8 | — | 8.0 | -2.2 | 7.5 |
| 18 | .0 | 2.5 | 6.2 | 3.2 | 12.2 | 8.3 | — | 8.4 | -2.8 | 6.7 |
| 19 | .0 | 1.6 | -.2 | -.1 | 9.4 | 1.6 | — | 3.8 | 13.0 | 1.9 |
| 20 | .0 | 1.2 | -4.5 | 2.5 | 11.3 | 1.4 | — | 8.1 | 8.9 | -4.8 |
| Mean | .0 | .5 | -.1 | .7 | 7.8 | 1.7 | 4.9 | 3.1 | 6.7 | 1.7 |
| rms | .0 | 1.8 | 4.2 | 2.2 | 3.4 | 3.9 | 5.9 | 5.6 | 8.1 | 4.3 |

(c) Z bias

Table 5.12: Orbit Bias in a Earth-Centered Earth-Fixed Frame for External Comparison

However, the combined orbits from CSR such as Orbit **csr1** and Orbit **csr2** with the dynamic approach appear to be comparable to the orbit **jpl**. The crossover RMSs of **csr1** (5.87 cm) and **csr2** (5.85 cm) are close or better than the crossover RMS of **jpl** (5.87 cm). Also, the SLR residual RMSs of **csr1** (0.87 cm) and **csr2** (0.90 cm) are much better than the SLR residual RMS of **jpl** (1.10 cm) with smaller scatter, which was expected since **Case csr1** and **Case csr2** included SLR data for the orbit processing. Especially in cycle 12 and 16, where the weak tracking of GPS occurred (see Figure 4.2(a) and Table 4.3), the orbit centering of **Case csr1** appears to be much better than **Case jpl**.

The orbit centering of **csr1** is the best among all the orbits, with the crossover Mean of $-0.7$ ($\pm 4.9$) mm, which is also the smallest scatter. On the other hand, the Orbit **csr2** with all three measurement systems shows slightly degraded orbit centering with the crossover Mean of $-1.9$ ($\pm 7.0$) mm. As discussed previously in Section 5.4, the degradation of the orbit centering of **Case csr2** against **Case csr1** is due to the addition of DORIS, which somehow can be redundant or actually degrade the orbits when there are adequate GPS and SLR tracking. When we compare the two reduced-dynamic approach orbits with GPS-only (**Case jpl**) and with GPS/DORIS (**Case willis**), the degradation from the addition of DORIS can be observed again. By addition of the DORIS data to GPS, the magnitude of the crossover Mean increased from $-0.7$ mm to $-4.1$ mm, also the crossover RMS and the SLR residual RMS increased from 5.87 cm to 5.91 cm, and from 1.10 cm to 1.21 cm respectively.

Table 5.12 shows the orbit bias in each direction of each orbit solution in the Earth-Centered Earth-Fixed (ECEF) frame compared to Orbit **csr1**. Orbit **csr1**, which is the orbit solution from combination of GPS and SLR, is assumed to be the true orbit. Most of SLR/DORIS orbits from the dynamic approach such as **csr3**, **nasa1** and **deos** show biases from **csr1** of $-2\sim -3$ cm in X-direction, $-4\sim -6$ cm in Y-direction, and $0\sim 2$ cm in Z-direction. However, Orbit **jpl** from reduced-dynamic approach with the GPS-only tracking shows biases less than 1 cm in all directions while Orbit **willis** from reduced-dynamic approach with combination of GPS and DORIS shows a bias as large as 8 cm in Z-direction. It is unclear if this was a processing problem or the result of adding DORIS without also including the SLR data.

In summary, among the orbit solutions with the dynamic approach, CSR's two combined orbit solutions, **csr1** and **csr2**, performed best. Orbit **csr1** were processed by combining GPS and SLR systems, and Orbit **csr2** were processed by combining GPS, SLR and DORIS systems. Among the orbit solutions with the reduced-dynamic approach, Orbit **jpl** with GPS-only system performed best. The crossover Means of **csr1**, **csr2** and **jpl** are -0.7($\pm$4.9) mm, -1.9($\pm$7.0) mm and -0.7($\pm$6.9) mm respectively. The crossover RMSs of **csr1**, **csr2** and **jpl** are 5.87($\pm$0.21) cm, 5.85($\pm$0.21) cm and 5.87($\pm$0.19) cm respectively. The SLR residual RMSs of **csr1**, **csr2** and **jpl** are 0.87($\pm$0.21) cm, 0.90($\pm$0.18) cm and 1.10($\pm$0.30) cm respectively. In both approaches, DORIS combined to GPS appears to be redundant or even degrade the orbit centering in those cases where the GPS tracking alone is adequate. Especially,

without support from SLR, DORIS may significantly degrade the orbit centering. Overall, in the dynamic approach, a combination of GPS and SLR appears to perform best.

# Chapter 6

# Orbit Improvement by Optimal Network Selection of GPS Stations

As of August 2002, 335 stations of the International GPS Service (IGS) are available at `http://igscb.jpl.nasa.gov/network/list.html`, and about 200 ITRF2000 GPS station coordinate solutions are available with the SINEX format at `ftp://schubert.ensg.ign.fr/pub/itrf/itrf2000/`. For GPS orbit processing, a good performing station set should be selected, since it would be unreasonable to process the GPS data from all the stations, and processing all the data does not necessarily guarantee the best orbit solution.

Since December 2, 2001, Analysis Centers of the IGS have been providing GPS satellite orbits (ephemerides) that are referenced to a new terrestrial reference frame, called IGS2000 (or IGS00). IGS00, which is the IGS realization of ITRF2000, is composed of 51[1] stations updated from the original 51 stations of IGS97. IGS00 was designed to be consistent 'on the average sense' with the International Terrestrial Reference Frame of 2000 (ITRF2000 or ITRF00). Thus, the best fitting Helmert transformation between IGS00 and

[1]For the complete list of IGS00, refer to `ftp://igscb.jpl.nasa.gov/igscb/station/coord/IGS00P04_RS51.SNX.Z`. The station set used is updated from 51 stations to 54 stations later with minor changes in `IGS01P37_RS54.snx.Z`.

ITRF2000 for the set of 51 well-established, international GPS satellite tracking sites is the identity function, even though the IGS00 position and velocity for any particular site may differ slightly from its corresponding ITRF2000 position and velocity.

As of 2002, for CSR's nominal GPS orbits, we use coordinate information for the 51 IGS00 stations (see Table 6.1) to process the GPS tracking data. Out of these stations, several stations are not utilized at CSR, mainly because the data from these stations might be redundant or simply because they do not track the Jason-1 satellite steadily and reliably over the cycles. Thus, the GPS tracking data from about 40 to 43 stations (the "Nominal Set") have usually been processed to obtain the nominal orbit solutions discussed in the previous chapters. The number of stations in the Nominal Set may vary each day depending on each station's scheduling. However, the question of whether the nominal orbit solutions from the Nominal Set are the best orbit solutions or not when compared with orbits from other station sets has never been fully investigated.

The objective of this chapter is to develop a method of selecting the best performing and geographically well-distributed optimal station sets, and to assess their orbit quality compared to the orbits from the Nominal Set. Selecting optimal sets is expected to improve orbit solutions and the tuned gravity solution, not only by reducing poorer performing redundant stations, but also by improving the centering of orbits with better distributed stations.

First, before the introduction of the optimal set selection in Section

| site Id | DOMES Number | Lon(W) (deg) | Lat(N) (deg) | Height (m) | Location | Country | Agency |
|---|---|---|---|---|---|---|---|
| algo | 40104M002 | 281.9286 | 45.9588 | 202.0000 | Algonquin Park | Canada | NRCan/GSD |
| areq | 42202M005 | 288.5072 | -16.4655 | 2488.9294 | Arequipa | Peru | NASA/JPL |
| auck | 50209M001 | 174.8344 | -36.6028 | 132.0000 | Whangaparaoa | New Zealand | IGNS-JPL |
| bahr | 24901M002 | 50.6081 | 26.2091 | -17.0300 | Manama | Bahrain | NIMA |
| braz | 41606M001 | 312.1222 | -15.9474 | 1106.0413 | Brasilia | Brazil | IBGE |
| brmu | 42501S004 | 295.3030 | 32.3700 | -10.6190 | Bermuda | U.K. | NOAA |
| cas1 | 66011M001 | 110.5197 | -66.2834 | 22.5500 | Casey | Antarctica | AUSLIG |
| chat | 50207M001 | 183.4342 | -43.9558 | 58.0000 | Waitangi | New Zealand | IGNS-JPL |
| dav1 | 66010M001 | 77.9726 | -68.5773 | 44.5000 | Davis | Antarctica | AUSLIG |
| fair | 40408M001 | 212.5008 | 64.9780 | 319.0097 | Fairbanks | USA | JPL-GSFC |
| fort | 41602M001 | 321.5744 | -3.8774 | 20.4918 | Eusebio, Fortaleza | Brazil | NOAA |
| gode | 40451M123 | 283.1732 | 39.0217 | 14.5082 | Greenbelt | USA | NASA/JPL |
| gold | 40405S031 | 243.1108 | 35.4251 | 986.6644 | Goldstone | USA | NASA/JPL |
| graz | 11001M002 | 15.4935 | 47.0671 | 538.2900 | Graz | Austria | ISR |
| guam | 50501M002 | 144.8683 | 13.5893 | 201.9220 | Dededo | Guam | NASA/JPL |
| hob2 | 50116M004 | 147.4387 | -42.8047 | 41.1263 | Hobart | Australia | AUSLIG |
| hrao | 30302M004 | 27.6870 | -25.8901 | 1414.1877 | Krugersdorp | South Africa | HRAO-JPL |
| irkt | 12313M001 | 104.3162 | 52.2190 | 503.3816 | Irkutsk | Russia | DUT |
| kerg | 91201M002 | 70.2555 | -49.3515 | 74.0583 | Port aux Francais | Kerguelen Islands | CNES |
| kit3 | 12334M001 | 66.8800 | 39.1400 | 643.0000 | Kitab | Uzbekistan | GFZ |
| kokb | 40424M004 | 200.3351 | 22.1263 | 1167.3680 | Kokee Park, Waimea, | USA | NASA/JPL |
| kosg | 13504M003 | 5.8096 | 52.1784 | 97.8617 | Kootwijk | The Netherlands | DUT |
| kour | 97301M210 | 307.1940 | 5.2522 | -25.5700 | Kourou | French Guyana | ESA |
| kwj1 | 50506M001 | 167.7302 | 8.7222 | 38.2688 | Kwajalein Atoll | Marshall Islands | NASA/JPL |
| lhas | 21613M001 | 91.1040 | 29.6573 | 3622.0000 | LHASA | China | BKG |
| mac1 | 50135M001 | 158.9358 | -54.4995 | -6.6900 | MacQuarie Island | Southern Ocean | AUSLIG |
| mali | 33201M001 | 40.1944 | -2.9959 | 22.7200 | Malindi | Kenya | ESA |
| mas1 | 31303M002 | 344.3667 | 27.7637 | 197.3000 | Maspalomas | Spain | ESA |
| mate | 12734M008 | 16.7045 | 40.6491 | 535.6000 | MATERA | ITALY | ASI |
| mcm4 | 66001M003 | 166.6693 | -77.8383 | 97.9201 | Ross Island | Antarctica | NASA/JPL |
| mdo1 | 40442M012 | 255.9850 | 30.6805 | 2005.4936 | Fort Davis | USA | NASA/JPL |
| nlib | 40465M001 | 268.4251 | 41.7716 | 207.0648 | North Liberty | USA | NASA/JPL |
| nyal | 10317M001 | 11.8700 | 78.9300 | 82.0000 | Ny-Alesund | Norway | NMA |
| ohig † | * | * | * | * | * | * | * |
| onsa | 10402M004 | 11.9255 | 57.3953 | 46.5789 | ONSALA | SWEDEN | OSO |
| pert | 50133M001 | 115.8852 | -31.8019 | 12.9200 | Perth | Australia | ESA |
| pie1 | 40456M001 | 251.8811 | 34.3015 | 2347.7250 | Pie Town | USA | NASA/JPL |
| pots | 14106M003 | 13.0700 | 52.3800 | 174.0000 | Potsdam | Germany | GFZ |
| sant | 41705M003 | 289.3314 | -33.1503 | 723.0399 | Santiago | Chile | NASA/JPL |
| shao | 21605M002 | 121.2004 | 31.0996 | 22.0933 | Sheshan | China | CAS-JPL |
| thu1 | 43001M001 | 291.2120 | 76.5373 | 55.0030 | Thule | Greenland | KMS-JPL |
| tidb | 50103M108 | 148.9800 | -35.3992 | 665.3818 | Tidbinbilla | Australia | NASA/JPL |
| trom | 10302M003 | 18.9383 | 69.6639 | 132.0000 | Tromsoe | Norway | NMA |
| tskb | 21730S005 | 140.0874 | 36.1057 | 67.3000 | Tsukuba | Japan | GSI |
| vill | 13406M001 | 356.0480 | 40.4436 | 647.5000 | Villafranca | Spain | ESA |
| wes2 | 40440S020 | 288.5060 | 42.6130 | 86.0170 | Westford | U.S.A. | NOAA |
| wtzr | 14201M010 | 12.8789 | 49.1442 | 666.0000 | Koetzting | Germany | BKG |
| yar1 | 50107M004 | 115.3470 | -29.0466 | 241.2967 | Mingenew | Australia | NASA/JPL |
| yell | 40127M003 | 245.5193 | 62.4809 | 181.0000 | Yellowknife | Canada | NRCan/GSD |
| zwen | 12330M001 | 36.7600 | 55.7000 | 270.0000 | Zwenigorod | Russia | GFZ |

† **ohig** is deactivated in 2002

Table 6.1: 51 Stations implemented in the TEXGAP software at CSR for nominal LEO orbits. It is based on IGS00

6.2, the orbit quality degradation affected by the reduced GPS tracking station numbers and by the hemispherical imbalanced distribution of tracking stations is examined in Section 6.1. Several experimental subsets out of the 51 IGS00 stations were selected, and their orbit solutions were compared with the solution from the Nominal Set. In Section 6.2, an optimal IGS network selection method is discussed. As a first step, to select the best performing stations out of over 300 IGS stations, 1) station coordinates accuracy, 2) station performance quality over a cycle, and 3) double-differenced observation numbers over a cycle are examined for each station in Section 6.2.1. Then, to measure the uniformity of distribution, a measure of the distribution uniformity ($u$) is defined in Section 6.2.2. The uniformity measure, $u$, was applied to find optimally distributed sets out of the best performing stations. To improve the global distribution of the network, the remotely located stations were weighted more in the selection process. The orbits with the optimal sets selected for cycle 8 to 10 were compared with the orbits from the Nominal Set by using several orbit performance measures in Section 6.3.

## 6.1 GPS Tracking station distribution and degradation of Orbit

For the ground station selection problem, there are two important aspects to consider: one is to find the optimal number of ground stations to process, the other is to find a uniformly distributed set in the geographical sense. In this section, we discuss the test results concerning 1) the relationship

between the ground station numbers and orbit quality, and 2) the relationship between the geographical distribution of stations and the orbit quality.

To investigate how a reduced number of stations affects the orbit quality, five sets with different ground station distributions were chosen with a uniform geographical distribution in mind. However, it is difficult to avoid some imbalance between the southern and northern hemispherical distributions. Their orbit solutions were compared with the orbit solution from the Nominal Set. Jason-1 GPS tracking data from the Nominal Set with 43 stations for cycle 8 and 10 were processed at CSR to get the nominal orbits discussed in the previous chapters. Although the Nominal Set composed of these 43 stations is almost globally distributed, it is not uniformly distributed, and there could still be redundancies.

As shown in Fig. 6.2, five ground stations are selected for Set 1. Eleven stations for Set 2, fifteen stations for Set 3, twenty stations for Set 4, and twenty four stations for Set 5 were selected. All of these stations are also members of the Nominal Set and they are also IGS00 stations. All other parameterizations were the same for each orbit determination process. The subarc lengths adopted for this experiment are 1.8738 hour for the estimation of CT, and 5.6214 hour for the estimation of the 1-cpr empirical forces, which were the same as the parameterization for the nominal orbit solutions.

Table 6.2 and Figure 6.3 compare the orbit performance of each station set. As expected, the orbit from Set 1 with only five ground stations performed worst in both cycles. Its crossover Mean, 1.62 cm, is particularly large com-

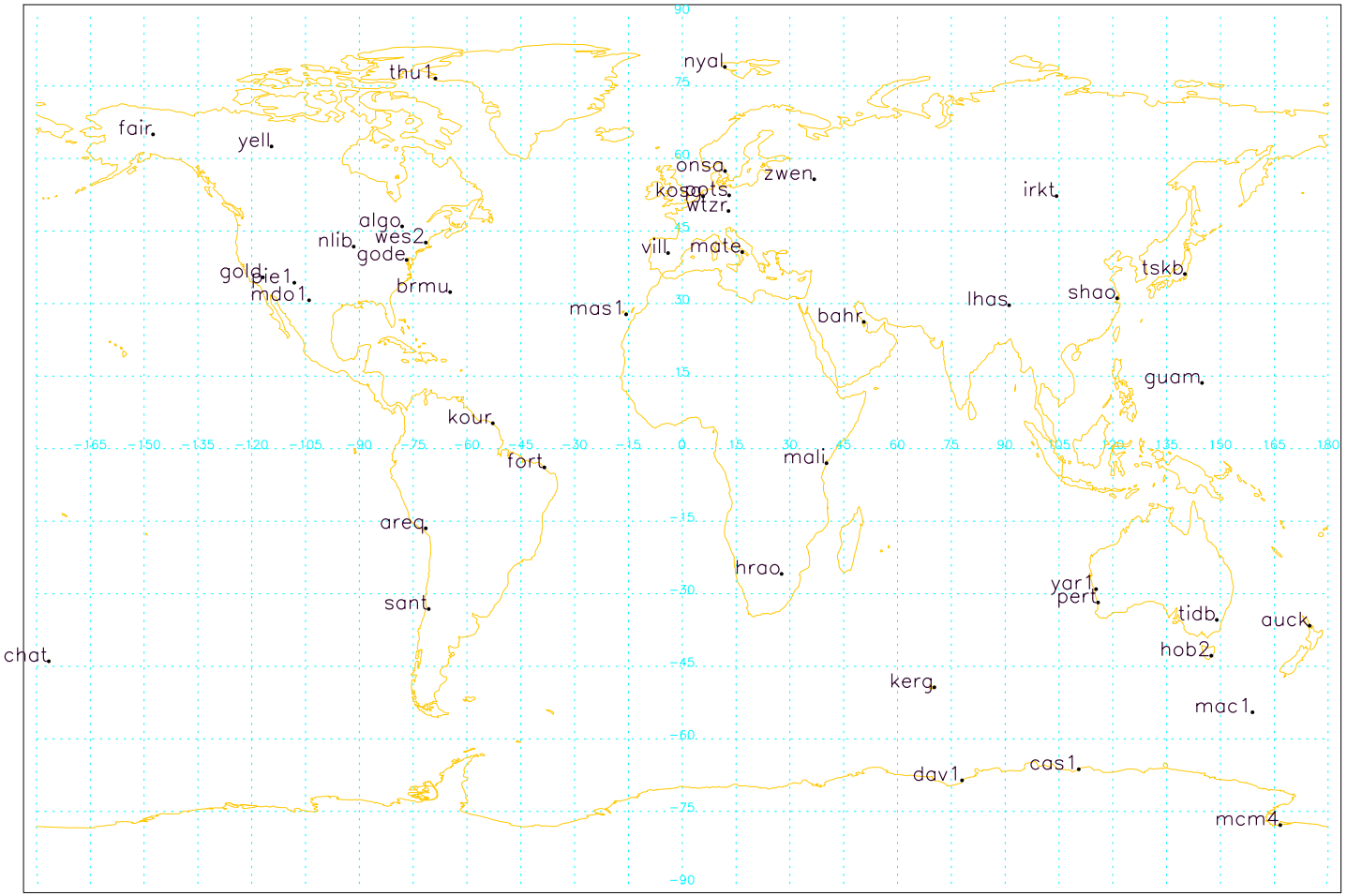


Figure 6.1: Nominal Set for Jason-1 POD at CSR (43 IGS00 stations).

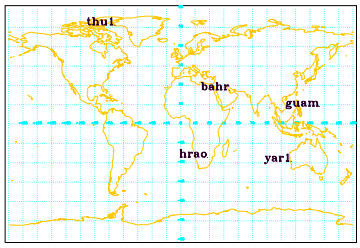


(a) Set 1 (5 stations)

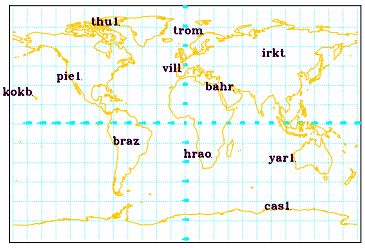


(b) Set 2 (11 stations)

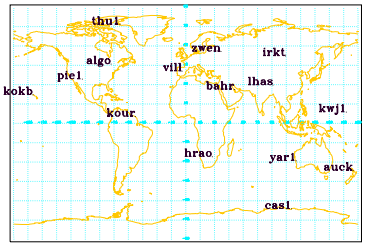


(c) Set 3 (15 stations)

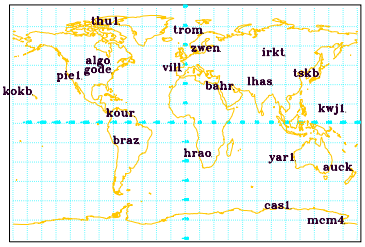


(d) Set 4 (20 stations)

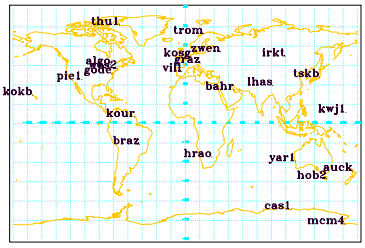


(e) Set 5 (24 stations)

Figure 6.2: Ground station set selection for the experiment to find optimal number of ground station for the precision orbit determination problem

pared to the crossover Mean of other orbits ranging 3 to 5 mm, which indicates that the orbit with so few tracking stations suffered from orbit miscentering. The orbit of cycle 8 from Set 2, and the orbit of cycle 10 from Set 1 were possibly miscentered too. The comparison of the crossover RMSs shows that the orbit from Set 3 with 15 stations performed close to the nominal orbit which was obtained from the Nominal Set with 43 stations. The orbits from Set 4 with 20 stations and Set 5 with 24 stations performed as good as the nominal orbit did in the sense of the crossover statistics and SLR residual tests. This strongly indicates that, for the Jason-1 precise orbit determination problem with GPS tracking data, only 20 to 30 well-distributed and well-performing GPS ground stations are required for a good quality orbit.

In summary, for the Jason-1 POD with GPS tracking data, tracking from well-distributed and the best-performing 20 to 30 GPS stations appears to be enough to obtain reasonably accurate orbit solutions. More tracking stations do not necessarily guarantee the orbit solution with better accuracy. Therefore, it is necessary to further search for the optimal sets composed of best performing and uniformly distributed ground stations. The optimal sets may further improve the orbit quality. In the next section, how to select the optimal ground station set will be discussed, also the orbit performance with the optimal station set will be assessed. Using the uniformly distributed station set is important for avoiding miscentering problems.

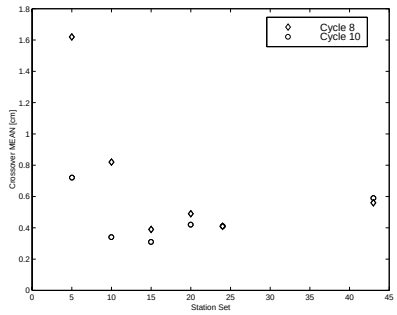


(a) Crossover Mean

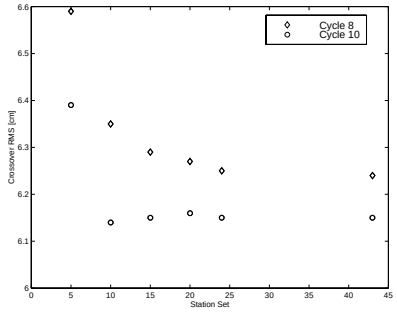


(b) Crossover RMS

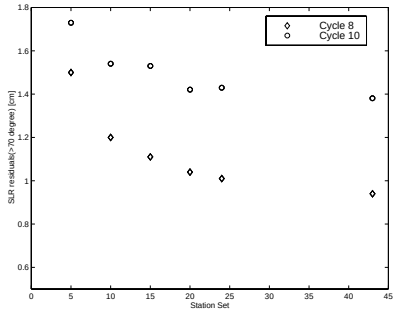


(c) SLR residuals

Figure 6.3: Orbit Performance Test for the Sets with Various Station Numbers. The orbits with 20∼25 stations perform as good as the orbits from the Nominal Set.

| station set | crossover residuals | | SLR residuals(>70°) | |
|---|---|---|---|---|
| | Mean | RMS | Mean | RMS |
| Set 1 (5 stations) | 16.2 | 65.9 | -.4 | 15.0 |
| Set 2 (11 stations) | 8.2 | 63.5 | .4 | 12.0 |
| Set 3 (15 stations) | 3.9 | 62.9 | .5 | 11.1 |
| Set 4 (20 stations) | 4.9 | 62.7 | .9 | 10.4 |
| Set 5 (24 stations) | 4.1 | 62.5 | .6 | 10.1 |
| Nominal Set | 5.6 | 62.4 | .0 | 9.4 |

(a) GPS-only orbit for cycle 8

| station set | crossover residuals | | SLR residuals(>70°) | |
|---|---|---|---|---|
| | Mean | RMS | Mean | RMS |
| Set 1 (5 stations) | 7.2 | 63.9 | -7.4 | 17.3 |
| Set 2 (11 stations) | 3.4 | 61.4 | -7.9 | 15.4 |
| Set 3 (15 stations) | 3.1 | 61.5 | -8.6 | 15.3 |
| Set 4 (20 stations) | 4.2 | 61.6 | -7.8 | 14.2 |
| Set 5 (24 stations) | 4.1 | 61.5 | -7.9 | 14.3 |
| Nominal Set | 5.9 | 61.5 | -7.5 | 13.8 |

(b) GPS-only orbit for cycle 10

Table 6.2: Station Number and Orbit Performance. In terms of the crossover RMS, the orbits with 20 or 24 stations perform as good as the orbits from the Nominal Set.

## 6.2 Optimal IGS Network Selection

A proof of concept for the International GPS Service for Geodynamics (IGS) was conducted with a three-month campaign during June through September 1992, and was continued through a Pilot-service until the establishment of the IGS in 1993 by the International Association of Geodesy (IAG). The IGS began formally on 1 January 1994. IGS is a member of the Federa-

tion of Astronomical and Geophysical Data Analysis Services (FAGS) and it operates in close cooperation with the International Earth Rotation Service (IERS). Due to the expansion of IGS objectives, the name of the service was changed to International GPS Service (IGS) on 1 January 1999.

IGS Stations provide continuous tracking using high accuracy receivers and have data transmission facilities allowing for a rapid (at least daily) data transmission to the data centers. The stations have to meet certain requirements, which are specified in a separate document available from the Central Bureau. The tracking data of IGS stations are regularly and continuously analyzed by at least one IGS Analysis Center or IGS Associate Analysis Center. These analyses must be available to, analyzed and published by the IERS for at least two consecutive years. During this initial period, the IGS Central Bureau can temporarily designate new tracking stations as IGS stations.

An IGS Station whose data is analyzed by at least three IGS Analysis Centers for the purpose of orbit generation, at least one of which lies on a different continent from the station considered, is called an IGS Global Station. As of August 2002, there are 335 IGS stations, of which 127 are designated as IGS Global stations (see Appendix F.1). Most of IGS00 stations are also IGS Global Stations. All IGS stations are qualified as reference stations for regional GPS analyses.

For the experiment to search for the optimal station sets, a new station information file (see Appendix F.3) for preprocessing in TEXGAP and the orbit estimation in MSODP was created independent of CSR's nominal

station information file, which is based on IGS00 and used for CSR's general LEO orbit determination purpose. To create the new MSODP station information file, 5-digit DOMES numbers for each antenna and their coordinates were taken from the ITRF2000 GPS SINEX file (see `ftp://schubert.ensg.ign.fr/pub/itrf/itrf2000/ITRF2000_GPS.SNX.gz`), and 4-character codes were used from the IGS SINEX file ( see `ftp://igscb.jpl.nasa.gov/igscb/station/general/igs.snx` or, `ftp://igs.ensg.ign.fr/pub/igscb/station/general/igs.snx`). It is not unusual that the coordinate solutions for the same antenna can be different between the two SINEX files. The ITRF2000 GPS SINEX file was the basis of the coordinates solution of the station information file in this experiment.

Although 335 IGS stations are available in the IGS SINEX solution as of August 2002, many stations are excluded in this experiment because:

1. Some stations were included in the IGS network after the establishment of the ITRF2000, so the ITRF2000 SINEX file do not provide their coordinates.

2. Some stations are not active any longer,

3. 4-character IDs of some stations in the ITRF2000 GPS SINEX file do not match with the IDs in the IGS SINEX file, although their 9-character DOMES numbers exactly coincide.

The DOMES number (e.g. 14001M004) is the only truly unique identifier of a marker within the network of permanent IGS stations. It has already been

defined by the IERS for the sites of other space technique sites such as VLBI and SLR. It contains: 1) one digit for the continent (e.g.: 1=Europe); 2) two for the country (40=Switzerland); 3) two for the site (01=Zimmerwald); 4) one character to distinguish between marker (M) and sensor (S); and 5) three digits for the marker (004). It is assigned to each marker by the IERS bureau on request. The 4-character station code used e.g., for the RINEX file naming, is not suited for such a unique identifier. Station names stored in the logs and the RINEX files are often difficult to relate to the specific marker.

Since the MSODP station information file uses only 5 digits for DOMES number, several antennas sharing the same 5-digit DOMES number, need to be assigned to new 5-digit DOMES numbers for MSODP. For the 5-digit DOMES numbers, 80000 to 89999 are allocated since these numbers are not assigned to any marker by IERS yet. For example, stations such as **bran** (DOMES number=40400M301), **cit1** (40400S201), **jplm** (40400M007), and **wlsn** (40400M101) are located close to each other, and share the same 5-digit DOMES number, 40400. For this experiment, 80028, 80027, 40400, and 80026 are assigned to each station respectively for the station information file as shown in Table F.3. Other neighboring antennas such as **harv** (40420M101) and **vndp** (40420M007) are also assigned to 80030 and 40420 respectively. Although all the GPS tracking data from these neighboring antennas are processed in the preprocessing stage with TEXGAP, ultimately one of the best performing antenna among them will be selected during the optimal distributed station selection process for the orbit estimation to be discussed later

in Section 6.2.3.

Stations like **ober**, **ohig**, **taiw**[2], and **upad** are not active and new antennas have substituted for them with new 4-character IDs by IGS, but with the same 5-digit DOMES numbers to the old antennas by IERS (e.g. **ober** to **obe2** and **obet**; **ohig** to **ohi2** and **ohiz**; and **upad** to **pado**). None of them, either old ones or new ones, are included in the new MSODP station information file because the coordinate solution of these new substitutes do not match to the 4-character IDs nor 9-character DOMES numbers in the ITRF2000 GPS SINEX file.

For the pairs such as **darr** and **darw**; **davr** and **dav1**; **gol2** and **gold**; **mad2** and **madr**; **nrc2** and **nrc1**; **os0g** and **onsa**; **tid1**, **tid2** and **tidb**; and, **yar2** and **yar1** (close to **yarr**), each site in pairs shares the exact same 9-character DOMES numbers with different 4-character IDs in the IGS SINEX file, while the ITRF 2000 GPS SINEX file provides only one coordinate solution for each DOMES number. Although all of the antennas in the pairs are active, only one antenna from each pair with the same 4-character IDs in the ITRF2000 GPS SINEX file was selected to process its GPS data. For this experiment, **darw**, **dav1**, **gold**, **madr**, **nrc1**, **onsa**, **tidb**, and **yar1** were included with the original 5-digit DOMES numbers. For the **darw** and **darr** pair, **darw** was chosen even though its coordinate solution is not available in the ITRF2000 GPS SINEX file since it is a fairly new station. Coordinates of

[2]no longer assigned to DOMES number 23601

**darw** were assumed to be the same to the coordinates of **darr**.

Since the station information file used in this experiment is based on the ITRF2000 GPS SINEX file, the station information is limited only to the stations available at the time of the ITRF2000 establishment. To use newly activated station information, the approximate positions and velocities should be taken from in the log file maintained by each station. In this experiment, no coordinate information from the log file of any site was taken. However, when the log file is used as a source for the coordinate information, care should be taken, because their solution may not be consistent with ITRF2000. Another station needs to be mentioned is **areq**. An earthquake occurred recently near the **areq** station after the ITRF2000 establishment, so its coordinate information in the ITRF2000 GPS SINEX file is outdated. The information of **areq** for the Nominal Set was from the ITRF2000 GPS SINEX file, but **areq** was excluded in the optimal set selection.

### 6.2.1 Selection Criteria

For the initial step to obtain optimal station sets, 208 ITRF2000 GPS stations were chosen for the preprocessing in TEXGAP and for the MSODP station information file. The coordinate information of the 208 stations is based on `ftp://schubert.ensg.ign.fr/pub/itrf/itrf2000/ITRF2000_GPS.SNX.gz`, and their 4-character IDs are based on `ftp://igscb.jpl.nasa.gov/igscb/station/general/igs.snx`.

All of the GPS tracking data from the 208 stations were preprocessed

to generate the Double-Differenced observation (DDobs), but all of the DDobs data were not necessarily processed in MSODP to get orbit solutions. Instead, the results of the DDobs numbers from the preprocessing were used as one of the criteria to select the best performing stations for the next step in the optimal station set selection process. The DDobs from finally selected optimal station sets were actually processed for the orbit solution in MSODP.

For the optimal selection process, there are two aspects to consider: one is to quantify each station's performance; the other is to examine the geographical distribution. To quantify the station performance, three criteria such as 1) Station Coordinates Accuracy, 2) Station Performance Quality, and 3) DDobs numbers are defined in this section. Another criteria to investigate the geographical distribution of networks will be defined in Section 6.2.2.

The Station Coordinates Accuracy is defined based on the coordinate solution accuracy in the ITRF2000 GPS SINEX file. The Station Performance Quality is based on the daily station performance report from JPL (see `ftp://igscb.jpl.nasa.gov/igscb/mail/igsnet/daily/`). The DDobs numbers are taken from the preprocessing of CSR's TEXGAP program. Once the best performing stations are screened based on the three criteria above, the uniformity indicator of the distribution is applied to get optimal station sets whose tracking data will be processed to get orbit solutions.

***Station Coordinates Accuracy (SIGMA)***

The total position accuracy for each station is calculated by using each component's sigma from the ITRF2000 solution as:

$$\sigma_{pos} = \sqrt{\sigma_x^2 + \sigma_y^2 + \sigma_z^2} \tag{6.1}$$

Likewise, the total velocity accuracy for each station is calculated as:

$$\sigma_{vel} = \sqrt{\sigma_{V_x}^2 + \sigma_{V_y}^2 + \sigma_{V_z}^2} \tag{6.2}$$

The coordinates accuracy of some stations such as **bili** (12.44 cm), **chwk** (10.86 cm), **drag** (19.57 cm), **ineg** (15.06 cm), etc. are noticeably larger (see Table F.4 for detailes). Their coordinates are poorly determined for one of several reasons: 1) some are located on very active, moving plates, 2) poor tracking history, 3) stations with poorly working GPS receivers, 4) recent earthquake occurrence and others. All stations with poor coordinates will be excluded in the process of selecting an optimal ground station set. Note that the coordinates accuracy of all 51 IGS00 stations is less than the 1-cm level.

***Station Performance Quality***

The daily performance qualities of 208 stations for cycle 8 were examined (see Table F.7 for details). For each station, daily performance quality values were averaged over one cycle period. The information listed in Table F.7 is from JPL IGS Analysis Center procedures based on RINEX data available from JPL's GPS Networks and Operations Group. The station report is generated periodically for the IGS Central Bureau by JPL's Satellite Geodesy and

Geodynamics System (SGGS) Group, based on Rinex data provided by the GPS Networks and Operations (GNO) Group. See Zumberge [1996] for details on the daily station performance definition.

The values of the performance quality in Table F.7 account for amount of data, number of phase breaks, formal errors of (precise) point-positioned coordinates, and pseudorange and phase residuals. (A dot means that no data from the site were processed at JPL for the days covered.) The quality is also the average over one or more days of a daily quality value. The daily quality value is based on several categories as shown in Table F.6. One quality point is awarded on each day for each of the following conditions:

1. there are at least 250 valid clock solutions
2. there are fewer than 100 phase bias resets (the last field in Table F.6 )
3. the 3d formal error of the solution for station location is less than 1 cm (this field is not in Table F.6, but is in a related database)
4. the pseudorange rms residuals (field 8 in Table F.6) are less than 86 cm (this is true 95% of the time), and the number of pseudorange measurements is at least 90% of the number of phase measurements
5. the phase rms residuals (field 10 in Table F.6) are less than 13 mm (also true 95% of the time)

Thus, one site can be awarded up to 5 quality points every day. The quality values in Table F.7 is calculated as:

$$quality =< P > /0.5 \tag{6.3}$$

where $< P >$ is the average number of points awarded over the period reported. In this study, the daily performance quality values were averaged again over 11 days, or approximately one Jason-1 repeat cycle. However, if there is no available performance information for some days over a cycle, only the available performance qualities data were averaged. Stations with consistently bad scores ranging between 0 and 6 out of 10 were excluded.

***Double-Differenced Observation numbers***

All of the GPS tracking data from the 208 stations were preprocessed in the TEXGAP software, but the Double-Differenced observation (DDobs) data only from the stations of the optimal set were processed to obtain orbits in MSODP. The results of the averaged daily DDobs numbers of each station over one Jason-1 repeat cycle from the preprocessing were taken to serve as one of the criteria in the process of the optimal ground station selection (see Tables F.8, F.9 and F.10 of the daily DDobs numbers for cycles 8, 9 and 10).

### 6.2.2 Measure of the Distribution of Stations

Along with the criteria discussed in the previous section, another important indicator to measure the distribution uniformity of ground stations is defined in Section 6.2.2.1. In Section 6.2.2.2, Girard's formula is introduced.

The formula is employed to define the distribution uniformity indicator. Section 6.2.2.3 shows the uniformity indicator values computed for the examples of experimental distribution.

#### 6.2.2.1 Definition of a Uniformity Measure

To define a distribution uniformity measure, all the stations on the globe are considered as vertices conforming a convex deltahedron (see Fig. 6.4). With sets of three vertices forming each triangle on the convex deltahedron, areas of the spherical triangles (or facets) were calculated by applying Girard's formula. A uniformity distribution measure ($u$) for the global distribution of the station network on the earth with assumed radius $R$ can be defined such as:

$$u \equiv 1 - \frac{\sqrt{N} \cdot \sqrt{\sum_{i=1}^{i=N} (S_i - \bar{S})^2}}{4\pi R^2} \tag{6.4}$$

$$= 1 - \frac{N}{4\pi R^2} \cdot \sigma \tag{6.5}$$

where, $N$ is the number of triangles of the deltahedrons, $S_i$ is the $i$-th spherical triangle's area fromed by three vertices, $\bar{S}$ is the mean value of the all the spherical triangle areas ($\bar{S} = \sum_{i=1}^{i=N} S_i/\mathrm{N}$), and $\sigma$ is the standard deviation of the spherical triangle areas ($\sigma = \sqrt{\sum_{i=1}^{i=N} (S_i - \bar{S})^2/N}$ ). For the perfect uniform distribution, $u = 1$. By the definition, $u$ always satisfies $0 < u \leq 1$.

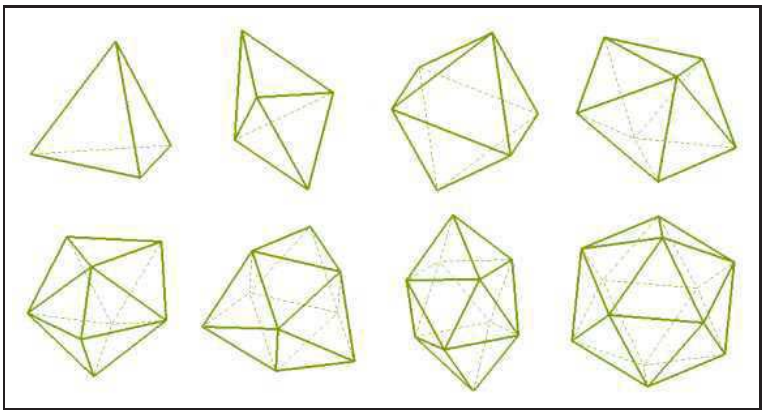

Figure 6.4: Convex Deltahedrons

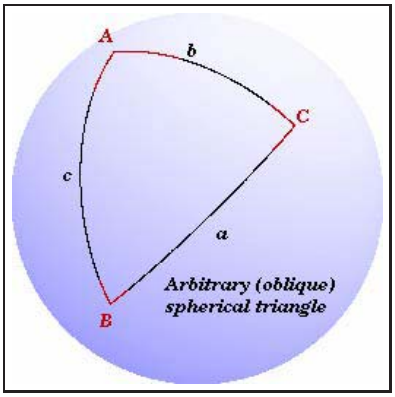


Figure 6.5: Girard Formula

#### 6.2.2.2 Girard's Formula for Spherical Triangle

A spherical triangle is a figure formed on the surface of a sphere by three great circles intersecting pairwise in three vertices. Thus, a spherical triangle consists of three points called *vertices*, the arcs of great circles that join the vertices, called the *sides*, and the *area* that is inclosed therein as shown

in Fig. 6.5. To avoid any ambiguity in the definition, we deal with only small triangles, which are assumed that given the three vertices, no pair of which are antipodal.

Let a spherical triangle have angles $A$, $B$, and $C$ (measured in radians at the vertices along the surface of the sphere) and let the radius of the sphere on which the spherical triangle sits is $R$. Also suppose that $a$, $b$, and $c$ are the arc lengths. Then, Girard formula gives the area of the spherical triangle, $S$, such as [Girard, 1629; Zwillinger, 1995]:

$$S = R^2 \cdot E = R^2 \cdot (A + B + C - \pi) \tag{6.6}$$

where $E$ is called the 'spherical excess', with $E = 0$ in the degenerate case of a planar triangle. When the radius $R$ is very large, and the area of the triangle is small, $E$ $(= S/R^2)$ gets extremely small. In such cases it would be difficult to distinguish the sum of the angles from 180 degrees.

When the vectors of three points are known, their sides, $a$, $b$, and $c$, can be obtained such as:

$$a = \arccos\left(\frac{\vec{r}_B \cdot \vec{r}_C}{|\vec{r}_B||\vec{r}_C|}\right) \tag{6.7a}$$

$$b = \arccos\left(\frac{\vec{r}_C \cdot \vec{r}_A}{|\vec{r}_C||\vec{r}_A|}\right) \tag{6.7b}$$

$$c = \arccos\left(\frac{\vec{r}_A \cdot \vec{r}_B}{|\vec{r}_A||\vec{r}_B|}\right) \tag{6.7c}$$

The vertex angles, $A$, $B$ and $C$ are computed by **the law of cosines for sides** as follows:

$$\cos a = \cos b \ \cos c + \sin b \ \sin c \ \cos A \tag{6.8a}$$

$$\cos b = \cos c \ \cos a + \sin c \ \sin a \ \cos B \tag{6.8b}$$

$$\cos c = \cos a \ \cos b + \sin a \ \sin b \ \cos C \tag{6.8c}$$

Other spherical trigonometric laws can also be used. **The law of sines** can be expressed as:

$$\frac{\sin a}{\sin A} = \frac{\sin b}{\sin B} = \frac{\sin c}{\sin C} \tag{6.9}$$

**The law of cosines for angles** can be expressed as:

$$\cos C = -\cos A \ \cos B \ + \sin A \ \sin B \ \cos c \tag{6.10}$$

The equation for the spherical excess, $E$, in terms of the side lengths ($a$, $b$, and $c$) known as l'Huilier's theorem [Beyer, 1987; Zwillinger, 1995] also can be used:

$$\tan \frac{1}{4}E = \sqrt{\tan \frac{1}{2}s \tan \frac{1}{2}(s-a) \tan \frac{1}{2}(s-b) \tan \frac{1}{2}(s-c)} \tag{6.11}$$

where $s$ is the semiperimeter. Perimeter is defined as the arc length along the boundary of a closed two-dimensional region.

Girard's theorem can easily be extended from spherical triangles to spherical polygons. A spherical polygon is a figure on the sphere which is

bounded by segments of great circles. The area for a spherical quadrilateral with angles $A$, $B$, $C$ and $D$ can be expressed as:

$$S = R^2 \cdot (A + B + C + D - 2\pi) \tag{6.12}$$

Also, the area of a spherical polygon with $n$ sides can be described as [Beyer, 1987]:

$$S = R^2 \cdot [\theta - (n - 2)\pi] \tag{6.13}$$

where, $\theta$ is the sum of the radian angles of a spherical polygon on a sphere of radius $R$.

#### 6.2.2.3 The Distribution Uniformity for Several Experiment Examples

Table 6.3 shows the distribution uniformity for several experiment examples. As expected, the distribution uniformity measure for regular uniform polyhedrons such as a cube in Table 6.3(a) are exactly one, because the areas of all the spherical triangles are the same. The distributions with different numbers of electrons and random points on a sphere were also tested. For the distribution test for the electrons, the inverse square law for the electrical force between electrons in the quasi-steady state was applied.

The uniformity indicator comparison of two distributions with the same number of electrons and randomly generated points on the sphere shows that the electron distribution are distributed closer to uniform than the random distribution on the sphere. But, in reality, the distribution of GPS ground

stations on the globe is far from the uniform distribution because of the nature of the vast oceans. Also, most of the GPS stations are located in North America or Europe. The uniformity indicator computed with 95 IGS "Global Stations" (as of June 2001) is 0.946, which is smaller than the uniformity indicator computed with 95 random point distribution, which is about 0.953∼0.958 as shown in Table 6.3(c) implying that the 95 IGS "Global Stations" are not close to the uniform distribution, nor a random distribution. It may be a rather biased distribution set.

| case | cube | electron | random |
|---|---|---|---|
| 1 | 1.0 | 0.993 | 0.713 |
| 2 | 1.0 | 0.993 | 0.641 |
| 3 | 1.0 | 0.993 | 0.770 |

(a) 8 points

| case | electron | random |
|---|---|---|
| 1 | 0.997 | 0.935 |
| 2 | 0.997 | 0.935 |
| 3 | 0.997 | 0.917 |

(b) 51 points

| case | electron | random |
|---|---|---|
| 1 | 0.998 | 0.954 |
| 2 | 0.998 | 0.953 |
| 3 | 0.998 | 0.958 |

(c) 95 points

| case | electron | random |
|---|---|---|
| 1 | 0.999 | 0.972 |
| 2 | 0.999 | 0.974 |
| 3 | 0.999 | 0.973 |

(d) 269 points

Table 6.3: Comparison of Uniformity Measures for Various Distributions. For "electron", given number of electrons were distributed on a sphere. For "random", given number of points were randomly generated.

With the GPS stations, a greater number of stations does not guarantee a better distribution uniformity. For the distribution on a sphere of electrons or random points, as the number of electrons or points increases, the distribution

uniformity also increases. Contrary to the distribution of electrons or random points, the uniformity indicator with an increase of GPS stations appears to get worse at some point. Also, as shown in Section 6.1, only 20-30 stations are enough for Jason-1 POD. Therefore, the goal of the next section will be to find an optimal number of best performing stations out of the IGS set producing the most uniform distribution. The optimal station selection process by using the previously discussed selection criteria such as 1) station coordinates accuracy, 2) station daily performance quality, 3) station's DDobs number and finally, 4) uniformity indicator to measure the distribution, is further discussed in the next section.

### 6.2.3 Optimal Station Networks

To select optimal sets for each cycle, two steps of selection process are applied as shown in Algorithm 1 and 2. First, for each cycle, the best stations are selected out of the initial 208 ITRF2000 stations based on 1) DDobs numbers, 2) station coordinates accuracy and 3) station performance quality according to Algorithm 1. For ordinary stations, 3000 for the averaged daily DDobs numbers, 6.0 for the station performance quality, and 3.0 cm for the station coordinates accuracy are applied as thresholds. Less stringent criteria are applied to the stations of the remote station set (see Table 6.4) such as 1000 for the averaged daily DDobs numbers, 3.0 for the station performance quality, and 20.0 cm for the station coordinates accuracy. The remote station set is composed of the stations located at remote islands or polar regions, thus

they have a better chance, first, to be selected as a member of the best station set, then next, to form the optimal station sets with the geographically better distribution.

Second, for each cycle, an optimal station set is formed as shown in Algorithm 2 by applying the uniformity measure to the the best station set previously obtained according to Algorithm 1. To do so, we define a fiducial station set composed of 6 globally-distributed and best-performing stations. Starting from a fiducial station set as an initial optimal set candidate, one station out of the best station set which will produce the best uniformity of the next optimal set candidate are iteratively searched and added to the previous optimal set candidate. If there is a station nearby within 7° radius with better coordinate accuracy and DDobs number, the neighboring station replaces the subject station that was to be added to the set. The optimal set is defined as the set of which the uniformity indicator reaches the maximum or near the maximum among the optimal set candidates in the station accumulation process.

Table 6.5 shows the 95 best stations selected for cycle 8 according to Algorithm 1. Two sets with 86 best stations are also selected independently for cycle 9 and cycle 10 as shown in Table 6.6 and Table 6.7 respectively. The daily performance quality of several stations such as **braz**, **goug**, **mas1** and **vesl** was not available from the JPL ftp site. However, they were included in the best station set, since they may produce better geographical distribution if they are selected as a member of the optimal station sets in the following

**Algorithm 1** Best Station Set Selection

- Start from Initial Station Set (208 ITRF2000 stations were chosen).
- Obtain each station's 1)DDobs Numbers, 2)Station Coordinates Accuracy($\sigma$), and 3)Station Performance Quality over a cycle.
- Select better stations based on the three criteria. If the subjected station is one of the Remote Station Set, loosen the criteria as follows.

**repeat**
- Get a station out of 208 ITRF2000 stations

**if** [the subjected station = Remote Station] **then**
**if** [ ($\sigma < 20.0cm$) and (Quality $\geq 3.0$) and (DDobsNumber $\geq 1000$) ] **then**
- Add the subjected station to the best station set

**else**
- Discard the subjected station

**end if**
**else**
**if** [ ($\sigma < 3.0cm$) and (Quality $\geq 6.0$) and (DDobsNumber $\geq 3000$) ] **then**
- Add the subjected station to the best station set

**else**
- Discard the subjected station

**end if**
**end if**

**until** [All 208 stations are checked]

- To get a Optimal Set from the best station set, apply the uniformity measure for the station members of the Best Station Set following Algorithm 2

**Algorithm 2** Optimal Set Selection

- Initialize Optimal Set candidate with no station
- Select fiducial stations from the best station set and Add fiducial stations to the optimal set candidate

**while** [station number of the best station set $\leq$ station number of the optimal set candidate] **do**

  **repeat**

    - choose a station out of the best station set

    **if** [there is any station nearby (neighborhood radius = 7°)] **then**

      **if** [ ($\text{DDobs}_{nghb}$ > 100+DDobs) and ($\sigma_{nghb} < \sigma/5$) and ($9 \leq \text{Quality}_{nghb} \leq 11$) ] **then**

        - Replace the subjected station to a neighborhood station

      **end if**

    **end if**

    - Add the subjected station to the previous optimal set candidate
    - Compute the uniformity of the new set and save the subjected station and uniformity

  **until** [All the stations of the best station set is processed]

  - The new optimal set candidate is formed by adding the station producing the maximal uniformity to the previous optimal set candidate
  - Compute the uniformity indicator of the new optimal set candidate and save it

**end while**

- An optimal set candidate with approximate maximal uniformity indicator ($u$) is defined as the optimal set

| site Id | DOMES Number | Lon(W) (deg) | Lat(N) (deg) | Height (m) | Location | Country | Agency |
|---|---|---|---|---|---|---|---|
| asc1 | 30602M001 | 345.5880 | -7.9512 | 105.1508 | Ascension Island | Ascension Island | NASA/JPL |
| auck | 50209M001 | 174.8344 | -36.6028 | 132.0000 | Whangaparaoa | New Zealand | IGNS-JPL |
| bahr | 24901M002 | 50.6081 | 26.2091 | -17.0300 | Manama | Bahrain | NIMA |
| bili | 12363M001 | 166.4380 | 68.0761 | 456.2380 | Bilibino | Russian Federation | RDAAC-IRIS |
| brmu | 42501S004 | 295.3030 | 32.3700 | -10.6190 | Bermuda | U.K. | NOAA |
| cas1 | 66011M001 | 110.5197 | -66.2834 | 22.5500 | Casey | Antarctica | AUSLIG |
| chat | 50207M001 | 183.4342 | -43.9558 | 58.0000 | Waitangi | New Zealand | IGNS-JPL |
| coco | 50127M001 | 96.8339 | -12.1883 | -35.2212 | Cocos Island | Australia | AUSLIG |
| cro1 | 43201M001 | 295.4157 | 17.7568 | -31.8280 | Christiansted | U.S. Virgin Islands | NRAO-JPL |
| dav1 | 66010M001 | 77.9726 | -68.5773 | 44.5000 | Davis | Antarctica | AUSLIG |
| dgar | 30802M001 | 72.3702 | -7.2696 | -64.8965 | Diego Garcia Island | U.K. Territory | NASA/JPL |
| eisl | 41703M003 | 250.6167 | -27.1482 | 114.5179 | Easter Island | Chile | NASA/JPL |
| fair | 40408M001 | 212.5008 | 64.9780 | 319.0097 | Fairbanks | USA | JPL-GSFC |
| fort | 41602M001 | 321.5744 | -3.8774 | 20.4918 | Eusebio, Fortaleza | Brazil | NOAA |
| gala | 42005M001 | 269.6964 | -0.7426 | 7.4453 | Galapagos Island | Ecuador | NASA/JPL |
| goug | 30608M001 | 350.1333 | -40.3488 | 81.3000 | Gough Island | territory of the U.K. | AWI |
| guam | 50501M002 | 144.8683 | 13.5893 | 201.9220 | Dededo | Guam | NASA/JPL |
| hofn | 10204M002 | 344.8132 | 64.2673 | 82.5000 | Hoefn | Iceland | BKG |
| jama | 42601S001 | 283.2191 | 17.9390 | -2.9410 | Kingston | Jamaica | NGS/NOS/NOAA |
| kely | 43005M001 | 309.0550 | 66.9873 | 230.5636 | Kangerlussuaq | Greenland | NOAA |
| kerg | 91201M002 | 70.2555 | -49.3515 | 74.0583 | Port aux Francais | Kerguelen Islands | CNES |
| kokb | 40424M004 | 200.3351 | 22.1263 | 1167.3680 | Kokee Park, Waimea, | USA | NASA/JPL |
| kour | 97301M210 | 307.1940 | 5.2522 | -25.5700 | Kourou | French Guyana | ESA |
| kwj1 | 50506M001 | 167.7302 | 8.7222 | 38.2688 | Kwajalein Atoll | Marshall Islands | NASA/JPL |
| mac1 | 50135M001 | 158.9358 | -54.4995 | -6.6900 | MacQuarie Island | Southern Ocean | AUSLIG |
| mas1 | 31303M002 | 344.3667 | 27.7637 | 197.3000 | Maspalomas | Spain | ESA |
| maw1 | 66004M001 | 62.8707 | -67.6048 | 59.1840 | Mawson | Antarctica | AUSLIG |
| mcm4 | 66001M003 | 166.6693 | -77.8383 | 97.9201 | Ross Island | Antarctica | NASA/JPL |
| mkea | 40477M001 | 204.5437 | 19.8013 | 3754.7305 | Mauna Kea | USA | NASA/JPL |
| noum | 92701M003 | 166.4102 | -22.2699 | 83.0790 | NOUMEA | FRANCE | DITTT |
| ntus | 22601M001 | 103.6799 | 1.3458 | 79.0000 | Singapore | Republic of Singapore | NTU |
| nya1 | 10317M003 | 11.8653 | 78.9296 | 84.0000 | Ny-Alesund | Norway | NMA |
| nyal | 10317M001 | 11.8700 | 78.9300 | 82.0000 | Ny-Alesund | Norway | NMA |
| pimo | 22003M001 | 121.0777 | 14.6357 | 95.4934 | Quezon City | Phillipines | NASA/JPL |
| reyk | 10202M001 | 338.0445 | 64.1388 | 93.0950 | Reykjavik | Iceland | IfAG |
| riog | 41507M004 | 292.2500 | -53.7900 | 32.0000 | Rio Grande | Argentina | GFZ |
| sch2 | 40133M002 | 293.1674 | 54.8321 | 498.1800 | Schefferville | Canada | NRCan/GSD |
| sey1 | 39801M001 | 55.4794 | -4.6737 | 538.2248 | La Misere | Seychelles | JPL-IRIS/IDA |
| stjo | 40101M001 | 307.1889 | 47.5952 | 153.9000 | St. John's | Canada | NRCan/GSD |
| syog | 66006S002 | 39.5837 | -69.0070 | 50.0902 | East Ongle Island | Antarctica | GSI |
| thti | 92201M009 | 210.3937 | -17.5769 | 98.0400 | Papeete | Tahiti, French | CNES |
| thu1 | 43001M001 | 291.2120 | 76.5373 | 55.0030 | Thule | Greenland | KMS-JPL |
| tixi | 12360M001 | 128.8664 | 71.6345 | 46.9847 | Tixi | Russian Federation | RDAAC-IRIS |
| vesl | 66009M001 | 357.1583 | -71.6738 | 862.4000 | Sanae IV | Antarctica | AWI |
| whit | 40136M001 | 224.7779 | 60.7505 | 1427.0000 | WHITEHORSE | CANADA | NRCan/GSC |
| yell | 40127M003 | 245.5193 | 62.4809 | 181.0000 | Yellowknife | Canada | NRCan/GSD |
| ykro | 32601M001 | 354.7599 | 6.8706 | 270.4983 | Yamoussoukro | Cote d'Ivorie | NASA/JPL |

Table 6.4: "Remote Stations" selected for Algorithm 1 as of August, 2002. Stations at remote islands or polar regions are collected for Remote Stations.

process. The daily performance quality of **braz** was not available over cycle 8, but it was included in the best station of cycle 8. No daily performance quality of **goug** was available over cycle 8, and only 3 daily performance quality data were available over cycle 9, but **goug** was included in the best station set for both cycle 8 and 9. The daily performance quality of **mas1** and **vesl** was available for only several days, but they were also included in the best station sets of cycle 8 and 9. Note that the coordinates accuracy of **bili** is 12.44 cm, which is relatively large compared with the coordinates accuracies of other stations, but it is still within the range of the threshold of 20 cm of remote stations for the best station set selection.

In the best station sets for cycle 8, 9 and 10, the pairs such as **madr** – **vill**, **mdvo** – **zwen**, **nyal** – **nya1**, **tro1** – **trom**, **wsrt** – **kosg**, and, **usna** – **sol1** are located within the radius of 7°. Thus, only one of the pairs was selected by the condition of criteria of Algorithm 2 to form the optimal station sets.

The resulting optimal station set can be different depending on the initial selection of the fiducial stations in Algorithm 2. For this experiment, three different fiducial set, which are called **fidu1**, **fidu2** and **fidu3**, were chosen as core stations to accumulate one station, for each iteration, producing a maximal uniformity. The fiducial set of **fidu1** consists of **nya1**, **vesl**, **brmu**, **mas1**, **bahr**, and **guam**. For **fidu2**, **mag0**, **pol2**, **stjo**, **tidb**, **thti**, and **goug** are selected. The **fidu3** set are composed of **algo**, **pots**, **brmu**, **tixi**, **thti**, **goug**, and **guam**. For the fiducial sets, stations with relatively good DDobs

| site Id | daily DDobs | Quality N.A. | Quality daily | coordinates accuracy | site Id | daily DDobs | Quality N.A. | Quality daily | coordinates accuracy |
|---|---|---|---|---|---|---|---|---|---|
| algo | 3098.0 | 0 | 10.00000 | 0.30000 | mawl | 4131.0 | 1 | 8.18180 | 0.88000 |
| alic | 3557.2 | 0 | 10.00000 | 1.24000 | mcm4 | 4517.1 | 0 | 5.45450 | 0.33000 |
| ankr | 3579.6 | 1 | 9.09090 | 1.24000 | mdvo | 3481.3 | 2 | 6.9091 | 0.3700 |
| artu | 3776.7 | 0 | 10.00000 | 0.71000 | mets | 3880.7 | 1 | 9.09090 | 0.24000 |
| asc1 | 2776.8 | 1 | 8.90910 | 0.46000 | mkea | 2611.4 | 0 | 10.00000 | 0.30000 |
| auck | 3286.0 | 0 | 10.00000 | 0.30000 | nico | 3469.4 | 1 | 9.09090 | 0.58000 |
| bahr | 3326.2 | 1 | 8.72730 | 0.35000 | noum | 3376.8 | 2 | 8.18180 | 0.66000 |
| bili | 4021.0 | 0 | 10.00000 | 12.44000 | nrc1 | 3153.5 | 0 | 10.00000 | 0.37000 |
| bjfs | 3356.9 | 2 | 7.81820 | 2.91000 | ntus | 3838.4 | 2 | 8.18180 | 0.92000 |
| borl | 3250.0 | 1 | 9.09090 | 0.30000 | nya1 | 4372.4 | 2 | 4.36360 | 0.42000 |
| braz | 3116.9 | 11 | 0.00000 | 0.47000 | nyal | 4343.2 | 2 | 6.5455 | 0.3300 |
| brmu | 2771.4 | 0 | 10.00000 | 0.30000 | onsa | 3734.5 | 1 | 9.09090 | 0.24000 |
| brus | 3135.0 | 1 | 8.54550 | 0.30000 | pert | 3244.1 | 1 | 9.09090 | 0.30000 |
| cas1 | 4205.5 | 1 | 7.09090 | 0.37000 | petp | 3392.1 | 0 | 9.63640 | 1.21000 |
| chat | 3361.8 | 0 | 10.00000 | 0.30000 | pimo | 2441.5 | 0 | 7.09090 | 1.08000 |
| chur | 3101.3 | 1 | 8.90910 | 0.37000 | pol2 | 3535.0 | 0 | 10.00000 | 0.30000 |
| coco | 2912.3 | 2 | 8.18180 | 0.46000 | pots | 3568.3 | 1 | 9.09090 | 0.24000 |
| cro1 | 2987.8 | 0 | 10.00000 | 0.24000 | ramo | 3459.8 | 5 | 5.45450 | 1.17000 |
| dav1 | 3781.9 | 1 | 6.90910 | 0.33000 | reyk | 3872.1 | 1 | 8.72730 | 0.24000 |
| ebre | 3363.1 | 1 | 9.09090 | 0.44000 | riog | 3526.7 | 1 | 8.72730 | 0.54000 |
| eisl | 1433.5 | 0 | 7.81820 | 0.30000 | sant | 3307.3 | 0 | 9.81820 | 0.30000 |
| fair | 3157.9 | 0 | 7.45450 | 0.24000 | sch2 | 3274.5 | 0 | 10.00000 | 0.54000 |
| fort | 2513.8 | 0 | 8.36360 | 0.30000 | sey1 | 1568.0 | 0 | 5.81820 | 1.30000 |
| gala | 3009.0 | 0 | 10.00000 | 0.64000 | stjo | 3530.2 | 0 | 10.00000 | 0.24000 |
| glsv | 3653.5 | 1 | 9.09090 | 0.84000 | suth | 3115.8 | 0 | 10.00000 | 0.78000 |
| goug | 2759.6 | 11 | 0.00000 | 1.27000 | suwn | 3462.5 | 5 | 5.45450 | 0.98000 |
| gras | 3128.1 | 1 | 8.00000 | 0.30000 | syog | 3921.8 | 3 | 6.72730 | 0.79000 |
| graz | 3562.0 | 1 | 9.09090 | 0.30000 | thti | 2865.8 | 2 | 8.18180 | 0.52000 |
| guam | 3183.2 | 0 | 9.27270 | 0.35000 | thu1 | 2493.5 | 2 | 5.63640 | 0.33000 |
| hers | 3459.6 | 3 | 7.27270 | 0.51000 | tidb | 3452.2 | 0 | 10.00000 | 0.30000 |
| hob2 | 3316.4 | 2 | 7.63640 | 0.30000 | tixi | 4170.5 | 0 | 9.45450 | 1.24000 |
| hofn | 3856.6 | 1 | 8.36360 | 0.59000 | tow2 | 3527.7 | 0 | 10.00000 | 1.19000 |
| irkt | 3002.0 | 3 | 6.90910 | 0.30000 | tro1 | 4258.8 | 1 | 8.5455 | 0.9700 |
| joze | 3509.5 | 1 | 9.09090 | 0.30000 | trom | 4268.8 | 1 | 8.54550 | 0.33000 |
| karr | 3530.8 | 1 | 9.09090 | 1.27000 | urum | 3186.1 | 1 | 9.09090 | 0.90000 |
| kely | 2875.8 | 1 | 6.90910 | 0.33000 | usud | 3558.6 | 0 | 10.00000 | 0.35000 |
| kerg | 3195.7 | 1 | 8.00000 | 0.30000 | vesl | 4339.1 | 11 | 0.00000 | 0.62000 |
| kiru | 4158.8 | 1 | 8.90910 | 0.33000 | vill | 3370.8 | 1 | 9.09090 | 0.30000 |
| kosg | 3555.3 | 6 | 4.54550 | 0.24000 | whit | 3292.5 | 0 | 9.63640 | 0.33000 |
| kour | 2795.9 | 2 | 7.27270 | 0.30000 | wsrt | 3552.5 | 1 | 9.0909 | 0.3700 |
| lhas | 3118.3 | 4 | 6.36360 | 0.37000 | wtzr | 3630.5 | 1 | 9.09090 | 0.24000 |
| lpgs | 3129.3 | 1 | 8.90910 | 0.35000 | wuhn | 3355.0 | 2 | 6.36360 | 0.41000 |
| mac1 | 3481.4 | 1 | 8.90910 | 0.37000 | yell | 3402.7 | 0 | 9.27270 | 0.24000 |
| madr | 3255.4 | 0 | 10.00000 | 0.9700 | yssk | 3619.9 | 0 | 10.00000 | 1.39000 |
| mag0 | 3653.3 | 0 | 10.00000 | 0.78000 | zeck | 3563.5 | 10 | 0.90910 | 0.58000 |
| mali | 3171.3 | 0 | 9.63640 | 1.29000 | zimm | 3510.9 | 1 | 9.09090 | 0.37000 |
| mas1 | 2809.3 | 11 | 0.00000 | 0.24000 | zwen | 3750.4 | 1 | 8.54550 | 0.24000 |
| mate | 3332.7 | 1 | 7.81820 | 0.30000 | | | | | |

Table 6.5: 95 Best Stations for cycle 8, which were selected from 208 ITRF2000 stations according to Algorithm 1

| site Id | daily DDobs | Quality N.A. | Quality daily | coordinates accuracy | site Id | daily DDobs | Quality N.A. | Quality daily | coordinates accuracy |
|---|---|---|---|---|---|---|---|---|---|
| algo | 3216.6 | 0 | 10.00000 | 0.30000 | mcm4 | 4437.5 | 1 | 4.90910 | 0.33000 |
| alic | 3631.5 | 0 | 9.09090 | 1.24000 | mdvo | 3106.7 | 1 | 6.3636 | 0.3700 |
| artu | 3435.3 | 0 | 9.09090 | 0.71000 | mets | 3709.4 | 0 | 8.90910 | 0.24000 |
| asc1 | 2466.5 | 2 | 8.18180 | 0.46000 | mkea | 2322.4 | 0 | 9.81820 | 0.30000 |
| auck | 3281.6 | 0 | 9.63640 | 0.30000 | nico | 3181.1 | 0 | 9.09090 | 0.58000 |
| bahr | 3166.2 | 0 | 8.90910 | 0.35000 | noum | 3226.5 | 3 | 7.09090 | 0.66000 |
| bili | 1748.8 | 8 | 2.54550 | 12.44000 | nrc1 | 3248.9 | 0 | 10.00000 | 0.37000 |
| bor1 | 3116.9 | 0 | 9.09090 | 0.30000 | ntus | 3629.0 | 0 | 9.09090 | 0.92000 |
| brmu | 2791.5 | 0 | 10.00000 | 0.30000 | nya1 | 4166.5 | 0 | 5.81820 | 0.42000 |
| cas1 | 4394.5 | 0 | 6.36360 | 0.37000 | nyal | 4145.6 | 0 | 7.2727 | 0.3300 |
| cedu | 3036.6 | 1 | 8.18180 | 1.50000 | onsa | 3560.1 | 0 | 9.09090 | 0.24000 |
| chat | 3318.4 | 0 | 9.81820 | 0.30000 | pert | 3442.7 | 0 | 9.09090 | 0.30000 |
| chur | 3212.5 | 0 | 9.63640 | 0.37000 | pimo | 2455.5 | 0 | 7.81820 | 1.08000 |
| coco | 3370.9 | 0 | 9.09090 | 0.46000 | pol2 | 3033.4 | 0 | 8.90910 | 0.30000 |
| cro1 | 2950.7 | 1 | 9.09090 | 0.24000 | pots | 3381.9 | 0 | 9.09090 | 0.24000 |
| dav1 | 3933.3 | 1 | 6.18180 | 0.33000 | ramo | 3174.6 | 2 | 7.27270 | 1.17000 |
| ebre | 3223.9 | 1 | 8.18180 | 0.44000 | reyk | 3871.6 | 0 | 8.90910 | 0.24000 |
| eisl | 1634.4 | 0 | 7.81820 | 0.30000 | riog | 2275.3 | 7 | 3.63640 | 0.54000 |
| fair | 3046.2 | 0 | 7.45450 | 0.24000 | sant | 3362.5 | 0 | 9.81820 | 0.30000 |
| fort | 2066.8 | 1 | 6.54550 | 0.30000 | sch2 | 3306.8 | 0 | 10.00000 | 0.54000 |
| gala | 3079.7 | 0 | 10.00000 | 0.64000 | sey1 | 1523.6 | 0 | 5.81820 | 1.30000 |
| glsv | 3434.3 | 1 | 8.18180 | 0.84000 | sol1 | 3097.1 | 0 | 9.45450 | 0.37000 |
| goug | 2902.7 | 8 | 2.54550 | 1.27000 | stjo | 3502.0 | 0 | 10.00000 | 0.24000 |
| graz | 3216.8 | 1 | 8.00000 | 0.30000 | suth | 3166.6 | 0 | 9.09090 | 0.78000 |
| guam | 2518.8 | 0 | 9.09090 | 0.35000 | suwn | 3144.9 | 1 | 8.72730 | 0.98000 |
| hers | 3292.6 | 1 | 7.81820 | 0.51000 | syog | 4154.1 | 1 | 7.81820 | 0.79000 |
| hob2 | 3564.5 | 0 | 9.09090 | 0.30000 | thti | 3116.4 | 4 | 6.36360 | 0.52000 |
| hofn | 3817.5 | 0 | 8.72730 | 0.59000 | tidb | 3459.0 | 0 | 9.09090 | 0.30000 |
| joze | 3383.6 | 0 | 9.09090 | 0.30000 | tixi | 3981.2 | 0 | 8.90910 | 1.24000 |
| karr | 3608.5 | 0 | 9.09090 | 1.27000 | tow2 | 3471.0 | 0 | 9.63640 | 1.19000 |
| kely | 3360.6 | 0 | 8.72730 | 0.33000 | tro1 | 4088.4 | 0 | 8.9091 | 0.9700 |
| kerg | 3473.8 | 4 | 4.90910 | 0.30000 | trom | 4109.8 | 0 | 8.90910 | 0.33000 |
| kiru | 3921.1 | 0 | 9.09090 | 0.33000 | usud | 3087.3 | 0 | 10.00000 | 0.35000 |
| kokb | 2467.2 | 0 | 10.00000 | 0.30000 | vesl | 1906.4 | 11 | 0.00000 | 0.62000 |
| kosg | 3391.5 | 0 | 9.0909 | 0.2400 | vill | 3277.0 | 0 | 9.09090 | 0.30000 |
| kour | 3481.1 | 1 | 8.36360 | 0.30000 | whit | 3160.6 | 0 | 9.81820 | 0.33000 |
| mac1 | 3585.4 | 0 | 9.09090 | 0.37000 | wsrt | 3398.6 | 0 | 9.09090 | 0.37000 |
| madr | 3178.1 | 0 | 9.0909 | 0.9700 | wtzr | 3252.4 | 0 | 8.90910 | 0.24000 |
| mag0 | 3162.9 | 0 | 10.00000 | 0.78000 | yell | 3298.3 | 0 | 9.45450 | 0.24000 |
| mali | 3195.2 | 0 | 8.72730 | 1.29000 | yssk | 3150.6 | 0 | 10.00000 | 1.39000 |
| mas1 | 3200.2 | 10 | 0.90910 | 0.24000 | zeck | 3314.9 | 9 | 1.81820 | 0.58000 |
| mate | 3158.5 | 0 | 8.00000 | 0.30000 | zimm | 3306.1 | 2 | 7.27270 | 0.37000 |
| maw1 | 4245.5 | 0 | 8.36360 | 0.88000 | zwen | 3459.7 | 0 | 8.54550 | 0.24000 |

Table 6.6: 86 Best Stations for cycle 9, which were selected from 208 ITRF2000 stations according to Algorithm 1

| site | daily | Quality | | coordinates | site | daily | Quality | | coordinates |
|---|---|---|---|---|---|---|---|---|---|
| Id | DDobs | N.A. | daily | accuracy | Id | DDobs | N.A. | daily | accuracy |
| algo | 3461.0 | 1 | 8.72730 | 0.30000 | maw1 | 4449.6 | 1 | 7.27270 | 0.88000 |
| alic | 3544.8 | 1 | 8.72730 | 1.24000 | mcm4 | 4661.4 | 1 | 5.45450 | 0.33000 |
| amc2 | 3066.6 | 1 | 8.54550 | 1.64000 | mdvo | 3032.1 | 1 | 6.3636 | 0.3700 |
| artu | 3396.4 | 1 | 8.36360 | 0.71000 | mets | 3670.8 | 1 | 8.54550 | 0.24000 |
| asc1 | 2363.1 | 2 | 8.18180 | 0.46000 | mkea | 2585.3 | 1 | 8.54550 | 0.30000 |
| auck | 3220.0 | 1 | 8.72730 | 0.30000 | nico | 3206.5 | 1 | 8.36360 | 0.58000 |
| bahr | 3105.3 | 1 | 8.72730 | 0.35000 | nklg | 3117.0 | 1 | 8.54550 | 1.14000 |
| bili | 3624.7 | 1 | 7.81820 | 12.44000 | noum | 3114.1 | 5 | 5.45450 | 0.66000 |
| bor1 | 3181.9 | 1 | 8.72730 | 0.30000 | nrc1 | 3507.7 | 1 | 8.72730 | 0.37000 |
| brmu | 2427.4 | 3 | 6.90910 | 0.30000 | ntus | 3534.5 | 1 | 8.72730 | 0.92000 |
| cas1 | 4509.1 | 1 | 5.81820 | 0.37000 | nya1 | 1572.0 | 2 | 5.8182 | 0.4200 |
| cedu | 3138.5 | 1 | 8.54550 | 1.50000 | nyal | 4325.7 | 1 | 6.72730 | 0.33000 |
| chat | 3279.4 | 1 | 8.72730 | 0.30000 | onsa | 3705.7 | 1 | 8.72730 | 0.24000 |
| chur | 3409.3 | 1 | 7.27270 | 0.37000 | pert | 3425.5 | 1 | 8.54550 | 0.30000 |
| coco | 3340.5 | 1 | 8.54550 | 0.46000 | pimo | 2584.6 | 2 | 6.72730 | 1.08000 |
| cro1 | 3165.8 | 1 | 8.72730 | 0.24000 | pots | 3540.0 | 1 | 8.72730 | 0.24000 |
| daej | 3037.2 | 1 | 6.72730 | 0.81000 | prds | 3127.4 | 1 | 8.72730 | 0.81000 |
| dav1 | 3937.7 | 2 | 6.00000 | 0.33000 | ramo | 3138.4 | 2 | 7.63640 | 1.17000 |
| ebre | 3381.7 | 1 | 8.72730 | 0.44000 | reyk | 4029.2 | 1 | 8.00000 | 0.24000 |
| fair | 3117.4 | 1 | 6.00000 | 0.24000 | riog | 3541.6 | 1 | 8.90910 | 0.54000 |
| fort | 1982.7 | 2 | 6.18180 | 0.30000 | sant | 3191.1 | 1 | 8.36360 | 0.30000 |
| gala | 3229.7 | 1 | 8.72730 | 0.64000 | sch2 | 3488.8 | 1 | 8.36360 | 0.54000 |
| glsv | 3403.8 | 1 | 8.72730 | 0.84000 | sey1 | 1595.1 | 1 | 5.27270 | 1.30000 |
| goug | 2783.7 | 2 | 7.63640 | 1.27000 | soll | 3285.8 | 1 | 8.54550 | 0.37000 |
| graz | 3226.1 | 1 | 8.54550 | 0.30000 | stjo | 3683.7 | 1 | 8.72730 | 0.24000 |
| guam | 2740.2 | 1 | 8.00000 | 0.35000 | suth | 3040.1 | 1 | 8.72730 | 0.78000 |
| hers | 3438.3 | 1 | 8.72730 | 0.51000 | syog | 3924.7 | 2 | 6.72730 | 0.79000 |
| hob2 | 3525.5 | 1 | 8.72730 | 0.30000 | thti | 3105.2 | 2 | 7.81820 | 0.52000 |
| hofn | 3777.4 | 1 | 7.81820 | 0.59000 | thu1 | 1963.1 | 4 | 4.90910 | 0.33000 |
| joze | 3421.0 | 1 | 8.72730 | 0.30000 | tidb | 3388.4 | 1 | 8.72730 | 0.30000 |
| karr | 3165.6 | 2 | 7.45450 | 1.27000 | tixi | 3932.1 | 1 | 6.72730 | 1.24000 |
| kely | 2225.8 | 3 | 5.27270 | 0.33000 | tow2 | 3366.4 | 1 | 8.72730 | 1.19000 |
| kerg | 3380.2 | 1 | 7.27270 | 0.30000 | tro1 | 4163.0 | 1 | 7.81820 | 0.97000 |
| kiru | 4080.5 | 1 | 8.18180 | 0.33000 | trom | 3625.7 | 2 | 6.9091 | 0.3300 |
| kokb | 2670.8 | 1 | 8.54550 | 0.30000 | usna | 3023.8 | 1 | 8.1818 | 0.5400 |
| kosg | 3568.1 | 2 | 7.8182 | 0.2400 | vill | 3134.0 | 1 | 8.1818 | 0.3000 |
| kour | 3862.2 | 1 | 8.72730 | 0.30000 | whit | 3365.7 | 1 | 8.54550 | 0.33000 |
| mac1 | 3676.6 | 1 | 8.00000 | 0.37000 | wsrt | 3600.0 | 1 | 8.72730 | 0.37000 |
| madr | 3230.0 | 1 | 8.72730 | 0.97000 | wtzr | 3503.7 | 1 | 8.72730 | 0.24000 |
| mag0 | 3104.4 | 1 | 8.18180 | 0.78000 | yell | 3481.1 | 1 | 7.45450 | 0.24000 |
| mali | 3234.2 | 1 | 8.18180 | 1.29000 | zeck | 3277.3 | 4 | 6.36360 | 0.58000 |
| mas1 | 3135.5 | 9 | 1.81820 | 0.24000 | zimm | 3477.0 | 2 | 8.18180 | 0.37000 |
| mate | 3286.7 | 1 | 8.00000 | 0.30000 | zwen | 3467.2 | 1 | 8.54550 | 0.24000 |

Table 6.7: 86 Best Stations for cycle 10, which were selected from 208 ITRF2000 stations according to Algorithm 1

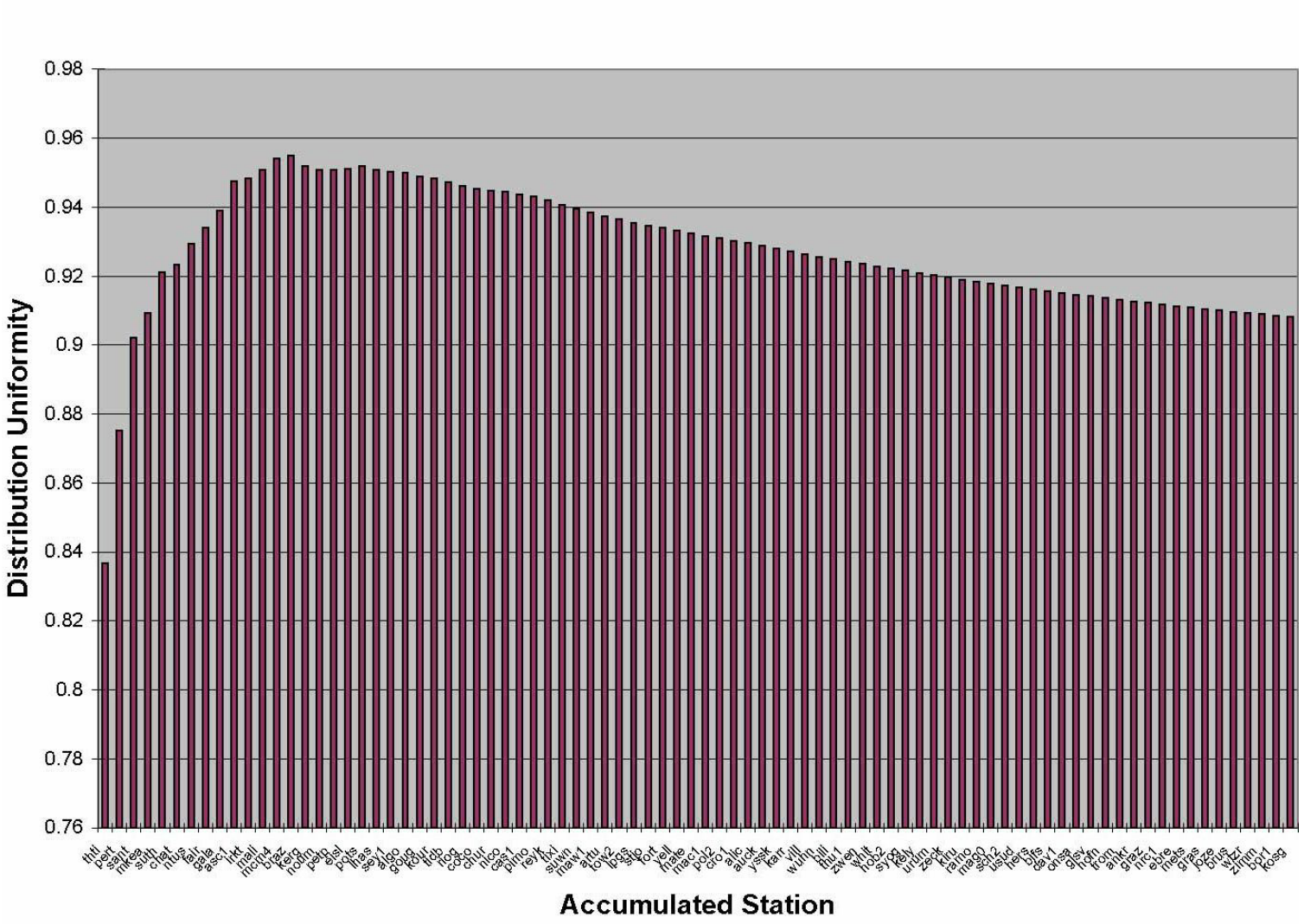


Figure 6.6: Distribution Uniformity ($u$) of each Accumulated Station Set for Cycle 8. Set **C8-fidu1** is defined as a set accumulated up to **pots** starting from the **fidu1** set, which is composed of nya1, vesl, brmu, mas1, bahr, and guam. Uniformity reaches its maximum with 20∼30 accumulated stations. Uniformity with other fiducial station sets or other cycles shows the same pattern.

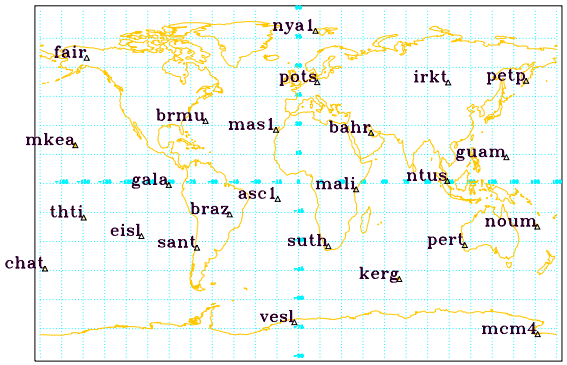


(a) Set **C8-fidu1** (25 stations, $u = 0.952$)

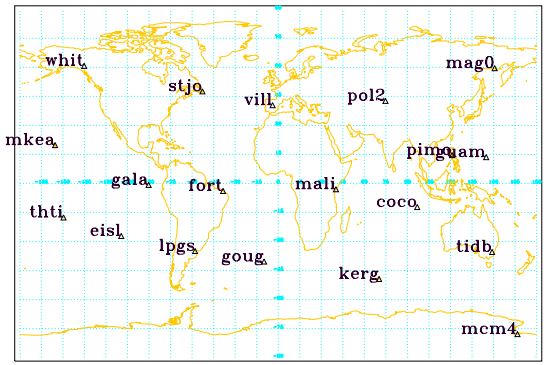


(b) Set **C8-fidu2** (19 stations, $u = 0.950$)

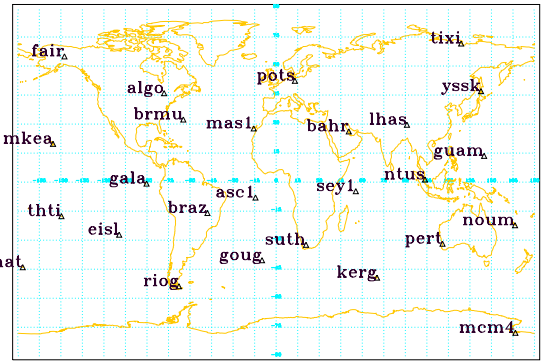


(c) Set **C8-fidu3** (26 stations, $u = 0.951$)

Figure 6.7: Optimal Sets for cycle 8. Set **C8-fidu1** (fiducial = nya1, vesl, brmu, mas1, bahr, guam ), Set **C8-fidu2** (fiducial = mag0, pol2, stjo, tidb, thti, goug ), and Set **C8-fidu3** (fiducial = algo, pots, brmu, tixi, thti, goug, guam ). Note that all three sets have nearly the same uniformity measure.

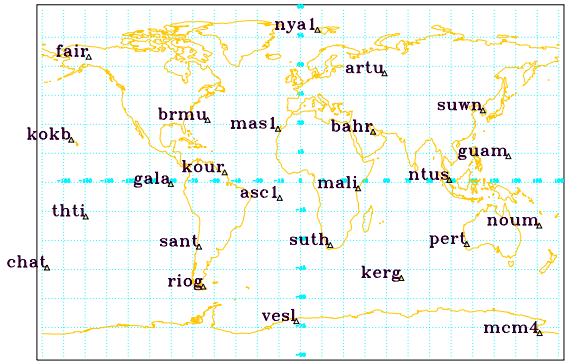


(a) Set **C9-fidu1** (24 stations, $u = 0.952$)

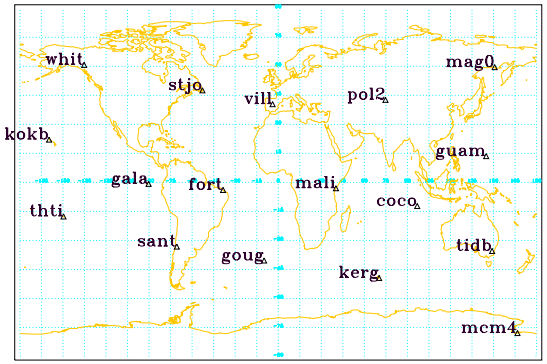


(b) Set **C9-fidu2** (17 stations, $u = 0.955$)

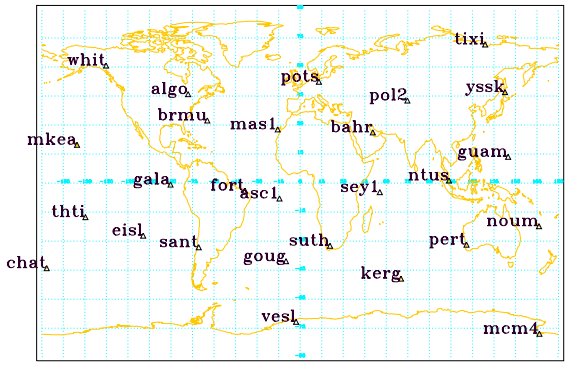


(c) Set **C9-fidu3** (27 stations, $u = 0.950$)

Figure 6.8: Optimal Sets for cycle 9. Set **C9-fidu1** (fiducial=nya1,vesl,brmu,mas1,bahr,guam.), Set **C9-fidu2** (fiducial=mag0,pol2,stjo,tidb,thti,goug.), and Set **C9-fidu3** (fiducial=algo,pots,brmu,tixi,thti,goug,guam.). Note that Set **C9-fidu2** has the highest uniformity, yet requires only 17 stations.

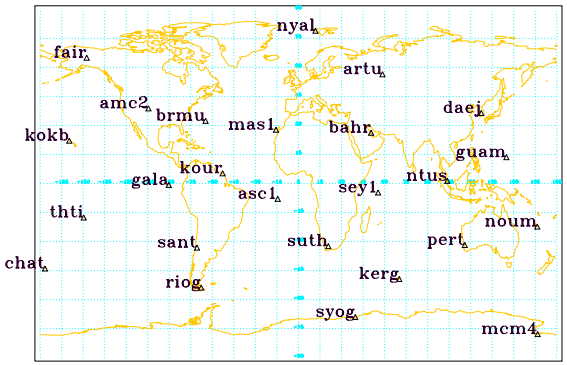


(a) Set **C10-fidu1**(25 stations, $u = 0.957$)

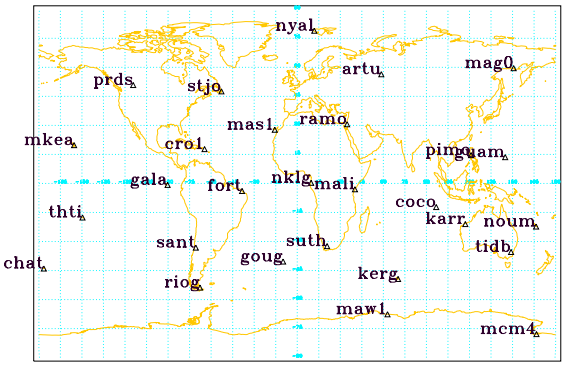


(b) Set **C10-fidu2**(28 stations, $u = 0.945$)

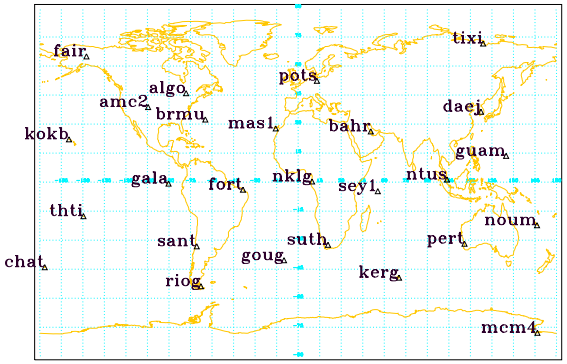


(c) Set **C10-fidu3**(26 stations, $u = 0.950$)

Figure 6.9: Optimal Sets for cycle 10. Set **C10-fidu1** (fiducial = nya1, syog, brmu, mas1, bahr, guam.), Set **C10-fidu2** (fiducial = mag0, artu, stjo, tidb, thti, goug.), and Set **C10-fidu3** (fiducial = algo, pots, brmu, tixi, thti, goug, guam.)

and coordinates accuracy are selected. For cycle 10, **vesl** was replaced by **syog** for **fidu1**, and **pol2** was replaced by **artu** for **fidu2**, since **vesl** and **pol2** are not included in best stations of cycle 10 (see Table 6.7).

Starting with these three different fiducial set, each station out of the best stations producing the maximal uniformity was accumulated following Algorithm 2. Figure 6.6 shows the distribution uniformity for each accumulated set in order of accumulation starting from the **fidu1** set for cycle 8. It shows that the sets with only 20∼30 accumulated stations (including fiducial stations) reach the approximate maximal distribution uniformity. The uniformity of the accumulated sets with different fiducial sets followed the same pattern. Cycles 9 and 10 also showed the same uniformity-changing pattern with the accumulation of stations. This implies that, in terms of the distribution uniformity, the optimal number of stations in a set may range from 20 to 30 regardless of the selection of fiducial stations.

Finally, the optimal station sets accumulated starting from each fiducial sets are shown in Figures 6.7, 6.8 and 6.9 for cycle 8, 9 and 10 respectively.

## 6.3 Orbit improvement with new tracking station sets and Summary

The Nominal Set is a subset of 51 IGS00 stations with high quality positions/velocities. Many of the 51 IGS00 stations are equipped with more

than one geodetic instrument[3] per site. More observing techniques generally provide better accuracy as well as a better integrity with the help of accurate tie information between the geodetic instruments. Thus, the 43 stations of the Nominal Set have high quality coordinates, but are not well-distributed.

On the other hand, the stations of the optimal sets were chosen out of 208 ITRF2000 stations by considering mostly the uniformity of distribution in mind. More than half of the stations in any optimal set do not belong to IGS00, and several stations located in remote regions are included in the optimal sets to maximize the uniformity of distribution of optimal sets, although their coordinate qualities are relatively low.

Table 6.9 shows the comparison of GPS-only orbits from the Nominal Set and three optimal station sets. The subarc length of 3 hours for estimation of the CT parameter and 9 hours for estimation of 1-cpr T & N parameters were applied for the orbit solutions (see **Case sub1.5-4.5** in Table 4.12(a)). For cycle 8, the crossover residuals (Mean=5.6 mm, RMS=6.24 cm) of the orbit from the Nominal Set are better than the orbits from the optimal sets. However, for cycle 9 and 10, the statistics of orbits from the Nominal Set and the optimal sets appear to be very close. Considering that the number of stations in the optimal sets are just half of the number of stations in the Nominal Set, and that individual station's quality in the optimal sets are not

[3]Each station of ITRF2000 uses geodetic techniques such as VLBI, SLR, GPS and DORIS. According to `http://lareg.ensg.ign.fr/ITRF`, 70 stations of ITRF2000 are collocated with 2 geodetic techniques, 25 stations of ITRF2000 are collocated with 3 geodetic techniques, and 6 stations of ITRF2000 are collocated with 4 geodetic techniques.

better than individual station's quality in the Nominal Set, it may indicate that the uniform distribution of optimal station sets contributed inertial centering to the orbit solutions preventing them from being worse. However, the fact that the orbits from the optimal sets are not significantly better than the orbits from the Nominal Set implies that not only uniformity of distribution is an important factor to improve the orbit accuracy, but the quality of the individual station is also an important factor to consider in choosing the station set.

| case | Internal Consistency | | | | SLR residuals(>70°) | | crossover residuals | |
|---|---|---|---|---|---|---|---|---|
| | R | T | N | RSS | Mean | RMS | Mean | RMS |
| cycle 8: | | | | | | | | |
| Nominal Set | 8.2 | 17.9 | 12.0 | 23.8 | -.2 | 7.6 | 3.9 | 61.2 |
| Set C8-fidu1 | 9.2 | 19.7 | 12.4 | 26.0 | .8 | 7.0 | 7.0 | 61.3 |
| Set C8-fidu2 | 8.9 | 18.7 | 12.8 | 25.3 | .4 | 7.1 | 7.1 | 61.4 |
| Set C8-fidu3 | 9.4 | 19.6 | 12.0 | 25.9 | .6 | 7.4 | 6.5 | 61.3 |
| cycle 9: | | | | | | | | |
| Nominal Set | 13.3 | 29.1 | 9.2 | 33.6 | -3.7 | 10.9 | 3.6 | 58.9 |
| Set C9-fidu1 | 13.3 | 28.8 | 9.1 | 33.3 | -3.2 | 10.5 | 4.3 | 58.9 |
| Set C9-fidu2 | 13.0 | 28.7 | 9.1 | 33.2 | -3.5 | 10.3 | 3.5 | 59.0 |
| Set C9-fidu3 | 13.1 | 29.4 | 9.2 | 33.8 | -3.4 | 10.6 | 3.8 | 58.9 |
| cycle 10: | | | | | | | | |
| Nominal Set | 10.7 | 20.7 | 10.1 | 25.5 | -5.7 | 10.0 | -1.6 | 59.2 |
| Set C10-fidu1 | 10.1 | 19.6 | 9.8 | 24.3 | -4.6 | 8.8 | 1.0 | 59.1 |
| Set C10-fidu2 | 13.0 | 28.7 | 9.1 | 33.2 | -4.8 | 8.8 | 1.0 | 59.2 |
| Set C10-fidu3 | 10.5 | 20.1 | 10.1 | 24.9 | -4.5 | 8.8 | .8 | 59.1 |

Table 6.8: Orbit Improvement for Mixed Orbits: SLR and crossover residuals

| case | Internal Consistency | | | | SLR residuals(>70°) | | crossover residuals | |
|---|---|---|---|---|---|---|---|---|
| | R | T | N | RSS | Mean | RMS | Mean | RMS |
| cycle 8: | | | | | | | | |
| Nominal Set | 14.5 | 30.0 | 12.5 | 36.0 | .0 | 9.4 | 5.6 | 62.4 |
| Set C8-fidu1 | 14.8 | 30.2 | 14.2 | 36.9 | 1.7 | 8.1 | 12.1 | 64.2 |
| Set C8-fidu2 | 14.5 | 29.4 | 14.0 | 36.0 | 1.0 | 8.9 | 11.4 | 63.6 |
| Set C8-fidu3 | 15.2 | 30.4 | 14.1 | 37.3 | 1.4 | 9.2 | 12.3 | 64.0 |
| cycle 9: | | | | | | | | |
| Nominal Set | 16.0 | 36.5 | 9.3 | 41.2 | -4.0 | 13.9 | 6.8 | 61.2 |
| Set C9-fidu1 | 15.7 | 35.5 | 9.8 | 40.3 | -3.8 | 14.1 | 7.3 | 61.2 |
| Set C9-fidu2 | 15.8 | 36.8 | 10.2 | 41.6 | -4.4 | 14.0 | 5.9 | 61.3 |
| Set C9-fidu3 | 16.2 | 38.3 | 9.9 | 43.0 | -4.3 | 14.3 | 6.0 | 61.0 |
| cycle 10: | | | | | | | | |
| Nominal Set | 13.1 | 24.6 | 9.9 | 29.9 | -7.5 | 13.8 | 5.9 | 61.5 |
| Set C10-fidu1 | 13.3 | 24.2 | 9.5 | 29.4 | -7.6 | 13.6 | 7.3 | 61.8 |
| Set C10-fidu2 | 13.0 | 24.0 | 10.1 | 29.2 | -8.1 | 13.7 | 7.1 | 61.8 |
| Set C10-fidu3 | 13.6 | 24.2 | 9.8 | 29.7 | -7.2 | 13.7 | 6.8 | 61.7 |

Table 6.9: Orbit Improvement for GPS-only Orbits: SLR and crossover residuals

Table 6.8 shows the comparison of SLR/DORIS/GPS orbits from the Nominal Set and the three optimal station sets. In Table 6.8 from GPS tracking combined with SLR/DORIS, the orbits from the Nominal Set and the optimal sets show less difference than in Table 6.9 mainly because of the contribution of SLR to the orbit centering. To see the influence of the distribution uniformity of the optimal station set on the orbit improvement, an extended investigation with more cycles and with more broad range of criteria of station qualities will be needed. At this point, it appears that we can only conclude that the optimal station selection provides almost the same orbit performance as the nominal selection, but generally requires fewer stations than the nominal selection in the process.

# Chapter 7

# Conclusions

## 7.1 Summary and Conclusions

In this study, the three tracking data types, SLR, DORIS and GPS, of Jason-1 for cycles 8 - 20 were processed either simultaneously or separately. The orbits of 30-hour arcs were integrated daily with 3-hour extension on both ends for the overlap test purpose. Then, each full cycle's orbits were obtained by merging the middle 24-hour arcs of the daily orbits. For the performance assessment of each orbit solution, the altimeter crossover data test and the SLR residual test were conducted as well as the overlap test for the internal consistency check. An external test with orbits from other institutes was also performed to compare the solutions from different approaches of each software with different combinations of measurement types.

One of the objectives of this research was to seek optimal models and parameterizations to get the best orbit solution by using GPS-only data or combined data in the dynamic approach. To achieve the most precise orbits that these tracking data could support, three areas required refinement; 1) the parameters related to the Center of Mass (CoM) or antenna phase center, 2) the empirical acceleration parameters to accommodate the surface force model

errors, and 3) the parameters related to the orbit element correction of GPS satellites.

First, the parameters related to the location of the antenna phase centers were estimated because of their contribution to the orbit improvement. Early analysis of Jason-1 tracking indicated likely errors in either the location of CoM, the antenna phase centers or both. Estimates of the phase center offset from different orbit analysis centers using different tracking data were compared to see whether there is an actual CoM error common to each measurement's tracking antenna or whether the shift of the phase center is peculiar to the GPS antenna alone. Because the estimated phase center offsets in the x-axis for both the LRA and the GPS antenna appeared to be the same - approximately 13 mm, it is far more likely that the estimated shift in the x-axis reflects an error in the nominal value for the CoM of the satellite rather than a phase center error in both antennas. In contrast, there was no observable bias along the z-axis for the LRA, implying that the GPS $L_C$ phase center location was offset from its true location by 34 mm. The new CoM location with respect to the reference point was estimated to be (955, 0, 0) mm at CSR. The new phase center location of the GPS antenna relative to the new CoM location estimated at CSR was (1434, $-218$, $-538$) mm. Furthermore, the orbits with the estimation of the z-directional change of the GPS phase center offset performed best in the low fixed yaw regime. For the sinusoidal yaw regime, the x- and z-directional changes of the GPS phase center offset had to be estimated simultaneously.

Second, the optimal subarc length for the estimation of empirical parameters was investigated. Finding an optimal frequency for the estimation of empirical acceleration parameters is very important to obtain an orbit solution with better accuracy. One of the benefits that the GPS data can provide for POD is its dense and homogeneous tracking capability, and with the dense observation set, a heavier level of parameterization is possible to accommodate the force model errors. The GPS-only orbit solutions using a subarc length of 3 hours for the estimation of CT and 9 hours for the 1-cpr T & N parameters performed best with a crossover RMS of 6.01 ($\pm$0.2) cm. The magnitudes of the crossover Means of cycle 11, 12, 16, 19 and 20 for GPS-only orbits were persistently larger than 1 cm regardless of the subarc length, which indicates that the orbits with GPS-only tracking are not well centered inertially especially for short terms. However, the averaged value of the crossover Means over cycles 8 to 20 was 0.06 cm, which indicates that they are well centered in the mean sense. The short-term instability of orbit centering for several cycles was also observed in SLR/DORIS orbits, which implies that the accuracy of the altimeter data for those cycles might be deteriorated. The averaged value of the SLR residual RMSs was 1.3 ($\pm$0.3) cm for the GPS-only orbits, which is an excellent result as a measure of the absolute radial orbit accuracy considering that the SLR data was not used to obtain the orbit.

When all three data types were used, it was possible to improve the results a little more. The optimal subarc lengths for the estimation of the empirical force parameters with the combined measurement system were de-

termined to be 3 hours for the estimation of CT and 6 hours for the estimation of 1-cpr T & N parameters, which were further shortened compared to the optimal subarc lengths of the GPS-only orbits due to the mutual support from each tracking system. However, the results of the crossover test and the SLR residual test of the combined orbits were not so sensitive to the subarc lengths in the range between 3 hours and 15 hours for the estimation of empirical parameters. The averaged crossover RMSs over the cycles of the combined orbits was 5.87($\pm$0.22) cm. The crossover Means, which are indicators of the orbit centering, were in the range of $-1\sim-2$ mm for the combined orbits. Their standard deviation ($\sim$7 mm) from cycle to cycle is smaller than the standard deviation ($\sim$10 mm) of cycles from the GPS-only orbits, which indicates that the orbits with combined measurement types are more stable in the sense of the orbit centering due to the SLR tracking. However, other tests also indicate that the DORIS data was not helpful in the orbit centering. The SLR residual RMSs of the combined orbits were less than 1 cm, even when the orbits of days 117 and 141 with the occurrence of tracking weakness were included. This is a very promising result to reach the goal of 1-cm radial orbit RMS error, since the SLR residual RMS is an absolute measure of the orbit accuracy.

Third, the GPS orbit element correction method was introduced to absorb the remaining orbit errors in the ephemerides of the GPS satellites by considering them as an empirical correction to the fixed GPS orbits provided by IGS. The correction of GPS satellite orbit elements rarely showed any orbit performance improvement. This implies that the orbit element correction

method is not sufficient to accommodate the remaining orbit errors in the ephemerides of the GPS satellites, or that the errors are now small enough not to have a significant impact on the orbit accuracy.

Fourth, to choose the best gravity model for the Jason-1 POD, out of 1) JGM-3, 2) EGM96, 3) TEG4 and 4) a preliminary GRACE gravity model, orbits from each gravity model were compared. Out of the four gravity models compared, orbits from the preliminary GRACE gravity model clearly outperformed the orbits from other gravity models in both aspects of the crossover test and the SLR residual test. Their averaged crossover RMS over the cycles was $5.83(\pm 0.23)$ cm, which was reduced modestly, when compared to the averaged crossover RMS of the orbits from JGM3, $5.87(\pm 0.21)$ cm. Their averaged crossover Mean was $-0.2(\pm 4.7)$ mm, which was better than $-0.7(\pm 4.9)$ mm of the orbits from JGM3.

The essential work of this dissertation, as presented in Chapter 5, was to explore the sensitivity of the orbit to changes in the relative weighting of each measurement type, to seek the optimal relative weighting of each measurement type, and to determine which combination of measurement types produced the best orbits. Jason-1 is the first platform to produce long term high precision data from three high quality tracking instruments. The GPS receiver on T/P had several limitations, the DORIS was not as precise as that flown on Jason-1 and the large LRA on T/P tended to introduce biases in the SLR data. The a priori sigmas sought for an optimal relative weighting for each measurement type were 25 cm for GPS and 2 mm/s for DORIS, when 10 cm for SLR was

adopted. We found that the weight for GPS was relatively insensitive between 15 and 35 cm. For the orbit solutions with the optimal relative weightings, the crossover RMS was 5.86 cm, the crossover Mean was $-1.6$ mm, and the SLR residual RMS was 0.91 cm. Upweighting DORIS degraded the orbit accuracy, implying that orbits from the combination of SLR and GPS without DORIS may perform better than orbits from combination of all three measurement types. In fact, except for the duration when GPS tracking is not adequate, DORIS appeared to be redundant or even degrade orbit centering when it was combined with GPS and SLR, if given too much weight. For all of the test cases with or without a combination of measurement types, the crossover Means ranged between 0 mm and $-2$ mm, the crossover RMSs ranged between 5.9 cm and 6.0 cm, and SLR residual RMSs ranged between 0.9 cm and 1.3 cm. The SLR residual RMSs from GPS-only orbits, and from orbits combined with GPS and DORIS were 1.3 cm and 1.2 cm respectively, which appear quite promising even without inclusion of SLR.

The orbits from UT/CSR were compared with the external orbits from other institutes such as CNES, DEOS, NASA/GSFC, and NASA/JPL. Both the altimeter crossover test and the SLR residual test show that CSR's and NASA's SLR/DORIS orbits were very close to each other, and in general, their orbits performed better than CNES's and DEOS's. Among the orbit solutions with the dynamic approach, CSR's two combined orbit solutions, **csr1** and **csr2**, performed best. Orbits **csr1** were processed by combining GPS and SLR systems, and Orbits **csr2** were processed by combining GPS, SLR and

DORIS systems. Among the orbit solutions with the reduced-dynamic approach, the orbits from JPL (**jpl**) with GPS-only system performed best. The crossover Means of **csr1**, **csr2** and **jpl** were $-0.7(\pm 4.9)$ mm, $-1.9(\pm 7.0)$ mm and $-0.7(\pm 6.9)$ mm respectively. The crossover RMSs of **csr1**, **csr2** and **jpl** were $5.87(\pm 0.21)$ cm, $5.85(\pm 0.21)$ cm and $5.87(\pm 0.19)$ cm respectively. The SLR residual RMSs of **csr1**, **csr2** and **jpl** were $0.87(\pm 0.21)$ cm, $0.90(\pm 0.18)$ cm and $1.10(\pm 0.30)$ cm respectively. Overall, in the dynamic approach, the combination of GPS and SLR appears to be the best combined systems.

In Chapter 6, a quantitative method for selecting the best performing and geographically well-distributed station network was developed, and the orbits from the optimal networks were compared to the orbits from the nominal network of approximately 43 stations. For the Jason-1 POD with GPS tracking data, tracking from the well-distributed and best-performing 20 to 30 GPS stations appeared to be sufficient. The optimal sets, which were obtained by applying the distribution uniformity measure of the network and each station's performance quality to 208 ITRF2000 stations, are usually composed of 20 - 30 stations. More tracking stations do not necessarily guarantee an orbit solution with better accuracy. The orbits from the optimal network appear to show no significant improvement over the orbits from the nominal network; however, they did not significantly underperform the orbits from the nominal network either. Considering that nominal network was composed of 43 best-performing stations compared to about 20 stations of the optimal network, it indicate that a uniform distribution of high performance station sets can produce a good

result with significantly less data and processing time.

## 7.2 Suggested Future Work

In order to meet the goal of the 1-cm radial RMS of Jason-1 orbit accuracy, many aspects of the dynamic and kinematic models used in the estimation process require optimization. For LEO POD in general, while gravity models are rapidly improving from the efforts made over the previous decade and now with the GRACE mission, non-conservative surface forces are becoming the largest source of satellite orbit errors. For Jason-1 in a higher altitude, drag became less important, while solar radiation pressure becomes increasingly important compared to gravity. In recent years, most of the research on solar radiation pressure has concentrated on empirical modeling. The empirical parameters tend to absorb the model error of solar radiation pressure as well as all of the other unmodeled forces, many of which are non-conservative and may be correlated with each other. Accounting analytically for solar radiation pressure as accurately as possible might free up the burden of the empirical parameters in order to improve the orbit solution. However, little work has been done to improve the accuracy of the solar radiation model for Jason-1. The model of Ziebart *et al.* [2002], one of the surface models for Jason-1, will be worth evaluating.

Estimation of the phase center offsets has become a standard operating procedure in POD because of its clear contribution to the orbit performance improvement. However, little study on the nature of the phase center change

of the GPS antenna in space has been done. Better understanding of the phase center offsets may improve the orbit accuracy. For short terms such as one cycle, GPS orbit centering was sometimes found to be inadequate. To improve this, more accurate modeling or optimized parameterization will be required. To see the influence of the distribution uniformity of the optimal station set on the orbit improvement, only 3 cycles were processed in this study, which were not enough to fully evaluate the effect of the optimal station network on the orbit improvement. An extended investigation with more cycles, exploring the effect of the geographical distribution uniformity of the network and each station's performance quality with varying thresholds, will be needed.

For the future altimetry mission, both SLR and GPS tracking systems are strongly recommended for the POD purpose.

# Appendices

# Appendix A

# Gravitational Force Models and Measurement Models

The equations of motion of a near-Earth satellite with respect to the J2000 geocentric inertial frame can be expressed as:

$$\ddot{\vec{r}} = \vec{a}_g + \vec{a}_{non} \tag{A.1}$$

where $\vec{r}$ is the position of the center of mass of the satellite, $\vec{a}_g$ is the sum of the gravitaional perturbations acting on the satellite, and $\vec{a}_{non}$ is the sum of the non-gravitaional perturbations acting on the satellite.

## A.1 Gravitational Perturbations

The gravitaional perturbations composed of the perturbations from the Earth,the other bodies such as the Sun, Moon, and other planets and the general relativity effect.

$$\vec{a}_g = \vec{P}_{geo} + \vec{P}_{stides} + \vec{P}_{otides} + \vec{P}_{rotdef} + \vec{P}_{Nbody} + \vec{P}_{rel} \tag{A.2}$$

where $\vec{P}_{geo}$ is the perturbations due to the geopotential of the Earth, $\vec{P}_{stides}$ is the perturbations due to the solid Earth tides, $\vec{P}_{otides}$ is the perturbations due

to the ocean tides, $\vec{P}_{rotdef}$ is the perturbations due to the rotational deformation, $\vec{P}_{Nbody}$ is the perturbations due to the Sun, moon and other planets, and $\vec{P}_{rel}$ is the perturbations due to the general relativity effect.

### A.1.1 Earth Geopotential

The perturbing force on a satellite due to the geopotential of the Earth can be expressed as the gradient of a potential function, $U$, which satisfies the Laplace equation, $\nabla^2 U = 0$. The potential function $U$ composes of the potential due to the non-spherical solid mass distribution($U_s$), the potential change due to the solid-body tides($\Delta U_{stides}$), the potential change due to the ocean tides($\Delta U_{otides}$), and the potential change due to the rotational deformations($\Delta U_{rotdef}$). So, by using the potential function, the force on the unit mass on the near of Earth can be also expressed as:

$$\begin{aligned} \nabla U &= \nabla(U_s + \Delta U_{stides} + \Delta U_{otides} + \Delta U_{rotdef}) \\ &= \vec{P}_{geo} + \vec{P}_{stides} + \vec{P}_{otides} + \vec{P}_{rotdef} \end{aligned} \tag{A.3}$$

The potential function for the non-spherical solid mass distribution of the Earth, $U_s$, can be expressed in terms of a spherical harmonic expansion with respect to a body-fixed reference frame as [Kaula, 1966]:

$$\begin{aligned} U_s(r,\phi,\lambda) &= \frac{GM_e}{r} + \\ &\quad \frac{GM_e}{r}\sum_{l=1}^{\infty}\sum_{m=0}^{l}\left(\frac{a_e}{r}\right)^l \bar{P}_{lm}(\sin\phi)\left[\bar{C}_{lm}\cos m\lambda + \bar{S}_{lm}\sin m\lambda\right] \end{aligned} \tag{A.4}$$

where $GM_e$ is the gravitational constant of the Earth; $a_e$ is the mean equatorial radius of the Earth; $\bar{C}_{lm}$ and $\bar{S}_{lm}$ are the normalized spherical harmonic

coefficients of degree $l$ and order $m$; $\bar{P}_{lm}(\sin\phi)$ is the normalized associated Legendre function of degree $l$ and order $m$; $r$, $\phi$, and $\lambda$ are the radial distance from the center of the Earth, the geometric latitude, and the longitude of the satellite respectively. The terms of degree 1 such as $\bar{C}_{10}$, $\bar{C}_{11}$, and $\bar{S}_{11}$ become zero, since the origin of the spherical coordinates coincides with the center of mass of the Earth. For the Jason-1 POD, the JGM-3 gravitational model [Tapley *et al.*, 1996] is used for the nominal orbits, and the coefficients up to degree and order 70 was used in the model. For the nominal orbits in this research, the GPS orbits were fixed to IGS orbits. However, to determine the GPS orbits simultaneously with the LEO orbit, the coefficients up to degree and order 12 are usually used.

### A.1.2 Solid Earth Tides

The mass distribution or the shape of the Earth can be changed due to the gravitational attraction especially by the Sun and Moon, because the Earth is not a rigid body. The tidal generating potential which is the disturbing potential of a particle on the surface of the Earth can be expressed in terms of a spherical harmonics expansion in the geocentric body-fixed refeernce frame as [Casotto, 1989]:

$$\begin{aligned} V_i &= g_i \sum_{l=2}^{\infty} \left(\frac{a_e}{r_i}\right)^{l+1} P_l\left(\cos\psi_i\right) \qquad \text{(A.5)} \\ &= g_i \sum_{l=2}^{\infty} \sum_{m=0}^{l} \left(\frac{a_e}{r_i}\right)^{l+1} (2-\delta_{0m}) \frac{(l-m)!}{(l+m)!} P_{lm}\left(\sin\phi\right) P_{lm}\left(\sin\phi\right) \cos m(\lambda-\lambda_i) \end{aligned}$$

where $g_i = GM_i/a_e$; $GM_i$ are the gravitational constant of the $i$-th perturbing body, either the Sun or the Moon; $r_i$, $\phi_i$, and $\lambda_i$ are geocentric distance, latitude, and longitude of the $i$-th perturbing body; $\phi$ and $\lambda$ are geograplhic latitude, and longitude of a particle on the Earth's surface; $\psi_i$ is the geocentric angular distance between the $i$-th perturbing body and a particle on the Earth's surface; $P_l$ is the Legendre polynomial; and, $P_{lm}$ is the associated Legendre function.

Following Cartwright & Taylor [1971], the tidal generating potential can be transformed from the time domain to the frequency domain. Thus, the periodic temporal variations which induced from the solid Earth tide can be approximated using frequency dependent Love numbers to scale the tidal generating potential as [Wahr, 1981]:

$$\begin{aligned} \Delta U_{stides} &= \frac{GM_e}{a_e^2} \sum_{l=2}^{(3)} \sum_{m=0}^{l} \sum_{k(l,m)} H_k e^{i(\Theta_k + \chi_k)} K_k^0 \\ &\quad \times \left[ \left( \frac{a_e}{r} \right)^{l+1} Y_m^l(\phi, \lambda) + K_k^+ \left( \frac{a_e}{r} \right)^{l+3} Y_m^{l+2}(\phi, \lambda) \right] \end{aligned} \tag{A.6}$$

where

$$Y_m^l(\phi, \lambda) = (-1)^m \sqrt{\frac{(2l+1)}{4\pi} \frac{(l-m)!}{(l+m)!}} P_{lm}(\sin\phi) e^{im\lambda} \tag{A.7}$$

and $P_{lm}(\sin\phi)$ is the associated Legendre function of degree $l$ and order $m$; $H_k$ is the frequency dependent tidal amplitude in meters; $\Theta_k$ and $\chi_k$ are the Doodson argument and phase correction for constituent $k$; $K_k^0$ and $K_k^+$ are the Love numbers for constituent $k$; and, $r$,$\lambda$ and $\phi$ are the geocentric body fixed coordinates of the satellite. The summarization over $k(l,m)$ means that each

different $l$,$m$ combination has a unique list of tidal frequencies $k$ over which to sum. A more direct and practical approach in modeling the tide generating potential is to consider it as variations in the standard normalized geopotential coefficients $\bar{C}_{nm}$ and $\bar{S}_{nm}$ [Eanes *et al.*, 1983]:

$$\Delta\bar{C}_{lm} = \frac{(-1)^m}{a_E\sqrt{4\pi(2-\delta_{0m})}}\sum_k K_k^0 H_k \begin{cases} \cos\Theta_k, & \text{l-m even} \\ \sin\Theta_k, & \text{l-m odd} \end{cases} \tag{A.8}$$

$$\Delta\bar{S}_{lm} = \frac{(-1)^m}{a_E\sqrt{4\pi(2-\delta_{0m})}}\sum_k K_k^0 H_k \begin{cases} -\sin\Theta_k, & \text{l-m even} \\ \cos\Theta_k, & \text{l-m odd} \end{cases} \tag{A.9}$$

where $\delta_{0m}$ is the Kronecker delta. This way simplify the coding to compute the net acceleration due to the solid tide by incorporating directly into the geopotential.

### A.1.3 Ocean Tides

The temporal variation of the free space geopotential induced from the ocean tide deformation may be computed by a surface integal of a thin layer of sea water over a sphere of radius $a_e$ as [Eanes *et al.*, 1983]:

$$\begin{aligned} \Delta U_{otides} &= 4\pi G\rho_w a_e \sum_k \sum_{l=0}^{\infty}\sum_{m=0}^{l}\sum_{+}^{-} \frac{1+k_l^{'}}{2l+1}\left(\frac{a_e}{r}\right)^{l+1} \\ &\quad \times \left[C_{klm}^{\pm}\cos(\Theta_k \pm m\lambda) + S_{klm}^{\pm}\sin(\Theta_k \pm m\lambda)\right] P_{lm}(\sin\phi) \end{aligned} \tag{A.10}$$

where $\rho_w$ is the mean density of sea water; $k$ is the ocean tide constituent index; $k_l^{'}$ is the load Love number of degree $l$; $C_{klm}^{\pm}$ and $S_{klm}^{\pm}$ are the unnormalized prograde and retrograde tide coefficients; and, $\Theta_k$ is the Doodson argument for constituent $k$.

In the same manner as with the solid earth tides, the potential variations due to the ocean tides can be expressed as variations with the normalized geopotential coefficients $\bar{C}_{nm}$ and $\bar{S}_{nm}$:

$$\begin{aligned} \Delta\bar{C}_{lm} &= F_{lm}\sum_{k} A_{klm} \\ \Delta\bar{S}_{lm} &= F_{lm}\sum_{k} B_{klm} \end{aligned} \tag{A.11}$$

where $F_{lm}$,$A_{klm}$ and $B_{klm}$ are defined as

$$F_{lm} = 4\pi a_e^2 \rho_w \sqrt{\frac{(l+m)!}{(l-m)!(2l+1)(2-\delta_{0m}}} \left(\frac{1+k_l^{'}}{2l+1}\right) \tag{A.12}$$

and

$$\left[\begin{array}{c} A_{klm} \\ B_{klm} \end{array}\right] = \left[\begin{array}{c} (C^{+}_{klm} + C^{-}_{klm}) \\ (S^{+}_{klm} - S^{-}_{klm}) \end{array}\right] \cos\Theta_k + \left[\begin{array}{c} (S^{+}_{klm} + S^{-}_{klm}) \\ (C^{+}_{klm} - C^{-}_{klm}) \end{array}\right] \sin\Theta_k \tag{A.13}$$

The ocean tide model used for this research is the CSR 3.0 ocean tide model [Eanes & Bettadpur, 1996].

### A.1.4 Rotational Deformation

Rotational deformation accounts for variations in the geopotential coefficients due to polar motion. The generating potential for Earth's rotational deformation is the centrigugal potential. This centrifugal potential $U_{cent}$ for a point on the Earth can be expressed by second degree spherical harmonics as [Lambeck, 1980]:

$$U_{cent} = \frac{1}{3}\omega^2 r^2 + \Delta U_{cent} \tag{A.14}$$

and

$$\begin{aligned}\Delta U_{cent} &= \frac{r^2}{6}(\omega_1^2+\omega_2^2-2\omega_3^2)P_{20}(\sin\phi) \\ &\quad -\frac{r^2}{3}(\omega_1\omega_3\cos\lambda+\omega_2\omega_3\sin\lambda)P_{21}(\sin\phi) \\ &\quad +\frac{r^2}{12}[(\omega_2^2-\omega_1^2)\cos 2\lambda-2\omega_1\omega_2\sin 2\lambda]P_{22}(\sin\phi)\end{aligned} \tag{A.15}$$

where $\omega^2 = (\omega_1^2+\omega_2^2\omega_3^2)$, $\omega_1 = m_1\Omega$, $\omega_2 = m_2\Omega$, and $\omega_3 = (1+m_3)\Omega$. $\Omega$ is the mean angular velocity of the Earth, $m_i$ are small dimensionless quantities which are related to the polar motion and the Earth rotation parameters such as:

$$\begin{aligned}m_1 &= x_p \\ m_2 &= -y_p \\ m_3 &= \frac{d(UT1-TAI)}{d(TAI)}\end{aligned} \tag{A.16}$$

where $x_p$,$y_p$ are the polar motion coordinates in radian of the instantaneous rotation axis, with respect to the Conventional Terrestrial System. $\frac{d(UT1-TAI)}{d(TAI)}$ is the length of day.

The first term of Equation A.14 results in a small and purely radial deformation in the variation of the geopotential, which is negligible. The variation of the free space geopotential outside of the Earth due to the rotational deformation, $\Delta U_{rotdef}$, can be expressed in terms of the deformation potential, $\Delta U_{cent}$, as:

$$\Delta U_{rotdef} = \left(\frac{a_e}{r}\right)^3 k_2 \Delta U_{cent}(a_e) \tag{A.17}$$

Again by using the approach to model variations in the standard geopotential coefficients, the corresponding variation of the second degree geopotential coefficients are given as:

$$\begin{aligned} \Delta C_{20} &\approx -\frac{a_e^2}{3GM_e}(1+2m_3)\Omega^2 k_2 \\ \Delta C_{21} &\approx -\frac{a_e^2}{3GM_e} m_1 \Omega^2 k_2 \\ \Delta S_{21} &\approx -\frac{a_e^2}{3GM_e} m_2 \Omega^2 k_2 \end{aligned} \tag{A.18}$$

and $\Delta C_{22} \approx 0$, $\Delta S_{22} \approx 0$.

Note that with variations in the standard normalized geopotential coefficients $\bar{C}_{nm}$ and $\bar{S}_{nm}$ from the solid earth tides, ocean tides and rotational deformation, the geogravitational potential of the Earth can be expressed similar to Equation A.5 as:

$$\begin{aligned} U_s(r,\phi,\lambda) &= \frac{GM_e}{r} + \frac{GM_e}{r}\sum_{l=1}^{\infty}\sum_{m=0}^{l}\left(\frac{a_e}{r}\right)^l \bar{P}_{lm}(\sin\phi) \\ &\quad \times \left[\left(\bar{C}_{lm}+\Delta\bar{C}_{lm}\right)\cos m\lambda + \left(\bar{S}_{lm}+\Delta\bar{S}_{lm}\right)\sin m\lambda\right] \end{aligned} \tag{A.19}$$

### A.1.5 N-body Perturbation

The gravitational perturbations of the Sun, Moon and other planets on the satellite other than the Earth can be modeled adequately by approximating the perturbing bodies as point masses. The N-body gravitational perturba-

tions can be expressed with respect to the geocentric inertial coordinates as:

$$\begin{aligned} \vec{P}_{Nbody} &= \sum_n GM_n \left( \frac{\vec{r}_n}{r_n^3} - \frac{\vec{\Delta}_n}{\Delta_n^3} \right) \\ &= \vec{\nabla} \sum_n V_n \\ &= \vec{\nabla} \sum_n GM_n \left( \frac{1}{\Delta_n} - \frac{\vec{r} \cdot \vec{r}_n}{r_n} \right) \end{aligned} \tag{A.20}$$

where $GM_n$ is the gravitational constant of the $n$-th perturbing body; $\vec{r}$ is the position vector of the satellite in geocentric inertial coordinates; $\vec{r}_n$ is the the position vector of the $n$-th perturbing body in geocentric inertial coordinates; $\vec{\Delta}_n = \vec{r}_n - \vec{r}$; and, $V_n$ is the disturbing potential of the $n$-th perturbing body.

The the position vector of the $n$-th perturbing body in geocentric inertial coordinates, $\vec{r}_n$, is obtained from a preintegrated planetary ephemerides. The JPL DE-200/LE-200 [Standish, 1982] is used for this research.

### A.1.6 General Relativity Perturbation

The perturbation due to general relativity acting on a near Earth satellite can be described as [Ries, 1989]:

$$\begin{aligned} \vec{P}_{rel} &= \frac{GM_e}{c^2 r^3} \left\{ \left[ 2(\beta + \gamma) \frac{GM_e}{r} - \gamma (\dot{\vec{r}} \cdot \dot{\vec{r}}) \right] \vec{r} + 2(1+\gamma)(\vec{r} \cdot \dot{\vec{r}}) \dot{\vec{r}} \right\} \\ &\quad + 2(\vec{\Omega} \times \dot{\vec{r}}) \\ &\quad + L(1+\gamma) \frac{GM_e}{c^2 r^3} \left[ \frac{3}{r^2} (\vec{r} \times \dot{\vec{r}})(\vec{r} \cdot \vec{J}) + (\dot{\vec{r}} \times \vec{J}) \right] \end{aligned} \tag{A.21}$$

and

$$\vec{\Omega} \approx \left( \frac{1+\gamma}{2} \right) (\dot{\vec{R}}_{ES}) \times \left[ \frac{-GM_s \vec{R}_{ES}}{c^2 R_{ES}^3} \right] \tag{A.22}$$

where $c$ is the speed of light in the geocentric frame; $\vec{r}$ and $\dot{\vec{r}}$ are the geocentric satellite position and velocity vectors; $\vec{R}_{ES}$ and $\dot{\vec{R}}_{ES}$ are the position and velocity of the Earth with respect to the Sun; $GM_e$ and $GM_s$ are the gravitational constants for the Earth and the Sun respectively; $\vec{J}$ is the Earth's angular momentum per unit mass; $L$ is the Lense-Thirring parameter; and, $\beta$ and $\gamma$ are the parameterized post-Newtonian parameters.

The first term in Equation A.22 is the Schwarzschild motion which describes the main effect on the satellite orbit with the precession of perigee. The second term in Equation A.22 is the effect of geodesic (or de Sitter) precession and the last term is the Lense-Thirring precession which is due to the angular monentum of the rotating Earth. The geodesic precession and Lense-Thirring precession are generally negligible relative to the other Newtonian error sources.

## A.2 Measurement Models for Each System

Satellite tracking involves the measurement of some physical properties of electromagnetic wave propagation between the tracking station and the satellite or between two satellites. The actual observations are generally preprocessed to correct for known effects such as clock offsets or timing biases, instrument-induced errors, antenna offsets from the spacecraft, or atmospheric refraction and any other corrections. Some corrections are applied to all the measurement type, some corrections can be different from each measurement type.

Based on a mathematical model of the dynamical and the measurement system, a computed measurement can be generated as functions of the nominal trajectory of the satellite as well as number of model parameters. The residuals (O-C), which are produced by differencing the actual observed measurements from the computed measurements, will show the nonzero difference due to the noise and biasing in making the measurements. In the following sections, the measurement models for each tracking systems used in this research, and the correction models to them are described.

### A.2.1 SLR Measurement Model

Basically, an electromagnetic signal is transmitted from the ground station at time $t_T$ and is received at the satellite at time $t_\nu$. The signal is then transmitted by the satellite and received at the ground station at time $t_R$. For laser tracking, the signal is immediately retransmitted to the ground by the retroreflectors at time $t_\nu$. For radio frequency ranging, the satellite transponder retransmits the signal at time $t_\nu + \Delta\tau$, where $\Delta\tau$ is the transponder delay time.

The relative motion of the satellite and the station which caused by the motion relative to inertial space while the signal is traveling, known as the light time solution, must be accounted for when determining the computed value of the observable. The range measurement is the average of the uplink propagation distance and the downlink propagation distance, which is computed from satellite ephemeris and station coordinates information.

***Observed Range***

The observed one-way range from the reference point of the ranging instrument to the retroreflector of the satellite, $\rho_o$, can be expressed as:

$$\rho_o = \frac{1}{2} c \cdot \Delta t + \varepsilon \tag{A.23}$$

where $\Delta t$ is the round trip light time, which is the primary measurement between the laser pulse transmission and the return of the satellite reflected energy to the optical receiver at the tracking station; $c$ is the speed of light in a vacuum; and $\varepsilon$ is the measurement error.

***Computed Range***

With the corrections for atmospheric refraction and instrument delays, the computed one-way range, $\rho_c$, can be described as:

$$\rho_c = |\vec{\rho}_{sat}| + \rho_{cm} + \rho_{trop} + \rho_{grel} + \rho_{bias} \tag{A.24}$$

where $\vec{\rho}_{sat}$ $(= \vec{r}_{sat} - \vec{r}_{sta})$ is the satellite center of mass position in topocentric coordinates, where $\vec{r}_{sat}$ is the satellite position in geocentric coordinates, and $\vec{r}_{sta}$ is the position of the tracking station in geocentric coordinates; $\rho_{cm}$ is the range correction for satellite center of mass offset from the retroreflector reference point; $\rho_{trop}$ is the atmospheric refraction correction; $\rho_{rel}$ is the correction due to the general relativistic effect; and $\rho_{bias}$ is the system bias.

The empirical systematic range bias and timing bias estimated with the orbit parameters are modeled as:

$$\rho_{bias} = b + \dot{\rho}\tau \tag{A.25}$$

where $b$ is the range bias error; $\tau$ is the timing bias error; and, $\dot{\rho}(= \vec{\rho}_{sat} \cdot \dot{\vec{\rho}}_{sat})$ is the range rate of the satellite with respect to the tracking station.

The corrections are further discussed in Section A.2.4. The model of Marini & Murray [1973] is used for the laser tropospheric refraction correction. The general relativity correction is the same for SLR, DORIS and GPS. However, the special relativity correction is not neccessary for SLR. The effects of the displacement caused by the crustral motions on the ground station location, $\vec{r}_{sta}$, will be also discussed in Section A.2.4.

### A.2.2 DORIS Measurement Model

The Doppler Orbitography and Radiopositioning Integrated by Satellite (DORIS) is a one-way, ascending Doppler system which utilizes a set of ground beacons. T/P was the first satellite to carry a DORIS receiver on board. The beacons in the ground stations broadcast the signal on two frequencies of 2036.25 and 401.25 MHz. A receiver on the satellite receives the signal and measures the Doppler shift, which the average range rate of the satellite relative to the beacon can be measured from. Average range rate is defined as the range change over a finite interval, which is usually 7 to 10 sec. Note that the data types of the TRANET and OPNET Doppler tracking systems, which were the primary means of tracking the U.S. Navy's Geodetic Satellite (Geosat) from 1985-1989, are also referred to as Doppler range-rate measurements [Anderle, 1986].

***Observed Doppler Range-rate***

The observed raw average range-rate can be measured using the number of cycles $N_{1,2}$ such as:

$$\dot{\bar{\rho}}_o = \frac{c}{f_t}\left[\frac{(N_{1,2} - N_{iono})}{(t_2 - t_1)} - (f_g - f_t)\right] + \varepsilon \tag{A.26}$$

where $c$ is the speed of light int he vacuum; $t_1$ is the time at the beginning of the count interval; $t_2$ is the time at the end of the count interval; $f_t$ is the transmitter reference freqency; $f_g$ is the ground receiver reference freqency; $N_{1,2}$ is the raw Doppler count over the interval $(t_1, t_1)$; $N_{iono}$ is the ionospheric refraction correction in Doppler count; and, $\varepsilon$ is the oservation noise. $N_{1,2}$ is the measurable physical quantitiy which is counted by the receiver at the ground tracking station between the count time intervals, $t_1$ and $t_2$. The signal can be transmitted from the satellite for one-way or from a tracking station for two-way Doppler data.

***Computed Range-rate***

The computed average range rate is the time average of the range difference over the count interval $(t_1, t_2)$ with the additional Doppler frequency shift due to the periodic relativistic effect for Doppler range measurement rate as:

$$\dot{\bar{\rho}}_c = \frac{1}{t_2 - t_1}\left[\Delta\rho + \Delta\rho_{cm} + \alpha\Delta\rho_{trop} + \Delta\rho_{grel} + \Delta\rho_{srel}\right] + \frac{c}{f_t}\Delta f \tag{A.27}$$

where $\Delta\rho$ is the difference of Euclidian ranges at time $t_1$ and $t_2$ ($\Delta\rho = |\vec{\rho}_{sat}|_2 - |\vec{\rho}_{sat}|_1$).

For the Doppler signal, the tropospheric refraction correction is from the modified Hopfield model [Goad & Goodman, 1974]. The scale factor $\alpha$ to be estimated to reduce the error was introduced. $\Delta\rho_{grel}$ is for the propagation correction due to the general ralativity. $\Delta\rho_{srel}$ is for the additional Doppler frequency shift correction due to the periodic relativistic effect. For more details for the corrections, Section A.2.4 can be referred.

The freqency offset parameter $\Delta f$ in Equation A.27 is estimated for each pass of the one-way range rate data to remove some uncertanty caused by inaccurate measurement of $(f_g - f_t)$ because of the different oscillator stability between the satellite transmitter and ground receiver. For two-way range measurement, this frequency offset is cancelled.

### A.2.3 GPS Measurement Model

In this section, a brief introduction of GPS measurement model will be summarized. More details about GPS signals and GPS sytem can be referred to Hofmann-Wellenhof *et al.* [1992]. Details about the GPS measurement model can be referred to Rim [1992].

#### *Code Pseudorange (PR) Model*

The observed measurement $\rho^O_{PR}$ and the computed measurement $\rho^C_{PR}$ of the Code Pseudorange can be expressed as:

$$\rho^O_{PR} = c \cdot \Delta t + \varepsilon = c \cdot (t_{rec} - t_{tr}) + \varepsilon \tag{A.28}$$

$$\rho^C_{PR} = |\vec{\rho}_{sat}| + \rho_{cm} + \rho_{iono} + \rho_{trop} + \rho_{grel} + \rho_{srel} + \rho_{bias} \tag{A.29}$$

where $t_{rec}$ and $t_{tr}$ are the time tags of the receiver and transmitter respectively; $\vec{\rho}_{sat}$ is the satellite center of mass position in topocentric coordinates; $\rho_{cm}$ is the range correction for satellite center of mass offset from the retroreflector reference point; $\rho_{trop}$ is the atmospheric refraction correction; and, $\rho_{grel}$ and $\rho_{srel}$ are the corrections due to the general relativistic effect and special relativistic effect respectively. The details of the correction model will be further discussed in Section A.2.4.

### *Carrier Phase Pseudorange (PPR) Model*

The observed carrier phase pseudorange (PPR) measurement between the $i$-th receiver and the $j$-th GPS satellite transmitter, $\rho_{i\,PPR}^{j\,O}$, is given as:

$$\begin{aligned} \rho_{i\,PPR}^{j\,O} &= \frac{c}{f_n}\Delta\phi_i^j + \varepsilon \\ &= \frac{c}{f_n}[\phi_i(t_R) - \phi^j(t_{T\to R})] + \varepsilon \end{aligned} \tag{A.30}$$

where $t_R$ is the received time of the $i$-th receiver, which can be located on a ground station or on an user satellite; $t_T$ is the transmitted time of the $j$-th GPS satellite transmitter; $\phi^j(t_{T\to R})$ is the received radio frequency phase of the $j$-th GPS satellite signal at the time of signal reception, $t_R$; $\phi_i(t_R)$ is the receiver reference phase at the same time, $t_R$; $c$ is the speed of light; and, $f_n$ is the nominal value for both the transmitting and the receiver mixing frequency.

The computed carrier phase pseudorange measurement between the $i$-th receiver and the $j$-th GPS satellite transmitter, $\rho_{i\,PPR}^{j\,C}$, can be modeled

as:

$$\rho_{i\,PPR}^{j\,C} = \frac{c}{f_n}[\phi_i(t_R) - \phi^j(t_{T\to R}) - N_i^j(t_{0/R})] \tag{A.31}$$

where $N_i^j(t_{0/R})$ is the integer bias which will be estimated. With the help of relationships such as $t_R = t_i - \delta t_i$, $t_T = t^j - \delta t^j$, and $t_{T\to R} = t_R - [\rho_i^j(t_R) + \rho_{i\,corr}^j]/c$, and by assuming highly stable oscillators of the transmitters on the GPS satellites as well as the receivers of the ground stations and of the user satellite, , Equation A.31 can be expressed as [Rim, 1992]:

$$\rho_{i\,PPR}^{j\,C} = \rho_i^j(t_i) + \rho_{i\,corr}^j + c(\delta t_i - \delta t^j) - \dot{\rho}_i^j(t_i)\delta t_i - \frac{c}{f_n}N_i^j \tag{A.32}$$

where $t_i$ is the time tag of the measurement in the $i$-th receiver; $t^j$ is the time tag of the measurement in the $j$-th transmitter; $t_R$ and $t_T$ are true signal received and transmitted times respectively; $\delta t_i$ is the clock error of the $i$-th receiver; $\delta t^j$ is the clock error of the $j$-th transmitter; $\rho_i^j(t_R)$ is the geometric line of sight range between $j$-th GPS satellite and $i$-th receiver; $\rho_{i\,corr}^j$ is the range correction from ionospheric delay, tropospheric delay, relativistic effects and phase-center corrections ($\rho_{i\,corr}^j = \rho_{i\,cm}^j + \rho_{i\,iono}^j + \rho_{i\,trop}^j + \rho_{i\,grel}^j + \rho_{i\,srel}^j$). The third term, $c(\delta t_i - \delta t^j)$, represents clock drifting effects between the transmitter and receiver clocks, and the fourth term, $\dot{\rho}_i^j\delta t_i$, is similar to the timing bias in Equation A.25. Therefore, Equation A.32 is similar to Equation A.29 except the integer ambiguity term. The ionospheric delay is corrected in the pre-processing stage with L1 and L2 linear combination, the corrections will be discussed further in Section A.2.4. The clock errors would be estimated for each epoch during the pre-processing stage.

***Single-Differenced Phase Pseudorange (SDPPR) Measurement***

A computed single-differenced phase pseudorange (SDPPR) measurement between the $j$-th and $k$-th GPS satellites for the $j$-th ground receiver and for the user satellite, $u$, can be formed as:

$$\Delta\rho^{j\ C}_{iu\,SDPPR} \equiv \rho^{j\,C}_{i\,PPR} - \rho^{j\,C}_{u\,PPR} \tag{A.33}$$

$$\Delta\rho^{k\ C}_{iu\,SDPPR} \equiv \rho^{k\,C}_{i\,PPR} - \rho^{k\,C}_{u\,PPR} \tag{A.34}$$

***Double-Differenced Phase Pseudorange (DDPPR) Measurement***

A computed double-differenced phase pseudorange (DDPPR) measurement can be formed by subtracting two single-differenced phase pseudorange measurements as:

$$\Delta\rho^{jk\,C}_{iu\,DDPPR} \equiv \Delta\rho^{j\ C}_{iu\,SDPPR} - \Delta\rho^{k\ C}_{iu\,SDPPR} \tag{A.35}$$

By using Equations, A.32, A.33 and A.34, Equation A.35 can be expressed as:

$$\begin{aligned}
\Delta\rho^{jk\,C}_{iu\,DDPPR} \;=\;& \rho^j_i(t_i) - \rho^j_u(t_u) - \rho^k_i(t_i) + \rho^k_u(t_u) \\
& - [\dot\rho^j_i(t_i) - \dot\rho^k_i(t_i)] \cdot \delta t_i + [\dot\rho^j_u(t_u) - \dot\rho^k_u(t_u)] \cdot \delta t_u \\
& + \rho^j_{i\,corr} - \rho^j_{ucorr} - \rho^k_{i\,corr} + \rho^k_{ucorr} \\
& + \frac{c}{f_n}[N^j_i - N^j_u - N^k_i + N^k_u]
\end{aligned} \tag{A.36}$$

This is the double-differenced phase pseudorange measurement model for high-low or low-low implemented in MSODP. Note that in the equation, all the clock error terms associated with the GPS satellite are cancelled by forming

double differenced measurement. The model was derived from the assumption of the highly stable oscillators of transmitters and receivers. Since the GPS satellites have highly stable oscillators with $10^{-11}$ to $10^{-12}$ clock drift rate, the frequencies of the clocks usually stay close to the nominal frequency, $f_n$. The receiver time tags both on the ground station and on-board in the third line of Equation A.36 are corrected by using independent information from the pseudo-range measurement in the preprocessing stage. If the independent clock information is not provided, it can be modeled with coefficients to be estimated such as $\delta t = a + b(t - t_0)$, where $a$ is the clock bias, $b$ is the clock drift coefficient, and $t_0$ is the reference time for clock parameters.

### A.2.4 Measurement Correction Models

When processing measurement data, the errors are corrected either in the preprocess stage or in the orbit estimation stage. The errors of measurement data can be categorized as: 1) ground station-related, 2) media-related, and 3) the instrument-related. The displacement of the tracking station location due to the solid earth tides as well as the ocean tide loading effects should be corrected for ground tracking stations. The media-related correction errors include refraction effects caused by the dry and wet components of the troposphere and the electron content of the ionosphere. The relativistic effects of gravity on the signal are also accounted for. The antenna phase center offsets and center of mass offsets of the satellite are also considered as in Section 2.4.

Each measurement shares ground-station-related effects. The instrument-

dependent errors such as the center of mass offset and antenna phase center offset need to be corrected with each different correction model. Each different signal is propagated through the atmosphere differently, so different atmospheric error correction models are applied to each measurement type.

#### A.2.4.1 Displacement of the Ground Station Location

The geocentric body-fixed coordinates of the tracking station reference point, $\vec{r}_{sta}$, is computed with corrections of the dispacements caused eccentricity from the geodetic marker, solid earth tides, rotational deformation, ocean loading, and tectonic motion such as:

$$\vec{r}_{sta} = (\vec{r}_{marker} + \vec{\Delta}_{tect} + \vec{\Delta}_{tide}) + \vec{\Delta}_{eccen} \tag{A.37}$$

and

$$\vec{\Delta}_{tide} = \vec{\Delta}_{dtide} + \vec{\Delta}_{otide} + \vec{\Delta}_{rotdef} \tag{A.38}$$

where $\vec{r}_{marker}$ is the position of the geodetic marker in the geocentric body-fixed coordinate system, $\vec{\Delta}_{tect}$ is the tectonic plate motion correction of the gedetic marker, $\vec{\Delta}_{dtide}$ is the solid Earth tide correction of the geodetic marker, $\vec{\Delta}_{otide}$ is the ocean loading correction of the geodetic marker, $\vec{\Delta}_{rotdef}$ is the rotational deformation correction of the geodetic marker, and $\vec{\Delta}_{eccen}$ is the correction from the geodetic marker to the instrument reference point.

The effect of plate tectonic motion is modeled as station velocities which cause the stations to move away from the nominal coordinates. The station

displacement vector at time $t$ from the original site position at time $t_0$ can be computed with the cartesian rotation vector as [Minster & Jordan, 1987]:

$$\vec{\Delta}_{tect} = \vec{\omega}_{plate} \times \vec{r}_{marker}(t - t_0) \tag{A.39}$$

where $\vec{\omega}_{plate}$ is the angular velocity of the plate; and $(t - t_0)$ is the time interval since the reference epoch $t_0$. For this research, more simplified model is used as:

$$\vec{\Delta}_{tect} = \vec{r}_{sta_0} + \dot{\vec{r}}_{sta}(t - t_0) \tag{A.40}$$

where $\vec{r}_{sta_0}$ is the Earth-fixed coordinates of the station at $t_0$; and, $\dot{\vec{r}}_{sta}$ is the station velocity with respect to the reference epoch. Station velocity informations are provided by IGS in the cartesian station coordinates with respect to the refernce epoch.

Ocean tide effects called also as ocean loading are due to the elastic response of the Earth's crust to ocean tides. The variation of station coordinates caused by ocean loading can be compiled into a table containing the amplitude and phase of the height displacement for each station which generated by the formula as [Schwiderski, 1978]:

$$\vec{\Delta}_{otide} = \sum_k A_k \cos(\Theta_k - \delta_k)\hat{e}_r \tag{A.41}$$

where $A_k$ is the amplitude of the radial (height) displacement for a specific station; $\delta_k$ is the phase of the radial (height) displacement for a specific station; $\Theta_k$ is the Doodson argument of constituent $k$; and, $\hat{e}_r$ is the unit vector in the radial direction for a specific station.

The solid earth and ocean tides and rotational deformation have a geometric effect on the ground station positions. The displacement due to the rotational deformation means the ground station displacement due to the elastic response of the Earth's crust to shifts in the spin axis orientation. The IERS Standards [McCarthy, 1996] for the tides has been used in MSODP.

#### A.2.4.2 Tropospheric path delay – wet and dry

The tropospheric delays composed of two components, wet and dry, can be expressed at any elevation angle as:

$$\rho_{trop} = \rho^z_{dry} m_{dry}(E) + \rho^z_{wet} m_{wet}(E) \tag{A.42}$$

where $E$ is the unrefracted elevation angle of the observation; $\rho^z_{dry}$ and $\rho^z_{wet}$ are the zenith delays for the dry component and the wet component respectively; and, $m_{dry}$ and $m_{wet}$ are the mapping functions. As shown in the equation, the tropospheric path delay is frequency-independent, thus, it can not be removed by using dual frequency.

The $\rho^z_{dry}$ can be modeled as [Saastamoinen, 1972; Davis *et al.*, 1985; Bevis *et al.*, 1992]:

$$\rho^z_{dry} = 0.0022768 \frac{P_s}{f(\phi, H_s)} \tag{A.43}$$

where $f(\phi, H_s) = 1 - 0.00266 \cos 2\phi - 0.00028 H_s$; $\phi$ is the geodetic latitude of the station; $H_s$ is the height of the station above the refernce ellipsoid; and, $P_s$ is the surface pressure at the station (in millibars).

Several mapping functions such as Chao [1974] model, the Modified Hopfield model [Goad & Goodman, 1974], and the Mapping Temperature Test (MTT) model [Herring, 1992] are implemented in MSODP for the radio frequency range measurement. The MTT model for GPS and the Modified Hopfield model for DORIS are applied for this research.

The mapping function needs the location and meterological information (such as temperature and pressure) of the station. When surface meteorological data are not provided for the station, nominal pressure is computed as a function of altitude by Vanicek & Krakiwsky [1986, p443], or 900 $m$bar and $17°C$ may be used in MSODP.

The wet component of delay contributes 20% of the tropospheric path delay, but is more difficult to model because of the lack of information of the spatial variation of its water vapor content. For MSODP, since the errors in the wet part of the calculated zenith delay are highly variable, the wet zenith parameters are estimated simultaneously with orbit parameters.

The most commonly used tropospheric refraction correction model for optical frequency range measurement is Marini & Murray [1973] model which is applied for SLR in this research:

$$\rho_{trop} = \frac{f(\lambda)}{f(\phi, H)} \frac{A + B}{\sin E + \frac{B/(A+B)}{\sin E + 0.01}} \tag{A.44}$$

and

$$
\begin{aligned}
A &= 0.002357P_0 + 0.000141e_0 \\
B &= (1.084 \times 10^{-8})P_0T_0K + (4.734 \times 10^{-8})\frac{P_0^2}{T_0}\frac{2}{(3 - 1/K)} \\
K &= 1.163 - 0.00968\cos 2\phi - 0.00104T_0 + 0.00001435P_0 \\
f(\lambda) &= 0.965 + 0.0164/\lambda^2 + 0.000228/\lambda^4 \\
f(\phi, H) &= 1 - 0.026\cos 2\phi - 0.00031H \\
e_0 &= \frac{R_h}{100} \times 6.11 \times 10^{[7.5(T_0-273.15)]/[273.3+(T_0-273.15)]}
\end{aligned}
$$

where $e_o$ is the water vapor pressure; $f(\lambda)$ is the laser wavelength ($\lambda$) parameter; $f(\phi, H)$ is the laser site function of site's latitude ($\phi$) and geodetic height ($H$); $E$ is the elevation of the satellite; $P_0$ is the atmospheric pressure at the laser site (milibars); $T_0$ is the atmospheric temperature at the laser site ($K$); and, $R_h$ is the atmospheric relative humidity (%).

#### A.2.4.3 Ionospheric path delay

The ionosphere is a region of the upper atmosphere ranging 100 km to 1000 km from the surface of the Earth. The presence of electrons and ions in the ionosphere delays the signal path proportionally to the number of electrons along the path and inverse-proportionally to the frequency of the signal.

The ionospheric path delay depends on the frequency of the radio signal varying 0.15 m to 50 m on L1 GPS measurement. To correct the ionospheric path delay for GPS, the dual frequency measurements [Ho, 1990] with a linear combination of the L1 and L2 signals are used in the pre-process. The

ionospheric free carrier phase observable ($\phi_{L_c}$) can be expressed as:

$$\phi_{L_c} = \frac{f_1^2}{f_1^2 - f_2^2}\phi_{L_1} - \frac{f_1 f_2}{f_1^2 - f_2^2}\phi_{L_2} \tag{A.45}$$

where, $f_1$ is $1575.42 \times 10^6$, and $f_2$ is $1227.60 \times 10^6$. The similar ionospheric correction can be also applied for Doppler range measurement.

#### A.2.4.4 Relativistic effect

The relativistic effects on the measurements have both aspects, special and gereral. The special relativistic effect causes an apparent shift in the frequency of the signal transmitted from the satellite due to the relative motion between the satellite (or transmitter) and the ground stations (or receiver). The constant drift shift can be removed by setting the clock frequency low before launch, and the periodic part of the shift can be modeled for range "difference" measurement as [Gibson, 1983]:

$$\Delta\rho_{srel} = \frac{2}{c}\left(\vec{r}(t_2) \times \dot{\vec{r}}(t_2) - \vec{r}(t_1) \times \dot{\vec{r}}(t_1)\right) \tag{A.46}$$

and for a high-low measurement as [Rim, 1992]:

$$\Delta\rho_{srel} = \frac{2}{c}\left(\vec{r}_l \times \dot{\vec{r}}_l - \vec{r}_h \times \dot{\vec{r}}_h\right) \tag{A.47}$$

where $c$ is the speed of light; $\vec{r}(t_2)$ and $\dot{\vec{r}}(t_2)$ are the position and velocity of the satellite at observation time $t_2$; $\vec{r}(t_1)$ and $\dot{\vec{r}}(t_1)$ are the position and velocity of the satellite at observation time $t_1$; $\vec{r}_h$ and $\dot{\vec{r}}_h$ are the position and velocity of a GPS satellite; and, $\vec{r}_l$ and $\dot{\vec{r}}_l$ are the position and velocity of the user satellite. This correction for "range differences" is cyclic, varying with the eccentric

anomaly of the satellite. It would be zero for a circular orbit and would be small enough to be negligible for many near-circular orbit satellites. However, for precision orbit determination, this correction needs to be accounted for. The special relativistic effect for the laser signal can be neglected, but needs to be added to DORIS and GPS.

The gravitational potential difference at the satellite and the station causes the general relativistic effect which can model a time delay due to the reduction of the coordinate speed of the measurement signal as the signal passes near the Earth as [Holdridge, 1967]:

$$\begin{aligned} \rho_{grel} &= (1+\gamma)\frac{GM_e}{c^2}\ln\left[\frac{|\vec{r}_{tr}|+|\vec{r}_{rec}|+|\vec{\rho}|}{|\vec{r}_{tr}|+|\vec{r}_{rec}|-|\vec{\rho}|}\right] + \\ & \quad (1+\gamma)\frac{GM_s}{c^2}\ln\left[\frac{|\vec{r}_{tr}-\vec{r}_s|+|\vec{r}_{rec}-\vec{r}_s|+|\vec{\rho}|}{|\vec{r}_{tr}-\vec{r}_s|+|\vec{r}_{rec}-\vec{r}_s|-|\vec{\rho}|}\right] \end{aligned} \tag{A.48}$$

where $\gamma$ is the parameterized post-Newtonian (PPN) parameter (=1 in General Relativity); $GM_e$ is the gravitational constant for the Earth; $|\vec{r}_{tr}|$ is the geocentric radial distance of the transmitter; $|\vec{r}_{rec}|$ is the geocentric radial distance of the receiver; $|\vec{r}_s|$ is the sun-vector; and, $|\vec{\rho}|$ is the relativistically uncorrelated range between the transmitter and the receiver. The general relativistic effect from the Sun ($GM_s$) is optional for MSODP. For high-low measurement, $\vec{r}_{tr}$ is changed to $\vec{r}_h$ and $\vec{r}_{rec}$ to $\vec{r}_l$.

# Appendix B

# Jason-1 Attitude Event Information

Table B.1: Jason-1 Attitude Event Information for cycle 1 - 20

| | EVENT | OBSERVED TIME (UTC) | Cycle | Pass |
|---|---|---|---|---|
| Set | Solar Array Pitch Bias (deg) = 0.00 | 2001-341T00:00:00 | 000 | 001 |
| Set | Limit Sinusoidal to Fixed (deg) = 15.00 | 2001-341T00:00:00 | 000 | 001 |
| Set | Limit Fixed to Sinusoidal (deg) = 15.00 | 2001-341T00:00:00 | 000 | 001 |
| Set | Limit Yaw Flip (deg) = 0.00 | 2001-341T00:00:00 | 000 | 001 |
| Roll | Bias (deg) = 0.00 | 2001-341T00:00:00 | 000 | 001 |
| Pitch | Bias (deg) = 0.00 | 2001-341T00:00:00 | 000 | 001 |
| Yaw | Bias (deg) = 0.00 | 2001-341T00:00:00 | 000 | 001 |
| Start | Yaw Ramp(Fixed to Sinusoid BETAP=+15.0) | 2001-344T00:00:00 | 900 | 001 |
| Stop | Yaw Ramp(Fixed to Sinusoidal) | 2001-344T00:01:00 | 900 | 001 |
| Start | Yaw Ramp(Sinusoid to Fixed BETAP=+15.0) | 2002-006T15:44:48 | 903 | 035 |
| Stop | Yaw Ramp(Sinusoidal to Fixed) | 2002-006T15:45:58 | 903 | 035 |
| Start | Yaw Flip | 2002-012T16:37:00 | 903 | 190 |
| Stop | Yaw Flip (Fly Backward) | 2002-012T16:52:00 | 903 | 190 |
| Start | Gyro Calibration Maneuver | 2002-017T10:35:00 | 001 | 058 |
| Stop | Gyro Calibration Maneuver | 2002-017T11:25:00 | 001 | 058 |
| Start | ALT Boresight Calibration Maneuver | 2002-017T18:25:00 | 001 | 066 |
| Stop | ALT Boresight Calibration Maneuver | 2002-017T18:30:00 | 001 | 066 |
| Start | Yaw Ramp(Fixed to Sinusoid BETAP=-15.0) | 2002-018T17:36:54 | 001 | 091 |
| Stop | Yaw Ramp(Fixed to Sinusoidal) | 2002-018T17:37:27 | 001 | 091 |
| Start | ALT Boresight Calibration Maneuver | 2002-025T08:05:00 | 002 | 006 |
| Stop | ALT Boresight Calibration Maneuver | 2002-025T08:30:00 | 002 | 006 |
| Start | ALT Boresight Calibration Maneuver | 2002-029T04:45:00 | 002 | 105 |
| Stop | ALT Boresight Calibration Maneuver | 2002-029T05:10:00 | 002 | 105 |
| Start | Gyro Calibration Maneuver | 2002-029T11:10:00 | 002 | 112 |
| Stop | Gyro Calibration Maneuver | 2002-029T12:10:00 | 002 | 113 |
| Start | Maneuver Burn | 2002-035T00:45:26 | 002 | 254 |
| Stop | maneuver burn | 2002-035T00:45:27 | 002 | 254 |
| Start | Maneuver Burn | 2002-035T01:41:39 | 003 | 001 |
| Stop | maneuver burn | 2002-035T01:41:40 | 003 | 001 |
| Start | ALT Boresight Calibration Maneuver | 2002-039T05:38:28 | 003 | 108 |
| Stop | ALT Boresight Calibration Maneuver | 2002-039T05:51:28 | 003 | 108 |
| Start | Gyro Calibration Maneuver | 2002-039T11:10:00 | 003 | 114 |
| Stop | Gyro Calibration Maneuver | 2002-039T12:10:00 | 003 | 115 |
| Start | ALT Boresight Calibration Maneuver | 2002-050T11:44:00 | 004 | 142 |
| Stop | ALT Boresight Calibration Maneuver | 2002-050T12:00:00 | 004 | 142 |
| Start | Gyro Calibration Maneuver | 2002-050T14:55:00 | 004 | 145 |
| Stop | Gyro Calibration Maneuver | 2002-050T15:44:00 | 004 | 146 |
| Start | Maneuver Burn | 2002-064T18:40:27 | 005 | 254 |
| Stop | maneuver burn | 2002-064T18:40:29 | 005 | 254 |
| Start | Maneuver Burn | 2002-064T19:36:40 | 006 | 001 |
| Stop | maneuver burn | 2002-064T19:36:42 | 006 | 001 |
| Start | Yaw Ramp(Sinusoid to Fixed BETAP=-15.0) | 2002-070T05:15:28 | 006 | 139 |
| Stop | Yaw Ramp(Sinusoidal to Fixed) | 2002-070T05:20:28 | 006 | 140 |
| Start | Yaw Flip | 2002-075T02:46:28 | 007 | 011 |
| Stop | Yaw Flip | 2002-075T02:54:28 | 007 | 011 |
| Start | Yaw Ramp(Fixed to Sinusoid BETAP=+15.0) | 2002-080T00:27:11 | 007 | 136 |
| Stop | Yaw Ramp(Fixed to Sinusoidal) | 2002-080T00:31:00 | 007 | 137 |
| Start | Eronous Pointing (star tracker) | 2002-094T10:36:00 | 008 | 252 |
| Stop | Eronous Pointing | 2002-094T16:30:00 | 009 | 004 |
| Start | Gyro Calibration Maneuver | 2002-101T06:29:00 | 009 | 173 |
| Stop | Gyro Calibration Maneuver | 2002-101T07:33:00 | 009 | 174 |
| Start | Gyro Calibration Maneuver | 2002-106T06:44:00 | 010 | 047 |
| ... | ... | ... | ... | ... |

Table B.1: Jason-1 Attitude Event Information for cycle 1 - 20 (continued)

| EVENT | | OBSERVED TIME (UTC) | Cycle | Pass |
|---|---|---|---|---|
| Stop | Gyro Calibration Maneuver | 2002-106T07:40:00 | 010 | 048 |
| Start | Yaw Ramp(Sinusoid to Fixed BETAP=+15.0) | 2002-131T12:16:04 | 012 | 186 |
| Stop | Yaw Ramp(Sinusoidal to Fixed) | 2002-131T12:19:47 | 012 | 186 |
| Start | Maneuver Burn | 2002-134T04:30:40 | 012 | 254 |
| Stop | maneuver burn | 2002-134T04:30:41 | 012 | 254 |
| Start | Maneuver Burn | 2002-134T05:26:53 | 013 | 001 |
| Stop | maneuver burn | 2002-134T05:26:55 | 013 | 001 |
| Start | Yaw Flip | 2002-137T16:41:07 | 013 | 086 |
| Stop | Yaw Flip | 2002-137T16:51:16 | 013 | 086 |
| Start | Yaw Ramp(Fixed to Sinusoid BETAP=-15.0) | 2002-143T13:52:03 | 013 | 241 |
| Stop | Yaw Ramp(Fixed to Sinusoidal) | 2002-143T13:55:47 | 013 | 241 |
| Start | ALT Boresight Calibration Maneuver | 2002-149T03:04:45 | 014 | 129 |
| Stop | ALT Boresight Calibration Maneuver | 2002-149T03:10:21 | 014 | 129 |
| Start | ALT Boresight Calibration Maneuver | 2002-149T03:11:45 | 014 | 129 |
| Stop | ALT Boresight Calibration Maneuver | 2002-149T03:17:20 | 014 | 129 |
| Start | Yaw Ramp(Sinusoid to Fixed BETAP=-15.0) | 2002-183T05:15:28P | 017 | 240 |
| Stop | Yaw Ramp(Sinusoidal to Fixed) | 2002-183T05:20:28P | 017 | 240 |
| Start | Maneuver Burn | 2002-183T18:23:19 | 017 | 254 |
| Stop | maneuver burn | 2002-183T18:23:20 | 017 | 254 |
| Start | Maneuver Burn | 2002-183T19:19:31 | 018 | 001 |
| Stop | maneuver burn | 2002-183T19:19:32 | 018 | 001 |

# Appendix C

# Orbit Determination Problem Overview

For a spacecraft whose equations of motion and initial state, $X_0$, at some initial time, $t_0$, are known, its state can be determined at any subsequent time $t \geq t_0$ by integrating the differential equations governing the motion of the vehicle. In reality, the errors in the initial state, the models, and the physical parameters in the differential equations cause the predicted trajectory to deviate from the true trajectory. Thus, to estimate the state closer to the true trajectory, the observations of the spacecraft, whether ground-based or space-based tracking, are necessary to combine with the dynamical equations.

The differential equations of the motion, Equation A.1, which are based on Newton's Second law, can be expressed as:

$$\begin{aligned} \dot{\vec{r}} &= \vec{v} \\ \dot{\vec{v}} &= \vec{a}_g + \vec{a}_{non} \end{aligned} \tag{C.1}$$

By defining the state vector $X$ composed of the position vector, $\vec{r}$, the velocity vector, $\vec{v}$, and the model parameters, $\vec{c}$, to be estimated, Equation C.1 can be rewritten as:

$$\dot{X} = F(X,t) = \begin{bmatrix} \vec{v} \\ \vec{a}_g + \vec{a}_{non} \\ \vec{0} \end{bmatrix}; \quad X(t_0) = X_0 \tag{C.2}$$

where $X^T = [\vec{r}\ \vec{v}\ \vec{c}]$, and $\vec{c}$ is a vector of unknown model constants which satisfies the relation $\dot{\vec{c}} = 0$. Equation C.2 represents a system of $n$ nonlinear first order ordinary differential equations.

Assuming that observations have been made at times $t_1, \ldots, t_l$, the functional form of the observation equation can also be expressed as:

$$Y_i = G(\vec{r}_i, \vec{r}_{si}, t_i) + \varepsilon_i \quad (i = 1, \ldots, l) \tag{C.3}$$

where $\vec{r}$ and $\vec{r}_s$ are the geocentric positions of the spacecraft and the tracking stations respectively at time $t_i$, and $\varepsilon$ is the measurement error, which is assumed to be Gaussian white noise. Applying the state vector, $X$, Equation C.3 can be expressed as:

$$Y_i = G(X_i, t_i) + \varepsilon_i \quad (i = 1, \ldots, l) \tag{C.4}$$

Thus, the actual observation $Y_i$ is assumed to be a nonlinear function of the true observation $G(X_i, t_i)$ and the random measurement noise $\varepsilon_i$.

To relate the state vector and observation vector in a linear manner, the linear estimation theory is applied. If the true trajectory denoted as $X$ and a reasonable reference trajectory denoted as $X^*$ remain close to each other throughout the time interval of interest, then a linear relation between the observation deviation, $y$, and the state deviation, $x$, can be obtained. In the linear orbit determination problem, the state deviation from some reference trajectory will be estimated.

By letting the state deviation, $x$, and observation deviation, $y$, be defined as:

$$x(t) = X(t) - X^*(t) \quad ; \; y(t) = Y(t) - Y^*(t) \tag{C.5}$$

and substituting them into Equations C.2 and C.4 to expand in a Taylor's series, Equations C.2 and C.4 can be expressed as linear differential equations with time dependent coefficients as:

$$\begin{aligned} \dot{x} &= A(t)x \\ y_i &= \tilde{H}_i x_i + \varepsilon_i \end{aligned} \tag{C.6}$$

where

$$A(t) = \frac{\partial F}{\partial X}(X^*, t) \;\; ; \tilde{H} = \frac{\partial G}{\partial X}(X^*, t) \tag{C.7}$$

The first equation of Equation C.6 has the solutions:

$$x(t) = \Phi(t, t_k)x_k \tag{C.8}$$

where $x(t)$ is the value of $x$ at a specific time, $t$, $\Phi(t_i, t_k)$ is the state transition matrix with properties such as; 1) $\Phi(t_k, t_k) = I$, 2) $\Phi(t_i, t_k) = \Phi(t_i, t_j)\Phi(t_j, t_k)$, and 3) $\Phi(t_i, t_k) = \Phi^{-1}(t_k, t_i)$.

By using Equation C.8, the first equation of Equation C.6 can be written in terms of the state at $t_0$ as:

$$\begin{aligned} y_1 &= \tilde{H}_1\Phi(t_1, t_0)x_0 + \varepsilon_1 \\ y_2 &= \tilde{H}_2\Phi(t_2, t_0)x_0 + \varepsilon_2 \\ &\vdots \qquad\quad \vdots \\ y_l &= \tilde{H}_l\Phi(t_l, t_0)x_0 + \varepsilon_l \end{aligned} \tag{C.9}$$

Equation C.9 can be further expressed as:

$$y = H x_0 + \varepsilon \tag{C.10}$$

where,

$$y = \begin{bmatrix} y_1 \\ y_2 \\ \vdots \\ y_l \end{bmatrix}; H = \begin{bmatrix} \tilde{H}_1 \Phi(t_1, t_0) \\ \tilde{H}_2 \Phi(t_2, t_0) \\ \vdots \\ \tilde{H}_l \Phi(t_l, t_0) \end{bmatrix}; \varepsilon = \begin{bmatrix} \varepsilon_1 \\ \varepsilon_2 \\ \vdots \\ \varepsilon_l \end{bmatrix} \tag{C.11}$$

It contains $m$ observations ($y$ is an $m \times 1$ vector) and $n$ unknown components of the state ($x$ is an $n \times 1$ vector), $\varepsilon$ is an $m \times 1$ vector, $H$ is an $m \times n$ mapping matrix. If $m > n$, the least squares solution for the best estimate of $x_0$, denoted as $\hat{x}_0$, can be obtained as:

$$\hat{x}_0 = (H^T H)^{-1} H^T y \tag{C.12}$$

Given a set of initial conditions $X^*(t_0)$, an a priori estimate $\bar{x}_0$ and associated covariance matrix $\bar{P}_0$, the computational algorithm for the batch processor generally uses the normal equation form for the state estimate $\hat{x}$ at the initial time as:

$$\hat{x} = (H^T R^{-1} H + \bar{P}_0^{-1})^{-1} (H^T R^{-1} y + \bar{P}_0^{-1} \bar{x}_0) \tag{C.13}$$

where $t_0$ can represent an arbitrary epoch associated with the initial time for a trajectory or a set of tracking data. For a more complete description of linear estimation theory applied to the orbit determination problem, Tapley [1973] can be referenced. For the details specific to the multisatellite orbit determination problem, Rim [1992] or Tapley & Ries [2003] can be referenced.

# Appendix D

# Surface Force Model Comparison: Box-wing Vs. Cannonball-wing

For Jason-1 POD, the surface force model error is one large factor that affects the radial orbit error, especially because of the significant improvement of the gravity model which had been a large error source. At a high altitude of 1336 kilometers above the Earth, acceleration due to atmospheric drag does not affect the satellite, but the accelerations due to solar radiation and Earth radiation on the satellite become greater. For Jason-1 in particular, the decreased mass-to-area ratio compared to T/P may increase the influence of the surface force model error on the orbit error.

For the surface force models, two kinds of shape models for Jason-1 are implemented in MSODP: one is a box-wing model, and the other is a cannonball-wing model, which is a simplified model generally used in UTOPIA for T/P. The solar radiation force based on the box-wing model is presented in Equation 2.5. The solar radiation forces on a body and on wings based on the cannonball-wing model are described in Equations 2.6 and 2.7, respectively. Equations 2.12 and 2.13 express the atmospheric drag forces from the box-wing model and from the cannonball-wing model respectively.

In this section, the effect of the two surface models on the orbit performance will be compared by applying each different drag and solar radiation model according to the two different shapes. The orbits from the box-wing model are expected to perform better than the orbits from the cannonball-wing, and how much they will be improved is a question to be answered in this experiment. The benefit of the introduction of empirical accelerations along with the surface force models is also re-examined. To that end, several experiments using the different surface force models are performed with and without empirical accelerations.

| Case | Model | Estimation Strategy |
|---|---|---|
| **Case b1** | box-wing | No empirical acceleration estimated |
| **Case c1** | cannon-wing | No empirical acceleration estimated |
| **Case b2** | box-wing | Only CT estimated |
| **Case c2** | cannon-wing | Only CT estimated |
| **Case b3** | box-wing | CT & 1-cpr T estimated |
| **Case c3** | cannon-wing | CT & 1-cpr T estimated |
| **Case b4** | box-wing | CT & 1-cpr N estimated |
| **Case c4** | cannon-wing | CT & 1-cpr N estimated |
| **Case b5** | box-wing | CT & 1-cpr T,N estimated |
| **Case c5** | cannon-wing | CT & 1-cpr T,N estimated |
| **Case b6** | box-wing | mixed measurements*; CT & 1-cpr T,N estimated |
| **Case c6** | cannon-wing | mixed measurements*; CT & 1-cpr T,N estimated |

* Mixed orbit with GPS+SLR+DORIS. See Chapter 5.
- For subarc length, **Case sub1.5-4.5** is applied.

Table D.1: Cases for Orbit Solution with Different Surface Force Models

Table D.1 summarizes all of the experimental cases with different surface force models and different empirical force parameterizations. **Case b1**

for the box-wing model and **Case c1** for the cannonball-wing model are processed without estimation of any empirical acceleration parameter to see the improvement of the orbit accuracy when compared with the orbits processed with the estimation of the empirical acceleration parameters. When empirical parameters are estimated, 1-cpr T and N parameters are estimated every 9 hours, and the CT parameter is estimated every 3 hours. The estimation of the empirical parameter, CT, in **Case b2** and in **Case c2** will accommodate the drag acceleration errors from the two different shape models, since CT was designed to accommodate the non-periodic along-track acceleration error. The estimation of the 1-cpr T and/or N parameters will accommodate the unmodeled radiation accelerations from the two different shapes. This will help in analyzing the effect of the radiation force differences from the two shapes on the orbit error. The 1-cpr T parameter in the along-track direction will accommodate most of the radiation force model errors from the solar-panels. Since the radiation force from the solar-panels, rather than the radiation force from the main body, will be the major radiation force source because of the broad area of solar arrays (see Table 2.3), whether to estimate the 1-cpr T parameter or not will make a large impact on the orbit accuracy. In Table D.1, the cases with the combined data of SLR/DORIS and GPS such as **Case b6** and **Case c6** were also processed for the shape model comparison. All other cases were processed with GPS-only data. More issues related to the use of SLR/DORIS and GPS simultaneously will be discussed in Chapter 5.

It is interesting that orbits from the box-wing model perform worse than

the orbits from the cannonball-wing model unless the 1-cpr T is estimated. When no empirical acceleration parameter is estimated, the crossover Mean of **Case b1** from the box-wing model is 4.90 (±3.14) cm, while the crossover Mean of **Case c1** from the cannonball-wing model is 2.99 (±2.80) cm (see Table D.2(a)). When the CT and 1-cpr N parameters are estimated, the crossover Means of **Case b4** and **Case c4** are 2.92 (±3.20) and 2.77 (±3.14) cm respectively. Generally, it appears that the orbit centering from the box-wing model is worse than the orbit centering from the cannonball-wing model when there is no estimation of 1-cpr T. This is also true for the comparison of the crossover RMS values from the two shape models without the estimation of 1-cpr T. The crossover RMS of the **Case b1** orbit from the box-wing model is 30.36 (±7.12) cm, while the crossover RMS of the **Case c1** orbit from the cannonball-wing model is 28.08 (±8.02) cm. The crossover RMS values of **Case b4** and **Case c4** are 29.56 (±11.83) and 27.26 (±13.04) cm, respectively (see Table D.2(b)).

With the estimation of the 1-cpr T parameter, however, the crossover statistics of the orbit solutions were dramatically improved from 3∼5 cm to ∼0.5 cm for the crossover Mean, and from ∼30 cm to 6-7 cm for the crossover RMS. This means that the 1-cpr T parameter affects the radial orbit accuracy very strongly. Also, when the 1-cpr T parameter is estimated, the orbits from the box-wing model perform better than the orbits from the cannonball-wing model. For example, the crossover Mean and crossover RMS of the orbits from **Case b3** are 4.7 (±8.0) mm and 6.70 (±0.64) cm respectively, which are

better than 5.6 (±9.4) mm and 6.82 (±0.74) cm respectively of the crossover Mean and crossover RMS of the orbits from **Case c3**. The large influence of the 1-cpr T parameter on the orbits indicates that the radiation acceleration error from the solar array is a major source of the orbit error because of its relatively large cross-sectional area with respect to the main body's. It also implies that there are more ways to improve the surface force model especially for the solar array.

The estimation of CT, whether along with the estimation of the 1-cpr N parameter or not, does not improve the orbits as significantly as the estimation of the 1-cpr T parameter does in both surface force models. It is probably because of limited impact of drag on the satellite. The CT parameter affects a mean motion, but it affects the radial orbit accuracy only weakly. For example, the crossover RMS of **Case c2** with the estimation of CT is 27.38 (±13.04) cm while the crossover RMS of **Case c4** with the estimation of the CT and 1-cpr N parameters is 27.26 (±13.04) cm. The crossover RMS of **Case c1** without the estimation of empirical parameters is 28.08 (±8.02) cm.

When the combined data of GPS and SLR/DORIS are simultaneously processed while estimating CT and 1-cpr N & T, the orbits with the box-wing model showed an improvement over the orbits with the cannonball-wing model, although it was not significant. For example, the crossover RMS of **Case b6** was 5.87 (±0.24) cm while the crossover RMS of **Case c6** was 5.89 (±0.23) cm. Also, overall the orbits with the combined data showed significant improvement over the orbits with GPS-only. The crossover RMS of **Case b6**

| Cyc | Crossover Mean for each Case of Surface Force Model | | | | | | | | | | | |
|---|---|---|---|---|---|---|---|---|---|---|---|---|
| | c1 | b1 | c2 | b2 | c3 | b3 | c4 | b4 | c5 | b5 | c6 | b6 |
| 8 | -4.1 | 35.5 | 50.6 | 47.3 | 16.2 | 10.9 | 45.6 | 44.2 | 5.9 | 2.1 | 3.8 | 2.9 |
| 9 | -13.6 | -21.6 | 3.5 | -2.8 | 4.9 | 3.3 | 5.2 | -.8 | 6.9 | 5.5 | 2.9 | 2.5 |
| 10 | 15.5 | 16.3 | 7.9 | 10.5 | 7.3 | 8.5 | 6.1 | 8.6 | 5.3 | 6.6 | -1.8 | -1.2 |
| 11 | 17.8 | 42.2 | 26.5 | 33.5 | 7.6 | 10.6 | 19.7 | 27.7 | -11.5 | -7.5 | -10.7 | -9.5 |
| 12 | 41.4 | 97.4 | 40.7 | 41.8 | 8.5 | 7.7 | 23.9 | 27.2 | -17.4 | -13.5 | -12.1 | -10.9 |
| 13 | 11.9 | 22.4 | 92.4 | 92.8 | 11.1 | 8.5 | 86.7 | 86.8 | 1.0 | -.5 | -1.3 | -2.3 |
| 14 | -5.5 | 50.3 | -10.5 | -5.6 | 1.4 | 3.9 | -8.7 | -4.9 | -3.8 | -1.1 | -5.6 | -4.8 |
| 15 | 64.4 | 81.0 | 15.9 | 19.8 | -5.2 | -4.7 | 17.1 | 20.7 | -7.3 | -6.5 | -6.5 | -6.2 |
| 16 | 55.3 | 67.3 | -4.5 | -4.2 | -13.5 | -14.0 | -2.7 | -2.7 | -11.1 | -12.0 | -7.6 | -7.9 |
| 17 | 35.5 | 53.7 | -9.9 | -14.3 | 4.1 | 1.8 | -6.9 | -10.6 | 8.0 | 5.6 | 6.6 | 5.9 |
| 18 | 44.2 | 71.2 | 42.5 | 54.8 | -4.4 | -2.4 | 47.4 | 54.5 | -2.5 | -.7 | -5.2 | -3.8 |
| 19 | 66.8 | 73.2 | 80.5 | 80.0 | 16.8 | 13.4 | 79.3 | 79.8 | 16.5 | 12.8 | 13.4 | 12.5 |
| 20 | 58.8 | 47.7 | 47.6 | 48.4 | 18.6 | 14.1 | 47.3 | 48.6 | 17.4 | 13.0 | 7.8 | 6.8 |
| Mean | 29.9 | 49.0 | 29.5 | 30.9 | 5.6 | 4.7 | 27.7 | 29.2 | 0.6 | 0.3 | -1.3 | -1.2 |
| rms | 28.0 | 31.4 | 33.3 | 33.9 | 9.4 | 8.0 | 31.4 | 32.0 | 10.7 | 8.5 | 7.7 | 7.0 |

(a) Crossover Mean

| Cyc | Crossover RMS for each Case of Surface Force Model | | | | | | | | | | | |
|---|---|---|---|---|---|---|---|---|---|---|---|---|
| | c1 | b1 | c2 | b2 | c3 | b3 | c4 | b4 | c5 | b5 | c6 | b6 |
| 8 | 289.2 | 295.8 | 250.7 | 278.6 | 74.6 | 72.0 | 248.9 | 277.3 | 62.1 | 61.8 | 61.3 | 61.3 |
| 9 | 151.1 | 182.6 | 127.0 | 166.2 | 59.0 | 58.9 | 126.9 | 166.0 | 59.5 | 59.3 | 58.6 | 58.5 |
| 10 | 139.0 | 175.6 | 124.6 | 167.7 | 64.2 | 64.3 | 124.1 | 167.2 | 61.1 | 61.3 | 59.5 | 59.4 |
| 11 | 292.4 | 326.9 | 272.0 | 310.4 | 82.6 | 80.7 | 269.4 | 308.0 | 61.7 | 60.9 | 61.5 | 61.2 |
| 12 | 365.6 | 372.6 | 339.1 | 339.8 | 71.6 | 70.4 | 334.1 | 335.0 | 56.9 | 55.7 | 54.9 | 54.6 |
| 13 | 428.2 | 426.8 | 648.4 | 635.8 | 72.9 | 68.9 | 648.8 | 641.8 | 63.2 | 63.1 | 61.2 | 61.2 |
| 14 | 322.8 | 348.4 | 297.7 | 300.7 | 68.3 | 68.0 | 296.4 | 299.4 | 58.5 | 58.4 | 58.1 | 58.0 |
| 15 | 246.5 | 286.8 | 215.4 | 241.1 | 61.2 | 61.3 | 215.6 | 241.2 | 60.2 | 60.1 | 57.1 | 57.0 |
| 16 | 224.8 | 262.1 | 197.5 | 224.7 | 62.6 | 62.8 | 197.5 | 224.8 | 62.7 | 62.9 | 61.8 | 61.8 |
| 17 | 292.4 | 311.0 | 276.8 | 287.4 | 63.3 | 62.3 | 276.2 | 287.0 | 60.0 | 59.6 | 59.7 | 59.5 |
| 18 | 336.1 | 369.1 | 316.4 | 351.4 | 58.5 | 58.4 | 316.4 | 350.4 | 55.6 | 55.6 | 55.1 | 55.0 |
| 19 | 312.1 | 313.5 | 277.8 | 291.8 | 75.4 | 73.4 | 276.0 | 290.6 | 60.6 | 59.6 | 59.3 | 59.0 |
| 20 | 250.7 | 275.5 | 216.0 | 255.3 | 72.8 | 70.1 | 214.1 | 253.9 | 59.3 | 58.2 | 57.0 | 56.9 |
| Mean | 280.8 | 303.6 | 273.8 | 296.2 | 68.2 | 67.0 | 272.6 | 295.6 | 60.1 | 59.7 | 58.9 | 58.7 |
| rms | 80.2 | 71.2 | 130.4 | 117.0 | 7.4 | 6.4 | 130.4 | 118.3 | 2.2 | 2.4 | 2.3 | 2.4 |

(b) Crossover RMS

| Cyc | SLR residual RMS (> 70 deg) for each Surface Force Model | | | | | | | | | | | |
|---|---|---|---|---|---|---|---|---|---|---|---|---|
| | c1 | b1 | c2 | b2 | c3 | b3 | c4 | b4 | c5 | b5 | c6 | b6 |
| 8 | 159.8 | 190.8 | 149.5 | 168.7 | 34.3 | 32.8 | 147.8 | 167.5 | 11.5 | 11.9 | 8.9 | 9.0 |
| 9 | 47.4 | 83.8 | 55.4 | 79.8 | 14.5 | 14.7 | 56.5 | 80.6 | 13.2 | 13.0 | 10.4 | 10.2 |
| 10 | 66.7 | 84.4 | 54.5 | 76.2 | 20.7 | 20.7 | 51.1 | 73.5 | 12.6 | 13.1 | 10.2 | 10.5 |
| 11 | 149.6 | 160.6 | 119.7 | 141.2 | 32.9 | 31.0 | 114.7 | 138.4 | 14.6 | 13.5 | 9.8 | 9.8 |
| 12 | 234.8 | 208.9 | 210.1 | 205.7 | 46.4 | 44.2 | 201.6 | 198.2 | 7.4 | 7.8 | 6.7 | 6.8 |
| 13 | 286.7 | 259.2 | 260.1 | 264.5 | 14.1 | 14.6 | 263.4 | 270.4 | 9.6 | 9.9 | 8.1 | 8.0 |
| 14 | 122.3 | 116.9 | 140.3 | 138.7 | 18.4 | 17.1 | 140.3 | 139.6 | 10.4 | 10.1 | 10.7 | 10.5 |
| 15 | 115.1 | 138.1 | 118.0 | 134.1 | 17.6 | 17.3 | 118.6 | 135.1 | 15.5 | 15.3 | 9.6 | 9.7 |
| 16 | 94.1 | 97.7 | 102.3 | 118.0 | 15.6 | 15.1 | 104.4 | 119.7 | 13.4 | 13.2 | 9.6 | 9.6 |
| 17 | 147.8 | 166.7 | 122.6 | 127.9 | 14.2 | 12.7 | 121.6 | 127.5 | 11.5 | 11.4 | 10.2 | 10.3 |
| 18 | 197.7 | 242.6 | 181.2 | 212.8 | 14.2 | 15.6 | 182.8 | 214.4 | 8.8 | 9.0 | 7.7 | 7.9 |
| 19 | 174.7 | 202.1 | 184.2 | 197.9 | 47.8 | 44.2 | 169.8 | 186.3 | 17.8 | 17.5 | 12.8 | 12.8 |
| 20 | 136.7 | 178.2 | 145.9 | 173.8 | 43.9 | 40.6 | 137.4 | 168.3 | 17.2 | 16.3 | 13.2 | 13.2 |
| Mean | 148.7 | 163.8 | 141.8 | 156.9 | 25.7 | 24.7 | 139.2 | 155.3 | 12.6 | 12.5 | 9.8 | 9.9 |
| rms | 65.6 | 57.5 | 57.8 | 54.1 | 13.4 | 12.1 | 57.3 | 54.1 | 3.2 | 2.9 | 1.8 | 1.8 |

(c) SLR residual RMS

Table D.2: Orbit Improvement with Box-wing Surface Force Model. Based on the crossover RMS, the box-wing model performed better than the cannonball-wing model in both GPS-only orbits and the 'mixed-data orbits'.

was 5.87 cm against 5.97 cm of **Case b5**.

In summary, constantly exerting drag force error is not an important error factor for Jason-1. Consequently, the estimation of CT does little to improve the orbit solution. However, the estimation of the 1-cpr T parameter in the along-track direction improves the orbits significantly, which indicates that the radiation force from the solar array is the main source for the surface force model error because of its relatively large cross-sectional area. It implies that there is room for improvement of the surface force model for Jason-1 in the future. With the estimation of empirical parameters, the orbits were significantly improved compared to the orbits without the estimation of the empirical parameters (i.e. in Table D.2(c), $\sim$16 cm was reduced to $\sim$1 cm in the SLR residual RMS sense, which is one of the indicators for the radial orbit error). When the CT parameter and, the 1-cpr N and T parameters were estimated, for both cases with GPS-only data and with the combined data, the orbits with the box-wing model performed better than the orbits with the cannonball-wing model. The box-wing model for the surface force model was adopted in this research.

# Appendix E

# Combining Data Types

## E.1 MSODP Job-deck for Mixed-data Orbit

```
# QSUB -s /bin/sh -eo -ro
# QSUB -r mix
# QSUB -lT 80000
# QSUB -lM 16Mw
# QSUB -q high
#
set -xS
#### change to temporary directory
#
cd $QSUB_TMPDIR
#
#### set the name of the log file and other variables
#
ID=`echo $QSUB_REQID | sed 's/\..*$//'`
LOG="${QSUB_WORKDIR}/${QSUB_REQNAME}.o${ID}"
#
WD="${QSUB_WORKDIR}"
YR="2002"
YR2=`echo $YR | awk '{ print substr($1,3,4) }'`
#
DAY=84
DDic="s+i"; DDd="s+i.over"
#
ICDAY=`expr $DAY - 1`
SEC="75600" # 21:00:00 GPS
#
if [ $DAY -lt 10 ]; then
  NDAY=00$DAY
elif [ $DAY -ge 10 ] && [ $DAY -le 99 ]; then
  NDAY=0$DAY
elif [ $DAY -ge 100 ]; then
  NDAY=$DAY
fi
#
if [ $ICDAY -lt 10 ]; then
  NICDAY=00$ICDAY
elif [ $ICDAY -ge 10 ] && [ $ICDAY -le 99 ]; then
  NICDAY=0$ICDAY
elif [ $ICDAY -ge 100 ]; then
  NICDAY=$ICDAY
fi
#
V="${DDd}.${NDAY}.${YR2}"
#
DIROUT="${WD}/out.${V}"
if [ ! -d $DIROUT ]
then
  mkdir $DIROUT
fi
#
#### start accounting
#
ja
#
###### Get Initial Condition for this job deck
#
```

```
cp /archive/utexas/csr/byaa713/msodp/pod/JASON/gps/mday.arc.24h/out.${DDic}.${NICDAY}.${YR2}/${DDic}.${NICDAY}.${YR2}.j2.stt stt1
trastrip stt1 stt
#
CASE="gps+leo"
LEOID="105501"
CORD="0"
msodp_ic1 $NICDAY $YR $SEC igs $CASE $LEOID stt $CORD > out3
###
cat > input << EOF
          JASON DOUBLE-DIFFERENCED HIGH-LOW MEAS PROCESSING
          AMBIGUITY, 2.5HR Z-DEL ESTIMATED
          GPS ORBIT FIXED TO IGS SOLUTION
          1r Cd, 3h 1/rev T,N ESTIMATED FOR JASON
          JASON02(99x99) GEOPOTENTIAL WITH OTIDES.TOPEX_3.0
          29 GPS SATELLITES+ JASON, 50 GS (ALL GS FIXED)
INITIAL
          CHECK  1
 CLAS01   SETID  1
 CLAS02   SETID  2
 GPS01    SATID  1                    1.0              975.00
 GPS02    SATID  1                    2.0              880.00
 GPS03    SATID  1                    3.0              975.00
 GPS04    SATID  1                    4.0              975.00
 GPS05    SATID  1                    5.0              975.00
 GPS06    SATID  1                    6.0              975.00
 GPS07    SATID  1                    7.0              975.00
 GPS08    SATID  1                    8.0              975.00
 GPS09    SATID  1                    9.0              975.00
 GPS10    SATID  1                   10.0              975.00
 GPS11    SATID  1                   11.0             1100.00
 GPS13    SATID  1                   13.0             1100.00
 GPS14    SATID  1                   14.0             1100.00
 GPS15    SATID  1                   15.0              880.00
 GPS17    SATID  1                   17.0              880.00
 GPS18    SATID  1                   18.0             1100.00
 GPS20    SATID  1                   20.0             1100.00
 GPS21    SATID  1                   21.0              880.00
 GPS22    SATID  1                   22.0              975.00
 GPS23    SATID  1                   23.0              975.00
 GPS24    SATID  1                   24.0              975.00
 GPS25    SATID  1                   25.0              975.00
 GPS26    SATID  1                   26.0              975.00
 GPS27    SATID  1                   27.0              975.00
 GPS28    SATID  1                   28.0             1100.00
 GPS29    SATID  1                   29.0              975.00
 GPS30    SATID  1                   30.0              975.00
 GPS31    SATID  1                   31.0              975.00
 JASON    SATID  2              105501.0              481.00
          EPOCH1                  2002.0                1.0                15.0
          EPOCH2                    23.0               59.0                47.0
 GPS01    POS    0 4   19528162.18000245    3744893.23199867   17797088.51899910
 GPS01    VEL          -1910.55570056738    1145.98405077404    1869.08183313358
 GPS02    POS    0 4   15333881.55199945    6185073.07799673  -20172143.10900426
 GPS02    VEL             58.08265020394    2720.92601636444     808.43464664462
 GPS03    POS    0 4   -2898339.58099890   18261181.11399817  -19075772.86000347
 GPS03    VEL          -2159.83033314810    1115.24995834429    1411.79319946853
 GPS04    POS    0 4    8924038.38499719  -12091166.05600119   21974273.46200097
 GPS04    VEL          2324.84419881208    1504.88458592688     -90.82838294926
 GPS05    POS    0 4  -12931889.54799992  -16004702.94199777   16813317.44700444
 GPS05    VEL           146.30376133409    -2154.68074128759   -1916.79530306711
 GPS06    POS    0 4  -23589610.97100353    2730529.17800197   12259256.90899706
 GPS06    VEL          1214.52169245305    -962.27618828032    2568.24782385693
 GPS07    POS    0 4   18996427.32600009  -17105845.56400025    7125119.18700302
 GPS07    VEL           913.45182336611    -153.58978182668   -2974.44794772417
 GPS08    POS    0 4   16608095.34099734   -5966508.87400076  -20142371.40700197
 GPS08    VEL          2035.86830461619    1455.84589114516    1242.17968470627
 GPS09    POS    0 4  -21655195.10300231  -15458968.07100022   -3449169.46199635
 GPS09    VEL           487.43335553384     -47.40483815084   -3074.80342205126
 GPS10    POS    0 4   -2078528.34800056  -26007267.74300134   -4280164.74200571
 GPS10    VEL           254.18310775745    -537.26115242286    3169.60820556672
 GPS11    POS    0 4   22236625.43100178   14268117.09400010   -2700942.09999579
 GPS11    VEL          -499.70088368906     195.16907427732   -3055.87754895032
 GPS13    POS    0 4   24158155.57700217   -5940132.03500250    9171686.49399686
 GPS13    VEL          -916.19519324080     758.32475495225    2911.35519456836
 GPS14    POS    0 4  -19327969.54499984   16609638.49800003    7679602.11400321
 GPS14    VEL          -963.23932929360     253.19722841572   -2979.94191692673
```

```
 GPS15    POS    0 4  -18496605.14899814    2610274.94900146  -19166797.58900607
 GPS15    VEL          -1868.28485279857   -1466.82500383275    1616.40019218762
 GPS17    POS    0 4  -21607774.19999886   -3760033.70599900  -15404647.23800272
 GPS17    VEL          -1450.38706281881   -1280.37730007318    2279.60563299221
 GPS18    POS    0 4  -15171141.92699987    5384211.18500468  -21118416.45699978
 GPS18    VEL           131.84279531935   -2678.19530902122    -789.12895346463
 GPS20    POS    0 4   13212800.89899999   12296582.90999788   19416882.27800167
 GPS20    VEL          -188.60134645809    2474.03284232330   -1438.41966533762
 GPS21    POS    0 4  -10876989.61699939   18203596.24000371  -15182842.59599817
 GPS21    VEL          -138.46586699202   -2029.16047470894   -2333.39473635529
 GPS22    POS    0 4    -566739.85599924   26143818.78500175    2189986.36799526
 GPS22    VEL          -433.36410495815    -306.72626596683    3126.84454865879
 GPS23    POS    0 4  -12430153.41699988  -11601500.39599615  -19946947.19900215
 GPS23    VEL           297.86584547556   -2619.56112800686    1290.34827738235
 GPS24    POS    0 4   -4427807.23600319  -18316146.89500141   19019258.54799926
 GPS24    VEL           2003.01429276897    1227.14238455603    1674.32963645025
 GPS25    POS    0 4   -4316079.94899574   15474357.73500121   21455884.37100136
 GPS25    VEL          -2375.27217679023   -1205.64946671537     382.18178130801
 GPS26    POS    0 4   -9910473.26900339  -11681872.22499746  -21871194.23400176
 GPS26    VEL           2414.02655864017   -1292.17947910590    -346.67981785989
 GPS27    POS    0 4   23461387.70699954    2725080.72299948  -12418680.13400626
 GPS27    VEL           1288.28473191032     990.20634788711    2526.77972562259
 GPS28    POS    0 4   12451732.49099934  -15831739.36500400  -17084949.71399856
 GPS28    VEL           130.34606066380    2205.34004143301   -1957.61982337051
 GPS29    POS    0 4  -17065569.17999959   17734959.67700040   10004589.97500402
 GPS29    VEL          -1194.13293423112     409.28135845822   -2846.70770308634
 GPS30    POS    0 4  -15408974.58899975   -3116813.66399652   21213595.58200276
 GPS30    VEL            45.09182792784   -2746.70965665906    -360.65222823860
 GPS31    POS    0 4   10385592.12700260   12046761.65799791  -21568380.36200106
 GPS31    VEL          -2301.93816019966    1370.07979297933    -314.33812184416
 JASON    POS    0 0   -1774009.87595063   -3152702.09599146   -6815750.81361818
 JASON    VEL           3873.52046491858   -5811.97344473365    1679.10648967836
          END
RUNMODE
          MODE   4
          ITER   6
          POSMIN       .00000001
          RMSFRA       .00000001
          RESTRT 0
          NARC   1
          END
FORCES
          GM              398600.4415
          GEO    1 0
 CLAS01   NJMAX 12
 CLAS01   NMAX  12
 CLAS01   MMAX  12
 CLAS02   NJMAX 99
 CLAS02   NMAX  99
 CLAS02   MMAX  99
          J2DOT  1        2446431.5              -26.0
          MOON   1
          SUN    1
          MERCUR 1
          VENUS  1
          MARS   1
          JUPITE 1
          SATURN 1
          URANUS 1
          NEPTUN 1
          INDRJ2 1 1
          ROTDEF 1                    0.3               0.046               0.294
          RELPRT 1
          DTIDES 1
          OTIDES 1
                   END
          GPSYAW 1
 JASON    ORIENT 4 0
 JASON    TPXYAW 2                              0.0
 JASON    RTNPRT 1
 JASON    THERMS 0
 JASON    YBIAS  1          374.0            187.0
 JASON    DRAGL  2
 JASON    DRAG   5                 20.           2.2
 JASON    DRAG1  2                  9.8           3.0           3.1
          FLUX   0               200.0                250.0              2.5
```

```
 JASON    BWSRP  1 8                                        1.0
 JASON    MACRO1 1   1.65  0.436  0.209 -0.001
 JASON    MACRO1 2   1.65  0.434  0.215  0.005
 JASON    MACRO1 3   3.0   0.357  0.375  0.271
 JASON    MACRO1 4   3.0   0.321  0.400  0.308
 JASON    MACRO1 5   3.1   0.240  0.402  0.330
 JASON    MACRO1 6   3.1   0.318  0.370  0.267
 JASON    MACRO1 7   9.8   0.344  0.006  0.647
 JASON    MACRO1 8   9.8   0.004  0.298  0.697
          BWPRNT 1
          SHADOW 2
 JASON    ERADP  1                3.1           0.3
 JASON    ERADP2 2 0
 JASON    ERADP1 2          2444960.5
          AL 0 0                        .34
          AL 1 0                        .00
          AL 2 0                        .29
          EM 0 0                        .68
          EM 1 0                        .00
          EM 2 0                       -.18
          AL 1 0   365.25               .10                      .00
          EM 1 0   365.25              -.07                      .00
END ERAD
          EPO    1
          END
FRAME
          POLMOT 2
          SPDUT1 1
          UT1TAI 2
          NUTCOR 1
          POLEPO                               0.0460               0.2940
          END
SUBARC
 JASON    DOEARC          1.0
 JASON    DRAGL       0.34492
 JASON    RTNPRT      1.03475
 JASON    CD        0      1.5
 JASON    RADIAL    0         0.                  0.
 JASON    TRANSV    0         0.                  0.
 JASON    NORMAL    0         0.                  0.
          END
INTEG/OUT
30h       TFDAYS               1.25
          TOVER     1         21600.0
          NPRINT9000
 CLAS01   FXSTEP  14               300.0             2.0E-12
 CLAS01   INTPOL   1
 CLAS01   EXTSYS   1
 CLAS01   EXTFRM   1
 CLAS02   FXSTEP  11        30.
          DTNEW                 604800.0
          DTOUT                 604800.0
          DTOBS                 604800.0
          CCMAX     0                0.9
          NPTAFT    2
          RMSPRN    3
          END
STA/OBS
 GPS01    CMOFF4    3          0.2794          0.0000          1.0230
 GPS02    CMOFF4    3          0.2794          0.0000          1.0230
 GPS03    CMOFF4    3          0.2794          0.0000          1.0230
 GPS04    CMOFF4    3          0.2794          0.0000          1.0230
 GPS05    CMOFF4    3          0.2794          0.0000          1.0230
 GPS06    CMOFF4    3          0.2794          0.0000          1.0230
 GPS07    CMOFF4    3          0.2794          0.0000          1.0230
 GPS08    CMOFF4    3          0.2794          0.0000          1.0230
 GPS09    CMOFF4    3          0.2794          0.0000          1.0230
 GPS10    CMOFF4    3          0.2794          0.0000          1.0230
 GPS11    CMOFF4    3          0.0000          0.0000          0.0000
 GPS13    CMOFF4    3          0.0000          0.0000          0.0000
 GPS14    CMOFF4    3          0.0000          0.0000          0.0000
 GPS15    CMOFF4    3          0.2749          0.0000          1.0230
 GPS17    CMOFF4    3          0.2749          0.0000          1.0230
 GPS18    CMOFF4    3          0.0000          0.0000          0.0000
 GPS20    CMOFF4    3          0.0000          0.0000          0.0000
 GPS21    CMOFF4    3          0.2749          0.0000          1.0230
```

```
 GPS22    CMOFF4    3          0.2749          0.0000          1.0230
 GPS23    CMOFF4    3          0.2749          0.0000          1.0230
 GPS24    CMOFF4    3          0.2749          0.0000          1.0230
 GPS25    CMOFF4    3          0.2749          0.0000          1.0230
 GPS26    CMOFF4    3          0.2749          0.0000          1.0230
 GPS27    CMOFF4    3          0.2749          0.0000          1.0230
 GPS28    CMOFF4    3          0.0000          0.0000          0.0000
 GPS29    CMOFF4    3          0.2749          0.0000          1.0230
 GPS30    CMOFF4    3          0.2749          0.0000          1.0230
 GPS31    CMOFF4    3          0.2749          0.0000          1.0230
 JASON    CMOFF4    3          1.4471         -0.2180         -0.5040
          MEAS1     1
          MEAS5     2       10000.0
          MEAS6     1       10000.0           4.0
          MEAS7     1
          MEAS14    1            0.03
          DECORR    1
          MXREAD  100
          TROPOS    1
          TROPRN    1
          TROLIM    1           900.0
          REFRAC    3
          ZENITH    0             0.2
          DDTROP                9000.0
          SATFRQ                                          1575.42
          MEASX     0
 JASON    CMOFF1    3           0.229           0.598           0.683          0.049
          ELMIN     1           15.0
          CUTOFF    1           90.0
          EDIT      1
          EDIT1     1
          EDIT2     1
          EDCRIT    1       1000.00          0.15             3.0
          EDCRIT    5         100.0           0.6             3.0
          EDCRIT    6         100.0           0.3             3.0
          EDCRIT    7      100000.0           0.3             3.0
          EDTPSS    1         10000.0           0.2           2.0
          EDCRIT   14      10000000.0          10.0           3.0
          GTIDES    1
          ROTDEF    1
          RELCOR    1
          ANTPHS    3
          ANTPCV    1
          DDPCC     1
          STAPRN    1
          INVBAR    1
 TEG2B    GEOIDC    2 62636858.76615
 .50      GEOIDC    2    62636856.61
          SSTCOR    1          25.            25.            25.
          H13EDT    1           0.0          10.0
          ABIAS                 0.0           0.0             0.0
          WTNODE    3       2445578.5            0.10
          WTNODE    4       2447000.5            0.10
          WTNODE    5       2449353.5            0.10
          END
 SOLVEPARAM
 CLAS01   SATEST      0
 CLAS02   SATEST      1
 JASON    DRAGL       1
 JASON    RTNEST      0 1 1
 JASON    COMDEL      1 0 1
 CLAS01   DELOE       0         86400.0
 CLAS01   DOEECC      1             1.0
 CLAS01   DOEINC      1             1.0
 CLAS01   DOESOM      1             1.0
 CLAS01   DOECOM      1             1.0
          DDBIAS  200 2
          ZENITH  150 2
          STAXYZ      0
 trom     STA   10302 0 0 0
 nyal     STA   10317 0 0 0
 onsa     STA   10402 0 0 0
 graz     STA   11001 0 0 0
 irkt     STA   12313 0 0 0
 zwen     STA   12330 0 0 0
 kit3     STA   12334 0 0 0
```

```
mate     STA   12734 0 0 0
vill     STA   13406 0 0 0
kosg     STA   13504 0 0 0
pots     STA   14106 0 0 0
wtzr     STA   14201 0 0 0
shao     STA   21605 0 0 0
lhas     STA   21613 0 0 0
tskb     STA   21730 0 0 0
bahr     STA   24901 0 0 0
hrao     STA   30302 0 0 0
mas1     STA   31303 0 0 0
mali     STA   33201 0 0 0
algo     STA   40104 0 0 0
drao     STA   40105 0 0 0
yell     STA   40127 0 0 0
gol2     STA   40405 0 0 0
fair     STA   40408 0 0 0
kokb     STA   40424 0 0 0
wes2     STA   40440 0 0 0
mdo1     STA   40442 0 0 0
gode     STA   40451 0 0 0
pie1     STA   40456 0 0 0
nlib     STA   40465 0 0 0
fort     STA   41602 0 0 0
braz     STA   41606 0 0 0
sant     STA   41705 0 0 0
areq     STA   42202 0 0 0
brmu     STA   42501 0 0 0
thu1     STA   43001 0 0 0
tidb     STA   50103 0 0 0
yar1     STA   50107 0 0 0
hob2     STA   50116 0 0 0
pert     STA   50133 0 0 0
mac1     STA   50135 0 0 0
chat     STA   50207 0 0 0
auck     STA   50209 0 0 0
guam     STA   50501 0 0 0
kwj1     STA   50506 0 0 0
ohig     STA   66008 0 0 0
mcm4     STA   66001 0 0 0
dav1     STA   66010 0 0 0
cas1     STA   66011 0 0 0
kerg     STA   91201 0 0 0
kour     STA   97301 0 0 0
         YBIAS       0      2000.0
         SSTEST      0 0 0
         ALPHA 4002 2
         ALPHA 4005 2
         ALPHA 4006 2
         ALPHA 4008 2
         ALPHA 4009 2
         ALPHA 4010 2
         ALPHA 4012 2
         ALPHA 4013 2
         ALPHA 4016 2
         ALPHA 4017 2
         ALPHA 4018 2
         ALPHA 4019 2
         ALPHA 4020 2
         ALPHA 4022 2
         ALPHA 4023 2
         ALPHA 4025 2
         ALPHA 4027 2
         ALPHA 4035 2
         ALPHA 4036 2
         ALPHA 4037 2
         ALPHA 4038 2
         ALPHA 4040 2
         ALPHA 4041 2
         ALPHA 4042 2
         ALPHA 4043 2
         ALPHA 4045 2
         ALPHA 4046 2
         ALPHA 4047 2
         ALPHA 4048 2
         ALPHA 4050 2
```

```
            ALPHA 4051 2
            ALPHA 4053 2
            ALPHA 4054 2
            ALPHA 4055 2
            ALPHA 4201 2
            ALPHA 4202 2
            ALPHA 4203 2
            ALPHA 4204 2
            ALPHA 4205 2
            ALPHA 4206 2
            ALPHA 4207 2
            ALPHA 4208 2
            ALPHA 4209 2
            ALPHA 4210 2
            ALPHA 4211 2
            ALPHA 4212 2
            ALPHA 4213 2
            ALPHA 4214 2
            ALPHA 4215 2
            ALPHA 4216 2
            ALPHA 4217 2
            ALPHA 4218 2
            ALPHA 4219 2
            ALPHA 4220 2
            ALPHA 4221 2
            ALPHA 4222 2
            ALPHA 4223 2
            ALPHA 4224 2
            ALPHA 4225 2
            ALPHA 4226 2
            ALPHA 4227 2
            ALPHA 4228 2
            ALPHA 4229 2
            ALPHA 4230 2
            ALPHA 4231 2
            ALPHA 4232 2
            ALPHA 4235 2
            ALPHA 4236 2
            ALPHA 4237 2
            ALPHA 4238 2
            ALPHA 4239 2
            ALPHA 4245 2
            ALPHA 4246 2
            ALPHA 4247 2
            ALPHA 4248 2
            ALPHA 4249 2
            ALPHA 4250 2
            ALPHA 4251 2
            ALPHA 4252 2
            ALPHA 4253 2
            ALPHA 4254 2
            ALPHA 4255 2
            ALPHA 4256 2
            ALPHA 4257 2
            ALPHA 4258 2
            ALPHA 4259 2
            ALPHA 4260 2
            ALPHA 4261 2
            ALPHA 4262 2
            ALPHA 4263 2
            ALPHA 4264 2
            ALPHA 4265 2
            ALPHA 4266 2
            ALPHA 4267 2
            ALPHA 4268 2
            ALPHA 4269 2
            ALPHA 4270 2
            ALPHA 4271 2
            ALPHA 4272 2
            ALPHA 4273 2
            ALPHA 4274 2
            ALPHA 4275 2
PDMB        ALPHA 4276 2
YELB        ALPHA 4277 2
AREB        ALPHA 4278 2
            ALPHA 4279 2
```

```
ALPHA 4280 2
ALPHA 4281 2
ALPHA 4282 2
ALPHA 4283 2
BIAS  4002 2
BIAS  4005 2
BIAS  4006 2
BIAS  4008 2
BIAS  4009 2
BIAS  4010 2
BIAS  4012 2
BIAS  4013 2
BIAS  4016 2
BIAS  4017 2
BIAS  4018 2
BIAS  4019 2
BIAS  4020 2
BIAS  4022 2
BIAS  4023 2
BIAS  4025 2
BIAS  4027 2
BIAS  4035 2
BIAS  4036 2
BIAS  4037 2
BIAS  4038 2
BIAS  4040 2
BIAS  4041 2
BIAS  4042 2
BIAS  4043 2
BIAS  4045 2
BIAS  4046 2
BIAS  4047 2
BIAS  4048 2
BIAS  4050 2
BIAS  4051 2
BIAS  4053 2
BIAS  4054 2
BIAS  4055 2
BIAS  4201 2
BIAS  4202 2
BIAS  4203 2
BIAS  4204 2
BIAS  4205 2
BIAS  4206 2
BIAS  4207 2
BIAS  4208 2
BIAS  4209 2
BIAS  4210 2
BIAS  4211 2
BIAS  4212 2
BIAS  4213 2
BIAS  4214 2
BIAS  4215 2
BIAS  4216 2
BIAS  4217 2
BIAS  4218 2
BIAS  4219 2
BIAS  4220 2
BIAS  4221 2
BIAS  4222 2
BIAS  4223 2
BIAS  4224 2
BIAS  4225 2
BIAS  4226 2
BIAS  4227 2
BIAS  4228 2
BIAS  4229 2
BIAS  4230 2
BIAS  4231 2
BIAS  4232 2
BIAS  4235 2
BIAS  4236 2
BIAS  4237 2
BIAS  4238 2
BIAS  4239 2
BIAS  4245 2
```

```
          BIAS  4246 2
          BIAS  4247 2
          BIAS  4248 2
          BIAS  4249 2
          BIAS  4250 2
          BIAS  4251 2
          BIAS  4252 2
          BIAS  4253 2
          BIAS  4254 2
          BIAS  4255 2
          BIAS  4256 2
          BIAS  4257 2
          BIAS  4258 2
          BIAS  4259 2
          BIAS  4260 2
          BIAS  4261 2
          BIAS  4262 2
          BIAS  4263 2
          BIAS  4264 2
          BIAS  4265 2
          BIAS  4266 2
          BIAS  4267 2
          BIAS  4268 2
          BIAS  4269 2
          BIAS  4270 2
          BIAS  4271 2
          BIAS  4272 2
          BIAS  4273 2
          BIAS  4274 2
          BIAS  4275 2
PDMB      BIAS  4276 2
YELB      BIAS  4277 2
AREB      BIAS  4278 2
          BIAS  4279 2
          BIAS  4280 2
          BIAS  4281 2
          BIAS  4282 2
          BIAS  4283 2
          BIAS  7237 1
          BIAS  8834 1
          END
FILES
          REPORT 1 1
          DDRES  1
          DUZWRT 0
          REGWRT 0
          OBSBIN 0
          OBSPOS 1
          GTRACK 2
          UTCWRT 2     10.
 CLAS02   NGAWRT 2 1
          SYSTEM 1
          END
PLOT
          IPLT       0
          IORBPL     1
          IORB1      1 1 1
          IORB2      1 1 0
          DIMXY      2
          END
FINIS
EOF
####### modify I.C. 1) for gps (from 'addic script), 2) for Jason-1 ###########
addic input ICFILE input1
addcmoff input1 CMOFF input2
#####################################
addsta input2 /archive/utexas/csr/byab343/topex/doris_network_itrf2000  input3
addsta input3 /archive/utexas/csr/byaa713/msodp/sta/g+s/s+gps_network_itrf2000.0     INPUT
rm -f input input2 input3 input1 input4 input5 input6 ICFILE CMOFF
cp /archive/utexas/csr/byab343/utopia/EPHDAT EPHDAT
cp /archive/utexas/csr/byab343/utopia/FLXDAT FLXDAT
cp /archive/utexas/csr/byab343/utopia/OLOAD.GCM NETWRK
cp /archive/utexas/csr/export/aux/EOPDAT EOPDAT
cp /archive/utexas/csr/byab343/utopia/JGM3.GEO GEO
cp /archive/utexas/csr/byab343/utopia/OTIDES.TOPEX_3.0 OTIDES
cp /archive/utexas/csr/byab343/jason/SOE SOE
```

```
cp /archive/utexas/csr/byaa766/Msodpmod/2001.1/Phase_correction/ANTCOR  ANTCOR
#### create direct-access ephemeris from sp3 file for gps
set `dn2gw $ICDAY $YR`; WK=$1; WKD=$2
sp3n2da $WK $WKD 3 igs
mv DAFILE EXTSTA
#
MRGYAW="/archive/utexas/csr/byaa713/msodp/pod/JASON/gps+doris+slr/bin/my_mrgyaw"
set `dn2gw $DAY $YR`; WK_YAW=$1; WKD_YAW=$2
${MRGYAW} $WK_YAW $WKD_YAW 1      #### this merges 3 days (left+middle+right)
#
# modify to /archive/utexas/csr/byab310/bin/catyaw: script for concatenate JPL's yaw rate files
cp /archive/utexas/csr/byab310/gps/yaw/nominal_yaw_rates YAWNMN
cp /archive/utexas/csr/byab310/gps/yaw/yaw_bias_table YAWBIA
#
cp /archive/utexas/csr/byaa713/gps/dd/JASON/${YR2}/${DDd}/met/jason${YR2}${NDAY}.met METDAT
cp /archive/utexas/csr/byaa713/msodp/obs/dd/JASON/dd/${DDd}/jason${YR2}${NDAY}.Rimsta.utfm  gps.tmp
grep -v '*' gps.tmp > gps
rm gps.tmp
cp /archive/utexas/csr/byab343/jason/tracking/SLR.NMPT.01 slr
cp /archive/utexas/csr/byab343/jason/tracking/DORIS.NEWOBS.01  doris.1
cp /archive/utexas/csr/byab343/jason/tracking/DORIS.NEWOBS.02  doris.2
sort -m -o OBSDAT -k 1.17,1.32 slr doris.1 doris.2 gps
#
#### execute msodp1 ( the script will read EPHDAT AND FLXDAT;  it will
#    also read defaults for GEO, OTIDES and EOPDAT if not provided by the user)
#########################
cp /archive/utexas/csr/byaa713/make/2001.2/mix+antcor+yaw/PATHLIST.mix+antcor+yaw.3 PATHLIST
make_ms 2001.2 update < INPUT > OUTPUT
#########################
cp OUTPUT   $DIROUT/$V.output
cp REPORT   $DIROUT/$V.rep
cp STATE    $DIROUT/$V.bf.stt
cp J2STATE  $DIROUT/$V.j2.stt
cp DDRES    $DIROUT/$V.ddr
#
#### close accounting
#
ls -al
set +xS
ja -csflht
#
# append log file to end of output and save in desired directory;
# log file will remain on original submission directory if any error
# occurs in copying log or saving output; output will also be in
# fortran carriage control form for printing
#
if nasa $LOG >> out.log
then
  if cp out.log $DIROUT/${V}.log
  then
    rm $LOG
  fi
else
  cp out.log $DIROUT/${V}.log
fi
```

## E.2 Modsets Used in Mixed-data Orbit

```
This document can also be found at http://www.csr.utexas.edu/internal/projects/grace/messages/

*****************************************************************************
GRACE Electronic Mail      Tue Feb 27 21:42:18 CST 2001         Message No. 0012
*****************************************************************************

 Author: Key-rok Choi
 Subject: Update of Mail #11

 Purpose of changes: - To process the multi-observation types (DDobs, SLR and DORIS added to MSODP)
                     - Added PASS EDITING function in the modset.
                       (now, the 'EDTPSS' card can be used for the mixing
                        process too)
                     - Statistics for GPS DD pass was added in the OUTPUT file,
                     - Adapted to the 2001.2 version

 Directory in which changes reside:
  /archive/utexas/csr/byaa713/make/2001.2/mix/src/ on Cray SV1.

 Subroutine(s) (to be) modified:
  BATCH.f90,  BATPRO.f90,  DELRHO.f90,  GIVENS.f90, GPSPAR.f90, HTIL2H.f90
  INDICE.f90, INTERP.f90, KPRSET.f90, OBSERV.f90, OCSAVE.f90, PKPPRO.f90
  READOB.f90, REPORT.f90, SIMOBS.f90

 Subroutine(s) (to be) created: GPSPAR.f90 ( Based on Dr. Rim's 9401 version)

 Subroutine(s) (to be) deleted: <none>

 Changes (to be) made:
   BATPRO.f90 : changed to get both statistics for pass and for stations from
                OCSAVE.f90.
   OCSAVE.f90 : M_RMSPRT is called to use the IRMSPR variable.
   REPORT.f90 : DD passes to be edited will be selected/printed for the mixing
                process and statistics for gps DD pass will be printed.
```

# Appendix F

# IGS Network

## F.1 IGS Network

Table F.1: IGS Stations(335) as of August, 2002

| site Id | DOMES Number | Lon(W) (deg) | Lat(N) (deg) | Height (m) | Location | Country | Agency |
|---|---|---|---|---|---|---|---|
| albh† | 40129M003 | 236.5126 | 48.3898 | 32.0000 | Victoria | Canada | NRCan/GSC |
| algo† | 40104M002 | 281.9286 | 45.9588 | 202.0000 | Algonquin Park | Canada | NRCan/GSD |
| alic† | 50137M001 | 133.8855 | -23.6701 | 603.3580 | Alice Springs | Australia | AUSLIG |
| amc2† | 40472S004 | 255.4754 | 38.8031 | 1911.0870 | Colorado Springs | U.S.A. | USNO |
| ammn | 22201M001 | 35.8800 | 32.0300 | 1055.8300 | Amman | Jordan | RJGC |
| ankr† | 20805M002 | 32.7586 | 39.8875 | 974.8000 | Ankara | Turkey | BKG and GCM |
| aoa1 | 40483S001 | 241.1697 | 34.1574 | 246.5566 | Westlake | USA | NASA/JPL |
| aoml† | 49914S001 | 279.8378 | 25.7347 | 0.0870 | Key Biscayne, Miami | USA | NOAA |
| areq | 42202M005 | 288.5072 | -16.4655 | 2488.9294 | Arequipa | Peru | NASA/JPL |
| artu† | 12362M001 | 58.5605 | 56.4298 | 247.5110 | Arti | Russian Federation | RDAAC-IRIS |
| asc1† | 30602M001 | 345.5880 | -7.9512 | 105.1508 | Ascension Island | Ascension Island | NASA/JPL |
| auck† | 50209M001 | 174.8344 | -36.6028 | 132.0000 | Whangaparaoa Peninsula | New Zealand | IGNS-JPL |
| azu1 | 49911M001 | 242.1000 | 34.1300 | 144.7800 | Azusa | USA | USGS |
| bahr† | 24901M002 | 50.6081 | 26.2091 | -17.0300 | Manama | Bahrain | NIMA |
| bako | 23101M002 | 106.8489 | -6.4911 | 158.1365 | Cibinong | Indonesia | BAKO |
| ban2 | 22306M003 | 77.5100 | 12.9500 | 732.9000 | Bangalore | India | GFZ |
| barb | 43401S001 | 300.3912 | 13.0878 | -86.2782 | Bridgetown | Barbados | NOAA |
| barh | 49927S001 | 291.7783 | 44.3950 | 7.3680 | Bar Harbor | U.S.A | NOAA |
| bili† | 12363M001 | 166.4380 | 68.0761 | 456.2380 | Bilibino | Russian Federation | RDAAC-IRIS |
| bill | 49916M001 | 242.9354 | 33.5782 | 470.0417 | Temecula | USA | SIO |
| bjfs† | 21601M001 | 115.8925 | 39.6086 | 87.4130 | BEIJING | P.R.C. | CASM |
| blyt | 40479M001 | 245.2900 | 33.6100 | 85.9200 | Blythe | USA | SIO |
| bogi‡ | 12207M003 | 21.0352 | 52.4750 | 139.9100 | Borowa Gora | POLAND | IGiK |
| bogt† | 41901M001 | 285.9191 | 4.6401 | 2577.0833 | Bogota | Colombia | INGM-JPL |
| bor1 | 12205M002 | 17.0668 | 52.1002 | 124.0000 | BOROWIEC | POLAND | SRC PAS |
| bran | 40400M301 | 241.7200 | 34.1800 | 246.2600 | Burbank | USA | USGS |
| braz† | 41606M001 | 312.1222 | -15.9474 | 1106.0413 | Brasilia | Brazil | IBGE |
| brew | 40473M001 | 240.3173 | 48.1313 | 290.0000 | Brewster | USA | JPL |
| brmu† | 42501S004 | 295.3030 | 32.3700 | -10.6190 | Bermuda | U.K. | NOAA |
| brus | 13101M004 | 4.3592 | 50.7978 | 149.7000 | Brussels | Belgium | ROB |
| bucu | 11401M001 | 26.1257 | 44.4639 | 143.2000 | Bucuresti | Romania | BKG |
| bzrg | 12751M001 | 11.3368 | 46.4990 | 328.8000 | Bolzano | Italy | BZgpsRATAA |
| cagl† | 12725M003 | 8.9728 | 39.1359 | 238.4000 | Cagliari | Italy | ASI |
| cags | 40147M001 | 284.1927 | 45.5850 | 235.0000 | Gatineau | Canada | NRCan/GSD |
| cagz‡ | 12725M004 | 8.9728 | 39.1359 | 238.0000 | CAPOTERRA | ITALY | DIST-Cagliari |
| carr | 40464M001 | 239.5700 | 35.8900 | 478.7400 | Parkfield | USA | USGS |
| cas1† | 66011M001 | 110.5197 | -66.2834 | 22.5500 | Casey | Antarctica | AUSLIG |
| casa | 40437M002 | 241.1034 | 37.6446 | 2390.4416 | Mammoth Lakes | USA | NASA/JPL |
| cat1 | 40488M001 | 241.5200 | 33.4500 | 3.9100 | Catalina | USA | USGS |
| cedu† | 50138M001 | 133.8098 | -31.8667 | 144.8021 | Ceduna | Australia | AUSLIG |
| cfag | 41517S001 | 291.7674 | -31.6022 | 703.0000 | Caucete | Argentina | CERI |
| chat† | 50207M001 | 183.4342 | -43.9558 | 58.0000 | Waitangi | New Zealand | IGNS-JPL |
| chil | 40484M001 | 241.9700 | 34.3300 | 1567.5200 | San Gabriel Mountains | USA | USGS |
| chpi | 41609M003 | 315.0102 | -22.6872 | 640.0000 | Cachoeira Paulista | Brazil | INPE |
| chum | 25601M001 | 74.7505 | 42.9983 | 766.1515 | Chumysh | Kazakhstan | JPL |
| chur† | 40128M002 | 265.9113 | 58.7591 | -18.9000 | Churchill | Canada | NRCan/GSD |
| chwk | 40142M001 | 237.9916 | 49.1566 | 170.0000 | Chilliwack | Canada | NRCan/GSC |
| cic1 | 40508M002 | 243.3342 | 31.8707 | 67.5000 | Ensenada | Mexico | CICESE-JPL |
| cit1 | 40400S201 | 241.8700 | 34.1400 | 215.3500 | Pasadena | USA | USGS |
| ... | ... | ... | ... | ... | ... | ... | ... |

Table F.1: IGS Stations(335) as of August, 2002. (continued)

| site Id | DOMES Number | Lon(W) (deg) | Lat(N) (deg) | Height (m) | Location | Country | Agency |
|---|---|---|---|---|---|---|---|
| clar | 49906M001 | 242.2900 | 34.1100 | 373.6400 | Claremont | USA | USGS |
| cmp9 | 49905M003 | 241.5900 | 34.3500 | 1138.0100 | Sylmar | USA | USGS |
| coco† | 50127M001 | 96.8339 | -12.1883 | -35.2212 | Cocos (Keeling) Island | Australia | AUSLIG |
| conz‡ | 41719M002 | 286.9745 | -36.8438 | 181.2000 | Concepcion | Chile | BKG |
| cord | 41511M001 | 295.5300 | -31.7102 | 747.0654 | Cordoba | Argentina | NASA/JPL |
| coso | 40469M001 | 242.1900 | 35.9800 | 1455.3800 | Coso Junction | USA | SIO |
| coyq | 41715S001 | 288.1079 | -45.5143 | 476.0000 | Coyhaique | Chile | PGPSF |
| crfp | 40481M001 | 242.9000 | 34.0400 | 688.8000 | Yucaipa | USA | SIO |
| cro1† | 43201M001 | 295.4157 | 17.7568 | -31.8280 | Christiansted | U.S. Virgin Islands (USA) | NRAO-JPL |
| csn1 | 49910S001 | 241.4800 | 34.2500 | 261.5200 | Northridge | USA | USGS |
| daej† | 23902M002 | 127.3745 | 36.3994 | 117.0370 | Taejon | Korea | KAO |
| darw† | 50134M001 | 131.1327 | -12.8438 | 125.1970 | Darwin | Australia | AUSLIG |
| dav1† | 66010M001 | 77.9726 | -68.5773 | 44.5000 | Davis | Antarctica | AUSLIG |
| davr‡ | 66010M001 | 77.9726 | -68.5773 | 44.5000 | Davis | Antarctica | GA |
| dgar | 30802M001 | 72.3702 | -7.2696 | -64.8965 | Diego Garcia Island | U.K. Territory | NASA/JPL |
| dhlg | 49904M001 | 244.2100 | 33.3900 | -83.0500 | Durmid Hill | USA | SIO |
| dlft‡ | 13502M006 | 4.3876 | 51.9860 | 74.3000 | Delft | Netherlands | DUT/MGP |
| drag | 20710S001 | 35.3924 | 31.5929 | 120.2782 | metzoki dragot | Israel | SIO |
| drao† | 40105M002 | 240.3750 | 49.3226 | 542.0000 | Penticton | Canada | NRCan/GSC |
| dubo† | 40137M001 | 264.1338 | 50.2588 | 251.0000 | Lac du Bonnet | Canada | NRCan/GSC |
| dubr | 11901M001 | 18.1104 | 42.6500 | 454.2800 | Dubrovnik | Croatia | IfAG |
| dwh1 | 49837S001 | 237.9198 | 47.7741 | 109.1000 | Woodinville | US | DWH |
| dyr2 | 20801M002 | 40.2764 | 37.9157 | 500.0000 | Diyarbakir | Turkey | UNV-JPL-GCM |
| ebre | 13410M001 | 0.4924 | 40.8209 | 107.9150 | Roquetes | Spain | ICC |
| eisl† | 41703M003 | 250.6167 | -27.1482 | 114.5179 | Easter Island | Chile | NASA/JPL |
| eprt | 49928S001 | 293.0079 | 44.9087 | 30.9880 | Eastport | U.S.A. | NOAA |
| esti | 41202S001 | 273.6380 | 13.0995 | 956.5000 | Esteli | Nicaragua | NGS/NOAA |
| fair† | 40408M001 | 212.5008 | 64.9780 | 319.0097 | Fairbanks | USA | JPL-GSFC |
| fale | 50601S001 | 188.0005 | -13.8322 | 48.0000 | Faleolo | Samoa | PGPSF |
| ffmj‡ | 14279M001 | 8.6650 | 50.0906 | 178.2000 | Frankfurt / Main | Germany | BKG |
| flin† | 40135M001 | 258.0220 | 54.7256 | 320.0000 | CFS Flin Flon | Canada | NRCan/GSC |
| fort | 41602M001 | 321.5744 | -3.8774 | 20.4918 | Eusebio, Fortaleza | Brazil | NOAA |
| free | 43605S001 | 281.0074 | 26.7025 | -26.0000 | Freeport | The Bahamas | PGPSF |
| gala† | 42005M001 | 269.6964 | -0.7426 | 7.4453 | Galapagos Island | Ecuador | NASA/JPL |
| geno | 12712M002 | 8.9211 | 44.4194 | 137.0000 | GENOVA | ITALY | ASI |
| glsv† | 12356M001 | 30.4967 | 50.3642 | 226.8000 | Kiev | Ukraine | MAO |
| gode† | 40451M123 | 283.1732 | 39.0217 | 14.5082 | Greenbelt | USA | NASA/JPL |
| gol2 | 40405S031 | 243.1108 | 35.4252 | 986.6759 | Goldstone | USA | NASA/JPL |
| gold† | 40405S031 | 243.1108 | 35.4251 | 986.6644 | Goldstone | USA | NASA/JPL |
| gope | 11502M002 | 14.7856 | 49.9137 | 592.6000 | Ondrejov | Czech Republic | RIGTC GOP |
| goug† | 30608M001 | 350.1333 | -40.3488 | 81.3000 | Gough Island | territory of the U.K. | AWI |
| gras | 10002M006 | 6.9206 | 43.7547 | 1320.3182 | Caussols | France | CNES |
| graz† | 11001M002 | 15.4935 | 47.0671 | 538.2900 | Graz | Austria | ISR |
| guam† | 50501M002 | 144.8683 | 13.5893 | 201.9220 | Dededo | Guam | NASA/JPL |
| guao | 21612m003 | 87.1773 | 43.4711 | 2049.2000 | URUMQI | CHINA | |
| guat | 40901S001 | 269.4802 | 14.5905 | 1552.0000 | Guatemala City | Guatemala | NGS/NOAA |
| harb† | 30302M009 | 27.7075 | -25.8869 | 1555.0000 | Pretoria | Republic of South Africa | CNES |
| harv | 40420M101 | 239.3179 | 34.4694 | 14.9941 | Vandenberg AFB | USA | NASA/JPL |
| helj‡ | 14264M001 | 7.8931 | 54.1745 | 48.6000 | Helgoland Island | Germany | BKG |
| herp‡ | 13212M009 | 0.3362 | 50.8675 | 72.5920 | Hailsham | England | NSGF |
| hers | 13212M007 | 0.3362 | 50.8673 | 76.4990 | Hailsham | England | NSGF |
| hflk | 11006S003 | 11.3861 | 47.3129 | 2383.0000 | Innsbruck | Austria | ISR |
| hilo | 49979S001 | 204.9473 | 19.7192 | 29.0000 | Hilo | USA | PGPSF |
| hnlc | 49970S001 | 202.1355 | 21.3033 | 22.0000 | Honolulu | USA | PGPSF |
| hnpt | 49913S001 | 283.8690 | 38.5880 | -27.4763 | Cambridge | USA | NOAA |
| hob2† | 50116M004 | 147.4387 | -42.8047 | 41.1263 | Hobart | Australia | AUSLIG |
| hofn† | 10204M002 | 344.8132 | 64.2673 | 82.5000 | Hoefn | Iceland | BKG |
| holb | 40130M001 | 231.8650 | 50.6404 | 560.0000 | Holberg | Canada | NRCan/GSC |
| holc | 40404M101 | 242.1500 | 34.4600 | 1238.1700 | Pearblossom | USA | USGS |
| holm | 40148M001 | 242.2391 | 70.7364 | 39.5000 | Holman (Victoria Island) | Canada | NRCan/GSD |
| holp | 49903M001 | 241.8300 | 33.9200 | -6.6700 | Hollydale | USA | USGS |
| hrao† | 30302M004 | 27.6870 | -25.8901 | 1414.1877 | Krugersdorp | South Africa | HRAO-JPL |
| hueg‡ | 14280M001 | 7.5962 | 47.8339 | 278.4000 | Huegelheim | Germany | BKG |
| iisc† | 22306M002 | 77.5700 | 13.0210 | 800.0000 | Bangalore | India | CMMACS-JPL |
| ineg | 40507M001 | 257.7158 | 21.8561 | 1888.3160 | Aguascalientes | Mexico | INEGI |
| invk | 40150M001 | 226.4730 | 68.3062 | 46.3600 | Inuvik | Canada | NRCan/GSD |
| irkt† | 12313M001 | 104.3162 | 52.2190 | 503.3816 | Irkutsk | Russia | DUT |
| ista | 20807M001 | 29.0193 | 41.1044 | 147.2000 | Istanbul | Turkey | BKG |
| jab1 | 50136M001 | 132.8939 | -12.6588 | 82.1140 | Jabiru | Australia | AUSLIG |
| jama† | 42601S001 | 283.2191 | 17.9390 | -2.9410 | Kingston | Jamaica | NGS/NOS/NOAA |
| ... | ... | ... | ... | ... | ... | ... | ... |

Table F.1: IGS Stations(335) as of August, 2002. (continued)

| site Id | DOMES Number | Lon(W) (deg) | Lat(N) (deg) | Height (m) | Location | Country | Agency |
|---|---|---|---|---|---|---|---|
| joze | 12204M001 | 21.0332 | 52.0863 | 141.0000 | JOZEFOSLAW | POLAND | IGGA-WUT |
| jplm† | 40400M007 | 241.8268 | 34.2048 | 423.9830 | Pasadena | USA | NASA/JPL |
| karr† | 50139M001 | 117.0972 | -20.9814 | 109.2463 | Karratha | Australia | AUSLIG |
| kely† | 43005M001 | 309.0550 | 66.9873 | 230.5636 | Kangerlussuaq | Greenland | NOAA |
| kerg† | 91201M002 | 70.2555 | -49.3515 | 74.0583 | Port aux Francais | Kerguelen Islands | CNES |
| kgn0 | 21704S006 | 139.4885 | 35.7068 | 128.5000 | Koganei | Japan | CRL |
| kgni | 21704S005 | 139.4881 | 35.7103 | 123.5000 | KOGANEI | JAPAN | RAAG-KSRC |
| kiru† | 10403M002 | 20.9684 | 67.8573 | 391.0600 | Kiruna | Sweden | ESA |
| kit3 | 12334M001 | 66.8800 | 39.1400 | 643.0000 | Kitab | Uzbekistan | GFZ |
| kodk† | 40419S003 | 207.5000 | 57.7300 | 78.5300 | Kodiak | USA | NASA |
| kokb† | 40424M004 | 200.3351 | 22.1263 | 1167.3680 | Kokee Park, Waimea, | USA | NASA/JPL |
| kosg† | 13504M003 | 5.8096 | 52.1784 | 97.8617 | Kootwijk (near Apeldoorn) | The Netherlands | DUT |
| kou1 | 97301M211 | 307.1940 | 5.2522 | -25.7450 | Kourou | French Guyana | |
| kouc | 92727S001 | 164.2873 | -20.5587 | 84.0000 | Koumac | New Caledonia | PGPSF |
| kour† | 97301M210 | 307.1940 | 5.2522 | -25.5700 | Kourou | French Guyana | ESA |
| kr0g‡ | 10422M001 | 21.0602 | 67.8775 | 498.0500 | Kiruna | Sweden | LMV |
| ksmv | 21701S007 | 140.6577 | 35.9554 | 57.9000 | KASHIMA | JAPAN | RAAG-KSRC |
| kstu† | 12349M002 | 92.7900 | 55.9900 | 210.0000 | Krasnoyarsk | Russia | GFZ |
| kunm† | 21609M001 | 102.7970 | 25.0290 | 2023.0000 | Kunming | China | NASA/JPL |
| kwj1† | 50506M001 | 167.7302 | 8.7222 | 38.2688 | Kwajalein Atoll | Marshall Islands | NASA/JPL |
| lae1† | 51002M001 | 146.9932 | -6.6737 | 140.3500 | Lae | Papua New Guinea | RSES |
| lama | 12209M001 | 20.6699 | 53.8924 | 187.0000 | OLSZTYN | POLAND | UWM_OLSZTYN |
| lbch | 40482M001 | 241.8000 | 33.7900 | -27.5600 | Long Beach | USA | USGS |
| leep | 49902M001 | 241.6800 | 34.1300 | 485.0600 | Hollywood | USA | USGS |
| leij‡ | 14267M001 | 12.3741 | 51.3540 | 178.4000 | Leipzig | Germany | BKG |
| lhas† | 21613M001 | 91.1040 | 29.6573 | 3622.0000 | LHASA | China | BKG |
| lhaz‡ | 21613M002 | 91.1040 | 29.6573 | 3622.0000 | Lhasa | China | BKG |
| lhue | 49980S001 | 200.6607 | 21.9846 | 46.0000 | Lihue, Kauai | USA | PGPSF |
| lind | 49767M001 | 239.4600 | 47.0000 | 471.9800 | Ellensburg | USA | |
| long | 40485M001 | 242.0000 | 34.1100 | 74.2900 | Irwindale | USA | USGS |
| lpgs† | 41510M001 | 302.0700 | -34.9100 | 254.0000 | La Plata | Argentina | GFZ |
| lroc | 10023M001 | 358.7807 | 46.1589 | 57.9000 | LA ROCHELLE | FRANCE | CLDG |
| mac1† | 50135M001 | 158.9358 | -54.4995 | -6.6900 | MacQuarie Island | Southern Ocean | AUSLIG |
| mad2 | 13407S012 | 355.7503 | 40.4292 | 829.4583 | Robledo | Spain | NASA/JPL |
| madr† | 13407S012 | 355.7504 | 40.4291 | 829.4574 | Robledo | Spain | NASA/JPL |
| mag0† | 12354M001 | 150.7700 | 59.5758 | 361.9266 | Magadan | Russian Federation | RDAAC-IRIS |
| mald | 22901S001 | 73.5263 | 4.1887 | -92.0000 | Male Airport | Republic of Maldives | PGPSF |
| mali† | 33201M001 | 40.1944 | -2.9959 | 22.7200 | Malindi | Kenya | ESA |
| mana | 41201S001 | 273.7513 | 12.1491 | 170.0000 | Managua | Nicaragua | NGS/NOAA |
| manz | 40513S001 | 255.7019 | 19.0639 | -14.0000 | Manzanillo | Mexico | PGPSF |
| mas1† | 31303M002 | 344.3667 | 27.7637 | 197.3000 | Maspalomas | Spain | ESA |
| mat1‡ | 12734M009 | 16.7045 | 40.6491 | 534.5000 | MATERA | ITALY | ASI |
| mate† | 12734M008 | 16.7045 | 40.6491 | 535.6000 | MATERA | ITALY | ASI |
| math | 40474M001 | 242.5600 | 33.8600 | 396.8900 | Lake Mathews Reservoir | USA | SIO |
| maui | 40445S008 | 203.7430 | 20.7067 | 3062.0000 | Haleakala, Maui | USA | PGPSF |
| maw1† | 66004M001 | 62.8707 | -67.6048 | 59.1840 | Mawson | Antarctica | AUSLIG |
| mbar† | 33901M001 | 30.7377 | -0.6013 | 1327.0000 | Mbarara | Uganda | NASA/JPL/IRIS |
| mcm4† | 66001M003 | 166.6693 | -77.8383 | 97.9201 | Ross Island | Antarctica | NASA/JPL |
| mdo1† | 40442M012 | 255.9850 | 30.6805 | 2005.4936 | Fort Davis | USA | NASA/JPL |
| mdvo | 12309M002 | 37.2236 | 56.0275 | 220.0326 | Mendeleevo, Moscow | Russia | IMVP-DUT |
| medi | 12711M003 | 11.6468 | 44.5199 | 50.0000 | MEDICINA (BOLOGNA) | ITALY | ASI |
| mets† | 10503S011 | 24.6953 | 60.2175 | 94.5680 | Kirkkonummi | Finland | FGI |
| metz‡ | 10503M005 | 24.3953 | 60.2175 | 94.5000 | Kirkkonummi | Finland | FGI |
| mikl‡ | 12335M001 | 31.9728 | 46.9728 | 94.7000 | Mykolaiv | Ukraine | RIGC |
| mizu | 21702M002 | 141.1300 | 39.1400 | 75.6000 | Mizusawa | Japan | GFZ |
| mkea† | 40477M001 | 204.5437 | 19.8013 | 3754.7305 | Mauna Kea | USA | NASA/JPL |
| mobn | 12365M001 | 36.5695 | 55.1149 | 182.6340 | Obninsk | Russian Federation | RDAAC-JPL-IRIS |
| monp | 40497M004 | 243.5800 | 32.8900 | 1842.5600 | Laguna Mountains | USA | SIO |
| mr6g‡ | 10405M002 | 17.2585 | 60.5951 | 75.4400 | Maartsbo | Sweden | LMV |
| msku† | 32810M001 | 13.5520 | -1.6312 | 387.0000 | Franceville | Gabon | JPL/IRIS |
| mtbg‡ | 11030M001 | 16.4043 | 47.7379 | 294.0000 | Mattersburg | Austria | BEWAG |
| mtka‡ | 21741S002 | 139.5614 | 35.6795 | 109.0000 | Mitaka | Japan | ENRI |
| nano | 40138M001 | 235.9135 | 49.2948 | 6.0000 | Nanoose Bay | Canada | NRCan/GSC |
| nico | 14302M001 | 33.3964 | 35.1409 | 155.0000 | Nicosia | Cyprus | BKG |
| nklg† | 32809M002 | 9.6698 | 0.3523 | 31.3870 | Libreville | Gabon | CNES |
| nlib† | 40465M001 | 268.4251 | 41.7716 | 207.0648 | North Liberty | USA | NASA/JPL |
| nnor‡ | 50181M001 | 116.1927 | -31.0487 | 234.9840 | New Norcia | Australia | |
| not1† | 12717M004 | 14.9898 | 36.8761 | 126.2000 | NOTO | ITALY | ASI |
| noto | 12717M003 | 14.9898 | 36.8761 | 126.2000 | NOTO | ITALY | ASI |
| noum† | 92701M003 | 166.4102 | -22.2699 | 83.0790 | NOUMEA | FRANCE | DITTT |
| ... | ... | ... | ... | ... | ... | ... | ... |

Table F.1: IGS Stations(335) as of August, 2002. (continued)

| site Id | DOMES Number | Lon(W) (deg) | Lat(N) (deg) | Height (m) | Location | Country | Agency |
|---|---|---|---|---|---|---|---|
| npld | 13234M003 | 359.6604 | 51.4210 | 72.7185 | Teddington | United Kingdom | NPL |
| nrc1† | 40114M001 | 284.3762 | 45.4542 | 82.4755 | Ottawa | Canada | NRCan/GSD |
| nrc2 | 40114M001 | 284.3762 | 45.4542 | 82.4755 | OTTAWA | CANADA | NRCan/GSD |
| nril† | 12364M001 | 88.3598 | 69.3618 | 47.8937 | Norilsk | Russian Federation | RDAAC-JPL-IRIS |
| nssp | 12312M001 | 44.5031 | 40.2265 | 1167.0000 | Yerevan | Republic of Armenia | NASA/JPL |
| ntus | 22601M001 | 103.6799 | 1.3458 | 79.0000 | Singapore | Republic of Singapore | NTU |
| nvsk | 12319M001 | 83.2355 | 54.8406 | 123.6429 | Novosibirsk | Russia | IGF SB RAS(A10) |
| nya1† | 10317M003 | 11.8653 | 78.9296 | 84.0000 | Ny-Alesund | Norway | NMA |
| nyal† | 10317M001 | 11.8700 | 78.9300 | 82.0000 | Ny-Alesund | Norway | NMA |
| oat2 | 40478S101 | 241.4000 | 34.3300 | 1112.6000 | Santa Susana Mountains | USA | USGS |
| obe2 | 14208M003 | 11.3000 | 48.1000 | 651.0000 | Oberpfaffenhofen | Germany | GFZ |
| obet‡ | 14208M004 | 11.2776 | 48.0843 | 635.9000 | Wessling | Germany | DLR-KN-NL |
| ohi2† | 66008M005 | 302.0997 | -63.3207 | 30.6210 | O'Higgins | Antarctic Peninsula | IfAG |
| ohiz‡ | 66008M004 | 302.0997 | -63.3207 | 30.6000 | O'Higgins | Antarctic Peninsula | BKG |
| onsa† | 10402M004 | 11.9255 | 57.3953 | 46.5789 | ONSALA | SWEDEN | OSO |
| orid | 15601M001 | 20.7940 | 41.1274 | 773.0000 | Ohrid | Macedonia | BKG |
| os0g‡ | 10402M004 | 11.9255 | 57.3953 | 46.5789 | Onsala | Sweden | |
| osje | 11902M001 | 18.6805 | 45.5608 | 153.8500 | Osijek | Croatia | IfAG |
| ous2 | 50212M002 | 170.5100 | -45.6800 | 26.1900 | Dunedin | New Zealand | GFZ |
| pado | 12750S001 | 11.8961 | 40.1479 | 64.7000 | PADOVA | ITALY | UPAD |
| parc | 41716S001 | 289.1201 | -53.1370 | 22.0000 | Punta Arenas | Chile | PGPSF |
| pdel† | 31906M004 | 334.3372 | 37.7477 | 110.8000 | Ponta Delgada | PORTUGAL | IGP |
| penc | 11206M006 | 19.2815 | 47.7896 | 291.7900 | Penc | Hungary | FOMI |
| pert† | 50133M001 | 115.8852 | -31.8019 | 12.9200 | Perth | Australia | ESA |
| petp† | 12355M002 | 158.6070 | 53.0667 | 211.0343 | Petropavlovsk-Kamchatka | Russian Federation | RDAAC-IRIS |
| pie1† | 40456M001 | 251.8811 | 34.3015 | 2347.7250 | Pie Town | USA | NASA/JPL |
| pimo† | 22003M001 | 121.0777 | 14.6357 | 95.4934 | Quezon City | Phillipines | NASA/JPL |
| pin1 | 40407M003 | 243.5400 | 33.6100 | 1256.2100 | Pinyon Flat | USA | SIO |
| pol2† | 12348M001 | 74.6943 | 42.6798 | 1714.2000 | Bishkek | Kyrghyzstan | UNAVCO-JPL |
| polv | 12336M001 | 34.5429 | 49.6026 | 178.1000 | Poltava | Ukraine | RIGK |
| pots† | 14106M003 | 13.0700 | 52.3800 | 174.0000 | Potsdam | Germany | GFZ |
| prds | 40124M001 | 245.7065 | 50.8713 | 1247.9400 | Calgary | Canada | NRCan/GSD |
| ptbb | 14234M001 | 10.4597 | 52.2962 | 130.2000 | Braunschweig | Germany | BKG |
| pvep | 40403M002 | 241.6000 | 33.7400 | 69.3900 | Palos Verdes | USA | USGS |
| qaq1 | 43007M001 | 313.9522 | 60.7152 | 110.3900 | Qaqortoq / Julianehaab | Denmark | NSC |
| quin | 40433M004 | 239.0556 | 39.9746 | 1105.7868 | Quincy | USA | NASA/JPL |
| rabt† | 35001M002 | 353.1450 | 33.9800 | 80.8000 | Rabat | Morocco | NASA/JPL |
| ramo | 20703S001 | 34.7631 | 30.5978 | 893.1000 | Mitzpe Ramon | Israel | SOI |
| rbay | 30315M001 | 32.0784 | -28.7956 | 34.2310 | Richardsbay | South Africa | HRAO-JPL |
| reso† | 40149M001 | 265.1067 | 74.6908 | 34.9000 | Resolute,Cornwallis Island | Canada | NRCan/GSD |
| reyk† | 10202M001 | 338.0445 | 64.1388 | 93.0950 | Reykjavik | Iceland | IfAG |
| reyz‡ | 10202M003 | 338.0445 | 64.1388 | 93.0000 | Reykjavik | Iceland | BKG |
| riog† | 41507M004 | 292.2500 | -53.7900 | 32.0000 | Rio Grande | Argentina | GFZ |
| riop | 42006M001 | 281.3480 | -1.6510 | 2816.0820 | Riobamba | Ecuador | NASA/JPL |
| roch | 40486M001 | 243.3900 | 33.6100 | 1393.7300 | Pinemeadow | USA | SIO |
| rock | 40478M002 | 241.3200 | 34.2400 | 553.3900 | Simi Valley | USA | USGS |
| sant† | 41705M003 | 289.3314 | -33.1503 | 723.0399 | Santiago | Chile | NASA/JPL |
| sch2† | 40133M002 | 293.1674 | 54.8321 | 498.1800 | Schefferville | Canada | NRCan/GSD |
| scip | 49915M001 | 241.5100 | 32.9100 | 452.8600 | San Clemente Island | USA | SIO |
| scub† | 40701M001 | 284.2377 | 20.0121 | 21.9500 | Santiago de Cuba | Cuba | GFZ |
| sele† | 12352M001 | 77.0168 | 43.1791 | 1340.0000 | Almaty | Kazakstan | IVTAN |
| sey1† | 39801M001 | 55.4794 | -4.6737 | 538.2248 | La Misere | Seychelles | JPL-IRIS/IDA |
| sfdm | 49826M001 | 241.2500 | 34.4600 | 291.5000 | Piru | USA | USGS |
| sfer | 13402M004 | 353.7944 | 36.4643 | 85.8300 | San Fernando (Cadiz) | Spain | ROA |
| shao† | 21605M002 | 121.2004 | 31.0996 | 22.0933 | Sheshan | China | CAS-JPL |
| simo | 30307M001 | 18.4395 | -34.1879 | 34.8510 | Simonstown | South Africa | HRAO/JPL/UNV |
| sio3 | 40460M004 | 242.7500 | 32.8600 | 34.9100 | La Jolla | USA | SIO |
| slor | 41102S001 | 272.5639 | 13.4241 | 41.0000 | San Lorenzo | Honduras | NOAA |
| sni1 | 49909S001 | 240.4800 | 33.2500 | 239.6900 | San Nicolas Island | USA | USGS |
| sofi | 11101M002 | 23.3947 | 42.5561 | 1119.6000 | Sofia | Bulgaria | BKG |
| sol1 | 49907S001 | 283.5460 | 38.3180 | -18.0699 | Solomons Island | U.S.A. | NOAA |
| spk1 | 40458M001 | 241.3500 | 34.0600 | 440.1300 | Saddle Peak | USA | USGS |
| spt0 | 10425M001 | 12.8913 | 57.7150 | 219.9190 | Boras | Sweden | OSO |
| ssia | 41401S001 | 270.8838 | 13.6973 | 664.4000 | San Salvador | El Salvador | NOAA |
| stjo† | 40101M001 | 307.1889 | 47.5952 | 153.9000 | St. John's | Canada | NRCan/GSD |
| str1 | 50119M002 | 149.0101 | -35.3155 | 799.9640 | Canberra | Australia | AUSLIG |
| str2‡ | 50119M001 | 149.0169 | -35.5319 | 799.9540 | Canberra | Australia | GA |
| sulp | 12366M001 | 24.0145 | 49.8356 | 370.5000 | Lviv | Ukraine | NULP |
| sunm‡ | 50143M001 | 153.0352 | -27.4849 | 92.0000 | BRISBANE | AUSTRALIA | NR&M |
| suth† | 30314M002 | 20.8105 | -32.3802 | 1799.7960 | Sutherland | South Africa | HRAO-JPL |
| ... | ... | ... | ... | ... | ... | ... | ... |

Table F.1: IGS Stations(335) as of August, 2002. (continued)

| site Id | DOMES Number | Lon(W) (deg) | Lat(N) (deg) | Height (m) | Location | Country | Agency |
|---|---|---|---|---|---|---|---|
| sutm | 30314M004 | 20.8100 | -32.2100 | 1797.6008 | Sutherland | South Africa | GFZ |
| suva | 50801S001 | 178.4252 | -18.1459 | 73.0000 | Suva | Fiji | PGPSF |
| suwn† | 23903M001 | 127.0542 | 37.2755 | 83.9322 | Suwon-shi | Korea | NGI |
| syog† | 66006S002 | 39.5837 | -69.0070 | 50.0902 | East Ongle Island | Antarctica | GSI |
| tabl | 49901M001 | 242.3200 | 34.3800 | 2228.0200 | Wrightwood | USA | USGS |
| tcms‡ | 23604S002 | 120.9874 | 24.7980 | 77.2000 | Hsinchu | Republic of China | NML |
| tegu | 41101S001 | 272.8000 | 14.1000 | 995.0000 | Tegucigalpa | Honduras | NGS/NOAA |
| tgcv | 39601S001 | 337.0172 | 16.7548 | 35.0000 | Palmeira | Republic of Cape Verde | PGPSF |
| thti† | 92201M009 | 210.3937 | -17.5769 | 98.0400 | Papeete | Tahiti, French Polynesia | CNES |
| thu1† | 43001M001 | 291.2120 | 76.5373 | 55.0030 | Thule | Greenland | KMS-JPL |
| thu3 | 43001M002 | 291.1750 | 76.5370 | 36.1000 | THULE AIRBASE | DENMARK | NSC |
| tid1 | 50103M108 | 148.9800 | -35.3992 | 665.3627 | (Near) Canberra | Australia | AUSLIG |
| tid2† | 50103M108 | 148.9800 | -35.3992 | 665.3627 | Tidbinbilla | Australia | NASA/JPL |
| tidb† | 50103M108 | 148.9800 | -35.3992 | 665.3818 | Tidbinbilla | Australia | NASA/JPL |
| titz‡ | 14278M001 | 6.4316 | 51.0353 | 155.6000 | Titz | Germany | BKG |
| tixi† | 12360M001 | 128.8664 | 71.6345 | 46.9847 | Tixi | Russian Federation | RDAAC-IRIS |
| tlse | 10003M009 | 1.4808 | 43.5607 | 211.6000 | Toulouse | France | CNES |
| tnml‡ | 23604S001 | 120.9873 | 24.7980 | 77.4553 | Hsinchu | Republic of China | NML |
| torp | 49912M001 | 241.6700 | 33.8000 | -5.2000 | Torrance | USA | USGS |
| tow2† | 50140M001 | 147.0557 | -19.2693 | 87.3860 | Cape Ferguson | Australia | GA |
| trab | 20808M001 | 39.7756 | 40.9947 | 99.2000 | Trabzon | Turkey | BKG |
| trak | 40480M001 | 242.2000 | 33.6200 | 115.5600 | Irvine | USA | SIO |
| tro1† | 10302M006 | 18.9396 | 69.6627 | 138.0000 | Tromsoe | Norway | NMA |
| trom | 10302M003 | 18.9383 | 69.6639 | 132.0000 | Tromsoe | Norway | NMA |
| tskb† | 21730S005 | 140.0874 | 36.1057 | 67.3000 | Tsukuba | Japan | GSI |
| tubi | 20806M001 | 29.4507 | 40.7867 | 221.8310 | Gebze | TURKEY | TUBITAK |
| twtf† | 23603S002 | 121.1645 | 24.9536 | 203.1220 | Taoyuan | Republic of China | NSTFL |
| uclp | 40487M002 | 241.5600 | 34.0700 | 111.5600 | Los Angeles | USA | USGS |
| uclu | 40140M001 | 234.4584 | 48.9256 | 10.0000 | Uclulet | Canada | NRCan/GSC |
| ulab | 24201M001 | 107.0500 | 47.6700 | 1611.7000 | Ulaanbataar | Mongolia | GFZ |
| unb1 | 40146S001 | 293.6170 | 45.5700 | 22.8100 | Fredericton | Canada | GGE-UNB |
| unsa† | 41514M001 | 294.5924 | -24.7275 | 1257.8000 | Salta | Argentina | GFZ |
| urum† | 21612M001 | 87.6300 | 43.5900 | 856.1000 | Urumqi | China | GFZ |
| usc1 | 40487M001 | 241.7100 | 34.0200 | 21.9400 | Los Angeles | USA | USGS |
| usn1 | 40451S006 | 282.9337 | 38.9205 | 57.4050 | Washington | U.S.A. | USNO |
| usna | 49908S001 | 283.5200 | 38.9830 | -26.3083 | Annapolis | U.S.A. | NOAA |
| usno† | 40451S003 | 282.9338 | 38.9190 | 48.8780 | Washington | U.S.A. | USNO/NOAA |
| usud† | 21729S007 | 138.3620 | 36.1331 | 1508.6328 | Usuda | Japan | NASA/JPL |
| uzhl | 12301M001 | 22.2976 | 48.6320 | 232.0000 | Uzhgorod | Ukraine | MAO |
| valp | 41712S001 | 288.3739 | -33.0272 | 31.0000 | Valparaiso | Chile | PGPSF |
| vene | 12741M001 | 12.3319 | 45.4369 | 67.1000 | VENEZIA | ITALY | ASI |
| vesl | 66009M001 | 357.1583 | -71.6738 | 862.4000 | Sanae IV | Antarctica | AWI |
| vill† | 13406M001 | 356.0480 | 40.4436 | 647.5000 | Villafranca | Spain | ESA |
| vndp | 40420M007 | 239.3800 | 34.5600 | -11.5200 | Vandenberg Air Force Base | USA | USGS |
| vs0g‡ | 10423M001 | 18.3673 | 57.6539 | 79.7660 | Visby | Sweden | LMV |
| wes2† | 40440S020 | 288.5060 | 42.6130 | 86.0170 | Westford | U.S.A. | NOAA |
| whc1 | 40461M001 | 241.9700 | 33.9800 | 94.2900 | Whittier | USA | USGS |
| whit† | 40136M001 | 224.7779 | 60.7505 | 1427.0000 | WHITEHORSE | CANADA | NRCan/GSC |
| widc | 49917M001 | 243.6100 | 33.9300 | 445.0200 | Sky Valley | USA | SIO |
| will | 40134M001 | 237.8322 | 52.2369 | 1096.0000 | Williams Lake | Canada | NRCan/GSC |
| wlsn | 40400M101 | 241.9400 | 34.2300 | 1705.2700 | Mt. Wilson | USA | USGS |
| wroc‡ | 12217M001 | 17.0619 | 51.1131 | 181.0000 | WROCLAW | POLAND | AUW DG&P |
| wslr | 40141M001 | 237.0788 | 50.1265 | 909.0000 | Whistler | Canada | NRCan/GSC |
| wsrt† | 13506M005 | 6.6045 | 52.9146 | 86.0000 | Westerbork | The Netherlands | DEOS |
| wtza | 14201M013 | 12.8789 | 49.1442 | 666.0000 | Koetzting | Germany | BKG |
| wtzj‡ | 14201M012 | 12.8789 | 49.1442 | 666.0000 | Koetzting | Germany | BKG |
| wtzr† | 14201M010 | 12.8789 | 49.1442 | 666.0000 | Koetzting | Germany | BKG |
| wtzt | 14201M011 | 12.8789 | 49.1442 | 666.0000 | Koetzting | Germany | BKG |
| wtzz | 14201M014 | 12.8789 | 49.1442 | 666.0000 | Koetzting | Germany | BKG |
| wuhn† | 21602M001 | 114.3573 | 30.5317 | 93.4000 | Wuhan City | P.R. China | WTUS |
| xian | 21614M001 | 109.2215 | 34.3687 | 81.5686 | Lintong | P.R.C. | CAS-JPL |
| yakt | 12353M002 | 129.6803 | 62.0310 | 103.3700 | Yakutsk | Russian Federation | RDAAC-IRIS |
| yakz | 12353M001 | 129.6810 | 62.0310 | 100.0644 | Yakutsk | Russian Federation | RDAAC-IRIS |
| yar1 | 50107M004 | 115.3470 | -29.0466 | 241.2967 | Mingenew | Australia | NASA/JPL |
| yar2 | 50107M004 | 115.3470 | -29.0466 | 241.2967 | Dongara | Australia | AUSLIG |
| yarr‡ | 50107M006 | 115.5860 | -29.0850 | 241.3820 | Dongara | Australia | GA |
| yebe | 13420M001 | 356.9114 | 40.5249 | 973.0000 | Yebes | Spain | IGN-E |
| yell† | 40127M003 | 245.5193 | 62.4809 | 181.0000 | Yellowknife | Canada | NRCan/GSD |
| ykro | 32601M001 | 354.7599 | 6.8706 | 270.4983 | Yamoussoukro | Cote d'Ivorie | NASA/JPL |
| yssk† | 12329M003 | 142.7167 | 47.0297 | 91.2887 | Yuzhno-Sakhalinsk | Russian Federation | RDAAC-IRIS |
| ... | ... | ... | ... | ... | ... | ... | ... |

Table F.1: IGS Stations(335) as of August, 2002. (continued)

| site Id | DOMES Number | Lon(W) (deg) | Lat(N) (deg) | Height (m) | Location | Country | Agency |
|---|---|---|---|---|---|---|---|
| zamb‡ | 34601M001 | 28.3110 | -15.3272 | 1321.0960 | Lusaka | Zambia | |
| zeck† | 12351M001 | 41.5651 | 43.2884 | 1166.8000 | Zelenchukskaya | Russia | BKG |
| zimj‡ | 14001M006 | 7.4651 | 46.8771 | 954.3000 | Zimmerwald | Switzerland | AIUB |
| zimm† | 14001M004 | 7.4653 | 46.8771 | 956.7000 | Zimmerwald | Switzerland | AIUB |
| zimz‡ | 14001M005 | 7.4651 | 46.8771 | 953.9000 | Zimmerwald | Switzerland | swisstopo |
| zwen† | 12330M001 | 36.7600 | 55.7000 | 270.0000 | Zwenigorod | Russia | GFZ |

† Designates a Global Station.
‡ Designates an site newer than 6 months to the IGS.

Table F.2: IGS ITRF Stations(52) as of August, 2002

| site Id | DOMES Number | Lon(W) (deg) | Lat(N) (deg) | Height (m) | Location | Country | Agency |
|---|---|---|---|---|---|---|---|
| algo | 40104M002 | 281.9286 | 45.9588 | 202.0000 | Algonquin Park | Canada | NRCan/GSD |
| asc1 | 30602M001 | 345.5880 | -7.9512 | 105.1508 | Ascension Island | Ascension Island | NASA/JPL |
| auck | 50209M001 | 174.8344 | -36.6028 | 132.0000 | Whangaparaoa Peninsula | New Zealand | IGNS-JPL |
| bahr | 24901M002 | 50.6081 | 26.2091 | -17.0300 | Manama | Bahrain | NIMA |
| brmu | 42501S004 | 295.3030 | 32.3700 | -10.6190 | Bermuda | U.K. | NOAA |
| cas1 | 66011M001 | 110.5197 | -66.2834 | 22.5500 | Casey | Antarctica | AUSLIG |
| cedu | 50138M001 | 133.8098 | -31.8667 | 144.8021 | Ceduna | Australia | AUSLIG |
| chat | 50207M001 | 183.4342 | -43.9558 | 58.0000 | Waitangi | New Zealand | IGNS-JPL |
| dav1 | 66010M001 | 77.9726 | -68.5773 | 44.5000 | Davis | Antarctica | AUSLIG |
| dgar† | 30802M001 | 72.3702 | -7.2696 | -64.8965 | Diego Garcia Island | U.K. Territory | NASA/JPL |
| drao | 40105M002 | 240.3750 | 49.3226 | 542.0000 | Penticton | Canada | NRCan/GSC |
| fair | 40408M001 | 212.5008 | 64.9780 | 319.0097 | Fairbanks | USA | JPL-GSFC |
| fort† | 41602M001 | 321.5744 | -3.8774 | 20.4918 | Eusebio, Fortaleza | Brazil | NOAA |
| gode | 40451M123 | 283.1732 | 39.0217 | 14.5082 | Greenbelt | USA | NASA/JPL |
| gol2† | 40405S031 | 243.1108 | 35.4252 | 986.6759 | Goldstone | USA | NASA/JPL |
| graz | 11001M002 | 15.4935 | 47.0671 | 538.2900 | Graz | Austria | ISR |
| guam | 50501M002 | 144.8683 | 13.5893 | 201.9220 | Dededo | Guam | NASA/JPL |
| hob2 | 50116M004 | 147.4387 | -42.8047 | 41.1263 | Hobart | Australia | AUSLIG |
| irkt | 12313M001 | 104.3162 | 52.2190 | 503.3816 | Irkutsk | Russia | DUT |
| kerg | 91201M002 | 70.2555 | -49.3515 | 74.0583 | Port aux Francais | Kerguelen Islands | CNES |
| kit3† | 12334M001 | 66.8800 | 39.1400 | 643.0000 | Kitab | Uzbekistan | GFZ |
| kokb | 40424M004 | 200.3351 | 22.1263 | 1167.3680 | Kokee Park, Waimea, | USA | NASA/JPL |
| kour | 97301M210 | 307.1940 | 5.2522 | -25.5700 | Kourou | French Guyana | ESA |
| kwj1 | 50506M001 | 167.7302 | 8.7222 | 38.2688 | Kwajalein Atoll | Marshall Islands | NASA/JPL |
| lhas | 21613M001 | 91.1040 | 29.6573 | 3622.0000 | LHASA | China | BKG |
| lpgs | 41510M001 | 302.0700 | -34.9100 | 254.0000 | La Plata | Argentina | GFZ |
| mac1 | 50135M001 | 158.9358 | -54.4995 | -6.6900 | MacQuarie Island | Southern Ocean | AUSLIG |
| mali | 33201M001 | 40.1944 | -2.9959 | 22.7200 | Malindi | Kenya | ESA |
| mas1 | 31303M002 | 344.3667 | 27.7637 | 197.3000 | Maspalomas | Spain | ESA |
| mate | 12734M008 | 16.7045 | 40.6491 | 535.6000 | MATERA | ITALY | ASI |
| mcm4 | 66001M003 | 166.6693 | -77.8383 | 97.9201 | Ross Island | Antarctica | NASA/JPL |
| mdo1 | 40442M012 | 255.9850 | 30.6805 | 2005.4936 | Fort Davis | USA | NASA/JPL |
| nlib | 40465M001 | 268.4251 | 41.7716 | 207.0648 | North Liberty | USA | NASA/JPL |
| nyal | 10317M001 | 11.8700 | 78.9300 | 82.0000 | Ny-Alesund | Norway | NMA |
| onsa | 10402M004 | 11.9255 | 57.3953 | 46.5789 | ONSALA | SWEDEN | OSO |
| pert | 50133M001 | 115.8852 | -31.8019 | 12.9200 | Perth | Australia | ESA |
| pie1 | 40456M001 | 251.8811 | 34.3015 | 2347.7250 | Pie Town | USA | NASA/JPL |
| pots | 14106M003 | 13.0700 | 52.3800 | 174.0000 | Potsdam | Germany | GFZ |
| riog | 41507M004 | 292.2500 | -53.7900 | 32.0000 | Rio Grande | Argentina | GFZ |
| sant | 41705M003 | 289.3314 | -33.1503 | 723.0399 | Santiago | Chile | NASA/JPL |
| shao | 21605M002 | 121.2004 | 31.0996 | 22.0933 | Sheshan | China | CAS-JPL |
| thu1 | 43001M001 | 291.2120 | 76.5373 | 55.0030 | Thule | Greenland | KMS-JPL |
| tidb | 50103M108 | 148.9800 | -35.3992 | 665.3818 | Tidbinbilla | Australia | NASA/JPL |
| trom† | 10302M003 | 18.9383 | 69.6639 | 132.0000 | Tromsoe | Norway | NMA |
| tskb | 21730S005 | 140.0874 | 36.1057 | 67.3000 | Tsukuba | Japan | GSI |
| vill | 13406M001 | 356.0480 | 40.4436 | 647.5000 | Villafranca | Spain | ESA |
| wes2 | 40440S020 | 288.5060 | 42.6130 | 86.0170 | Westford | U.S.A. | NOAA |
| wsrt | 13506M005 | 6.6045 | 52.9146 | 86.0000 | Westerbork | The Netherlands | DEOS |
| wtzr | 14201M010 | 12.8789 | 49.1442 | 666.0000 | Koetzting | Germany | BKG |
| yar1† | 50107M004 | 115.3470 | -29.0466 | 241.2967 | Mingenew | Australia | NASA/JPL |
| yell | 40127M003 | 245.5193 | 62.4809 | 181.0000 | Yellowknife | Canada | NRCan/GSD |
| zwen | 12330M001 | 36.7600 | 55.7000 | 270.0000 | Zwenigorod | Russia | GFZ |

† : not a Global Station.

Table F.3: MSODP implemented Stations(208) for the Optimal Set Study

| site ID | DOMES | X[m] | Y[m] | Z[m] |
|---|---|---|---|---|
| albh | 40129 | -2341332.886 | -3539049.513 | 4745791.371 |
| algo† | 40104 | 918129.499 | -4346071.239 | 4561977.824 |
| alic | 50137 | -4052051.830 | 4212836.100 | -2545105.836 |
| amc2 | 40472 | -1248596.070 | -4819428.229 | 3976506.042 |
| ankr | 20805 | 4121948.594 | 2652187.938 | 4069023.685 |
| aoal | 40483 | -2547879.914 | -4628773.880 | 3561049.917 |
| aoml | 49914 | 982296.803 | -5664607.228 | 2752614.479 |
| areq | 42202 | 1942826.728 | -5804070.256 | -1796893.968 |
| artu | 12362 | 1843956.907 | 3016203.039 | 5291261.706 |
| ascl† | 30602 | 6118526.077 | -1572344.698 | -876451.166 |
| auck† | 50209 | -5105681.003 | 461564.048 | -3782181.752 |
| azu1 | 49911 | -2472979.158 | -4671338.256 | 3558107.694 |
| bahr† | 24901 | 3633909.050 | 4425275.467 | 2799861.271 |
| bako | 23101 | -1836968.965 | 6065617.193 | -716257.776 |
| barb | 43401 | 3143384.507 | -5359714.632 | 1434871.503 |
| bili | 12363 | -2321892.971 | 560096.878 | 5894691.764 |
| bjfs | 21601 | -2148743.784 | 4426641.236 | 4044655.935 |
| blyt | 40479 | -2223206.565 | -4830299.786 | 3510587.672 |
| bogt | 41901 | 1744399.096 | -6116037.813 | 512731.625 |
| bor1 | 12205 | 3738358.598 | 1148173.582 | 5021815.705 |
| bran | 80028 | -2502254.466 | -4651654.382 | 3563569.196 |
| braz | 41606 | 4115014.087 | -4550641.532 | -1741444.061 |
| brmu† | 42501 | 2304703.582 | -4874817.178 | 3395186.895 |
| brus | 13101 | 4027893.852 | 307045.689 | 4919475.037 |
| bucu | 11401 | 4093760.981 | 2007793.635 | 4445129.877 |
| bzrg | 12751 | 4312657.614 | 864634.517 | 4603844.341 |
| cagl | 12725 | 4893378.933 | 772649.625 | 4004182.063 |
| casl† | 66011 | -901776.162 | 2409383.419 | -5816748.420 |
| casa | 40437 | -2444430.296 | -4428687.799 | 3875747.438 |
| cat1 | 40488 | -2540621.963 | -4682555.618 | 3495319.216 |
| cedu† | 50138 | -3753472.231 | 3912740.984 | -3347960.860 |
| chat† | 50207 | -4590670.912 | -275482.993 | -4404596.777 |
| chil | 40484 | -2478003.030 | -4655349.280 | 3577932.197 |
| chur | 40128 | -236438.708 | -3307616.791 | 5430049.174 |
| chwk | 40142 | -2215259.730 | -3543996.846 | 4802098.800 |
| cic1 | 40508 | -2433176.853 | -4845045.125 | 3348295.738 |
| cit1 | 80027 | -2491489.941 | -4660803.503 | 3559128.869 |
| clar | 49906 | -2458218.162 | -4680467.713 | 3556758.387 |
| cmp9 | 49905 | -2508505.849 | -4637175.117 | 3579499.854 |
| coco | 50127 | -741950.006 | 6190961.630 | -1337768.586 |
| cord | 41511 | 2345503.864 | -4910842.804 | -3316365.439 |
| coso | 40469 | -2411148.241 | -4571430.495 | 3727461.547 |
| crfp | 40481 | -2410446.534 | -4710490.586 | 3550422.388 |
| cro1 | 43201 | 2607771.157 | -5488076.781 | 1932767.685 |
| csn1 | 49910 | -2520225.756 | -4637082.562 | 3569875.398 |
| daej | 23902 | -3120041.778 | 4084614.970 | 3764027.006 |
| darw | 50134 | -4091358.781 | 4684606.724 | -1408580.460 |
| dav1† | 80043 | 486854.548 | 2285099.302 | -5914955.683 |
| dgar† | 30802 | 1916269.771 | 6029977.317 | -801720.175 |
| dhlg | 49904 | -2319099.063 | -4799846.543 | 3490090.466 |
| drag | 20710 | 4432980.874 | 3149431.992 | 3322110.339 |
| drao† | 40105 | -2059164.684 | -3621108.394 | 4814432.379 |
| dubo | 40137 | -417603.554 | -4064529.811 | 4881432.198 |
| ebre | 13410 | 4833520.246 | 41536.947 | 4147461.448 |
| eisl | 41703 | -1884951.760 | -5357595.877 | -2892890.504 |
| fair† | 40408 | -2281621.431 | -1453595.793 | 5756961.909 |
| flin | 40135 | -766174.416 | -3611375.303 | 5184056.250 |
| fort† | 41602 | 4985386.627 | -3954998.587 | -428426.482 |
| gala | 42005 | -33796.116 | -6377522.655 | -82120.899 |
| geno | 12712 | 4507892.447 | 707621.329 | 4441603.426 |
| glsv | 12356 | 3512889.114 | 2068979.763 | 4888903.141 |
| gode† | 80032 | 1130773.867 | -4831253.583 | 3994200.409 |
| gold | 40405 | -2353614.181 | -4641385.388 | 3676976.454 |
| gope | 11502 | 3979316.259 | 1050312.340 | 4857067.020 |
| goug | 30608 | 4795578.541 | -835299.537 | -4107634.065 |
| gras | 10002 | 4581691.012 | 556114.680 | 4389360.696 |
| graz† | 11001 | 4194423.960 | 1162702.549 | 4647245.328 |
| guam† | 50501 | -5071312.800 | 3568363.492 | 1488904.316 |
| harv | 80030 | -2686069.302 | -4527084.330 | 3589502.308 |
| ... | ... | ... | ... | ... |

Table F.3: MSODP implemented Stations(208) for the Optimal Set Study. (continued)

| site ID | DOMES | X[m] | Y[m] | Z[m] |
|---|---|---|---|---|
| hers | 13212 | 4033470.217 | 23672.770 | 4924301.233 |
| hflk | 11006 | 4248505.175 | 855575.595 | 4667172.195 |
| hnpt | 49913 | 1196626.466 | -4846358.507 | 3956723.098 |
| hob2† | 50116 | -3950071.361 | 2522415.185 | -4311638.362 |
| hofn | 10204 | 2679690.006 | -727951.336 | 5722789.146 |
| holb | 40130 | -2503040.416 | -3188233.336 | 4908701.563 |
| holc | 40404 | -2459517.947 | -4655992.282 | 3589168.804 |
| holp | 49903 | -2500945.815 | -4670473.245 | 3539500.425 |
| hrao | 30302 | 5085352.489 | 2668395.670 | -2768731.676 |
| iisc | 22306 | 1337936.813 | 6070317.106 | 1427876.516 |
| ineg | 40507 | -1260435.744 | -5788547.698 | 2360340.250 |
| irkt† | 12313 | -968332.190 | 3794425.411 | 5018167.758 |
| jab1 | 50136 | -4236442.824 | 4559929.623 | -1388624.653 |
| jama | 42601 | 1388059.738 | -5909149.083 | 1951963.837 |
| joze | 12204 | 3664940.315 | 1409153.741 | 5009571.323 |
| jplm | 40400 | -2493304.198 | -4655215.451 | 3565497.383 |
| karr | 50139 | -2713832.258 | 5303935.087 | -2269515.012 |
| kely | 43005 | 1575559.280 | -1941827.932 | 5848076.502 |
| kerg† | 91201 | 1406337.336 | 3918161.100 | -4816167.355 |
| kiru | 10403 | 2251420.923 | 862817.135 | 5885476.614 |
| kit3† | 12334 | 1944945.356 | 4556652.193 | 4004325.976 |
| kokb† | 40424 | -5543838.118 | -2054587.260 | 2387809.705 |
| kosg | 13504 | 3899225.245 | 396731.809 | 5015078.351 |
| kour† | 97301 | 3839591.421 | -5059567.553 | 579956.935 |
| kr0g | 10422 | 2248123.320 | 865686.592 | 5886425.686 |
| kstu | 12349 | -174281.721 | 3571333.012 | 5264196.061 |
| kunm | 21609 | -1281255.473 | 5640746.079 | 2682880.117 |
| kwj1† | 50506 | -6160881.013 | 1339882.959 | 960810.459 |
| lama | 12209 | 3524523.073 | 1329693.519 | 5129846.289 |
| lbch | 40482 | -2507798.449 | -4676370.054 | 3526890.666 |
| leep | 49902 | -2507463.082 | -4652632.264 | 3559086.685 |
| lhas† | 21613 | -106937.669 | 5549269.591 | 3139215.762 |
| long | 40485 | -2482077.362 | -4667439.251 | 3556771.594 |
| lpgs† | 41510 | 2780102.969 | -4437418.863 | -3629404.583 |
| mac1† | 50135 | -3464038.501 | 1334172.763 | -5169224.323 |
| madr | 13407 | 4849202.462 | -360329.081 | 4114913.083 |
| mag0 | 12354 | -2825810.143 | 1581232.927 | 5477005.540 |
| mali† | 33201 | 4865366.477 | 4110737.432 | -331121.706 |
| mas1† | 31303 | 5439192.252 | -1522055.633 | 2953454.722 |
| mate† | 12734 | 4641949.707 | 1393045.271 | 4133287.343 |
| math | 40474 | -2443215.352 | -4706037.477 | 3533477.600 |
| mawl | 66004 | 1111287.166 | 2168911.279 | -5874493.595 |
| mcm4† | 66001 | -1311703.250 | 310815.104 | -6213255.125 |
| mdo1† | 40442 | -1329998.678 | -5328393.387 | 3236504.199 |
| mdvo | 12309 | 2844672.267 | 2161070.079 | 5266363.806 |
| medi | 12711 | 4461400.895 | 919593.423 | 4449504.682 |
| mets | 80005 | 2892570.923 | 1311843.330 | 5512634.057 |
| mkea | 40477 | -5464105.097 | -2495166.895 | 2148290.939 |
| monp | 40497 | -2386246.845 | -4802359.598 | 3444902.121 |
| mr6g | 10405 | 2998189.527 | 931451.662 | 5533398.581 |
| nano | 40138 | -2335726.738 | -3451608.345 | 4812009.996 |
| nico | 14302 | 4359415.849 | 2874116.974 | 3650777.712 |
| nklg | 32809 | 6287385.842 | 1071574.385 | 39132.745 |
| nlib† | 40465 | -130934.482 | -4762291.737 | 4226854.669 |
| noto | 12717 | 4934528.655 | 1321262.222 | 3806479.519 |
| noum | 92701 | -5739971.535 | 1387563.663 | -2402123.551 |
| nrc1 | 40114 | 1112777.321 | -4341475.826 | 4522955.775 |
| nssp | 12312 | 3478646.842 | 3418805.729 | 4097987.116 |
| ntus | 22601 | -1508022.690 | 6195576.699 | 148799.482 |
| nya1 | 80003 | 1202433.960 | 252632.229 | 6237772.513 |
| nyal† | 10317 | 1202430.643 | 252626.646 | 6237767.533 |
| oat2 | 80033 | -2524553.534 | -4630094.340 | 3577352.088 |
| onsa† | 10402 | 3370658.663 | 711877.023 | 5349786.877 |
| penc | 11206 | 4052449.626 | 1417680.986 | 4701407.038 |
| pert† | 50133 | -2368686.968 | 4881316.517 | -3341796.161 |
| petp | 12355 | -3576239.756 | 1401003.444 | 5075177.505 |
| piel† | 40456 | -1640916.793 | -5014781.204 | 3575447.142 |
| pimo | 22003 | -3186294.170 | 5286624.093 | 1601158.176 |
| pol2 | 12348 | 1239971.586 | 4530790.055 | 4302578.777 |
| pots† | 14106 | 3800689.768 | 882077.259 | 5028791.246 |
| ... | ... | ... | ... | ... |

Table F.3: MSODP implemented Stations(208) for the Optimal Set Study. (continued)

| site ID | DOMES | X[m] | Y[m] | Z[m] |
|---|---|---|---|---|
| prds | 40124 | -1659602.844 | -3676725.756 | 4925493.611 |
| pvep | 40403 | -2525523.162 | -4670030.707 | 3522843.104 |
| quin | 40433 | -2517231.003 | -4198595.164 | 4076531.251 |
| ramo | 20703 | 4514722.017 | 3133507.725 | 3228024.574 |
| reyk | 10202 | 2587384.489 | -1043033.504 | 5716563.979 |
| riog† | 41507 | 1429907.727 | -3495354.740 | -5122698.672 |
| riop | 42006 | 1255144.990 | -6253609.537 | -182569.867 |
| roch | 40486 | -2382183.274 | -4755085.074 | 3511367.707 |
| rock | 40478 | -2533219.884 | -4631543.705 | 3568400.368 |
| sant† | 41705 | 1769693.337 | -5044574.148 | -3468321.048 |
| sch2 | 40133 | 1448636.903 | -3385243.649 | 5191046.936 |
| scip | 49915 | -2556587.402 | -4711014.066 | 3446241.381 |
| sele | 12352 | 1046790.836 | 4540257.051 | 4342920.758 |
| sey1 | 39801 | 3602870.766 | 5238174.329 | -516275.514 |
| sfer | 13402 | 5105519.055 | -555146.005 | 3769803.246 |
| shao† | 21605 | -2831733.268 | 4675666.039 | 3275369.521 |
| sio3 | 40460 | -2455456.521 | -4767480.705 | 3441383.654 |
| sni1 | 49909 | -2631346.566 | -4646278.982 | 3477113.259 |
| sofi | 11101 | 4319372.228 | 1868687.631 | 4292063.865 |
| sol1 | 49907 | 1173608.863 | -4871160.862 | 3933263.105 |
| spk1 | 40458 | -2535991.605 | -4642435.287 | 3552148.093 |
| stjo | 40101 | 2612631.229 | -3426807.026 | 4686757.805 |
| suth | 30314 | 5041274.808 | 1916053.992 | -3397076.074 |
| suwn | 23903 | -3062022.653 | 4055448.089 | 3841818.340 |
| syog | 66006 | 1766207.841 | 1460290.350 | -5932297.680 |
| tabl | 49901 | -2448549.823 | -4668099.290 | 3582740.937 |
| thti | 92201 | -5246415.202 | -3077260.424 | -1913842.475 |
| thu1† | 43001 | 538981.422 | -1388714.794 | 6181005.139 |
| tidb† | 50103 | -4460996.129 | 2682557.076 | -3674443.693 |
| tixi | 12360 | -1264873.036 | 1569455.795 | 6031003.458 |
| torp | 49912 | -2517894.221 | -4670260.212 | 3527827.455 |
| tow2 | 50140 | -5054582.693 | 3275504.449 | -2091539.703 |
| trab | 20808 | 3705250.492 | 3084421.557 | 4162044.636 |
| trak | 40480 | -2480029.028 | -4703111.049 | 3511298.477 |
| tro1 | 80002 | 2102928.615 | 721619.378 | 5958196.182 |
| trom† | 10302 | 2102940.337 | 721569.379 | 5958192.113 |
| tskb† | 21730 | -3957199.240 | 3310199.668 | 3737711.708 |
| uclp | 80034 | -2519006.908 | -4650672.626 | 3552862.645 |
| uclu | 40140 | -2440669.053 | -3416437.076 | 4785136.866 |
| urum | 21612 | 193030.873 | 4606851.324 | 4393311.421 |
| usc1 | 40487 | -2507564.595 | -4659953.553 | 3548660.889 |
| usna | 49908 | 1160668.929 | -4826883.325 | 3990863.060 |
| usno | 40451 | 1112189.893 | -4842955.037 | 3985352.249 |
| usud | 21729 | -3855262.998 | 3427432.519 | 3741020.362 |
| vene | 12741 | 4379724.871 | 957495.734 | 4521605.129 |
| vesl | 66009 | 2009329.713 | -99741.474 | -6033158.472 |
| vill† | 13406 | 4849833.786 | -335049.186 | 4116014.840 |
| vndp | 40420 | -2678089.919 | -4525437.661 | 3597431.568 |
| vs0g | 10423 | 3246470.378 | 1077900.392 | 5365278.018 |
| wes2† | 40440 | 1492233.369 | -4458089.483 | 4296046.010 |
| whc1 | 40461 | -2488199.015 | -4673487.488 | 3544649.152 |
| whit | 40136 | -2218337.816 | -2201205.112 | 5543057.583 |
| widc | 49917 | -2354850.049 | -4745524.099 | 3540692.991 |
| will | 40134 | -2084258.009 | -3313872.988 | 5019853.098 |
| wlsn | 80026 | -2483640.617 | -4660073.111 | 3568172.089 |
| wroc | 12217 | 3835751.428 | 1177249.830 | 4941605.159 |
| wslr | 40141 | -2227013.617 | -3439649.113 | 4872522.251 |
| wsrt† | 13506 | 3828735.985 | 443304.827 | 5064884.632 |
| wtzr† | 14201 | 4075580.685 | 931853.660 | 4801568.054 |
| wuhn | 21602 | -2267749.162 | 5009154.325 | 3221290.762 |
| xian | 21614 | -1735212.505 | 4976840.109 | 3580538.372 |
| yakz | 12353 | -1915023.239 | 2308213.235 | 5610225.002 |
| yar1† | 50107 | -2389025.536 | 5043316.872 | -3078530.731 |
| yell† | 40127 | -1224452.501 | -2689216.107 | 5633638.278 |
| ykro | 32601 | 6306439.987 | -578381.058 | 757956.265 |
| yssk | 12329 | -3465320.798 | 2638269.400 | 4644085.493 |
| zeck | 12351 | 3451174.880 | 3060335.313 | 4391955.568 |
| zimm | 14001 | 4331297.177 | 567555.732 | 4633133.840 |
| zwen† | 12330 | 2886325.543 | 2155998.399 | 5245816.145 |

## F.2 Optimal Set Selection Criteria

### F.2.1 Station Coordinates Accuracy

Table F.4: IGS Stations SIGMA

| site Id | DOMES Number | position | | | Velocity | | | Total | |
|---|---|---|---|---|---|---|---|---|---|
| | | $\sigma_x$ (cm) | $\sigma_y$ (cm) | $\sigma_z$ (cm) | $\sigma_{Vx}$ (cm/yr) | $\sigma_{Vy}$ (cm/yr) | $\sigma_{Vz}$ (cm/yr) | $\sigma_{pos}$ (cm) | $\sigma_{vel}$ (cm/yr) |
| albh | 40129M003 | 0.10 | 0.10 | 0.20 | 0.04 | 0.05 | 0.07 | 0.24 | 0.09 |
| algo | 40104M002 | 0.10 | 0.20 | 0.20 | 0.01 | 0.03 | 0.04 | 0.30 | 0.05 |
| alic | 50137M001 | 0.80 | 0.80 | 0.50 | 0.29 | 0.30 | 0.19 | 1.24 | 0.46 |
| amc2 | 40472S004 | 0.50 | 1.20 | 1.00 | 0.17 | 0.42 | 0.34 | 1.64 | 0.57 |
| ankr | 20805M002 | 0.80 | 0.50 | 0.80 | 0.08 | 0.06 | 0.08 | 1.24 | 0.13 |
| aoa1 | 40483S001 | 0.40 | 0.60 | 0.40 | 0.22 | 0.31 | 0.23 | 0.82 | 0.44 |
| aoml | 49914S001 | 0.20 | 0.60 | 0.30 | 0.09 | 0.21 | 0.11 | 0.70 | 0.25 |
| areq | 42202M005 | 0.10 | 0.20 | 0.10 | 0.03 | 0.04 | 0.03 | 0.24 | 0.06 |
| artu | 12362M001 | 0.30 | 0.40 | 0.50 | 0.10 | 0.10 | 0.12 | 0.71 | 0.19 |
| asc1 | 30602M001 | 0.40 | 0.20 | 0.10 | 0.15 | 0.07 | 0.04 | 0.46 | 0.17 |
| auck | 50209M001 | 0.20 | 0.10 | 0.20 | 0.08 | 0.04 | 0.07 | 0.30 | 0.11 |
| azu1 | 49911M001 | 0.80 | 1.10 | 0.80 | 0.43 | 0.65 | 0.46 | 1.58 | 0.90 |
| bahr | 24901M002 | 0.20 | 0.20 | 0.20 | 0.08 | 0.09 | 0.06 | 0.35 | 0.13 |
| bako | 23101M002 | 0.60 | 0.60 | 0.30 | 0.24 | 0.27 | 0.12 | 0.90 | 0.38 |
| barb | 43401S001 | 0.50 | 0.70 | 0.30 | 0.19 | 0.29 | 0.11 | 0.91 | 0.36 |
| bili | 12363M001 | 4.40 | 3.80 | 11.00 | 1.53 | 1.31 | 3.80 | 12.44 | 4.30 |
| bjfs | 21601M001 | 1.40 | 1.90 | 1.70 | 0.40 | 0.55 | 0.49 | 2.91 | 0.84 |
| blyt | 40479M001 | 2.20 | 3.20 | 2.30 | 0.27 | 0.45 | 0.32 | 4.51 | 0.61 |
| bogt | 41901M001 | 0.30 | 0.50 | 0.10 | 0.15 | 0.27 | 0.06 | 0.59 | 0.31 |
| bor1 | 12205M002 | 0.20 | 0.10 | 0.20 | 0.05 | 0.02 | 0.06 | 0.30 | 0.08 |
| bran | 40400M301 | 0.20 | 0.30 | 0.20 | 0.04 | 0.06 | 0.06 | 0.41 | 0.09 |
| braz | 41606M001 | 0.30 | 0.30 | 0.20 | 0.16 | 0.17 | 0.08 | 0.47 | 0.25 |
| brmu | 42501S004 | 0.10 | 0.20 | 0.20 | 0.03 | 0.05 | 0.04 | 0.30 | 0.07 |
| brus | 13101M004 | 0.20 | 0.10 | 0.20 | 0.05 | 0.02 | 0.06 | 0.30 | 0.08 |
| bucu | 11401M001 | 1.40 | 1.00 | 1.40 | 0.48 | 0.34 | 0.47 | 2.22 | 0.75 |
| bzrg | 12751M001 | 0.90 | 0.50 | 0.90 | 0.40 | 0.21 | 0.42 | 1.37 | 0.62 |
| cagl | 12725M003 | 0.20 | 0.10 | 0.20 | 0.07 | 0.03 | 0.07 | 0.30 | 0.10 |
| cas1 | 66011M001 | 0.10 | 0.20 | 0.30 | 0.04 | 0.05 | 0.10 | 0.37 | 0.12 |
| casa | 40437M002 | 1.40 | 2.20 | 1.80 | 0.54 | 0.91 | 0.76 | 3.17 | 1.30 |
| cat1 | 40488M001 | 0.40 | 0.60 | 0.50 | 0.26 | 0.36 | 0.26 | 0.88 | 0.51 |
| cedu | 50138M001 | 0.90 | 0.90 | 0.80 | 0.33 | 0.34 | 0.29 | 1.50 | 0.56 |
| chat | 50207M001 | 0.20 | 0.10 | 0.20 | 0.07 | 0.04 | 0.07 | 0.30 | 0.11 |
| chil | 40484M001 | 0.20 | 0.30 | 0.20 | 0.10 | 0.14 | 0.11 | 0.41 | 0.20 |
| chur | 40128M002 | 0.10 | 0.20 | 0.30 | 0.03 | 0.07 | 0.10 | 0.37 | 0.13 |
| chwk | 40142M001 | 5.10 | 6.10 | 7.40 | 1.92 | 2.31 | 2.78 | 10.86 | 4.09 |
| cic1 | 40508M002 | 0.90 | 1.40 | 1.00 | 0.31 | 0.49 | 0.34 | 1.94 | 0.67 |
| cit1 | 40400S201 | 0.30 | 0.50 | 0.40 | 0.04 | 0.06 | 0.06 | 0.71 | 0.09 |
| clar | 49906M001 | 0.20 | 0.30 | 0.20 | 0.10 | 0.14 | 0.11 | 0.41 | 0.20 |
| cmp9 | 49905M003 | 0.20 | 0.30 | 0.30 | 0.09 | 0.14 | 0.10 | 0.47 | 0.19 |
| coco | 50127M001 | 0.10 | 0.40 | 0.20 | 0.06 | 0.16 | 0.06 | 0.46 | 0.18 |
| cord | 41511M001 | 0.50 | 0.70 | 0.60 | 0.11 | 0.11 | 0.11 | 1.05 | 0.19 |
| coso | 40469M001 | 0.60 | 0.90 | 0.70 | 0.36 | 0.52 | 0.40 | 1.29 | 0.75 |
| crfp | 40481M001 | 0.20 | 0.30 | 0.30 | 0.10 | 0.14 | 0.11 | 0.47 | 0.20 |
| cro1 | 43201M001 | 0.10 | 0.20 | 0.10 | 0.03 | 0.06 | 0.04 | 0.24 | 0.08 |
| csn1 | 49910S001 | 2.30 | 3.10 | 2.30 | 0.37 | 0.53 | 0.39 | 4.49 | 0.75 |
| daej | 23902M002 | 0.40 | 0.50 | 0.50 | 0.12 | 0.15 | 0.14 | 0.81 | 0.24 |
| darw | 50134M001 | 2.30 | 2.60 | 1.10 | 0.75 | 0.83 | 0.36 | 3.64 | 1.18 |
| dav1 | 66010M001 | 0.10 | 0.10 | 0.30 | 0.04 | 0.04 | 0.06 | 0.33 | 0.08 |
| dgar | 30802M001 | 0.20 | 0.40 | 0.20 | 0.09 | 0.18 | 0.05 | 0.49 | 0.21 |
| dhlg | 49904M001 | 2.50 | 3.70 | 2.60 | 0.36 | 0.57 | 0.40 | 5.17 | 0.78 |
| drag | 20710S001 | 12.80 | 11.00 | 9.90 | 3.54 | 3.05 | 2.75 | 19.57 | 5.42 |
| drao | 40105M002 | 0.10 | 0.10 | 0.20 | 0.03 | 0.04 | 0.06 | 0.24 | 0.08 |
| dubo | 40137M001 | 0.10 | 0.30 | 0.30 | 0.05 | 0.12 | 0.14 | 0.44 | 0.19 |
| ebre | 13410M001 | 0.30 | 0.10 | 0.30 | 0.13 | 0.03 | 0.11 | 0.44 | 0.17 |
| eisl | 41703M003 | 0.10 | 0.20 | 0.20 | 0.04 | 0.05 | 0.04 | 0.30 | 0.08 |
| fair | 40408M001 | 0.10 | 0.10 | 0.20 | 0.02 | 0.02 | 0.04 | 0.24 | 0.05 |
| flin | 40135M001 | 0.10 | 0.20 | 0.20 | 0.03 | 0.07 | 0.10 | 0.30 | 0.13 |
| fort | 41602M001 | 0.20 | 0.20 | 0.10 | 0.04 | 0.04 | 0.03 | 0.30 | 0.06 |
| gala | 42005M001 | 0.20 | 0.60 | 0.10 | 0.09 | 0.22 | 0.05 | 0.64 | 0.24 |
| geno | 12712M002 | 0.90 | 0.30 | 0.90 | 0.37 | 0.11 | 0.36 | 1.31 | 0.53 |
| glsv | 12356M001 | 0.50 | 0.30 | 0.60 | 0.19 | 0.12 | 0.25 | 0.84 | 0.34 |
| gode | 40451M123 | 0.10 | 0.20 | 0.20 | 0.01 | 0.03 | 0.03 | 0.30 | 0.04 |
| gold | 40405S031 | 0.10 | 0.20 | 0.20 | 0.02 | 0.03 | 0.04 | 0.30 | 0.05 |
| ... | ... | ... | ... | ... | ... | ... | ... | ... | ... |

Table F.4: IGS Stations SIGMA (continued)

| site Id | DOMES Number | position $\sigma_x$ (cm) | position $\sigma_y$ (cm) | position $\sigma_z$ (cm) | Velocity $\sigma_{Vx}$ (cm/yr) | Velocity $\sigma_{Vy}$ (cm/yr) | Velocity $\sigma_{Vz}$ (cm/yr) | Total $\sigma_{pos}$ (cm) | Total $\sigma_{vel}$ (cm/yr) |
|---|---|---|---|---|---|---|---|---|---|
| gope | 11502M002 | 0.20 | 0.10 | 0.20 | 0.07 | 0.03 | 0.09 | 0.30 | 0.12 |
| goug | 30608M001 | 0.90 | 0.40 | 0.80 | 0.39 | 0.18 | 0.34 | 1.27 | 0.55 |
| gras | 10002M006 | 0.20 | 0.10 | 0.20 | 0.03 | 0.01 | 0.04 | 0.30 | 0.05 |
| graz | 11001M002 | 0.20 | 0.10 | 0.20 | 0.03 | 0.01 | 0.04 | 0.30 | 0.05 |
| guam | 50501M002 | 0.20 | 0.20 | 0.20 | 0.09 | 0.07 | 0.05 | 0.35 | 0.12 |
| harv | 40420M101 | 0.60 | 1.00 | 0.80 | 0.32 | 0.44 | 0.34 | 1.41 | 0.64 |
| hers | 13212M007 | 0.30 | 0.10 | 0.40 | 0.02 | 0.01 | 0.03 | 0.51 | 0.04 |
| hflk | 11006S003 | 0.30 | 0.10 | 0.30 | 0.13 | 0.04 | 0.14 | 0.44 | 0.20 |
| hnpt | 49913S001 | 0.30 | 0.50 | 0.40 | 0.15 | 0.26 | 0.20 | 0.71 | 0.36 |
| hob2 | 50116M004 | 0.20 | 0.10 | 0.20 | 0.04 | 0.03 | 0.05 | 0.30 | 0.07 |
| hofn | 10204M002 | 0.30 | 0.10 | 0.50 | 0.13 | 0.06 | 0.24 | 0.59 | 0.28 |
| holb | 40130M001 | 1.10 | 1.20 | 1.50 | 0.47 | 0.54 | 0.70 | 2.21 | 1.00 |
| holc | 40404M101 | 1.10 | 1.40 | 1.10 | 0.10 | 0.15 | 0.11 | 2.09 | 0.21 |
| holp | 49903M001 | 0.20 | 0.30 | 0.30 | 0.11 | 0.15 | 0.11 | 0.47 | 0.22 |
| hrao | 30302M004 | 0.30 | 0.20 | 0.20 | 0.05 | 0.03 | 0.04 | 0.41 | 0.07 |
| iisc | 22306M002 | 0.20 | 0.30 | 0.20 | 0.09 | 0.07 | 0.05 | 0.41 | 0.12 |
| ineg | 40507M001 | 3.90 | 13.30 | 5.90 | 1.33 | 4.43 | 1.95 | 15.06 | 5.02 |
| irkt | 12313M001 | 0.10 | 0.20 | 0.20 | 0.04 | 0.06 | 0.08 | 0.30 | 0.11 |
| jab1 | 50136M001 | 3.00 | 3.20 | 1.10 | 1.27 | 1.37 | 0.48 | 4.52 | 1.93 |
| jama | 42601S001 | 12.20 | 39.10 | 15.40 | 4.06 | 12.95 | 5.12 | 43.76 | 14.51 |
| joze | 12204M001 | 0.20 | 0.10 | 0.20 | 0.06 | 0.03 | 0.08 | 0.30 | 0.10 |
| jplm | 40400M007 | 0.10 | 0.20 | 0.20 | 0.04 | 0.06 | 0.06 | 0.30 | 0.09 |
| karr | 50139M001 | 0.60 | 1.00 | 0.50 | 0.22 | 0.37 | 0.18 | 1.27 | 0.47 |
| kely | 43005M001 | 0.10 | 0.10 | 0.30 | 0.05 | 0.05 | 0.13 | 0.33 | 0.15 |
| kerg | 91201M002 | 0.10 | 0.20 | 0.20 | 0.05 | 0.07 | 0.08 | 0.30 | 0.12 |
| kiru | 10403M002 | 0.10 | 0.10 | 0.30 | 0.04 | 0.03 | 0.10 | 0.33 | 0.11 |
| kit3 | 12334M001 | 0.10 | 0.20 | 0.20 | 0.04 | 0.07 | 0.06 | 0.30 | 0.10 |
| kokb | 40424M004 | 0.20 | 0.10 | 0.20 | 0.03 | 0.02 | 0.04 | 0.30 | 0.05 |
| kosg | 13504M003 | 0.10 | 0.10 | 0.20 | 0.04 | 0.01 | 0.05 | 0.24 | 0.06 |
| kour | 97301M210 | 0.20 | 0.20 | 0.10 | 0.07 | 0.08 | 0.03 | 0.30 | 0.11 |
| kr0g | 10422M001 | 0.50 | 0.20 | 1.30 | 0.25 | 0.12 | 0.65 | 1.41 | 0.71 |
| kstu | 12349M002 | 0.20 | 0.30 | 0.50 | 0.07 | 0.15 | 0.21 | 0.62 | 0.27 |
| kunm | 21609M001 | 1.00 | 2.20 | 1.20 | 0.37 | 0.83 | 0.43 | 2.70 | 1.01 |
| kwj1 | 50506M001 | 0.30 | 0.20 | 0.20 | 0.16 | 0.08 | 0.06 | 0.41 | 0.19 |
| lama | 12209M001 | 0.10 | 0.10 | 0.20 | 0.05 | 0.02 | 0.07 | 0.24 | 0.09 |
| lbch | 40482M001 | 0.70 | 1.10 | 0.80 | 0.53 | 0.75 | 0.55 | 1.53 | 1.07 |
| leep | 49902M001 | 0.20 | 0.30 | 0.20 | 0.10 | 0.14 | 0.11 | 0.41 | 0.20 |
| lhas | 21613M001 | 0.10 | 0.30 | 0.20 | 0.05 | 0.11 | 0.07 | 0.37 | 0.14 |
| long | 40485M001 | 0.20 | 0.30 | 0.30 | 0.11 | 0.16 | 0.12 | 0.47 | 0.23 |
| lpgs | 41510M001 | 0.20 | 0.20 | 0.20 | 0.06 | 0.09 | 0.08 | 0.35 | 0.13 |
| mac1 | 50135M001 | 0.20 | 0.10 | 0.30 | 0.06 | 0.04 | 0.08 | 0.37 | 0.11 |
| madr | 13407S012 | 0.70 | 0.30 | 0.60 | 0.05 | 0.02 | 0.05 | 0.97 | 0.07 |
| mag0 | 12354M001 | 0.40 | 0.30 | 0.60 | 0.14 | 0.11 | 0.23 | 0.78 | 0.29 |
| mali | 33201M001 | 0.90 | 0.90 | 0.20 | 0.14 | 0.13 | 0.04 | 1.29 | 0.20 |
| mas1 | 31303M002 | 0.20 | 0.10 | 0.10 | 0.07 | 0.03 | 0.05 | 0.24 | 0.09 |
| mate | 12734M008 | 0.20 | 0.10 | 0.20 | 0.03 | 0.01 | 0.04 | 0.30 | 0.05 |
| math | 40474M001 | 0.20 | 0.30 | 0.20 | 0.08 | 0.12 | 0.09 | 0.41 | 0.17 |
| maw1 | 66004M001 | 0.20 | 0.30 | 0.80 | 0.08 | 0.12 | 0.28 | 0.88 | 0.31 |
| mcm4 | 66001M003 | 0.10 | 0.10 | 0.30 | 0.04 | 0.04 | 0.13 | 0.33 | 0.14 |
| mdo1 | 40442M012 | 0.10 | 0.20 | 0.20 | 0.01 | 0.03 | 0.03 | 0.30 | 0.04 |
| mdvo | 12309M002 | 0.20 | 0.10 | 0.30 | 0.08 | 0.07 | 0.15 | 0.37 | 0.18 |
| medi | 12711M003 | 0.20 | 0.10 | 0.20 | 0.04 | 0.02 | 0.04 | 0.30 | 0.06 |
| mets | 10503S011 | 0.10 | 0.10 | 0.20 | 0.03 | 0.02 | 0.06 | 0.24 | 0.07 |
| mkea | 40477M001 | 0.20 | 0.10 | 0.20 | 0.05 | 0.04 | 0.05 | 0.30 | 0.08 |
| monp | 40497M004 | 0.10 | 0.20 | 0.20 | 0.02 | 0.03 | 0.03 | 0.30 | 0.05 |
| mr6g | 10405M002 | 0.60 | 0.20 | 1.00 | 0.28 | 0.11 | 0.49 | 1.18 | 0.57 |
| nano | 40138M001 | 1.40 | 1.80 | 2.10 | 0.67 | 0.83 | 1.00 | 3.10 | 1.46 |
| nico | 14302M001 | 0.40 | 0.30 | 0.30 | 0.17 | 0.12 | 0.14 | 0.58 | 0.25 |
| nklg | 32809M002 | 0.70 | 0.80 | 0.40 | 0.22 | 0.24 | 0.13 | 1.14 | 0.35 |
| nlib | 40465M001 | 0.10 | 0.20 | 0.20 | 0.01 | 0.03 | 0.04 | 0.30 | 0.05 |
| noto | 12717M003 | 0.20 | 0.10 | 0.20 | 0.04 | 0.02 | 0.04 | 0.30 | 0.06 |
| noum | 92701M003 | 0.50 | 0.30 | 0.30 | 0.18 | 0.11 | 0.11 | 0.66 | 0.24 |
| nrc1 | 40114M001 | 0.10 | 0.20 | 0.30 | 0.05 | 0.09 | 0.10 | 0.37 | 0.14 |
| nssp | 12312M001 | 1.10 | 1.10 | 1.10 | 0.55 | 0.55 | 0.58 | 1.91 | 0.97 |
| ntus | 22601M001 | 0.40 | 0.80 | 0.20 | 0.14 | 0.31 | 0.07 | 0.92 | 0.35 |
| nya1 | 10317M003 | 0.10 | 0.10 | 0.40 | 0.02 | 0.01 | 0.06 | 0.42 | 0.06 |
| nyal | 10317M001 | 0.10 | 0.10 | 0.30 | 0.02 | 0.01 | 0.06 | 0.33 | 0.06 |
| oat2 | 40478S101 | 0.40 | 0.50 | 0.40 | 0.10 | 0.14 | 0.11 | 0.75 | 0.20 |
| onsa | 10402M004 | 0.10 | 0.10 | 0.20 | 0.02 | 0.01 | 0.04 | 0.24 | 0.05 |
| ... | ... | ... | ... | ... | ... | ... | ... | ... | ... |

Table F.4: IGS Stations SIGMA (continued)

| site Id | DOMES Number | position $\sigma_x$ (cm) | position $\sigma_y$ (cm) | position $\sigma_z$ (cm) | Velocity $\sigma_{Vx}$ (cm/yr) | Velocity $\sigma_{Vy}$ (cm/yr) | Velocity $\sigma_{Vz}$ (cm/yr) | Total $\sigma_{pos}$ (cm) | Total $\sigma_{vel}$ (cm/yr) |
|---|---|---|---|---|---|---|---|---|---|
| penc | 11206M006 | 0.30 | 0.10 | 0.30 | 0.12 | 0.05 | 0.14 | 0.44 | 0.19 |
| pert | 50133M001 | 0.10 | 0.20 | 0.20 | 0.04 | 0.07 | 0.06 | 0.30 | 0.10 |
| petp | 12355M002 | 0.70 | 0.40 | 0.90 | 0.26 | 0.15 | 0.33 | 1.21 | 0.45 |
| pie1 | 40456M001 | 0.10 | 0.20 | 0.20 | 0.02 | 0.03 | 0.04 | 0.30 | 0.05 |
| pimo | 22003M001 | 0.60 | 0.80 | 0.40 | 0.11 | 0.12 | 0.12 | 1.08 | 0.20 |
| pol2 | 12348M001 | 0.10 | 0.20 | 0.20 | 0.05 | 0.09 | 0.09 | 0.30 | 0.14 |
| pots | 14106M003 | 0.10 | 0.10 | 0.20 | 0.03 | 0.02 | 0.05 | 0.24 | 0.06 |
| prds | 40124M001 | 0.40 | 0.50 | 0.50 | 0.17 | 0.20 | 0.23 | 0.81 | 0.35 |
| pvep | 40403M002 | 0.70 | 1.00 | 0.80 | 0.25 | 0.41 | 0.30 | 1.46 | 0.57 |
| quin | 40433M004 | 0.10 | 0.20 | 0.20 | 0.02 | 0.03 | 0.04 | 0.30 | 0.05 |
| ramo | 20703S001 | 0.80 | 0.60 | 0.60 | 0.32 | 0.24 | 0.23 | 1.17 | 0.46 |
| reyk | 10202M001 | 0.10 | 0.10 | 0.20 | 0.04 | 0.03 | 0.08 | 0.24 | 0.09 |
| riog | 41507M004 | 0.20 | 0.30 | 0.40 | 0.07 | 0.09 | 0.11 | 0.54 | 0.16 |
| riop | 42006M001 | 2.50 | 4.40 | 1.10 | 0.82 | 1.58 | 0.38 | 5.18 | 1.82 |
| roch | 40486M001 | 0.30 | 0.50 | 0.40 | 0.17 | 0.24 | 0.18 | 0.71 | 0.34 |
| rock | 40478M002 | 0.20 | 0.30 | 0.20 | 0.10 | 0.14 | 0.11 | 0.41 | 0.20 |
| sant | 41705M003 | 0.10 | 0.20 | 0.20 | 0.04 | 0.06 | 0.05 | 0.30 | 0.09 |
| sch2 | 40133M002 | 0.20 | 0.30 | 0.40 | 0.08 | 0.13 | 0.18 | 0.54 | 0.24 |
| scip | 49915M001 | 0.70 | 1.10 | 0.80 | 0.34 | 0.50 | 0.35 | 1.53 | 0.70 |
| sele | 12352M001 | 0.20 | 0.40 | 0.40 | 0.09 | 0.19 | 0.17 | 0.60 | 0.27 |
| sey1 | 39801M001 | 0.80 | 1.00 | 0.20 | 0.35 | 0.44 | 0.09 | 1.30 | 0.57 |
| sfer | 13402M004 | 0.70 | 0.20 | 0.50 | 0.25 | 0.06 | 0.19 | 0.88 | 0.32 |
| shao | 21605M002 | 0.10 | 0.20 | 0.20 | 0.04 | 0.05 | 0.05 | 0.30 | 0.08 |
| sio3 | 40460M004 | 0.50 | 0.80 | 0.60 | 0.26 | 0.40 | 0.28 | 1.12 | 0.55 |
| sni1 | 49909S001 | 0.70 | 1.00 | 0.80 | 0.37 | 0.52 | 0.38 | 1.46 | 0.74 |
| sofi | 11101M002 | 0.50 | 0.20 | 0.40 | 0.26 | 0.13 | 0.25 | 0.67 | 0.38 |
| sol1 | 49907S001 | 0.10 | 0.30 | 0.20 | 0.07 | 0.12 | 0.10 | 0.37 | 0.17 |
| spk1 | 40458M001 | 0.50 | 0.70 | 0.50 | 0.28 | 0.39 | 0.28 | 0.99 | 0.56 |
| stjo | 40101M001 | 0.10 | 0.10 | 0.20 | 0.03 | 0.04 | 0.05 | 0.24 | 0.07 |
| suth | 30314M002 | 0.60 | 0.30 | 0.40 | 0.22 | 0.12 | 0.15 | 0.78 | 0.29 |
| suwn | 23903M001 | 0.50 | 0.60 | 0.60 | 0.23 | 0.28 | 0.26 | 0.98 | 0.45 |
| syog | 66006S002 | 0.30 | 0.20 | 0.70 | 0.08 | 0.08 | 0.18 | 0.79 | 0.21 |
| tabl | 49901M001 | 0.20 | 0.40 | 0.30 | 0.12 | 0.18 | 0.14 | 0.54 | 0.26 |
| thti | 92201M009 | 0.30 | 0.30 | 0.30 | 0.07 | 0.08 | 0.07 | 0.52 | 0.13 |
| thu1 | 43001M001 | 0.10 | 0.10 | 0.30 | 0.02 | 0.03 | 0.10 | 0.33 | 0.11 |
| tidb | 50103M108 | 0.20 | 0.10 | 0.20 | 0.04 | 0.03 | 0.05 | 0.30 | 0.07 |
| tixi | 12360M001 | 0.40 | 0.40 | 1.10 | 0.13 | 0.14 | 0.39 | 1.24 | 0.43 |
| torp | 49912M001 | 0.90 | 1.20 | 0.90 | 0.49 | 0.70 | 0.50 | 1.75 | 0.99 |
| tow2 | 50140M001 | 0.90 | 0.60 | 0.50 | 0.33 | 0.24 | 0.17 | 1.19 | 0.44 |
| trab | 20808M001 | 14.70 | 13.40 | 15.20 | 4.19 | 3.80 | 4.33 | 25.03 | 7.12 |
| trak | 40480M001 | 0.20 | 0.30 | 0.30 | 0.11 | 0.15 | 0.12 | 0.47 | 0.22 |
| tro1 | 10302M006 | 0.30 | 0.20 | 0.90 | 0.04 | 0.03 | 0.08 | 0.97 | 0.09 |
| trom | 10302M003 | 0.10 | 0.10 | 0.30 | 0.04 | 0.03 | 0.08 | 0.33 | 0.09 |
| tskb | 21730S005 | 0.20 | 0.20 | 0.20 | 0.05 | 0.05 | 0.06 | 0.35 | 0.09 |
| uclp | 40487M002 | 0.40 | 0.50 | 0.40 | 0.18 | 0.25 | 0.19 | 0.75 | 0.36 |
| uclu | 40140M001 | 1.40 | 1.60 | 1.90 | 0.64 | 0.76 | 0.92 | 2.85 | 1.35 |
| urum | 21612M001 | 0.30 | 0.60 | 0.60 | 0.09 | 0.22 | 0.20 | 0.90 | 0.31 |
| usc1 | 40487M001 | 0.40 | 0.50 | 0.40 | 0.18 | 0.25 | 0.19 | 0.75 | 0.36 |
| usna | 49908S001 | 0.20 | 0.40 | 0.30 | 0.12 | 0.21 | 0.17 | 0.54 | 0.30 |
| usno | 40451S003 | 0.10 | 0.20 | 0.20 | 0.02 | 0.03 | 0.03 | 0.30 | 0.05 |
| usud | 21729S007 | 0.20 | 0.20 | 0.20 | 0.05 | 0.05 | 0.06 | 0.35 | 0.09 |
| vene | 12741M001 | 0.40 | 0.10 | 0.40 | 0.18 | 0.05 | 0.18 | 0.57 | 0.26 |
| vesl | 66009M001 | 0.30 | 0.20 | 0.50 | 0.09 | 0.09 | 0.11 | 0.62 | 0.17 |
| vill | 13406M001 | 0.20 | 0.10 | 0.20 | 0.05 | 0.02 | 0.05 | 0.30 | 0.07 |
| vndp | 40420M007 | 0.50 | 0.70 | 0.60 | 0.06 | 0.09 | 0.08 | 1.05 | 0.13 |
| vs0g | 10423M001 | 0.60 | 0.20 | 1.00 | 0.30 | 0.12 | 0.48 | 1.18 | 0.58 |
| wes2 | 40440S020 | 0.20 | 0.40 | 0.40 | 0.01 | 0.02 | 0.03 | 0.60 | 0.04 |
| whc1 | 40461M001 | 0.40 | 0.60 | 0.50 | 0.25 | 0.35 | 0.26 | 0.88 | 0.50 |
| whit | 40136M001 | 0.10 | 0.10 | 0.30 | 0.05 | 0.05 | 0.10 | 0.33 | 0.12 |
| widc | 49917M001 | 0.50 | 0.80 | 0.60 | 0.24 | 0.37 | 0.27 | 1.12 | 0.52 |
| will | 40134M001 | 0.20 | 0.20 | 0.30 | 0.07 | 0.09 | 0.13 | 0.41 | 0.17 |
| wlsn | 40400M101 | 0.50 | 0.70 | 0.50 | 0.04 | 0.06 | 0.06 | 0.99 | 0.09 |
| wroc | 12217M001 | 0.60 | 0.20 | 0.80 | 0.37 | 0.13 | 0.47 | 1.02 | 0.61 |
| wslr | 40141M001 | 1.30 | 1.60 | 1.90 | 0.64 | 0.79 | 0.95 | 2.80 | 1.39 |
| wsrt | 13506M005 | 0.20 | 0.10 | 0.30 | 0.09 | 0.04 | 0.12 | 0.37 | 0.16 |
| wtzr | 14201M010 | 0.10 | 0.10 | 0.20 | 0.02 | 0.01 | 0.04 | 0.24 | 0.05 |
| wuhn | 21602M001 | 0.20 | 0.30 | 0.20 | 0.07 | 0.12 | 0.09 | 0.41 | 0.17 |
| xian | 21614M001 | 0.10 | 0.30 | 0.20 | 0.08 | 0.17 | 0.13 | 0.37 | 0.23 |
| yakz | 12353M001 | 0.30 | 0.30 | 0.60 | 0.11 | 0.13 | 0.23 | 0.73 | 0.29 |
| ... | ... | ... | ... | ... | ... | ... | ... | ... | ... |

Table F.4: IGS Stations SIGMA (continued)

| site Id | DOMES Number | position | | | Velocity | | | Total | |
|---|---|---|---|---|---|---|---|---|---|
| | | $\sigma_x$ (cm) | $\sigma_y$ (cm) | $\sigma_z$ (cm) | $\sigma_{Vx}$ (cm/yr) | $\sigma_{Vy}$ (cm/yr) | $\sigma_{Vz}$ (cm/yr) | $\sigma_{pos}$ (cm) | $\sigma_{vel}$ (cm/yr) |
| yarl | 50107M004 | 0.10 | 0.20 | 0.20 | 0.02 | 0.03 | 0.04 | 0.30 | 0.05 |
| yell | 40127M003 | 0.10 | 0.10 | 0.20 | 0.02 | 0.03 | 0.06 | 0.24 | 0.07 |
| ykro | 32601M001 | 2.00 | 0.60 | 0.50 | 0.12 | 0.11 | 0.11 | 2.15 | 0.20 |
| yssk | 12329M003 | 0.80 | 0.70 | 0.90 | 0.23 | 0.22 | 0.25 | 1.39 | 0.40 |
| zeck | 12351M001 | 0.30 | 0.30 | 0.40 | 0.13 | 0.12 | 0.15 | 0.58 | 0.23 |
| zimm | 14001M004 | 0.20 | 0.10 | 0.30 | 0.04 | 0.02 | 0.05 | 0.37 | 0.07 |
| zwen | 12330M001 | 0.10 | 0.10 | 0.20 | 0.05 | 0.04 | 0.08 | 0.24 | 0.10 |

Table F.5: MSODP's IGS ITRF Ref Stations (52) SIGMA

| site Id | DOMES Number | position | | | Velocity | | | Total | |
|---|---|---|---|---|---|---|---|---|---|
| | | $\sigma_x$ (cm) | $\sigma_y$ (cm) | $\sigma_z$ (cm) | $\sigma_{Vx}$ (cm/yr) | $\sigma_{Vy}$ (cm/yr) | $\sigma_{Vz}$ (cm/yr) | $\sigma_{pos}$ (cm) | $\sigma_{vel}$ (cm/yr) |
| algo | 40104M002 | 0.10 | 0.20 | 0.20 | 0.01 | 0.03 | 0.04 | 0.30 | 0.05 |
| ascl | 30602M001 | 0.40 | 0.20 | 0.10 | 0.15 | 0.07 | 0.04 | 0.46 | 0.17 |
| auck | 50209M001 | 0.20 | 0.10 | 0.20 | 0.08 | 0.04 | 0.07 | 0.30 | 0.11 |
| bahr | 24901M002 | 0.20 | 0.20 | 0.20 | 0.08 | 0.09 | 0.06 | 0.35 | 0.13 |
| brmu | 42501S004 | 0.10 | 0.20 | 0.20 | 0.03 | 0.05 | 0.04 | 0.30 | 0.07 |
| casl | 66011M001 | 0.10 | 0.20 | 0.30 | 0.04 | 0.05 | 0.10 | 0.37 | 0.12 |
| cedu | 50138M001 | 0.90 | 0.90 | 0.80 | 0.33 | 0.34 | 0.29 | 1.50 | 0.56 |
| chat | 50207M001 | 0.20 | 0.10 | 0.20 | 0.07 | 0.04 | 0.07 | 0.30 | 0.11 |
| davl | 66010M001 | 0.10 | 0.10 | 0.30 | 0.04 | 0.04 | 0.06 | 0.33 | 0.08 |
| dgar | 30802M001 | 0.20 | 0.40 | 0.20 | 0.09 | 0.18 | 0.05 | 0.49 | 0.21 |
| drao | 40105M002 | 0.10 | 0.10 | 0.20 | 0.03 | 0.04 | 0.06 | 0.24 | 0.08 |
| fair | 40408M001 | 0.10 | 0.10 | 0.20 | 0.02 | 0.02 | 0.04 | 0.24 | 0.05 |
| fort | 41602M001 | 0.20 | 0.20 | 0.10 | 0.04 | 0.04 | 0.03 | 0.30 | 0.06 |
| gode | 40451M123 | 0.10 | 0.20 | 0.20 | 0.01 | 0.03 | 0.03 | 0.30 | 0.04 |
| gol2 | 40405S031 | 0.10 | 0.20 | 0.20 | 0.02 | 0.03 | 0.04 | 0.30 | 0.05 |
| graz | 11001M002 | 0.20 | 0.10 | 0.20 | 0.03 | 0.01 | 0.04 | 0.30 | 0.05 |
| guam | 50501M002 | 0.20 | 0.20 | 0.20 | 0.09 | 0.07 | 0.05 | 0.35 | 0.12 |
| hob2 | 50116M004 | 0.20 | 0.10 | 0.20 | 0.04 | 0.03 | 0.05 | 0.30 | 0.07 |
| irkt | 12313M001 | 0.10 | 0.20 | 0.20 | 0.04 | 0.06 | 0.08 | 0.30 | 0.11 |
| kerg | 91201M002 | 0.10 | 0.20 | 0.20 | 0.05 | 0.07 | 0.08 | 0.30 | 0.12 |
| kit3 | 12334M001 | 0.10 | 0.20 | 0.20 | 0.04 | 0.07 | 0.06 | 0.30 | 0.10 |
| kokb | 40424M004 | 0.20 | 0.10 | 0.20 | 0.03 | 0.02 | 0.04 | 0.30 | 0.05 |
| kour | 97301M210 | 0.20 | 0.20 | 0.10 | 0.07 | 0.08 | 0.03 | 0.30 | 0.11 |
| kwjl | 50506M001 | 0.30 | 0.20 | 0.20 | 0.16 | 0.08 | 0.06 | 0.41 | 0.19 |
| lhas | 21613M001 | 0.10 | 0.30 | 0.20 | 0.05 | 0.11 | 0.07 | 0.37 | 0.14 |
| lpgs | 41510M001 | 0.20 | 0.20 | 0.20 | 0.06 | 0.09 | 0.08 | 0.35 | 0.13 |
| macl | 50135M001 | 0.20 | 0.10 | 0.30 | 0.06 | 0.04 | 0.08 | 0.37 | 0.11 |
| mali | 33201M001 | 0.90 | 0.90 | 0.20 | 0.14 | 0.13 | 0.04 | 1.29 | 0.20 |
| masl | 31303M002 | 0.20 | 0.10 | 0.10 | 0.07 | 0.03 | 0.05 | 0.24 | 0.09 |
| mate | 12734M008 | 0.20 | 0.10 | 0.20 | 0.03 | 0.01 | 0.04 | 0.30 | 0.05 |
| mcm4 | 66001M003 | 0.10 | 0.10 | 0.30 | 0.04 | 0.04 | 0.13 | 0.33 | 0.14 |
| mdol | 40442M012 | 0.10 | 0.20 | 0.20 | 0.01 | 0.03 | 0.03 | 0.30 | 0.04 |
| nlib | 40465M001 | 0.10 | 0.20 | 0.20 | 0.01 | 0.03 | 0.04 | 0.30 | 0.05 |
| nyal | 10317M001 | 0.10 | 0.10 | 0.30 | 0.02 | 0.01 | 0.06 | 0.33 | 0.06 |
| onsa | 10402M004 | 0.10 | 0.10 | 0.20 | 0.02 | 0.01 | 0.04 | 0.24 | 0.05 |
| pert | 50133M001 | 0.10 | 0.20 | 0.20 | 0.04 | 0.07 | 0.06 | 0.30 | 0.10 |
| piel | 40456M001 | 0.10 | 0.20 | 0.20 | 0.02 | 0.03 | 0.04 | 0.30 | 0.05 |
| pots | 14106M003 | 0.10 | 0.10 | 0.20 | 0.03 | 0.02 | 0.05 | 0.24 | 0.06 |
| riog | 41507M004 | 0.20 | 0.30 | 0.40 | 0.07 | 0.09 | 0.11 | 0.54 | 0.16 |
| sant | 41705M003 | 0.10 | 0.20 | 0.20 | 0.04 | 0.06 | 0.05 | 0.30 | 0.09 |
| shao | 21605M002 | 0.10 | 0.20 | 0.20 | 0.04 | 0.05 | 0.05 | 0.30 | 0.08 |
| thul | 43001M001 | 0.10 | 0.10 | 0.30 | 0.02 | 0.03 | 0.10 | 0.33 | 0.11 |
| tidb | 50103M108 | 0.20 | 0.10 | 0.20 | 0.04 | 0.03 | 0.05 | 0.30 | 0.07 |
| trom | 10302M003 | 0.10 | 0.10 | 0.30 | 0.04 | 0.03 | 0.08 | 0.33 | 0.09 |
| tskb | 21730S005 | 0.20 | 0.20 | 0.20 | 0.05 | 0.05 | 0.06 | 0.35 | 0.09 |
| vill | 13406M001 | 0.20 | 0.10 | 0.20 | 0.05 | 0.02 | 0.05 | 0.30 | 0.07 |
| wes2 | 40440S020 | 0.20 | 0.40 | 0.40 | 0.01 | 0.02 | 0.03 | 0.60 | 0.04 |
| wsrt | 13506M005 | 0.20 | 0.10 | 0.30 | 0.09 | 0.04 | 0.12 | 0.37 | 0.16 |
| wtzr | 14201M010 | 0.10 | 0.10 | 0.20 | 0.02 | 0.01 | 0.04 | 0.24 | 0.05 |
| yarl | 50107M004 | 0.10 | 0.20 | 0.20 | 0.02 | 0.03 | 0.04 | 0.30 | 0.05 |
| yell | 40127M003 | 0.10 | 0.10 | 0.20 | 0.02 | 0.03 | 0.06 | 0.24 | 0.07 |
| zwen | 12330M001 | 0.10 | 0.10 | 0.20 | 0.05 | 0.04 | 0.08 | 0.24 | 0.10 |

### F.2.2 Station daily performance quality

Table F.6: Station Performance Sample(Jan 21, 2002)

| site Id | epochs | clock | p-code Residual | Phase Residual | phase breaks | days Processed | Days Since Last Day processed |
|---|---|---|---|---|---|---|---|
| agmt | 273.31 | 42.18 | 33.33 | 5.55 | 53.10 | 494 | 2 |
| albh | 285.07 | 12641.97 | 46.55 | 5.91 | 56.16 | 2226 | 2 |
| algo | 285.29 | 48.73 | 48.66 | 5.67 | 53.22 | 2234 | 2 |
| alic | 280.34 | 96.04 | 50.40 | 6.77 | 50.10 | 424 | 2 |
| amc2 | 280.43 | 7.09 | 41.54 | 6.60 | 52.35 | 425 | 2 |
| ankr | 273.87 | 745.91 | 65.06 | 7.63 | 58.20 | 1615 | 2 |
| aoa1 | 282.52 | 335.39 | 61.84 | 7.09 | 56.35 | 2208 | 2 |
| azry | 281.91 | 3766.83 | 35.88 | 6.79 | 65.23 | 643 | 2 |
| azu1 | 280.84 | 2226876.19 | 44.43 | 7.14 | 61.73 | 1611 | 3 |
| bahr | 283.50 | 2054.03 | 43.98 | 9.15 | 64.64 | 1690 | 2 |
| bako | 260.38 | 283160.81 | 71.19 | 9.25 | 63.66 | 495 | 112 |
| barb | 269.45 | 82.33 | 36.37 | 8.52 | 53.37 | 372 | 431 |
| barh | 277.71 | 288045.89 | 62.34 | 7.29 | 61.59 | 316 | 109 |
| bbry | 282.60 | 29514.69 | 73.42 | 6.82 | 60.29 | 745 | 3 |
| bgis | 281.28 | 1026.38 | 70.72 | 7.44 | 64.13 | 679 | 3 |
| bili | 274.64 | 2778.03 | 38.26 | 6.38 | 100.30 | 232 | 2 |
| bill | 278.78 | 838.62 | 51.48 | 6.41 | 76.94 | 961 | 2 |
| bkms | 283.04 | 681.41 | 48.27 | 6.69 | 57.26 | 1018 | 3 |
| blyt | 283.40 | 153358.40 | 39.28 | 7.60 | 52.52 | 2087 | 2 |
| bmhl | 268.89 | 1049.53 | 50.72 | 5.80 | 83.60 | 394 | 2 |
| bmry | 283.15 | 1215.99 | 59.66 | 6.29 | 56.07 | 694 | 2 |
| bogt | 262.64 | 2456.49 | 75.54 | 8.06 | 81.93 | 981 | 778 |
| borl | 284.71 | 6463.14 | 53.53 | 6.50 | 65.84 | 2190 | 2 |
| bran | 284.19 | 8310.47 | 86.47 | 7.39 | 57.93 | 2061 | 3 |
| braz | 276.75 | 46228.27 | 60.02 | 9.74 | 73.33 | 680 | 468 |
| brib | 281.14 | 251141.40 | 63.39 | 8.55 | 47.27 | 1493 | 729 |
| brmu | 283.63 | 191.54 | 45.57 | 7.21 | 52.68 | 2160 | 2 |
| bru1 | 279.97 | 290313.58 | 120.25 | 11.19 | 58.22 | 881 | 876 |
| brus | 280.89 | 298.35 | 59.34 | 6.54 | 71.57 | 2162 | 2 |
| bsry | 283.03 | 1458.96 | 54.69 | 6.62 | 63.45 | 900 | 3 |
| btdm | 272.03 | 620.86 | 43.04 | 5.78 | 49.56 | 209 | 3 |
| bucu | 278.14 | 288971.22 | 39.12 | 6.67 | 56.23 | 417 | 2 |
| bzrg | 279.15 | 68.09 | 95.37 | 7.74 | 44.20 | 427 | 2 |
| cact | 277.44 | 504.24 | 47.96 | 6.39 | 59.40 | 202 | 2 |
| cagl | 280.11 | 29539.70 | 55.66 | 7.02 | 63.19 | 1469 | 2 |
| canb | 276.04 | 304.03 | 7.99 | 6.84 | 53.61 | 2096 | 2 |
| carr | 287.25 | 110.34 | 54.50 | 9.15 | 55.45 | 20 | 1444 |
| cas1 | 275.73 | 354453.93 | 38.09 | 8.19 | 101.02 | 1810 | 2 |
| casa | 274.09 | 252566.76 | 42.55 | 6.37 | 70.48 | 1908 | 3 |
| cat1 | 284.48 | 430.43 | 42.36 | 6.49 | 54.33 | 2043 | 3 |
| cat2 | 269.36 | 319.34 | 29.59 | 5.13 | 56.79 | 211 | 2 |
| cbhs | 276.16 | 2544.31 | 53.48 | 6.39 | 61.68 | 659 | 2 |
| ccco | 274.15 | 2299.98 | 54.65 | 6.21 | 97.50 | 824 | 3 |
| cccs | 283.60 | 1113.60 | 51.72 | 6.54 | 60.00 | 843 | 2 |
| cedu | 279.74 | 178.99 | 33.27 | 6.22 | 52.45 | 419 | 4 |
| chab | 280.16 | 194467.44 | 56.48 | 7.69 | 51.38 | 1380 | 732 |
| chat | 284.97 | 93.34 | 79.95 | 8.96 | 60.37 | 2057 | 2 |
| chil | 274.81 | 127722.98 | 45.47 | 7.45 | 48.72 | 2032 | 3 |
| chms | 278.27 | 1001.73 | 49.62 | 6.42 | 63.14 | 555 | 3 |
| chur | 281.57 | 8295.47 | 36.31 | 6.55 | 90.41 | 1797 | 2 |
| chwk | 281.47 | 119.07 | 67.57 | 6.10 | 59.58 | 434 | 2 |
| cic1 | 279.73 | 90.01 | 55.68 | 5.61 | 51.07 | 432 | 2 |
| cice | 282.13 | 9046.48 | 35.52 | 6.28 | 52.96 | 1323 | 1033 |
| cit1 | 279.93 | 2747.04 | 49.76 | 6.10 | 54.73 | 2035 | 3 |
| cjms | 281.33 | 633.25 | 61.20 | 7.12 | 56.80 | 685 | 3 |
| clar | 281.92 | 141690.81 | 79.31 | 7.12 | 50.82 | 2099 | 3 |
| cmbb | 274.21 | 354413.74 | 80.85 | 9.32 | 68.32 | 1360 | 748 |
| cmp9 | 276.09 | 220480.97 | 54.58 | 7.72 | 65.60 | 1905 | 3 |
| cnpp | 275.01 | 458.74 | 45.81 | 5.87 | 56.72 | 194 | 2 |
| coat | 244.27 | 12646.55 | 44.16 | 7.84 | 239.07 | 154 | 1367 |
| coco | 270.01 | 12205.19 | 45.16 | 8.50 | 134.99 | 1489 | 2 |
| cord | 266.60 | 30.23 | 69.55 | 6.06 | 81.93 | 405 | 2 |
| coso | 277.94 | 153364.66 | 52.18 | 6.89 | 54.67 | 1772 | 4 |
| cotd | 280.53 | 470.73 | 45.22 | 8.59 | 62.89 | 430 | 2 |
| crfp | 283.64 | 128790.24 | 45.76 | 7.25 | 52.14 | 2132 | 2 |
| crhs | 282.41 | 693.51 | 41.16 | 6.45 | 57.76 | 560 | 43 |
| cro1 | 278.03 | 2915.15 | 47.49 | 7.58 | 75.03 | 1980 | 2 |
| ... | ... | ... | ... | ... | ... | ... | ... |

Table F.6: Station Performance Sample(Jan 21, 2002). (continued)

| site Id | epochs | clock | p-code Residual | Phase Residual | phase breaks | days Processed | Days Since Last Day processed |
|---|---|---|---|---|---|---|---|
| crrs | 281.04 | 2514.74 | 32.35 | 6.35 | 70.51 | 846 | 2 |
| cru1 | 278.47 | 950.09 | 55.42 | 5.81 | 62.64 | 329 | 2 |
| csdh | 281.21 | 1102.53 | 42.73 | 6.10 | 73.48 | 1024 | 3 |
| csn1 | 256.95 | 4606.13 | 55.69 | 6.77 | 96.21 | 1666 | 4 |
| ctms | 281.92 | 250.22 | 46.71 | 6.42 | 61.28 | 676 | 3 |
| cuhs | 280.34 | 203.49 | 71.36 | 7.03 | 56.51 | 354 | 3 |
| cvhs | 274.59 | 1368.17 | 62.86 | 6.65 | 59.70 | 978 | 3 |
| daej | 279.25 | 1300.09 | 78.35 | 7.12 | 69.33 | 400 | 3 |
| dam1 | 283.12 | 296080.10 | 44.43 | 7.26 | 46.12 | 1536 | 657 |
| dam2 | 277.44 | 140393.36 | 73.58 | 7.56 | 44.68 | 1673 | 3 |
| darw | 269.18 | 245269.25 | 39.64 | 7.35 | 64.08 | 373 | 2 |
| dav1 | 259.03 | 2903.55 | 90.89 | 7.93 | 107.05 | 1750 | 2 |
| denc | 285.93 | 289043.80 | 57.14 | 5.39 | 256.76 | 137 | 2258 |
| dgar | 239.12 | 51238.94 | 62.51 | 9.38 | 71.49 | 1547 | 429 |
| dhlg | 281.65 | 104160.37 | 26.41 | 6.64 | 60.30 | 1683 | 2 |
| drao | 287.86 | 5.66 | 34.86 | 6.62 | 54.76 | 21 | 1444 |
| dshs | 245.35 | 1040.47 | 52.40 | 6.50 | 61.22 | 554 | 3 |
| dssc | 282.57 | 1304.63 | 70.21 | 6.71 | 54.64 | 858 | 2 |
| dubo | 285.03 | 272.91 | 44.96 | 5.74 | 66.04 | 1640 | 2 |
| dvpb | 269.58 | 684.26 | 44.23 | 5.99 | 53.76 | 294 | 2 |
| dyhs | 273.01 | 9615.34 | 56.43 | 7.05 | 67.97 | 1015 | 13 |
| ebre | 282.76 | 286547.75 | 51.34 | 7.21 | 66.51 | 1623 | 2 |
| ecco | 281.59 | 266.46 | 42.73 | 7.23 | 58.20 | 697 | 3 |
| edpp | 136.52 | 22.02 | 32.52 | 5.58 | 165.00 | 31 | 138 |
| eisl | 275.47 | 1312423.85 | 57.39 | 10.40 | 60.49 | 1887 | 2 |
| elsc | 282.08 | 395.40 | 60.72 | 6.67 | 65.39 | 611 | 3 |
| engl | 278.51 | 278165.40 | 103.07 | 12.44 | 48.82 | 1098 | 876 |
| eprt | 276.98 | 289407.93 | 68.76 | 6.39 | 67.37 | 429 | 2 |
| fort | 269.12 | 5219.88 | 68.21 | 9.43 | 84.08 | 2140 | 2 |
| fvpk | 283.76 | 306.81 | 36.71 | 6.30 | 57.51 | 892 | 2 |
| fxhs | 264.83 | 1239.74 | 64.14 | 6.85 | 51.70 | 556 | 4 |
| fzhs | 283.93 | 409.77 | 44.86 | 6.97 | 52.64 | 982 | 3 |
| gala | 273.84 | 309141.62 | 50.27 | 8.12 | 72.23 | 1257 | 2 |
| geno | 279.86 | 288016.11 | 74.39 | 7.21 | 61.92 | 416 | 2 |
| ggao | 276.44 | 38866.84 | 43.92 | 6.72 | 56.60 | 2118 | 2 |
| ghrp | 245.08 | 63.37 | 56.66 | 5.91 | 58.55 | 230 | 2 |
| glrs | 270.22 | 38.46 | 58.33 | 5.33 | 62.44 | 9 | 60 |
| glsv | 275.29 | 288470.75 | 52.78 | 6.48 | 73.19 | 359 | 2 |
| gmrc | 251.48 | 212.41 | 54.40 | 6.51 | 50.01 | 354 | 3 |
| gnps | 281.15 | 1060.49 | 90.79 | 6.63 | 53.79 | 246 | 90 |
| gode | 284.61 | 53.64 | 50.22 | 6.00 | 57.89 | 18 | 1445 |
| gol2 | 278.52 | 173.58 | 57.67 | 5.52 | 110.52 | 1969 | 2 |
| gold | 266.77 | 583.30 | 9.32 | 5.41 | 59.01 | 2023 | 2 |
| gope | 281.53 | 220247.74 | 49.99 | 8.77 | 49.69 | 1868 | 2 |
| goug | 281.02 | 288987.55 | 62.98 | 8.02 | 59.91 | 241 | 18 |
| graz | 278.23 | 3690.15 | 60.13 | 6.65 | 64.83 | 2096 | 2 |
| guam | 277.07 | 80514.35 | 66.95 | 8.73 | 58.38 | 2133 | 2 |
| hark | 281.51 | 37364.37 | 77.04 | 8.76 | 82.25 | 907 | 526 |
| hart | 271.83 | 103.15 | 29.95 | 7.90 | 53.64 | 688 | 1673 |
| harv | 280.43 | 6092143.55 | 67.98 | 7.39 | 50.37 | 2060 | 4 |
| hbco | 273.70 | 327.81 | 62.88 | 6.72 | 73.39 | 181 | 2 |
| hbrk | 279.77 | 286349.24 | 48.56 | 7.34 | 70.44 | 794 | 1547 |
| hcmn | 273.71 | 1747.45 | 48.03 | 6.18 | 75.30 | 320 | 2 |
| hers | 267.76 | 3185.02 | 11.51 | 6.55 | 68.15 | 1921 | 2 |
| hflk | 281.83 | 908075.58 | 76.79 | 6.45 | 72.86 | 1349 | 2 |
| hivi | 278.80 | 114.70 | 79.21 | 8.26 | 73.67 | 272 | 2 |
| hklo | 280.77 | 282860.59 | 49.44 | 7.32 | 94.09 | 817 | 1547 |
| hnps | 256.64 | 424.09 | 28.12 | 7.02 | 51.28 | 301 | 90 |
| hnpt | 279.67 | 5669.47 | 58.61 | 6.03 | 58.70 | 1312 | 2 |
| hob2 | 273.95 | 7354.92 | 51.34 | 7.69 | 92.95 | 1785 | 2 |
| hofn | 278.60 | 287607.48 | 51.82 | 7.63 | 95.30 | 1086 | 2 |
| holb | 280.33 | 28943.28 | 48.41 | 5.50 | 51.39 | 418 | 12 |
| holc | 276.63 | 162002.20 | 96.82 | 8.57 | 63.10 | 1941 | 56 |
| holp | 278.34 | 110836.00 | 60.56 | 8.64 | 73.92 | 1994 | 3 |
| hopb | 282.07 | 258231.67 | 59.27 | 6.90 | 59.86 | 1216 | 730 |
| hrao | 281.90 | 17986.23 | 63.36 | 7.77 | 71.45 | 1291 | 2 |
| hvlk | 281.97 | 288381.62 | 70.50 | 8.30 | 53.36 | 359 | 1499 |
| iid2 | 275.16 | 671.27 | 65.23 | 6.11 | 58.81 | 202 | 2 |
| iisc | 262.58 | 32554.54 | 75.66 | 10.00 | 63.26 | 1744 | 6 |
| ... | ... | ... | ... | ... | ... | ... | ... |

Table F.6: Station Performance Sample(Jan 21, 2002). (continued)

| site Id | epochs | clock | p-code Residual | Phase Residual | phase breaks | days Processed | Days Since Last Day processed |
|---|---|---|---|---|---|---|---|
| imps | 262.00 | 66.58 | 26.45 | 6.74 | 49.26 | 278 | 90 |
| ineg | 270.05 | 288850.00 | 60.29 | 5.75 | 182.09 | 220 | 5 |
| irkt | 282.71 | 8840.68 | 62.77 | 8.54 | 66.69 | 1946 | 3 |
| islk | 280.58 | 1297.22 | 30.93 | 6.73 | 52.79 | 421 | 3 |
| ivco | 277.01 | 961.15 | 62.06 | 6.34 | 54.74 | 234 | 2 |
| jab1 | 250.83 | 1788.98 | 49.96 | 6.36 | 179.40 | 366 | 65 |
| joze | 280.67 | 55741.66 | 62.44 | 8.09 | 64.88 | 2169 | 2 |
| jplm | 282.38 | 78368.41 | 41.20 | 5.85 | 51.90 | 2195 | 2 |
| karr | 272.12 | 59.31 | 41.05 | 7.00 | 63.80 | 388 | 23 |
| kely | 223.58 | 11767.18 | 55.72 | 7.04 | 81.97 | 1755 | 3 |
| kerg | 273.22 | 58090.94 | 16.00 | 7.95 | 70.79 | 1876 | 2 |
| kiru | 280.08 | 748.84 | 55.48 | 7.75 | 68.66 | 2132 | 2 |
| kit3 | 281.68 | 3782.68 | 68.10 | 9.29 | 75.79 | 1404 | 53 |
| kok2 | 266.16 | 692.49 | 44.26 | 9.62 | 51.94 | 166 | 2203 |
| kokb | 271.86 | 2060.18 | 58.04 | 6.78 | 66.83 | 2166 | 2 |
| kosg | 281.58 | 4295.25 | 41.20 | 6.17 | 66.21 | 2121 | 5 |
| kour | 258.25 | 24075.46 | 43.10 | 9.08 | 66.08 | 1962 | 76 |
| krak | 262.01 | 330.39 | 64.87 | 7.19 | 44.64 | 1172 | 591 |
| kstu | 255.67 | 105.11 | 40.78 | 7.68 | 110.87 | 755 | 26 |
| kunm | 231.38 | 1245.14 | 83.79 | 6.88 | 53.35 | 425 | 2 |
| kwj1 | 272.27 | 34065.60 | 67.09 | 7.95 | 79.45 | 1551 | 2 |
| lama | 268.04 | 83131.75 | 45.86 | 6.45 | 71.22 | 1739 | 2 |
| lanl | 147.00 | 85.20 | 37.50 | 6.00 | 27.50 | 2 | 2187 |
| lapc | 263.35 | 995.97 | 41.65 | 6.13 | 53.10 | 173 | 4 |
| lasc | 282.66 | 98332.10 | 42.46 | 6.64 | 64.98 | 839 | 3 |
| lbc1 | 282.16 | 1024.93 | 38.53 | 7.29 | 56.96 | 772 | 3 |
| lbc2 | 282.47 | 491.23 | 47.26 | 6.67 | 59.52 | 775 | 3 |
| lbch | 253.16 | 4104.65 | 61.96 | 6.42 | 219.03 | 1878 | 3 |
| ldes | 280.62 | 549.54 | 75.02 | 6.40 | 68.98 | 683 | 3 |
| ldsw | 273.05 | 597.41 | 45.01 | 5.92 | 61.34 | 196 | 2 |
| leep | 279.91 | 131784.72 | 67.70 | 6.72 | 51.61 | 1994 | 3 |
| lexi | 282.92 | 383.65 | 48.14 | 6.72 | 68.41 | 1923 | 2 |
| lfrs | 282.53 | 725.98 | 56.79 | 7.00 | 52.69 | 747 | 3 |
| lhas | 266.92 | 5955.19 | 57.32 | 9.14 | 68.12 | 1557 | 2 |
| llas | 276.98 | 784.48 | 77.37 | 6.58 | 76.33 | 563 | 3 |
| lmno | 283.83 | 288536.41 | 56.21 | 7.39 | 78.62 | 824 | 1547 |
| long | 276.47 | 148118.32 | 86.52 | 8.79 | 61.67 | 1985 | 3 |
| lors | 282.56 | 464.07 | 34.50 | 5.87 | 60.49 | 599 | 3 |
| lpgs | 263.72 | 104878.53 | 55.72 | 8.21 | 102.22 | 1677 | 7 |
| lphs | 280.64 | 1290.64 | 71.35 | 7.50 | 60.17 | 848 | 3 |
| lvms | 278.34 | 428.95 | 83.41 | 6.46 | 64.44 | 426 | 3 |
| mac1 | 273.36 | 1641.57 | 36.88 | 7.41 | 80.51 | 1784 | 2 |
| mad2 | 273.04 | 1401.77 | 65.89 | 6.66 | 121.71 | 1419 | 2 |
| madr | 266.00 | 242.69 | 10.99 | 6.75 | 66.52 | 2084 | 2 |
| mag0 | 278.74 | 19990.40 | 42.82 | 7.09 | 64.85 | 363 | 2 |
| mali | 264.65 | 32407.92 | 58.11 | 10.16 | 74.70 | 1797 | 2 |
| mas1 | 277.11 | 2511.64 | 45.65 | 6.72 | 62.91 | 1944 | 2 |
| mate | 265.92 | 1242.20 | 32.42 | 6.82 | 112.52 | 2175 | 2 |
| math | 282.72 | 289636.44 | 59.03 | 7.58 | 46.24 | 1246 | 11 |
| maw1 | 276.80 | 30.39 | 35.98 | 6.32 | 108.94 | 432 | 2 |
| mcm4 | 276.27 | 1106.61 | 43.44 | 8.27 | 92.96 | 2150 | 2 |
| mdo1 | 283.96 | 7631.48 | 45.29 | 6.19 | 54.15 | 2182 | 2 |
| mdvo | 272.08 | 22817.17 | 71.53 | 8.42 | 78.57 | 2091 | 2 |
| medi | 279.56 | 385.50 | 43.83 | 6.62 | 65.86 | 1460 | 2 |
| mets | 280.79 | 5094.31 | 52.73 | 6.27 | 72.86 | 2009 | 2 |
| mhms | 272.39 | 22970.94 | 74.64 | 8.37 | 63.50 | 317 | 3 |
| mig1 | 278.15 | 570.33 | 63.72 | 6.05 | 61.56 | 280 | 2 |
| mins | 277.43 | 285020.55 | 50.87 | 7.25 | 50.49 | 146 | 1321 |
| mkea | 280.61 | 230.33 | 49.45 | 7.64 | 66.18 | 1680 | 2 |
| mlfp | 282.78 | 1381.18 | 50.22 | 6.21 | 65.20 | 819 | 2 |
| moin | 278.24 | 1046.03 | 66.93 | 10.63 | 67.80 | 387 | 1397 |
| mola | 283.96 | 288050.37 | 64.19 | 8.45 | 44.41 | 675 | 1476 |
| monp | 280.84 | 143447.69 | 47.18 | 6.61 | 56.12 | 2060 | 2 |
| mpwd | 227.13 | 2163.67 | 51.43 | 5.49 | 252.29 | 782 | 2 |
| msob | 276.91 | 2643.79 | 56.73 | 6.73 | 75.85 | 850 | 2 |
| musd | 283.26 | 516.63 | 74.26 | 6.78 | 58.63 | 939 | 3 |
| mvfd | 278.89 | 938.68 | 68.36 | 7.32 | 84.26 | 691 | 2 |
| nall | 239.23 | 717.37 | 15.13 | 6.84 | 104.74 | 1811 | 2 |
| nano | 279.36 | 1625.82 | 61.69 | 5.73 | 79.51 | 435 | 2 |
| ... | ... | ... | ... | ... | ... | ... | ... |

Table F.6: Station Performance Sample(Jan 21, 2002). (continued)

| site Id | epochs | clock | p-code Residual | Phase Residual | phase breaks | days Processed | Days Since Last Day processed |
|---|---|---|---|---|---|---|---|
| nbps | 271.63 | 1416.86 | 126.15 | 6.01 | 59.94 | 390 | 2 |
| nico | 265.91 | 211.51 | 42.21 | 7.79 | 57.48 | 1054 | 2 |
| nist | 287.73 | 2.24 | 102.55 | 7.53 | 63.08 | 40 | 2185 |
| nlib | 284.31 | 2733.31 | 54.12 | 5.97 | 56.21 | 2216 | 2 |
| noco | 263.57 | 352.04 | 35.63 | 5.24 | 119.02 | 197 | 2 |
| nopk | 232.36 | 521.36 | 42.02 | 6.51 | 59.73 | 207 | 2 |
| noto | 284.30 | 15902.18 | 50.96 | 7.64 | 56.21 | 1564 | 502 |
| noum | 267.78 | 291278.22 | 69.80 | 7.67 | 88.22 | 930 | 2 |
| nrc1 | 285.01 | 29.23 | 63.78 | 6.11 | 56.88 | 1632 | 2 |
| nrc2 | 278.66 | 7.04 | 47.29 | 5.73 | 56.67 | 428 | 2 |
| nssp | 278.06 | 24.09 | 60.94 | 5.38 | 48.88 | 16 | 2 |
| ntus | 260.22 | 811.16 | 76.54 | 8.98 | 76.54 | 1032 | 3 |
| nune | 284.70 | 288396.67 | 40.85 | 7.92 | 43.03 | 721 | 1030 |
| nya1 | 279.26 | 21.53 | 32.26 | 5.52 | 123.84 | 421 | 2 |
| oaes | 280.92 | 917.82 | 59.88 | 6.50 | 61.11 | 657 | 3 |
| oat2 | 282.91 | 700.88 | 40.35 | 6.16 | 56.35 | 1821 | 429 |
| ober | 284.12 | 643.93 | 104.85 | 7.24 | 68.05 | 1415 | 429 |
| oghs | 281.53 | 1209.65 | 58.26 | 6.65 | 61.27 | 475 | 9 |
| ohig | 264.12 | 59412.48 | 56.43 | 9.59 | 85.40 | 1216 | 2 |
| onsa | 281.10 | 2400.44 | 44.00 | 6.13 | 78.46 | 2096 | 2 |
| opcl | 267.00 | 1294.14 | 33.31 | 5.68 | 106.79 | 397 | 2 |
| opcx | 271.65 | 4523.20 | 45.63 | 5.62 | 67.93 | 393 | 2 |
| oprd | 253.51 | 4358.77 | 50.98 | 5.82 | 148.07 | 328 | 2 |
| ores | 278.78 | 423.40 | 56.83 | 6.27 | 53.06 | 389 | 3 |
| ovls | 282.38 | 458.29 | 57.70 | 6.52 | 58.29 | 508 | 2 |
| oxyc | 258.19 | 45.25 | 34.29 | 5.79 | 56.02 | 360 | 3 |
| pama | 261.68 | 600.68 | 58.43 | 15.91 | 80.70 | 674 | 1743 |
| penc | 281.61 | 27267.49 | 55.71 | 8.32 | 63.11 | 1424 | 2 |
| pent | 285.62 | 18981.22 | 35.31 | 6.16 | 56.84 | 2224 | 2 |
| pert | 280.44 | 328.27 | 56.18 | 6.97 | 57.01 | 1991 | 2 |
| petp | 224.99 | 338.33 | 39.55 | 5.89 | 327.47 | 423 | 2 |
| phlb | 270.19 | 533.29 | 104.94 | 6.22 | 63.97 | 288 | 2 |
| pie1 | 284.87 | 19780.55 | 48.85 | 6.14 | 55.60 | 2228 | 2 |
| pimo | 249.44 | 34.51 | 91.28 | 6.90 | 63.43 | 348 | 2 |
| pin1 | 285.94 | 289125.00 | 38.31 | 9.44 | 45.38 | 16 | 1447 |
| pin2 | 283.39 | 47051.99 | 58.68 | 6.84 | 55.24 | 892 | 2 |
| piny | 281.40 | 167572.01 | 37.84 | 7.14 | 52.78 | 2142 | 2 |
| pltc | 283.90 | 289036.71 | 53.95 | 6.82 | 103.32 | 899 | 1548 |
| pmhs | 281.97 | 1257.89 | 69.65 | 6.61 | 62.97 | 1006 | 3 |
| pmob | 277.53 | 9090.59 | 46.65 | 6.27 | 61.98 | 775 | 2 |
| pol2 | 280.95 | 68748.14 | 55.18 | 8.65 | 63.77 | 1646 | 71 |
| potm | 265.54 | 228.47 | 70.79 | 6.54 | 57.04 | 484 | 1327 |
| pots | 280.86 | 2739.15 | 93.00 | 6.62 | 72.18 | 2145 | 2 |
| ppbf | 263.49 | 1351.65 | 42.28 | 6.09 | 163.16 | 784 | 2 |
| prds | 284.10 | 501.57 | 67.38 | 6.05 | 60.04 | 1300 | 2 |
| psap | 280.44 | 419.60 | 60.89 | 6.29 | 62.24 | 431 | 2 |
| psdm | 280.76 | 795.64 | 70.32 | 6.13 | 52.90 | 353 | 3 |
| pvep | 282.86 | 156668.04 | 67.69 | 9.37 | 57.01 | 1857 | 533 |
| pvhs | 281.62 | 333.57 | 75.43 | 6.46 | 62.84 | 651 | 3 |
| pvrs | 275.97 | 1398.80 | 61.61 | 7.47 | 106.82 | 830 | 3 |
| qhtp | 253.26 | 2177.59 | 55.39 | 6.35 | 115.67 | 288 | 2 |
| quin | 257.67 | 42371.10 | 57.89 | 6.71 | 51.12 | 1761 | 8 |
| ramo | 271.79 | 896.78 | 60.41 | 7.57 | 83.04 | 394 | 15 |
| rcm5 | 272.11 | 377.16 | 41.35 | 8.06 | 53.24 | 510 | 1905 |
| rcm6 | 283.75 | 124.02 | 71.69 | 8.19 | 56.59 | 632 | 1216 |
| rdmt | 272.32 | 1107.29 | 48.60 | 5.90 | 59.49 | 367 | 2 |
| reyk | 281.84 | 485.55 | 61.14 | 7.67 | 74.60 | 1802 | 2 |
| rhcl | 283.20 | 659.88 | 57.38 | 7.26 | 58.80 | 692 | 3 |
| riog | 264.00 | 1062.11 | 32.32 | 7.42 | 73.67 | 415 | 2 |
| riop | 234.51 | 386.10 | 64.90 | 6.48 | 75.60 | 523 | 22 |
| roch | 282.64 | 43662.66 | 47.32 | 7.30 | 54.75 | 1227 | 2 |
| rock | 283.00 | 166462.47 | 49.99 | 8.36 | 52.75 | 1867 | 3 |
| rstp | 279.92 | 2486.58 | 66.01 | 5.63 | 60.93 | 267 | 2 |
| rths | 267.27 | 7845.25 | 77.15 | 6.34 | 94.98 | 992 | 2 |
| sacy | 258.37 | 192.09 | 44.56 | 6.48 | 61.52 | 464 | 4 |
| sant | 249.70 | 37743.11 | 34.49 | 6.89 | 79.87 | 2089 | 2 |
| sbcc | 278.67 | 838.84 | 59.59 | 5.96 | 63.15 | 151 | 4 |
| sch2 | 283.63 | 3425.48 | 58.86 | 6.12 | 73.30 | 1348 | 2 |
| scia | 248.59 | 1982.11 | 48.09 | 5.65 | 139.81 | 658 | 3 |
| ... | ... | ... | ... | ... | ... | ... | ... |

Table F.6: Station Performance Sample(Jan 21, 2002). (continued)

| site Id | epochs | clock | p-code Residual | Phase Residual | phase breaks | days Processed | Days Since Last Day processed |
|---|---|---|---|---|---|---|---|
| scip | 279.59 | 1422.30 | 45.79 | 5.70 | 69.79 | 725 | 85 |
| scms | 280.19 | 1249.23 | 61.81 | 7.49 | 97.06 | 647 | 182 |
| sele | 281.57 | 150.54 | 58.45 | 7.98 | 61.29 | 1250 | 2 |
| sey1 | 229.21 | 1169699.85 | 73.39 | 11.25 | 66.53 | 308 | 2 |
| sfdm | 270.77 | 1958.96 | 58.81 | 5.85 | 51.10 | 195 | 2 |
| sfer | 272.00 | 3906.82 | 74.09 | 6.69 | 86.95 | 946 | 2 |
| sghs | 280.74 | 784.80 | 48.80 | 6.67 | 57.40 | 426 | 4 |
| sgps | 195.02 | 66.20 | 56.95 | 6.67 | 63.90 | 120 | 2 |
| shao | 283.66 | 4275.15 | 79.14 | 8.33 | 61.11 | 1509 | 2 |
| shk1 | 276.95 | 288061.30 | 83.27 | 8.51 | 49.61 | 715 | 1067 |
| silk | 274.39 | 1328.66 | 57.47 | 6.25 | 69.25 | 202 | 3 |
| sio3 | 274.57 | 142875.69 | 48.30 | 6.72 | 59.02 | 2048 | 2 |
| skyb | 281.30 | 19.74 | 55.83 | 6.13 | 46.70 | 23 | 182 |
| slms | 247.15 | 2271.79 | 49.46 | 5.77 | 235.56 | 418 | 2 |
| snhs | 280.98 | 861.71 | 59.55 | 7.32 | 69.11 | 692 | 2 |
| sni1 | 265.89 | 27161.39 | 34.45 | 6.06 | 61.32 | 1377 | 3 |
| sofi | 265.47 | 106.68 | 54.21 | 6.94 | 56.10 | 770 | 2 |
| soll | 281.08 | 9867.40 | 60.59 | 8.30 | 60.03 | 1934 | 2 |
| spk1 | 265.34 | 530204.25 | 35.75 | 6.28 | 68.69 | 1793 | 3 |
| spms | 281.46 | 10733.21 | 58.27 | 6.37 | 64.83 | 899 | 3 |
| stjo | 282.96 | 16018.37 | 46.20 | 6.29 | 59.62 | 2212 | 2 |
| stl3 | 274.02 | 287822.37 | 104.56 | 10.08 | 57.89 | 859 | 876 |
| str1 | 280.30 | 33.81 | 33.85 | 6.42 | 49.31 | 428 | 4 |
| strl | 281.50 | 384.91 | 54.56 | 6.58 | 56.54 | 614 | 1615 |
| suth | 275.28 | 80.07 | 74.18 | 6.11 | 55.50 | 357 | 2 |
| suwn | 279.34 | 230720.97 | 68.93 | 7.32 | 60.15 | 343 | 3 |
| syog | 277.61 | 129025.30 | 62.44 | 7.91 | 85.30 | 369 | 7 |
| tabl | 272.07 | 109166.08 | 140.91 | 6.86 | 62.78 | 1795 | 3 |
| taej | 278.91 | 159862.56 | 48.03 | 9.08 | 52.09 | 1002 | 1219 |
| tahi | 268.99 | 1126.47 | 80.17 | 11.74 | 61.89 | 254 | 1327 |
| tais | 261.45 | 83280.09 | 0.00 | 9.16 | 125.23 | 860 | 1511 |
| thti | 280.49 | 156998.65 | 78.63 | 8.30 | 74.46 | 412 | 2 |
| thu1 | 279.92 | 182.30 | 48.65 | 7.01 | 95.00 | 1806 | 78 |
| tibb | 276.13 | 356510.58 | 69.91 | 9.18 | 49.86 | 1190 | 730 |
| tid2 | 282.45 | 49.92 | 40.61 | 6.21 | 137.66 | 1980 | 98 |
| tidb | 284.60 | 14.15 | 66.27 | 12.27 | 60.20 | 15 | 1444 |
| tixi | 279.42 | 3336.08 | 41.74 | 6.58 | 92.93 | 397 | 2 |
| tmap | 280.03 | 308.25 | 40.03 | 6.38 | 59.08 | 426 | 2 |
| tmgo | 284.88 | 155.94 | 43.35 | 6.45 | 53.76 | 897 | 1548 |
| torp | 278.49 | 669.60 | 48.61 | 6.10 | 88.82 | 1393 | 3 |
| tost | 280.76 | 2036.84 | 53.27 | 6.24 | 60.53 | 418 | 2 |
| toul | 282.82 | 219.80 | 69.00 | 7.21 | 59.99 | 749 | 430 |
| tow2 | 279.99 | 78.65 | 20.96 | 6.83 | 52.95 | 415 | 2 |
| trak | 279.25 | 144476.27 | 76.55 | 7.67 | 47.39 | 1837 | 2 |
| tro1 | 281.30 | 20.51 | 58.74 | 6.83 | 96.74 | 423 | 2 |
| trom | 241.11 | 100459.41 | 14.65 | 6.62 | 91.14 | 1473 | 2 |
| tskb | 283.96 | 76796.84 | 53.96 | 7.42 | 54.66 | 2113 | 3 |
| uclp | 284.73 | 1579.43 | 36.53 | 6.36 | 52.75 | 2016 | 3 |
| uclu | 280.37 | 62.34 | 53.81 | 5.92 | 70.12 | 410 | 2 |
| ucsb | 282.12 | 526.37 | 45.87 | 7.06 | 57.32 | 701 | 2 |
| upad | 272.53 | 420760.88 | 70.97 | 8.29 | 89.92 | 1704 | 61 |
| urum | 281.49 | 180.30 | 37.50 | 8.05 | 59.95 | 384 | 2 |
| usc1 | 283.07 | 621.27 | 61.27 | 7.42 | 52.34 | 2096 | 3 |
| usgc | 277.91 | 157.75 | 41.62 | 5.74 | 54.69 | 202 | 2 |
| usna | 282.89 | 531.31 | 66.83 | 6.94 | 64.38 | 1827 | 2 |
| usno | 280.96 | 7.20 | 56.29 | 7.12 | 54.51 | 1360 | 2 |
| usud | 285.05 | 386.88 | 42.12 | 6.64 | 56.06 | 2161 | 2 |
| uzhl | 270.69 | 288929.96 | 92.01 | 7.05 | 62.58 | 257 | 3 |
| vcio | 280.71 | 289017.12 | 53.47 | 7.61 | 82.89 | 876 | 1548 |
| vene | 273.45 | 134348.41 | 61.10 | 6.53 | 57.66 | 411 | 2 |
| vesl | 281.16 | 289692.77 | 58.05 | 7.96 | 86.80 | 166 | 33 |
| vill | 280.26 | 426.78 | 51.81 | 6.79 | 55.92 | 2080 | 2 |
| vims | 285.71 | 101.36 | 43.59 | 6.70 | 55.13 | 922 | 896 |
| vncx | 242.75 | 1668.35 | 60.54 | 6.62 | 65.11 | 493 | 3 |
| vndp | 280.32 | 129241.02 | 36.50 | 6.67 | 54.06 | 2086 | 3 |
| vnps | 279.48 | 189.94 | 43.05 | 6.56 | 55.28 | 399 | 3 |
| vtis | 267.89 | 1276.34 | 37.51 | 5.95 | 91.50 | 685 | 3 |
| vyas | 283.29 | 975.25 | 52.44 | 6.68 | 56.16 | 1015 | 3 |
| wchs | 282.41 | 1257.70 | 65.35 | 6.90 | 59.99 | 815 | 3 |
| ... | ... | ... | ... | ... | ... | ... | ... |

Table F.6: Station Performance Sample(Jan 21, 2002). (continued)

| site Id | epochs | clock | p-code Residual | Phase Residual | phase breaks | days Processed | Days Since Last Day processed |
|---|---|---|---|---|---|---|---|
| wes2 | 287.86 | 43.11 | 69.46 | 5.60 | 59.46 | 35 | 991 |
| west | 278.88 | 9024.26 | 54.44 | 6.42 | 65.55 | 1939 | 2 |
| wetb | 258.83 | 9.61 | 0.00 | 7.43 | 103.58 | 642 | 1814 |
| wgpp | 160.81 | 27.83 | 48.25 | 6.31 | 40.28 | 32 | 138 |
| whcl | 283.90 | 337465.36 | 46.95 | 6.55 | 54.99 | 2070 | 3 |
| whil | 276.30 | 29814.26 | 57.51 | 6.36 | 50.88 | 809 | 1649 |
| whit | 281.72 | 6916.32 | 56.85 | 6.05 | 86.24 | 1788 | 2 |
| widc | 283.99 | 4093.05 | 47.82 | 7.57 | 56.06 | 1033 | 2 |
| will | 281.59 | 302.47 | 36.22 | 5.53 | 63.91 | 432 | 2 |
| wint | 280.20 | 252288.67 | 66.29 | 7.60 | 51.28 | 1399 | 735 |
| wkpk | 263.55 | 313.25 | 60.13 | 7.09 | 68.88 | 220 | 2 |
| wlps | 285.27 | 134.50 | 95.83 | 7.25 | 50.78 | 805 | 1322 |
| wlsn | 273.24 | 744.74 | 63.48 | 8.02 | 55.04 | 2089 | 3 |
| wmap | 282.56 | 4724.02 | 52.12 | 7.56 | 58.81 | 831 | 3 |
| womt | 277.94 | 1832.62 | 42.98 | 6.18 | 58.34 | 200 | 2 |
| wrhs | 238.01 | 2609.42 | 50.40 | 6.43 | 76.81 | 422 | 3 |
| wslr | 281.68 | 4611.62 | 32.17 | 5.82 | 52.14 | 432 | 2 |
| wsmn | 280.17 | 287508.23 | 61.94 | 8.42 | 109.56 | 887 | 1548 |
| wsrt | 280.68 | 32298.80 | 36.20 | 6.34 | 70.58 | 1260 | 2 |
| wtzr | 277.41 | 828.04 | 61.48 | 6.89 | 61.19 | 1905 | 2 |
| wtzt | 260.17 | 286693.74 | 71.41 | 6.01 | 260.33 | 431 | 2 |
| wuhn | 277.97 | 6513.08 | 59.62 | 8.99 | 62.56 | 1789 | 2 |
| xian | 279.30 | 27809.16 | 51.75 | 9.17 | 59.50 | 999 | 803 |
| yakz | 283.27 | 878.30 | 51.81 | 7.48 | 72.25 | 222 | 430 |
| yarl | 273.42 | 38048.49 | 31.60 | 5.99 | 65.43 | 2082 | 2 |
| yell | 284.31 | 1974.99 | 45.86 | 6.14 | 96.29 | 2223 | 2 |
| yssk | 281.10 | 1238.98 | 46.38 | 6.95 | 55.83 | 423 | 2 |
| zeck | 283.24 | 1186.64 | 55.59 | 7.30 | 65.03 | 1120 | 7 |
| zimm | 275.70 | 280414.97 | 63.88 | 7.60 | 76.82 | 2156 | 2 |
| zwen | 273.50 | 5178.07 | 65.46 | 7.57 | 77.37 | 1944 | 2 |

Table F.7: Daily Performance of Stations for cyc 8

| site | day 84 | day 85 | day 86 | day 87 | day 88 | day 89 | day 90 | day 91 | day 92 | day 93 | day 94 |
|---|---|---|---|---|---|---|---|---|---|---|---|
| albh | . | 10 | 10 | 10 | 10 | 10 | 10 | 10 | 10 | 10 | 10 |
| algo | 10 | 10 | 10 | 10 | 10 | 10 | 10 | 10 | 10 | 10 | 10 |
| alic | 10 | 10 | 10 | 10 | 10 | 10 | 10 | 10 | 10 | 10 | 10 |
| amc2 | 10 | 10 | 10 | 10 | 10 | 10 | 10 | 10 | 10 | 10 | 10 |
| ankr | . | 10 | 10 | 10 | 10 | 10 | 10 | 10 | 10 | 10 | 10 |
| aoa1 | 10 | 10 | 10 | 10 | 10 | 10 | 10 | 10 | 10 | 10 | 10 |
| aoml | 10 | 10 | 10 | 10 | 10 | 10 | 10 | 10 | 10 | 8 | 10 |
| areq | 10 | 10 | 10 | 10 | . | . | . | . | . | . | . |
| artu | 10 | 10 | 10 | 10 | 10 | 10 | 10 | 10 | 10 | 10 | 10 |
| asc1 | 10 | 10 | 8 | 10 | . | 10 | 10 | 10 | 10 | 10 | 10 |
| auck | 10 | 10 | 10 | 10 | 10 | 10 | 10 | 10 | 10 | 10 | 10 |
| azu1 | 10 | 10 | 10 | 10 | 10 | 10 | 8 | 10 | 10 | 10 | 10 |
| bahr | . | 10 | 10 | 8 | 10 | 10 | 10 | 10 | 10 | 10 | 8 |
| bako | . | . | . | . | . | . | . | . | . | . | . |
| barb | . | . | . | . | . | . | . | . | . | . | . |
| bili | 10 | 10 | 10 | 10 | 10 | 10 | 10 | 10 | 10 | 10 | 10 |
| bjfs | . | . | 8 | 10 | 10 | 8 | 10 | 10 | 10 | 10 | 10 |
| blyt | 10 | 10 | 10 | 10 | 10 | 10 | 10 | 10 | 10 | 10 | 10 |
| bogt | . | . | . | . | . | . | . | . | . | . | . |
| bor1 | . | 10 | 10 | 10 | 10 | 10 | 10 | 10 | 10 | 10 | 10 |
| bran | 10 | 10 | 10 | 10 | 10 | 10 | 10 | 10 | 10 | 10 | 10 |
| braz | . | . | . | . | . | . | . | . | . | . | . |
| brmu | 10 | 10 | 10 | 10 | 10 | 10 | 10 | 10 | 10 | 10 | 10 |
| brus | . | 8 | 10 | 10 | 10 | 10 | 10 | 10 | 10 | 10 | 6 |
| bucu | . | 10 | 10 | 10 | 10 | 10 | 10 | 10 | 10 | 10 | 10 |
| bzrg | . | 8 | 10 | 8 | 10 | 10 | 10 | 10 | 10 | 10 | 10 |
| cagl | . | 10 | 10 | 10 | 10 | 10 | 6 | 10 | 10 | 10 | 10 |
| cas1 | 8 | . | 8 | 8 | 8 | 6 | 8 | 8 | 8 | 8 | 8 |
| casa | 10 | 10 | 8 | 8 | 8 | 10 | 10 | 10 | 10 | 10 | 10 |
| cat1 | 10 | 10 | 10 | 10 | 10 | 10 | 10 | 10 | 10 | 10 | 10 |
| cedu | . | . | 10 | 10 | 10 | 10 | 10 | 10 | . | 10 | 10 |
| chat | 10 | 10 | 10 | 10 | 10 | 10 | 10 | 10 | 10 | 10 | 10 |
| chil | 10 | 10 | 10 | 10 | 10 | 10 | 10 | 10 | 10 | 10 | 10 |
| chur | 10 | 8 | 10 | 10 | 10 | 10 | . | 10 | 10 | 10 | 10 |
| chwk | . | 10 | 10 | 10 | 10 | 10 | 10 | 10 | 10 | 8 | 8 |
| cic1 | 8 | 10 | 10 | 10 | 10 | 10 | 10 | 10 | 10 | 10 | 10 |
| cit1 | 10 | 10 | 10 | 10 | 10 | 10 | 10 | 10 | 10 | 10 | 10 |
| clar | . | . | . | . | . | . | . | . | . | . | . |
| cmp9 | . | . | . | 10 | 10 | 10 | 10 | 10 | 10 | 10 | 10 |
| coco | . | . | 10 | 10 | 10 | 10 | 10 | 10 | 10 | 10 | 10 |
| cord | . | . | . | . | . | . | . | . | . | . | . |
| coso | 10 | 10 | 10 | 10 | 10 | 10 | 10 | 10 | 10 | 10 | . |
| crfp | 10 | 10 | 10 | 10 | 10 | 10 | 10 | 10 | 10 | 10 | 10 |
| cro1 | 10 | 10 | 10 | 10 | 10 | 10 | 10 | 10 | 10 | 10 | 10 |
| csn1 | 10 | 10 | 10 | 10 | 10 | 10 | 10 | 10 | 10 | 10 | 10 |
| daej | . | . | 8 | 8 | 8 | 8 | 8 | . | 8 | 8 | 8 |
| darw | . | . | . | . | . | . | . | . | . | 8 | 0 |
| dav1 | 8 | 8 | 8 | . | 8 | 6 | 8 | 6 | 8 | 8 | 8 |
| dgar | . | . | . | . | . | . | . | . | . | . | . |
| dhlg | . | . | . | . | . | . | . | . | . | 10 | 10 |
| drag | 4 | 6 | 2 | . | . | . | . | . | . | . | . |
| drao | . | 10 | 10 | 10 | 10 | 10 | 10 | 10 | 10 | 10 | 10 |
| dubo | . | 10 | 10 | 10 | 10 | 10 | 10 | 10 | 10 | 10 | 10 |
| ebre | . | 10 | 10 | 10 | 10 | 10 | 10 | 10 | 10 | 10 | 10 |
| eisl | 8 | 8 | 8 | 8 | 8 | 8 | 8 | 8 | 8 | 6 | 8 |
| fair | 8 | 8 | 8 | 8 | 8 | 6 | 8 | 6 | 6 | 8 | 8 |
| flin | . | 10 | 10 | 10 | 10 | 10 | 10 | 10 | 10 | 10 | 10 |
| fort | 8 | 10 | 8 | 10 | 8 | 8 | 8 | 10 | 8 | 8 | 6 |
| gala | 10 | 10 | 10 | 10 | 10 | 10 | 10 | 10 | 10 | 10 | 10 |
| geno | . | 10 | 10 | 10 | 10 | 10 | 10 | 10 | 10 | 10 | 10 |
| glsv | . | 10 | 10 | 10 | 10 | 10 | 10 | 10 | 10 | 10 | 10 |
| gode | 8 | 10 | 6 | 6 | 4 | 6 | 4 | . | . | . | . |
| gold | 10 | 10 | 10 | 10 | 10 | 10 | 8 | 10 | 10 | 10 | 10 |
| gope | . | 10 | 10 | 10 | 10 | 10 | 10 | 10 | 10 | 10 | 10 |
| goug | . | . | . | . | . | . | . | . | . | . | . |
| gras | . | 10 | 8 | 10 | 10 | 10 | 8 | 8 | 8 | 8 | 8 |
| graz | . | 10 | 10 | 10 | 10 | 10 | 10 | 10 | 10 | 10 | 10 |
| guam | 8 | 10 | 8 | 8 | 8 | 10 | 10 | 10 | 10 | 10 | 10 |
| harv | 10 | 8 | 10 | 10 | 10 | 10 | 10 | 10 | 10 | 10 | 10 |
| hers | . | 10 | 10 | 10 | 10 | 10 | 10 | 10 | 10 | . | . |
| hflk | . | 10 | 10 | 10 | 10 | 10 | 10 | 10 | 10 | 10 | 10 |
| ... | ... | ... | ... | ... | ... | ... | ... | ... | ... | ... | ... |

Table F.7: Daily Performance of Stations for cyc 8. (continued)

| site | day 84 | day 85 | day 86 | day 87 | day 88 | day 89 | day 90 | day 91 | day 92 | day 93 | day 94 |
|---|---|---|---|---|---|---|---|---|---|---|---|
| hnpt | 10 | 10 | 10 | 10 | 10 | 10 | 10 | 10 | 10 | 10 | 10 |
| hob2 | 8 | 8 | . | . | 10 | 8 | 10 | 10 | 10 | 10 | 10 |
| hofn | . | 10 | 10 | 10 | 10 | 8 | 8 | 8 | 10 | 8 | 10 |
| holb | . | 10 | 10 | 10 | 10 | 10 | 10 | 10 | 8 | 10 | 10 |
| holc | 8 | 8 | 8 | 8 | 10 | 8 | 8 | 8 | 8 | 8 | 8 |
| holp | . | . | . | 0 | 8 | 0 | 10 | 10 | 10 | 10 | 10 |
| hrao | 10 | 10 | 10 | 10 | 10 | 10 | 10 | 10 | 10 | 10 | 10 |
| iisc | . | . | . | . | 8 | 8 | 10 | 10 | 10 | 8 | 8 |
| ineg | . | . | . | . | . | . | . | . | . | . | . |
| irkt | . | 10 | 10 | 8 | . | 10 | 10 | 10 | 10 | . | 8 |
| jab1 | . | . | . | . | . | . | . | . | . | . | . |
| jama | 10 | 10 | 8 | . | 8 | 10 | . | . | . | 10 | 8 |
| joze | . | 10 | 10 | 10 | 10 | 10 | 10 | 10 | 10 | 10 | 10 |
| jplm | 10 | 10 | 10 | 10 | 10 | 10 | 10 | 10 | 10 | 10 | 10 |
| karr | 10 | . | 10 | 10 | 10 | 10 | 10 | 10 | 10 | 10 | 10 |
| kely | 8 | 6 | . | 8 | 10 | 6 | 8 | 8 | 8 | 6 | 8 |
| kerg | . | 10 | 10 | 10 | 10 | 10 | 8 | 10 | 6 | 8 | 6 |
| kiru | . | 8 | 10 | 10 | 10 | 10 | 10 | 10 | 10 | 10 | 10 |
| kit3 | . | . | . | . | . | . | . | . | . | . | . |
| kokb | . | . | . | . | . | . | . | . | . | 10 | 10 |
| kosg | . | . | . | . | . | . | 10 | 10 | 10 | 10 | 10 |
| kour | . | . | 8 | 8 | 10 | 10 | 8 | 10 | 10 | 8 | 8 |
| kr0g | | | | | | | | | | | |
| kstu | . | . | . | 10 | 10 | 10 | 10 | 10 | 10 | 10 | 10 |
| kunm | 6 | 4 | 4 | 4 | 4 | 4 | 4 | 4 | 4 | 0 | 6 |
| kwj1 | 4 | 6 | 4 | 2 | 2 | 4 | 6 | 4 | 4 | 2 | 4 |
| lama | . | 10 | 10 | 10 | 10 | 10 | 10 | 10 | 10 | 10 | 10 |
| lbch | 10 | 10 | 10 | 10 | 10 | 10 | 10 | 10 | 10 | 10 | 10 |
| leep | 10 | 10 | 10 | 10 | 10 | 10 | 10 | 10 | 10 | 10 | 10 |
| lhas | 10 | . | 10 | . | . | . | 10 | 10 | 10 | 10 | 10 |
| long | 10 | 10 | 10 | 10 | 10 | 10 | 10 | 10 | 10 | 10 | 10 |
| lpgs | . | 10 | 10 | 10 | 10 | 10 | 8 | 10 | 10 | 10 | 10 |
| mac1 | 10 | . | 10 | 10 | 10 | 8 | 10 | 10 | 10 | 10 | 10 |
| madr | 10 | 10 | 10 | 10 | 10 | 10 | 10 | 10 | 10 | 10 | 10 |
| mag0 | 10 | 10 | 10 | 10 | 10 | 10 | 10 | 10 | 10 | 10 | 10 |
| mali | 8 | 10 | 8 | 10 | 10 | 10 | 10 | 10 | 10 | 10 | 10 |
| mas1 | . | . | . | . | . | . | . | . | . | . | . |
| mate | . | 6 | 8 | 10 | 10 | 10 | 10 | 10 | 10 | 4 | 8 |
| math | . | . | . | . | . | . | . | . | . | . | . |
| maw1 | 10 | . | 10 | 10 | 10 | 8 | 8 | 8 | 8 | 8 | 10 |
| mcm4 | 6 | 4 | 6 | 6 | 6 | 6 | 6 | 4 | 4 | 6 | 6 |
| mdo1 | 10 | 10 | 10 | 10 | 10 | 10 | 10 | 10 | 10 | 10 | 10 |
| mdvo | 8 | 10 | 10 | . | . | 10 | 6 | 6 | 10 | 8 | 8 |
| medi | . | 10 | 10 | 10 | 10 | 10 | 10 | 10 | 10 | 10 | 10 |
| mets | . | 10 | 10 | 10 | 10 | 10 | 10 | 10 | 10 | 10 | 10 |
| mkea | 10 | 10 | 10 | 10 | 10 | 10 | 10 | 10 | 10 | 10 | 10 |
| monp | . | 10 | . | . | . | . | 10 | 10 | 10 | 10 | 10 |
| mr6g | | | | | | | | | | | |
| nano | . | 8 | 10 | 10 | 6 | 10 | 10 | 10 | 8 | 8 | 10 |
| nico | . | 10 | 10 | 10 | 10 | 10 | 10 | 10 | 10 | 10 | 10 |
| nklg | . | 10 | 10 | 10 | . | 10 | 10 | 10 | 10 | 10 | 10 |
| nlib | 10 | 10 | 10 | 10 | 10 | 10 | 10 | 10 | 10 | 10 | 10 |
| noto | . | . | . | . | . | . | . | . | . | . | . |
| noum | . | 10 | 10 | 10 | . | 10 | 10 | 10 | 10 | 10 | 10 |
| nrc1 | 10 | 10 | 10 | 10 | 10 | 10 | 10 | 10 | 10 | 10 | 10 |
| nssp | . | . | . | . | . | . | . | . | . | . | . |
| ntus | . | 10 | 10 | 10 | 10 | . | 10 | 10 | 10 | 10 | 10 |
| nya1 | . | 4 | 6 | 6 | 6 | . | 6 | 6 | 4 | 4 | 6 |
| nyal | . | 8 | 8 | 8 | 8 | . | 8 | 8 | 8 | 8 | 8 |
| oat2 | . | . | . | . | . | . | . | . | . | . | . |
| onsa | . | 10 | 10 | 10 | 10 | 10 | 10 | 10 | 10 | 10 | 10 |
| penc | . | 10 | 10 | 10 | 10 | 10 | 10 | 10 | 10 | 10 | 10 |
| pert | . | 10 | 10 | 10 | 10 | 10 | 10 | 10 | 10 | 10 | 10 |
| petp | 6 | 10 | 10 | 10 | 10 | 10 | 10 | 10 | 10 | 10 | 10 |
| pie1 | 10 | 10 | 10 | 10 | 10 | 10 | 10 | 10 | 10 | 10 | 10 |
| pimo | 6 | 8 | 6 | 8 | 6 | 8 | 10 | 8 | 8 | 4 | 6 |
| pol2 | 10 | 10 | 10 | 10 | 10 | 10 | 10 | 10 | 10 | 10 | 10 |
| pots | . | 10 | 10 | 10 | 10 | 10 | 10 | 10 | 10 | 10 | 10 |
| prds | 10 | 10 | 10 | 10 | 10 | 10 | 10 | 10 | 10 | 10 | 10 |
| pvep | . | . | . | . | . | . | . | . | . | . | . |
| ... | ... | ... | ... | ... | ... | ... | ... | ... | ... | ... | ... |

Table F.7: Daily Performance of Stations for cyc 8. (continued)

| site | day 84 | day 85 | day 86 | day 87 | day 88 | day 89 | day 90 | day 91 | day 92 | day 93 | day 94 |
|---|---|---|---|---|---|---|---|---|---|---|---|
| quin | 10 | 10 | 10 | 10 | 10 | 10 | 10 | 10 | 10 | 10 | 10 |
| ramo | 10 | 10 | 10 | 10 | 10 | 10 | . | . | . | . | . |
| reyk | . | 10 | 10 | 10 | 10 | 8 | 10 | 10 | 10 | 8 | 10 |
| riog | . | 10 | 10 | 10 | 10 | 8 | 10 | 8 | 10 | 10 | 10 |
| riop | . | . | . | . | . | . | . | . | . | . | . |
| roch | 10 | 10 | 10 | 10 | 10 | 10 | 10 | 10 | 10 | 10 | 10 |
| rock | 10 | 10 | 10 | 10 | 10 | 10 | 10 | 10 | 10 | 10 | 10 |
| sant | 10 | 10 | 10 | 10 | 10 | 10 | 10 | 10 | 10 | 10 | 8 |
| sch2 | 10 | 10 | 10 | 10 | 10 | 10 | 10 | 10 | 10 | 10 | 10 |
| scip | 10 | 10 | 10 | 10 | 10 | 10 | 10 | 10 | 10 | 10 | 10 |
| sele | 10 | 10 | 10 | 10 | 10 | 10 | 10 | 10 | 10 | 10 | . |
| sey1 | 6 | 4 | 6 | 6 | 6 | 6 | 6 | 6 | 6 | 6 | 6 |
| sfer | . | 6 | 4 | 4 | 4 | . | 4 | 8 | 10 | 10 | 10 |
| shao | 8 | 4 | 6 | 8 | 8 | 8 | 8 | 8 | 8 | 8 | 8 |
| sio3 | 10 | 10 | 10 | 10 | 10 | 10 | 10 | 10 | 10 | 10 | 10 |
| snil | 10 | 10 | 10 | 10 | 10 | 10 | 10 | 10 | 10 | 10 | 10 |
| sofi | . | 10 | 10 | 10 | . | 10 | 10 | 10 | 10 | 10 | 10 |
| sol1 | 10 | 10 | 10 | 10 | 10 | 10 | 10 | 10 | 10 | 10 | 10 |
| spk1 | 10 | 10 | 10 | 10 | 10 | 10 | 10 | 10 | 10 | 10 | 10 |
| stjo | 10 | 10 | 10 | 10 | 10 | 10 | 10 | 10 | 10 | 10 | 10 |
| suth | 10 | 10 | 10 | 10 | 10 | 10 | 10 | 10 | 10 | 10 | 10 |
| suwn | . | . | . | 10 | . | 10 | 10 | 10 | 10 | 10 | . |
| syog | . | 10 | 10 | . | . | 8 | 10 | 8 | 8 | 10 | 10 |
| tabl | 8 | 8 | 8 | 8 | 8 | 8 | 8 | 8 | 8 | 8 | 8 |
| thti | . | . | 10 | 10 | 10 | 10 | 10 | 10 | 10 | 10 | 10 |
| thu1 | . | . | 8 | 8 | 8 | 8 | 0 | 8 | 8 | 8 | 6 |
| tidb | 10 | 10 | 10 | 10 | 10 | 10 | 10 | 10 | 10 | 10 | 10 |
| tixi | 8 | 8 | 10 | 10 | 10 | 8 | 10 | 10 | 10 | 10 | 10 |
| torp | . | . | . | . | . | . | . | . | . | . | . |
| tow2 | 10 | 10 | 10 | 10 | 10 | 10 | 10 | 10 | 10 | 10 | 10 |
| trab | . | 8 | 10 | 10 | 10 | 10 | 10 | 10 | 10 | 10 | 10 |
| trak | 10 | 10 | 10 | 10 | 10 | 10 | 10 | . | . | . | 10 |
| tro1 | . | 10 | 10 | 10 | 10 | 8 | 8 | 10 | 10 | 8 | 10 |
| trom | . | 10 | 10 | 10 | 10 | 8 | 8 | 10 | 10 | 8 | 10 |
| tskb | . | 10 | 10 | . | . | 8 | 8 | 10 | 8 | 8 | 10 |
| uclp | 10 | 10 | 10 | 10 | 10 | 10 | 10 | 10 | 10 | 10 | 10 |
| uclu | . | 10 | 10 | 10 | 10 | 10 | 10 | 10 | 10 | 10 | 10 |
| urum | 10 | 10 | . | 10 | 10 | 10 | 10 | 10 | 10 | 10 | 10 |
| usc1 | 10 | 10 | 10 | 10 | 10 | 10 | 10 | 10 | 10 | 10 | 10 |
| usna | 10 | 8 | 8 | 10 | 10 | 10 | 8 | 10 | 10 | 10 | 10 |
| usno | . | . | . | . | . | . | . | . | . | . | . |
| usud | 10 | 10 | 10 | 10 | 10 | 10 | 10 | 10 | 10 | 10 | 10 |
| vene | . | 10 | 10 | 6 | 8 | 10 | 10 | 10 | 10 | 10 | 10 |
| vesl | . | . | . | . | . | . | . | . | . | . | . |
| vill | . | 10 | 10 | 10 | 10 | 10 | 10 | 10 | 10 | 10 | 10 |
| vndp | . | 10 | 10 | 10 | 10 | 10 | 10 | 10 | 10 | 10 | 10 |
| vs0g | | | | | | | | | | | |
| wes2 | 8 | . | . | . | . | . | . | . | 10 | 10 | 8 |
| whc1 | 10 | 10 | 10 | 10 | 10 | 10 | 10 | 10 | 10 | 10 | 10 |
| whit | 10 | 10 | 10 | 10 | 10 | 8 | 10 | 8 | 10 | 10 | 10 |
| widc | 10 | 10 | 10 | 10 | 10 | 10 | 10 | 10 | 10 | 10 | 10 |
| will | . | 10 | 10 | 10 | 10 | 10 | 10 | 10 | 10 | 10 | 10 |
| wlsn | 10 | 10 | 10 | 10 | 10 | 10 | 10 | 10 | 10 | 10 | 10 |
| wroc | | | | | | | | | | | |
| wslr | . | 10 | 10 | 10 | 10 | 10 | 10 | 10 | 10 | 10 | 10 |
| wsrt | . | 10 | 10 | 10 | 10 | 10 | 10 | 10 | 10 | 10 | 10 |
| wtzr | . | 10 | 10 | 10 | 10 | 10 | 10 | 10 | 10 | 10 | 10 |
| wuhn | . | 0 | 8 | 8 | 8 | 10 | 10 | . | 8 | 8 | 10 |
| xian | . | . | . | . | . | . | . | . | . | . | . |
| yakz | . | . | . | . | . | . | . | . | . | . | . |
| yar1 | 8 | 10 | 10 | 10 | 8 | 10 | 8 | 10 | 10 | 10 | 10 |
| yell | 10 | 8 | 10 | 10 | 10 | 8 | 10 | 8 | 10 | 8 | 10 |
| ykro | . | . | . | . | . | . | . | . | . | . | . |
| yssk | 10 | 10 | 10 | 10 | 10 | 10 | 10 | 10 | 10 | 10 | 10 |
| zeck | . | . | 10 | . | . | . | . | . | . | . | . |
| zimm | . | 10 | 10 | 10 | 10 | 10 | 10 | 10 | 10 | 10 | 10 |
| zwen | . | 10 | 10 | 10 | 10 | 10 | 10 | 10 | 10 | 8 | 6 |

### F.2.3 Station daily DDobs numbers

Table F.8: Daily DDobs numbers for cycle 8

| site ID | day 84 | day 85 | day 86 | day 87 | day 88 | day 89 | day 90 | day 91 | day 92 | day 93 | day 94 |
|---|---|---|---|---|---|---|---|---|---|---|---|
| albh | 54 | 89 | 135 | 113 | 164 | 119 | 15 | 39 | 129 | 202 | 113 |
| algo | 3264 | 3014 | 2994 | 3071 | 3410 | 2812 | 2830 | 3337 | 3315 | 3105 | 2926 |
| alic | 3608 | 3530 | 3527 | 3437 | 3574 | 3476 | 3321 | 3866 | 3690 | 3495 | 3605 |
| amc2 | 3170 | 2873 | 2755 | 2713 | 3224 | 2496 | 2589 | 3138 | 3091 | 2635 | 2674 |
| ankr | 3767 | 3644 | 3682 | 3673 | 3641 | 3306 | 3584 | 3738 | 3600 | 3477 | 3264 |
| aoa1 | 2604 | 2349 | 2283 | 2327 | 2668 | 2309 | 2283 | 2579 | 2415 | 2245 | 2429 |
| aoml | 2628 | 2390 | 2388 | 2097 | 2781 | 2433 | 2277 | 2287 | 2578 | 2254 | 2329 |
| areq | 3389 | 3219 | 3098 | 3240 | 1913 | 0 | 0 | 0 | 0 | 0 | 0 |
| artu | 3818 | 3817 | 3830 | 3584 | 3663 | 3862 | 3775 | 3868 | 3916 | 3788 | 3623 |
| asc1 | 3414 | 3029 | 2856 | 2556 | 0 | 2453 | 3130 | 3377 | 3231 | 3272 | 3227 |
| auck | 3247 | 3496 | 3312 | 3004 | 3293 | 3524 | 3232 | 3226 | 3357 | 3269 | 3186 |
| azu1 | 0 | 0 | 0 | 0 | 0 | 0 | 0 | 0 | 0 | 0 | 0 |
| bahr | 3416 | 3397 | 3447 | 3282 | 2951 | 3146 | 3479 | 3555 | 3488 | 3204 | 3223 |
| bako | 0 | 0 | 0 | 0 | 0 | 0 | 0 | 0 | 0 | 0 | 0 |
| barb | 0 | 0 | 0 | 0 | 0 | 0 | 0 | 0 | 0 | 0 | 0 |
| bili | 4459 | 4197 | 4071 | 3740 | 4189 | 4071 | 3868 | 4164 | 3977 | 3649 | 3846 |
| bjfs | 3602 | 3351 | 3440 | 3283 | 3195 | 3500 | 3421 | 3653 | 3283 | 3012 | 3186 |
| blyt | 0 | 0 | 0 | 0 | 0 | 0 | 0 | 0 | 0 | 0 | 0 |
| bogt | 0 | 0 | 0 | 0 | 0 | 0 | 0 | 0 | 0 | 0 | 0 |
| bor1 | 3132 | 3142 | 3461 | 3460 | 3077 | 2956 | 3318 | 3575 | 3262 | 3301 | 3066 |
| bran | 0 | 0 | 0 | 0 | 0 | 0 | 0 | 0 | 0 | 0 | 0 |
| braz | 3504 | 2908 | 3079 | 2486 | 2973 | 2724 | 3156 | 3697 | 3211 | 3149 | 3399 |
| brmu | 2937 | 2838 | 2662 | 2862 | 2839 | 2422 | 2405 | 3060 | 3110 | 2884 | 2466 |
| brus | 1790 | 1521 | 3547 | 3745 | 3575 | 3253 | 3271 | 3684 | 3674 | 3390 | 3035 |
| bucu | 0 | 0 | 0 | 0 | 0 | 0 | 0 | 0 | 0 | 0 | 0 |
| bzrg | 0 | 0 | 0 | 0 | 0 | 0 | 0 | 0 | 0 | 0 | 0 |
| cagl | 0 | 0 | 0 | 0 | 0 | 0 | 0 | 0 | 0 | 0 | 0 |
| cas1 | 4240 | 3962 | 4153 | 3981 | 4430 | 4346 | 3929 | 4305 | 4357 | 4394 | 4163 |
| casa | 2528 | 2211 | 2024 | 2141 | 2531 | 2315 | 2196 | 2561 | 2387 | 2187 | 2192 |
| cat1 | 0 | 0 | 0 | 0 | 0 | 0 | 0 | 0 | 0 | 0 | 0 |
| cedu | 0 | 0 | 3119 | 3247 | 3451 | 3279 | 2961 | 3062 | 0 | 2954 | 3215 |
| chat | 3366 | 3459 | 3379 | 3123 | 3672 | 3518 | 3234 | 3257 | 3427 | 3242 | 3303 |
| chil | 0 | 0 | 0 | 0 | 0 | 0 | 0 | 0 | 0 | 0 | 0 |
| chur | 3400 | 3054 | 3316 | 3068 | 3389 | 2680 | 2996 | 3512 | 3144 | 2831 | 2724 |
| chwk | 2779 | 2316 | 2438 | 2178 | 2816 | 2240 | 2409 | 2566 | 2598 | 2321 | 2256 |
| cic1 | 1951 | 1922 | 2085 | 2063 | 2385 | 2019 | 2117 | 2467 | 2212 | 2159 | 2362 |
| cit1 | 0 | 0 | 0 | 0 | 0 | 0 | 0 | 0 | 0 | 0 | 0 |
| clar | 0 | 0 | 0 | 0 | 0 | 0 | 0 | 0 | 0 | 0 | 0 |
| cmp9 | 0 | 0 | 0 | 0 | 0 | 0 | 0 | 0 | 0 | 0 | 0 |
| coco | 1762 | 3453 | 3447 | 2973 | 3003 | 0 | 3262 | 3668 | 3605 | 3501 | 3361 |
| cord | 0 | 0 | 0 | 0 | 0 | 0 | 0 | 0 | 0 | 0 | 0 |
| coso | 0 | 0 | 0 | 0 | 0 | 0 | 0 | 0 | 0 | 0 | 0 |
| crfp | 0 | 0 | 0 | 0 | 0 | 0 | 0 | 0 | 0 | 0 | 0 |
| cro1 | 2991 | 2775 | 2801 | 3037 | 3200 | 2838 | 2702 | 3108 | 3409 | 3142 | 2863 |
| csn1 | 0 | 0 | 0 | 0 | 0 | 0 | 0 | 0 | 0 | 0 | 0 |
| daej | 0 | 0 | 3235 | 3428 | 3601 | 3984 | 3729 | 3755 | 3592 | 3505 | 3644 |
| darw | 0 | 0 | 0 | 0 | 0 | 0 | 0 | 0 | 0 | 2608 | 3622 |
| dav1 | 4130 | 4011 | 3890 | 0 | 4038 | 4344 | 3889 | 4532 | 4219 | 4389 | 4159 |
| dgar | 0 | 0 | 0 | 0 | 0 | 0 | 0 | 0 | 0 | 0 | 0 |
| dhlg | 0 | 0 | 0 | 0 | 0 | 0 | 0 | 0 | 0 | 0 | 0 |
| drag | 3034 | 1710 | 2273 | 2102 | 2228 | 2021 | 1316 | 0 | 2447 | 2872 | 1527 |
| drao | 54 | 89 | 130 | 108 | 171 | 126 | 16 | 41 | 124 | 196 | 113 |
| dubo | 2900 | 2640 | 2567 | 2487 | 2973 | 2455 | 2354 | 2853 | 2648 | 2573 | 2548 |
| ebre | 3347 | 3358 | 3269 | 3639 | 3444 | 3159 | 3052 | 3632 | 3558 | 3435 | 3101 |
| eisl | 1648 | 1190 | 1297 | 1639 | 1989 | 1494 | 1468 | 1336 | 1258 | 940 | 1509 |
| fair | 3294 | 2991 | 3230 | 3269 | 3559 | 2729 | 2980 | 3537 | 3282 | 2817 | 3049 |
| flin | 696 | 673 | 713 | 999 | 849 | 572 | 476 | 935 | 1137 | 890 | 726 |
| fort | 2479 | 2421 | 2635 | 2433 | 2653 | 2277 | 2684 | 2688 | 2466 | 2290 | 2626 |
| gala | 3627 | 2929 | 3049 | 2385 | 2746 | 3166 | 3371 | 3261 | 3092 | 2670 | 2803 |
| geno | 0 | 0 | 0 | 0 | 0 | 0 | 0 | 0 | 0 | 0 | 0 |
| glsv | 3619 | 3729 | 3755 | 3685 | 3655 | 3553 | 3603 | 3827 | 3623 | 3657 | 3482 |
| gode | 2682 | 2875 | 1241 | 636 | 686 | 444 | 878 | 0 | 0 | 0 | 0 |
| gold | 3044 | 2595 | 2659 | 2733 | 3240 | 2445 | 2267 | 2948 | 3050 | 2628 | 2541 |
| gope | 0 | 0 | 0 | 0 | 0 | 0 | 0 | 0 | 0 | 0 | 0 |
| goug | 0 | 2642 | 3084 | 3047 | 3110 | 2901 | 2899 | 3321 | 3154 | 3114 | 3084 |
| gras | 3141 | 3111 | 3133 | 3365 | 3102 | 2784 | 3028 | 3584 | 3235 | 3078 | 2848 |
| graz | 3567 | 3568 | 3513 | 3877 | 3597 | 3217 | 3356 | 3849 | 3772 | 3522 | 3344 |
| guam | 3045 | 3129 | 3006 | 3042 | 2679 | 3513 | 3563 | 3326 | 3581 | 3410 | 2721 |
| ... | ... | ... | ... | ... | ... | ... | ... | ... | ... | ... | ... |

Table F.8: Daily DDobs numbers for cycle 8. (continued)

| site ID | day 84 | day 85 | day 86 | day 87 | day 88 | day 89 | day 90 | day 91 | day 92 | day 93 | day 94 |
|---|---|---|---|---|---|---|---|---|---|---|---|
| harv | 3131 | 2434 | 2544 | 2641 | 3191 | 2626 | 2511 | 3033 | 3054 | 2640 | 2526 |
| hers | 3431 | 3367 | 3477 | 3665 | 3569 | 3320 | 3185 | 3671 | 3559 | 3575 | 3237 |
| hflk | 0 | 0 | 0 | 0 | 0 | 0 | 0 | 0 | 0 | 0 | 0 |
| hnpt | 2642 | 2567 | 2683 | 2615 | 2796 | 2492 | 2476 | 2802 | 2848 | 2528 | 2552 |
| hob2 | 3250 | 3236 | 2935 | 2733 | 3679 | 3353 | 3339 | 3214 | 3432 | 3608 | 3701 |
| hofn | 4002 | 3693 | 3797 | 4009 | 4216 | 3314 | 3440 | 4334 | 4298 | 3758 | 3562 |
| holb | 54 | 88 | 134 | 146 | 197 | 119 | 16 | 49 | 142 | 206 | 113 |
| holc | 0 | 0 | 0 | 0 | 0 | 0 | 0 | 0 | 0 | 0 | 0 |
| holp | 0 | 0 | 0 | 0 | 0 | 0 | 0 | 0 | 0 | 0 | 0 |
| hrao | 2662 | 2708 | 3363 | 3038 | 2901 | 2692 | 2872 | 2894 | 2608 | 2293 | 2678 |
| iisc | 0 | 0 | 0 | 0 | 620 | 2661 | 3471 | 3582 | 3473 | 3114 | 2588 |
| ineg | 0 | 0 | 0 | 0 | 0 | 0 | 0 | 0 | 0 | 0 | 0 |
| irkt | 3628 | 2979 | 2912 | 2111 | 2763 | 3225 | 3180 | 3145 | 3116 | 2897 | 3066 |
| jab1 | 0 | 0 | 0 | 0 | 0 | 0 | 0 | 0 | 0 | 0 | 0 |
| jama | 3247 | 3069 | 2032 | 463 | 2308 | 2002 | 149 | 0 | 729 | 2644 | 1875 |
| joze | 3632 | 3730 | 3533 | 3637 | 3481 | 3326 | 3395 | 3717 | 3550 | 3411 | 3193 |
| jplm | 2608 | 2406 | 2360 | 2338 | 2679 | 2391 | 2291 | 2571 | 2435 | 2287 | 2464 |
| karr | 3642 | 3713 | 3679 | 3093 | 3269 | 3668 | 3370 | 3624 | 3507 | 3531 | 3743 |
| kely | 4064 | 1620 | 0 | 3074 | 3901 | 1297 | 3114 | 4073 | 3806 | 3512 | 3173 |
| kerg | 3076 | 3346 | 3504 | 2984 | 3124 | 3341 | 2886 | 3323 | 3008 | 3138 | 3423 |
| kiru | 4409 | 4133 | 4044 | 3980 | 4268 | 4135 | 3969 | 4376 | 4364 | 4270 | 3799 |
| kit3 | 0 | 0 | 0 | 0 | 0 | 0 | 0 | 0 | 0 | 0 | 0 |
| kokb | 0 | 0 | 0 | 0 | 0 | 0 | 0 | 0 | 0 | 2550 | 2563 |
| kosg | 3668 | 3521 | 3500 | 3790 | 3747 | 3260 | 3289 | 3717 | 3759 | 3605 | 3252 |
| kour | 1771 | 932 | 1784 | 2492 | 3282 | 3462 | 2209 | 3625 | 3835 | 3769 | 3594 |
| kr0g | 0 | 0 | 0 | 0 | 0 | 0 | 0 | 0 | 0 | 0 | 0 |
| kstu | 0 | 0 | 827 | 3201 | 3327 | 3497 | 3426 | 2954 | 3169 | 3132 | 3357 |
| kunm | 1636 | 1982 | 2024 | 1871 | 1950 | 2260 | 2273 | 2351 | 1971 | 1889 | 1803 |
| kwj1 | 0 | 0 | 0 | 0 | 0 | 0 | 0 | 0 | 0 | 0 | 0 |
| lama | 0 | 0 | 0 | 0 | 0 | 0 | 0 | 0 | 0 | 0 | 0 |
| lbch | 0 | 0 | 0 | 0 | 0 | 0 | 0 | 0 | 0 | 0 | 0 |
| leep | 0 | 0 | 0 | 0 | 0 | 0 | 0 | 0 | 0 | 0 | 0 |
| lhas | 3231 | 3294 | 3123 | 3028 | 2843 | 3210 | 3177 | 3166 | 3104 | 2945 | 3180 |
| long | 0 | 0 | 0 | 0 | 0 | 0 | 0 | 0 | 0 | 0 | 0 |
| lpgs | 3274 | 3106 | 2818 | 3032 | 3320 | 3122 | 2939 | 3074 | 3136 | 3285 | 3316 |
| mac1 | 3236 | 3422 | 3469 | 3331 | 3505 | 3569 | 3494 | 3538 | 3450 | 3557 | 3724 |
| madr | 3360 | 3262 | 3307 | 3670 | 3370 | 3097 | 2905 | 3410 | 3284 | 3360 | 2784 |
| mag0 | 4068 | 3794 | 3519 | 3284 | 3869 | 3883 | 3629 | 3522 | 3610 | 3541 | 3467 |
| mali | 3004 | 3368 | 3328 | 2855 | 2913 | 3401 | 3515 | 3309 | 3022 | 2921 | 3248 |
| mas1 | 0 | 2621 | 2788 | 2992 | 2991 | 3072 | 2974 | 3579 | 3523 | 3325 | 3037 |
| mate | 3524 | 3065 | 3370 | 3642 | 3426 | 3107 | 3271 | 3548 | 3380 | 3171 | 3156 |
| math | 0 | 0 | 0 | 0 | 0 | 0 | 0 | 0 | 0 | 0 | 0 |
| maw1 | 3894 | 4030 | 4394 | 3947 | 4168 | 4228 | 3996 | 4283 | 4214 | 4170 | 4117 |
| mcm4 | 4193 | 4462 | 4805 | 4264 | 4627 | 4514 | 4545 | 4553 | 4515 | 4464 | 4746 |
| mdo1 | 2420 | 1600 | 2159 | 2176 | 2534 | 2049 | 1972 | 2601 | 2460 | 2196 | 2252 |
| mdvo | 3713 | 3929 | 3852 | 3742 | 3711 | 3616 | 1936 | 2855 | 3771 | 3661 | 3508 |
| medi | 0 | 0 | 0 | 0 | 0 | 0 | 0 | 0 | 0 | 0 | 0 |
| mets | 3904 | 3993 | 3788 | 3828 | 3868 | 3792 | 3732 | 4034 | 4070 | 3911 | 3768 |
| mkea | 3143 | 2619 | 2326 | 2377 | 2806 | 2727 | 2563 | 2587 | 2483 | 2565 | 2529 |
| monp | 3124 | 2615 | 2650 | 2742 | 3305 | 2626 | 2488 | 2970 | 3106 | 2716 | 2645 |
| mr6g | 0 | 0 | 0 | 0 | 0 | 0 | 0 | 0 | 0 | 0 | 0 |
| nano | 643 | 619 | 495 | 707 | 790 | 483 | 406 | 723 | 864 | 872 | 587 |
| nico | 3610 | 3556 | 3534 | 3607 | 3444 | 3100 | 3504 | 3640 | 3527 | 3304 | 3337 |
| nklg | 3345 | 3300 | 3199 | 2876 | 2665 | 3059 | 2791 | 2867 | 2729 | 3017 | 2944 |
| nlib | 2668 | 2526 | 2175 | 2230 | 2733 | 2274 | 2040 | 2546 | 2558 | 2309 | 2176 |
| noto | 0 | 0 | 0 | 0 | 0 | 0 | 0 | 0 | 0 | 0 | 0 |
| noum | 3656 | 3494 | 3318 | 3027 | 3686 | 3407 | 3195 | 3273 | 3356 | 3318 | 3415 |
| nrc1 | 3364 | 3031 | 3051 | 3120 | 3439 | 2918 | 2815 | 3334 | 3422 | 3193 | 3001 |
| nssp | 0 | 0 | 0 | 0 | 0 | 0 | 0 | 0 | 0 | 0 | 0 |
| ntus | 4090 | 3924 | 3825 | 3792 | 3481 | 3862 | 3685 | 3907 | 4045 | 3764 | 3847 |
| nya1 | 4742 | 4435 | 4275 | 4306 | 4746 | 4239 | 4016 | 4552 | 4655 | 4390 | 3740 |
| nyal | 4688 | 4371 | 4260 | 4293 | 4699 | 4187 | 3975 | 4550 | 4684 | 4391 | 3677 |
| oat2 | 0 | 0 | 0 | 0 | 0 | 0 | 0 | 0 | 0 | 0 | 0 |
| onsa | 3895 | 3562 | 3669 | 3983 | 3976 | 3549 | 3441 | 3851 | 3951 | 3772 | 3431 |
| penc | 0 | 0 | 0 | 0 | 0 | 0 | 0 | 0 | 0 | 0 | 0 |
| pert | 3171 | 3276 | 3311 | 2935 | 2913 | 3304 | 3056 | 3630 | 3426 | 3246 | 3417 |
| petp | 3624 | 3539 | 3303 | 2903 | 3556 | 3717 | 3421 | 3322 | 3276 | 3324 | 3328 |
| pie1 | 2533 | 2167 | 2251 | 2347 | 2728 | 2187 | 2212 | 2478 | 2685 | 2236 | 2354 |
| pimo | 3622 | 2280 | 1811 | 2178 | 1029 | 1899 | 3078 | 2693 | 3842 | 2775 | 1650 |
| pol2 | 3564 | 3697 | 3515 | 3270 | 3407 | 3669 | 3611 | 3560 | 3701 | 3469 | 3422 |
| pots | 3709 | 3541 | 3537 | 3933 | 3731 | 3284 | 3057 | 3493 | 3873 | 3690 | 3403 |
| ... | ... | ... | ... | ... | ... | ... | ... | ... | ... | ... | ... |

Table F.8: Daily DDobs numbers for cycle 8. (continued)

| site ID | day 84 | day 85 | day 86 | day 87 | day 88 | day 89 | day 90 | day 91 | day 92 | day 93 | day 94 |
|---|---|---|---|---|---|---|---|---|---|---|---|
| prds | 3199 | 2736 | 2749 | 2729 | 3273 | 2641 | 2788 | 3045 | 3066 | 2832 | 2635 |
| pvep | 0 | 0 | 0 | 0 | 0 | 0 | 0 | 0 | 0 | 0 | 0 |
| quin | 2430 | 2159 | 2026 | 2095 | 2454 | 2135 | 2197 | 2529 | 2318 | 2079 | 2158 |
| ramo | 3632 | 3586 | 3463 | 3597 | 3471 | 3238 | 3482 | 3584 | 3476 | 3222 | 3307 |
| reyk | 4061 | 3787 | 3848 | 3981 | 4139 | 3444 | 3586 | 4291 | 4286 | 3732 | 3438 |
| riog | 3195 | 3632 | 3635 | 3308 | 3627 | 2849 | 3743 | 3780 | 3536 | 3697 | 3792 |
| riop | 0 | 0 | 0 | 0 | 0 | 0 | 0 | 0 | 0 | 0 | 0 |
| roch | 0 | 0 | 0 | 0 | 0 | 0 | 0 | 0 | 0 | 0 | 0 |
| rock | 0 | 0 | 0 | 0 | 0 | 0 | 0 | 0 | 0 | 0 | 0 |
| sant | 3512 | 3291 | 3200 | 3027 | 3502 | 3252 | 3329 | 3442 | 3482 | 3469 | 2874 |
| sch2 | 3581 | 3149 | 3224 | 3219 | 3631 | 3015 | 2955 | 3504 | 3552 | 3278 | 2912 |
| scip | 0 | 0 | 0 | 0 | 0 | 0 | 0 | 0 | 0 | 0 | 0 |
| sele | 3097 | 3199 | 2935 | 2800 | 2880 | 3252 | 3026 | 2897 | 3018 | 3012 | 975 |
| sey1 | 1264 | 1479 | 1652 | 1734 | 1532 | 1507 | 1631 | 1624 | 1709 | 1674 | 1442 |
| sfer | 0 | 0 | 0 | 0 | 0 | 0 | 0 | 0 | 0 | 0 | 0 |
| shao | 2993 | 916 | 2369 | 2830 | 2754 | 3075 | 3258 | 3270 | 2945 | 2563 | 2992 |
| sio3 | 54 | 22 | 23 | 68 | 159 | 114 | 0 | 22 | 96 | 108 | 77 |
| sni1 | 0 | 0 | 0 | 0 | 0 | 0 | 0 | 0 | 0 | 0 | 0 |
| sofi | 0 | 0 | 0 | 0 | 0 | 0 | 0 | 0 | 0 | 0 | 0 |
| sol1 | 3025 | 2718 | 2895 | 2760 | 3247 | 2610 | 2541 | 3324 | 3313 | 3025 | 2972 |
| spk1 | 0 | 0 | 0 | 0 | 0 | 0 | 0 | 0 | 0 | 0 | 0 |
| stjo | 3703 | 3476 | 3474 | 3572 | 3786 | 3214 | 3169 | 3909 | 3819 | 3513 | 3197 |
| suth | 3163 | 3121 | 3363 | 3187 | 3049 | 2890 | 2999 | 3424 | 2995 | 2938 | 3145 |
| suwn | 3116 | 3492 | 3486 | 3341 | 3424 | 3801 | 3566 | 3654 | 3391 | 3307 | 3509 |
| syog | 3858 | 3864 | 4206 | 3828 | 4180 | 3958 | 3698 | 3921 | 3901 | 3840 | 3886 |
| tabl | 0 | 0 | 0 | 0 | 0 | 0 | 0 | 0 | 0 | 0 | 0 |
| thti | 2916 | 0 | 3057 | 3220 | 3211 | 3251 | 3290 | 3335 | 2890 | 2988 | 3366 |
| thu1 | 3347 | 2123 | 2432 | 2994 | 3028 | 2334 | 2083 | 2601 | 2395 | 2205 | 1886 |
| tidb | 3708 | 3644 | 3434 | 2913 | 3415 | 3661 | 3329 | 3363 | 3395 | 3543 | 3569 |
| tixi | 3204 | 4383 | 4255 | 4158 | 4320 | 4344 | 4189 | 4352 | 4336 | 4128 | 4206 |
| torp | 0 | 0 | 0 | 0 | 0 | 0 | 0 | 0 | 0 | 0 | 0 |
| tow2 | 3517 | 3432 | 3838 | 3304 | 3516 | 3419 | 3628 | 3563 | 3499 | 3370 | 3719 |
| trab | 0 | 0 | 0 | 0 | 0 | 0 | 0 | 0 | 0 | 0 | 0 |
| trak | 0 | 0 | 0 | 0 | 0 | 0 | 0 | 0 | 0 | 0 | 0 |
| tro1 | 4501 | 4359 | 4199 | 4151 | 4378 | 4085 | 3957 | 4398 | 4537 | 4372 | 3910 |
| trom | 4672 | 4294 | 4133 | 4072 | 4333 | 4152 | 4037 | 4436 | 4579 | 4366 | 3883 |
| tskb | 2312 | 2074 | 2289 | 2146 | 2384 | 2431 | 2165 | 2221 | 2323 | 2100 | 2299 |
| uclp | 0 | 0 | 0 | 0 | 0 | 0 | 0 | 0 | 0 | 0 | 0 |
| uclu | 54 | 89 | 135 | 113 | 171 | 126 | 16 | 41 | 134 | 206 | 113 |
| urum | 3708 | 3306 | 0 | 3056 | 3484 | 3735 | 3731 | 3862 | 3532 | 3401 | 3232 |
| usc1 | 0 | 0 | 0 | 0 | 0 | 0 | 0 | 0 | 0 | 0 | 0 |
| usna | 2525 | 2593 | 2603 | 2503 | 2778 | 2351 | 2398 | 2767 | 2919 | 2714 | 2597 |
| usno | 147 | 93 | 61 | 153 | 317 | 250 | 25 | 50 | 189 | 256 | 154 |
| usud | 3989 | 3414 | 3612 | 3328 | 3632 | 3638 | 3693 | 3780 | 3464 | 3228 | 3367 |
| vene | 0 | 0 | 0 | 0 | 0 | 0 | 0 | 0 | 0 | 0 | 0 |
| vesl | 4458 | 4118 | 4512 | 4226 | 4673 | 4201 | 4037 | 4513 | 4335 | 4260 | 4397 |
| vill | 3419 | 3347 | 3293 | 3687 | 3446 | 3200 | 3014 | 3626 | 3513 | 3491 | 3043 |
| vndp | 616 | 413 | 339 | 705 | 827 | 544 | 360 | 800 | 927 | 763 | 581 |
| vs0g | 0 | 0 | 0 | 0 | 0 | 0 | 0 | 0 | 0 | 0 | 0 |
| wes2 | 65 | 0 | 0 | 0 | 0 | 0 | 0 | 53 | 219 | 255 | 122 |
| whc1 | 0 | 0 | 0 | 0 | 0 | 0 | 0 | 0 | 0 | 0 | 0 |
| whit | 3688 | 3211 | 3048 | 3079 | 3768 | 3126 | 3081 | 3488 | 3408 | 3279 | 3042 |
| widc | 0 | 0 | 0 | 0 | 0 | 0 | 0 | 0 | 0 | 0 | 0 |
| will | 2804 | 2389 | 2291 | 2125 | 2910 | 2283 | 2409 | 2688 | 2624 | 2509 | 2252 |
| wlsn | 0 | 0 | 0 | 0 | 0 | 0 | 0 | 0 | 0 | 0 | 0 |
| wroc | 0 | 0 | 0 | 0 | 0 | 0 | 0 | 0 | 0 | 0 | 0 |
| wslr | 608 | 592 | 444 | 600 | 705 | 470 | 380 | 589 | 749 | 855 | 568 |
| wsrt | 3656 | 3497 | 3494 | 3782 | 3783 | 3303 | 3289 | 3713 | 3751 | 3666 | 3143 |
| wtzr | 3635 | 3664 | 3546 | 3932 | 3703 | 3273 | 3541 | 3878 | 3841 | 3547 | 3376 |
| wuhn | 3705 | 3812 | 3707 | 3246 | 3376 | 3805 | 3642 | 1434 | 3135 | 3404 | 3639 |
| xian | 0 | 0 | 0 | 0 | 0 | 0 | 0 | 0 | 0 | 0 | 0 |
| yakz | 0 | 0 | 0 | 0 | 0 | 0 | 0 | 0 | 0 | 0 | 0 |
| yar1 | 2181 | 2730 | 2426 | 2145 | 2179 | 2418 | 2391 | 2503 | 2226 | 2294 | 2559 |
| yell | 3712 | 3553 | 3422 | 3114 | 3783 | 3230 | 3189 | 3487 | 3519 | 3287 | 3134 |
| ykro | 0 | 0 | 0 | 0 | 0 | 0 | 0 | 0 | 0 | 0 | 0 |
| yssk | 4148 | 3549 | 3555 | 3429 | 3834 | 3730 | 3417 | 3816 | 3532 | 3459 | 3350 |
| zeck | 3562 | 3418 | 3716 | 3539 | 3420 | 3500 | 3728 | 3711 | 3679 | 3480 | 3446 |
| zimm | 3600 | 3450 | 3540 | 3794 | 3700 | 3270 | 3370 | 3683 | 3453 | 3500 | 3260 |
| zwen | 3867 | 4150 | 3719 | 3567 | 3808 | 3679 | 3855 | 3697 | 3736 | 3717 | 3459 |

Table F.9: Daily DDobs numbers for cycle 9

| site ID | day 94 | day 95 | day 96 | day 97 | day 98 | day 99 | day 100 | day 101 | day 102 | day 103 | day 104 |
|---|---|---|---|---|---|---|---|---|---|---|---|
| albh | 113 | 39 | 43 | 174 | 237 | 195 | 183 | 65 | 179 | 335 | 169 |
| algo | 2926 | 2987 | 3477 | 3347 | 3182 | 2990 | 3013 | 3069 | 3452 | 3420 | 3520 |
| alic | 3605 | 3886 | 3826 | 3722 | 3567 | 3445 | 3679 | 3370 | 3491 | 3479 | 3877 |
| amc2 | 2674 | 2955 | 3082 | 2868 | 2858 | 2964 | 2696 | 2689 | 3057 | 3395 | 3205 |
| ankr | 3264 | 3526 | 3733 | 3304 | 3233 | 3030 | 1115 | 0 | 3226 | 3387 | 3269 |
| aoa1 | 2429 | 2488 | 2504 | 2476 | 2495 | 2302 | 2092 | 2462 | 2402 | 2258 | 2363 |
| aoml | 2329 | 2326 | 2697 | 2642 | 2566 | 2567 | 2324 | 2292 | 2700 | 2724 | 2558 |
| areq | 0 | 0 | 0 | 0 | 0 | 0 | 0 | 0 | 0 | 0 | 0 |
| artu | 3623 | 3789 | 3660 | 3427 | 3511 | 3232 | 3034 | 3206 | 3357 | 3397 | 3552 |
| asc1 | 3227 | 3214 | 3296 | 2912 | 0 | 0 | 2458 | 2943 | 2980 | 3148 | 2953 |
| auck | 3186 | 3489 | 3478 | 3267 | 3303 | 3260 | 3278 | 2917 | 3303 | 3330 | 3287 |
| azu1 | 0 | 0 | 0 | 0 | 0 | 0 | 0 | 0 | 0 | 0 | 0 |
| bahr | 3223 | 3429 | 3454 | 3252 | 3123 | 2909 | 2860 | 3014 | 3136 | 3280 | 3148 |
| bako | 0 | 0 | 0 | 0 | 0 | 0 | 0 | 0 | 0 | 0 | 0 |
| barb | 0 | 0 | 0 | 0 | 0 | 0 | 0 | 0 | 0 | 0 | 0 |
| bili | 3846 | 4004 | 3792 | 3630 | 847 | 0 | 0 | 0 | 0 | 0 | 3118 |
| bjfs | 3186 | 3581 | 3128 | 2876 | 2951 | 2992 | 2606 | 2549 | 2886 | 3006 | 3090 |
| blyt | 0 | 0 | 0 | 0 | 0 | 0 | 0 | 0 | 0 | 0 | 0 |
| bogt | 0 | 0 | 0 | 0 | 0 | 0 | 0 | 0 | 0 | 0 | 0 |
| bor1 | 3066 | 3439 | 3368 | 2933 | 3010 | 3004 | 3039 | 2763 | 3033 | 3305 | 3326 |
| bran | 0 | 0 | 0 | 0 | 0 | 0 | 0 | 0 | 0 | 0 | 0 |
| braz | 3399 | 3419 | 3409 | 3828 | 3424 | 3401 | 2868 | 3237 | 3672 | 1960 | 0 |
| brmu | 2466 | 2645 | 3115 | 3045 | 2641 | 2640 | 2764 | 2710 | 2874 | 2846 | 2960 |
| brus | 3035 | 3284 | 3604 | 3498 | 3304 | 3160 | 3175 | 2103 | 1834 | 0 | 1689 |
| bucu | 0 | 0 | 0 | 0 | 0 | 0 | 0 | 0 | 0 | 0 | 0 |
| bzrg | 0 | 0 | 0 | 0 | 0 | 0 | 0 | 0 | 0 | 0 | 0 |
| cagl | 0 | 0 | 0 | 0 | 0 | 0 | 0 | 0 | 0 | 0 | 0 |
| cas1 | 4163 | 4497 | 4800 | 4877 | 4479 | 4051 | 4103 | 4155 | 4499 | 4214 | 4501 |
| casa | 2192 | 2398 | 2430 | 2604 | 2411 | 2123 | 2040 | 2403 | 2606 | 2431 | 2253 |
| cat1 | 0 | 0 | 0 | 0 | 0 | 0 | 0 | 0 | 0 | 0 | 0 |
| cedu | 3215 | 3339 | 3179 | 0 | 3039 | 3174 | 3541 | 3454 | 3440 | 3364 | 3658 |
| chat | 3303 | 3311 | 3434 | 3576 | 3402 | 3055 | 3152 | 3266 | 3451 | 3187 | 3365 |
| chil | 0 | 0 | 0 | 0 | 0 | 0 | 0 | 0 | 0 | 0 | 0 |
| chur | 2724 | 3436 | 3339 | 3243 | 2899 | 3392 | 3034 | 3065 | 3181 | 3538 | 3486 |
| chwk | 2256 | 2576 | 2522 | 2753 | 2419 | 2306 | 2077 | 2550 | 2713 | 2637 | 2397 |
| cic1 | 2362 | 2393 | 2363 | 2296 | 2214 | 2121 | 1841 | 2114 | 2317 | 2331 | 2132 |
| cit1 | 0 | 0 | 0 | 0 | 0 | 0 | 0 | 0 | 0 | 0 | 0 |
| clar | 0 | 0 | 0 | 0 | 0 | 0 | 0 | 0 | 0 | 0 | 0 |
| cmp9 | 0 | 0 | 0 | 0 | 0 | 0 | 0 | 0 | 0 | 0 | 0 |
| coco | 3361 | 3641 | 3491 | 3599 | 3401 | 3115 | 3393 | 3404 | 3305 | 3190 | 3180 |
| cord | 0 | 0 | 0 | 0 | 0 | 0 | 0 | 0 | 0 | 0 | 0 |
| coso | 0 | 0 | 0 | 0 | 0 | 0 | 0 | 0 | 0 | 0 | 0 |
| crfp | 0 | 0 | 0 | 0 | 0 | 0 | 0 | 0 | 0 | 0 | 0 |
| cro1 | 2863 | 2920 | 3205 | 3326 | 3023 | 2988 | 2728 | 2778 | 2785 | 2785 | 3057 |
| csn1 | 0 | 0 | 0 | 0 | 0 | 0 | 0 | 0 | 0 | 0 | 0 |
| daej | 3644 | 3473 | 3259 | 3208 | 3385 | 619 | 0 | 2559 | 3449 | 3340 | 3104 |
| darw | 3622 | 3412 | 957 | 0 | 0 | 0 | 0 | 0 | 0 | 0 | 0 |
| dav1 | 4159 | 4703 | 4834 | 4811 | 4423 | 4274 | 4425 | 3878 | 3706 | 0 | 4053 |
| dgar | 0 | 0 | 0 | 0 | 0 | 0 | 0 | 0 | 0 | 0 | 0 |
| dhlg | 0 | 0 | 0 | 0 | 0 | 0 | 0 | 0 | 0 | 0 | 0 |
| drag | 1527 | 0 | 0 | 0 | 0 | 912 | 2292 | 0 | 0 | 0 | 0 |
| drao | 113 | 39 | 44 | 175 | 293 | 289 | 221 | 66 | 193 | 398 | 485 |
| dubo | 2548 | 2806 | 2855 | 2892 | 2732 | 2673 | 2421 | 2674 | 2824 | 3100 | 3049 |
| ebre | 3101 | 3182 | 3525 | 3157 | 3218 | 3179 | 3228 | 2983 | 3216 | 3313 | 3361 |
| eisl | 1509 | 1576 | 1610 | 1818 | 1555 | 1870 | 1172 | 1681 | 1830 | 1587 | 1770 |
| fair | 3049 | 3137 | 3304 | 2938 | 3031 | 2907 | 2861 | 2930 | 2966 | 3217 | 3168 |
| flin | 726 | 820 | 1026 | 1150 | 1061 | 1057 | 1024 | 1044 | 1040 | 1229 | 1207 |
| fort | 2626 | 2170 | 0 | 2555 | 2271 | 1975 | 2051 | 1993 | 2358 | 2496 | 2240 |
| gala | 2803 | 2828 | 3054 | 3412 | 2890 | 2952 | 2788 | 2801 | 3437 | 3440 | 3472 |
| geno | 0 | 0 | 0 | 0 | 0 | 0 | 0 | 0 | 0 | 0 | 0 |
| glsv | 3482 | 3701 | 3737 | 3291 | 3554 | 3096 | 3332 | 3231 | 3569 | 3353 | 3431 |
| gode | 0 | 0 | 0 | 0 | 0 | 0 | 0 | 0 | 0 | 0 | 0 |
| gold | 2541 | 2789 | 3140 | 3034 | 2781 | 2517 | 2529 | 2844 | 3072 | 3118 | 2895 |
| gope | 0 | 0 | 0 | 0 | 0 | 0 | 0 | 0 | 0 | 0 | 0 |
| goug | 3084 | 3193 | 3119 | 3285 | 3136 | 2848 | 2704 | 2811 | 2405 | 2695 | 2650 |
| gras | 2848 | 3042 | 3201 | 2776 | 2770 | 2791 | 2860 | 2529 | 2657 | 2912 | 3086 |
| graz | 3344 | 3532 | 3718 | 3274 | 2008 | 2776 | 3296 | 3236 | 3336 | 3462 | 3403 |
| guam | 2721 | 2730 | 1789 | 2420 | 2112 | 2376 | 2321 | 2688 | 2936 | 3037 | 2577 |
| harv | 2526 | 2795 | 2938 | 2929 | 2649 | 2535 | 2539 | 2786 | 3103 | 3009 | 2766 |
| hers | 3237 | 3285 | 3484 | 3499 | 3234 | 3008 | 3098 | 3208 | 3436 | 3407 | 3323 |
| hflk | 0 | 0 | 0 | 0 | 0 | 0 | 0 | 0 | 0 | 0 | 0 |
| ... | ... | ... | ... | ... | ... | ... | ... | ... | ... | ... | ... |

Table F.9: Daily DDobs numbers for cycle 9. (continued)

| site ID | day 94 | day 95 | day 96 | day 97 | day 98 | day 99 | day 100 | day 101 | day 102 | day 103 | day 104 |
|---|---|---|---|---|---|---|---|---|---|---|---|
| hnpt | 2552 | 2637 | 2776 | 2942 | 2384 | 44 | 483 | 2556 | 2975 | 3212 | 3100 |
| hob2 | 3701 | 3535 | 3654 | 3822 | 3679 | 3346 | 3235 | 3576 | 3694 | 3599 | 3369 |
| hofn | 3562 | 4029 | 4240 | 3798 | 3697 | 3712 | 3578 | 3654 | 3819 | 4008 | 3895 |
| holb | 113 | 39 | 60 | 35 | 53 | 156 | 139 | 49 | 169 | 285 | 353 |
| holc | 0 | 0 | 0 | 0 | 0 | 0 | 0 | 0 | 0 | 0 | 0 |
| holp | 0 | 0 | 0 | 0 | 0 | 0 | 0 | 0 | 0 | 0 | 0 |
| hrao | 2678 | 3253 | 2888 | 2812 | 3079 | 3179 | 2734 | 2664 | 2925 | 2547 | 2486 |
| iisc | 2588 | 2492 | 1775 | 1083 | 1972 | 2790 | 2656 | 2603 | 2468 | 2932 | 3198 |
| ineg | 0 | 0 | 0 | 0 | 0 | 0 | 0 | 0 | 0 | 0 | 0 |
| irkt | 3066 | 3246 | 3077 | 2770 | 2952 | 2833 | 2501 | 2857 | 2806 | 2775 | 2756 |
| jab1 | 0 | 0 | 0 | 0 | 0 | 0 | 0 | 0 | 0 | 0 | 0 |
| jama | 1875 | 2145 | 2678 | 1632 | 1020 | 1915 | 1908 | 2055 | 2347 | 1106 | 1901 |
| joze | 3193 | 3508 | 3760 | 3212 | 3460 | 3097 | 3272 | 3106 | 3460 | 3591 | 3561 |
| jplm | 2464 | 2467 | 2594 | 2602 | 2516 | 2257 | 2109 | 2464 | 2721 | 2657 | 2452 |
| karr | 3743 | 3867 | 3663 | 3674 | 3711 | 3453 | 3427 | 3320 | 3640 | 3700 | 3495 |
| kely | 3173 | 3714 | 4064 | 3205 | 2929 | 3603 | 3088 | 1901 | 3515 | 4014 | 3761 |
| kerg | 3423 | 3634 | 3402 | 3725 | 3764 | 3314 | 3273 | 3248 | 3662 | 3588 | 3179 |
| kiru | 3799 | 3974 | 4359 | 4096 | 3718 | 3569 | 3809 | 3568 | 3951 | 4088 | 4201 |
| kit3 | 0 | 0 | 0 | 0 | 1436 | 1166 | 2316 | 2346 | 669 | 1561 | 2934 |
| kokb | 2563 | 2739 | 2041 | 2698 | 2450 | 2449 | 2276 | 2427 | 2744 | 2449 | 2303 |
| kosg | 3252 | 3357 | 3689 | 3528 | 3368 | 3136 | 3205 | 3285 | 3454 | 3507 | 3525 |
| kour | 3594 | 2647 | 3356 | 4162 | 3854 | 2121 | 3173 | 3315 | 3886 | 4290 | 3894 |
| kr0g | 0 | 0 | 0 | 0 | 0 | 0 | 0 | 0 | 0 | 0 | 0 |
| kstu | 3357 | 2847 | 2178 | 2349 | 3096 | 2876 | 2478 | 2816 | 2815 | 2677 | 681 |
| kunm | 1803 | 2273 | 2144 | 1681 | 2042 | 1437 | 1793 | 1892 | 1344 | 2135 | 1491 |
| kwj1 | 0 | 0 | 0 | 0 | 0 | 0 | 0 | 0 | 0 | 0 | 0 |
| lama | 0 | 0 | 0 | 0 | 0 | 0 | 0 | 0 | 0 | 0 | 0 |
| lbch | 0 | 0 | 0 | 0 | 0 | 0 | 0 | 0 | 0 | 0 | 0 |
| leep | 0 | 0 | 0 | 0 | 0 | 0 | 0 | 0 | 0 | 0 | 0 |
| lhas | 3180 | 3246 | 2777 | 2769 | 2836 | 2683 | 2517 | 2563 | 2548 | 2786 | 2704 |
| long | 0 | 0 | 0 | 0 | 0 | 0 | 0 | 0 | 0 | 0 | 0 |
| lpgs | 3316 | 3429 | 3352 | 3459 | 2973 | 2968 | 2702 | 2857 | 3001 | 0 | 0 |
| mac1 | 3724 | 3648 | 3409 | 3642 | 3575 | 3341 | 3548 | 3359 | 3676 | 3695 | 3822 |
| madr | 2784 | 2922 | 3443 | 3180 | 3043 | 3169 | 3275 | 2960 | 3161 | 3572 | 3450 |
| mag0 | 3467 | 3358 | 2951 | 3170 | 3192 | 3266 | 2889 | 3121 | 3026 | 3209 | 3143 |
| mali | 3248 | 3273 | 3195 | 3442 | 3245 | 2998 | 2948 | 3322 | 3483 | 3080 | 2913 |
| mas1 | 3037 | 3218 | 3552 | 3410 | 3129 | 2927 | 2940 | 2907 | 3404 | 3437 | 3241 |
| mate | 3156 | 3325 | 3561 | 3253 | 2948 | 2706 | 3039 | 3149 | 3247 | 3297 | 3063 |
| math | 0 | 0 | 0 | 0 | 0 | 0 | 0 | 0 | 0 | 0 | 0 |
| maw1 | 4117 | 2921 | 4519 | 4725 | 4427 | 4193 | 4433 | 4185 | 4544 | 4236 | 4401 |
| mcm4 | 4746 | 4861 | 4721 | 4971 | 4810 | 4484 | 1895 | 4170 | 4818 | 4644 | 4692 |
| mdo1 | 2252 | 2602 | 2520 | 2509 | 2238 | 2250 | 2120 | 2238 | 2241 | 2496 | 2484 |
| mdvo | 3508 | 3572 | 3633 | 1899 | 3127 | 2654 | 2984 | 3459 | 3294 | 3488 | 2556 |
| medi | 0 | 0 | 0 | 0 | 0 | 0 | 0 | 0 | 0 | 0 | 0 |
| mets | 3768 | 3922 | 4064 | 3601 | 3657 | 3392 | 3532 | 3384 | 3734 | 3969 | 3780 |
| mkea | 2529 | 2541 | 2458 | 2624 | 2296 | 2344 | 1839 | 1741 | 2703 | 2196 | 2275 |
| monp | 2645 | 2897 | 3078 | 3030 | 2806 | 2716 | 2590 | 2893 | 3076 | 3114 | 2923 |
| mr6g | 0 | 0 | 0 | 0 | 0 | 0 | 0 | 0 | 0 | 0 | 0 |
| nano | 587 | 551 | 654 | 921 | 918 | 692 | 725 | 816 | 1016 | 1020 | 843 |
| nico | 3337 | 3408 | 3547 | 3221 | 3265 | 2917 | 2989 | 3040 | 2943 | 3283 | 3042 |
| nklg | 2944 | 2947 | 2930 | 2924 | 3013 | 2721 | 2565 | 2728 | 2887 | 3238 | 2663 |
| nlib | 2176 | 2417 | 2503 | 2044 | 1868 | 1515 | 984 | 607 | 1482 | 2581 | 2590 |
| noto | 0 | 0 | 0 | 0 | 0 | 0 | 0 | 0 | 0 | 0 | 0 |
| noum | 3415 | 3514 | 3324 | 3334 | 3233 | 3167 | 2978 | 3117 | 3201 | 3151 | 3057 |
| nrc1 | 3001 | 2990 | 3524 | 3437 | 3265 | 2998 | 2963 | 3069 | 3509 | 3480 | 3502 |
| nssp | 0 | 0 | 0 | 0 | 0 | 0 | 0 | 0 | 0 | 0 | 0 |
| ntus | 3847 | 3738 | 3825 | 3625 | 3496 | 3537 | 3610 | 3485 | 3675 | 3552 | 3529 |
| nya1 | 3740 | 3978 | 4421 | 4404 | 4051 | 3798 | 4052 | 4179 | 4350 | 4289 | 4570 |
| nyal | 3677 | 4081 | 4329 | 4437 | 3969 | 3716 | 4072 | 4156 | 4314 | 4243 | 4608 |
| oat2 | 0 | 0 | 0 | 0 | 0 | 0 | 0 | 0 | 0 | 0 | 0 |
| onsa | 3431 | 3597 | 3997 | 3575 | 3513 | 3290 | 3412 | 3432 | 3631 | 3552 | 3731 |
| penc | 0 | 0 | 0 | 0 | 0 | 0 | 0 | 0 | 0 | 0 | 0 |
| pert | 3417 | 3640 | 3654 | 3589 | 3105 | 3123 | 3592 | 3276 | 3273 | 3502 | 3699 |
| petp | 3328 | 3073 | 2938 | 2927 | 3114 | 2948 | 2639 | 2853 | 2650 | 2960 | 2796 |
| pie1 | 2354 | 2696 | 2642 | 2331 | 2142 | 2258 | 2028 | 2192 | 2218 | 2668 | 2488 |
| pimo | 1650 | 2715 | 3022 | 2350 | 2203 | 2454 | 2654 | 2515 | 1940 | 2596 | 2912 |
| pol2 | 3422 | 2669 | 3387 | 3224 | 3264 | 2968 | 2821 | 2956 | 3085 | 2720 | 2851 |
| pots | 3403 | 3298 | 3869 | 3405 | 3248 | 3146 | 3276 | 3121 | 3455 | 3450 | 3530 |
| prds | 2635 | 3056 | 3031 | 3038 | 2872 | 2884 | 2709 | 2820 | 3094 | 3103 | 3030 |
| pvep | 0 | 0 | 0 | 0 | 0 | 0 | 0 | 0 | 0 | 0 | 0 |
| quin | 2158 | 2397 | 2432 | 2435 | 2261 | 2074 | 2032 | 2318 | 1990 | 2335 | 2249 |
| ... | ... | ... | ... | ... | ... | ... | ... | ... | ... | ... | ... |

Table F.9: Daily DDobs numbers for cycle 9. (continued)

| site ID | day 94 | day 95 | day 96 | day 97 | day 98 | day 99 | day 100 | day 101 | day 102 | day 103 | day 104 |
|---|---|---|---|---|---|---|---|---|---|---|---|
| ramo | 3307 | 3403 | 3526 | 3184 | 3201 | 2885 | 2936 | 2906 | 3245 | 3377 | 2951 |
| reyk | 3438 | 3943 | 4258 | 3876 | 3686 | 3729 | 3603 | 3666 | 4005 | 4296 | 4088 |
| riog | 3792 | 3340 | 0 | 0 | 0 | 0 | 3112 | 3629 | 3548 | 3903 | 3704 |
| riop | 0 | 0 | 0 | 0 | 0 | 0 | 0 | 0 | 0 | 0 | 0 |
| roch | 0 | 0 | 0 | 0 | 0 | 0 | 0 | 0 | 0 | 0 | 0 |
| rock | 0 | 0 | 0 | 0 | 0 | 0 | 0 | 0 | 0 | 0 | 0 |
| sant | 2874 | 3499 | 3401 | 3752 | 3444 | 3231 | 2921 | 3392 | 3618 | 3697 | 3158 |
| sch2 | 2912 | 3285 | 3528 | 3453 | 3068 | 3170 | 3009 | 3250 | 3634 | 3533 | 3533 |
| scip | 0 | 0 | 0 | 0 | 0 | 0 | 0 | 0 | 0 | 0 | 0 |
| sele | 975 | 0 | 724 | 2461 | 2801 | 2582 | 2459 | 948 | 2158 | 2665 | 2777 |
| sey1 | 1442 | 1603 | 1709 | 1601 | 1354 | 1337 | 1722 | 1648 | 1440 | 1408 | 1496 |
| sfer | 0 | 0 | 0 | 0 | 0 | 0 | 0 | 0 | 0 | 0 | 0 |
| shao | 2992 | 3230 | 2708 | 2463 | 2870 | 2729 | 2425 | 2456 | 2600 | 2855 | 2718 |
| sio3 | 77 | 85 | 60 | 77 | 157 | 283 | 238 | 64 | 33 | 253 | 472 |
| sni1 | 0 | 0 | 0 | 0 | 0 | 0 | 0 | 0 | 0 | 0 | 0 |
| sofi | 0 | 0 | 0 | 0 | 0 | 0 | 0 | 0 | 0 | 0 | 0 |
| sol1 | 2972 | 2939 | 3498 | 3154 | 2881 | 2899 | 3001 | 2955 | 3291 | 3241 | 3237 |
| spk1 | 0 | 0 | 0 | 0 | 0 | 0 | 0 | 0 | 0 | 0 | 0 |
| stjo | 3197 | 3590 | 3743 | 3574 | 3392 | 3385 | 3251 | 3188 | 3757 | 3823 | 3622 |
| suth | 3145 | 3432 | 3386 | 3276 | 3155 | 3157 | 3161 | 2900 | 3074 | 3093 | 3054 |
| suwn | 3509 | 3339 | 3068 | 3027 | 3328 | 3129 | 2776 | 2832 | 3310 | 3264 | 3012 |
| syog | 3886 | 4507 | 4536 | 4485 | 4237 | 4053 | 4278 | 4044 | 4073 | 3583 | 4013 |
| tabl | 0 | 0 | 0 | 0 | 0 | 0 | 0 | 0 | 0 | 0 | 0 |
| thti | 3366 | 3322 | 3196 | 3179 | 2793 | 3162 | 2546 | 2878 | 3257 | 3161 | 3420 |
| thu1 | 1886 | 1641 | 0 | 0 | 0 | 0 | 0 | 0 | 0 | 2387 | 2385 |
| tidb | 3569 | 3428 | 3350 | 3729 | 3544 | 3236 | 3341 | 3469 | 3622 | 3383 | 3378 |
| tixi | 4206 | 4172 | 4071 | 3645 | 4045 | 4008 | 3595 | 3704 | 3913 | 4241 | 4193 |
| torp | 0 | 0 | 0 | 0 | 0 | 0 | 0 | 0 | 0 | 0 | 0 |
| tow2 | 3719 | 3837 | 3598 | 3511 | 3510 | 3376 | 3230 | 3333 | 3211 | 3449 | 3407 |
| trab | 0 | 0 | 0 | 0 | 0 | 0 | 0 | 0 | 0 | 0 | 0 |
| trak | 0 | 0 | 0 | 0 | 0 | 0 | 0 | 0 | 0 | 0 | 0 |
| tro1 | 3910 | 4197 | 4472 | 4220 | 3982 | 3829 | 3959 | 3808 | 4104 | 4309 | 4182 |
| trom | 3883 | 4148 | 4562 | 4244 | 4001 | 3788 | 4035 | 3855 | 4127 | 4314 | 4251 |
| tskb | 2299 | 2354 | 1891 | 1691 | 1843 | 1839 | 1458 | 1583 | 1747 | 1813 | 1720 |
| uclp | 0 | 0 | 0 | 0 | 0 | 0 | 0 | 0 | 0 | 0 | 0 |
| uclu | 113 | 39 | 44 | 175 | 214 | 174 | 152 | 49 | 174 | 291 | 370 |
| urum | 3232 | 0 | 2773 | 2799 | 0 | 2590 | 2731 | 2943 | 3111 | 3059 | 3186 |
| uscl | 0 | 0 | 0 | 0 | 0 | 0 | 0 | 0 | 0 | 0 | 0 |
| usna | 2597 | 2546 | 2964 | 2793 | 2632 | 2504 | 2581 | 2449 | 2816 | 3145 | 3061 |
| usno | 154 | 61 | 46 | 155 | 304 | 413 | 274 | 43 | 235 | 543 | 636 |
| usud | 3367 | 3499 | 3204 | 2863 | 3065 | 3303 | 2979 | 2616 | 2799 | 3187 | 3078 |
| vene | 0 | 0 | 0 | 0 | 0 | 0 | 0 | 0 | 0 | 0 | 0 |
| vesl | 4397 | 4713 | 4532 | 4802 | 2526 | 0 | 0 | 0 | 0 | 0 | 0 |
| vill | 3043 | 3211 | 3599 | 3322 | 3057 | 3170 | 3291 | 3003 | 3306 | 3590 | 3455 |
| vndp | 581 | 632 | 781 | 898 | 802 | 710 | 861 | 831 | 882 | 938 | 945 |
| vs0g | 0 | 0 | 0 | 0 | 0 | 0 | 0 | 0 | 0 | 0 | 0 |
| wes2 | 122 | 61 | 66 | 183 | 146 | 452 | 274 | 43 | 235 | 543 | 636 |
| whc1 | 0 | 0 | 0 | 0 | 0 | 0 | 0 | 0 | 0 | 0 | 0 |
| whit | 3042 | 3183 | 3342 | 3366 | 3247 | 2818 | 2803 | 3079 | 3417 | 3253 | 3217 |
| widc | 0 | 0 | 0 | 0 | 0 | 0 | 0 | 0 | 0 | 0 | 0 |
| will | 2252 | 2678 | 2632 | 2801 | 2483 | 2484 | 2198 | 2533 | 2779 | 2765 | 2542 |
| wlsn | 0 | 0 | 0 | 0 | 0 | 0 | 0 | 0 | 0 | 0 | 0 |
| wroc | 0 | 0 | 0 | 0 | 0 | 0 | 0 | 0 | 0 | 0 | 0 |
| wslr | 568 | 456 | 609 | 934 | 816 | 568 | 629 | 793 | 976 | 915 | 733 |
| wsrt | 3143 | 3354 | 3703 | 3580 | 3388 | 3152 | 3186 | 3345 | 3499 | 3498 | 3537 |
| wtzr | 3376 | 3495 | 3828 | 2841 | 2387 | 3112 | 3280 | 3235 | 3365 | 3403 | 3454 |
| wuhn | 3639 | 3622 | 2857 | 2606 | 3528 | 3339 | 2957 | 2966 | 3341 | 3485 | 3385 |
| xian | 0 | 0 | 0 | 0 | 0 | 0 | 0 | 0 | 0 | 0 | 0 |
| yakz | 0 | 0 | 0 | 0 | 0 | 0 | 0 | 0 | 0 | 0 | 0 |
| yar1 | 2559 | 2710 | 2463 | 2382 | 2200 | 2346 | 2498 | 1501 | 0 | 2006 | 2561 |
| yell | 3134 | 3274 | 3334 | 3337 | 3287 | 3277 | 2972 | 3147 | 3566 | 3621 | 3332 |
| ykro | 0 | 0 | 0 | 0 | 0 | 0 | 0 | 0 | 0 | 0 | 0 |
| yssk | 3350 | 3460 | 3174 | 3117 | 3071 | 3265 | 3101 | 2990 | 2841 | 3069 | 3219 |
| zeck | 3446 | 3621 | 3510 | 3086 | 3518 | 3172 | 3095 | 3038 | 3426 | 3299 | 3253 |
| zimm | 3260 | 3247 | 3611 | 3273 | 3209 | 3150 | 3185 | 3259 | 3305 | 3474 | 3394 |
| zwen | 3459 | 3588 | 3594 | 3534 | 3507 | 3140 | 3407 | 3443 | 3399 | 3351 | 3635 |

Table F.10: Daily DDobs numbers for cycle 10

| site ID | day 104 | day 105 | day 106 | day 107 | day 108 | day 109 | day 110 | day 111 | day 112 | day 113 | day 114 |
|---|---|---|---|---|---|---|---|---|---|---|---|
| albh | 169 | 109 | 123 | 97 | 306 | 535 | 399 | 103 | 110 | 449 | 677 |
| algo | 3520 | 3408 | 3488 | 3276 | 3451 | 3419 | 3416 | 3346 | 3316 | 3696 | 3735 |
| alic | 3877 | 3464 | 3166 | 3326 | 3830 | 3764 | 3433 | 3287 | 3369 | 3639 | 3838 |
| amc2 | 3205 | 2926 | 3077 | 3203 | 3149 | 2788 | 2892 | 3036 | 3182 | 3041 | 3234 |
| ankr | 3269 | 3479 | 3101 | 0 | 3026 | 3214 | 3570 | 3145 | 2940 | 3213 | 3621 |
| aoa1 | 2363 | 2495 | 2555 | 2469 | 2379 | 2533 | 2586 | 2339 | 2419 | 2584 | 2905 |
| aoml | 2558 | 2611 | 2574 | 2502 | 2780 | 2646 | 2607 | 2337 | 2260 | 287 | 2055 |
| areq | 0 | 0 | 0 | 0 | 0 | 0 | 0 | 0 | 0 | 0 | 0 |
| artu | 3552 | 3835 | 3251 | 3192 | 3426 | 3423 | 3483 | 3191 | 3137 | 3320 | 3550 |
| asc1 | 2953 | 2627 | 2527 | 2911 | 3487 | 2410 | 0 | 0 | 2847 | 3289 | 2943 |
| auck | 3287 | 3235 | 2897 | 2878 | 3341 | 3326 | 3124 | 3115 | 3240 | 3547 | 3430 |
| azu1 | 0 | 0 | 0 | 0 | 0 | 0 | 0 | 0 | 0 | 0 | 0 |
| bahr | 3148 | 3149 | 3109 | 3291 | 3465 | 3065 | 3172 | 2726 | 2741 | 3011 | 3281 |
| bako | 0 | 0 | 0 | 0 | 0 | 0 | 0 | 0 | 0 | 0 | 0 |
| barb | 0 | 0 | 0 | 0 | 0 | 0 | 0 | 0 | 0 | 0 | 0 |
| bili | 3118 | 4052 | 3811 | 3608 | 3735 | 3431 | 3409 | 3620 | 3707 | 3623 | 3758 |
| bjfs | 3090 | 2729 | 2743 | 2732 | 2874 | 2515 | 2599 | 2821 | 2577 | 2587 | 2743 |
| blyt | 0 | 0 | 0 | 0 | 0 | 0 | 0 | 0 | 0 | 0 | 0 |
| bogt | 0 | 0 | 0 | 0 | 0 | 0 | 0 | 0 | 0 | 0 | 0 |
| bor1 | 3326 | 3037 | 3164 | 3139 | 3624 | 3127 | 3059 | 2938 | 3263 | 3200 | 3124 |
| bran | 0 | 0 | 0 | 0 | 0 | 0 | 0 | 0 | 0 | 0 | 0 |
| braz | 0 | 1536 | 3274 | 3139 | 3148 | 3175 | 3257 | 3013 | 3070 | 3456 | 3473 |
| brmu | 2960 | 2788 | 0 | 0 | 2623 | 3214 | 3064 | 2946 | 2579 | 3226 | 3301 |
| brus | 1689 | 1945 | 886 | 0 | 0 | 1997 | 3687 | 3435 | 3428 | 3246 | 3367 |
| bucu | 0 | 0 | 0 | 0 | 0 | 0 | 0 | 0 | 0 | 0 | 0 |
| bzrg | 0 | 0 | 0 | 0 | 0 | 0 | 0 | 0 | 0 | 0 | 0 |
| cagl | 0 | 0 | 0 | 0 | 0 | 0 | 0 | 0 | 0 | 0 | 0 |
| cas1 | 4501 | 4158 | 4208 | 4533 | 4666 | 4550 | 4479 | 4600 | 4628 | 4554 | 4723 |
| casa | 2253 | 2521 | 2435 | 2320 | 2333 | 2570 | 2638 | 2297 | 2252 | 2591 | 2901 |
| cat1 | 0 | 0 | 0 | 0 | 0 | 0 | 0 | 0 | 0 | 0 | 0 |
| cedu | 3658 | 3397 | 3301 | 3158 | 3628 | 3801 | 3646 | 3035 | 3223 | 3677 | 0 |
| chat | 3365 | 3435 | 3031 | 2845 | 3356 | 3452 | 3346 | 3003 | 3214 | 3483 | 3543 |
| chil | 0 | 0 | 0 | 0 | 0 | 0 | 0 | 0 | 0 | 0 | 0 |
| chur | 3486 | 3438 | 3260 | 3159 | 3598 | 3420 | 3273 | 3065 | 3410 | 3692 | 3701 |
| chwk | 2397 | 2590 | 2786 | 2616 | 2492 | 2625 | 2867 | 2738 | 2563 | 2588 | 3096 |
| cic1 | 2132 | 2112 | 2058 | 2212 | 2292 | 2427 | 2394 | 2207 | 2238 | 2352 | 2743 |
| cit1 | 0 | 0 | 0 | 0 | 0 | 0 | 0 | 0 | 0 | 0 | 0 |
| clar | 0 | 0 | 0 | 0 | 0 | 0 | 0 | 0 | 0 | 0 | 0 |
| cmp9 | 0 | 0 | 0 | 0 | 0 | 0 | 0 | 0 | 0 | 0 | 0 |
| coco | 3180 | 3361 | 3354 | 3061 | 3439 | 3516 | 3488 | 3098 | 3073 | 3440 | 3735 |
| cord | 0 | 0 | 0 | 0 | 0 | 0 | 0 | 0 | 0 | 0 | 0 |
| coso | 0 | 0 | 0 | 0 | 0 | 0 | 0 | 0 | 0 | 0 | 0 |
| crfp | 0 | 0 | 0 | 0 | 0 | 0 | 0 | 0 | 0 | 0 | 0 |
| cro1 | 3057 | 3138 | 3222 | 3118 | 3307 | 3099 | 3158 | 3065 | 3247 | 3151 | 3262 |
| csn1 | 0 | 0 | 0 | 0 | 0 | 0 | 0 | 0 | 0 | 0 | 0 |
| daej | 3104 | 3093 | 3319 | 2911 | 2846 | 2951 | 3144 | 3259 | 2801 | 2869 | 3112 |
| darw | 0 | 2501 | 2991 | 3338 | 3651 | 3382 | 3065 | 3387 | 3585 | 3578 | 3411 |
| dav1 | 4053 | 4290 | 4347 | 4444 | 4637 | 4550 | 4386 | 4437 | 4042 | 0 | 4129 |
| dgar | 0 | 0 | 0 | 0 | 0 | 0 | 0 | 0 | 0 | 0 | 0 |
| dhlg | 0 | 0 | 0 | 0 | 0 | 0 | 0 | 0 | 0 | 0 | 0 |
| drag | 0 | 0 | 0 | 0 | 0 | 0 | 2747 | 1431 | 201 | 201 | 0 |
| drao | 485 | 375 | 125 | 158 | 388 | 543 | 399 | 103 | 110 | 452 | 680 |
| dubo | 3049 | 2826 | 2671 | 2834 | 2898 | 2886 | 2682 | 2842 | 2981 | 3159 | 3131 |
| ebre | 3361 | 3311 | 3344 | 3382 | 3718 | 3225 | 3346 | 3293 | 3396 | 3461 | 3362 |
| eisl | 1770 | 1293 | 366 | 705 | 359 | 342 | 0 | 704 | 982 | 767 | 598 |
| fair | 3168 | 3334 | 3208 | 2973 | 3157 | 2885 | 3068 | 2910 | 2914 | 3069 | 3605 |
| flin | 1207 | 1101 | 994 | 1089 | 1332 | 1259 | 1109 | 976 | 1128 | 1336 | 1320 |
| fort | 2240 | 2001 | 2250 | 2193 | 2089 | 2155 | 2559 | 2443 | 1778 | 1872 | 230 |
| gala | 3472 | 2885 | 2785 | 3224 | 3194 | 3009 | 3113 | 3125 | 3644 | 3597 | 3479 |
| geno | 0 | 0 | 0 | 0 | 0 | 0 | 0 | 0 | 0 | 0 | 0 |
| glsv | 3431 | 3617 | 3506 | 3222 | 3569 | 3360 | 3552 | 3243 | 3263 | 3203 | 3476 |
| gode | 0 | 0 | 0 | 1522 | 2665 | 2985 | 1708 | 2670 | 2103 | 0 | 2550 |
| gold | 2895 | 3078 | 2939 | 2770 | 2736 | 2891 | 3092 | 2775 | 2770 | 2783 | 3343 |
| gope | 0 | 0 | 0 | 0 | 0 | 0 | 0 | 0 | 0 | 0 | 0 |
| goug | 2650 | 2611 | 2554 | 2910 | 2719 | 2574 | 2871 | 2943 | 2858 | 2901 | 3030 |
| gras | 3086 | 2936 | 3001 | 2883 | 2743 | 0 | 3014 | 3025 | 3107 | 3207 | 2961 |
| graz | 3403 | 3560 | 3446 | 3308 | 3575 | 3460 | 3597 | 3310 | 3364 | 3125 | 1339 |
| guam | 2577 | 2950 | 2719 | 2471 | 2741 | 2604 | 3012 | 2790 | 2426 | 2746 | 3106 |
| harv | 2766 | 3065 | 3051 | 2844 | 2689 | 2329 | 0 | 0 | 0 | 0 | 0 |
| hers | 3323 | 3398 | 3607 | 3427 | 3613 | 3258 | 3644 | 3335 | 3342 | 3283 | 3591 |
| hflk | 0 | 0 | 0 | 0 | 0 | 0 | 0 | 0 | 0 | 0 | 0 |
| ... | ... | ... | ... | ... | ... | ... | ... | ... | ... | ... | ... |

Table F.10: Daily DDobs numbers for cycle 10. (continued)

| site ID | day 104 | day 105 | day 106 | day 107 | day 108 | day 109 | day 110 | day 111 | day 112 | day 113 | day 114 |
|---|---|---|---|---|---|---|---|---|---|---|---|
| hnpt | 3100 | 3144 | 2840 | 2719 | 2860 | 2893 | 2521 | 2600 | 2807 | 3299 | 3238 |
| hob2 | 3369 | 3461 | 3415 | 3330 | 3538 | 3595 | 3751 | 3525 | 3285 | 3496 | 4016 |
| hofn | 3895 | 4380 | 3993 | 3433 | 3327 | 3353 | 3429 | 3906 | 3926 | 3814 | 4095 |
| holb | 353 | 333 | 109 | 81 | 272 | 506 | 399 | 103 | 85 | 333 | 586 |
| holc | 0 | 0 | 0 | 0 | 0 | 0 | 0 | 0 | 0 | 0 | 0 |
| holp | 0 | 0 | 0 | 0 | 0 | 0 | 0 | 0 | 0 | 0 | 0 |
| hrao | 2486 | 2763 | 2744 | 3151 | 2938 | 2583 | 2386 | 1962 | 2381 | 2929 | 2841 |
| iisc | 3198 | 2846 | 2546 | 2634 | 3170 | 2459 | 3136 | 2878 | 2730 | 2739 | 2732 |
| ineg | 0 | 0 | 0 | 0 | 0 | 0 | 0 | 0 | 0 | 0 | 0 |
| irkt | 2756 | 3167 | 2854 | 2675 | 2968 | 2721 | 2855 | 2718 | 2766 | 2575 | 2872 |
| jab1 | 0 | 0 | 0 | 0 | 0 | 0 | 0 | 0 | 0 | 0 | 0 |
| jama | 1901 | 2338 | 2141 | 1405 | 1580 | 1535 | 939 | 167 | 448 | 386 | 0 |
| joze | 3561 | 3621 | 3501 | 3314 | 3621 | 3416 | 3550 | 3314 | 3230 | 3227 | 3276 |
| jplm | 2452 | 2716 | 2642 | 2519 | 2403 | 2510 | 2524 | 2394 | 2398 | 2574 | 3071 |
| karr | 3495 | 0 | 2956 | 3588 | 3780 | 3558 | 3532 | 3531 | 3318 | 3377 | 3687 |
| kely | 3761 | 2297 | 0 | 0 | 3599 | 3773 | 3124 | 0 | 1634 | 2834 | 3462 |
| kerg | 3179 | 2979 | 3349 | 3614 | 3429 | 3105 | 3523 | 3688 | 3479 | 3155 | 3682 |
| kiru | 4201 | 4494 | 4205 | 4225 | 4260 | 4148 | 4026 | 3871 | 3773 | 3813 | 3869 |
| kit3 | 2934 | 2977 | 1776 | 2011 | 661 | 0 | 0 | 0 | 0 | 0 | 1216 |
| kokb | 2303 | 2615 | 2797 | 2575 | 2619 | 2673 | 2748 | 2650 | 2738 | 2726 | 2935 |
| kosg | 3525 | 3589 | 3617 | 3453 | 3799 | 3492 | 3685 | 3492 | 3472 | 3492 | 3633 |
| kour | 3894 | 3755 | 3903 | 3958 | 3914 | 3590 | 3854 | 3633 | 3921 | 4025 | 4037 |
| kr0g | 0 | 0 | 0 | 0 | 0 | 0 | 0 | 0 | 0 | 0 | 0 |
| kstu | 681 | 2658 | 2813 | 2849 | 2814 | 2791 | 2738 | 2680 | 2391 | 1648 | 2066 |
| kunm | 1491 | 1577 | 1819 | 1221 | 1790 | 1922 | 2018 | 1216 | 1335 | 1485 | 1235 |
| kwj1 | 0 | 0 | 0 | 0 | 0 | 0 | 0 | 0 | 0 | 0 | 0 |
| lama | 0 | 0 | 0 | 0 | 0 | 0 | 0 | 0 | 0 | 0 | 0 |
| lbch | 0 | 0 | 0 | 0 | 0 | 0 | 0 | 0 | 0 | 0 | 0 |
| leep | 0 | 0 | 0 | 0 | 0 | 0 | 0 | 0 | 0 | 0 | 0 |
| lhas | 2704 | 2740 | 2673 | 2694 | 2778 | 2762 | 2821 | 2671 | 2467 | 2578 | 2715 |
| long | 0 | 0 | 0 | 0 | 0 | 0 | 0 | 0 | 0 | 0 | 0 |
| lpgs | 0 | 1797 | 2937 | 3249 | 3076 | 2815 | 2681 | 3091 | 3180 | 3401 | 3218 |
| mac1 | 3822 | 3472 | 3361 | 3411 | 3841 | 3843 | 3707 | 3493 | 3515 | 3973 | 4005 |
| madr | 3450 | 3273 | 3151 | 3222 | 3648 | 3189 | 2989 | 2469 | 3432 | 3372 | 3335 |
| mag0 | 3143 | 3419 | 3181 | 2803 | 3219 | 3055 | 3035 | 2975 | 3030 | 3117 | 3171 |
| mali | 2913 | 3139 | 3292 | 3433 | 3222 | 2973 | 3431 | 3460 | 3035 | 3149 | 3529 |
| mas1 | 3241 | 3397 | 3445 | 3150 | 3339 | 3064 | 3431 | 3051 | 3051 | 2239 | 3083 |
| mate | 3063 | 3413 | 3487 | 3187 | 3377 | 3272 | 3585 | 3249 | 2976 | 3064 | 3481 |
| math | 0 | 0 | 0 | 0 | 0 | 0 | 0 | 0 | 0 | 0 | 0 |
| maw1 | 4401 | 4239 | 3992 | 4323 | 4551 | 4685 | 4253 | 4273 | 4660 | 4781 | 4788 |
| mcm4 | 4692 | 4404 | 4503 | 4637 | 4667 | 4699 | 4628 | 4681 | 4600 | 4713 | 5051 |
| mdo1 | 2484 | 2215 | 2373 | 2451 | 2648 | 2529 | 2572 | 2097 | 2430 | 2610 | 2816 |
| mdvo | 2556 | 2973 | 3073 | 3360 | 3563 | 3507 | 3473 | 2481 | 2407 | 2591 | 3369 |
| medi | 0 | 0 | 0 | 0 | 0 | 0 | 0 | 0 | 0 | 0 | 0 |
| mets | 3780 | 3918 | 3609 | 3721 | 3756 | 3654 | 3728 | 3556 | 3481 | 3573 | 3603 |
| mkea | 2275 | 2579 | 2711 | 2601 | 2464 | 2666 | 2736 | 2529 | 2453 | 2447 | 2977 |
| monp | 2923 | 3111 | 3086 | 2882 | 2753 | 2828 | 3084 | 2675 | 2757 | 2328 | 0 |
| mr6g | 0 | 0 | 0 | 0 | 0 | 0 | 0 | 0 | 0 | 0 | 0 |
| nano | 843 | 877 | 906 | 933 | 810 | 868 | 987 | 884 | 874 | 0 | 1184 |
| nico | 3042 | 3280 | 3312 | 3268 | 3288 | 3124 | 3473 | 3198 | 2870 | 3065 | 3352 |
| nklg | 2663 | 2755 | 2810 | 3299 | 3472 | 3023 | 3498 | 3168 | 3171 | 3084 | 3344 |
| nlib | 2590 | 2457 | 2553 | 2520 | 2691 | 2483 | 2735 | 1056 | 0 | 2733 | 3064 |
| noto | 0 | 0 | 0 | 0 | 0 | 0 | 0 | 0 | 0 | 0 | 0 |
| noum | 3057 | 3205 | 3049 | 2919 | 3154 | 3023 | 3203 | 2904 | 2978 | 3137 | 3626 |
| nrc1 | 3502 | 3501 | 3550 | 3291 | 3462 | 3524 | 3481 | 3357 | 3334 | 3780 | 3803 |
| nssp | 0 | 0 | 0 | 0 | 0 | 0 | 0 | 0 | 0 | 0 | 0 |
| ntus | 3529 | 3528 | 3662 | 3488 | 3572 | 3630 | 3571 | 3382 | 3221 | 3573 | 3723 |
| nya1 | 4570 | 4629 | 4451 | 3642 | 0 | 0 | 0 | 0 | 0 | 0 | 0 |
| nyal | 4608 | 4602 | 4375 | 4094 | 4383 | 4171 | 4570 | 4020 | 3986 | 4375 | 4399 |
| oat2 | 0 | 0 | 0 | 0 | 0 | 0 | 0 | 0 | 0 | 0 | 0 |
| onsa | 3731 | 3974 | 3831 | 3515 | 3870 | 3682 | 3862 | 3514 | 3555 | 3502 | 3727 |
| penc | 0 | 0 | 0 | 0 | 0 | 0 | 0 | 0 | 0 | 0 | 0 |
| pert | 3699 | 3233 | 3148 | 3427 | 3667 | 3530 | 3365 | 3294 | 3352 | 3529 | 3437 |
| petp | 2796 | 3021 | 2847 | 2467 | 2728 | 2704 | 2648 | 1084 | 0 | 0 | 0 |
| pie1 | 2488 | 2351 | 2165 | 2419 | 2586 | 2518 | 2498 | 2188 | 2465 | 2614 | 2836 |
| pimo | 2912 | 2615 | 0 | 2429 | 2928 | 3230 | 3170 | 2382 | 2621 | 3135 | 3009 |
| pol2 | 2851 | 3299 | 2716 | 2400 | 2738 | 2915 | 3182 | 2801 | 2646 | 2760 | 3145 |
| pots | 3530 | 3635 | 3538 | 3385 | 3855 | 3572 | 3483 | 3329 | 3476 | 3555 | 3582 |
| prds | 3030 | 3030 | 3269 | 3195 | 3210 | 2922 | 3196 | 3089 | 3028 | 3027 | 3405 |
| pvep | 0 | 0 | 0 | 0 | 0 | 0 | 0 | 0 | 0 | 0 | 0 |
| quin | 2249 | 2395 | 2138 | 2176 | 2197 | 2515 | 2527 | 2224 | 2210 | 2708 | 2888 |
| ... | ... | ... | ... | ... | ... | ... | ... | ... | ... | ... | ... |

Table F.10: Daily DDobs numbers for cycle 10. (continued)

| site ID | day 104 | day 105 | day 106 | day 107 | day 108 | day 109 | day 110 | day 111 | day 112 | day 113 | day 114 |
|---|---|---|---|---|---|---|---|---|---|---|---|
| ramo | 2951 | 3202 | 3242 | 3221 | 3199 | 3118 | 3223 | 3160 | 2971 | 2964 | 3271 |
| reyk | 4088 | 4159 | 4021 | 3910 | 4089 | 3992 | 4061 | 3976 | 3830 | 3982 | 4213 |
| riog | 3704 | 3463 | 3027 | 3580 | 3540 | 3521 | 3340 | 3193 | 3767 | 4023 | 3800 |
| riop | 0 | 0 | 0 | 0 | 0 | 0 | 0 | 0 | 0 | 0 | 0 |
| roch | 0 | 0 | 0 | 0 | 0 | 0 | 0 | 0 | 0 | 0 | 0 |
| rock | 0 | 0 | 0 | 0 | 0 | 0 | 0 | 0 | 0 | 0 | 0 |
| sant | 3158 | 3193 | 3057 | 2965 | 3105 | 3089 | 3259 | 3171 | 3157 | 3293 | 3655 |
| sch2 | 3533 | 3659 | 3626 | 3409 | 3507 | 3049 | 3214 | 3557 | 3282 | 3659 | 3882 |
| scip | 0 | 0 | 0 | 0 | 0 | 0 | 0 | 0 | 0 | 0 | 0 |
| sele | 2777 | 2661 | 2498 | 2559 | 2844 | 2667 | 2917 | 2497 | 2433 | 2394 | 2489 |
| sey1 | 1496 | 1597 | 1612 | 1582 | 1741 | 1488 | 1483 | 1627 | 1520 | 1627 | 1773 |
| sfer | 0 | 0 | 0 | 0 | 0 | 0 | 0 | 0 | 0 | 0 | 0 |
| shao | 2718 | 2545 | 2395 | 2321 | 2649 | 2667 | 2434 | 2636 | 2468 | 2412 | 2498 |
| sio3 | 472 | 375 | 109 | 78 | 293 | 511 | 399 | 103 | 81 | 294 | 550 |
| sni1 | 0 | 0 | 0 | 0 | 0 | 0 | 0 | 0 | 0 | 0 | 0 |
| sofi | 0 | 0 | 0 | 0 | 0 | 0 | 0 | 0 | 0 | 0 | 0 |
| sol1 | 3237 | 3418 | 3044 | 2928 | 3040 | 3557 | 3327 | 3116 | 3156 | 3690 | 3631 |
| spk1 | 0 | 0 | 0 | 0 | 0 | 0 | 0 | 0 | 0 | 0 | 0 |
| stjo | 3622 | 3851 | 3875 | 3747 | 3776 | 3602 | 3532 | 3501 | 3435 | 3741 | 3839 |
| suth | 3054 | 2724 | 2675 | 3231 | 3091 | 2824 | 3031 | 3241 | 3220 | 3134 | 3216 |
| suwn | 3012 | 2982 | 3162 | 2872 | 2692 | 2435 | 2640 | 3155 | 2727 | 2725 | 2913 |
| syog | 4013 | 3905 | 3487 | 3514 | 3492 | 3857 | 3461 | 4237 | 4457 | 4354 | 4395 |
| tabl | 0 | 0 | 0 | 0 | 0 | 0 | 0 | 0 | 0 | 0 | 0 |
| thti | 3420 | 3006 | 2720 | 2924 | 3510 | 3167 | 2919 | 2815 | 3094 | 3245 | 3337 |
| thu1 | 2385 | 0 | 0 | 1989 | 0 | 2958 | 2090 | 2735 | 2952 | 3226 | 3259 |
| tidb | 3378 | 3364 | 3314 | 3207 | 3222 | 3379 | 3567 | 3381 | 3158 | 3302 | 4000 |
| tixi | 4193 | 4225 | 4106 | 3904 | 3800 | 3754 | 3906 | 3844 | 3831 | 3691 | 3999 |
| torp | 0 | 0 | 0 | 0 | 0 | 0 | 0 | 0 | 0 | 0 | 0 |
| tow2 | 3407 | 3391 | 3136 | 3151 | 3421 | 3472 | 3342 | 3024 | 3164 | 3480 | 4042 |
| trab | 0 | 0 | 0 | 0 | 0 | 0 | 0 | 0 | 0 | 0 | 0 |
| trak | 0 | 0 | 0 | 0 | 0 | 0 | 0 | 0 | 0 | 0 | 0 |
| tro1 | 4182 | 4570 | 4232 | 4040 | 4276 | 4066 | 4202 | 4003 | 4019 | 4126 | 4077 |
| trom | 4251 | 4717 | 4281 | 4010 | 4408 | 4233 | 4340 | 3998 | 3471 | 0 | 2174 |
| tskb | 1720 | 1553 | 1702 | 1354 | 2021 | 2374 | 2017 | 2371 | 1758 | 1739 | 1756 |
| uclp | 0 | 0 | 0 | 0 | 0 | 0 | 0 | 0 | 0 | 0 | 0 |
| uclu | 370 | 348 | 121 | 93 | 291 | 522 | 399 | 103 | 100 | 355 | 593 |
| urum | 3186 | 3209 | 3109 | 2999 | 3250 | 2965 | 2994 | 2890 | 2604 | 0 | 2535 |
| uscl | 0 | 0 | 0 | 0 | 0 | 0 | 0 | 0 | 0 | 0 | 0 |
| usna | 3061 | 3178 | 3015 | 2861 | 3008 | 3162 | 3002 | 2824 | 2841 | 3127 | 3183 |
| usno | 636 | 423 | 125 | 229 | 608 | 748 | 424 | 86 | 232 | 561 | 674 |
| usud | 3078 | 2955 | 2778 | 2714 | 2888 | 2701 | 2560 | 2824 | 2716 | 2759 | 2809 |
| vene | 0 | 0 | 0 | 0 | 0 | 0 | 0 | 0 | 0 | 0 | 0 |
| vesl | 0 | 0 | 0 | 0 | 0 | 0 | 0 | 0 | 0 | 0 | 0 |
| vill | 3455 | 3311 | 3434 | 3342 | 3664 | 2177 | 3014 | 3212 | 2414 | 3068 | 3383 |
| vndp | 945 | 974 | 883 | 811 | 855 | 1020 | 991 | 695 | 715 | 969 | 1138 |
| vs0g | 0 | 0 | 0 | 0 | 0 | 0 | 0 | 0 | 0 | 0 | 0 |
| wes2 | 636 | 406 | 108 | 229 | 608 | 732 | 408 | 86 | 233 | 648 | 760 |
| whc1 | 0 | 0 | 0 | 0 | 0 | 0 | 0 | 0 | 0 | 0 | 0 |
| whit | 3217 | 3425 | 3660 | 3418 | 3163 | 3180 | 3514 | 3404 | 3033 | 3246 | 3763 |
| widc | 0 | 0 | 0 | 0 | 0 | 0 | 0 | 0 | 0 | 0 | 0 |
| will | 2542 | 2700 | 2940 | 2804 | 2704 | 2685 | 2931 | 2892 | 2685 | 2609 | 2982 |
| wlsn | 0 | 0 | 0 | 0 | 0 | 0 | 0 | 0 | 0 | 0 | 0 |
| wroc | 0 | 0 | 0 | 0 | 0 | 0 | 0 | 0 | 0 | 0 | 0 |
| wslr | 733 | 823 | 917 | 892 | 730 | 845 | 931 | 709 | 519 | 871 | 1167 |
| wsrt | 3537 | 3681 | 3691 | 3478 | 3811 | 3520 | 3735 | 3467 | 3483 | 3508 | 3689 |
| wtzr | 3454 | 3633 | 3485 | 3358 | 3709 | 3589 | 3616 | 3366 | 3331 | 3457 | 3543 |
| wuhn | 3385 | 3123 | 3292 | 3075 | 3027 | 2816 | 2981 | 0 | 2788 | 2758 | 3046 |
| xian | 0 | 0 | 0 | 0 | 0 | 0 | 0 | 0 | 0 | 0 | 0 |
| yakz | 0 | 0 | 0 | 0 | 0 | 0 | 0 | 0 | 0 | 0 | 0 |
| yar1 | 2561 | 1988 | 2196 | 2376 | 1975 | 1932 | 2517 | 2428 | 1579 | 1986 | 2293 |
| yell | 3332 | 3616 | 3704 | 3464 | 3334 | 3343 | 3454 | 3571 | 3280 | 3426 | 3768 |
| ykro | 0 | 0 | 0 | 0 | 0 | 0 | 0 | 0 | 0 | 0 | 0 |
| yssk | 3219 | 3246 | 3037 | 2719 | 2938 | 2972 | 2987 | 2923 | 2857 | 2961 | 3119 |
| zeck | 3253 | 3406 | 3350 | 3287 | 3464 | 3154 | 3316 | 3193 | 3091 | 3218 | 3318 |
| zimm | 3394 | 3500 | 3455 | 3413 | 3659 | 3431 | 3607 | 3326 | 3353 | 3537 | 3572 |
| zwen | 3635 | 3767 | 3286 | 3492 | 3758 | 3492 | 3469 | 3145 | 3139 | 3447 | 3509 |

Table F.11: Daily DDobs numbers for cycle 11

| site ID | day 114 | day 115 | day 116 | day 117 | day 118 | day 119 | day 120 | day 121 | day 122 | day 123 | day 124 |
|---|---|---|---|---|---|---|---|---|---|---|---|
| albh | 677 | 479 | 134 | 0 | 318 | 613 | 433 | 138 | 88 | 389 | 579 |
| algo | 3735 | 3540 | 3545 | 2568 | 2492 | 3516 | 3369 | 3589 | 3728 | 3530 | 3440 |
| alic | 3838 | 3654 | 3611 | 2972 | 3105 | 3412 | 3696 | 3406 | 2959 | 1868 | 3078 |
| amc2 | 3234 | 3274 | 3390 | 2380 | 2345 | 3281 | 3079 | 3206 | 3275 | 3221 | 3218 |
| ankr | 3621 | 3343 | 3147 | 2119 | 2669 | 3403 | 3264 | 3059 | 3400 | 2868 | 2552 |
| aoa1 | 2905 | 2590 | 2404 | 1957 | 2120 | 2785 | 2554 | 2466 | 2650 | 2431 | 2608 |
| aoml | 2055 | 2643 | 2404 | 1835 | 1848 | 2579 | 2291 | 2594 | 2388 | 522 | 1645 |
| areq | 0 | 0 | 0 | 0 | 0 | 0 | 0 | 0 | 0 | 0 | 0 |
| artu | 3550 | 3163 | 2974 | 2080 | 2787 | 2964 | 3123 | 3151 | 3252 | 2628 | 2600 |
| asc1 | 2943 | 3059 | 3655 | 2862 | 2628 | 3292 | 1637 | 2724 | 2273 | 0 | 2368 |
| auck | 3430 | 3488 | 3538 | 2941 | 2943 | 3377 | 3616 | 3309 | 3378 | 3260 | 3187 |
| azu1 | 0 | 0 | 0 | 0 | 0 | 0 | 0 | 0 | 0 | 0 | 0 |
| bahr | 3281 | 3240 | 3035 | 2191 | 2545 | 3155 | 3265 | 2890 | 3105 | 2515 | 2485 |
| bako | 0 | 0 | 0 | 0 | 0 | 0 | 0 | 0 | 0 | 0 | 0 |
| barb | 0 | 0 | 0 | 0 | 0 | 0 | 0 | 0 | 0 | 0 | 0 |
| bili | 3758 | 3799 | 3551 | 2772 | 3183 | 3487 | 3590 | 3511 | 3818 | 3266 | 3551 |
| bjfs | 2743 | 2895 | 2551 | 2057 | 2339 | 2621 | 2727 | 2604 | 2531 | 2198 | 2489 |
| blyt | 0 | 0 | 0 | 0 | 0 | 0 | 0 | 0 | 0 | 0 | 0 |
| bogt | 0 | 0 | 0 | 0 | 0 | 0 | 0 | 0 | 0 | 0 | 0 |
| bor1 | 3124 | 3214 | 3114 | 2098 | 2209 | 3050 | 3220 | 3244 | 3042 | 2518 | 2585 |
| bran | 0 | 0 | 0 | 0 | 0 | 0 | 0 | 0 | 0 | 0 | 0 |
| braz | 3473 | 2981 | 0 | 2294 | 2819 | 3589 | 2821 | 3122 | 3107 | 0 | 2769 |
| brmu | 3301 | 2904 | 2881 | 2158 | 2366 | 3020 | 2592 | 2908 | 3064 | 3029 | 2801 |
| brus | 3367 | 3514 | 3543 | 2306 | 2349 | 3358 | 3556 | 3540 | 3382 | 3005 | 2971 |
| bucu | 0 | 0 | 0 | 0 | 0 | 0 | 0 | 0 | 0 | 0 | 0 |
| bzrg | 0 | 0 | 0 | 0 | 0 | 0 | 0 | 0 | 0 | 0 | 0 |
| cagl | 0 | 0 | 0 | 0 | 0 | 0 | 0 | 0 | 0 | 0 | 0 |
| cas1 | 4723 | 4858 | 4917 | 3755 | 3844 | 4871 | 4913 | 4573 | 4607 | 4579 | 4416 |
| casa | 2901 | 2505 | 2239 | 1917 | 2032 | 2614 | 2416 | 2302 | 2681 | 2591 | 2442 |
| cat1 | 0 | 0 | 0 | 0 | 0 | 0 | 0 | 0 | 0 | 0 | 0 |
| cedu | 0 | 3552 | 3497 | 2944 | 3224 | 3228 | 3215 | 3334 | 3455 | 2948 | 0 |
| chat | 3543 | 3465 | 3517 | 2995 | 3096 | 3495 | 3438 | 3606 | 3543 | 3482 | 3292 |
| chil | 0 | 0 | 0 | 0 | 0 | 0 | 0 | 0 | 0 | 0 | 0 |
| chur | 3701 | 3194 | 3473 | 2567 | 2614 | 3287 | 3348 | 3855 | 3811 | 3356 | 3317 |
| chwk | 3096 | 2921 | 2601 | 1918 | 2296 | 2922 | 2677 | 2533 | 2795 | 2861 | 2674 |
| cic1 | 2743 | 2441 | 1860 | 1723 | 1776 | 2429 | 2105 | 2008 | 2312 | 2184 | 1924 |
| cit1 | 0 | 0 | 0 | 0 | 0 | 0 | 0 | 0 | 0 | 0 | 0 |
| clar | 0 | 0 | 0 | 0 | 0 | 0 | 0 | 0 | 0 | 0 | 0 |
| cmp9 | 0 | 0 | 0 | 0 | 0 | 0 | 0 | 0 | 0 | 0 | 0 |
| coco | 3735 | 3635 | 3155 | 2677 | 2960 | 3591 | 3431 | 3274 | 3326 | 2791 | 3077 |
| cord | 0 | 0 | 0 | 0 | 0 | 0 | 0 | 0 | 0 | 0 | 0 |
| coso | 0 | 0 | 0 | 0 | 0 | 0 | 0 | 0 | 0 | 0 | 0 |
| crfp | 0 | 0 | 0 | 0 | 0 | 0 | 0 | 0 | 0 | 0 | 0 |
| cro1 | 3262 | 3251 | 3503 | 2378 | 2200 | 3342 | 2943 | 3293 | 3257 | 3217 | 2961 |
| csn1 | 0 | 0 | 0 | 0 | 0 | 0 | 0 | 0 | 0 | 0 | 0 |
| daej | 3112 | 3293 | 2872 | 2168 | 2732 | 2988 | 3101 | 2797 | 2972 | 2281 | 2889 |
| darw | 3411 | 3508 | 3735 | 2956 | 2882 | 3224 | 3992 | 3550 | 2937 | 2784 | 3640 |
| dav1 | 4129 | 4937 | 4805 | 3936 | 3803 | 4802 | 4830 | 4624 | 4884 | 4550 | 4344 |
| dgar | 0 | 0 | 0 | 0 | 0 | 0 | 0 | 0 | 0 | 0 | 0 |
| dhlg | 0 | 0 | 0 | 0 | 0 | 0 | 0 | 0 | 0 | 0 | 0 |
| drag | 0 | 6 | 0 | 0 | 0 | 1230 | 685 | 23 | 29 | 0 | 0 |
| drao | 680 | 479 | 134 | 0 | 339 | 648 | 455 | 146 | 88 | 402 | 591 |
| dubo | 3131 | 2947 | 2825 | 1893 | 2208 | 2992 | 2925 | 3036 | 3100 | 2896 | 2931 |
| ebre | 3362 | 3345 | 3445 | 2321 | 2367 | 3186 | 3404 | 3521 | 3360 | 2798 | 2927 |
| eisl | 598 | 2320 | 887 | 0 | 2142 | 2399 | 2224 | 2444 | 2359 | 2390 | 2101 |
| fair | 3605 | 3199 | 2928 | 2276 | 2940 | 3082 | 2683 | 2638 | 3264 | 3082 | 2935 |
| flin | 1320 | 1081 | 1010 | 651 | 850 | 1317 | 1059 | 914 | 902 | 1176 | 1274 |
| fort | 230 | 1867 | 2589 | 1743 | 1941 | 2345 | 2240 | 2120 | 2180 | 2422 | 2217 |
| gala | 3479 | 3378 | 3542 | 3051 | 2769 | 3451 | 2911 | 3221 | 3546 | 3484 | 3135 |
| geno | 0 | 0 | 0 | 0 | 0 | 0 | 0 | 0 | 0 | 0 | 0 |
| glsv | 3476 | 3426 | 3187 | 2133 | 2541 | 3460 | 3528 | 3374 | 3408 | 2827 | 2859 |
| gode | 2550 | 2055 | 2041 | 1796 | 1830 | 0 | 2553 | 3131 | 3210 | 1422 | 0 |
| gold | 3343 | 3298 | 2881 | 2201 | 2566 | 3394 | 2704 | 2715 | 3378 | 3333 | 3041 |
| gope | 0 | 0 | 0 | 0 | 0 | 0 | 0 | 0 | 0 | 0 | 0 |
| goug | 3030 | 0 | 2964 | 2832 | 2794 | 3117 | 2993 | 2887 | 3249 | 3192 | 2612 |
| gras | 2961 | 3101 | 3138 | 2166 | 2176 | 2802 | 3249 | 3127 | 2909 | 2347 | 2514 |
| graz | 1339 | 2899 | 3425 | 2379 | 2516 | 3329 | 3457 | 3557 | 3517 | 2904 | 2750 |
| guam | 3106 | 2672 | 0 | 1977 | 2906 | 2643 | 2459 | 1590 | 2729 | 2227 | 2917 |
| harv | 0 | 872 | 2898 | 2178 | 2655 | 3341 | 2918 | 3022 | 3433 | 3356 | 3090 |
| hers | 3591 | 3646 | 3526 | 2312 | 2319 | 3364 | 3536 | 3417 | 3007 | 3031 | 3054 |
| hflk | 0 | 0 | 0 | 0 | 0 | 0 | 0 | 0 | 0 | 0 | 0 |
| ... | ... | ... | ... | ... | ... | ... | ... | ... | ... | ... | ... |

Table F.11: Daily DDobs numbers for cycle 11. (continued)

| site ID | day 114 | day 115 | day 116 | day 117 | day 118 | day 119 | day 120 | day 121 | day 122 | day 123 | day 124 |
|---|---|---|---|---|---|---|---|---|---|---|---|
| hnpt | 3238 | 2954 | 2887 | 2155 | 2212 | 2961 | 2573 | 2871 | 2911 | 648 | 512 |
| hob2 | 4016 | 3865 | 3871 | 2773 | 3215 | 3725 | 3982 | 3413 | 3515 | 3538 | 3736 |
| hofn | 4095 | 4040 | 4039 | 2490 | 3040 | 4068 | 3876 | 3866 | 4047 | 3763 | 3452 |
| holb | 586 | 465 | 131 | 0 | 339 | 676 | 420 | 83 | 88 | 385 | 562 |
| holc | 0 | 0 | 0 | 0 | 0 | 0 | 0 | 0 | 0 | 0 | 0 |
| holp | 0 | 0 | 0 | 0 | 0 | 0 | 0 | 0 | 0 | 0 | 0 |
| hrao | 2841 | 2675 | 2593 | 2486 | 2373 | 3129 | 3114 | 3009 | 3461 | 2897 | 2826 |
| iisc | 2732 | 2862 | 2703 | 1598 | 2247 | 2902 | 2768 | 2809 | 2059 | 1824 | 2462 |
| ineg | 0 | 0 | 0 | 0 | 0 | 0 | 0 | 0 | 0 | 0 | 0 |
| irkt | 2872 | 2878 | 2664 | 2015 | 2521 | 2652 | 2653 | 2642 | 2774 | 2285 | 2272 |
| jab1 | 0 | 0 | 0 | 0 | 0 | 0 | 0 | 0 | 0 | 0 | 0 |
| jama | 0 | 0 | 0 | 0 | 0 | 410 | 624 | 757 | 1281 | 1991 | 2092 |
| joze | 3276 | 3438 | 3405 | 2250 | 2445 | 3367 | 3539 | 3337 | 3382 | 2775 | 2894 |
| jplm | 3071 | 2812 | 2468 | 1967 | 2201 | 2716 | 2426 | 2501 | 2754 | 2669 | 2549 |
| karr | 3687 | 3926 | 3728 | 2764 | 2969 | 3627 | 3812 | 3414 | 3402 | 3061 | 3666 |
| kely | 3462 | 4070 | 3354 | 2544 | 3110 | 2956 | 2247 | 3057 | 4271 | 3241 | 3352 |
| kerg | 3682 | 3655 | 3747 | 3094 | 2889 | 3829 | 3758 | 3377 | 3687 | 3330 | 3417 |
| kiru | 3869 | 3950 | 3797 | 2331 | 2950 | 3736 | 3767 | 3694 | 3847 | 3313 | 3310 |
| kit3 | 1216 | 719 | 0 | 0 | 1961 | 345 | 0 | 0 | 0 | 0 | 0 |
| kokb | 2935 | 2872 | 2690 | 2361 | 2637 | 1739 | 2895 | 2861 | 2841 | 2762 | 2844 |
| kosg | 3633 | 3623 | 3537 | 2313 | 2317 | 3442 | 3542 | 3551 | 3430 | 3043 | 2988 |
| kour | 4037 | 3816 | 4242 | 3122 | 3073 | 4071 | 3685 | 4125 | 4067 | 3943 | 3700 |
| kr0g | 0 | 0 | 0 | 0 | 0 | 0 | 0 | 0 | 0 | 0 | 0 |
| kstu | 2066 | 2830 | 2524 | 1805 | 1950 | 2621 | 2616 | 2486 | 2671 | 2142 | 2047 |
| kunm | 1235 | 1441 | 1189 | 525 | 1415 | 1164 | 1883 | 1561 | 1264 | 674 | 866 |
| kwj1 | 0 | 0 | 0 | 0 | 0 | 0 | 0 | 0 | 0 | 0 | 0 |
| lama | 0 | 0 | 0 | 0 | 0 | 0 | 0 | 0 | 0 | 0 | 0 |
| lbch | 0 | 0 | 0 | 0 | 0 | 0 | 0 | 0 | 0 | 0 | 0 |
| leep | 0 | 0 | 0 | 0 | 0 | 0 | 0 | 0 | 0 | 0 | 0 |
| lhas | 2715 | 2888 | 2635 | 1940 | 2349 | 2728 | 2776 | 2611 | 2608 | 2201 | 2559 |
| long | 0 | 0 | 0 | 0 | 0 | 0 | 0 | 0 | 0 | 0 | 0 |
| lpgs | 3218 | 3440 | 3478 | 2934 | 2604 | 3414 | 3271 | 3208 | 3122 | 3129 | 2689 |
| mac1 | 4005 | 3864 | 4076 | 3261 | 3254 | 3791 | 3963 | 3776 | 3574 | 3704 | 3716 |
| madr | 3335 | 3371 | 3603 | 2356 | 2347 | 3089 | 3147 | 3541 | 3351 | 2877 | 2854 |
| mag0 | 3171 | 3154 | 2873 | 2423 | 2753 | 3038 | 2950 | 3173 | 3218 | 2800 | 2860 |
| mali | 3529 | 3533 | 3369 | 2439 | 2652 | 3679 | 3417 | 3086 | 3653 | 3252 | 2736 |
| mas1 | 3083 | 3196 | 3359 | 2311 | 2431 | 3277 | 3124 | 3384 | 3415 | 3046 | 2890 |
| mate | 3481 | 3362 | 3074 | 2096 | 2507 | 3116 | 3070 | 3308 | 3486 | 2937 | 2762 |
| math | 0 | 0 | 0 | 0 | 0 | 0 | 0 | 0 | 0 | 0 | 0 |
| maw1 | 4788 | 4815 | 4164 | 3488 | 3166 | 4888 | 4724 | 4242 | 4909 | 4369 | 4126 |
| mcm4 | 5051 | 5220 | 5066 | 4106 | 4233 | 5252 | 5164 | 4699 | 4799 | 4954 | 4592 |
| mdo1 | 2816 | 2377 | 2489 | 1873 | 1917 | 2740 | 2265 | 2545 | 2550 | 2442 | 2385 |
| mdvo | 3369 | 1349 | 255 | 1246 | 2632 | 3178 | 3338 | 3425 | 961 | 1862 | 2677 |
| medi | 0 | 0 | 0 | 0 | 0 | 0 | 0 | 0 | 0 | 0 | 0 |
| mets | 3603 | 3578 | 3697 | 2189 | 2757 | 3460 | 3926 | 3607 | 3632 | 3039 | 3164 |
| mkea | 2977 | 2816 | 2548 | 2290 | 2763 | 2896 | 2609 | 2766 | 2780 | 2698 | 2647 |
| monp | 0 | 2968 | 2819 | 2231 | 2576 | 3365 | 2688 | 2735 | 3374 | 3377 | 3070 |
| mr6g | 0 | 0 | 0 | 0 | 0 | 0 | 0 | 0 | 0 | 0 | 0 |
| nano | 1184 | 1092 | 784 | 408 | 708 | 1165 | 923 | 605 | 579 | 995 | 977 |
| nico | 3352 | 3290 | 3132 | 2069 | 2372 | 3147 | 3209 | 2867 | 3269 | 2706 | 2451 |
| nklg | 3344 | 3161 | 3401 | 2599 | 2580 | 3450 | 3618 | 3191 | 3343 | 3185 | 2952 |
| nlib | 3064 | 2821 | 2804 | 1987 | 2109 | 3048 | 2719 | 2680 | 2716 | 2712 | 2594 |
| noto | 0 | 0 | 0 | 0 | 0 | 0 | 0 | 0 | 0 | 0 | 0 |
| noum | 3626 | 3342 | 955 | 2398 | 3030 | 3248 | 3546 | 3184 | 3249 | 2965 | 0 |
| nrc1 | 3803 | 3563 | 3587 | 2564 | 2657 | 3569 | 3361 | 3588 | 3772 | 3626 | 3433 |
| nssp | 0 | 0 | 0 | 0 | 0 | 0 | 0 | 0 | 0 | 0 | 0 |
| ntus | 3723 | 3671 | 3544 | 2335 | 3114 | 3532 | 3488 | 3191 | 3267 | 2956 | 3240 |
| nya1 | 0 | 0 | 0 | 0 | 0 | 0 | 0 | 4314 | 4376 | 3820 | 3496 |
| nyal | 4399 | 3934 | 0 | 2145 | 3331 | 4128 | 3993 | 4247 | 4390 | 3845 | 3840 |
| oat2 | 0 | 0 | 0 | 0 | 0 | 0 | 0 | 0 | 0 | 0 | 0 |
| onsa | 3727 | 3742 | 3611 | 2340 | 2642 | 3679 | 3698 | 3641 | 3517 | 3145 | 3088 |
| penc | 0 | 0 | 0 | 0 | 0 | 0 | 0 | 0 | 0 | 0 | 0 |
| pert | 3437 | 3559 | 3675 | 3056 | 2869 | 3478 | 3666 | 3485 | 3476 | 3127 | 3474 |
| petp | 0 | 497 | 2230 | 1407 | 2461 | 2751 | 883 | 1648 | 2578 | 2511 | 2409 |
| pie1 | 2836 | 2488 | 2499 | 1867 | 1869 | 2747 | 2239 | 2395 | 2452 | 2554 | 2388 |
| pimo | 3009 | 2446 | 2438 | 2080 | 2779 | 2518 | 2192 | 2450 | 2790 | 1878 | 2509 |
| pol2 | 3145 | 2898 | 2567 | 1965 | 2472 | 2711 | 2695 | 2441 | 2829 | 2239 | 2423 |
| pots | 3582 | 3418 | 3320 | 2098 | 2406 | 3424 | 3622 | 3702 | 3472 | 2904 | 2779 |
| prds | 3405 | 3174 | 3212 | 2302 | 2477 | 3068 | 3192 | 3224 | 3268 | 3159 | 3098 |
| pvep | 0 | 0 | 0 | 0 | 0 | 0 | 0 | 0 | 0 | 0 | 0 |
| quin | 2888 | 2517 | 2182 | 1876 | 2163 | 2733 | 2321 | 2479 | 2703 | 2562 | 2432 |
| ... | ... | ... | ... | ... | ... | ... | ... | ... | ... | ... | ... |

Table F.11: Daily DDobs numbers for cycle 11. (continued)

| site ID | day 114 | day 115 | day 116 | day 117 | day 118 | day 119 | day 120 | day 121 | day 122 | day 123 | day 124 |
|---|---|---|---|---|---|---|---|---|---|---|---|
| ramo | 3271 | 3332 | 3057 | 2141 | 2444 | 3077 | 1215 | 2421 | 3084 | 2546 | 2475 |
| reyk | 4213 | 4277 | 4035 | 2456 | 2950 | 4055 | 3773 | 3823 | 3931 | 3761 | 3501 |
| riog | 3800 | 3535 | 3877 | 3642 | 3336 | 3635 | 3403 | 3006 | 3741 | 3787 | 3247 |
| riop | 0 | 0 | 0 | 0 | 0 | 0 | 0 | 0 | 0 | 0 | 0 |
| roch | 0 | 0 | 0 | 0 | 0 | 0 | 0 | 0 | 0 | 0 | 0 |
| rock | 0 | 0 | 0 | 0 | 0 | 0 | 0 | 0 | 0 | 0 | 0 |
| sant | 3655 | 3497 | 3440 | 3109 | 3193 | 3600 | 3284 | 3162 | 3633 | 3811 | 3127 |
| sch2 | 3882 | 3621 | 3481 | 2486 | 2685 | 3589 | 3331 | 3663 | 3814 | 3560 | 3337 |
| scip | 0 | 0 | 0 | 0 | 0 | 0 | 0 | 0 | 0 | 0 | 0 |
| sele | 2489 | 2570 | 2380 | 1585 | 1880 | 2335 | 2377 | 2341 | 2441 | 1710 | 1978 |
| sey1 | 1773 | 1637 | 1666 | 877 | 889 | 1682 | 1678 | 1672 | 1754 | 1276 | 1212 |
| sfer | 0 | 0 | 0 | 0 | 0 | 0 | 0 | 0 | 0 | 0 | 0 |
| shao | 2498 | 2667 | 2516 | 1808 | 2437 | 2334 | 2579 | 2227 | 2393 | 1872 | 2289 |
| sio3 | 550 | 337 | 0 | 0 | 235 | 463 | 367 | 165 | 75 | 225 | 393 |
| sni1 | 0 | 0 | 0 | 0 | 0 | 0 | 0 | 0 | 0 | 0 | 0 |
| sofi | 0 | 0 | 0 | 0 | 0 | 0 | 0 | 0 | 0 | 0 | 0 |
| sol1 | 3631 | 3478 | 3445 | 2526 | 2493 | 3556 | 3176 | 3537 | 3879 | 3546 | 3299 |
| spk1 | 0 | 0 | 0 | 0 | 0 | 0 | 0 | 0 | 0 | 0 | 0 |
| stjo | 3839 | 3901 | 3759 | 2515 | 2717 | 3796 | 3506 | 3756 | 3838 | 3694 | 3462 |
| suth | 3216 | 3319 | 3417 | 2977 | 2820 | 3348 | 3392 | 3349 | 3658 | 3337 | 2969 |
| suwn | 2913 | 3154 | 2719 | 2092 | 2568 | 2868 | 3052 | 562 | 2696 | 2174 | 2788 |
| syog | 4395 | 4308 | 4567 | 3640 | 3457 | 4453 | 4373 | 4247 | 4703 | 4131 | 3964 |
| tabl | 0 | 0 | 0 | 0 | 0 | 0 | 0 | 0 | 0 | 0 | 0 |
| thti | 3337 | 3440 | 3287 | 3033 | 2854 | 3565 | 3134 | 3497 | 3338 | 3411 | 3172 |
| thu1 | 3259 | 2930 | 2774 | 1884 | 1868 | 0 | 2446 | 2766 | 2805 | 2397 | 2543 |
| tidb | 4000 | 3761 | 3502 | 2749 | 3248 | 3889 | 3750 | 3222 | 3360 | 3502 | 3575 |
| tixi | 3999 | 3951 | 899 | 0 | 0 | 0 | 0 | 2944 | 3880 | 3513 | 3569 |
| torp | 0 | 0 | 0 | 0 | 0 | 0 | 0 | 0 | 0 | 0 | 0 |
| tow2 | 4042 | 3592 | 3585 | 2830 | 3180 | 3432 | 3780 | 3242 | 3338 | 3331 | 3549 |
| trab | 0 | 0 | 0 | 0 | 0 | 0 | 0 | 0 | 0 | 0 | 0 |
| trak | 0 | 0 | 0 | 0 | 0 | 0 | 0 | 0 | 0 | 0 | 0 |
| tro1 | 4077 | 4130 | 3906 | 2420 | 2947 | 3778 | 4011 | 4082 | 4095 | 3618 | 3545 |
| trom | 2174 | 4166 | 3963 | 2508 | 3107 | 3903 | 4045 | 4103 | 4202 | 3699 | 3557 |
| tskb | 1756 | 1936 | 1694 | 1103 | 2040 | 1831 | 2256 | 2056 | 1960 | 1378 | 1628 |
| uclp | 0 | 0 | 0 | 0 | 0 | 0 | 0 | 0 | 0 | 0 | 0 |
| uclu | 593 | 471 | 135 | 0 | 338 | 630 | 375 | 83 | 88 | 385 | 563 |
| urum | 2535 | 3119 | 2684 | 2022 | 2558 | 2830 | 2720 | 0 | 2628 | 2362 | 2458 |
| uscl | 0 | 0 | 0 | 0 | 0 | 0 | 0 | 0 | 0 | 0 | 0 |
| usna | 3183 | 3033 | 2814 | 1865 | 2096 | 2871 | 2660 | 2823 | 3166 | 2966 | 2784 |
| usno | 674 | 453 | 139 | 17 | 410 | 672 | 309 | 47 | 174 | 574 | 701 |
| usud | 2809 | 2760 | 2679 | 2262 | 2809 | 2506 | 2768 | 2647 | 2906 | 2145 | 2610 |
| vene | 0 | 0 | 0 | 0 | 0 | 0 | 0 | 0 | 0 | 0 | 0 |
| vesl | 0 | 0 | 0 | 0 | 0 | 0 | 0 | 0 | 0 | 0 | 0 |
| vill | 3383 | 3487 | 3599 | 2339 | 2373 | 3334 | 3352 | 3526 | 3390 | 2914 | 2905 |
| vndp | 1138 | 924 | 706 | 470 | 747 | 1114 | 696 | 491 | 665 | 972 | 983 |
| vs0g | 0 | 0 | 0 | 0 | 0 | 0 | 0 | 0 | 0 | 0 | 0 |
| wes2 | 760 | 453 | 139 | 17 | 433 | 713 | 361 | 105 | 233 | 616 | 708 |
| whc1 | 0 | 0 | 0 | 0 | 0 | 0 | 0 | 0 | 0 | 0 | 0 |
| whit | 3763 | 3765 | 3272 | 2243 | 2933 | 3605 | 3294 | 3128 | 3465 | 3411 | 3179 |
| widc | 0 | 0 | 0 | 0 | 0 | 0 | 0 | 0 | 0 | 0 | 0 |
| will | 2982 | 2866 | 2752 | 1995 | 2362 | 2866 | 2793 | 2644 | 2816 | 2702 | 2683 |
| wlsn | 0 | 0 | 0 | 0 | 0 | 0 | 0 | 0 | 0 | 0 | 0 |
| wroc | 0 | 0 | 0 | 0 | 0 | 0 | 0 | 0 | 0 | 0 | 0 |
| wslr | 1167 | 1044 | 707 | 389 | 725 | 1186 | 870 | 539 | 546 | 950 | 967 |
| wsrt | 3689 | 3674 | 3549 | 2288 | 2415 | 3517 | 3640 | 3581 | 3452 | 3069 | 3004 |
| wtzr | 3543 | 3474 | 3563 | 2462 | 2502 | 3360 | 3577 | 3636 | 3450 | 2918 | 2849 |
| wuhn | 3046 | 3329 | 3199 | 2274 | 2635 | 2991 | 3146 | 2896 | 2863 | 2386 | 2836 |
| xian | 0 | 0 | 0 | 0 | 0 | 0 | 0 | 0 | 0 | 0 | 0 |
| yakz | 0 | 0 | 0 | 0 | 0 | 0 | 0 | 0 | 0 | 0 | 0 |
| yar1 | 2293 | 2185 | 2827 | 1681 | 1289 | 2634 | 2743 | 2601 | 2379 | 2030 | 2477 |
| yell | 3768 | 3794 | 3627 | 2497 | 2947 | 3750 | 3531 | 3537 | 3648 | 3529 | 3438 |
| ykro | 0 | 0 | 0 | 0 | 0 | 0 | 0 | 0 | 0 | 0 | 0 |
| yssk | 3119 | 2910 | 2726 | 1917 | 2934 | 2834 | 2800 | 2788 | 3126 | 2614 | 2724 |
| zeck | 3318 | 3427 | 3106 | 2069 | 2534 | 1482 | 2938 | 3095 | 3250 | 2639 | 2543 |
| zimm | 3572 | 3389 | 3479 | 2357 | 2411 | 3303 | 3564 | 3553 | 3406 | 2848 | 2877 |
| zwen | 3509 | 3365 | 3391 | 2226 | 2651 | 3128 | 3368 | 3234 | 3179 | 2549 | 2808 |

## F.3 IGS Organization (agency)

Table F.12: IGS Organization (agency)

| IGS Organization(agency) | |
|---|---|
| AEC | Ohio University Avionics Engineering Center |
| ASDC | American Samoa Department of Commerce |
| BAYONET | Bayonet Network |
| BLM | Bureau of Land Management (NOAA) |
| CCO | Carbon County, UT |
| CETI | Condor Earth Technologies Inc |
| CNMI | Commonwealth of the Northern Marianas Islands, TQ |
| CofC | City of Cincinnati, OH |
| CofHP | City of High Point, NC |
| CofS | City of Scottsdale, AZ |
| CofT | City of Tucson, AZ |
| CWU | Central Washington University (PANGA) |
| DEDP | Delaware Department of Parks and Recreation |
| FLDOT | Florida Department of Transportation |
| FSL | Forecast System Laboratory (NOAA) |
| GTI | Greenville Technical Institute |
| HCC | Hagerstown Community College, MD |
| HGCSD | Harris Galveston Coastal Subsidence District |
| HSCfA | Harvard-Smithsonian Center for Astrophysics (BARGN) |
| IDDOT | Idaho Department of Transportation |
| IGN | Instituto Geografico Nacional (NOAA) |
| INETER | Instituto Nicaraguense de Estudios Territoriales (NOAA) |
| INUN | Indiana University, IN |
| JAMET | Jamaica Meterological Service (NOAA) |
| JPL | Jet Propulsion Laboratory |
| LAMT | Lamont Earth Observatory, NY |
| LCDT | Lake County Division of Transportation |
| LLNL | Lawrence Livermore National Laboratory, CA |
| LVVWD | Las Vegas Valley Water District |
| MDOT | Michigan Department of Transportation |
| NCAD | NCAD Corporation, KY |
| NCGS | North Carolina Geodetic Survey |
| NDDOT | North Dakota Dept. of Transportation |
| NGS | National Geodetic Survey (NOAA) |
| NJIT | New Jersey Institute of Technology |
| ODOT | Ohio Department of Transportation |
| OKDOT | Oklahoma Department of Transportation |
| OSPA | Oswego Port Authority |
| OSU | Oregon State University (PANGA) |
| PADOT | Pennsylvania Department of Transportation |
| PGPSF | Pacific GPS Facility |
| PSC | Paul Smith's College |
| SRP | Salt River Project, AZ |
| SATLOC | SATLOC Inc |
| SCGS | South Carolina Geodetic Survey |
| SLCSO | Salt Lake County Surveyor's Office |
| SOPAC | Scripps Orbit and Permanent Array Center (SCIGN) |
| SOPAC | Scripps Orbit and Permanent Array Center (RIVCOFLOOD) |
| SPSU | Southeastern Polytechnic University, GA |
| TRS | Columbia County, GA |
| TSEA | The Surveyors Exchange, AK |
| TXDOT | Texas Department of Transportation |
| UCB | University of California, Berkeley (BARD) |
| UIUC | University of |
| UNAVCO | University of Utah |
| USACE | US Army Corps of Engineers |
| USCG | US Coast Guard |
| USDOT | US Department of Transportation (USCG) |
| USGS | US Geological Survey (BARD) |
| USGS | US Geological Survey (SCIGN) |
| USNO | US Naval Observatory (JPL) |
| UVA | University of Virginia |
| UWA | University of Washington (PANGA) |
| VAOT | Vermont Agency of Transportation |
| VDOT | Virginia Department of Transportation |
| VIMS | Virginia Institute of Marine Science |

# Appendix G

# Acronyms

Table G.1: Acronyms

| | |
|---|---|
| 1-cpr | once per revolution |
| AAC | Associate Analysis Center |
| AC | Analysis Center |
| AS | anti-spoofing |
| BRD | broadcast ephemeris |
| CA | coarse acquisition |
| CDDIS | Crustal Dynamics Data Information System, USA |
| CNES | Centre National d'Etudes Spatiales, France |
| CODE | Center for Orbit Determination in Europe |
| CoM | Center of Mass |
| CSR | Center for Space Research, USA |
| DDobs | Double-Differenced Observation |
| DEOS | Delft Institute for Earth-Oriented Space Research |
| DORIS | Doppler Orbitography and Radiopositioning Integrated by Satellite |
| DUT | Delft University of Technology |
| ECEF | Earth-Centered-Earth-Fixed |
| EOP | Earth orientation parameter |
| FAGS | Federation of Astronomical and Geophysical Data Analysis Services |
| FLIN | Flin Flon: a new Canadian deformation array site |
| GFZ | GeoForschungsZentrum, Germany |
| GMST | Greenwich mean sidereal time |
| GPS | Global Positioning System |
| GSFC | Goddard Space Flight Center, USA |
| IAG | International Association of Geodesy |
| IAU | International Astronomical Union |
| ICRF | International Celestial Reference Frame |
| IERS | International Earth Rotation Service |
| IGS | International GPS Service |
| ILRS | International Laser Ranging Service |
| ITRF | International Terrestrial Reference Frame |
| ITRS | International Terrestrial Reference System |
| IUGG | International Union of Geodesy and Geophysics |
| JPL | Jet Propulsion Laboratory, USA |
| LEO | Low Earth Orbiters |
| LRA | Laser Retro-reflector Array |
| MSODP | Multi-Satellite Orbit Determination Program |
| NASA | National Aeronautics and Space Administration, USA |
| NAVSOL | Navigation Solution software |
| NGS | National Geodetic Survey |
| NOAA | National Oceanic and Atmospheric Administration, USA |
| OSTM | Ocean Surface Topography Mission |
| POD | Precision Orbit Determination |
| RINEX | Receiver-Independent Exchange format |
| rms | root mean square |
| SA | Selective Availability |
| SINEX | Software-Independent Exchange format |
| SLR | satellite laser ranging |
| TEC | total electron content |
| TEXGAP | university of TEXas Gps Analysis Program |
| TRSR | Turbo Rogue Space Receiver |
| UTOPIA | the University of Texas Orbit Processor |
| VLBI | very long baseline radio interferometry |

# Index

# Bibliography

Anderle, R.J. (1973). Geodetic Analysis Through Numerical Integration. In *Proceedings of the International Symposium on the Use of Artificial Satellites for Geodesy and Geodynamics*, Athens, Greece.

Anderle, R.J. (1986). Doppler satellite measurements and their interpretation. In A.J. Anderson & A. Cazenave, eds., *Space Geodesy and Geodynamics*, pp113–167, Academic Press, London.

Barlier, F., Berger, C., Falin, J., Kockarts, G. & Thuiller, G. (1977). A thermospheric Model Based on Satellite Drag Data. *Aeronomica Acta*, **185**.

Barotto, B. (1995). *Introduction of stochastic parameters to improve the estimation of the trajectories of a dynamical system by a least-squares method. Application to centimeter-level orbit determination of a satellite*. Ph.D. thesis, L'Universite Paul Sabatier, Toulouse, France.

Berger, C., Biancale, R., Ill, M. & Barlier, F. (1998). Improvement of the empirical thermospheric model DTM: DTM94 - a comparative review of various temporal variations and prospects in space geodesy applications. *Journal of Geodesy*, **72(3)**, pp161–178.

Bertiger, W., Bar-Sever, Y., Christensen, E., Davis, E., Guinn, J., Haines, B., Ibanez-Meier, R., Jee, J., Melbourne, S.L.W., Muellerschoen, R., Munson,

T., Vigue, Y., Wu, S., Yunck, T., Schutz, B., Abusali, P., Rim, H., Watkins, M. & Willis, P. (1994). GPS precise tracking of TOPEX/POSEIDON: results and implications. *J. Geophys. Res.*, **99(C12)**, pp24449–24464.

Bevis, M., Businger, S., Herring, T., Rocken, C., Anthes, R. & Ware, R. (1992). GPS methodology: Remote sensing of atmospheric water vapor using the global positioning system. *Journal of Geophysical Research*, **97(D14)**, pp15787–15801.

Beyer, W., ed. (1987). *CRC Standard Mathematical Tables*. CRC Press, Boca Raton, FL, 28th edn.

Cartwright, D. & Taylor, R. (1971). New computations of the tide generating potential. *Geopysical Journal of the Royal Astronomical Society*, **23**, pp45–74.

Casotto, S. (1989). *Ocean Tide Models for Topex Precise Orbit Determination*. Ph.D. thesis, Department of Aerospace Engineering and Engineering Mechanics, The University of Texas at Austin.

Casotto, S. (1993). Position and velocity perturbations in the orbital frame in terms of classical element perturbations. *Cel. Mech.*, **55**, pp209–221.

Chao, C. (1974). The tropospheric calibration model for Mariner Mars 1971. Tech. Rep. 32-1587, JPL, Pasadena, CA.

Chelton, D., Ries, J., Haines, B., Fu, L.L. & Callahan, P. (2001). Satellite Altimetry. In L.L. Fu & A. Cazenave, eds., *Satellite Altimetry and Earth*

*Sciences: A Handbook for Techniques and Applications*, chap. 1, Academic Press.

Choi, K.R., Ries, J.C. & Tapley, B.D. (2002). Jason-1 POD. In Y. Menard, ed., *Minutes of the fourth Joint TOPEX/POSEIDON and JASON-1 Scientific Working Team Meeting*, TP2-J0-CR-2156-CNES, Biarritz, France, presented at Jason-1 and T/P Scientific Working Team Meeting, June 10-12, 2002.

Colombo, O.L. (1989). The dynamics of Global Positioning System orbits and the determination of precise ephemerides. *Journal of Geophysical Research*, **94**, pp9167–9182.

Davis, J., Herring, T., Shapiro, I., Rogers, A. & Elgered, G. (1985). Geodesy by Radio Interferometry:Effects of Atmospheric Modeling Errors on Estimated Baseline Length. *Radio Science*, **20(6)**, pp1593–1607.

Eanes, R. & Bettadpur, S. (1996). The CSR 3.0 global ocean tide model. Tech. Rep. CSR TM 95-06, Center for Space Research, The University of Texas at Austin.

Eanes, R., Schutz, B. & Tapley, B. (1983). Earth and ocean tide effects on Lageos and Starlette. In *Proceedings of the 9th International Symposium on Earth Tides*, In J.T. Kuo (Ed.).

Eanes, R.J. (1995). *A study of temporal variations in Earth's Gravitational*

*Filed Using LAGEOS-1 Laser Range Observations*. Ph.D. thesis, The University of Texas at Austin.

Feulner, M.R. (1990). *The Numerical Integration of Near Earth Satellite Orbits Across SRP Boundaries Using the Method of Modified Back Differences*. Master's thesis, Department of Aerospace Engineering and Engineering Mechanics, The University of Texas at Austin.

Fu, L.L. *et al.* (1994). TOPEX/POSEIDON mission overview. *Journal of Geophysical Research*, **99**, pp24,369–24,381.

Gibson, L. (1983). A Derivation of Relativistic Effects in Satellite Tracking. Tech. Rep. TR 83-55, Naval Surface Weapons Center.

Girard, A. (1629). *Invention nouvelle en algebra*. Amsterdam, Netherlands.

Goad, C. (1980). Gravimetric Tidal Loading Computed from Integrated Green's Functions. *Journal of Geophysical Research*, **85**, pp2679–2683.

Goad, C. & Goodman, L. (1974). A Modified Hopfield Tropospheric Refraction Correction Model, presented at the AGU Fall Meeting, San Francisco, CA.

Haines, B., Bertiger, W., Desai, S., Kuang, D., Munson, T., Young, L. & Willis, P. (2002). Initial Orbit Determination Results for Jason-1: Towards a 1-cm Orbit. In *Proceedings of ION GPS 2002*, Portland, Oregon.

Hatanaka, Y. (1998). Compact RINEX Format. `ftp://igscb.jpl.nasa.gov/igscb/software/rnxcmp_2.4.0/docs/crinex.txt`.

Herring, T. (1992). Modeling atmospheric delays in the analysis of space geodetic data. In J.D. Munck & T. Spoelstra, eds., *Refraction of Transatmospheric Signals In Geodesy*, 36, pp157–164, Netherlands Geodetic Commission Publications in Geodesy.

Ho, C. (1990). *Precision Orbit Determination of Global Positioning System Satellites*. Ph.D. thesis, The University of Texas at Austin.

Hofmann-Wellenhof, B., Lichtenegger, H. & Collins, J. (1992). *GPS:Theory and Practice*. Springer-Verlag, Wien, New York, 2nd edn.

Holdridge, D. (1967). An alternate expression for light time using general relativity. *JPL Space Program Summary, 37-38*, pp2–4.

Imel, D. (1994). Evaluation of the TOPEX/POSEIDON dual-frequency ionosphere correction. *J. Geophys. Res.*, **99**, pp24,895–24,906.

Jacchia, L. (1977). Thermospheric Temperature Density and Computation:New Models. *Smith. Astrophys. Obs. Spec. Rep.*, **375**.

Kaula, W. (1966). *Theory of Satellite Geodesy*. Blaisdell, Waltham, Mass.

Kaula, W.E. (1970). The Terrestrial Environment: Solid Earth and Ocean Physics,(Williamstown Report). Tech. Rep. Report CR-1579, NASA.

Knocke, P. (1989). *Earth radiation presure effects on satellites*. Ph.D. thesis, University of Texas at Austin.

Lambeck, K. (1980). *The Earth's Variable Rotation: Geophysical Causes and Consequences*. Cambridge University Press.

Leick, A., ed. (1995). *GPS Satellite Surveying*. A Wiley Interscience Publication, New York, 2nd edn.

Lemoine, F.G. *et al.* (1998). The Development of the Joint NASA GSFC and NIMA Geopotential Model EGM96. Tech. Rep. TM-1998-206861, NASA.

Lerch, F.J., Wagner, C.A., Klosko, S.M. & Putney, B.H. (1981). Goddard Earth models for oceanographic applications (GEM 10B and 10C). *Mar. Geod.*, **5**, 2–43.

Lerch, F.J., Marsh, J.G., Klosko, S.M. & Williamson, R.G. (1982). Gravity model improvement for SEASAT. *J. Geophys. Res.*, **87**, 3281–3296.

Luthcke, S. & Marshall, J. (1992). Nonconservative force model parameter estimation strategy for TOPEX/POSEIDON precision orbit determination. Tech. Rep. Technical Memorandom 104575, NASA.

Luthcke, S.B. *et al.* (2002). Jason-1/TOPEX POD at NASA GSFC using GPS, SLR and DORIS Tracking. New Orleans, Louisiana, presented at the Jason-1 and T/P Scientific Working Team Meeting, 21-23 October, 2002.

Marini, J. & Murray, C. (1973). Correction for Laser Range Tracking for Atmosphere Refraction at Elevation above 10 Degrees. Tech. Rep. Technical Memorandom X-70555, GSFC, Greenbelt, Maryland.

Marshall, J., Luthcke, S., Antreasian, P. & Rosborogh, G. (1992). Modeling Radiation Forces Acting on TOPEX/POSEIDON for Precise Orbit Determination. Tech. Rep. Technical Memorandom 104564, NASA.

Marshall, J., Zelensky, N., Klosko, S., Chinn, D., Luthcke, S., Rachlin, K. & Williamson, R. (1995). The temporal ans spatial characteristics of the TOPEX/POSEIDON radial orbit error. *J. Geophys. Res.*, **100(C12)**.

McCarthy, D., Boucher, C., Eans, E., Fukushima, T., Herring, T., Lieske, J., Ma, C., Montag, H., Paquet, P., Reigber, C., Ries, J., Schutz, B., Standish, E., Veillet, C. & Wahr, J. (1989). IERS Standards. Tech. Rep. Note 3, IERS.

McCarthy, D.D. (1996). IERS Standards 1996. Tech. Rep. Note 21, Observatoire de Paris.

Melbourne, W.G., Davis, E.S., Yunck, T.P. & Tapley, B.D. (1994). The GPS flight experiment on TOPEX/POSEIDON. *Geophys. Res. Lett.*, **21**, pp2171–2174.

Minster, R. & Jordan, T. (1987). Vector constraints on western U.S. deformation from space geodesy, neotectonics, and plate motions. *J. Geophys. Res.*, **92(B6)**.

Moyer, T.D. (1981). Transformation from proper time on earth to coordinate time in solar system barycentric space-time frame of reference. *Celestial Mechanics*, **23**, pp33–68.

Nerem, R.S. *et al.* (1994). Gravity model development for TOPEX/POSEIDON:Joint Gravity Model-1 and 2. *J. Geophys. Res.*, **99**, pp 24421–24447.

Nöuel, F., Bardina, J., Jayles, C., Labrune, Y. & Troung, B. (1988). DORIS: A precise satellite positioning doppler system. In J.S. et al., ed., *Adv. Astron. Sci.*, vol. 65, 311–320.

Perrygo, C. (1987). TOPEX Satellite Yaw Maneuvers. Tech. Rep. REF:968:SE:87-074, Fairchild Space Company Inter-Office Communication.

Ries, J. (1989). Simulation of an experiment to measure the Lense-Thirring precession using a second Lageos satellite. Tech. Rep. CSR 89-5, Center for Space Research, The University of Texas at Austin.

Ries, J., Huang, C. & Watkins, M. (1988). Effect of General Relativity on a near-Earth satellite in the geocentric and barycentric reference frames. *Phys. Rev. Lett.*, **61**, pp903.

Ries, J.C. & Tapley, B.D. (1999). Centimeter level orbit determination for the TOPEX/POSEIDON altimeter satellite. *Adv. Astronautical Sci.*, **102**, 583–598.

Ries, J.C., Choi, K.R. & Tapley, B.D. (2000). Jason-1 and TOPEX/POSEIDON Precision Orbit Determination: Status and Plans. In L.L. Fu, ed., *Minutes of the third Joint TOPEX/POSEIDON and JASON-1 Scientific Working Team Meeting*, JPL D-20240, Miami, Florida, presented

at Jason-1 and T/P Scientific Working Team Meeting, November 15-17, 2000.

Ries, J.C., Chambers, D.P., Choi, K.R. & Eanes, R.J. (2001). Effect of ITRF2000 on TOPEX/POSEIDON Orbit Determination and Mean Sea Level Time Series. AGU, San Francisco, CA., presented at Fall AGU, 2001.

Ries, J.C., Choi, K.R. & Tapley, B.D. (2002). Jason-1 POD. In Y. Menard, ed., *Minutes of the fourth Joint TOPEX/POSEIDON and JASON-1 Scientific Working Team Meeting*, TP2-J0-CR-2156-CNES, Biarritz, France, presented at Jason-1 and T/P Scientific Working Team Meeting, June 10-12, 2002.

Rim, H. (1992). *TOPEX orbit determination using GPS tracking system.* Ph.D. thesis, The University of Texas at Austin.

Rodríguez, E. & Martin, J.M. (1994). Estimation of the electromagnetic bias from retracked TOPEX data. *J. Geophys. Res.*, **99**, pp24,971–24,979.

Rosborough, G.W. (1986). Satellite orbit perturbations due to the geopotential. Tech. Rep. CSR 86-1, Center for Space Research, The University of Texas at Austin.

Ruf, C., Keihm, S., Subramanya, B. & Janssen, M. (1994). TOPEX/POSEIDON microwave radiometer performance and in-flight calibration. *J. Geophys. Res.*, **99**, pp24,915–24,926.

Saastamoinen, J. (1972). Atmospheric Correction for the Troposphere and Stratosphere in Radio Ranging of Satellites. In *The Use of Artificial Satellites for Geodesy*, vol. 15, Geophysics Monograph Series, American Geophysical Union, Washington D.C.

Schutz, B., Tapley, B., Abusali, P. & Rim, H. (1994). Dynamic orbit determination using GPS measurements from TOPEX/POSEIDON. *Geophys. Res. Lett.*, **21(19)**.

Schwiderski, E. (1978). Global Ocean Tides Part 1: A Detailed Hydrodynamical Model. Tech. Rep. TR-3866, U.S. Naval Surface Weapons Center.

Shum, C.K., Zhang, B.H., Schutz, B.E. & Tapley, B.D. (1990). Altimeter Crossover Methods for Precision Orbit Determination and Mapping of Geophysical Parameter. *The Jounal of the Astronautical Sciences*, **38(3)**, 355–368.

Standish, E. (1982). Orientation of the JPL Ephemerides, DE200/LE200, to the Dynamical Equinox of J2000. *Astronomy and Astrophysics*, **114**, pp297–302.

Stephens, G., Campbell, G. & Harr, T.V. (1981). Earth Radiation Budgets. *J. Geophys. Res.*, **86(C10)**, pp9739–9760.

Stewart, R., Fu, L.L. & Lefebvre, M. (1986). Science opportunities from the TOPEX/POSEIDON mission. Tech. Rep. JPL Publication 86-18.

Tapley, B., Schutz, B., Ries, J. & Shum, C. (1990). Precision Orbit Determination for Topex. *Adv. Space Res.*, **10(3-4)**, pp(3)239–(3)247.

Tapley, B., Schutz, B., Eanes, R., Ries, J. & Watkins, M. (1993). Lageos laser ranging contributions to geodynamics, geodesy, and orbital dynamics. In *Space Geodesy and Geodynamics, Crustal Dynamics Project Monograph*, AGU.

Tapley, B., Watkins, M., Ries, J., Davis, G., Eans, R., Pool, S., Rim, H., Schutz, B., Shum, C., Nerem, R., Lerch, F., Marshall, J., Klosko, S., Pavlis, N. & Williamson, R. (1996). The JGM-3 geopotential model. *J. Geophys. Res.*, **101(B12)**, pp28029–28049.

Tapley, B.D. (1973). Statistical orbit determination theory. In B.D. Tapley & V. Szebehely, eds., *Recent Advances in Dynamical Astronomy*, D. Reidel, Hingham, MA.

Tapley, B.D. & Ries, J.C. (2003). Precision Orbit Determination for Earth Observation Systems. In *Encyclopedia of Space Science and Technology*, pp341–355, Wylie and Sons, Hoboken, New Jersey.

Tapley, B.D. *et al.* (1994). Precision orbit determination for TOPEX/POSEIDON. *J. Geophys. Res.*, **99**, pp24383–24404.

Theillier, F. (1988). Effects of Solar Array Pitch Angle Error, Thermal Imbalance and Warping on TOPEX Satellite Orbit. Tech. Rep. CSR TM 88-02, Center for Space Research, The University of Texas at Austin.

Vanicek, P. & Krakiwsky, E. (1986). *Geodesy:The Concepts*. North-Holland Publishing Company.

Wahr, J. (1981). The forced nutations of an elliptical, rotating, elastic, and oceanless earth. *Geophysical Journal of the Royal Astronomical Society*, **64**, pp705–727.

Willis, P. *et al.* (2002). TOPEX/JASON combined GPS/DORIS orbit determination in the tandem phase. COSPAR01-A-00547.

Wu, S.C., Yunck, T.P. & Thornton, C.L. (1989). Reduced-Dynamic Technique for Precise Orbit Determination of Low Earth Satellite. In *AAS/AIAA Astrodynamics Specialist Conf. Proceedings*, AAS-87-410, Kalispell, Montana.

Wu, S.C., Yunck, T.P. & Thornton, C.L. (1991). Reduced-Dynamic Technique for Precise Orbit Determination of Low Earth Satellite. *J. Guid. Control Dynam.*, **14**, pp24–30.

Yuan, D.N. (1991). *The Determination and Error Assessment of the Earth's Gravity Field Model*. Ph.D. thesis, Department of Aerospace Engineering and Engineering Mechanics, The University of Texas at Austin.

Yunck, T.P. & Wu, S. (1986). Non-dynamic decimeter tracking of earth satellites using global positioning system. In *AIAA 24th Aerospace Sciences Meeting*, AIAA-86-0404, Reno, Nevada.

Yunck, T.P. *et al.* (1994). First assessment of GPS-based reduced dynamic orbit determination on TOPEX/POSEIDON. *Geophys. Res. Lett.*, **21**, pp541–544.

Zelensky, N.P. *et al.* (2002). Jason-1 POD with SLR and DORIS Tracking. New Orleans, Louisiana, presented at the Jason-1 and T/P Scientific Working Team Meeting, 21-23 October, 2002.

Ziebart, M., Adhya, S. & Cross, P. (2002). Pixel Array Solar and Thermal Force Modelling for JASON: Initial Results. New Orleans, Louisiana, presented at the Jason-1 and T/P Scientific Working Team Meeting, 21-23 October, 2002.

Zumberge, J. (1996). Station Report. `ftp://igscb.jpl.nasa.gov/igscb/data/network/igsnet.doc`.

Zwillinger, D., ed. (1995). *CRC Standard Mathematical Tables and Formulae*. CRC Press, Boca Raton, FL.

# Vita

Key-Rok Choi was born in Kwan-Chon, Jeon-Book Province of South Korea on 20 October 1968, the son of Tae-Sung Choi and In-Soon Lee. He received the Bachelor of Science degree in Astronomy in 1991 from the Seoul National University at Seoul in Korea and served in the Korean Defence Army in 1991-1992. After the national guard service, he returned to the school to continue Master program in Astronomy. In 1996, he applied to the University of Texas at Austin for enrollment in their Aerospace program. He was accepted and started graduate studies in August, 1996. While pursuing the Ph.D. degree, he joined the Center for Space Research of the University of Texas at Austin in January of 1997. He currently is working at the University of Texas/Center for Space Research.

Permanent address: 2005 W.Loop Apt.C
Austin, Texas 78758

This dissertation was typeset with LaTeX[†] by the author.

[†]LaTeX is a document preparation system developed by Leslie Lamport as a special version of Donald Knuth's TeX Program.